Edited by François Diederich,
Peter J. Stang, and Rik R. Tykwinski

WILEY-VCH

Modern Supramolecular Chemistry

Strategies for Macrocycle Synthesis

Modern Supramolecular Chemistry

Edited by
François Diederich, Peter J. Stang,
and Rik R. Tykwinski

Related Titles

Schalley, C. A. (ed.)

Analytical Methods in Supramolecular Chemistry

2007
ISBN: 978-3-527-31505-5

Dodziuk, H. (ed.)

Cyclodextrins and Their Complexes

Chemistry, Analytical Methods, Applications

2006
ISBN: 978-3-527-31280-1

Cragg, P.

A Practical Guide to Supramolecular Chemistry

2005
ISBN: 978-0-470-86654-2

Gleiter, R., Hopf, H. (eds.)

Modern Cyclophane Chemistry

2004
ISBN: 978-3-527-30713-5

Modern Supramolecular Chemistry

Strategies for Macrocycle Synthesis

Edited by
François Diederich, Peter J. Stang, and Rik R. Tykwinski

WILEY-
VCH

WILEY-VCH Verlag GmbH & Co. KGaA

The Editors

Prof. Dr. François Diederich
ETH Hönggerberg, HCI
Laboratory for Organic Chemistry
Wolfgang-Pauli-Str. 10
8093 Zürich
Switzerland

Prof. Dr. Peter J. Stang
University of Utah
Department of Chemistry
Henry Eyring Building
Salt Lake City, UT 84112
USA

Prof. Dr. Rik R. Tykwinski
University of Alberta
Department of Chemistry
Edmonton, Alberta, T6G 2G2
Canada

Contents

Preface

The 1987 Nobel Prize in Chemistry was awarded to Donald J. Cram, Jean-Marie Lehn, and Charles J. Pedersen for "their development and use of molecules with structure-specific interactions of high selectivity". At this time, the award was bestowed for the synthesis of molecules that mimicked important biological processes – what Lehn deemed supramolecular chemistry. In the two decades that have followed, this field has expanded greatly, and supramolecular breakthroughs in organic synthesis, molecular electronics, and materials science have now been realized. It is interesting to note, however, that in many respects supramolecular chemistry has remained close to its roots. The pioneering efforts that merited the Nobel Prize were based primarily on the synthesis of macrocycles. These were the crown ethers, the cryptands, the cavitands, and other host molecules that ultimately provide a welcoming and selective environment for a particular guest species, whether it be a neutral molecule, a cation, or an anion.

Both historically and in the present day, supramolecular chemistry beautifully marries two scientific disciplines: organic synthesis and physical organic chemistry. It is here that the most modern aspects of this field of chemistry share the spotlight. No longer is the objective simply to mimic biological systems such as enzymes, but rather, today's supramolecular chemist is limited only by his or her imagination as to the role that a macrocycle might play in some well-orchestrated chemical scheme.

The goal of the present monograph is to tie together these seemingly diverse achievements under a common heading: the synthesis of macrocycles for use in supramolecular chemistry. To this end, the biological relevance of macrocycles continues to play a pivotal role, as illustrated by a chapter on macrocyclic peptides by Liskamp and co-workers. The emergence of ring-closing metathesis as a pre-eminent synthetic strategy for constructing naturally occurring macrocycles is described next by Prunet *et al.* Synthetic efforts toward macrocycles continue to be inspired by Nature, and these stories are recounted by de Mendoza and Ballester (hydrogen-bonding assembly), Isaacs and coworkers (curcurbiturils), Böhmer and Podoprygorina (tetra-urea calixarenes), and Sessler and coworkers (anion-binding macrocycles). From here, supramolecular chemistry melds into materials chemistry, where shape-persistent macrocycles (Tykwinski and Sadowy), three-dimensional

architectures (Dalcanale and Pirondini), molecular containers (Fujita and Yoshizawa), and rotaxanes (Wisner and Blight) share the stage. While it is not possible to review comprehensively each of the above topics, we believe this monograph provides expert insight and advice, covering both synthetic endeavors and applications of the resulting products. Most of all, however, we hope that these 10 chapters will instill the inspiration to further expand the boundaries of this captivating field of research.

This book results from the substantial efforts of a number of people. Most importantly, we appreciate the contributions of the authors. In this era of dwindling time and funding, their efforts and expertise have provided a monograph that is both interesting to read and a scientific resource. We express our gratitude to Ms. Annie Tykwinski for the original illustration that became the cover of this book, and we would like to thank Drs. Manfred Köhl and Andreas Sendtko at Wiley-VCH, as well as the production staff, for their aid in preparing this monograph.

November 2007

François Diederich
Peter J. Stang
Rik R. Tykwinski
Zurich, Salt Lake City, Edmonton

List of Contributors

Saskia E. Bakker
Utrecht University
Faculty of Science
Department of Pharmaceutical Sciences
Medicinal Chemistry and Chemical
Biology
P.O. Box 80082
3508 TB Utrecht
The Netherlands

Pablo Ballester
Institute of Chemical Research of
Catalonia (ICIQ) and
Institució Catalana de Recerca i Estudis
Avançats (ICREA)
Avda. Països Catalans, 16
43007 Tarragona
Spain

Barry A. Blight
University of Western Ontario
Faculty of Science
Department of Chemistry
1151 Richmond St., Chemistry Building
London, Ontario, N6A 5B7
Canada

Volker Böhmer
Johannes Gutenberg-Universität
Mainz
Fachbereich Chemie, Pharmazie
und Geowissenschaften
Duesbergweg 10–14
55099 Mainz
Germany

Enrico Dalcanale
Università di Parma
Dipartimento di Chimica Organica e
Industriale
Viale G. Usberti 17/A
43100 Parma
Italy

Jean-Pierre Férézou
École Polytechnique
Laboratoire de Synthèse Organique,
DCSO
CNRS UMR 7652
91128 Palaiseau
France

Makoto Fujita
University of Tokyo
Department of Applied Chemistry
School of Engineering
and CREST (Core Research for
Evolution Science and Technology)
Japan Science and Technology Agency
(JST)
7-3-1 Hongo, Bunkyo-ku
Tokyo 113-8656
Japan

Wei-Hao Huang
University of Maryland
Department of Chemistry and
Biochemistry
College Park, MD 20742
USA

Lyle Isaacs
University of Maryland
Department of Chemistry and
Biochemistry
College Park, MD 20742
USA

Evgeny A. Katayev
Russian Academy of Sciences
A.N. Nesmeyanov Institute of
Organoelement Compounds
Vavilov St., 28
119899 Moscow
Russia

Rob M. J. Liskamp
Utrecht University
Faculty of Science
Department of Pharmaceutical Sciences
Medicinal Chemistry and
Chemical Biology
P.O. Box 80082
3508 TB Utrecht
The Netherlands

Simin Liu
University of Maryland
Department of Chemistry and
Biochemistry
College Park, MD 20742
USA

Patricia J. Melfi
University of Texas at Austin
Department of Chemistry and
Biochemistry
1 University Station - A5300
Austin, Texas 78712
USA

Javier de Mendoza
Institute of Chemical Research of
Catalonia (ICIQ)
Avda. Països Catalans, 16
43007 Tarragona
Spain

Laura Pirondini
Università di Parma
Dipartimento di Chimica Organica e
Industriale
Viale G. P. Usberti 17/A
43100 Parma
Italy

Ganna Podoprygorina
Johannes Gutenberg-Universität Mainz
Fachbereich Chemie, Pharmazie und
Geowissenschaften
Duesbergweg 10–14
55099 Mainz
Germany

Joëlle Prunet
École Polytechnique
Laboratoire de Synthèse Organique,
DCSO
CNRS UMR 7652
91128 Palaiseau
France

Dirk T. S. Rijkers
Utrecht University
Faculty of Science
Department of Pharmaceutical Sciences
Medicinal Chemistry and Chemical
Biology
P.O. Box 80082
3508 TB Utrecht
The Netherlands

Amber L. Sadowy
University of Alberta
Department of Chemistry
Edmonton, Alberta, T6G 2G2
Canada

Anderson Rouge dos Santos
Universidade Federal do Rio de Janeiro
Instituto de Química
Caixa Postal 068534
Ilha do Fundão, CT, Bloco A
CEP 21941-972 Rio de Janeiro RJ
Brazil

Jonathan L. Sessler
University of Texas at Austin
Department of Chemistry and
Biochemistry
1 University Station - A5300
Austin, Texas 78712
USA

Rik R. Tykwinski
University of Alberta
Department of Chemistry
Edmonton, Alberta, T6G 2G2
Canada

James A. Wisner
University of Western Ontario
Faculty of Science
Department of Chemistry
1151 Richmond St., Chemistry Building
London, Ontario, N6A 5B7
Canada

Michito Yoshizawa
Department of Applied Chemistry
School of Engineering
The University of Tokyo
and CREST (Core Research for
Evolution Science and Technology)
Japan Science and Technology Agency
(JST)
7-3-1 Hongo, Bunkyo-ku, Tokyo
113-8656
Japan

1
Bioactive Macrocyclic Peptides and Peptide Mimics

Rob M.J. Liskamp, Dirk T.S. Rijkers, and Saskia E. Bakker

1.1
Introduction

The number of both naturally occurring and synthesized biologically active cyclic peptides, modified peptides, and peptide mimics is rapidly increasing. So far, many of these sometimes biologically very potent peptides have unfortunately unknown molecular targets or mechanisms of action. This certainly opens up very interesting and challenging research areas with respect to uncovering these targets and/or molecular mechanisms of biological activity, which – depending on the biological action – can be very promising, for example, for the development of new drugs. However, merely a review of most biologically active cyclic peptides – if this were possible at all – is not the aim of this chapter. Instead, we wish to focus on selected bioactive macrocyclic peptide systems with known molecular *peptide* or *protein* targets as well as details about their molecular interaction mechanism. Where possible, we would like to discuss the contribution of the *cyclic* nature of the peptides to the molecular mechanism of interaction and the ensuing biological activity. We will therefore not include cyclic peptides and mimics merely interacting with membrane lipids or cyclic peptides interacting with DNA or RNA. Each of these topics deserves a review on its own, especially in light of the increasing interest in membrane proteins and transcription activators/regulators.

The selection of cyclic peptides interacting with known molecular targets in this chapter is largely determined by their relevance in relation to possible treatments of diseases. In this respect, probably vancomycin and cyclosporin are the most well-known cyclic peptides containing modified amino acids, which have had a profound influence on the treatment of life-threatening diseases. The vancomycin-related antibiotics [1] are outstanding examples of cyclic peptide systems containing multiple knotted side chains by which almost absolute control over the shape of the molecule is achieved, leading to efficient binding of crucial fragments of the cell-wall precursor of disease-causing bacteria.

In the larger peptide antibiotic compounds comprising the class of lantibiotics, the shape of the molecule is determined by several cyclic peptides, including two annulated peptide rings, present within one molecule, giving the lantibiotic a unique way to interact with the target molecule lipid II and subsequent pore-forming capabilities in phospholipid membranes [2].

In an increasing number of examples, the diversity of functions and activities of proteins can be reflected in their smaller peptide counterparts, and this is especially prominent in RGD-containing cyclic peptides and peptide mimics derived from the corresponding RGD sequence in proteins. These are capable of interacting with a variety of integrin receptors ($\alpha_V\beta_3$ and $\alpha_{IIb}\beta_3$) involved in cellular adhesion and migration [3]. As a result, the RGD sequence is, for example, crucial in the construction of (cyclic) peptide compounds used for molecular imaging and treatment of diseases such as cancer and infections.

However, it is good to realize that many biologically relevant cyclic peptides are not derived from or do not correspond to particular peptide sequence(s) in a larger protein molecule. These cyclic peptides are produced by micro-organisms, and although they are macrocyclic structures, they are of course much smaller than proteins. In addition to vancomycin and the lantibiotics mentioned above, other important examples are cyclosporin A [4] and cyclotheonamide [5]. The former cyclic peptide is the widely used immunosuppressive drug while the latter is capable of specifically interacting with thrombin, a crucial serine protease in the blood clotting cascade. As a consequence, cyclotheonamide and chemically synthesized analogs are potentially important for modulating blood clotting.

In principle, there is no limitation to the nature of the biological process or cascade, which can be influenced by (cyclic) peptides and their derivatives, and it should be emphasized that cyclic peptides and mimics derived thereof could be powerful instruments in modulating signal transduction. This is apparent, for example, from the interaction of cyclic peptides with SH2-domains involved in, among others, allergy, cancer and other diseases.

At present many biologically extremely important cyclic peptides and derivatives such as octreotide/octreotate [6] fall outside the scope of this contribution, simply because their exact molecular interaction mechanism together with their biological target are still unknown [7], which certainly poses a challenge for future research directed toward unraveling their biomolecular mechanisms of action. In addition, in many cases the molecular events subsequent to the specific interaction with a receptor are still unknown, leaving many unanswered questions with respect to the ultimate biological effects.

Cyclization of a linear peptide (Figure 1.1) endows the cyclic peptide first of all with a considerably reduced flexibility as compared to the parent peptide, which is (generally consisting of up to about ten amino acid residues) a very flexible molecule. Each amino acid residue contributes two single bonds to the conformational flexibility of the molecule, and generally speaking the only relatively rigid bond (*trans* and *trans/cis* in proline and *N*-alkylated amino acid-containing peptides) is the amide bond. After approximately ten to twenty amino acid residues, secondary structure elements (such as α-helices [8], turns, and β-strands) start to form. The reduced

"head to tail" cyclization

side chain to side chain cyclization

backbone to backbone cyclization

X = NH
X = O (depsipeptide)

X = NH (peptide amide)
X = O (peptide acid)

Y = ~S–S~ (disulfide bridge)
Y = ~S~ (thio ether or sulfide bridge)
Y = ~NH-C(O)~ (lactam bridge)
Y = ~O-C(O)~ (depsipeptide; lactone bridge)
Y = ~CH=CH~ (alkene bridge)
Y = ~C≡C~ (alkyne bridge)

X = NH (peptide amide)
X = O (peptide acid)

Y = ~S–S~ (disulfide bridge)
Y = ~NH-C(O)~ (lactam bridge)
Y = ~O-C(O)~ (depsipeptide; lactone bridge)
Y = ~CH=CH~ (alkene bridge)

side chain to C-terminus cyclization

side chain to N-terminus cyclization

X = NH
X = O (depsipeptide)

X = NH (peptide amide)
X = O (peptide acid)

Y = NH (lactam bridge)
Y = O (depsipeptide)

Figure 1.1 Different ways of peptide cyclization.

flexibility of the cyclic peptide derivative as compared to the open form is a distinct advantage for interaction with a potential molecular target. In general, provided that no significant enthalpy-entropy compensation takes place [9], a cyclized peptide which is less flexible and therefore more pre-organized, will display a higher affinity because it will lose less entropy upon interaction with its molecular target. As such, cyclization is also a universal first approach to increase the affinity of a peptide. An associated advantage of a cyclic peptide structure is the decreased sensitivity to proteolytic degradation, especially by exoproteases, which will be favorable for the half-life of the (cyclic) peptide and thereby its bioavailability.

1.2
Selected Cyclic Peptides

For this review we have selected the cyclic modified peptides mentioned above, i.e. vancomycin, nisin, cyclosporin, and cyclotheonamide, as well as two examples, i.e. RGD-containing cyclic peptides and SH2 domain binding cyclic peptides, which were inspired by proteins.

1.2.1
Vancomycin

Vancomycin (**1**, Figures 1.2 and 1.3) is a glycopeptide antibiotic with high activity against Gram-positive bacteria and is particularly renowned for its activity against the feared methicillin-resistant *Staphylococcus aureus* (MRSA) species [1b]. Vancomycin is produced by *Amycolatopsis orientalis*, a bacterium originally found in a soil

1
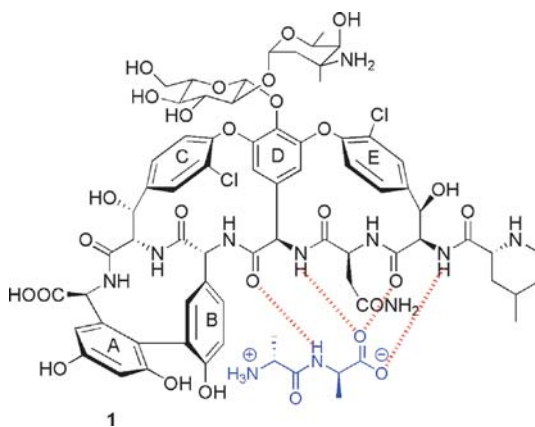
Figure 1.2 Structure of vancomycin (**1**). The dipeptide ligand D-Ala-D-Ala is shown in blue and the hydrogen bonds are shown in red. In the case of the D-Ala-D-lactate ligand, one hydrogen bond is lost and replaced by a repulsion due to the free electron pairs on oxygen.
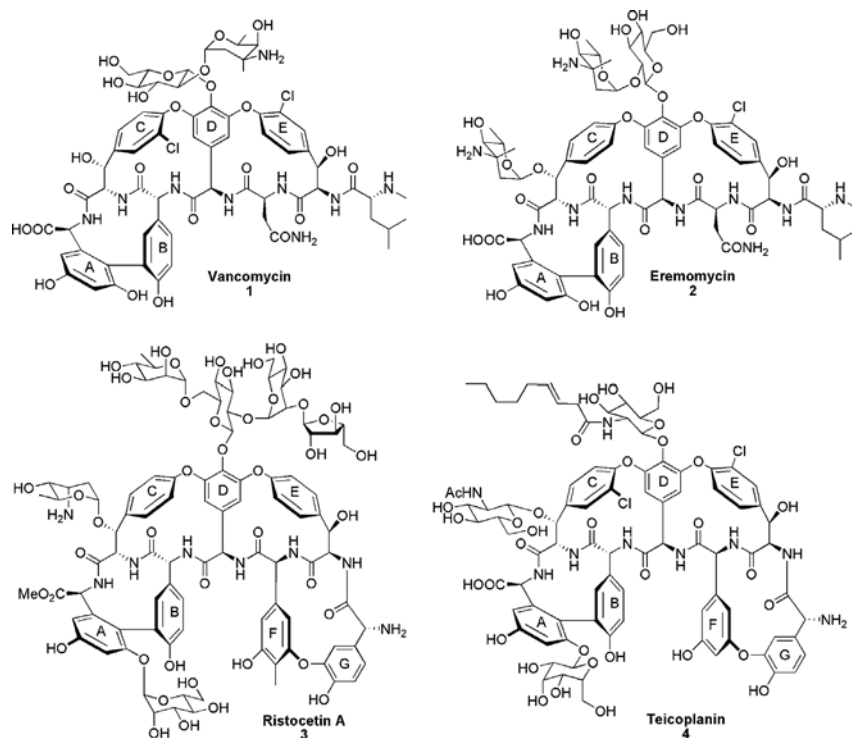
Figure 1.3 Chemical structures of glycopeptides antibiotics
vancomycin (**1**) [1], eremomycin (**2**) [15a], ristocetin A (**3**) [15b],
and teicoplanin (**4**) [15c].

sample from Borneo, Indonesia. The biosynthetic pathway and the total syntheses of
vancomycin and related structures have been reviewed in a comprehensive account
by Nicolaou and coworkers [1b]. Vancomycin is one of the representatives of the
glycopeptide family [1]. The vancomycin aglycon consists of a heptapeptide with
several non-proteinogenic amino acids. Residues 4, 5, and 7 are phenylglycine deri-
vatives with different substitution patterns of the aromatic ring, while residues 2 and 6
are β-hydroxytyrosines with chlorine substituents in the *ortho* position. The side chains
are involved in the formation of three macrocycles named after the component re-
sidues: residues 5 and 7 form the *A-B* biaryl system, while residues 2, 4, and 6 form the
two bisaryl ether systems *C-D* and *D-E*, respectively (Figures 1.2 and 1.3). The sugar
moieties are glucose and vancosamine [1b].

Vancomycin and other glycopeptides inhibit cell wall synthesis by non-covalent
binding to the D-Ala-D-Ala peptide motif of the cell wall precursor lipid II [10]. Four
hydrogen bonds are formed when vancomycin binds the D-Ala-D-Ala motif, and all of
these involve the peptide backbone [1,10], as shown in Figure 1.2.

Dimerization of vancomycin and other glycopeptide antibiotics, as well as anchor-
ing of glycopeptides in the bacterial cell membrane, contribute favorably to the

antibacterial effect [1]. Although eremomycin (**2**, Figure 1.3) has a lower affinity for model peptides *in vitro*, *in vivo* it is consistently more active than vancomycin. It seems that the actual activity of glycopeptide antibiotics depends on a balance between the dimerization constant and the affinity for model peptides *in vitro* [11]. The dimerization constant increases when ligand is added and *vice versa* [12], except in the case of ristocetin A [11] (**3**, Figure 1.3). Anchoring of the antibiotic to the bacterial cell wall by a lipophilic chain, as is the case with teicoplanin (**4**, Figure 1.3), also enhances antibacterial activity [13]. In both cases the enhanced activity can be explained by a decrease in entropy of binding, because the binding of the antibiotic to the target peptide becomes effectively intramolecular [1,12,13]. Cell wall synthesis may be inhibited because the enzymes involved in this can no longer bind to the peptide [10].

Resistance to vancomycin can follow three patterns [14]. In both VanA- and VanB-type resistance, the terminal D-alanine residue of the peptidoglycan cell wall precursor is replaced by a D-lactate. Because this changes the amide bond into an ester, a hydrogen bond donor is lost and repulsion between the carbonyl oxygen and lactate-ester oxygen is present, resulting in a thousand-fold loss of affinity (Figure 1.2). The VanA Enterococci (*E. faecium, E. faecalis*) are resistant to high concentrations of vancomycin and also clinically used teicoplanin (**4**), whereas VanB Enterococci are resistant to a wider range of vancomycin concentrations but remain susceptible to teicoplanin [14]. In VanC-type resistance (*E. gallinarum, E. casseliflavus*), the terminal amino acid D-alanine is replaced by D-serine, and loss of activity is probably due to steric hindrance from the serine side chain [1,14]. Knowing the molecular nature of resistance may be very important for the development of new antibiotics to fight resistant micro-organisms.

Although the total syntheses of vancomycin and derivatives can be heralded as top achievements in organic synthesis [1], they are of course not practical for obtaining these compounds for application purposes. Therefore, there has been considerable interest in the preparation of simplified mimics of vancomycin, having especially (part of) the binding cavity for D-Ala-D-Ala.

With respect to this, Ellman and coworkers [16], Zhu and coworkers [17], Arnusch and Pieters [18], and Liskamp and coworkers [19] have prepared (monocyclic) mimics of the *D-E* part of the cavity of these antibiotics *via* an intramolecular nucleophilic aromatic substitution [16–18] or a Sonogashira-based macrocyclization [19] (Figure 1.4). Recently, a bicyclic mimic of the *C-D-E* cavity, which was prepared by a Stille reaction followed by tandem ring-closing metathesis (**9**, Figure 1.4), was described by Liskamp and coworkers [20]. Considerable challenges lie ahead for the synthetic chemist in order to develop practical syntheses of mimics of vancomycin capable of binding not only D-Ala-D-Ala, but also cell wall parts of resistant bacteria, i.e. D-Ala-D-lactate.

1.2.2
Lantibiotic: Nisin

Nisin is a peptide-based antibiotic from the lantibiotic (*lant*hionine-containing an-t*ibiotic*) family [2]. It is produced by certain strains of *Lactococcus lactis* and is active
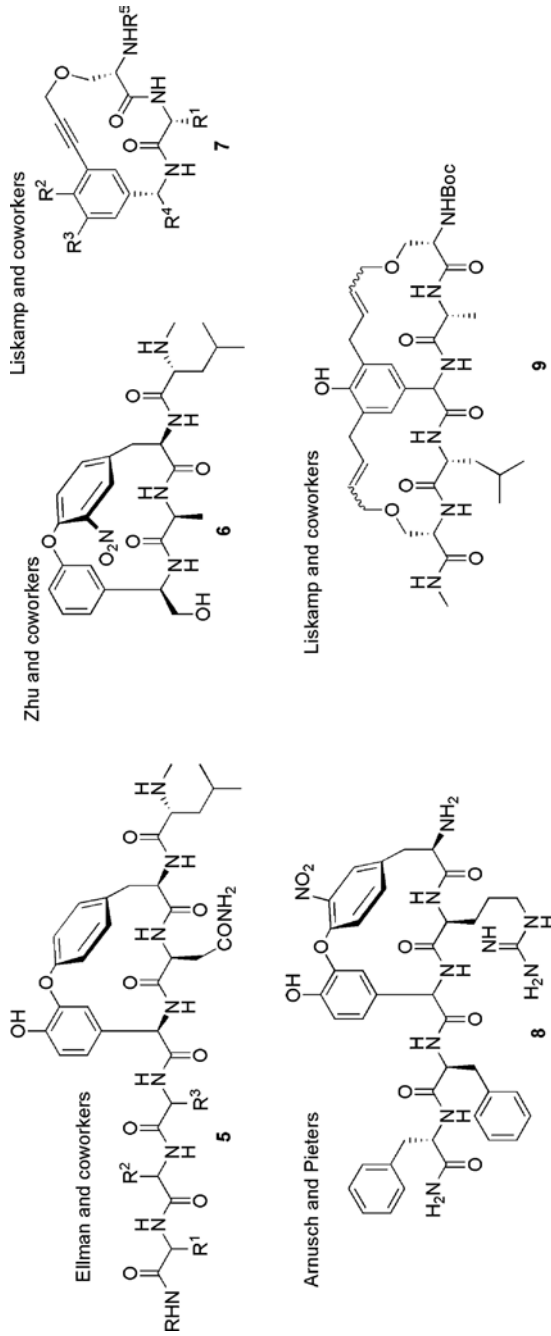
Figure 1.4 Structures of vancomycin mimics as described by Ellman and coworkers (**5**) [16], Zhu and coworkers (**6**) [17], Arnusch and Pieters (**8**) [18], and Liskamp and coworkers (**7**) [19] and (**9**) [20].
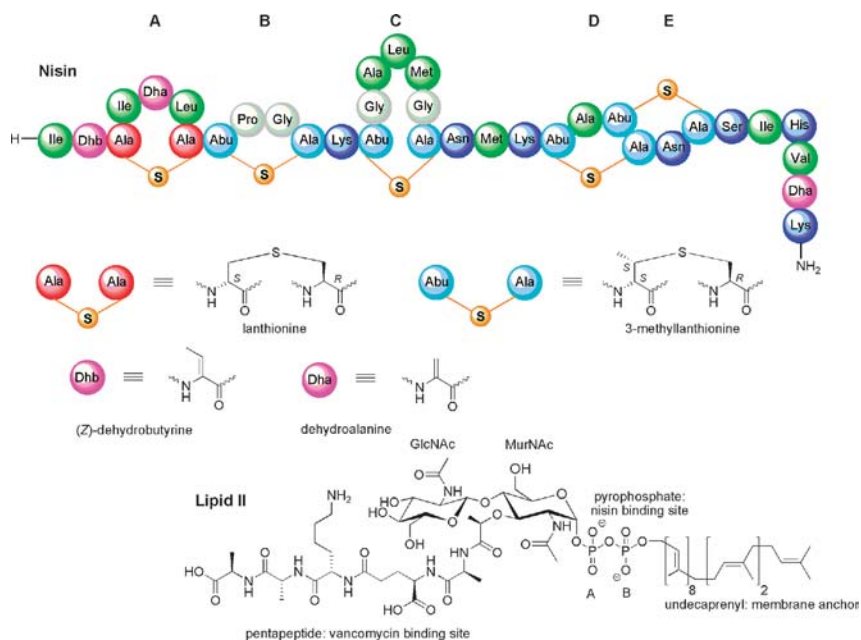
Figure 1.5 Representation of the structure of nisin. Hydrophobic amino acid residues are shown in green, polar residues in blue, and unsaturated amino acids in purple. The lanthionine ring is shown in red and the 3-methyllanthionine rings in turquoise.
The structural formulas of lanthionine, 3-methyllanthionine, dehydroalanine, and (Z)-dehydrobutyrine are also shown. The chemical structure of lipid II is shown, and the binding sites of vancomycin and nisin are indicated.

against most Gram-positive bacteria. Its antimicrobial effect has been long known, and nisin has been used as a food preservative for over 30 years. Its structure [21] is characterized by several connected cyclic peptides, including an annulated cyclic peptide system, providing the peptide with a unique shape (or shapes) which could not have been achieved by the corresponding linear sequences (Figure 1.5). Like other antimicrobial peptides, e.g., magainin, nisin has a net positive charge and an amphiphatic character. In addition to the cyclic peptide structures that are so characteristic for the lantibiotics, it contains the unusual amino acids lanthionine and 3-methyllanthionine as well as the unsaturated amino acids dehydroalanine and (Z)-dehydrobutyrine (Figure 1.5).

In 1960, Ramseier [22] discovered that nisin causes leakage of intracellular molecules from cells. Later, it was shown that it disturbs the membrane potential and interferes with energy transduction [23]. In addition, it causes inhibition of biosynthesis of the cell wall processes by blocking the synthesis of peptidoglycans [24] and by binding to the precursor lipid II [25]. However, micromolar amounts of nisin are needed to permeate artificial membranes [26,27] or to inhibit cell wall synthesis *in vitro* [28], while the *in vivo* activity of nisin is in the nanomolar range. As vancomycin, which binds to the peptide motif in lipid II, inhibited the antibacterial activity and
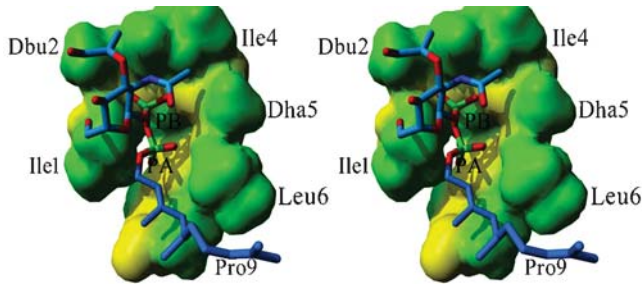
Figure 1.6 The pyrophosphate cage structure of nisin bound to lipid II. Side chains of nisin are depicted in green, backbone in yellow. Lipid II is depicted in blue [PDB entry code: 1WCO [32], molecular graphics created with YASARA (www.yasara.org) and PovRay (www.povray.org)].

membrane leakage by nisin in intact cells, Breukink *et al.* [26] concluded that lipid II is necessary for a high specific nisin activity and resulting pore formation. Studies with artificial membranes containing lipid II confirmed this conclusion [26].

The N-terminal fragment of nisin (1–12) has been shown to act as a nisin antagonist [29]. Mutation data have shown that changes in the N-terminal fragment reduced nisin activity [30]. NMR data showed that solvent accessibility of the A, B, and C rings of nisin decreased when it bound lipid II [31]. These data independently led to the conclusion that the N-terminal fragment of nisin, notably the ring structure A to C, is involved in lipid II binding. This was confirmed when the NMR structure of the nisin-lipid II complex was determined [32]. Rings A and B of nisin form a cage-like structure around the pyrophosphate moiety of lipid II. This structure shows that hydrogen bonds are formed between backbone amides of nisin and phosphate oxygens, while side chain interactions are of only minor importance. Only leucine residue six is conserved as a hydrophobic residue and interacts with the prenyl chain of lipid II (Figure 1.6).

In a model for pore formation, Hsu *et al.* proposed that after initial binding of nisin to the lipid II pyrophosphate, the C-ring embeds in the membrane, followed by a turn around the flexible hinge region and insertion of the C-terminus [31]. The size of these pores was calculated to be about 2 nm [33]. Studies with pyrene-labeled lipid II enabled Hasper *et al.* to calculate that a single nisin-lipid II pore consists of four lipid II molecules and eight nisin molecules (Figure 1.7). The pores are highly stable, even on addition of detergents that cause disruption of membranes [34].

Other lantibiotics that do not have the ability to form pores and indeed do not cause cell leakage have nevertheless still an impressive antibacterial effect *in vivo*. With respect to this, an alternative mechanism of antibacterial activity was recently described by which members of the lantibiotic family kill Gram-positive bacteria by binding lipid II and removing it from the cell division site (or septum) and thus block cell wall synthesis [35].

The cyclic peptide systems in nisin can be considered as side chain-cyclized peptide derivatives. However, they do not contain *disulfide* bridges, which is the most common
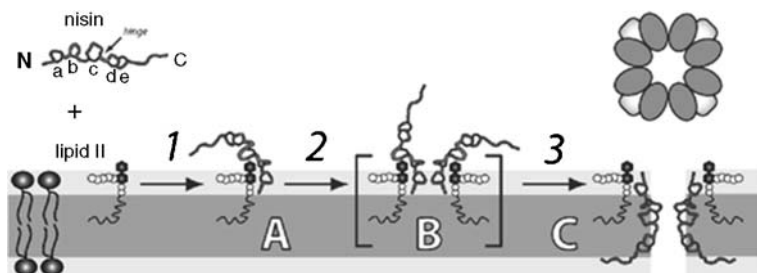
Figure 1.7 Interaction of nisin with phospholipid model membranes: mechanism of pore formation (reprinted with permission from Ref. [34]. Copyright 2007 © American Chemical Society).

way of generating side chain-cyclized peptides. In contrast they have *sulfide* or *thioether* bridges as part of their ring structures, which are introduced biosynthetically by post-translational modification. This rather unusual cyclization moiety enticed us to start investigating whether also "bridges" other than thioether bridges could be introduced as cyclization elements for obtaining mimics of the nisin ring structures [36]. Attention was directed towards designing and synthesizing alkene, alkyne, and alkane mimics of the thioether bridge, using ring-closing alkene and alkyne metathesis, sometimes followed by hydrogenation. Thus mimics of the A (**10**, **11**, and **14**), AB (**12**), C, and D/E (**16**) ring systems were prepared (Scheme 1.1). Apparently, the backbone structure of the D/E ring system has a predisposition towards a knotted ring structure, since it was possible to obtain an alkene mimic (**16**) directly in good yield (95%) from a double ring closing metathesis reaction of the tetra-allylglycine containing linear precursor (**15**) in a single reaction step [36d] (Scheme 1.1).

Based on the pyrophosphate cage structure of nisin bound to lipid II, a tricyclic mimic was designed and synthesized in which a lactam bridge connects the B-ring mimic with the A-ring mimic. The biological activity data are very promising and justify further improvement of the designed lipid II pyrophosphate binders. The inherent flexibility of a peptide, even when it is cyclized, challenges us to control its shape by alternative constraints to those already present.

1.2.3
Cyclosporin A

Cyclosporin was isolated from the fungus *Tolypocladium inflatum*. Its immunosuppressive activity was discovered in 1976 [4]. Although since then many analogs have been prepared and investigated, cyclosporin A (CsA, Sandimmune, **17**) remains the most effective cyclic peptide and is the major immunosuppressant drug to prevent graft rejection after transplant surgery.

CsA is a cyclic undecapeptide consisting completely of hydrophobic amino acids, as shown in Figure 1.8 [37]. Additional structural features are a threonine-derived butenyl-containing amino acid derivative as well as six *N*-methylated amino acid residues. In addition to reducing the proteolytic degradation rate and increasing the

Alkene-bridged nisin AB-ring mimic

1. RCM
2. peptide synthesis

1. peptide synthesis B-ring
2. RCM
3. fragment coupling
4. deprotection

$R^1 =$

$R^2 =$

Scheme 1.1 Synthesis and structures of alkane- and alkyne-bridged nisin mimics [36].
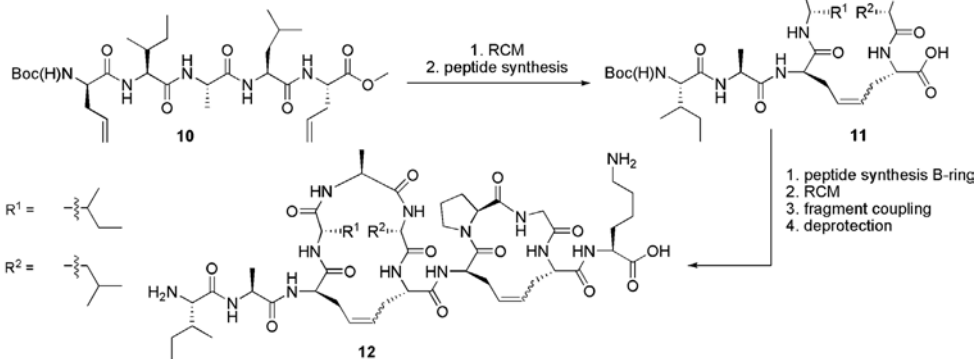
Alkyne-bridged nisin A-ring mimic

RCAM
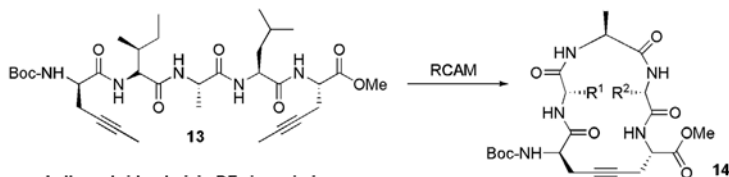
Crossed alkene-bridged nisin DE-ring mimic

RCM

Cyclosporin A (CsA)
17

$R =$
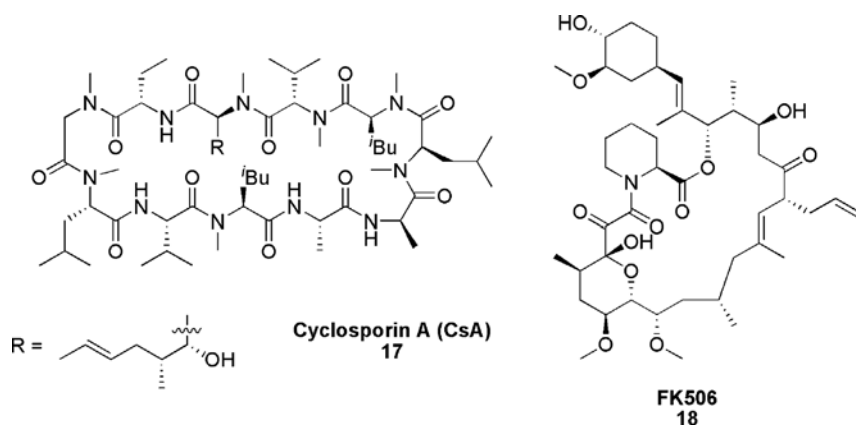
FK506
18

Figure 1.8 Structural formulas of cyclosporin A and FK506.

hydrophobicity, the influence of these *N*-methylated residues on the flexibility of the cyclic peptide system could be interesting.

The molecular basis of CsA's biological activity is the formation of a complex with the immunophilin cyclophilin A (CyPA) in such a way that the CsA-CyPA complex can associate with calcineurin (CN), which is a Ca^{2+}/calmodulin-dependent Ser/Thr phosphatase. As a result, dephosphorylation of a nuclear factor of activated T-cells (NFAT) is inhibited.

X-ray structures [38] of the CsA-CyPA complex show that one side of the CsA ring, comprising the residues 1–3 and 9–11, fits into a groove on CyPA, leaving the opposite side free to interact with CN. Interestingly, CyPA is a *cis-trans* proline isomerase, but this enzymatic activity does not play a role in CN inhibition. It seems that CsA interacts with CyPA to create a larger complex capable of interacting with CN. X-ray structures of the CsA-CyPA-CN complexes (Figure 1.9) show that the conformation of the CsA backbone and the side chains interacting with CyPA in this ternary complex are very similar to those in the binary CsA-CyPA complex. However, the side chains of the CN-binding moiety of CsA have undergone significant conformational changes.

CsA as well as FK506 (**18**), a completely unrelated non-peptide natural product with similar activity to CsA, have resisted many efforts to improve them as drugs. However, the X-ray structures of the ternary complex may help to stimulate the design of superior immunosuppressants.
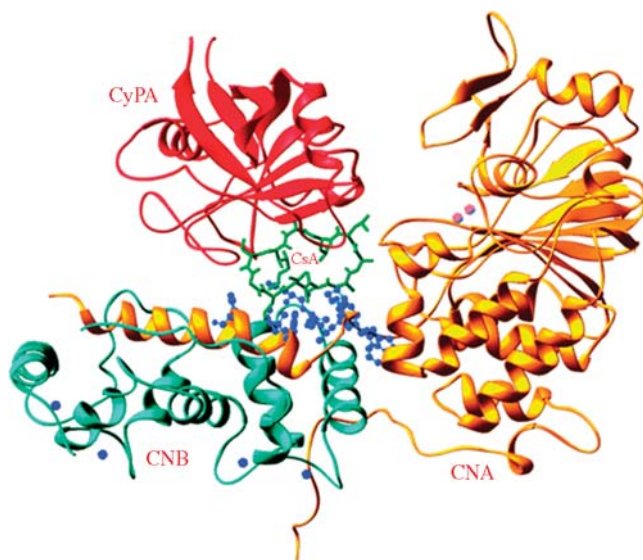
Figure 1.9 Ribbon representation of CyPA-CsA-CN. The catalytic subunit (CNA) of CN is shown in gold, the regulatory subunit (CNB) of CN cyan, cyclosporin (CsA) green, cyclophylin (CyPA) red, the Zn^{2+} and Fe^{3+} ions pink, and the Ca^{2+} ions blue. The residues from CN involved in binding of CyPA-CsA are shown as a blue ball-stick representation (reprinted with permission from Ref. [38]. Copyright 2007 © National Academy of Sciences, USA.)

1.2.4
Cyclotheonamide A and B

In the early 1990s, Fusetani and Matsunaga isolated two substances from marine sponges of the genus *Theonella*, which were called cyclotheonamide A and B (CtA **19** and CtB **20**, respectively), and were found to be potent inhibitors of various proteinases, especially the blood coagulation enzyme thrombin [5,39]. After structural elucidation by extensive NMR analysis [40], the cyclotheonamides were found to be cyclic pentapeptides having a 19-membered ring and containing a D-phenylalanine (D-Phe), an L-proline (L-Pro), an L-2,3-diaminopropionic acid (L-Dpr) with either a formylated (For, CtA **19**) or an acetylated (Ac, CtB **20**) N^2-amino moiety, a vinylogous L-tyrosine (L-vTyr), and an α-ketoarginine (L-kArg) residue (Figure 1.10).

Noteworthy are the presence of the uncommon non-proteinogenic amino acids L-α-ketoarginine (α-oxo-L-β-homoarginine) and vinylogous L-tyrosine (L-tyrosine-derived α,β-unsaturated γ-amino acid). More important, however, is the presence of the α-ketoamide moiety indicating the possible mechanism of action of the cyclotheonamides as potent serine protease inhibitors by serving as an electrophilic trap to form a tetrahedral intermediate (a transition state analog) with the hydroxyl group of Ser195, part of the catalytic triad His57-Asp102-Ser195 of the proteinase.

To obtain insight into the molecular basis of action of the cyclotheonamides and to explain the high affinity as a serine protease inhibitor, complexes of CtA with α-thrombin [41a,c] and β-trypsin [41b,c], respectively, were studied by X-ray crystallography.

Thrombin is the pivotal trypsin-like protease for the regulation of thrombosis and hemostasis. Thrombin hydrolyzes its natural substrates by recognition of the Pro-Arg motif in the apolar S2- and the primary specificity S1 pocket [42]. The molecular structure of the thrombin-CtA complex (Figure 1.11) showed that CtA was bound to the active site of the enzyme. The arginine side chain formed an electrostatic interaction with Asp189, located at the bottom of the S1 binding pocket.

R = H: cyclotheonamide A (CtA) **19**
R = CH$_3$: cyclotheonamide B (CtB) **20**
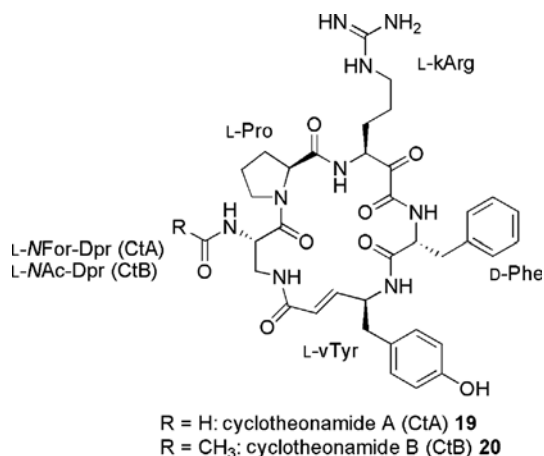
Figure 1.10 Structure of cyclotheonamide A and B.
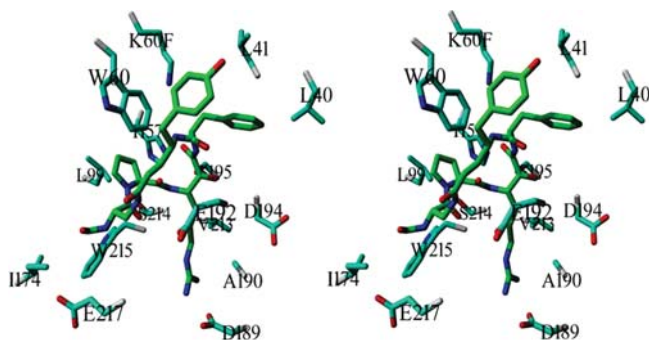
Figure 1.11 Stereoview of CtA **19** bound in the active-site cleft of α-thrombin [PDB entry code: 1TMB [41a], molecular graphics created with YASARA (www.yasara.org) and PovRay (www. povray.org)].

Furthermore, the backbone of the Pro-Arg segment formed a hydrogen-bonded antiparallel β-chain with the Ser214-Gly216 sequence in thrombin.

Both features were highly similar to what was observed for the binding of the high-affinity active site-directed thrombin inhibitor H-D-Phe-Pro-Arg chloromethyl ketone [42]. A well-defined continuous electron density between Ser195 and the carbonyl carbon of the α-ketoamide was observed, which was a strong indication of a "covalent complex" through the formation of a tetrahedral hemiketal. The other carbonyl oxygen was involved in a hydrogen-bonding network in the oxyanion hole formed by Gly193 and Ser195. X-ray analysis of the trypsin-CtA complex showed that the gross structural features were similar to thrombin. However, the higher degree of specificity for trypsin (K_i 0.023 μM versus 0.18 μM) is fairly well explained by the Trp60A-Thr60I insertion loop of thrombin [42], which narrows the active-site binding cleft and thus results in less favorable interaction with the D-Phe and L-vTyr residues.

The interesting macrocyclic pentapeptide scaffold prompted several research groups to design new total synthesis routes for cyclotheonamide [40,41a,b,43] and derivatives thereof [44], mainly for SAR-studies for targeting the development of novel synthetic thrombin inhibitors. The first total synthesis of CtB **20** was published by Hagihara and Schreiber [40]. This synthesis (Scheme 1.2) defined the true stereochemical structure of cyclotheonamide, which had previously been reported incorrectly.

The linear CtB precursor **21** was synthesized from dipeptide Ac-Dpr(Boc)-Pro-OPac **22**, following three amide coupling reactions in the C → N direction. The vinylogous tyrosine derivative **23** was synthesized from the protected Weinreb amide **24** that was obtained from the aldehyde intermediate in a Wittig homologation followed by conversion into an active pentafluorophenyl ester. Boc-D-Phe-OH was coupled with BOP/DMAP as the condensing agents. The α-hydroxy acid **25** was prepared from the protected arginine Weinreb amide derivative **26**. To avoid an intramolecular nucleophilic attack of the guanidinium moiety at the intermediate arginine aldehyde, it was doubly protected with Boc and Mtr groups. Finally, macrolactamization was achieved by a four-step process. Deprotection of the
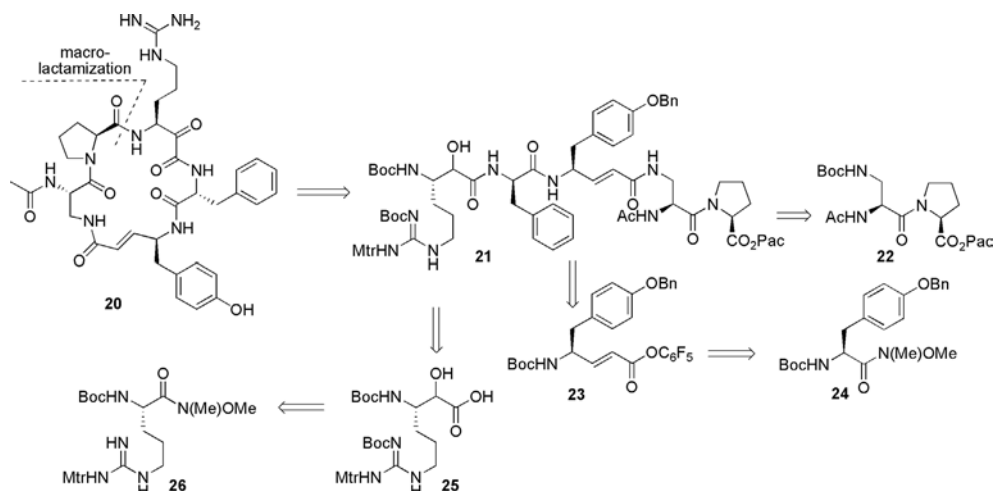
Scheme 1.2 Retrosynthesis of the first total synthesis of CtB **20**
as described by Hagihara and Schreiber [40].

phenacyl ester was followed by conversion into the active pentafluorophenyl
ester. Then, the N-terminal Boc functionality was selectively removed by *p*TsOH.
Neutralization with DIPEA and treatment with DMAP resulted in a smooth con-
version into the protected peptide macrocycle. After oxidation of the hydroxyl
functionality, all remaining protecting groups were removed by treatment with
TFA in the presence of thioanisole as scavenger to give CtB **20** in 3% overall yield
over 16 reaction steps.

The total synthesis of CtA **19**, which was used in the first X-ray studies to elucidate
the structure of the CtA – α-thrombin complex (Figure 1.11), is shown in Scheme 1.3.

This synthesis, as described by Maryanoff *et al.* [41a], was based on a convergent
[3 + 2] fragment condensation route (Scheme 1.3). The two segments **28** and **29** were
synthesized from their requisite protected amino acid building blocks **30**, **31** and **32**,
33 respectively. Coupling of **28** and **29** to give linear intermediate **27** proceeded in
65% yield. After selective removal of the N- and C-terminal protecting groups on **27**,
the critical macrocyclization was effected in 65% yield under high dilution condi-
tions. The intermediate protected macrocycle was then processed in four steps
(removal of the phthaloyl functionality and subsequent formylation of the α-amino
group, Dess-Martin oxidation to the α-ketoamide, and finally treatment with HF to
remove the tosyl protecting group) to give CtA **19**.

Since also many linear peptides that are powerful inhibitors of thrombin [45], have
been synthesized it is difficult to evaluate to what extent the cyclic nature of peptide
in cyclotheonamide contributes to the activity. Nevertheless, the cyclic nature is
advantageous for possible *in vivo* activity, because of the absence of polar end groups
and the greater steric hindrance. With respect to the latter, this can confer greater
resistance to degradation by peptidases and enhanced ability to traverse membrane
barriers. Unfortunately, cyclotheonamide and congeners have not been further
developed into suitable compounds for anticoagulation therapy.
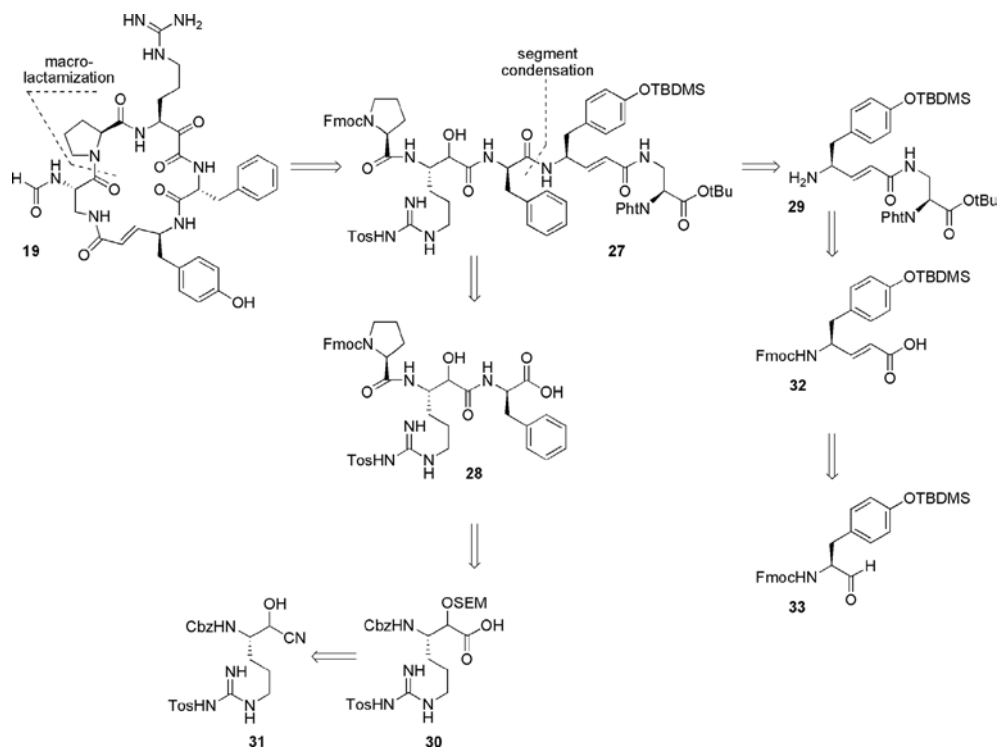
Scheme 1.3 Retrosynthesis of the total synthesis of CtA **19**, which was used in the X-ray analysis as a complex with α-thrombin [41a].

1.2.5
cyclo RGD Peptides as α$_V$β$_3$ Antagonists

So far, naturally occurring cyclic peptides and mimics thereof have been discussed, in which the cyclic character plays an essential role with respect to affinity and activity in particular. However, this could also be the case for suitable sequences present in proteins, which upon incorporation into macrocyclic peptide structures could lead to molecular constructs with similar or even enhanced affinity and activity without the requirement for the entire protein or a large derivative. This is an exceptional challenge, which could lead to a variety of new biologically active peptides. Although it is a realistic strategy, as is evidenced from the vast number of biologically active cyclic peptides, it may be sometimes a prolonged process and an integral approach featuring an iterative design-synthesis-activity-structure cycle seems to be essential.

Two important examples of cyclic peptides will be highlighted in which amino acid sequences of larger proteins have been successfully used as part of macrocyclic peptide structures to mimic in an almost "*pars pro toto*" approach important properties of the parent protein.

Integrins are a class of heterodimeric transmembrane proteins [46] which play an important role in cell signaling, cell-cell adhesion, apoptosis, and cell-matrix interactions [47]. Integrin $\alpha_V\beta_3$, which binds to Arg-Gly-Asp (RGD) tripeptide motif-containing ligands [48], plays a pivotal role in tumor angiogenesis and metastasis and is expressed on activated endothelial cells during tumor-induced angiogenesis and on various tumor cell types (e.g., breast, ovarian, and prostate cancers), whereas it is absent on quiescent endothelial cells and normal tissues [47]. Evidence exists that inhibition of $\alpha_V\beta_3$ integrin function prevents tumor growth and induces tumor regression by antagonizing angiogenesis [49]. Several peptidic [3] and peptidomimetic [50] $\alpha_V\beta_3$ antagonists have been synthesized. Among these, the *cyclo*[Arg-Gly-Asp-D-Phe-Val] (c[RGDfV]) (**34**), as developed by Kessler and coworkers, is one of the most active and selective antagonists for the $\alpha_V\beta_3$ integrin [51] (Figure 1.12).

Structure-activity relationship studies on this cyclic pentapeptide showed that the exchange of the valine by a lysine residue (Lys, K) (compound **36**) did not significantly influence activity and selectivity [52]. Because the ε-amino moiety of the lysine residue can easily be modified, numerous applications of *c*[RGDfK] have been studied for tumor targeting and imaging [53].

The linear precursor of, for example, **34** [51] was obtained by solid-phase peptide synthesis performed on an SASRIN®-resin applying the Fmoc/^{t}Bu strategy. This allowed the preparation of a protected peptide with both free amino and carboxylic acid termini, which were head-to-tail cyclized using diphenylphosphorylazide, leading to the protected cyclic peptide. Removal of side chain protecting groups afforded **34**.

The structural basis for binding of the prototypical Arg-Gly-Asp sequence to the $\alpha_V\beta_3$ integrin was recently provided by the crystal structure of **35** complexed with the extracellular segment of integrin $\alpha_V\beta_3$ [48] as shown in Figure 1.13.

34
cyclo[Arg-Gly-Asp-D-Phe-Val]
c[RGDfV]

35
cyclo[Arg-Gly-Asp-D-Phe-*N*MeVal]
c[RGDf-{*N*Me}V]

36
cyclo[Arg-Gly-Asp-D-Phe-Lys]
c[RGDfK]
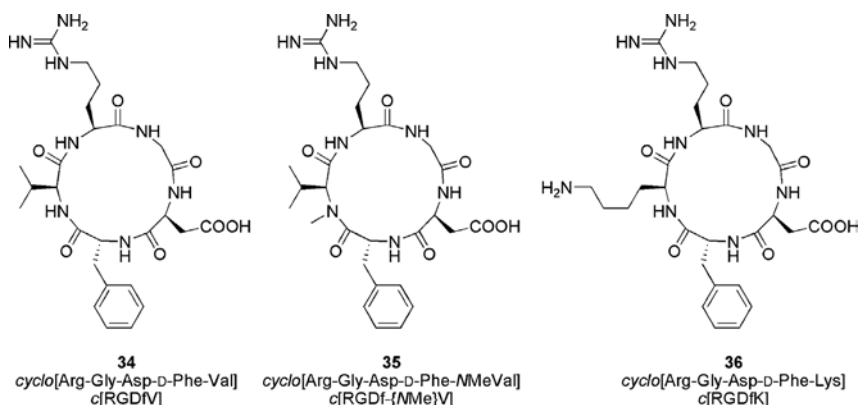
Figure 1.12 Structures of cyclic pentapeptides as potent antagonists of the $\alpha_V\beta_3$ integrin.
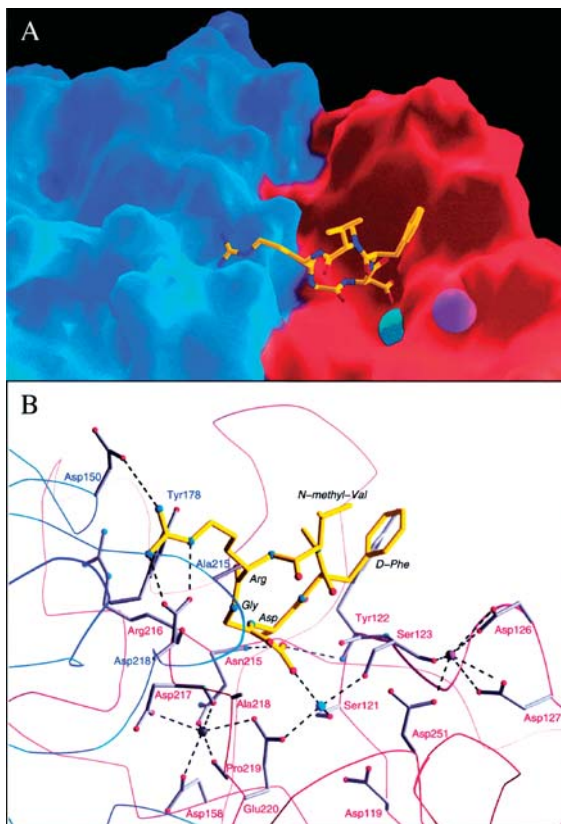
Figure 1.13 The ligand-integrin binding site. (A) Surface representation of the ligand-binding site, with the ligand peptide (**35**, Fig. 1.12) shown as ball-and-stick model. (B) Interactions between ligand and integrin. The peptide (yellow) and residues interacting with the ligand or with Mn^{2+} ions are shown in ball-and-stick representation. α_V and β_3 residues are labeled blue and red, respectively. Oxygen and nitrogen atoms are in red and blue, respectively. Hydrogen bonds and salt bridges (distance cutoff, 3.5 Å) are represented with dotted lines (reprinted with permission from Ref. [48]. Copyright 2007 © American Association for the Advancement of Science).

The interaction with the Arg-Gly-Asp ligand triggers the structural rearrangements of the $\alpha_V\beta_3$ integrin which are necessary for cell signaling pathways. Cyclic RGD peptide **35** binds at the major interface between the α_V and β_3 subunits. The arginine side chain inserts into a narrow groove forming a bidentate salt bridge to Asp218 and Asp150. The carboxylate moiety and the aspartic acid residue of **35** form an extensive network of polar interactions with the protein and are completely buried in the complex. The glycine residue undergoes several hydrophobic interactions and lies at the interface between the α and β subunits. The other two residues of the cyclic RGD pentapeptide point into the solution and do not have structural interactions with the $\alpha_V\beta_3$ integrin. Comparison of the X-ray structures of the unbound

and the RGD-bound $\alpha_V\beta_3$ integrin revealed many conformational rearrangements within the protein which may form a structural basis for receptor activation. The backbone conformation of the Arg-Gly-Asp tripeptide motif in the pentapeptide is almost identical to that of the RGD sequence in the natural ligand Echistatin, which is a 49 amino acid protein isolated from the venom of *Echis carinatus* and is one of the smallest natural ligands that interacts with integrin-type receptors through an Arg-Gly-Asp sequence [54]. This suggests that this X-ray structure [48] (Figure 1.13) may provide a basis for obtaining insight into the molecular interaction details of integrins with other and larger RGD-containing ligands.

1.2.6
SH2 Domain-Binding Peptides

The class of Src homology 2 (SH2) domains is the largest class of phosphotyrosine-recognizing protein domains. They occur in different protein groups that are mostly involved in signaling and regulation, and thus perform several functions within the cell [55]. Mutations in SH2 domains are implicated in many human diseases, of which a complete overview is given by Liu *et al.* [55a]. The SH2 domains are approximately 100 amino acids in size and have a well-defined structure, consisting of a central antiparallel β-sheet and two flanking α-helices, followed by a second, two-strand sheet, as elucidated by X-ray crystallography and NMR spectroscopy (Figure 1.14) [56,57].
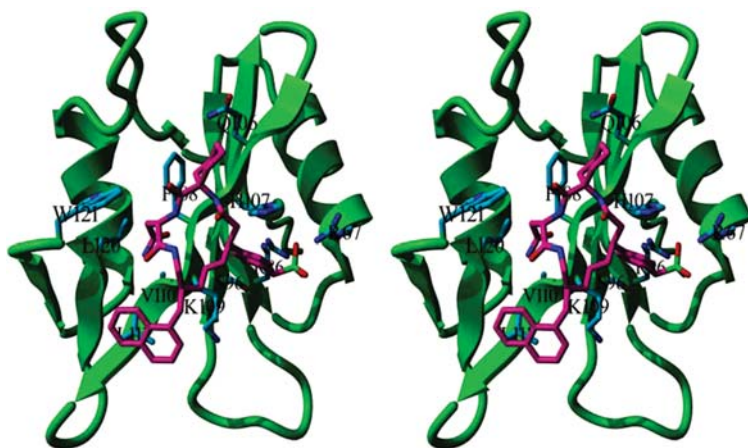
Figure 1.14 NMR-structure of the Grb2-SH2 domain in complex with inhibitor **39**. A central antiparallel β-sheet in the protein is flanked by two α-helices, with peptide binding mediated by the sheet, intervening loops, and one of the helices. The specific recognition of phospho-tyrosine involves cation-π interactions between lysine and arginine side chains and the aromatic tyrosine side chain, in addition to hydrogen-bond interactions with the phosphate moiety [57] [PDB entry code: 1X0N [57], molecular graphics created with YASARA (www.yasara.org) and PovRay (www.povray.org)].
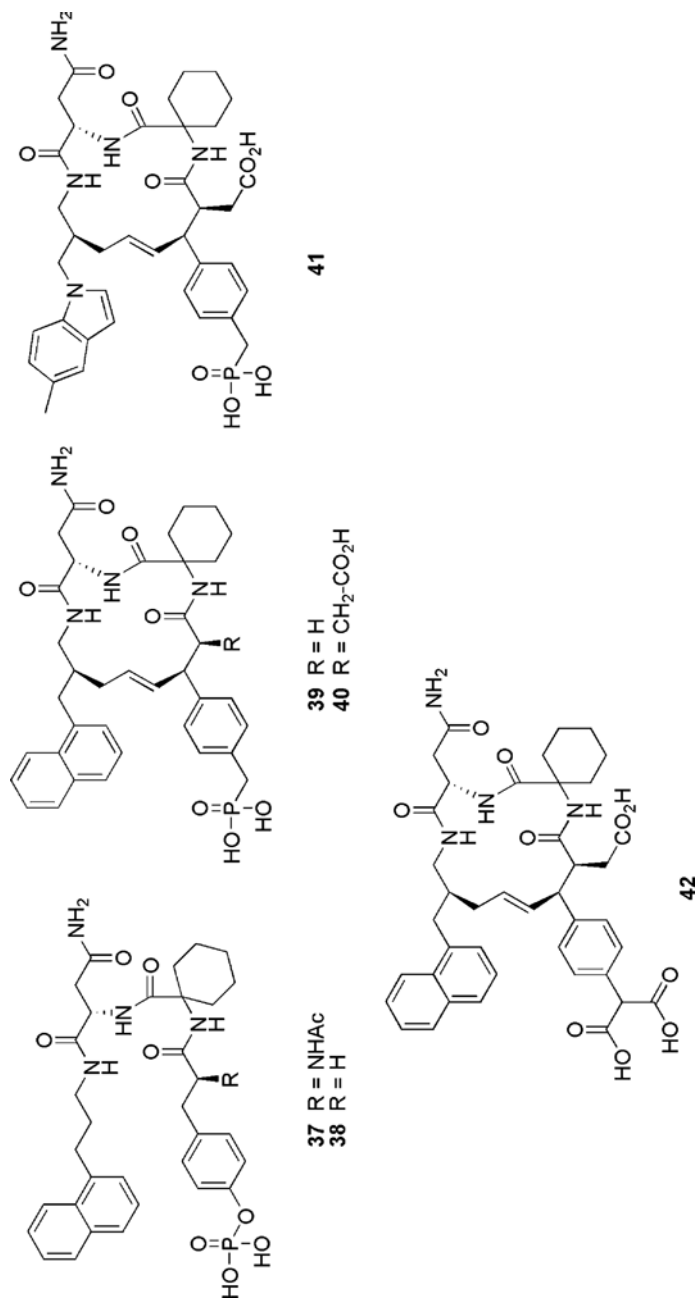
Figure 1.15 Structures of synthetic Grb2 SH2 domain-binding analogs [58–60].

The recognition of phosphorylated peptides by SH2 domains depends on the phosphorylated residue. Specificity is determined by one or two nearby residues. Apart from the phosphotyrosine-specific recognition, SH2-domains can interact in different ways with other proteins [55]. This paragraph focuses on the interactions mediated by the conventional phosphopeptide recognition region. (The Grb2 SH2 domain plays a crucial role in the Ras signal transduction pathway, which is an important regulator of cell growth and differentiation.) Although most SH2 domains bind their phosphorylated peptide ligands in an extended, β-strand-like conformation, the Grb2 SH2 domain binds the natural ligand in a type I β-turn conformation [58]. High-affinity binding and recognition processes are mediated by the pTyr-Xaa-Asn motif. In tripeptide **37** (Figure 1.15), the amino acid at the second position is a 1-aminocyclohexanecarboxylic acid residue, which induces a β-turn conformation. This results in a high binding affinity of the peptide for the Grb2 SH2 domain. Removal of the acetylated amino functionality of the pTyr residue (compound **38**, Figure 1.15) led to a 100-fold lower affinity, but cyclization restored this loss. However, in an intracellular assay, the cyclic peptide without α substitution (compound **39**, Figure 1.15) was markedly less active than the linear peptide with this substitution [58]. A K_D value of 75 pM was reported when the naphthyl group was replaced by a 5-methylindole and the α substitution was restored (compound **41**, Figure 1.15). In cell assays, the compound was an effective inhibitor of mitosis in breast cancer cell culture [59].

Cyclization of peptides containing phosphate group mimics (**42**) increased binding affinities about five-fold in ELISA assays compared to their linear equivalents [60]. However, one should not consider cyclization as a panacea. Recently, we found, for example, that cyclization by ring-closing metathesis of a phosphopeptide interacting with the Grb2 SH2 domain did not give rise to improvement of binding affinity (Figure 1.16) [61].
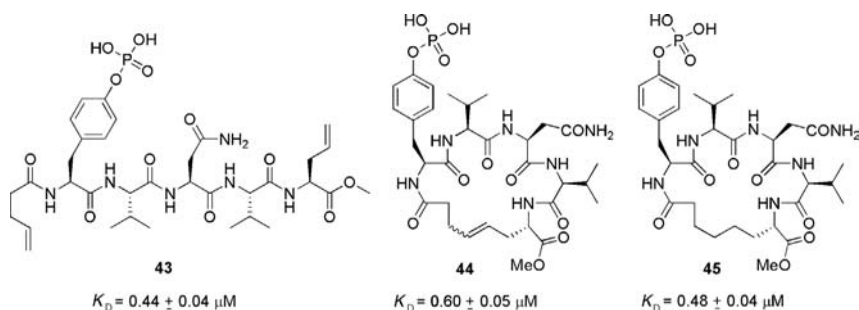
Figure 1.16 Linear phosphopeptide **43** and cyclic phosphopeptide ligands **44** and **45** obtained by ring-closing metathesis showing virtually no difference in affinity for the Grb2 SH2 domain as measured by a surface plasmon resonance assay [61].

1.3
Conclusions

The very limited number of bioactive (macro)cyclic peptides and peptide mimics for which molecular details of the interactions with targets are known stands in striking contrast to the vast and still increasing number of bioactive cyclic peptides. This calls for approaches to the elucidation of molecular mechanisms of interaction and target identification, since the biological activity of many of those peptides is extremely interesting, varying from antibiotic or anti-cancer activity to epigenetic behavior, or activity in signal transduction mechanisms. The studies could form a basis for the design and development of new generations of bioactive compounds also capable of interacting with large surfaces involved in many important protein-protein interactions. In this respect, macrocyclic *peptide* structures are particularly interesting because, in addition to the possibility of offering a large surface, the amino acid residues of which they are composed can offer a large diversity of functionalities for interaction. Since, in principle, there are no limitations to the preparation of macrocyclic peptide molecular constructs, there are plenty of opportunities for design and synthesis in the promising bio-supramolecular chemistry area.

1.4
Experimental: Selected Procedures

1.4.1
Synthesis of Bicyclic Peptide 9: an Alkene-bridged Mimic of the Vancomycin C-D-E Cavity

The original synthesis of this compound was described in Ref. [20]. The linear pentapeptide precursor, N^α-(*tert*-butyloxycarbonyl)-seryl(allyl)-D-alanyl-R,S-4-hydroxy-3,5-bisallyl-phenylglycyl-D-leucyl-serine(allyl) methyl amide (20 mg, 0.025 mmol) was dissolved in a mixture of TCE (12 mL) and DMF (0.5 mL). This solution was purged with N_2 and heated to 80 °C followed by the addition of the 2nd generation Grubbs' catalyst (21 mg, 0.025 mmol). After 10 min the reaction was complete according to TLC and ES-MS. Subsequently, the solvent was removed under reduced pressure and the residue was purified by column chromatography (eluent: $CH_2Cl_2 \rightarrow CH_2Cl_2/$ MeOH 95:5, v/v). The tandem ring-closed pentapeptide **9** was obtained as a slightly brownish solid in 67% yield (13 mg). HPLC analysis showed that the product was 92% pure (based on the diastereomers). HR-MS calcd. for $[M+H]^+$: $C_{37}H_{54}N_6O_{10}^+$: 743.3979; found m/z $[M+H]^+$: 743.3969.

1.4.2
Synthesis of Cyclic Peptide 14: an Alkyne-bridged Mimic of the Nisin A-Ring Fragment

The original synthesis of this compound was described in Ref. [36b]. The ring-closing alkyne metathesis reaction was carried out under argon in flame-dried

glassware using Schlenk techniques. The linear pentapeptide precursor, N^{α}-(*tert*-butyloxycarbonyl)-(2-butyne-glycyl)-isoleucyl-alanyl-leucyl-(2-butyne-glycine) methyl ester (46 mg, 0.070 mmol) was dissolved in dry toluene (200 mL), and the tungsten-alkylidyne catalyst (${}^{t}\text{BuO})_3 W \equiv C^{t}\text{Bu}$ (4 mg, 9 µmol) was added. The obtained reaction mixture was heated to 80 °C and stirred for 2 h. The reaction was monitored by TLC until no changes in product distribution could be observed. Then, H_2O (1 mL) was added to quench the catalyst, and the solvent was removed by evaporation. The residue was purified by column chromatography with CH_2Cl_2/MeOH 97.5:2.5, *v*/*v* as the eluent. Cyclic pentapeptide **14** was obtained as an off-white powder in 42% yield (18 mg). HR-MS calcd for $[M+H]^+$: $C_{29}H_{47}N_5O_8^+$: 616.33218; found *m/z* $[M+H]^+$: 616.33223.

Abbreviations

Abu	2-aminobutyric acid
Ac	acetyl
Ala	alanine (A)
Arg	arginine (R)
kArg	α-ketoarginine; α-oxo-L-β-homoarginine
Asn	asparagine (N)
Asp	aspartic acid (D)
Boc	*tert*-butyloxycarbonyl
BOP	benzotriazol-1-yloxy-tris(dimethylamino)phosphonium hexafluorophosphate
Bn	benzyl
^{i}Bu	*iso*-butyl
^{t}Bu	*tert*-butyl
Cbz	carbobenzyloxy
CN	calcineurin
CsA	cyclosporin A
CtA	cyclotheonamide A
CtB	cyclotheonamide B
CyPA	cyclophilin A
Dha	dehydroalanine
Dhb	(*Z*)-dehydrobutyrine
DIPEA	diisopropylethylamine
DMAP	4-dimethylaminopyridine
DMF	dimethylformamide
Dpr	2,3-diaminopropionic acid
ELISA	enzyme linked immunosorbent assay
ES-MS	electrospray mass spectrometry
Fmoc	9-fluorenylmethyloxycarbonyl
For	formyl
GlcNAc	*N*-acetyl glucosamine

Gly	glycine (G)
Grb2	growth factor receptor-bound protein 2
His	histidine (H)
HPLC	high-pressure liquid chromatography
HR-MS	high-resolution mass spectrometry
Ile	isoleucine (I)
Leu	leucine (L)
Lys	lysine (K)
Me	methyl
Met	methionine (M)
MRSA	methicillin resistant *Staphylococcus aureus*
Mtr	4-methoxy-2,3,6-trimethylbenzenesulfonyl
MurNAc	*N*-acetyl muramic acid
NFAT	nuclear factor of activated T-cells
NMR	nuclear magnetic resonance
Pac	phenacyl
Phe	phenylalanine (F)
Pht	phthaloyl
Pro	proline (P)
RCAM	ring-closing alkyne metathesis
RCM	ring-closing metathesis
SAR	structure-activity relationship
SASRIN	2-amino-4-alkoxybenzylalcohol resin
SEM	2-(trimethylsilyl)ethoxymethyl
Ser	serine (S)
SH2	Src homology 2
TBDMS	*tert*-butyl dimethyl silyl
TCE	1,1,2-trichloroethane
TFA	trifluoroacetic acid
Thr	threonine (T)
TLC	thin layer chromatography
Tos	tosyl
Trp	tryptophan (W)
Trt	trityl
*p*TsOH	*para*-toluenesulfonic acid
Tyr	tyrosine (Y)
vTyr	vinylogous tyrosine; L-tyrosine-derived α,β-unsaturated γ-amino acid
Val	valine (V)
VanA	resistance to vancomycin of type A
VanB	resistance to vancomycin of type B
VanC	resistance to vancomycin of type C
Xaa	unspecified amino acid residue

References

1 (a) Boger, D.L. (2001) *Med. Res. Rev.*, **21** (5), 356–381; (b) Nicolaou, K.C., Boddy, C.N.C., Bräse, S. and Winssinger, N. (1999) *Angew. Chem.*, **111**, 2230–2287. *Angew. Chem. Int. Ed.*, **38**, 2096–2152; (c) Rao, A.V.R., Gurjar, M.K., Reddy, K.L. and Rao, A.S. (1995) *Chem. Rev.*, **95**, 2135–2167.

2 Chatterjee, C., Paul, M., Xie, L. and van der Donk, W.A. (2005) *Chem. Rev.*, **105**, 633–684.

3 Haubner, R., Finsinger, D. and Kessler, H. (1997) *Angew. Chem.*, **109**, 1440–1456; *Angew. Chem. Int. Ed.*, **36**, 1374–1389.

4 Rüegger, A., Kuhn, M., Lichti, H., Loosli, H.-R., Huguenin, R., Quiquerez, C. and von Wartburg, A. (1976) *Helv. Chim. Acta*, **59**, 1075–1092.

5 Fusetani, N., Matsunaga, S., Matsumoto, H. and Takebayashi, Y. (1990) *J. Am. Chem. Soc.*, **112**, 7053–7054.

6 Froideveaux, S. and Eberle, A.N. (2002) *Biopolymers (Peptide Science)*, **66**, 161–183.

7 X-ray structure of octreotide: Pohl, E., Heine, A., Sheldrick, G.M., Dauter, Z., Wilson, K.S., Kallen, J., Huber, W. and Pfäffli, P.J. (1995) *Acta Crystallogr.*, Sect. D, **51**, 48–59.

8 Rohl, C.A., Chakrabartty, A. and Baldwin, R.L. (1996) *Protein Science*, **5**, 2623–2637.

9 (a) Benfield, A.P., Teresk, M.G., Plake, H.R., DeLorbe, J.E., Millspaugh, L.E. and Martin, S.F. (2006) *Angew. Chem.*, **118**, 6984–6989; *Angew. Chem. Int. Ed.*, **45**, 6830–6835; (b) de Mol, N.J., Catalina, M.I., Dekker, F.J., Fischer, M.J.E., Heck, A.J.R. and Liskamp, R.M.J. (2005) *ChemBioChem.*, **6**, 2261–2270.

10 Knox, J.R. and Pratt, R.F. (1990) *Antimicrob. Agents Chemother.*, **34**, 1342–1347.

11 Mackay, J.P., Gerhard, U., Beauregard, D.A., Maplestone, R.A. and Williams, D.H. (1994) *J. Am. Chem. Soc.*, **116**, 4573–4580.

12 Williams, D.H., Maguire, A.J., Tsuzuki, W. and Westwell, M.S. (1998) *Science*, **280**, 711–714.

13 Mackay, J.P., Gerhard, U., Beauregard, D.A., Westwell, M.S., Searle, M.S. and Williams, D.H. (1994) *J. Am. Chem. Soc.*, **116**, 4581–4590.

14 (a) Süssmuth, R.D. (2002) *ChemBioChem*, **3**, 295–298; (b) Walsh, C. T., Fisher, S.L., Park, I.-S., Prahalad, M. and Wu, Z. (1996) *Chem. Biol.*, **3**, 21–28.

15 (a) Printsevskaya, S.S., Pavlov, A.Y., Olsufyeva, E.N., Mirchnink, E.P., Isakova, E.B., Reznikova, M.I., Goldman, R.C., Branstrom, A.A., Baizman, E.R., Longley, C.B., Sztaricskai, F., Batta, G. and Preobrazhenskaya, M.N. (2002) *J. Med. Chem.*, **45**, 1340–1347; (b) Crowley, B.M., Mori, Y., McComas, C.C., Tang, D. and Boger, D.L. (2004) *J. Am. Chem. Soc.*, **126**, 4310–4317; (c) Boger, D.L., Kim, S. H., Mori, Y., Weng, J.-H., Rogel, O., Castle, S.L. and McAtee, J.J. (2001) *J. Am. Chem. Soc.*, **123**, 1862–1871.

16 Xu, R., Greiveldinger, G., Marenus, L.E., Cooper, A. and Ellman, J.A. (1999) *J. Am. Chem. Soc.*, **121**, 4898–4899.

17 Bois-Choussy, M., Neuville, L., Beugelmans, R. and Zhu, J. (1996) *J. Org. Chem.*, **61**, 9309–9322.

18 Arnusch, C.J. and Pieters, R.J. (2003) *Eur. J. Org. Chem.*, 3131–3138.

19 ten Brink, H.T., Rijkers, D.T.S. and Liskamp, R.M.J. (2006) *J. Org. Chem.*, **71**, 1817–1824.

20 ten Brink H.T., Rijkers D.T.S., Kemmink J., Hilbers H.W. and Liskamp R.M.J. (2004) *Org. Biomol. Chem.*, **2**, 2658–2663.

21 Gross, E. and Morell, J.L. (1971) *J. Am. Chem. Soc.*, **93**, 4634–4635.

22 Ramseier, H.R. (1960) *Arch. Microbiol.*, **37**, 57–94.

23 Ruhr, E. and Sahl, H.-G. (1985) *Antimicrob. Agents Chemother.*, **27**, 841–845.

24 Linnett, P.E. and Strominger, J.L. (1973) *Antimicrob. Agents Chemother.*, **4**, 231–236.

25 Reisinger, P., Seidel, H., Tschesche, H. and Hammes, W.P. (1980) *Arch. Microbiol.*, **127**, 187–193.

26 Breukink, E., Wiedemann, I., van Kraaij, C., Kuipers, O.P., Sahl, H.-G. and de Kruijff, B. (1999) *Science*, **286**, 2361–2364.

27 Hoffmann, A., Pag, U., Wiedemann, I. and Sahl, H.-G. (2001) *Il Farmaco*, **57**, 685–691.

28 Brötz, H., Josten, M., Wiedemann, I., Schneider, U., Götz, F., Bierbaum, G. and Sahl, H.-G. (1998) *Mol. Microbiol.*, **30**, 317–327.

29 Chan, W.C., Leyland, M., Clark, J., Dodd, H.M., Lian, L.-Y., Gasson, M.J., Bycroft, B.W. and Roberts, G.C.K. (1996) *FEBS Lett.*, **390**, 129–132.

30 Wiedemann, I., Breukink, E., van Kraaij, C., Kuipers, O.P., Bierbaum, G., de Kruijff, B. and Sahl, H.-G. (2001) *J. Biol. Chem.*, **276**, 1772–1779.

31 Hsu, S.-T.D., Breukink, E., de Kruijff, B., Kaptein, R., Bonvin, A.M.J.J. and van Nuland, N.A.J. (2002) *Biochemistry*, **41**, 7670–7676.

32 Hsu, S.-T.D., Breukink, E., Tischenko, E., Lutters, M.A.G., de Kruijff, B., Kaptein, R., Bonvin, A.M.J.J. and van Nuland, N.A.J. (2004) *Nat. Struct. Mol. Biol.*, **11**, 963–967.

33 van Heusden, H.E., de Kruijff, B. and Breukink, E. (2002) *Biochemistry*, **41**, 12171–12178.

34 Hasper, H.E., de Kruijff, B. and Breukink, E. (2004) *Biochemistry*, **43**, 11567–11575.

35 Hasper, H.E., Kramer, N.E., Smith, J.L., Hillman, J.D., Zachariah, C., Kuipers, O.P., de Kruijff, B. and Breukink, E. (2006) *Science*, **313**, 1636–1637.

36 (a) Ghalit, N., Rijkers, D.T.S., Kemmink, J., Versluis, C. and Liskamp, R.M.J. (2005) *Chem. Commun.*, 192–194; (b) Ghalit, N., Poot, A.J., Fürstner, A. and Rijkers, D.T.S. and Liskamp, R.M.J. (2005) *Org. Lett.*, **7**, 2961–2964; (c)

Ghalit, N., Rijkers, D.T.S. and Liskamp, R.M.J. (2006) *J. Mol. Catal. A: Chem.*, **254**, 68–77; (d) Ghalit, N., Kemmink, J., Hilbers, H.W., Versluis, C., Rijkers, D.T.S. and Liskamp, R.M.J. (2007) *Org. Biomol. Chem.*, **5**, 924–934.

37 For a solid phase synthesis: Angell, Y.M., Thomas, T.L., Flentke, G.R. and Rich, D.H. (1995) *J. Am. Chem. Soc.*, **117**, 7279–7280.

38 Huai, Q., Kim, H.-Y., Liu, Y., Zhao, Y., Mondragon, A., Liu, J.O. and Ke, H. (2002) *Proc. Natl. Acad. Sci. U.S.A.*, **99**, 12037–12042.

39 For a review on sponge peptides: Fusetani, N. and Matsunaga, S. (1993) *Chem. Rev.*, **93**, 1793–1806.

40 Since the original paper by Fusetani and Matsunaga [39], Hagihara and Schreiber reassigned the stereochemistry of the vinylogous tyrosine- and α-ketoarginine residue to be of the *S*-configuration Hagihara, M. and Schreiber, S.L. (1992) *J. Am. Chem. Soc.*, **114**, 6570–6571.

41 (a) Maryanoff, B.E., Qiu, X., Padmanabhan, K.P., Tulinsky, A., Almond, H.R. Jr., Andrade-Gordon, P., Greco, M.N., Kauffman, J.A., Nicolaou, K.C., Liu, A., Brungs, P.H. and Fusetani, N. (1993) *Proc. Natl. Acad. Sci. U.S.A.*, **90**, 8048–8052; (b) Lee, A.Y., Hagihara, M., Karmacharya, R., Albers, M.W., Schreiber, S.L. and Clardy, J. (1993) *J. Am. Chem. Soc.*, **115**, 12619–12620; (c) Ganesh, V., Lee, A.Y., Clardy, J. and Tulinsky, A. (1996) *Protein Sci.*, **5**, 825–835.

42 Bode, W., Mayr, I., Baumann, U., Huber, R., Stone, S.R. and Hofsteenge, J. (1989) *EMBO J.*, **8**, 3467–3475.

43 (a) Wipf, P. and Kim, H. (1993) *J. Org. Chem.*, **58**, 5592–5594; (b) Deng, J., Hamada, Y., Shioiri, T., Matsunaga, S. and Fusetani, N. (1994) *Angew. Chem.*, **106**, 1811–1813; *Angew. Chem. Int. Ed. Engl.*, **33**, 1729–1731; (c) Maryanoff, B.E., Greco, M.N., Zhang, H.-C., Andrade-Gordon, P., Kauffman, J.A., Nicolaou, K.C., Liu, A. and Brungs, P.H. (1995) *J. Am. Chem. Soc.*, **117**, 1225–1239; (d)

Bastiaans, H.H.M., van der Baan, J.L. and Ottenheijm, H.C.J. (1997) *J. Org. Chem.*, **62**, 3880–3889.

44 (a) Maryanoff, B.E., Zhang, H.-C., Greco, M.N., Glover, K.A., Kauffman, J.A. and Andrade-Gordon, P. (1995) *Bioorg. Med. Chem.*, **3**, 1025–1038; (b) Nakao, Y., Matsunaga, S. and Fusetani, N. (1995) *Bioorg. Med. Chem.*, **3**, 1115–1122.

45 For a review see: Gustafsson, D., Bylund, R., Antonsson, T., Nilsson, I., Nyström, J.-E., Eriksson, U., Bredberg, U. and Teger-Nilsson, A.-C. (2004) *Nat. Rev. Drug Discovery*, **3**, 649–659.

46 (a) Plow, E.F., Haas, T.A., Zhang, L., Loftus, J. Smith, J.W. (2000) *J. Chem. Biol.*, **275**, 21785–21788; (b) Gottschalk, K.-E. and Kessler, H. (2002) *Angew. Chem.*, **114**, 3919–3927; *Angew. Chem. Int. Ed.*, **41**, 3767–3774.

47 (a) Hynes, R.O. (1992) *Cell*, **69**, 11–25; (b) Brooks, P.C., Clark, R.A. and Cheresh, D.A. (1994) *Science*, **264**, 569–571; (c) Hynes, R.O. (2002) *Nat. Med.*, **8**, 918–921.

48 Xiong, J.-P., Stehle, T., Zhang, R., Joachimiak, A., Frech, M., Goodman, S. L. and Arnaout, M.A. (2002) *Science*, **296**, 151–155.

49 Brooks, P.C., Montgomery, A.M.P., Rosenfeld, M., Reisfeld, R.A., Hu, T., Klier, G. and Cheresh, D.A. (1994) *Cell*, **79**, 1157–1164.

50 Hood, J.D., Bednarski, M., Frausto, R., Guccione, S., Reisfeld, R.A., Xiang, R. and Cheresh, D.A. (2002) *Science*, **296**, 2404–2407.

51 Gurrath, M., Müller, G., Kessler, H., Aumailley, M. and Timpl, R. (1992) *Eur. J. Biochem.*, **210**, 911–921.

52 Haubner, R., Gratias, R., Diefenbach, B., Goodman, S.L., Jonczyk, A. and Kessler, H. (1996) *J. Am. Chem. Soc.*, **118**, 7461–7472.

53 Haubner, R., Wester, H.-J., Reuning, U., Senekowitsch-Schmidtke, R., Diefenbach, B., Kessler, H., Stöcklin, G. and Schwaiger, M. (1999) *J. Nucl. Med.*, **40**, 1061–1071.

54 (a) For the chemical synthesis of Echistatin, see: Garsky, V.M., Lumma, P.K., Freidinger, R.M., Pitzenberger, S.M., Randall, W.C., Veber, D.F., Gould, R.J. and Friedman, P.A. (1989) *Proc. Natl. Acad. Sci. U.S.A.*, **86**, 4022–4026; (b) For the structural elucidation by NMR, see: Saudek, V., Atkinson, R.A. and Pelton, J.T. (1991) *Biochemistry*, **30**, 7369–7372.

55 (a) Liu, B.A., Jablonowski, K., Raina, M., Arcé, M., Pawson, T. and Nash, P.D. (2006) *Mol. Cell*, **22**, 851–868; (b) Machida, K. and Mayer, B.J. (2005) *Biochim. Biophys. Acta*, **1747**, 1–25.

56 (a) Overduin, M., Rios, C.B., Mayer, B.J., Baltimore, D. and Cowburn, D. (1992) *Cell*, **70**, 697–704; (b) Waksman, G., Kominos, D., Robertson, S.C., Pant, N., Baltimore, D., Birge, R.B., Cowburn, D., Hanafusa, H., Mayer, B.J., Overduin, M., Resh, M.D., Rios, C.B., Silverman, L. and Kuriyan, J. (1992) *Nature*, **358**, 646–653; (c) Booker, G.W., Breeze, A.L., Downing, A.K., Panayotou, G., Gout, I., Waterfield, M.D. and Campbell, I.D. (1992) *Nature*, **358**, 684–687.

57 Ogura, K., Shiga, T., Yuzawa, S., Yokochi, M., Burke, T.R. and Inagaki, F., unpublished results: PDB access code: 1X0N.

58 Gao, Y., Voigt, J., Wu, J.X., Yang, D. and Burke, T.R. Jr. (2001) *Bioorg. Med. Chem. Lett.*, **11**, 1889–1892.

59 Shi, Z.-D., Lee, K., Liu, H., Zhang, M., Roberts, L.R., Worthy, K.M., Fivash, M. J., Fisher, R.J., Yang, D. and Burke, T.R. Jr. (2003) *Biochem. Biophys. Res. Commun.*, **310**, 378–383.

60 Shi, Z.-D., Wei, C.-Q., Lee, K., Liu, H., Zhang, M., Araki, T., Roberts, L.R., Worthy, K.M., Fisher, R.J., Neel, B.G., Kelley, J.A., Yang, D. and Burke, T.R. Jr. (2004) *J. Med. Chem.*, **47**, 2166–2169.

61 Dekker, F.J., de Mol, N.J., Fischer, M.J. E., Kemmink, J. and Liskamp, R.M.J. (2003) *Org. Biomol. Chem.*, **1**, 3297–3303.

2
Macrocycles by Ring-closure Metathesis

Joëlle Prunet, Anderson Rouge dos Santos, and Jean-Pierre Férézou

2.1
Introduction

This chapter concerns the preparation of macrocyclic products by ring-closing metathesis (RCM) or related processes combining RCM with other types of metathesis, starting from suitably substituted diene, ene-yne, or diyne precursors. Macrocyclic rings of 10 or more members have been taken in consideration. Such macrocycles can exist individually or as part of a polycyclic system of the bridged, fused, or ansa type.

This review is not intended to be comprehensive, but should be regarded as a critical overview of the scope and limitations of RCM as applied for the formation of macrocycles. We have tried to adopt a plan that reflects the different types of problems/solutions encountered throughout the huge number of methodological or synthetic studies devoted to the application of macrocycle ring-closing metathesis (M-RCM) to the construction of macrocycles during the past decade. Some "case" studies that involve particularly biologically and/or structurally interesting families of compounds for which, in some cases, several synthetic and methodological RCM strategies have been developed, will be presented in the last part of the review.

One of the main – and also more complex – areas of application of M-RCM is the field of natural product chemistry [1]. Natural macrocycles frequently show remarkable pharmacological properties, exhibiting, for example, antibiotic, immunosuppressant, antifungal, and anticancer activities, some of them being potent inhibitors of specific enzymes associated with several target diseases [2]. The main types of skeletons encountered in natural macrocycles include diterpenes, macrolactones, macrolactams, macroketides (macrocyclic polyketides), or cyclic peptides *inter alia*. This unique profile continues to inspire huge efforts for their total synthesis and for the development of more specific or simplified pharmacologically targeted analogs. This is especially the case for natural macrocycles (such as those of marine origin)

which are difficult to access and only available in minute quantities, insufficient for pharmacological trials. Synthesis is also sometimes the only way to determine their chemical structure with certainty. Whatever the object of performing such complex synthetic tasks, one common feature of most of these natural macrocyclic molecules is their complex structure, which often includes various substituents, polar functional groups and/or unsaturations on a skeleton bearing several stereogenic centers. The construction of these molecules requires specific chemo-, regio-, and stereoselective reactions among which a key one is the formation of the macrocycle itself, generally in one of the late steps of the synthesis, when the required acyclic precursor already comprises most of these complex functionalities. M-RCM has quickly emerged as one of the most useful tools for such a decisive purpose because of its ease of operation and its excellent functional group tolerance. These advantages are quite obvious when considering the spectacular speed at which it is supplanting classical well-established key macrocycle-closing methodologies such as macrolactonization, macrolactamization, or Wittig/Horner-Emmons reactions.

Furthermore, application of M-RCM is not restricted to complex natural products or their pharmacologically significant analogs. Alone, or in combination with other metathesis or non-metathesis processes, it has also been applied to the construction of several non-natural macrocyclic substrates such as catenanes, rotaxanes, etc. Complex strategies involving M-RCM as a key step in various tandem, domino, or even some multicomponent reaction chemistry (RCM) processes are also appearing, offering a promising entry into the diversity-oriented construction of macrocycles.

The advent of RCM [3] as an essential tool for the synthesis of macrocycles undoubtedly arose from two decisive factors:

- The development of stable metal-carbene precatalysts (called catalysts for sake of simplicity throughout this review) – easy to handle and exhibiting exceptional functional-group tolerance. Nowadays, the ruthenium catalysts are the most popular.
- The second factor, as a practical consequence of the first, has been the early commercial availability of some of these catalysts, particularly the first generation catalyst **G1** in 1996 and, some years later (1999), the second generation catalyst **G2** (Figure 2.1). These catalysts are now routinely used in organic chemistry laboratories.

Historically, two remarkable well-defined families of complexes were designed in the early 1990s. The first-generation metal-carbene of practical synthetic utility was the very active molybdenum catalyst **S1** developed by Schrock and coworkers in 1990 [4]. A little while after this, the first-generation stable ruthenium five-coordinate 16-electron alkylidene(II) complex **G0** was prepared by Nguyen and Grubbs, showing rather low reactivity [5]. The Grubbs research group succeeded in developing a practical large-scale production of the more reactive *bis*(PCy$_3$)ruthenium alkylidene complex **G1** by substituting the Ru=CH−CH=CPh$_2$ carbene unit by the Ru=CH−Ph moiety [6]. This second first-generation carbene rapidly became universally used for a huge number of synthetic applications.
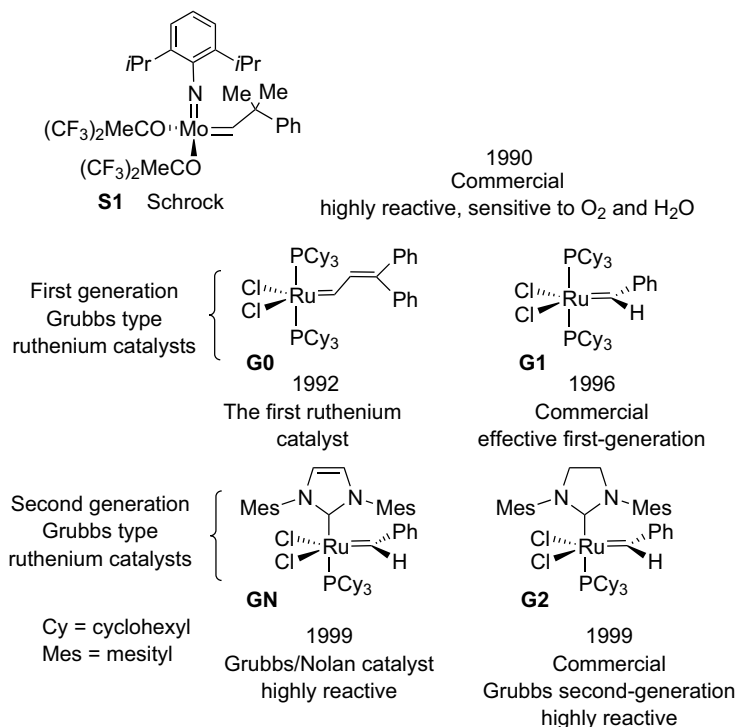
Figure 2.1 The most popular catalysts for RCM.

However, the lack of reactivity of **G1** with tri- and tetrasubstituted olefins led the Grubbs group to develop a second generation of catalysts bearing *N*-heterocyclic carbene ligands, with a remarkable metathesis activity together with an improved stability. Among these new super-catalysts was the ruthenium complex **GN** bearing a *bis*-mesitylimidazol-2-ylidene ligand, which was almost simultaneously developed by the Grubbs [7] and Nolan [8] groups. Subsequently, the catalyst **G2** with a *bis*-mesityl-4,5-dihydroimidazol-2-ylidene ligand [9] appeared, and received more attention from synthetic chemists. Nowadays, the commercial second-generation catalyst **G2** is routinely utilized by synthetic organic chemists.

Most of the recent synthetic applications of M-RCM involve one of the above catalysts, particularly **G1** or **G2**, chosen as a function of its own reactivity profile, generally after preliminary reaction assays on the genuine substrate or specific model compounds. The sensitivity of the RCM reaction to steric hindrance is well established. These ruthenium catalysts exhibit high affinity for carbon-carbon double bonds and are compatible with the presence of many functional groups, even the presence of free polar hydroxyl or amino groups. Their use does not require special conditions such as glove boxes, which are required when using Schrock's molybdenum catalyst.

2.2
How to Cyclize?

From the huge number of model studies and synthetic applications realized during the last ten years, it is possible nowadays to delineate the main factors that affect the course of M-RCM. The following section, through convenient examples, illustrates some of the most representative studies that have helped to establish the scope and limitations of the application of RCM to the synthesis of macrocycles. These contributions have made the use of RCM a predictive tool particularly well suited for the closing key step. However, as will be seen later, some complex situations can still occur where the course of the RCM reaction remains unpredictable and continues to require further studies.

Two main questions are to be asked when envisioning M-RCM as a key step in a synthetic strategy:

- What are the best conditions to perform the cyclization reaction?
- Is it possible to orientate the reaction to get an exclusive *E* or *Z* double bond accordingly?

This second – more complex – point only arises when the final synthetic target contains the newly formed double bond itself or one stereoselective transformation adduct of it. However, application of RCM to the synthesis of macrocycles is facilitated by the fact that many target macrocycles do not include double bonds or are constructed using synthetic strategies that design the closing reaction at a sigma bond. In both cases, the initial RCM closing step is followed by a subsequent hydrogenation reaction that obviously closes the stereochemical debate.

Many reviews deal with the main mechanistic aspects of the metathesis reaction [10]. There are three basic metathesis reactions (apart from polymerization reactions): the ring-closing metathesis (RCM), the cross-metathesis (CM) and the ring-opening metathesis (ROM) [11]. Among the fundamental aspects that govern the reaction course, the thermodynamic *versus* kinetic issue is particularly important when considering the application of RCM to the construction of macrocycles.

Basically, the metathesis reaction consists of reversible $[2 + 2]$-cycloaddition processes between two unsaturated partners, leading to equilibrium mixtures where kinetic, thermodynamic, and entropic parameters are decisive. The main steps are summarized in Scheme 2.1.

2.2.1
A Thermodynamic versus Kinetic Issue

As can be seen from Scheme 2.1, under appropriate equilibrating conditions, the macrocycle will be produced as the thermodynamic product. This clearly appears in the following example (Scheme 2.2). During the synthesis of the 14-membered lactam fluvirucin B_1 by Hoveyda and coworkers from diene **1**, only the dimer **2** resulting from the head-to-head coupling between the less substituted double bond
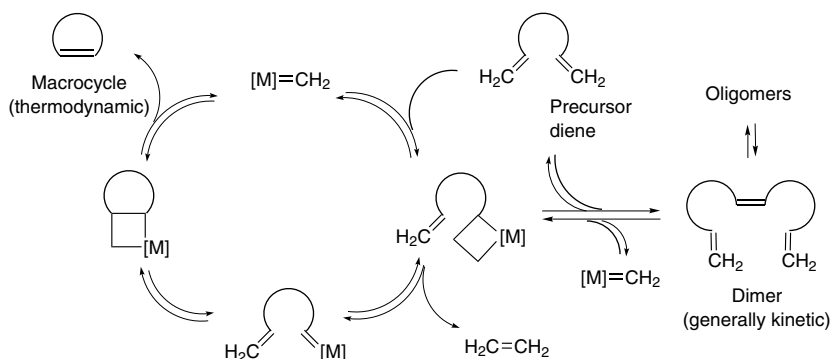
Scheme 2.1 Mechanism of RCM.

of the dienic substrate is formed when using **G1** catalysis [12]. With the more reactive molybdenum catalyst **S1**, the cyclic precursor **3** of fluvirucin is produced in excellent yield. Interestingly, direct treatment of the preceding dimer **2** (the kinetic product of metathesis) with **S1** also furnished **3** (the thermodynamic product of metathesis), which was subsequently transformed into the aglycon of fluvirucin B$_1$ (Sch 38516). Conversion of a head-to-head dimer to the corresponding macrocycle has also been effected during the synthesis of cylindrocyclophane precursors by Smith and coworkers (see Section 2.5.1).

A similar reaction profile was observed by Hagiwara *et al*. when synthesizing muscone from citronellal [13]. When diene **4** (R=Me) is exposed to catalyst **G1**, only the corresponding dimer is formed (Scheme 2.3). However, with terminal olefin **5**
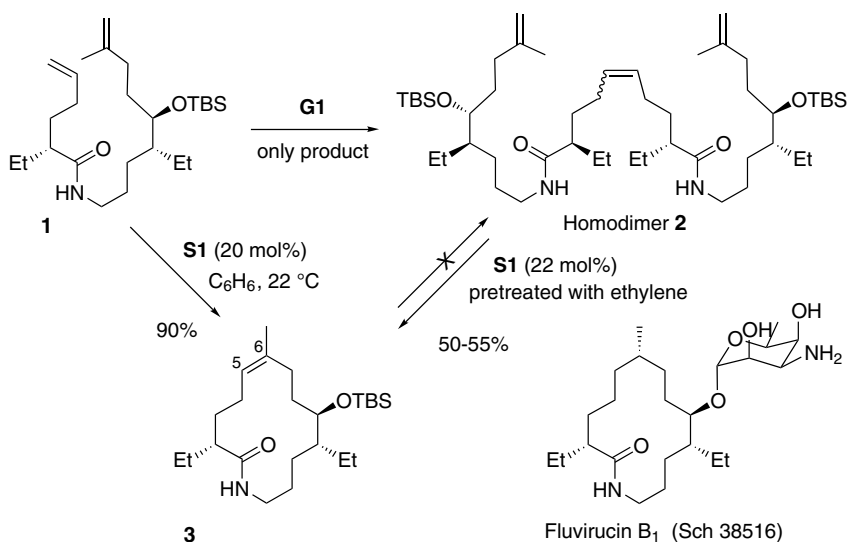
Scheme 2.2 Kinetics versus thermodynamics: catalyst effect.
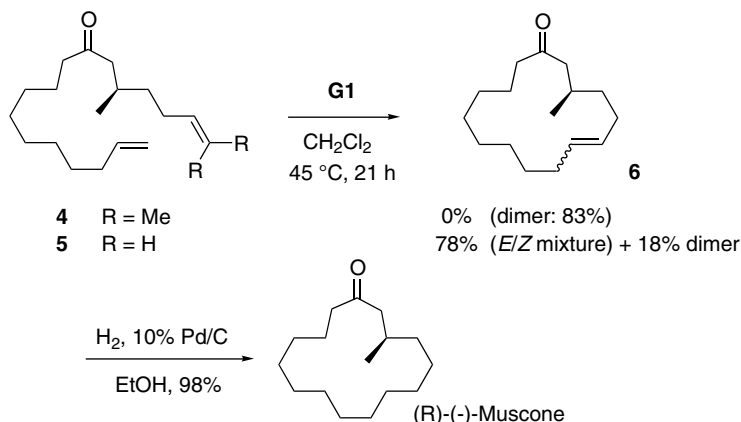
Scheme 2.3 Kinetics versus thermodynamics: influence of the olefin substitution.

(R=H), the desired product **6** is obtained in excellent yield. By lessening the steric hindrance of the olefin, the macrocyclic compound can be reached with **G1**, showing once again that this catalyst is unable to react with hindered olefins. On the other hand, the alcohol corresponding to **4** (**68** in Scheme 2.26), does cyclize with catalyst **G2** (see Section 2.5.5).

2.2.2
General Experimental Conditions

We have seen that the appropriate choice of the catalyst and/or the olefin substitution pattern can dramatically shift the equilibrium in favor of the macrocyclic product. Other factors are important as well, such as the general experimental conditions. Danishefsky and coworkers have highlighted the effects of solvent, temperature, and concentration on the yield of macrocycle RCM for the synthesis of analogs of epothilone 490 [14]. As shown in Scheme 2.4, RCM of compound **7** in
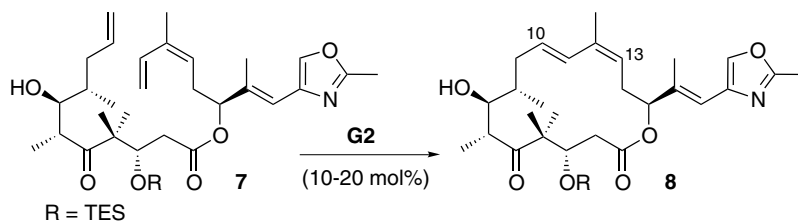
Solvent	Temp.	Time	Conc.	Yield
CH$_2$Cl$_2$	40 °C	6 h	2 mM	<20%
PhMe	110 °C	25 min	2 mM	30%
PhMe	110 °C	15 min	0.5 mM	65%

Scheme 2.4 Temperature and solvent effects.

refluxing dichloromethane affords only a poor yield of macrocycle **8**. When the reaction is performed in toluene at 110 °C, the yield slightly increases. At higher temperature *and* dilution, the yield improves to 65%.

2.2.3
Influence of Polar Complexing Groups

2.2.3.1 A Decisive Factor for Success
A key factor for the success of M-RCM is the presence of a properly positioned polar complexing group in the dienic substrate, which serves as an anchor group for the catalyst, as shown by Fürstner and Langemann [15]. Metathesis of hexadeca-2,15-diene with catalyst **G0** in dichloromethane does not lead to the desired 14-membered olefin **9**, but only to oligomers (Figure 2.2). When an ester function is present, compound **10** is obtained in 52% yield under the same conditions. However, the position of the carbonyl moiety relative to the olefin is of crucial importance: lactone **11** cannot be obtained by RCM with **G0**, while its regioisomer **12** is produced in good yield (Figure 2.2).

This difference in behavior is explained in Figure 2.3. If the ruthenium is too tightly complexed by the polar group (such as in 5- or 6-membered chelates), the metathesis reaction can be inhibited.

A thorough study by Weiler *et al.* [16] also illustrates this point: in the case of $n = 1$ or 9, 5- and 6-membered chelates, respectively, are formed as intermediates, and the RCM yields of lactones or lactams **14** are poor (Scheme 2.5). For $n = 5$, the chelate is a 10- or 11-membered ring, which is a favorable case for RCM (see Figure 2.3).

9 0%   **10** 52%   **11** 0%   **12** 84%
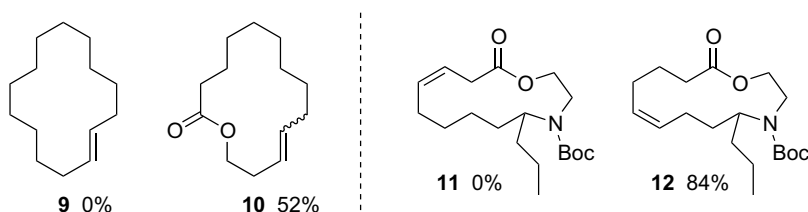
Figure 2.2 Influence of polar groups.

Favorable case   Unfavorable cases
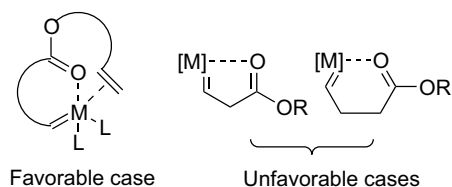
Figure 2.3 Possible chelation.

			Yield	
X	**n**	**Hours**	**Product**	**Start. mat.**
O	1	30	11%	41%
	5	"	62%	11%
	9	"	0%	66%
NH	1	24	0%	82%
	5	1	87%	12%
	9	26.5	7%	83%
NBoc	1	24	0%	93%
	5	8	62%	11%
	9	24	20%	67%

Scheme 2.5 Importance of polar group localization.

2.2.3.2 The Titanium Trick

Fürstner and Langemann devised a means of disrupting the chelate that is compatible with the metathesis catalysts. By using a mild Lewis acid, Ti(OiPr)$_4$, which is complexed by the carbonyl group and thus releases the ruthenium, RCM of esters **15** proceeds in 79–80% yield (Scheme 2.6) [17]. No trace of the desired macrocycles **16** was observed in the absence of Lewis acid. Compound **16** (R=SiMe$_2$tBu) is then converted to gloeosporone by KMnO$_4$ oxidation of the olefin into the corresponding diketone and deprotection of the silyl ether.

| **15** | R = Bn | 79% | (E/Z 3.6:1) | **16** |
| | R = SiMe$_2$tBu | 80% | (E/Z 2.7:1) | |

No reaction without Lewis acid
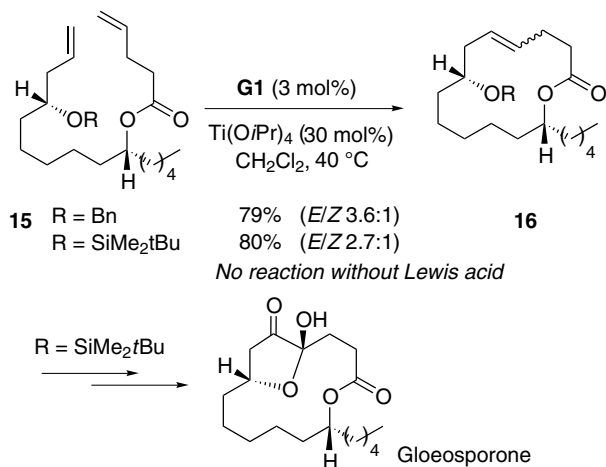
Scheme 2.6 The titanium trick.

Another example deals with the synthesis of 6-nor-analogs of fluvirucin reported by Bracher and Baltrusch [18], where the yield of the RCM step improves from 0% to 72% by addition of 30 mol% of titanium isopropoxide.

2.2.3.3 A Particularly Favorable Case: The Template-Directed RCM

One specific case of favorable conformational benefit for a RCM is the template-directed RCM where non-covalent interactions around an appropriate acidic and/or metal template serve to favor productive conformations. This has been found to be useful for linear substrates devoid of intrinsic conformational constraints [19]. RCM of ether **17** in the presence of lithium ions gives the best yield of product **18**, in accordance with the preferential binding of Li^+ by [12]crown-4, which resembles diene **17** (Scheme 2.7).

2.2.4
Chemoselectivity

Olefin metathesis is very sensitive to steric hindrance, and in particular to the substitution pattern of the reacting olefins. In the course of their total synthesis of the first proposed structure of amphidinolide A, Maleczka *et al.* nicely illustrated this feature [20]. Although the yield is modest and the catalyst loading high, RCM of polyene **19** with catalyst **G2** furnished only macrocycle **20** (Scheme 2.8), by preferential reaction of the terminal olefins versus the 1,1- and 1,2-disubstituted and trisubstituted alkenes. It is worth noting that the less reactive first-generation Grubbs catalyst **G1** only truncated the allylic alcohol to furnish the corresponding methyl ketone [21].

In the case of an approach toward cytotrienins, Panek and coworkers achieved different chemoselectivity according to the catalyst they employed [22]. They first tried RCM of polyene **21** with catalyst **G2** (Scheme 2.9). Unexpectedly, only the macrocyclic conjugated diene **22** is obtained; presumably, initiation of the metathesis reaction occurs at the internal bond of one of the dienes. On the other hand, use of catalyst **G1** leads to the expected conjugated triene **23** in 73% yield.

No salt	39% (*Z/E* 38:62)
LiClO₄	>95% (*Z/E* 100:0)
NaClO₄	42% (*Z/E* 62:38)
KClO₄	36% (*Z/E* 36:64)
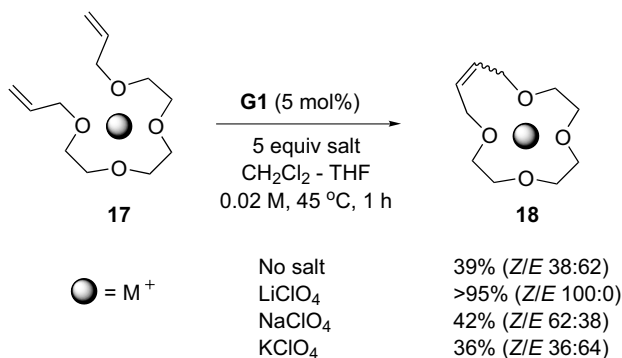
Scheme 2.7 Template-directed metathesis.
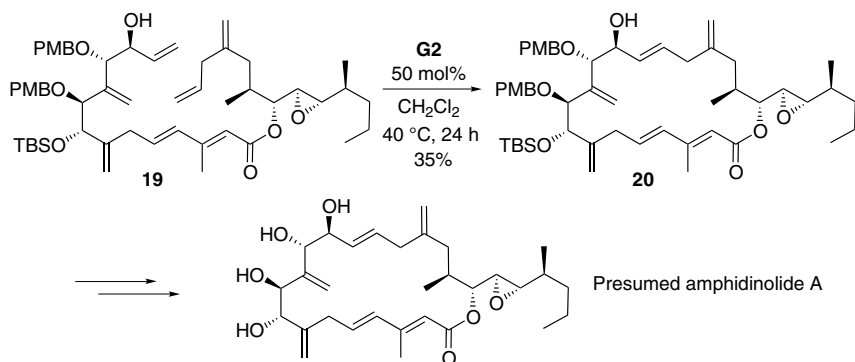
Scheme 2.8 Highly chemoselective RCM in the synthesis of presumed amphidinolide A.
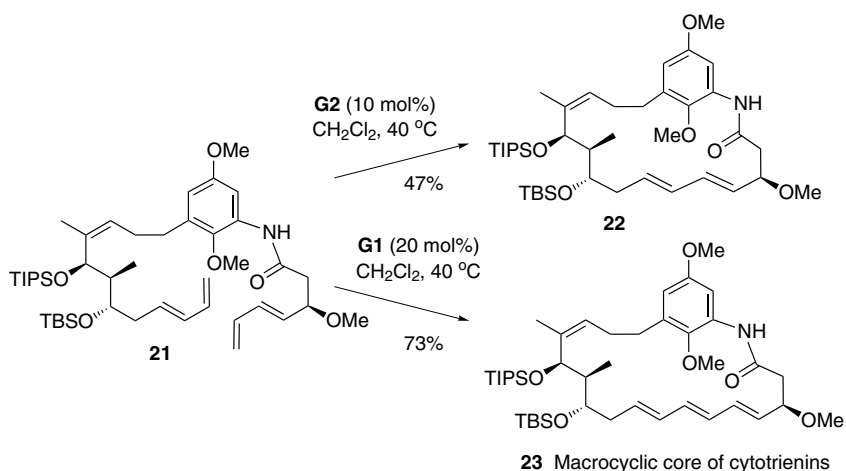
Scheme 2.9 Effect of catalyst on chemoselectivity.

2.2.5
Substrate "Tuning"

Among the factors affecting the course of the RCM reaction, those depending on substituent configuration and/or functional group protection are among the most difficult to anticipate. Several cases illustrate the important influence on the course of the reaction of apparently insignificant structural modifications to the precursor backbone.

2.2.5.1 Configurational/Conformational Aspect

One single inverted stereocenter can dramatically affect the course of the metathesis reaction. Schreiber and his group obtained substrates **24** and **25** by acylation of a
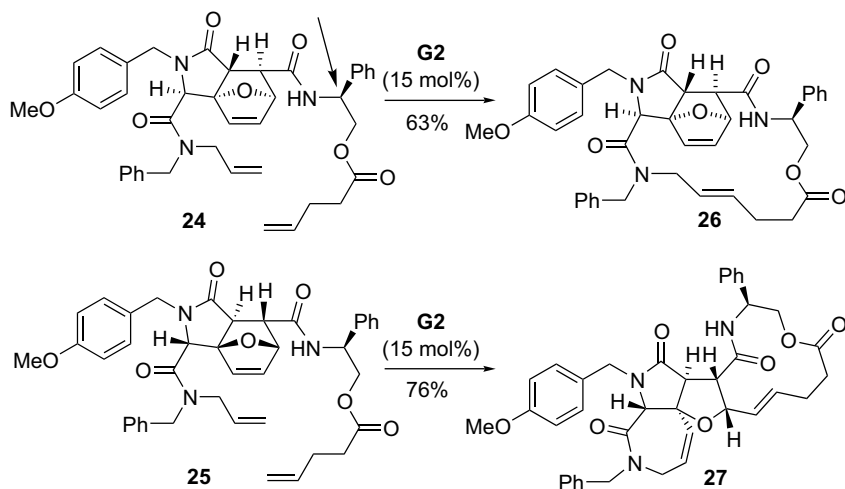
Scheme 2.10 Effect of a single stereocenter on the RCM outcome.

chiral amine by a racemic mixture of products of a Ugi 4CC-IMDA sequence, so they differ by the stereocenter marked in Scheme 2.10 (to be rigorously exact, **24** and the enantiomer of **25** are epimeric at this center [23]). In the case of **24**, a simple RCM takes place, leading to the 17-membered macrolactone **26**. For **25**, the reaction follows a totally different pathway: RCM/ROM, forming the seven-membered lactam and simultaneously opening the oxo-bridged bicycle, is accompanied by RCM which leads to the 12-membered lactam **27**. The pathway selectivity is very high: none of the product resulting from the alternative pathway is observed in either case.

2.2.5.2   Influence of Functional Group Protection
Cyclic diol protecting groups are not always conducive to a successful RCM. For example, when Banwell and McRae submitted acetonide-protected 1,3-diol **28** to the Grubbs first-generation catalyst, none of the desired macrocyle was produced, but cyclohexene **29** was obtained in 81% yield, probably because the acetonide protecting group facilitated interaction of the double bonds of the carboxylic acid portion of the molecule (Scheme 2.11) [24]. To circumvent this problem, substrate **30** was synthesized, where the diol was protected as two silyl ethers, and RCM of this compound led to the desired 18-membered lactone **31** in 70% yield under the same reaction conditions.

2.3
Factors Influencing the Double-Bond Configuration

A key challenge in M-RCM, especially for the construction of unsaturated targets in which the olefin moiety is installed during the metathesis reaction, is the control of the *E*/*Z* selectivity. This applies not only to macrocycles but also to medium-size
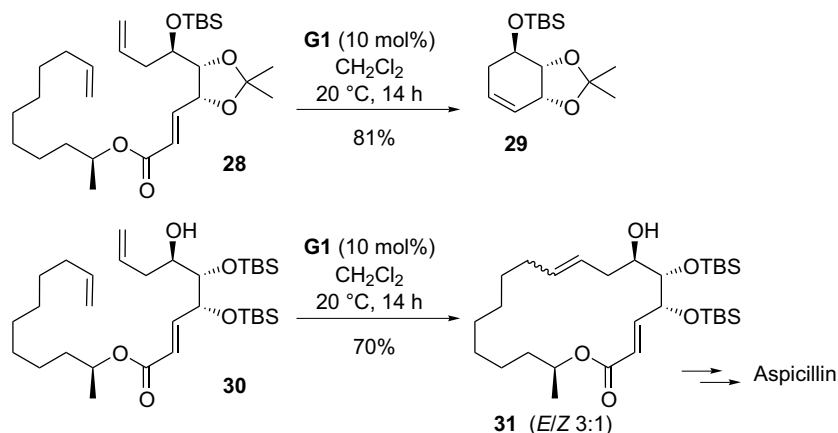
Scheme 2.11 Influence of protecting groups.

cycles starting from 8-membered rings. All prerequisite requirements described above for M-RCM cyclization to take place were based on more-or-less objective rationales in relation to the structure/configuration of the putative dienic precursor. However, the design of an appropriate substrate leading to the desired configuration of the incipient double bond is far more complex and therefore difficult to anticipate. In addition, several factors can also influence the stereoselectivity of the RCM reaction [25].

2.3.1
A Thermodynamic versus Kinetic Issue

As we have seen before, the RCM reaction is generally under thermodynamic control. The influence of the nature of the catalyst on the RCM selectivity was observed by Grubbs *et al.* (Scheme 2.12) [26]. By submitting **32** to a more active
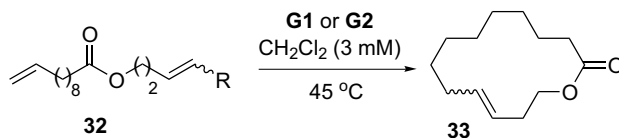
Entry	R	Cat.	(mol%)	Time	Yield	E/Z
1	H	**G2**	(1.0)	40 min	100%	11.5:1
2	"	**G1**	(5.0)	5 h	97%	4.5:1
3	Et (*Z*)	**G2**	(0.5)	30 min	100%	9.7:1
4	"	**G1**	(5.0)	6.5 h	77%	4.5:1
5	(CH$_2$)$_4$Me (*Z*)	**G2**	(0.5)	40 min	100%	10.8:1
6	CH$_2$OAc (*E*)	"	(2.0)	3 h	80%	9.7:1

Scheme 2.12 Influence of the nature of the catalyst on the *E/Z* ratio.
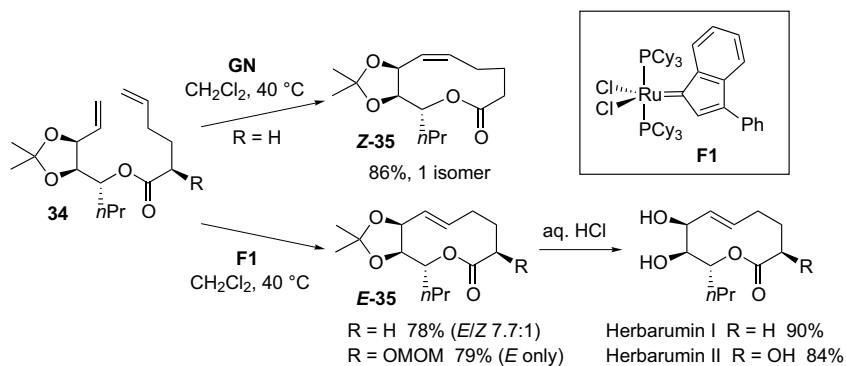
Scheme 2.13 E/Z selectivity by choice of the catalyst: synthesis of herbarumin I and II.

catalyst, a higher proportion of the E-isomer of lactone **33** is produced. The E/Z ratio does not significantly evolve with time when using catalyst **G1**, while it increases from 4.8:1 at 20% conversion to 11.5:1 at 100% conversion with **G2**. The authors also reported that a 4:1 E/Z mixture of lactone **33** can be transformed into a 12:1 mixture of E/Z isomers with **G2**, while the ratio does not change in the presence of **G1**. This increase in the E/Z ratio may be due to secondary metathical isomerization with the more active catalyst **G2**, ultimately leading to the thermodynamic equilibrium of the ring-closure product.

In some cases, the proper selection of the catalyst can lead selectively either to the thermodynamic or the kinetic metathesis product [27]. Fürstner *et al.* nicely illustrated this trend during their synthesis of herbarumin I and II from ester **34** [28] (Scheme 2.13). Semiempirical calculations showed that model lactone **Z-35** is ca. $3.5 \, \text{kcal} \, \text{mol}^{-1}$ more stable than the corresponding lactone **E-35** (R=H), suggesting that thermodynamic control would likely give the undesired isomer for the synthesis of the target molecules. This prediction was verified when compound **34** was submitted to the second-generation complex **GN**: the more stable **Z-35** lactone is produced as the only isomer. When catalyst **F1** is employed, whose activity is comparable to that of first-generation Grubbs catalyst **G1**, the E-isomer is obtained as the major product. The E/Z ratio does not evolve with time, proving that the reaction is under kinetic control with this catalyst. Herbarumin II precursor **E-35** (R=OMOM) is also synthesized with an excellent selectivity using **F1**.

A similar observation was made by Marco and coworkers when synthesizing microcarpalide [29]. In the case of the cyclization of acetonide **36**, the Z-olefin is the thermodynamic product, produced with the second-generation catalyst **G2**, while use of **G1** gives a 2:1 mixture of E/Z alkenes **37** (Scheme 2.14). These compounds could be separated by chromatography and the E-isomer was subsequently converted to microcarpalide by removal of the MOM and the acetonide protecting groups.
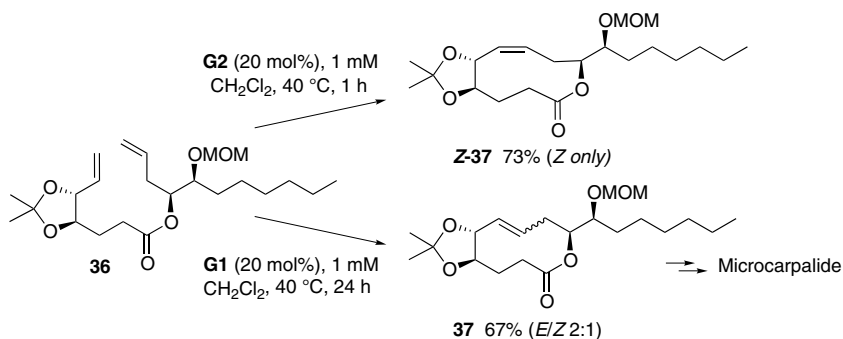
Scheme 2.14 Orientation of the *E/Z*-selectivity by choice of the catalyst: synthesis of microcarpalide.

2.3.2
General Experimental Conditions

The experimental conditions can also affect the stereoselectivity of the M-RCM reaction. For example, the key step of the synthesis of recifeiolide from ester **38** with catalyst **G0** by Fürstner and Langemann proceeds in good yield, but the *E/Z* ratio depends on the temperature of the reaction (Scheme 2.15) [15]. Nakagawa *et al.* also reported a variation of the *E/Z* ratio with the reaction temperature during the formation of azacycloundecenes in the presence of **G1**: it changes from 12.5:1 at 20 °C to 5.2:1 at 50 °C [30].

In the reaction shown in Scheme 2.15, the selectivity could also depend on the solvent, as it is the case for **39**, used for the preparation of the 17-membered diether **40** using catalyst **G1** by Tori *et al.*: in ether, the macrocyclic alkene is obtained as a 1:1 mixture of *E*- and *Z*-olefins, and in dichloromethane, the *E*-isomer of **40** is produced exclusively (Scheme 2.16) [31]. No rational explanation is given for the effect of solvent or temperature.

2.3.3
Substrate "Tuning"

In the course of total synthesis of highly functionalized targets, protecting groups are easily modifiable. They often have a dramatic influence on the stereochemical

| CH₂Cl₂, 40 °C | 80% (*E/Z* 4.7:1) |
| Toluene, 80 °C | 77% (*E/Z* 3.3:1) |
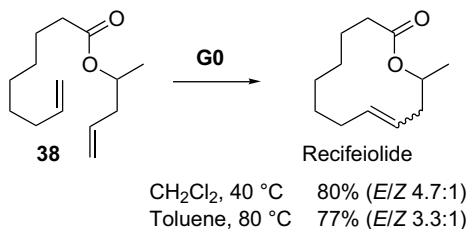
Scheme 2.15 Influence of temperature.
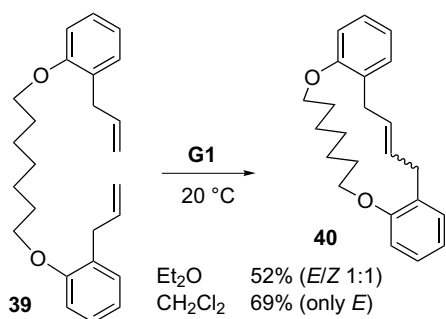
Scheme 2.16 Influence of solvent.

outcome of RCM, especially if a cyclic protecting group is employed. When designing the retrosynthesis of tonantzitlolone, Kirschning and his group envisaged an intermediate with an olefin moiety at C4–C5, which could be *Z* or *E*, as it was to be subsequently oxidized to a hydroxy ketone [32]. Diol **41** was first protected as the corresponding acetonide **42**, which furnished the *Z*-olefin **43** by RCM with good stereoselectivity (Scheme 2.17). Unfortunately, dihydroxylation of this alkene proved
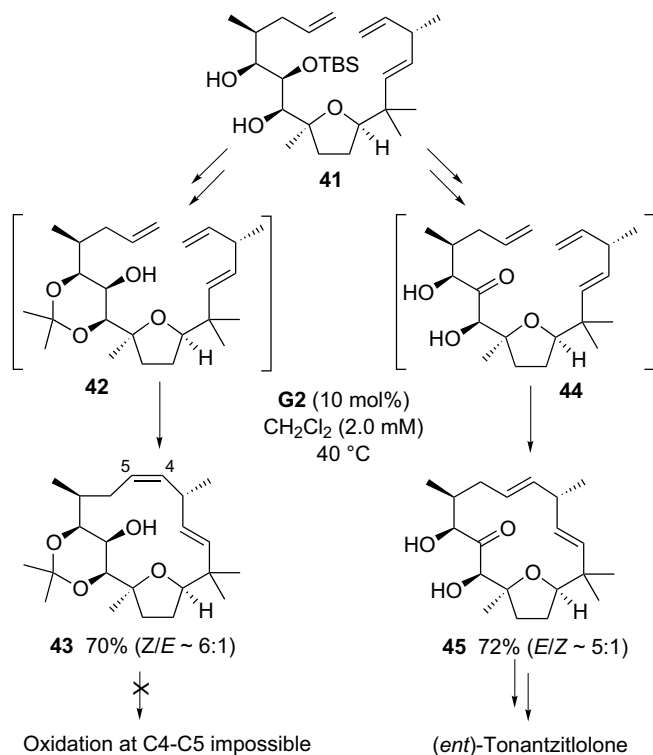
Scheme 2.17 Influence of a diol cyclic protecting group on the stereochemical outcome of RCM.

46a X = α-OTBS, Y = O, R = TBS   **47a** 86% (*E/Z* 1:1.7)
46b X = β-OH, Y = α-OTPS, R = TBS   **47b** 81% (*E/Z* 9:1)

47a →   Epothilone A
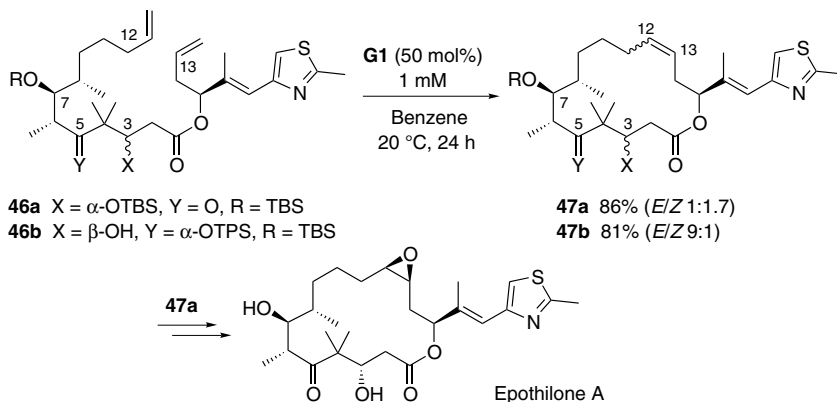
Scheme 2.18 Influence of remote substituents.

impossible. However, cyclization of keto diol **44**, derived from the same precursor **41**, led to the *E*-isomer **45**, which could be transformed into the enantiomer of tonantzitlolone. Presumably, the conformational constraint induced by the acetonide prevents the formation of the *E*-olefin, which is the more stable product in the absence of diol protecting group.

Precursors of epothilone A (with a *Z*-12,13-double bond which will lead to the required *cis* 12,13-epoxide) figure among the most studied macrocycles formed by RCM, and they are good examples of the influence of remote substituents on the *E/Z*-selectivity. In the synthesis by Nicolaou's group, the best proportion of *Z*-isomer is 1:1 [33]. In a similar approach toward this natural product, Danishefsky and coworkers showed that substituents far away from the reaction site (at C3, C5, or the C7 hydroxyl protecting group) have a profound influence on the selectivity of the alkene formation (Scheme 2.18) [34]. The best result in view of the epothilone A synthesis was a 1:1.7 *E/Z* ratio in the case of **46a**, which was eventually converted into the target molecule. For **46b**, which is epimeric at C3 and possesses a protected alcohol instead of a ketone at C5, the *E/Z* ratio switches to 9:1. It seems that there is no reliable method to predict the outcome of this RCM reaction. Alternative strategies for this total synthesis include either formation of the *Z*-alkene on a linear precursor and macrolactonization to close the 16-membered ring [35] or ring-closing alkyne metathesis followed by partial reduction of the newly created triple bond (see Section 2.3.4).

Other examples of the influence of remote substituents on the stereoselectivity of RCM will be detailed in Section 2.6.1.

2.3.4
Solutions

As we have just seen, olefin metathesis is a powerful method to synthesize large rings containing alkenes, but the *E/Z* selectivity is variable and rarely predictable. The answer may lie in an indirect methodology reported by Fürstner and coworkers.
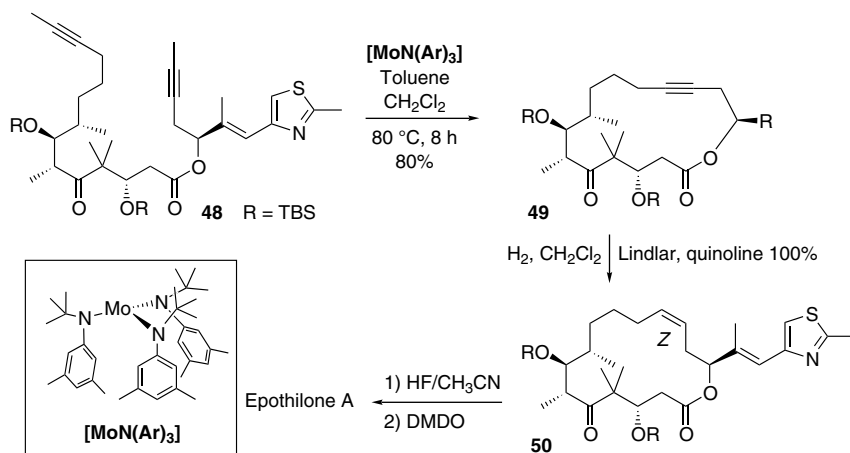
Scheme 2.19 RCAM: the solution to reliable stereoselectivity for alkene formation in macrocycles.

Ring-closing alkyne metathesis (RCAM) leads to alkyne macrocycles in excellent yields [36]. When combined with hydrogenation using a Lindlar-type catalyst, it is a convenient pathway to macrocyclic Z-cycloalkenes. Fürstner and coworkers utilized this strategy for numerous total syntheses of natural products [37], epothilone A being one of them [38].

The metathesis step is effected with the molybdenum precatalyst **[MoN(Ar)₃]** (Scheme 2.19). In the presence of dichloromethane, the active catalyst (the exact structure of which is unknown) reacts with **48** to give alkyne **49** in 80% yield. Hydrogenation of **49** exclusively leads to Z-olefin **50**. It is interesting to note that the olefin metathesis reported by Nicolaou with the diene analog of **48** gives a 1:1 ratio of E/Z isomers [33].

The macrocyclic alkynes can also be reduced in a two-step fashion (E-selective Ru-catalyzed hydrosilylation followed by desilylation with AgF) to furnish E-cycloalkenes with selectivities ranging from 90:10 to >98:2, as described by Fürstner and Radkowski [39].

2.4
Ene-yne M-RCM

Along with diene and diyne metathesis, ene-yne metathesis has also been employed to form macrocycles. This type of metathesis is performed with the catalysts used for olefin metathesis, and the yields are improved in the presence of ethylene, which forms the highly reactive [Ru]=CH₂ species. Shair and coworkers took advantage of this reaction twice in the course of their total synthesis of longithorone A [40]. When ene-ynes **51** and **52** are treated with ruthenium complex **G1** under an atmosphere of
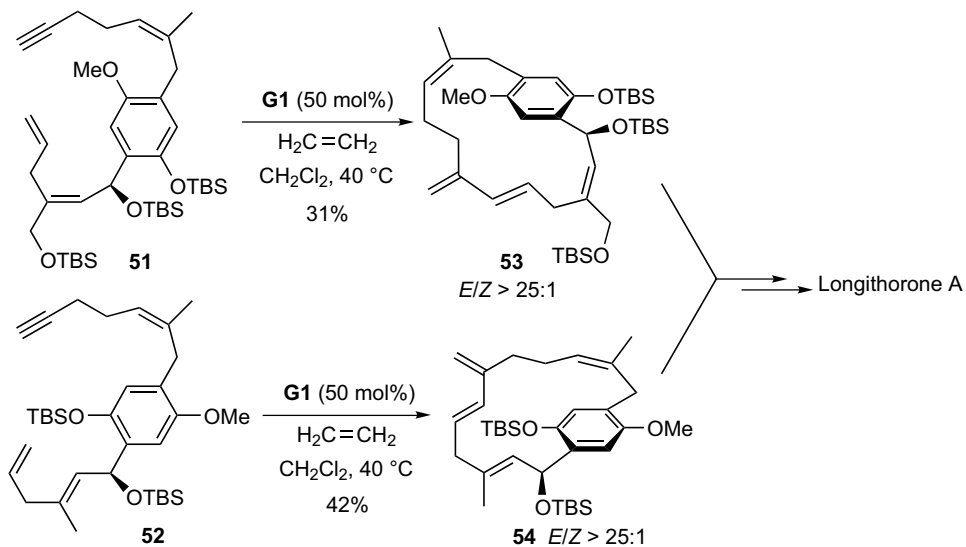
Scheme 2.20 Ene-yne RCM in the synthesis of longithorone A.

Intramolecular pathway:
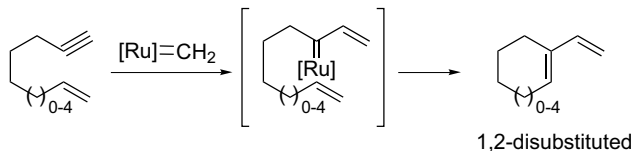
Intermolecular pathway:
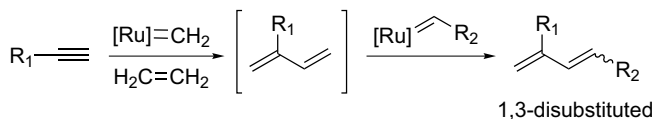
Scheme 2.21 Intramolecular and intermolecular ene-yne metathesis pathways.

ethylene, macrocycles **53** and **54** are produced as single atropdiastereomers, and with a *E/Z* selectivity better than 25:1 (Scheme 2.20).

Both compounds bear a 1,3-disubstituted diene, proving that RCM occurs through the intermolecular ene-yne metathesis pathway (Scheme 2.21), which is usually the case for rings of size 12 or greater.

2.5
Tandem Processes Involving M-RCM

A few examples of tandem processes have been designed for the synthesis or the transformation of natural products.

2.5.1
Tandem CM/RCM

The Smith group reported a very elegant synthesis of cylindrocyclophanes A and F
[41]. Dimerization of *bis*-olefin **55** with first-generation Grubbs catalyst **G1**, followed
by ring-closing metathesis of the resulting dimer furnishes exclusively the [7,7]-
paracyclophane **56** in 61% yield as a single (*E,E*)-isomer (Scheme 2.22). The yield is
not improved with catalyst **G2**, but use of Shrock molybdenum catalyst **S1** gives
optimum result (72% yield). None of the "head-to-head" dimerization products are
observed during this reaction. In a very interesting experiment, these dimers, pre-
pared by another route, were independently submitted to catalyst **S1**, and compound
56 was obtained as the exclusive product in each case. The [8,6]-cyclophanes were not
detected. The dimers probably undergo a cascade of metathesis reactions leading to
the most stable product [7,7]-paracyclophane **56**. This intermediate was subsequent-
ly converted to cylindrocyclophane F by hydrogenation of the olefins and deprotec-
tion of the methyl ethers.

2.5.2
Tandem ROM/RCM

Lazarova *et al.* described the ring contraction of 16-membered ring macrolide anti-
biotics such as josamycin (**57**) to their 14-membered analogs [42]. In the presence of
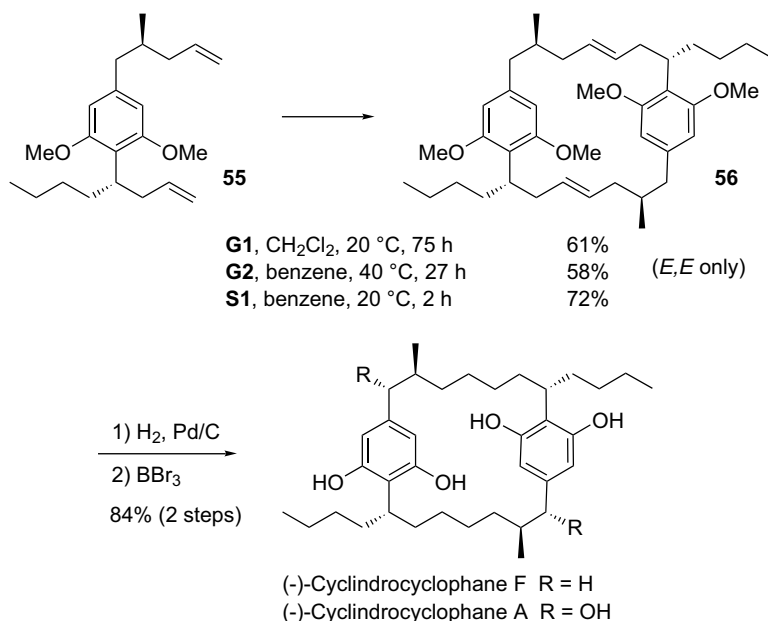
Scheme 2.22 Tandem CM/RCM process in the synthesis of cylindrocyclophanes.
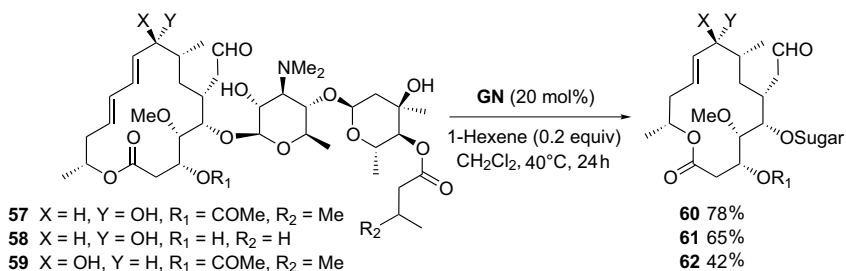
Scheme 2.23 Tandem ROM/RCM process in the synthesis of 14-membered macrolides.

catalyst **G2** and 1-hexene, the 16-membered macrocycles **57–59** are cleanly converted to their derivatives **60–62** by a ring-opening/ring-closing metathesis sequence (Scheme 2.23). Catalyst **G1** is ineffective for this transformation. The 1-hexene additive is a non-gaseous ethylene equivalent: it allows the formation of the [Ru]=CH$_2$ complex both from the original **G2** catalyst and from the conjugated carbene released after the ring-contraction operation. Titanium isopropoxide, which probably disrupts the chelate between the carbene and the lactone carbonyl moiety (see Section 2.2.3), can serve as an alternative to 1-hexene. Without these additives, the reaction is stoichiometric in ruthenium complex, and the percentage conversion is proportional to the amount of catalyst used.

2.5.3
Tandem RCM/ROM/RCM

During their studies toward the total synthesis of coleophomones, Nicolaou and his group uncovered a stereospecific RCM transformation of two regioisomeric enol ethers (this reaction will be detailed in Section 2.6.3). Vassilikogiannakis *et al.* prepared model systems of these enol ethers to try to understand the rationale for this selectivity [43]. During this work, they discovered a dramatic effect of the substitution of one of the olefinic partners on the metathesis outcome (Scheme 2.24). While compound **63a** (R=Me), submitted to catalyst **G2**, undergoes straightforward RCM reaction to give 11-membered ring **64a**, the terminal olefin **63b** (R=H) goes through an RCM/ROM/RCM cascade: after formation of the macrocycle **64b**, this ring is reopened and the resulting carbene reacts with the remaining isoprenyl unit to form the spiro compound **65**. In the case of **64a**, the trisubstitued alkene is too hindered to permit further ring-opening. This ring-opening is possible for **64b**, which is ultimately transformed into the thermodynamic product, 5-membered ring **65**.

2.5.4
Ring-Expansion Metathesis

This reaction was first reported by Grubbs and his group [44]. An ROM/CM sequence between cyclooctene and one of the unsaturated ketones of **66** is followed by
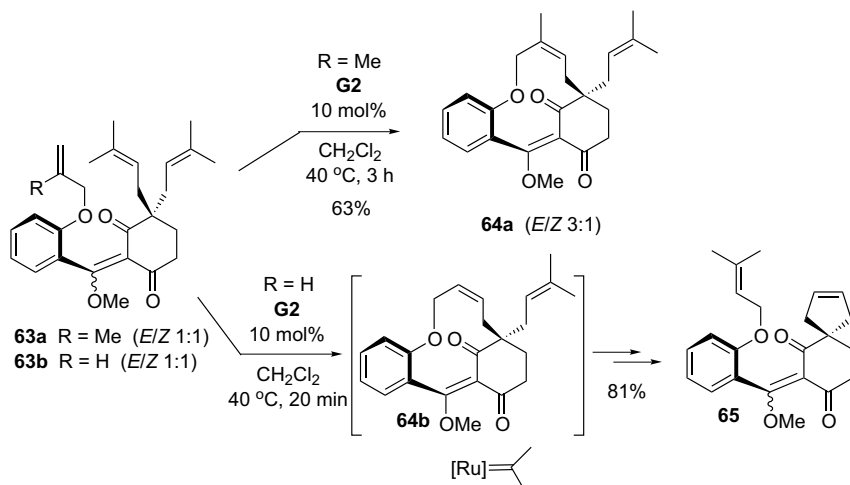
Scheme 2.24 Dramatic effect of olefin substitution on the RCM outcome.
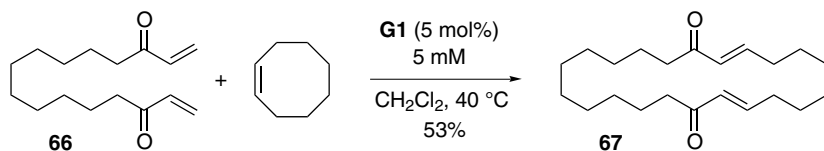
Scheme 2.25 Ring-expansion metathesis reaction.

an RCM to form macrocycle **67**. The authors have used other cycloalkenes for this ring-expansion reaction, ranging from cyclopentene to cyclododecene (see Scheme 2.25).

2.5.5
Other One-Pot Multistep Processes

Grubbs and coworkers have also shown that catalysts **G1** and **G2**, treated with hydrogen, afford the corresponding hydride complexes capable of performing hydrogenation reactions [45]. One-pot tandem RCM/hydrogenation or CM/hydrogenation products are easily obtained by pressurizing the reaction flask with hydrogen after the metathesis reaction is complete. Similarly, transfer hydrogenation with isopropanol (for reduction of ketones) or 3-pentanone (for oxidation of alcohols) can be effected by addition of H_2 and NaOH to the metathesis-reaction vessel. A 3-step one-pot RCM/transfer hydrogenation/hydrogenation was reported by the same
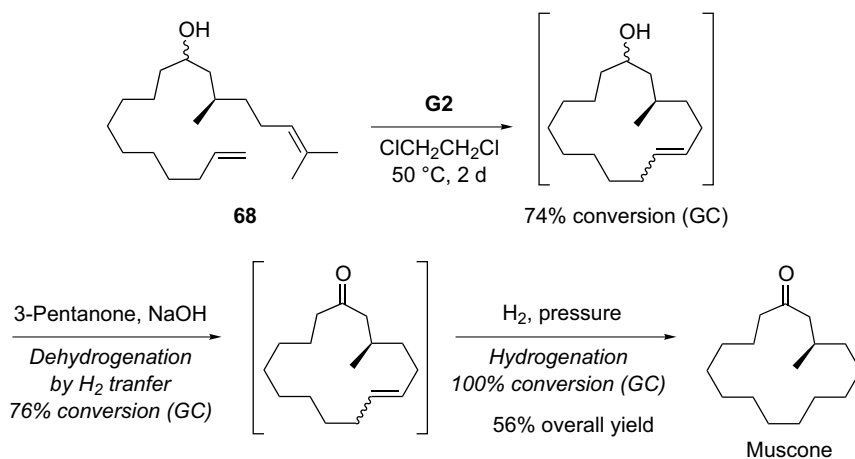
Scheme 2.26 Tandem metathesis/hydrogen transfer/hydrogenation sequence.

authors, resulting in a short and efficient synthesis of muscone from alcohol **68** (Scheme 2.26) [45].

2.5.6
M-RCM as Part of MCR Strategies

In term of diversity-oriented strategies, multicomponent reactions (MCR) represent an attractive and rapid access to libraries of macrocycles inspired by biologically active natural products. Combined with Passerini and Ugi reactions, M-RCM has already shown promising synthetic potential, as illustrated by the pioneering work of Dömling and coworkers [46]. Condensation of isocyanide **69** with carboxylic acid **70** in the presence of paraformaldehyde leads to *bis*-olefin **71**, which is subsequently submitted to RCM in the presence of **G1** and titanium isopropoxide to give the 22-membered macrocycle **72** (Scheme 2.27).

2.6
Representative Synthetic Applications

Numerous total syntheses of macrocycles involve RCM as the key step. For some popular targets, the metathesis disconnection has been designed at the same bond by almost all the groups working on their synthesis, so the effects of multiple factors on the outcome of the metathesis reaction can be outlined. A recent review on the metathesis approach to biologically active macrocycles by Van de Weghe and Eustache [47] reports the case of epothilones and peptidomimetic agents, so these compounds will not be mentioned in the following examples.
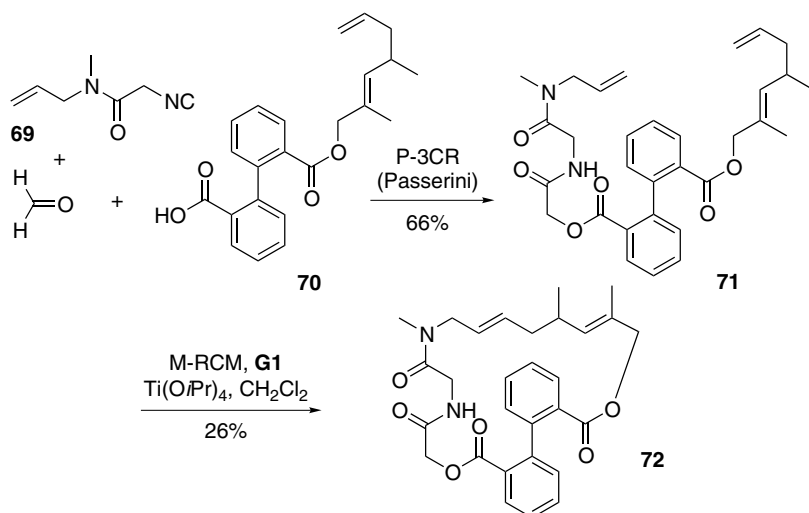
Scheme 2.27 M-RCM in MCR process.

2.6.1
Salicylihalamides/Oximidines: Potent Antitumor Agents with Selective anti-V-ATPase Activity

Salicylic enamides represent a new family of biologically active secondary metabolites of marine origin. These metabolites with promising antitumoral activities are 12-membered lactones, among which salicylihalamide A and oximidine III are two representative leads which have particularly focused the interest of organic chemists (Figure 2.4).

An excellent review was written by Yet in 2003 on the chemistry and biology of salicylihalamides, oximidines, and related compounds [48]. Since that year, a few more studies on the synthesis of these compounds have appeared in the literature. In this section, we will try to examine the factors influencing the *E/Z* selectivity in

Figure 2.4 Salicylihalamide A and Oximidine III.

Scheme 2.28 Influence of the catalyst: kinetics versus thermodynamics.
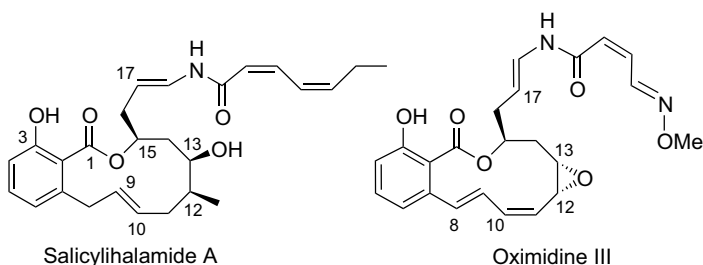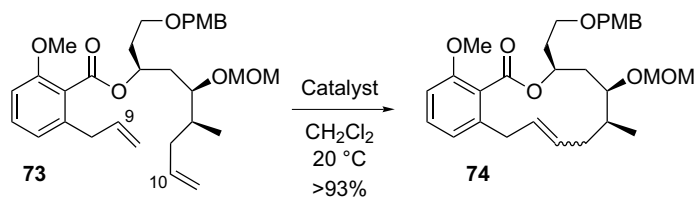
Catalyst	Time (h)	E/Z
G1	1.3	90:10
	6.3	88:12
	18.3	80:20
G2	1.3	66:34
	6.3	68:32
	18.3	67:33

the formation of the 12-membered ring of the salicylihalamide derivatives and illustrate the application of relay RCM to the synthesis of oximidine III.

2.6.1.1 Salicylihalamides: Influence of the Catalyst

In the course of their synthesis of salicylihalamide A, De Brabander *et al.* thoroughly studied the influence of the catalyst on the outcome of the RCM for **73**, which forms the C9–C10 bond [49]. They showed that the first-generation catalyst **G1** gives better *E* selectivity than the more active **G2** complex (Scheme 2.28). The ratio of *E/Z* isomers of **74** does not evolve in time with **G2**, proving that the thermodynamic mixture of products is obtained in this case. On the other hand, kinetic product ratios are probably observed with **G1**, as the *E* selectivity decreases with longer reaction times.

Maier and coworkers reported the same trend with the similar substrate **75** (Scheme 2.29) [50].
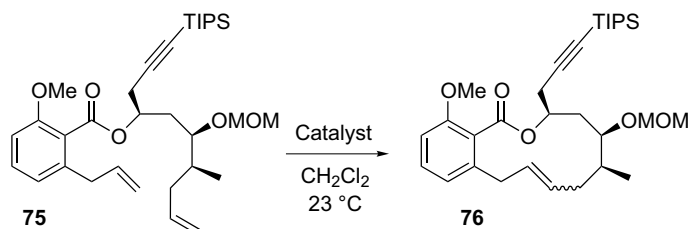
Catalyst	Yield	E/Z
G2	76%	69:31
G1	94%	97:03

Scheme 2.29 Influence of the catalyst.
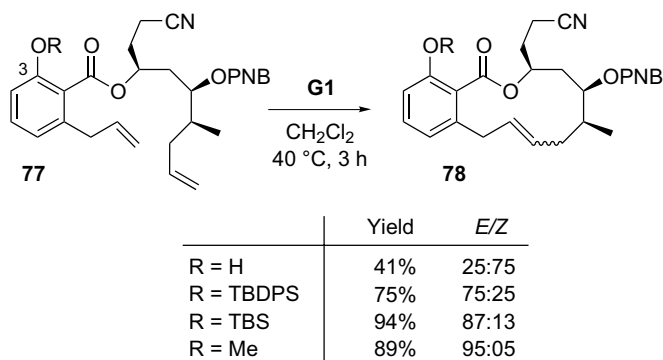
Scheme 2.30 Influence of the phenol protecting group with catalyst **G1**.

	Yield	*E/Z*
R = H	41%	25:75
R = TBDPS	75%	75:25
R = TBS	94%	87:13
R = Me	89%	95:05

2.6.1.2 Salicylihalamides: Influence of the Phenol Protecting Group

The phenol-protecting group has a dramatic effect on the selectivity of the RCM employed to form the 12-membered cycle of salicylihalamides. Georg and his group submitted compounds **77** to catalyst **G1**: the best *E/Z* ratio for **78** is obtained with R=Me, while bulkier protecting groups such as TBS or TBDPS give inferior results (Scheme 2.30) [51]. The unprotected phenol is the only substrate which predominantly leads to the *Z* isomer. This result was also observed by the same group on cyclic precursors of salicylihalamide A [52].

Fürstner *et al.* reported the same protecting-group effect using complex **GN**, with the free phenol **79** exclusively furnishing **Z-80** (Scheme 2.31) [53]. They ruled out the interaction of the free phenol with the catalyst, and proved by semi-empirical calculations that there is no correlation between the *E/Z* ratios and the thermodynamic stabilities of the products, so this effect remains unexplained. The first-generation catalyst **G1** is unable to react with the trisubstituted olefin at C10.
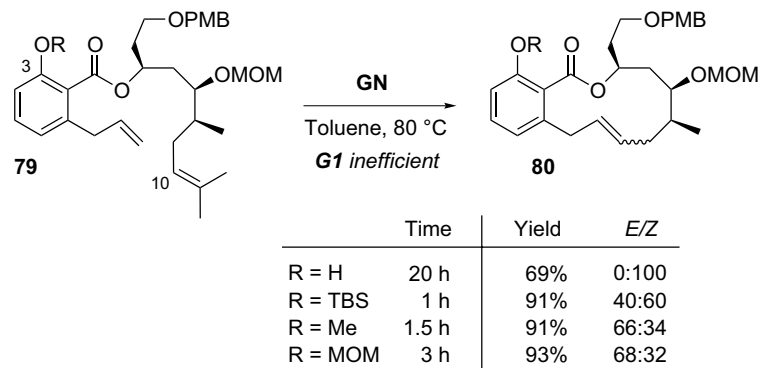
Scheme 2.31 Influence of the phenol protecting group with catalyst **GN**.

	Time	Yield	*E/Z*
R = H	20 h	69%	0:100
R = TBS	1 h	91%	40:60
R = Me	1.5 h	91%	66:34
R = MOM	3 h	93%	68:32

Scheme 2.32 shows compound **81** converting to **82** with G1, CH$_2$Cl$_2$, 40 °C, 3 h.
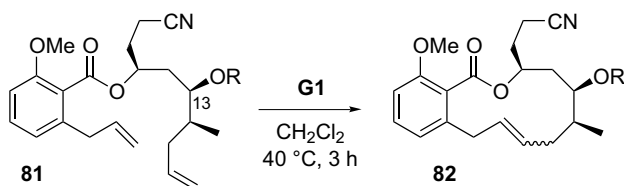
	Yield	E/Z
R = H	44%	97:03
R = Ac	87%	96:04
R = MOM	84%	96:04
R = Piv	94%	96:04
R = PNB	89%	95:05
R = TBS	94%	94:06

Scheme 2.32 Influence of the alcohol protecting group at C13.

2.6.1.3 Salicylihalamides: Influence of the Alcohol-Protecting Group at C13

The alcohol-protecting group at C13 has a slight effect on the RCM selectivity for **81**, as shown by Georg and coworkers [51], but the E/Z ratios of anisoles **82** are all good (Scheme 2.32).

2.6.1.4 Salicylihalamides: Influence of the Nature of the C15 Side Chain

Several groups (Labrecque [54], Smith and Zheng [55], Yadav and Srihari [56], Georg [51], and Snider [57]) have described total or formal syntheses of salicylihalamide A. Various intermediates **83** have been submitted to complex **G1**, and the selectivity does not vary much with the nature of the C15 side chain (Scheme 2.33). Once again, the E/Z ratios for **84** are lower when the phenol is protected as a TBS- rather than a Me-ether.
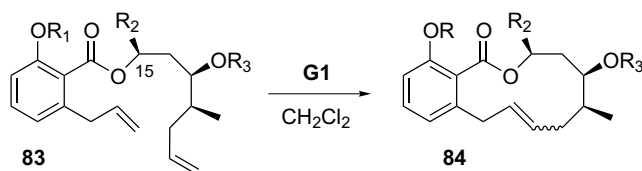
R_1	R_2	R_3	Yield	E/Z	Ref
Me	(CH$_2$)$_3$OBn	TBDPS	75%	90:10	54
	(E)-CH$_2$CH=CHCH$_2$OPMB	TBS	85%	91:09	55
	(CH$_2$)$_2$OTBS	MOM	85%	90:10	56
	(CH$_2$)$_2$CN		84%	96:04	51
TBS	(E)-CH$_2$CH=CHCOOMe	TBS	71%	81:19	57
	(CH$_2$)$_2$CN	PNB	94%	88:12	51

Scheme 2.33 Influence of the nature of the C15 side-chain.

In the same fashion, the C15 side chain does not seem to have a great impact on the selectivity observed with **G2**. Compounds **74** (Scheme 2.28) and **76** (Scheme 2.29) are obtained as 66:34 and 69:31 mixtures of *E/Z* isomers, respectively, when treating dienes **73** and **75** with **G2** in CH_2Cl_2 at ambient temperature. However, Maier and coworkers reported an example which seemingly shows some deviation from this behavior: if a substrate very similar to **73** (with an extra methylene in the side chain) is reacted with **G2** in toluene at 70 °C, the selectivity increases to 86:14 [58]. However, in this example the effects of solvent and temperature cannot be ruled out.

2.6.1.5 Salicylihalamides: Miscellaneous

We have seen in Section 2.2.5 that the inversion of a single stereocenter of a substrate can orientate the RCM in a totally different fashion. De Brabander *et al.* [49] verified this fact when they submitted substrate **85** (whose enantiomer is epimeric at C15 with the natural salicilyhalamide precursors) to RCM: macrocycle **86** is obtained as a 20:80 mixture of *E/Z* isomers (Scheme 2.34). In comparison, natural salicilyhalamide intermediates **83** (entries 2 and 3 of Scheme 2.33 for example) lead to 90:10 *E/Z* ratios for **84**.

Maier and coworkers reported the RCM with **G2** of an analog of substrate **75** devoid of substituents at C12 and C13, which leads to a 81:19 *E/Z* ratio of products [50] (compare with the 69:31 ratio obtained with **75**, Scheme 2.29). Finally, Rizzacasa *et al.* described the metathesis of a substrate with no phenolic OH and no C15 side-chain with a 77:23 *E/Z* selectivity [59].

In conclusion, general trends seem to emerge from the previously described RCM on salicylihalamide precursors, but no rational explanation of these effects has been put forward.

2.6.1.6 Oximidines: Use of Relay Ring-closing Metathesis

Porco and coworkers employed a M-RCM to synthesize the 12-membered ring of oximidine III [60]. When *bis*-diene **87** is engaged in a metathesis reaction with catalyst **HG** [61], whose activity is similar to that of complex **G2**, diene **88** is produced in only 15% yield, presumably because the ruthenium carbene formed at C10 is unreactive (Scheme 2.35). To circumvent this problem, they used the relay RCM strategy first developed by Hoye *et al.* [62]. The first carbene is formed at the terminal olefin of compound **89**, and an RCM furnishes the corresponding carbene at C11 (along with cyclopentene), which undergoes a second RCM to produce the desired oximidine core **88** in 71% yield. In this fashion, formation of the stable conjugated carbene at C10 is avoided.
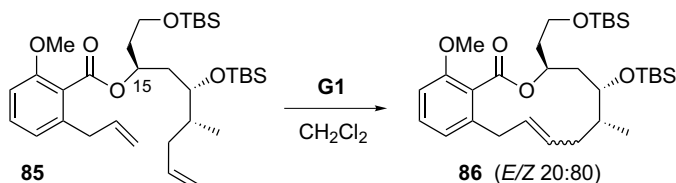
Scheme 2.34 Effect of the configuration of the C15 stereocenter.

Scheme 2.35 Relay RCM in the synthesis of oximidine III.

2.6.2
Radicicol-Type Macrolides: a Promising Family of Anticancer Resorcylides

The tolerance of the RCM reaction to diverse functional groups is illustrated by the synthesis of 14-membered macrocycles monocillin I and radicicol, reported by Danishefsky and coworkers [63]. In the presence of catalyst **G2**, cyclization of dienic substrates **90** and **91**, which comprise an allylic epoxide and a ketone function protected as a dithiane, occurs in 55–60% yields, generating intermediate macrocyclic dienes **92** and **93** of 6E,8Z stereochemistry (Scheme 2.36). It is interesting to

Scheme 2.36 Synthesis of monocillin I and radicicol by M-RCM.

Scheme 2.37 Problematic RCM in the synthesis of cycloproparadicicol.

Conditions			95	Dimer
CH$_2$Cl$_2$	42 °C	19 h	16%	30%
Toluene	42 °C	19 h	27%	48%
Toluene	110 °C	10 min	55%	-

note that the absence of protection of the phenolic hydroxyl groups lead to a less efficient RCM reaction. Difficulties encountered for the demethylation of the phenolic hydroxyl groups compelled the authors to use the silylated intermediate **93**, which can be transformed into monocillin I. Subsequent regioselective chlorination (SOCl$_2$ in Et$_2$O) furnishes radicicol in 58% yield.

In order to optimize the antitumoral properties of radicicol, particularly *in vivo*, the same group synthesized the analogous cycloproparadicicol, where the epoxide function is replaced by a cyclopropane [64]. Submitted to the conditions of the previous RCM reaction (CH$_2$Cl$_2$, 42 °C, 19 h), cyclopropyl triene **94** leads to the expected macrolide **95** in only 16% yield, along with 30% of the corresponding 28-membered dimeric macrocycle (Scheme 2.37). After numerous assays, the best conditions tested (toluene, 110 °C, 10 min) brought the yield up to 55%. In this case, the balance between thermodynamic and kinetic factors seems decisive for the course of the reaction. The fact that the monomeric product is predominant at elevated temperature indicates that this form is entropically favored.

With a view to scaling up the preparation of analogs of radicicol, Yang and Danishefsky developed an "ynolide" alternative strategy, using the alkyne intermediate **96** [65]. In this route, the macrocycle is constructed without the aromatic nucleus, which is elaborated after formation of the macrocycle by a Diels-Alder reaction with the appropriate cyclohexadiene. However, alkyne **96**, when submitted to the RCM conditions, does not furnish macrocycle **97**, probably because of the conformational constraints imposed by the triple bond and the *trans*-disubstituted cyclopropane (Scheme 2.38). Deactivation of the catalyst by complexation with the alkyne moiety could also have blocked the metathesis reaction. The problem was circumvented by formation of cobalt complex **98**, which possesses an angular conformation (140° angle), allowing the formation of macrocycle **99** with catalyst **G2** in 57% yield. The macrocycle was subsequently treated with ceric ammonium nitrate to produce cyclic diene **100**, which was converted to cycloproparadicicol by a sequence of reactions involving a Diels-Alder reaction to form the aromatic ring.
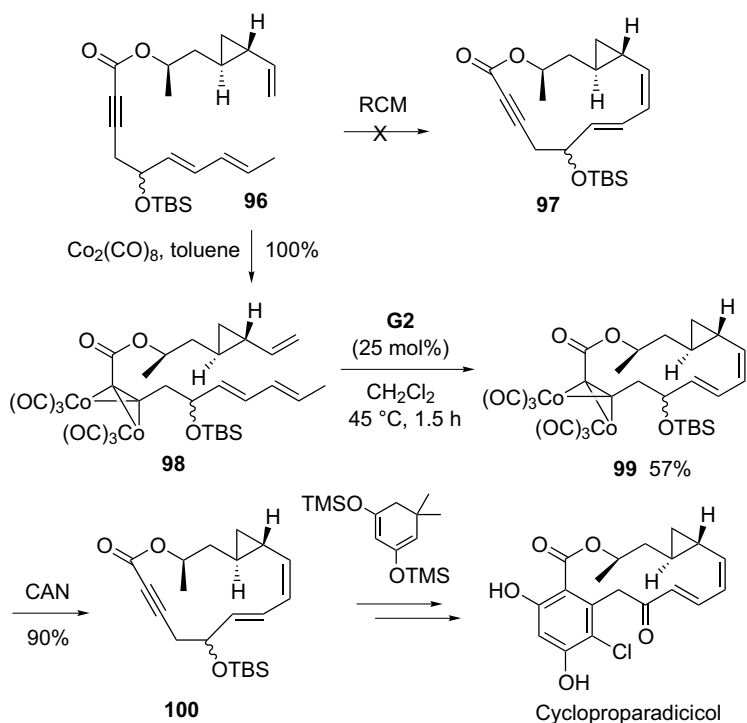
Scheme 2.38 Synthesis of cycloproparadicicol: the ynolide strategy.

This "ynolide" strategy was applied to the synthesis of the macrolide aigialomycin D by Geng and Danishefsky [66].

2.6.3
Coleophomones: a Versatile Access to this Class of Complex Polycyclic Diterpenes

Coleophomones, isolated by Shionogi Pharmaceutical Co. and later by Merck, are compact fungal diterpenes possessing a strained 11-membered central core. In the final strategy adopted by Nicolaou and his group for the synthesis of these challenging molecules, the labile triketone precursor **101** was protected as the mixture of enol ethers **102** and **103** (Scheme 2.39) [67]. After chromatographic separation, these regioisomers were independently submitted to RCM in the presence of **G2** to give in each case a single regio- and stereoisomer, the 11-membered rings **104** and **105** possessing an *E*- and a *Z*-trisubstituted double bond, respectively. Because of the absence of the more thermodynamically stable cyclopentene adducts, these products were claimed to be the kinetic products of the reaction.
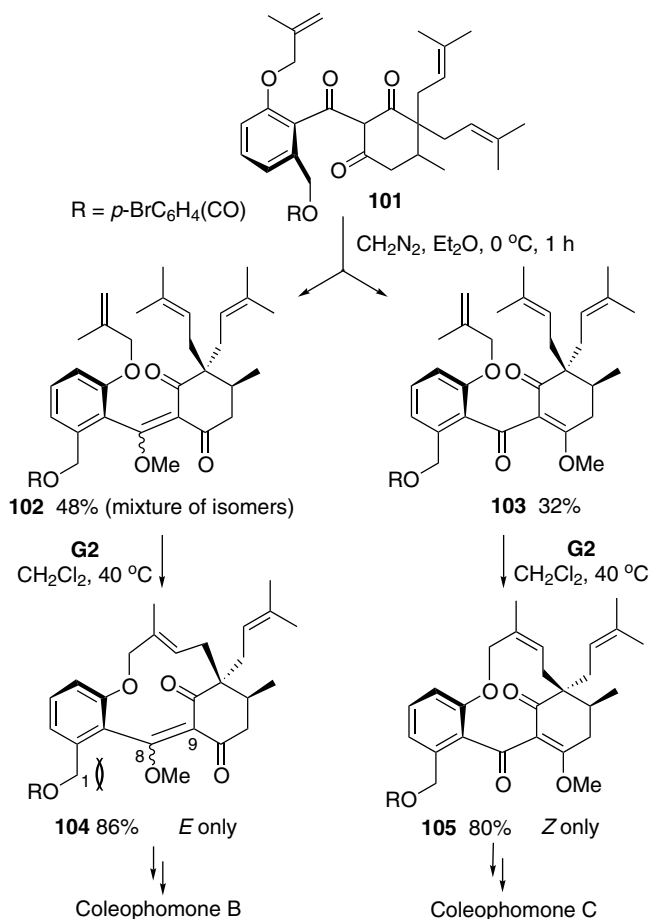
Scheme 2.39 Synthesis of Coleophomones B and C.

2.6.4
RCM in Supramolecular Chemistry

Because of its versatility, high functional-group compatibility, and exceptional cata-
lytic reactivity, the RCM reaction is particularly well suited for supramolecular
chemistry applications such as the synthesis of catenanes, rotaxanes, molecular
knots, dendrimer-type molecules, etc. [68]. One key strategic point in the construc-
tion of such molecular architectures is the application of intermediate use of tem-
plates to favor interlocking thermodynamically. Metal-based templation strategy has
been successfully applied to the construction of numerous supramolecular edifices.
Pioneering work from Grubbs [69] and Sauvage [70] groups, respectively, led to the
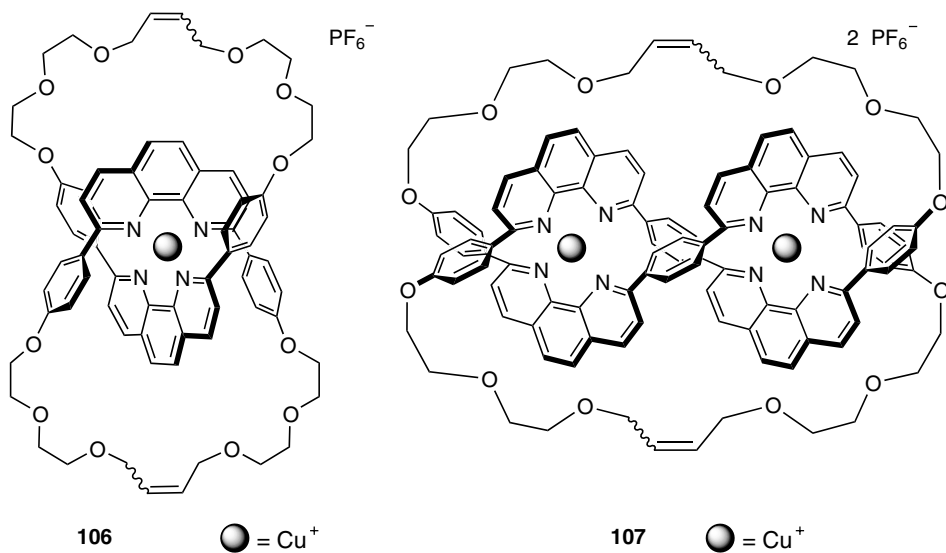
Figure 2.5 First catenane and molecular knot synthesized by RCM.

formation of the first catenane (**106**) and molecular knot (**107**) (Figure 2.5) using **G1**-catalyzed RCM of pre-assembled polyolefinic copper complexes.

Among the interesting applications of RCM to supramolecular chemistry, the synthesis of molecular gyroscopes containing an internal rotator domain [Fe (CO)$_3$] that can rotate independently of the external stator bearing easily adjustable spokes depending on the diphosphane olefinic chain length has been reported by Gladysz and coworkers [71]. RCM/hydrogenation sequence from the appropriate precursors **108** led to 13-, 15-, and 17-membered gyroscopes **109** (Scheme 2.40).

M-RCM supramolecule formation using metal-based templation strategies involving intermediate metal complexes to organize the reacting partners continue to receive much attention since their domain of application can be extended to numerous types of complex products. Conformational constraints such as those dictated by pincer-pyridine complexes clearly favor RCM of terminal olefins **110b** and **110c** (M=Pd or Pt) when compared with the unprotected pyridine analog **110a**. Final
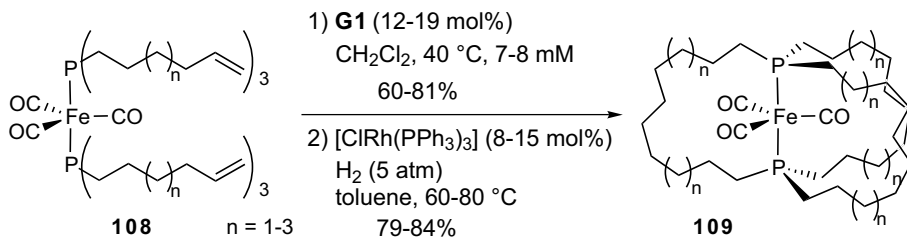
Scheme 2.40 Formation of molecular gyroscopes by RCM.

Scheme 2.41 Use of pincer-pyridine complexes to favor RCM reaction.
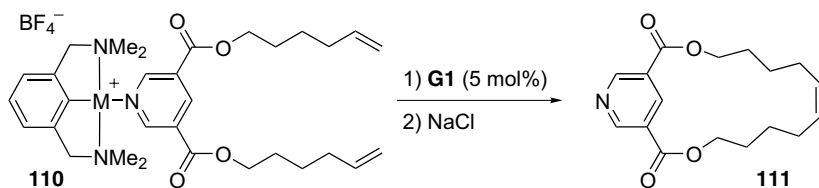
	M	Time	Macrocycle 111	Isomerized product
110a	No metal	16 h	20%	-
110b	Pd	5 d	50%	50%
110c	Pt	2 h	100%	0%

detachment of the pyridine ligands is realized in the presence of NaCl in biphasic systems (Scheme 2.41) [72].

Tripincer template-directed cyclization of a dienic pyridine precursor leads to the formation of the 69-membered ring trimeric heterocycle **112** (Figure 2.6). Decomplexation of the tripincer from the product is realized with NaCl [72]. The synthesis of a [2]rotaxane by M-RCM using a similar pincer-pyridine complex for pre-assembly was also reported by Leigh *et al.* [73].

Head-to-head α- and β-cyclodextrin homodimers, in which the two primary rims are doubly ligated through alkyl chains, have been efficiently synthesized by Sinaÿ and his groups by a CM followed by an RCM reaction sequence [74].
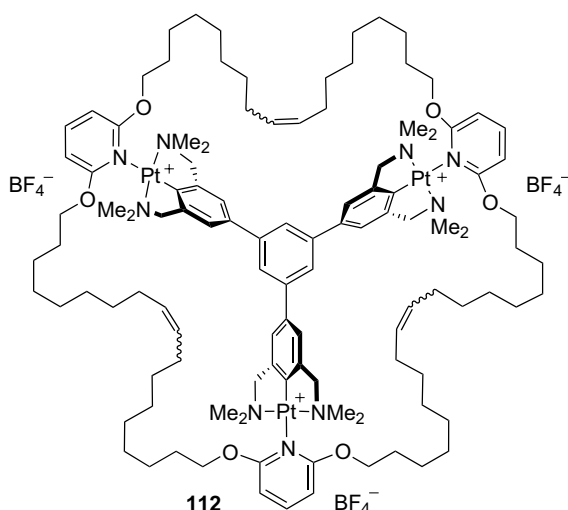
Figure 2.6 Synthesis of a 69-membered ring by M-RCM.

2.7
Conclusion and Perspectives

Ring-closing metathesis has been applied to the synthesis of very diverse macro-cycles, ranging from medium to very large rings and containing a wide range of functional groups. These macrocycles can be natural products or complex supra-molecular edifices.

One key argument that makes a given methodology useful in designing a syn-thetic process is its predictability, i.e. the possibility of anticipating an expected result from the accumulated knowledge – the state of the art – at a given time. Undoubt-edly, today, after no more than ten years of application in macrocyclization applica-tions, the RCM reaction has gained this status and therefore has become an essential tool for achieving the key cyclization steps in macrocycle synthesis. However, some decisive features such as the prevision of the *E*- or *Z*-configuration of the resulting double bond have still to be addressed. Several practical solutions to this problem have been proposed and obviously are still going to be found.

2.8
Experimental: Selected Procedures

2.8.1
Synthesis of Compound 3 with Catalyst S1 [12]

Molybdenum catalyst **S1** (9 mg, 0.01 mmol) was weighed in a glove box in a 10-mL round-bottom three-necked flask equipped with a reflux condenser and a rubber septum. The reaction vessel was subsequently removed from the glove box and maintained under an atmosphere of argon. The catalyst was then dissolved in anhydrous benzene (6.0 mL), and diene **1** (20 mg, 0.04 mmol) was added as a solu-tion in anhydrous benzene (0.60 mL). The reaction flask was immersed in an oil bath that was previously warmed to 50 °C, and the mixture was allowed to stir for 14 h. After this period, the reaction vessel was allowed to cool to 22 °C. The mixture was stirred in the presence of air (septum was removed) for approximately 2 h. Removal of solvent *in vacuo* afforded a black solid. Purification through silica gel chromatog-raphy (10:1 hexanes/ethyl acetate followed by 4:1 hexanes/ethyl acetate) delivered **3** as a white solid (18.1 mg, 90% yield).

2.8.2
Synthesis of Compound 6 with Catalyst G1 [13]

To a solution of **5** (30 mg, 0.114 mmol) in dry degassed CH_2Cl_2 (25 mL) was added, via syringe, a solution of ruthenium alkylidene catalyst **G1** (5 mg, 0.006 mmol) predissolved in CH_2Cl_2 (6 mL). The resulting purple solution was heated to 45 °C for 21 h and then concentrated under reduced pressure to afford an oily brown residue. Purification by MPLC [pre-packed silica gel column 2 × 50 cm, eluent: ethyl

acetate/*n*-hexane (1:9)] provided **6** (20.9 mg, 78%). The fractions also provided the cyclic dimer (5 mg, 18%).

2.8.3
Synthesis of Compound 8 with Catalyst G2 [14b]

A stirred solution of diene **7** in anhydrous toluene (0.2 mM) under argon was heated to 110 °C (reflux), and 5–10 mol% **G2** was added to the refluxing solution. Stirring was continued for 15 min, and then the flask was immersed in an ice bath. The reaction mixture was passed through a pad of silica gel, which was rinsed with CH_2Cl_2 and concentrated, and compound **8** was purified by flash chromatography.

2.8.4
Synthesis of Compound 16 (R=SiMe$_2$tBu) with Catalyst G1/Ti(OiPr)$_4$ [17]

The silyl ether **15** (R=SiMe$_2$*t*Bu) (200 mg, 0.46 mmol) and Ti(O*i*Pr)$_4$ (39 mg, 0.14 mmol, 41 µL, 0.3 equiv) were dissolved in CH_2Cl_2 (180 mL), and the mixture was refluxed for 1 h. The ruthenium carbene **G1** (8 mg, 0.01 mmol, 2 mol%) in CH_2Cl_2 (2 mL) was then added, and reflux was continued for 24 h, after which an additional 4 mg (0.005 mmol, 1 mol%) of **G1** in CH_2Cl_2 (2 mL) was added. After an additional 24 h, the mixture was cooled to ambient temperature and filtered through a short pad of silica gel. The solvent was removed *in vacuo*, and the residue was purified by flash chromatography (hexanes/ethyl acetate 100:1) to give the macrolide **16** as a colorless syrup (151 mg, 80%).

2.8.5
Synthesis of Compound 49 by RCAM [38]

Diyne **48** (120 mg, 0.14 mmol) was added to a solution of complex [MoN(Ar)$_3$] (12 mg, 0.02 mmol) in toluene (10 mL) and CH_2Cl_2 (0.3 mL), and the resulting mixture was stirred at 80 °C for 8 h. All volatiles were then evaporated, and the residue was purified by flash chromatography (pentane/Et$_2$O 20:1) to afford cycloalkyne **49** as a colorless syrup (84 mg, 80%).

2.8.6
Synthesis of Compound 53 with G1 by ene-yne RCM [40a]

To a solution of Grubbs catalyst **G1** (943 mg, 1.15 mmol, 0.4 equiv) in CH_2Cl_2 (900 mL) was added a solution of enyne **51** (2.00 g, 2.86 mmol, 1.0 equiv) in toluene (100 mL). The reaction was purged with ethylene and stirred at 45 °C under an atmosphere of ethylene for 40 h. The crude mixture was treated with ethyl vinyl ether (1 mL) and concentrated to a black oil. Purification by silica gel chromatography (doped with triethylamine, 5–6% in CH_2Cl_2/hexane) afforded cyclophane **53** (624 mg, 31%).

Acknowledgments

Abbreviations

4CC-IMDA	4-component condensation/intramolecular Diels-Alder reaction sequence
Ac	acetyl
Bn	benzyl
Boc	*tert*-butyloxycarbonyl
CAN	ceric ammonium nitrate
CM	cross-metathesis
Cy	cyclohexyl
DMDO	dimethyldioxirane
M-RCM	macrocycle ring-closing metathesis
MCR	multicomponent reaction
Mes	mesityl
MOM	methoxymethyl
P-3CR	Passerini 3-component reaction
Piv	pivaloyl
PMB	*p*-methoxybenzyl
PNB	*p*-nitrobenzoyl
RCM	ring-closing metathesis
RCAM	ring-closing alkyne metathesis
ROM	ring-opening metathesis
TBDPS	*tert*-butyldiphenylsilyl
TBS	*tert*-butyldimethylsilyl
TES	triethylsilyl
TIPS	triisopropylsilyl
TPS	triphenylsilyl

References

1 Wessjohann, L.A., Ruijter, E., Garcia-Rivera, D. and Brandt, W. (2005) *Mol. Diversity*, **9**, 171–186.

2 (a) Balunas, M.J. and Kinghorn, A.D. (2005) *Life Sci.*, **78**, 431–441; (b) Butler, M.S. (2004) *J. Nat. Prod.*, **67**, 2141–2153; erratum, *ibid.* 2006, **69**, 172; (c) Shu, Y.-Z. (1998) *J. Nat. Prod.*, **61**, 1053–1071.

3 (a) For a comprehensive review on metathesis, see: Grubbs, R.H. (ed.) (2003) *Handbook of Metathesis*, Wiley-VCH, Weinheim; (b) for a review of M-RCM in natural product synthesis, see:Gradillas, A. and Pérez-Castells, J. (2006) *Angew. Chem.*, **118**, 6232–6247; *Angew. Chem. Int. Ed.*, **45**, 6086–6101.

4 (a) Schrock, R.R., Murdzek, J.S., Bazan, G.C., Robbins, J., DiMare, M. and O'Regan, M. (1990) *J. Am. Chem. Soc.*, **112**, 3875–3886; (b) For a review:

Schrock, R.R. and Hoveyda, A.H. (2003) *Angew. Chem.*, **115**, 4740–4782; (c) Schrock, R.R. and Hoveyda, A.H. (2003) *Angew. Chem. Int. Ed.*, **42**, 4592–4633.

5 Nguyen, S.T., Grubbs, R.H. and Ziller, J.W. (1993) *J. Am. Chem. Soc.*, **115**, 9858–9859.

6 (a) Schwab, P., France, M.B., Ziller, J.W. and Grubbs, R.H. (1995) *Angew. Chem.*, **107**, 2179–2181; *Angew. Chem. Int. Ed.*, **34**, 2039–2041; (b) Schwab, P., Grubbs, R.H. and Ziller, J.W. (1996) *J. Am. Chem. Soc.*, **118**, 100–110.

7 Scholl, M., Trnka, T.M., Morgan, J.P. and Grubbs, R.H. (1999) *Tetrahedron Lett.*, **40**, 2247–2250.

8 (a) Huang, J., Stevens, E.D., Nolan, S.P. and Petersen, J.L. (1999) *J. Am. Chem. Soc.*, **121**, 2674–2678; (b) Jafarpour, L., Hillier, A.C. and Nolan, S.P. (2002) *Organometallics*, **21**, 442–444.

9 Scholl, M., Ding, S., Lee, C.W. and Grubbs, R.H. (1999) *Org. Lett.*, **1**, 953–956.

10 (a) Astruc, D. (2005) *New J. Chem.*, **29**, 42–56; *ibid.* (2006), **30**, 1848–1852; (b) Katz, T.J. (2006) *New J. Chem.*, **30**, 1844–1847.

11 Nicolaou, K.C., Bulger, P.G. and Sarlah, D. (2005) *Angew. Chem.*, **117**, 4564–4601; *Angew. Chem. Int. Ed.*, **44**, 4490–4527.

12 Xu, Z., Johannes, C.W., Houri, A.F., La, D.S., Cogan, D.A., Hofilena, G.E. and Hoveyda, A.H. (1997) *J. Am. Chem. Soc.*, **119**, 10302–10316.

13 Kamat, V.P., Hagiwara, H., Katsumi, T., Hoshi, T., Suzuki, T. and Ando, M. (2000) *Tetrahedron*, **56**, 4397–4403.

14 (a) Yamamoto, K., Biswas, K., Gaul, C. and Danishefsky, S.J. (2003) *Tetrahedron Lett.*, **44**, 3297–3299; (b) See also: Biswas, K., Lin, H., Njardarson, J.T., Chappell, M.D., Chou, T.-C., Guan, Y., Tong, W.P., He, L., Horwitz, S.B. and Danishefsky, S.J. (2002) *J. Am. Chem. Soc.*, **124**, 9825–9832.

15 Fürstner, A. and Langemann, K. (1997) *Synthesis*, 792–803.

16 Goldring, W.P.D., Hodder, A.S. and Weiler, L. (1998) *Tetrahedron Lett.*, **39**, 4955–4958.

17 Fürstner, A. and Langemann, K. (1997) *J. Am. Chem. Soc.*, **119**, 9130–9136.

18 (a) Baltrusch, A.W. and Bracher, F. (2002) *Synlett*, 1724–1726; (b) for yet another example of the use of $Ti(OiPr)_4$ in M-RCM, see: Eh, M. (2003) *Synthesis*, 365–370.

19 Marsella, M.J., Maynard, H.D. and Grubbs, R.H. (1997) *Angew. Chem.*, **109**, 1147–1150; *Angew. Chem. Int. Ed.*, **36**, 1101–1103.

20 Maleczka, R.E., Jr, Terrell, L.R., Geng, F. and Ward III, J.S., (2002) *Org. Lett.*, **4**, 2841–2844.

21 Hoye, T.R. and Zhao, H. (1999) *Org. Lett.*, **1**, 1123–1125.

22 Evano, G., Schaus, J.V. and Panek, J.S. (2004) *Org. Lett.*, **6**, 525–528.

23 Sello, J.K., Andreana, P.R., Lee, D. and Schreiber, S.L. (2003) *Org. Lett.*, **5**, 4125–4127.

24 Banwell, M.G. and McRae, K.J. (2000) *Org. Lett.*, **2**, 3583–3586.

25 For a review on the *E/Z* selectivity in M-RCM reactions, see: Prunet, J. (2003) *Angew. Chem.*, **115**, 2932–2936; *Angew. Chem. Int. Ed.*, **42**, 2826–2830; erratum, *Angew. Chem.* (2003), **115**, 3444; (2003) *Angew. Chem. Int. Ed.*, **42**, 3322.

26 Lee, C.W. and Grubbs, R.H. (2000) *Org. Lett.*, **2**, 2145–2147; erratum, *ibid.* 2000, **2**, 2558.

27 (a) For the first example of such a control in RCM, see: Bourgeois, D., Pancrazi, A., Ricard, L. and and Prunet, J. (2000) *Angew. Chem.*, **112**, 741–744; (2000) *Angew. Chem. Int. Ed.*, **39**, 725–728; (b) Bourgeois, D., Mahuteau, J., Pancrazi, A., Nolan, S.P. and Prunet, J. (2000) *Synthesis*, 869–882.

28 Fürstner, A., Radkowski, K., Wirtz, C., Goddard, R., Lehmann, C.W. and Mynott, R. (2002) *J. Am. Chem. Soc.*, **124**, 7061–7069.

29 Garcia-Fortanet, J., Murga, J., Falomir, E., Carda, M. and Marco, J.A. (2005) *J. Org. Chem.*, **70**, 9822–9827.

30 Arisawa, M., Kato, C., Kaneko, H., Nishida, A. and Nakagawa, M. (2000)

J. Chem. Soc., Perkin Trans. 1, 1873–1876.

31 Nakashima, K., Ito, R., Sono, M. and Tori, M. (2000) *Heterocycles*, **53**, 301–314.

32 Jasper, C., Wittenberg, R., Quitschalle, M., Jakupovic, J. and Kirschning, A. (2005) *Org. Lett.*, **7**, 479–482 erratum, *ibid.* 2005, **7**, 1885.

33 Nicolaou, K.C., He, Y., Vourloumis, D., Vallberg, H., Roschangar, F., Sarabia, F., Ninkovic, S., Yang, Z. and Trujillo, J.I. (1997) *J. Am. Chem. Soc.*, **119**, 7960–7973.

34 Meng, D., Su, D.-S., Balog, A., Bertinato, P., Sorensen, E.J., Danishefsky, S.J., Zheng, Y.-H., Chou, T.-C., He, L. and Horwitz, S.B. (1997) *J. Am. Chem. Soc.*, **119**, 2733–2734.

35 Nicolaou, K.C., Ninkovic, S., Sarabia, F., Vourloumis, D., He, Y., Vallberg, H., Finlay, M.R.V. and Yang, Z. (1997) *J. Am. Chem. Soc.*, **119**, 7974–7991.

36 Fürstner, A. and Seidel, G. (1998) *Angew. Chem.*, **110**, 1758–1760; *Angew. Chem. Int. Ed.*, **37**, 1734–1736.

37 (a) Other syntheses by Fürstner *et al.* using this strategy: prostaglandin E_2-1,15-lactone: Fürstner, A., Grela, K., Mathes, C. and Lehmann, C.W. (2000) *J. Am. Chem. Soc.*, **122**, 11799–11805; (b) sophorolipid lactone: Fürstner, A., Radkowski, K., Grabowski, J., Wirtz, C. and Mynott, R. (2000) *J. Org. Chem.*, **65**, 8758–8762; (c) ambrettolide and yuzu lactone: Fürstner, A., Guth, O., Rumbo, A. and Seidel, G. (1999) *J. Am. Chem. Soc.*, **121**, 11108–11113; (d) motuporamine C: Fürstner, A. and Rumbo, A. (2000) *J. Org. Chem.*, **65**, 2608–2611; (e) civetone: Fürstner, A. and Seidel, G. (2000) *J. Organomet. Chem.*, **606**, 75–78; (f) turrianes: Fürstner, A., Stelzer, F., Rumbo, A. and Krause, H. (2002) *Chem. Eur. J.*, **8**, 1856–1871.

38 Fürstner, A., Mathes, C. and Lehmann, C.W. (2001) *Chem. Eur. J.*, **7**, 5299–5317.

39 Fürstner, A. and Radkowski, K. (2002) *Chem. Commun.*, 2182–2183.

40 (a) Layton, M.E., Morales, C.A. and Shair, M.D. (2002) *J. Am. Chem. Soc.*, **124**, 773–775; (b) Morales, C.A., Layton, M.E. and Shair, M.D. (2004) *Proc. Natl. Acad. Sci. USA*, **101**, 12036–12041.

41 Smith, A.B., III, Adams, C.M., Kozmin, S.A. and Paone, D.V. (2001) *J. Am. Chem. Soc.*, **123**, 5925–5937.

42 Lazarova, T.I., Binet, S.M., Vo, N.H., Chen, J.S., Phan, L.T. and Or, Y.S. (2003) *Org. Lett.*, **5**, 443–445.

43 Vassilikogiannakis, G., Margaros, I. and Tofi, M. (2004) *Org. Lett.*, **6**, 205–208.

44 Lee, C.W., Choi, T.-L. and Grubbs, R.H. (2002) *J. Am. Chem. Soc.*, **124**, 3224–3225. See also Ref. 3, Vol. 2, p. 238 for a review on ring-expansion metathesis.

45 Louie, J., Bielawski, C.W. and Grubbs, R.H. (2001) *J. Am. Chem. Soc.*, **123**, 11312–11313.

46 (a) Beck, B., Larbig, G., Mejat, B., Magnin-Lachaux, M., Picard, A., Herdtweck, E. and Dömling, A. (2003) *Org. Lett.*, **5**, 1047–1050; (b) Dömling, A. (2006) *Chem. Rev.*, **106**, 17–89.

47 Van de Weghe, P. and Eustache, J. (2005) *Curr. Top. Med. Chem.*, **5**, 1495–1519. See also Ref. 3a, Vol. 2, p. 353 for epothilones and p. 54 for peptidomimetics.

48 Yet, L. (2003) *Chem. Rev.*, **103**, 4283–4306.

49 Wu, Y., Liao, X., Wang, R., Xie, X.-S. and De Brabander, J.K. (2002) *J. Am. Chem. Soc.*, **124**, 3245–3253.

50 Herb, C., Dettner, F. and Maier, M.E. (2005) *Eur. J. Org. Chem.*, 728–739.

51 Haack, T., Haack, K.L., Diederich, W.E., Blackman, B., Roy, S., Pusuluri, S. and Georg, G.I. (2005) *J. Org. Chem.*, **70**, 7592–7604.

52 Georg, G.I., Ahn, Y.M., Blackman, B., Farokhi, F., Flaherty, P.T., Mossman, C.J., Roy, S. and Yang, K.L. (2001) *Chem. Commun.*, 255–256.

53 Fürstner, A., Dierkes, T., Thiel, O.R. and Blanda, G. (2001) *Chem. Eur. J.*, **7**, 5286–5298.

54 Labrecque, D., Charron, S., Rej, R., Blais, C. and Lamothe, S. (2001) *Tetrahedron*

Lett., **42**, 2645–2648. The metathesis reaction is performed on the enantiomer of **83** in this case.

55 Smith, A.B., III and Zheng, J. (2002) *Tetrahedron*, **58**, 6455–6471.

56 Yadav, J.S. and Srihari, P. (2004) *Tetrahedron: Asymmetry*, **15**, 81–89.

57 Snider, B.B. and Song, F. (2001) *Org. Lett.*, **3**, 1817–1820.

58 Herb, C., Bayer, A. and Maier, M.E. (2004) *Chem. Eur. J.*, **10**, 5649–5660.

59 Feutrill, J.T., Holloway, G.A., Hilli, F., Hügel, H.M. and Rizzacasa, M.A. (2000) *Tetrahedron Lett.*, **41**, 8569–8572.

60 Wang, X., Bowman, E.J., Bowman, B.J. and Porco, J.A., Jr (2004) *Angew. Chem.*, **116**, 3685–3689; *Angew. Chem. Int. Ed.*, **43**, 3601–3605.

61 Garber, S.B., Kingsbury, J.S., Gray, B.L. and Hoveyda, A.H. (2000) *J. Am. Chem. Soc.*, **122**, 8168–8179; erratum, *ibid.* 2001, **123**, 3186.

62 (a) Hoye, T.R., Jeffrey, C.S., Tennakoon, M.A., Wang, J. and Zhao, H. (2004) *J. Am. Chem. Soc.*, **126**, 10210–10211; (b) for a review on relay RCM, see: Wallace, D.J. (2005) *Angew. Chem.*, **117**, 1946–1949; *Angew. Chem. Int. Ed.*, **44**, 1912–1915.

63 Garbaccio, R.M., Stachel, S.J., Baeschlin, D.K. and Danishefsky, S.J. (2001) *J. Am. Chem. Soc.*, **123**, 10903–10908.

64 Yamamoto, K., Garbaccio, R.M., Stachel, S.J., Solit, D.B., Chiosis, G., Rosen, N.

and Danishefsky, S.J. (2003) *Angew. Chem.*, **115**, 1318–1322; *Angew. Chem. Int. Ed.*, **42**, 1280–1284.

65 Yang, Z.-Q. and Danishefsky, S.J. (2003) *J. Am. Chem. Soc.*, **125**, 9602–9603.

66 Geng, X. and Danishefsky, S.J. (2004) *Org. Lett.*, **6**, 413–416.

67 Nicolaou, K.C., Montagnon, T., Vassilikogiannakis, G. and Mathison, C. J.N. (2005) *J. Am. Chem. Soc.*, **127**, 8872–8888.

68 For reviews on RCM in supramolecular chemistry, see Ref. 3a, Vol. 2, pp. 96 and 410.

69 Weck, M., Mohr, B., Sauvage, J.-P. and Grubbs, R.H. (1999) *J. Org. Chem.*, **64**, 5463–5471.

70 Dietrich-Buchecker, C., Rapenne, G. and Sauvage, J.-P. (1997) *Chem. Commun.*, 2053–2054.

71 Shima, T., Hampel, F. and Gladysz, J.A. (2004) *Angew. Chem.*, **116**, 5653–5656; *Angew. Chem. Int. Ed.*, **43**, 5537–5540.

72 Chase, P.A., Lutz, M., Spek, A.L., van Klink, G.P.M. and van Koten, G. (2006) *J. Mol. Catal. A*, **254**, 2–19.

73 Fuller, A.-M., Leigh, D.A., Lusby, P.J., Oswald, I.D.H., Parsons, S. and Walker, D.B. (2004) *Angew. Chem.*, **116**, 4004–4008; *Angew. Chem. Int. Ed.*, **43**, 3914–3918.

74 Lecourt, T., Mallet, J.-M. and Sinaÿ, P. (2003) *Eur. J. Org. Chem.*, 4553–4560.

3
Supramolecular Macrocycle Synthesis by H-bonding Assembly

Pablo Ballester and Javier de Mendoza

3.1
Introduction

A supramolecular macrocycle can be considered as a non-covalent cyclic oligomer formed by n monomers of the same or different chemical type. The formation of such architecture requires the establishment, of at least $n - 1$ intermolecular interactions and one intramolecular interaction. In fact, the intramolecular interaction appears as the necessary requisite to produce large, complex but discrete and defined oligomers in solution [1]. From this definition it can be inferred that the molecular components of supramolecular macrocycles have to be multitopic. For example, the self-assembly of a simple two-dimensional cyclic structure from a single component demands a difunctional monomer. Because of the non-covalent character of supramolecular assembly, the products are equilibrating structures. Therefore, the self-assembly of a cyclic oligomer will always be in competition with the self-assembly of linear oligomers and possibly other cyclic aggregates.

This chapter deals with formation of cyclic 2D and 3D structures in solution by self-assembly of two or more components using hydrogen bonds as the major interactions. Obviously, the formation of a defined supramolecular aggregate stabilized by non-covalent forces is a thermodynamically driven process which reflects a balance between enthalpy and entropy. Consequently, the product of a non-covalent macrocyclic synthesis must be evaluated and predicted in terms of thermodynamic minima in an equilibrium mixture.

In chloroform solution, the enthalpy of an isolated neutral hydrogen bond ranges from 1 to 7 kcal mol^{-1}. Because of the enthalpy-entropy compensation effect, the entropic cost for the formation of a bimolecular aggregate stabilized by hydrogen bonds could also be quite variable. In addition, use of multiple hydrogen bonds can yield a stronger interaction than that provided by the sum of individual donor-acceptor partners, because of secondary attractive interactions. Thus, the free enthalpy (ΔG) of binding of neutral hydrogen-bonded complexes can be estimated and used in a predictable manner for a number of systems [2]. In chloroform, for instance, and

based on the relative hydrogen-bonding affinities of imides and lactams, it is possible to assign a free enthalpy change of -1.5 to $-1.9\,\text{kcal mol}^{-1}$ for the establishment of a primary $N-H\cdots O=C$ hydrogen bond and a cost of 0.6–$0.7\,\text{kcal mol}^{-1}$ for each secondary repulsive interaction between spectator oxygen atoms [3]. However, a secondary interaction of attractive nature will contribute to the stability of the complex to a similar extent. This simple "back-of-the-envelope" approximation is not quantitatively perfect, but it does reflect some fundamental variations in systems stabilized by hydrogen-bonded arrays [4].

The theoretical treatment for the self-assembly of a molecular entity into rings or cages occurring under thermodynamic control is based on two fundamental physicochemical quantities: the effective molarity (EM) of the intramolecular interaction of the cyclic n-mer and the value of the stability constant of the intermolecular interaction (K_{inter}) [5]. The following formula has been derived by Ercolani and allows calculation of the minimum value of the product $K_{\text{inter}}EM$ to obtain a virtually complete self-assembled macrocycle at certain monomer concentration:

$$K_{\text{inter}}EM \geq \left(185\,\frac{N^2}{B}\right)^{1/(B-N+1)}$$

where N is the number of molecular units involved in the supramolecular structure of the macrocycle (minimum 2) and B the overall number of intermolecular bonds holding these units together. Thus, it turns out that for $N = 2$ and $B = 2$ the complete self-assembly requires a driving force $K_{\text{inter}}EM \geq 370$. The upper limit of the EM of a supramolecular macrocycle stabilized by intermolecular interactions has been estimated on the order of $10\,\text{M}$ [2]. Consequently, because of the low gain of free enthalpy obtained in the formation of a single intermolecular hydrogen bond (-1.5 kcal mol^{-1}, $K_{\text{inter}} = 12\,\text{M}^{-1}$), the efficient and complete self-assembly of a supramolecular macrocycle using neutral hydrogen bonds requires the use of subunits containing multiple hydrogen bonds. As the equation points out, an increase in the number of bonds (B) holding together the pieces of an assembly decreases the required driving force of the assembly. The increase of the K_{inter} favors the fulfillment of the above-mentioned relationship.

In 1992, Zimmerman and Duerr reported the use of the hydrogen bond-mediated cyclic aggregation strategy in the construction of cyclic trimer **1** from monomer **2** as opposed to dimer **3** or the open trimer **4** (Scheme 3.1) [6]. The cyclic structure of the aggregate and its corresponding trimerization constant ($K_{\text{trimer}} = 20000\,\text{M}^{-2}$) were estimated from the Saunders-Hyne analysis of the ^1H NMR dilution shifts of **1** in 10% $(\text{CD}_3)_2\text{SO/CDCl}_3$.

Model systems **5** and **6** did not self-associate or bind to one another to a significant extent in the same solvent mixture. Consequently, the authors assigned values of $K_7 < 3\,\text{M}^{-1}$ for the formation of the complex **7** and $K_{\text{dimer}} < 3\,\text{M}^{-1}$ for self-aggregation (Scheme 3.2).

The value of $K_7 \approx 3\,\text{M}^{-1}$ could be used as a reference for the equilibrium constant of the intermolecular interaction (K_{inter}) of the cyclic trimer **1**. Consequently, since $K_{\text{trimer}} = EM K_{\text{inter}}^3$, from $K_{\text{trimer}} = 20000\,\text{M}^{-2}$ an $EM \approx 740\,\text{M}$ can be calculated.
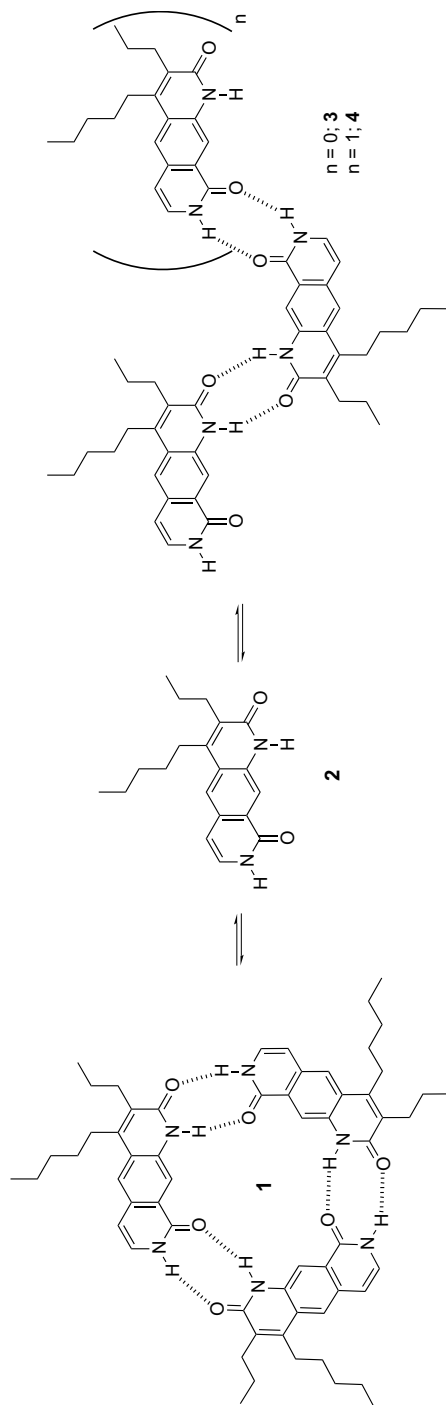
Scheme 3.1 Self-assembly of a cyclic trimer and open oligomers.
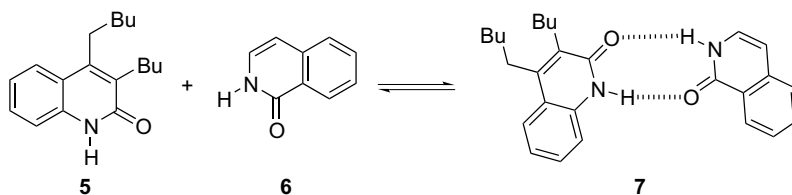
Scheme 3.2 Heterodimer formation.

According to the equation derived by Ercolani, this *EM* value is compatible with the complete assembly of the trimer ($K_{inter}EM = 3 \times 740 \geq 185 \times n = 185 \times 3$) at certain concentrations of the monomer. The calculated speciation profiles during the range of concentration of the dilution experiment are shown in Figure 3.1.

The binding model used for the simulation assumes the formation of trimer **1** and two other species: dimer **3** ($n = 0$) and an open trimer **4** ($n = 1$). The stability constants for these aggregates were estimated as $K_3 = K_7$ and $K_4 = K_7^2$. As shown in Figure 3.1, the molar fraction that could be reached for the macrocycle in the experimental range of monomer concentration is about 85%. A quantitative formation of the macrocycle (>98%) would require working at a monomer concentration close to 2 M. The take-home message is that even a supramolecular macrocyclic system having a high stability constant and fulfilling Ercolani's equation may require a high concentration of the monomer to be formed quantitatively. If we assume that the *EM* value has a limit close to a two-digit number, then the only practical way to reduce the monomer concentration and to achieve a quantitative cyclic assembly stabilized by hydrogen bonds is to increase the value of the intermolecular interaction (K_{inter}). For the case at hand, maintaining the same *EM* value and increasing the K_{inter} just one order of magnitude, i.e. from 3 M^{-1} to 30 M^{-1}, the quantitative formation of the cyclic trimer would require a monomer concentration of just 5×10^{-2} M, that is, 40-fold smaller than before.

The most intuitive way to increase the stability of an intermolecular interaction established through hydrogen bonds is to increase the number of hydrogen bonds formed or, alternatively, to work in less competitive solvents. The use of hydrogen bond-mediated cyclic aggregation for the effective synthesis of macrocycles requires
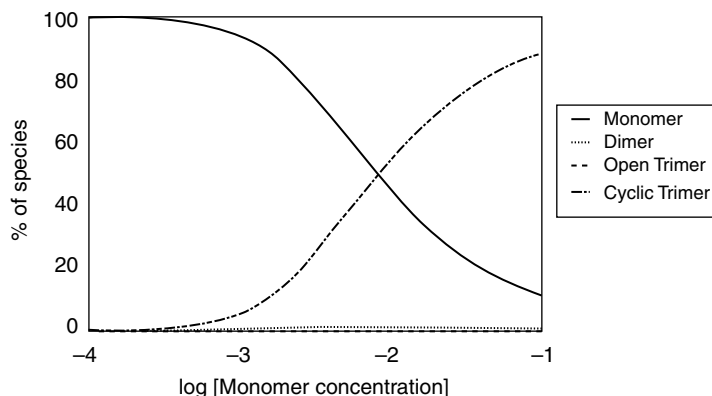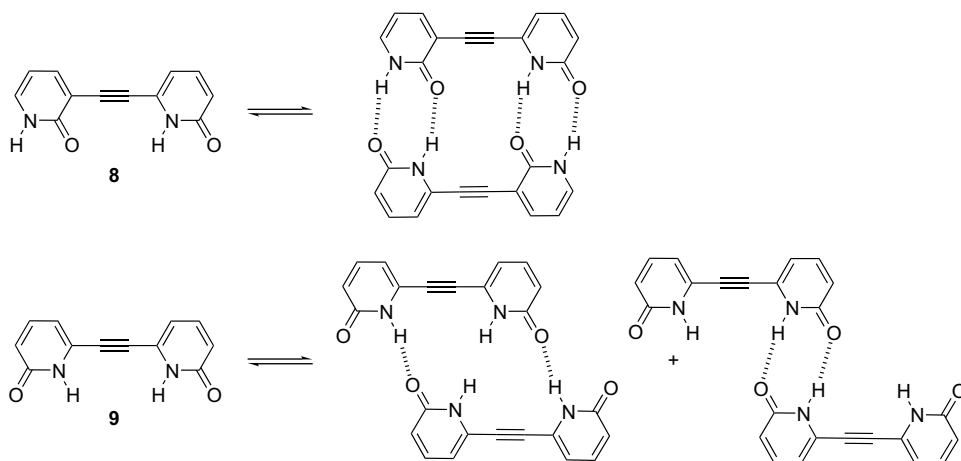

Figure 3.1 Calculated speciation profile during Zimmerman's dilution experiment [6].

Scheme 3.3 Self-assembly behavior of self-complementary (**8**) and non-self-complementary (**9**) dipyridone modules.

the formation of multiple arrays of intermolecular hydrogen bonds between its molecular components.

Four years before Zimmerman and Duerr's publication, Ducharme and Wuest [7] showed how the design of intermolecular hydrogen bonding arrays between ditopic monomers could be used to control molecular aggregation. The self-complementary asymmetric dipyridone **8** forms almost exclusively and quantitatively a dimer (Scheme 3.3) in chloroform at monomer concentrations as low as 3.6×10^{-4} M. The authors estimated that the stability constant for the dimer was higher than $5 \times 10^4 \, \mathrm{M}^{-1}$. They also calculated a $K_{\mathrm{dimer}} = 95 \, \mathrm{M}^{-1}$ for the dimerization of 2-pyridone under the same conditions. Taking this value as reference for the K_{inter} an $EM = 6.48 \, \mathrm{M}$ can be calculated for Wuest's system. The dimer is stabilized by the formation of two hydrogen bonds at each of the sticky ends.

Because of geometric constraints, the symmetric dipyridone isomer **9** is only capable of establishing two intermolecular hydrogen bonds when forming a cyclic or an open dimer. Assigning an $EM = 6.48 \, \mathrm{M}$ as calculated for **8** and a $K_{\mathrm{inter}} = 12 \, \mathrm{M}^{-1}$ (in chloroform $\Delta G° \approx -1.5 \, \mathrm{kcal/mol}$ for an NH$\cdots$O=C hydrogen bond), Ercolani's equation ($K_{\mathrm{inter}} EM = 77 < 370$) predicts the cyclic dimer not to be formed completely at any monomer concentration. From the calculated dimerization value for 2-pyridone ($K_{\mathrm{dimer}} = 95 \, \mathrm{M}^{-1}$) we estimate the stability constant for the open dimer as $K_{\mathrm{opendimer}}$ $4 \times 95 = 380 \, \mathrm{M}^{-1}$. The infrared spectrum of dipyridone **9** indicates only 20% of dimerization at a monomer concentration of $1.1 \times 10^{-3} \, \mathrm{M}$. This is a concentration value three times higher than that required for the quantitative formation of the cyclic dimer of **8**. In the solid state it was observed that **9** adopts a polymeric motif of the open dimer.

With the above simple examples we wish to emphasize that the synthetic use of hydrogen bonding assemblies in the effective formation of supramolecular macrocycles relies on high EM values and on the establishment of stable intermolecular arrays of hydrogen bonds capable of affording a high enthalpic gain to compensate for the entropic cost of the assembly.
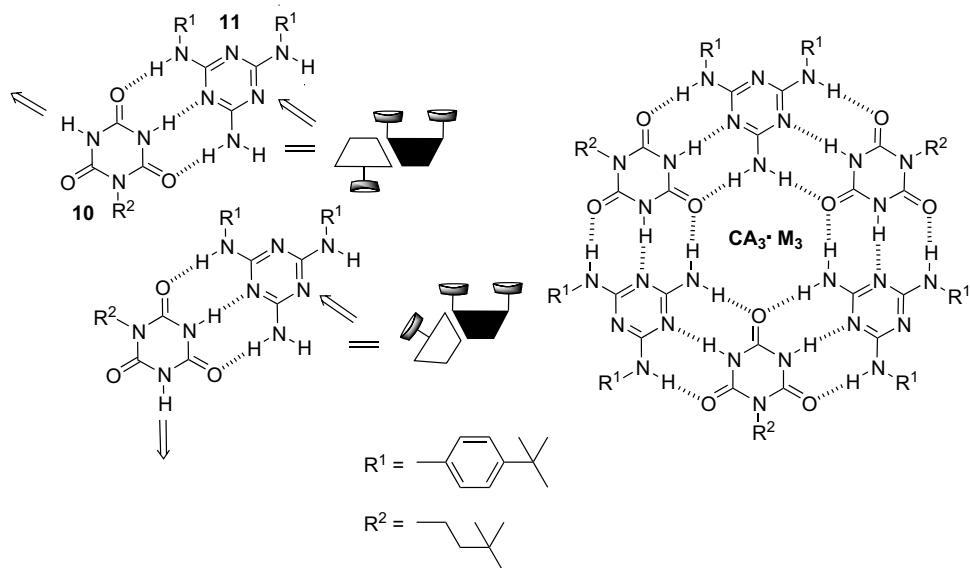
Scheme 3.4 Tape vs. hexagonal rosette formation in Whitesides' melamine-cyanurate aggregates [10].

3.2
Strategies to Build up Supramolecular Macrocycles Based on Hydrogen Bonds

The cyclic aggregate $CA_3 \cdot M_3$ "rosette" system introduced by Seto and Whitesides in 1993 elegantly illustrates most of the principles discussed in the Introduction (Scheme 3.4) [8]. This system utilizes the hydrogen-bonded pattern of the cyanuric acid CA (**10**) - melamine M (**11**) lattice [9,10]. The components of the CA-M dimer are two heterocyclic units acting as difunctional monomers ideally designed for the construction of linear and cyclic motifs. The maximum enthalpy for the formation of the cyclic aggregate in the simple $CA_3 \cdot M_3$ motif corresponds to 18 hydrogen bonds.

In chloroform, the authors estimated an enthalpic gain upon formation of such a hydrogen-bonded network of ca. $24 \, \text{kcal mol}^{-1}$ ($1.3 \, \text{kcal mol}^{-1}$ for each hydrogen bond).[1] However, formation of a cyclic aggregate by interaction of six molecules

---

[1] Our simple "back-of-the-envelope" approximation assigns a $K_{\text{inter}} = 100 \, \text{M}^{-1}$ (three primary interactions and four repulsive secondary interactions). Assuming an $EM = 10$, it turns out that $K_{\text{inter}} EM = 1000$. Ercolani's minimum value to obtain a virtually complete self-assembled macrocycle for such a system (considering each triply hydrogen-bonded interaction as one intermolecular interaction) turns out to be 1110. The similarity of these two values indicates that the complete self-assembly of the macrocycle requires high concentrations of the monomers and reflects a low thermodynamic stability. In fact, without preorganization via the hub and the spokes, CA and M derivatives associate in solution to form hydrogen-bonded oligomers that exchange rapidly at room temperature. Only at $-60\,^\circ\text{C}$ do the NH protons that are broad at room temperature become sharp and shift downfield, indicating the existence of a predominant geometry, probably the cyclic hexamer.

involves a high entropic loss. The translational and rotational entropic costs of bringing together two molecules to form a complex stabilized by two hydrogen bonds has been estimated to be about 3–4.5 kcal mol^{-1} in chloroform [11]. Therefore, the sum of all unfavorable entropy contributions (18–27 kcal mol^{-1}) [12] could hardly be balanced by the overall enthalpic gain (24 kcal mol^{-1}), and the rosette should not form, unless something is done to reduce the entropy penalty. Preorganization and peripheral crowding were employed by Whitesides and coworkers in their rosettes as successful strategies [9]. Preorganization lies at the foundation of molecular recognition [13], and the concept directly points to a reduction of the entropic cost by conformational control, usually introduced during the synthesis of the molecular components that self-assemble. This means that in a simple bimolecular aggregate some molecular components are introduced during the synthesis of the interacting partners that shape their conformations close to those found in the complex. For a rosette with multiple contacts, however, the concept must not only be applied to the conformational organization of the melamine subunits close to that achieved on complexation but also to reduction of the number of degrees of rotational and translational freedom that are lost upon aggregation. The covalent attachment of three components of the rosette (usually the melamines for synthetic reasons) to a common hub by appropriate connectors restricts the rotations into a conformation close to that observed in the $CA_3 \cdot M_3$ assembly. It also diminishes from 3 to 1 the number of melamine molecules that will lose translational and rotational entropy after self-assembly. The unfavorable conformational, translational, and rotational entropic penalties associated with the formation of the aggregate have been partially paid off by the new tripodal melamine component.

Although less effective, intermolecular steric hindrance between substituents is another approach to achieving selection of the cyclic $CA_3 \cdot M_3$ rosette in preference to competitive linear motifs in both the solid and solution states (Figure 3.2) [14]. Choosing the substituents on the melamine and cyanuric acid groups in such a
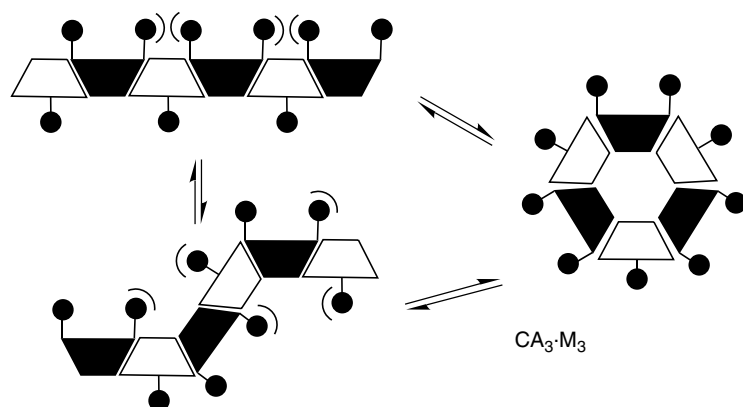

$CA_3 \cdot M_3$

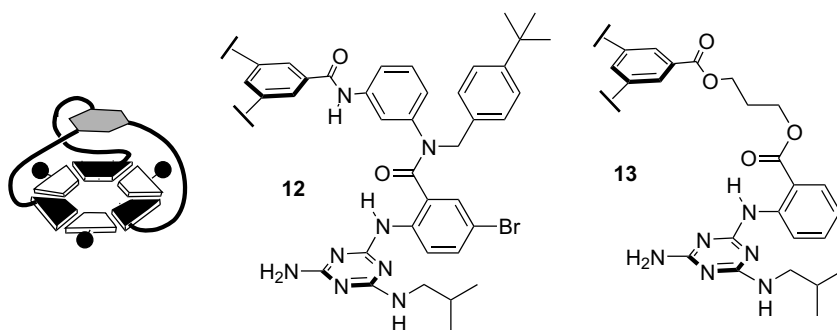**Figure 3.2** Peripheral crowding as a strategy to prevent linear aggregates.
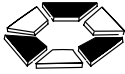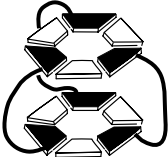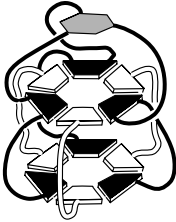
Figure 3.3 Schematic representation of tripodal melamines with linkers (**12** and **13**) to promote formation of rosettes [9].

way that non-cyclic structures become energetically less favored (for steric reasons) promotes formation of the cyclic assembly. This is another example of preorganization which relies on enthalpic rather than entropic control. Complexes with higher enthalpies having a similar entropic component will be formed to a lesser extent. Furthermore, the cyclic oligomer may also be favored relative to open oligomers because the interaction that closes the cycle is intramolecular and can benefit from the chelate effect (effective molarity).

In many cases, however, the preorganization of a receptor makes it difficult to separate the effects of entropy and enthalpy upon binding. Conformational preorganization of a receptor may induce repulsive enthalpic interactions between nearby functional groups or substituents (i.e. melamine residues of the tripodal construct). The elimination or reduction of this enthalpic destabilization in the free preorganized unit can be the main driving force for complex formation instead of simple preorganization. The observed difference in stability of the rosette complexes formed with tripodal melamine subunits having the rigid (**12**) or the more flexible (**13**) is consistent with the entropy gain due to restricted conformational flexibility of three single bonds (Figure 3.3).

Whitesides combined both strategies to create a wide range of self-assembled oligocyclic aggregates containing mono- and bis-rosette motifs. He undertook a complete, detailed and accurate experimental program to study and characterize the structures and to measure their relative stabilities [10]. A related thermodynamic analysis was carried out by Hunter and coworkers using the strict self-assembly of cyclic porphyrin oligomers [15]. One of the most important conclusions of these studies is that the $\Delta G°$ value is not an appropriate parameter to compare the relative stability of cyclic multiparticle aggregates containing different numbers of molecular components. This is because the effect of concentration (and, therefore, entropy) is not indicated in $\Delta G°$ (which assumes that aggregates and components are at 1 M). Let us compare the CA-M dimer to the cyclic hexameric aggregates with estimated $K_{CA-M} = K_{inter} = 10^2 \, M^{-1}$ and $K_{cyclic(CA-M)6} = (K_{inter})^6 \, EM = (10^2)^6 \times 10 = 10^{13} \, M^{-5}$ [2)]. Initially, it might be wrongly concluded that the hexamer is always more "stable", as it has the highest K value and, consequently, a more negative $\Delta G°$.

Table 3.1 Stability indices for hydrogen-bonded rosettes.

N^a	6	9	4	4
HB^b	18	36	18	36
$HB/(N-1)^c$	3.6	4.5	6	12
χ^{DMSOd}	0.04	0.23	0.4	0.7

[a]Number of molecules;
[b]Number of hydrogen bonds;
[c]This ratio reflects the competition contributions of enthalpy and entropy;
[d]Mole fraction of DMSO in chloroform where half of the aggregate has decomposed into components.

A simple speciation simulation, however, shows that at $[CA]_o = [M]_o = 1$ mM the rosette $CA_3 \cdot M_3$ is almost not formed at all (only around 1.5% of the components are self-assembled this way), whereas the dimer CA-M consumes more than 8% of the components. At this concentration ca. 90% of the components are free. A ten-fold increase in concentration, $[CA]_o = [M]_o = 10$ mM, highly favors the conversion of monomers to assemblies and changes the ratio of the formed aggregates. Up to 70% of monomers are now assembled as hexamers and only 6% as dimers.[3] The percentage of conversion of monomers to assemblies depends strongly on the number of monomers N and the concentration used for the self-assembly experiment. It is worthy of note that K_a or ΔG° do not correlate in a simple way to the conversion of the monomeric components into the full assembly. To overcome this limitation, Whitesides and coworkers introduced three indices to estimate the relative stability of hydrogen-bonded cyclic assemblies based on N (number of molecules) and HB (number of hydrogen bonds). Conceptually, the ratio $HB/(N$ 1) reflects the competition contributions of enthalpy (ΔH is proportional to HB) and entropy (ΔS is proportional to N). The authors observed that the stability measured experimentally from studies of de-aggregation in DMSO correlates with the value of the ratio $HB/(N-1)$. Table 3.1 shows the corresponding values for selected aggregates [9,10].

The most stable aggregate of Whitesides' rosettes family shown in Table 3.1 uses a combination of preorganization (sideways connection of the cyanurate subunits) and peripheral crowding of the melamine subunits for the preferential formation of

3) For $K_{CA-M} = 10^3$ M^{-1} and $K_{cyclic(CA-M)6} = 10^{13}$ M^{-5} at $[CA]_o = [M]_o = 10$ mM, 45% of monomers are assembled as dimers and only 32% as hexamers.
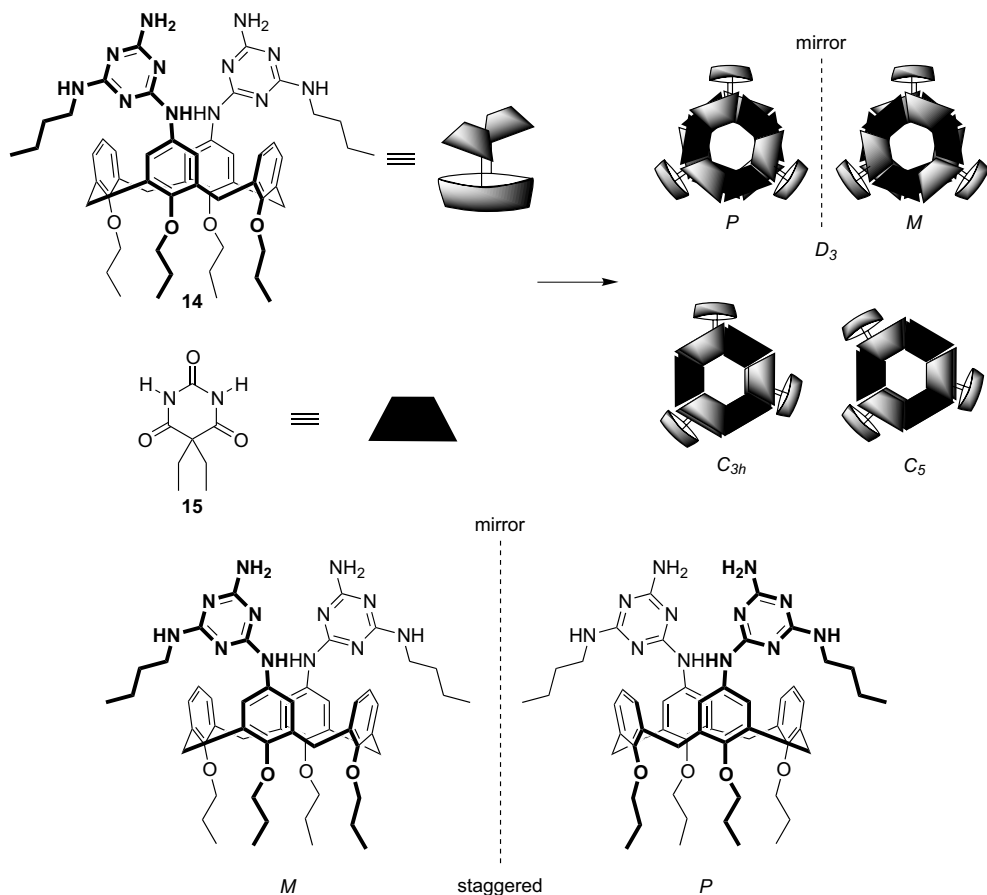
Figure 3.4 Origin of chirality in Reinhoudt's double rosettes.

the rosette. Reindhoudt and coworkers showed that pinched-cone calix[4]arenes serve as excellent linkers for double rosette assemblies ($HB/(N-1) = 4.5$) [16]. The diametrical substitution of a calix[4]arene with two melamine fragments at the upper rim (**14**) provides sufficient preorganization for the efficient self-assembly with two equivalents of cyanurate or barbiturate (**15**) into double rosettes with improved thermodynamic stability as compared to that of single rosettes (Figure 3.4).

These assemblies can exist in three different conformations with D_3, C_{3h}, or C_5 symmetries. In the D_3 conformation, the two melamine fragments of the calix[4] arene component adopt an antiparallel (staggered) orientation, which renders the assembly chiral. The chirality arises from the fact that the two melamines can adopt either a clockwise (*P*) or counter-clockwise (*M*) orientation (Figure 3.4).

Once formed, the double rosette is kinetically stable, and both enantiomers do not interconvert in organic solvents, as this would require an almost complete
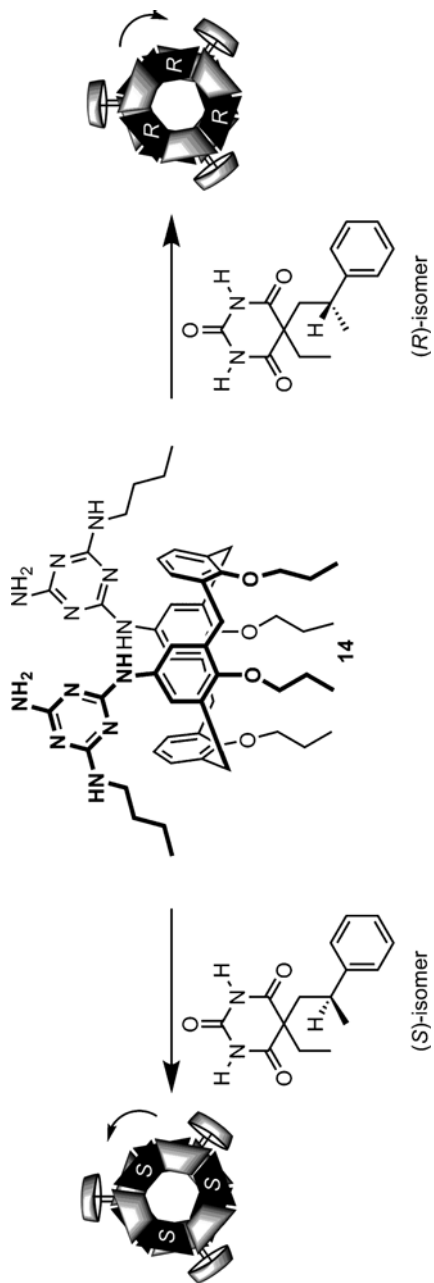
Scheme 3.5 Diastereoselective formation of double rosettes.
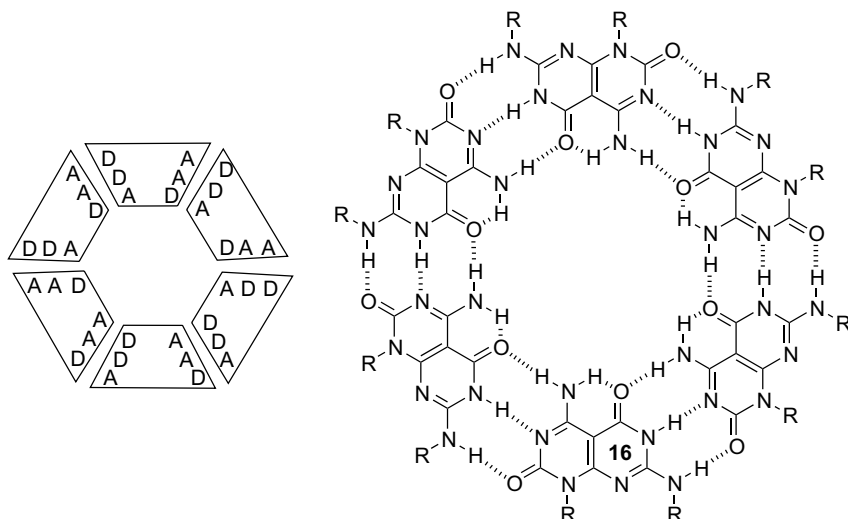
Figure 3.5 Proposed self-assembly of the self-complementary molecule **16** ($R = C_8H_{17}$) into a supramolecular macrocycle; schematic (left, A = acceptor, D = donor) and structural (right) representation.

dissociation of the aggregate, a too energetically costly process [17]. Introduction of one chiral component into the mixture, such as a chiral barbiturate or a chiral melamine, results in the remarkable formation of a preferred diastereoisomer in high stereoselectivity (Scheme 3.5) [18]. Moreover, once chirality has been induced via an enantiomerically pure barbiturate, the chiral component can be replaced in the rosette by an achiral cyanurate without destroying the *P* or *M* self-assembly (chiral memory concept) [17,19].

Unlike Whitesides' rosettes, based on "symmetric" ADA-DAD (A = acceptor, D donor) triple hydrogen-bonding motifs, introduction of DAA and ADD edges within a 60° angle in a planar molecule would also result in hexameric macrocycles, without competition with linear aggregates (Figure 3.5). Such "Janus type" molecules (**16**), hydrogen-bond-programmed to self-assemble into cyclic arrays, were first reported by Lehn and coworkers in 1994 [20]. Aggregation was studied by NMR spectroscopy, and vapor pressure osmometry (VPO) and gel permeation chromatography (GPC) measurements reasonably agreed with the formation of hexameric rosettes.

Similar molecules (**17**) were described by Mascal as G-C DNA base hybrids [21]. In this case, the hexameric macrocycle was beautifully evidenced in the solid state by an X-ray structure (Figure 3.6).

The limited solubility in organic solvents of most monomers endowed with hydrogen-bonding edges often prevents the achievement of the high concentrations (high *EM* values) required for complete cyclization. Therefore, efforts have concentrated on enhancing the intermolecular contacts to raise the enthalpy gain of the interaction. The two strategies most frequently applied are: (a) to add new contacts at

17
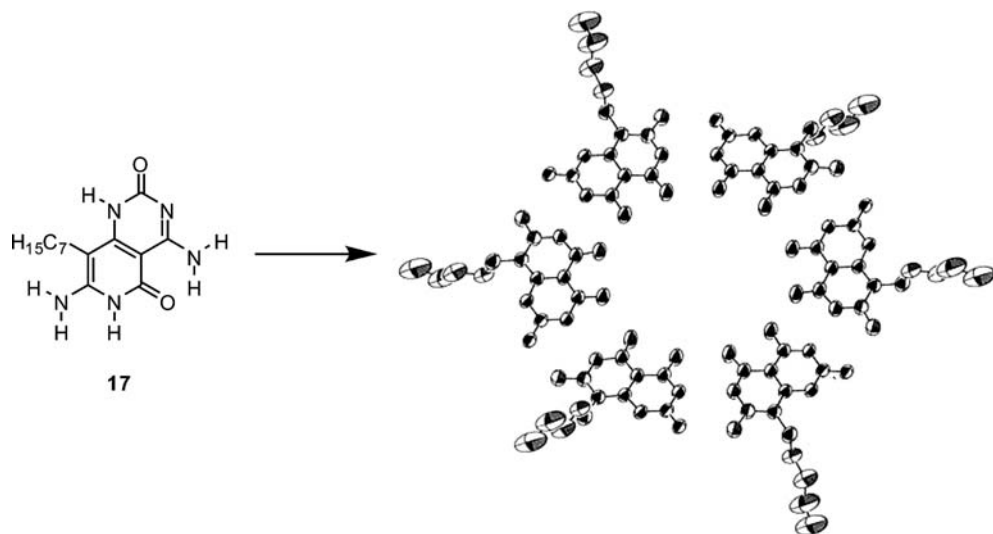
Figure 3.6 Mascal's G-C DNA base hybrids in the solid state. Reproduced with permission of Ref. [21b].

18 R =
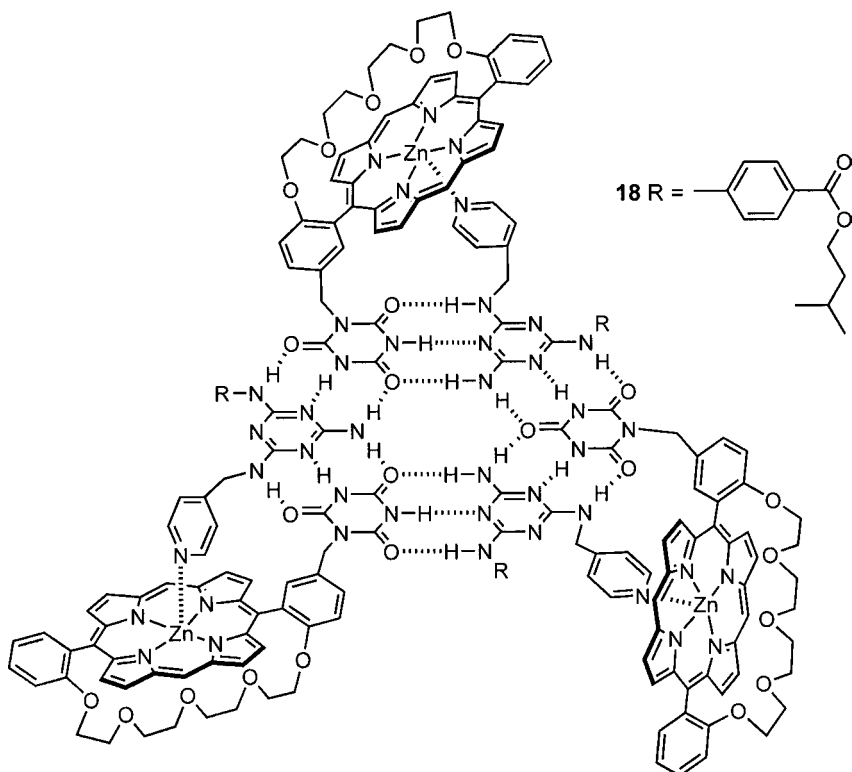
Figure 3.7 A rosette with peripheral stabilization by metal coordination [22].
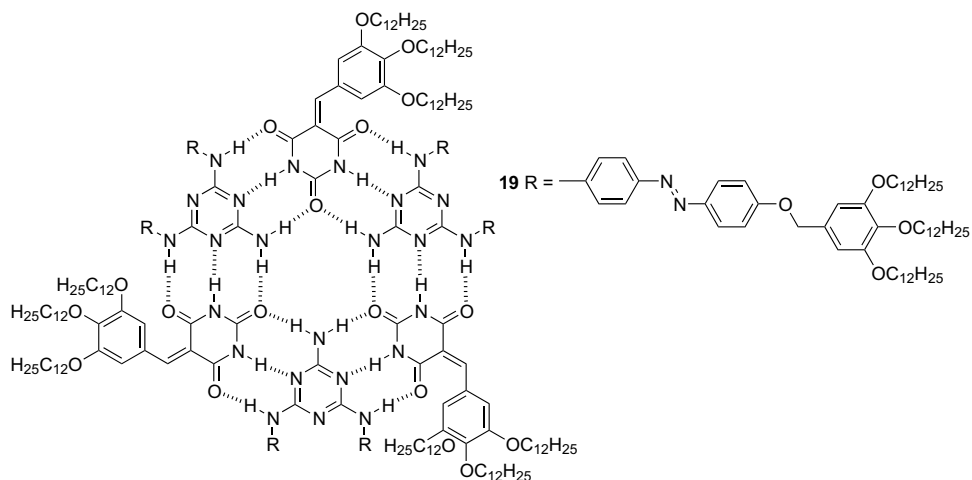
Figure 3.8 Photoswitchable peripheral crowding of a hexagonal rosette [23].

the periphery of the rosette, such as metal coordination, aromatic stacking, or ion pairing, in addition to peripheral crowding, and (b) to introduce more and/or more robust hydrogen bonding scaffolds.

Li's porphyrin rosettes (**18**) [22], Yagai's photoswitchable rosettes (**19**) [23], and Fenniri's nanotubes (**20**) [24] nicely illustrate the former approach. Thus, $CA_3 \cdot M_3$ rosettes (Figure 3.7) endowed with a pyridine moiety at the melamine component and a strapped Zn-porphyrin (to enhance coordination from only one side of the ring) at the cyanuric acid component are more stable than the $CA_3 \cdot M_3$ model rosette initially reported by Whitesides. Even more complex versions of the same concept, involving one *all*-pyridine rosette and one *all*-porphyrin rosette to self-assemble into double rosettes were studied, although only NMR evidence was presented [22].

Yagai *et al.* have recently reported rosette **19** with an azobenzene-appended mela-mine and barbiturate, both possessing bulky tridodecyloxyphenyl (TDP) wedges for peripheral crowding, which is quite stable in chloroform or toluene, as established by GPC, dynamic light scattering, and NMR and UV spectroscopy [23]. It is likely UV-vis that the multiple aromatic face-to-face stacking interactions contribute to the overall stability. The geometrical *EE*-isomer (bearing two *E*-azobenzene moieties) was unusually stable to *E-Z* photoisomerization because of the steric crowding of the TDP wedges, whereas UV-irradiation of the monomeric melamine resulted in the *ZZ* isomer as expected. However, this isomer was unable to form a rosette because of the intermolecular steric hindrance between the folded TDP wedges. This is a remarkable example of photo-regulated self-assembly (Figure 3.8).

Another interesting example of peripheral stabilization was provided by Fenniri [24]. Compound **20** is a DDA-AAD monomer, similar to those described by Lehn or Mascal, with a pending free amino acid that establishes further contacts via ion-pairing and hydrogen bonding to stabilize the rosette and to hierarchically favor
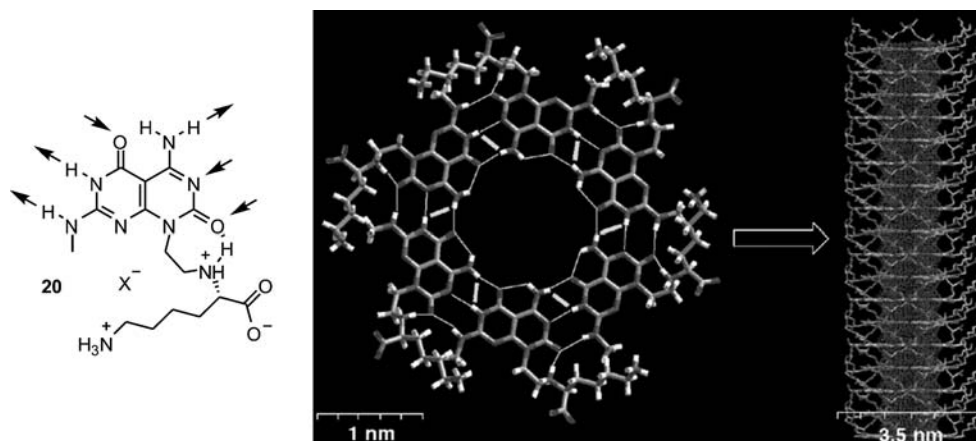
Figure 3.9 Hierarchical self-assembly of rosette nanotubes from module **20**. Reproduced with permission of Ref. [24].

stacking of the resulting hollow hexameric disks into nanotubular structures of ca. 4.0 nm outer diameter, that were studied by circular dichroism (CD) and transmission electron microscopy (TEM) (Figure 3.9).

Another general strategy to increase the enthalpy of the intermolecular interactions is based upon the use of strong DDAA-AADD quadruple hydrogen bond motifs, such as those of 2-ureido-4-pyrimidinones (UPys), reported by Meijer and coworkers (Scheme 3.6) [28,29]. UPy dimers (**21**) are formed in chloroform with exceedingly high binding constants ($K_{dim} > 10^7 M^{-1}$), a fact that could be explained by the favorable secondary interactions between the DD-AA pairs [4,27]. Among the possible tautomeric forms that UPy can display, the pyridine-4-ol tautomer also forms strong DADA-ADAD dimers (**22**). Although these tautomers do not display favorable secondary interactions, their strongly acidic OH contributes to enhance the binding. UPy dimers have been used mainly to form interesting solvent-sensitive polymers [28], but also to prepare fullerene dimers [29], dendrimers [30], or polymers [31].
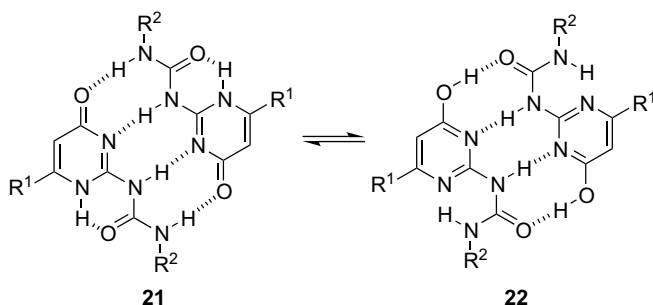
Scheme 3.6 Tautomeric equilibria between DDAA-AADD (**21**) and DADA-ADAD (**22**) UPy dimers.
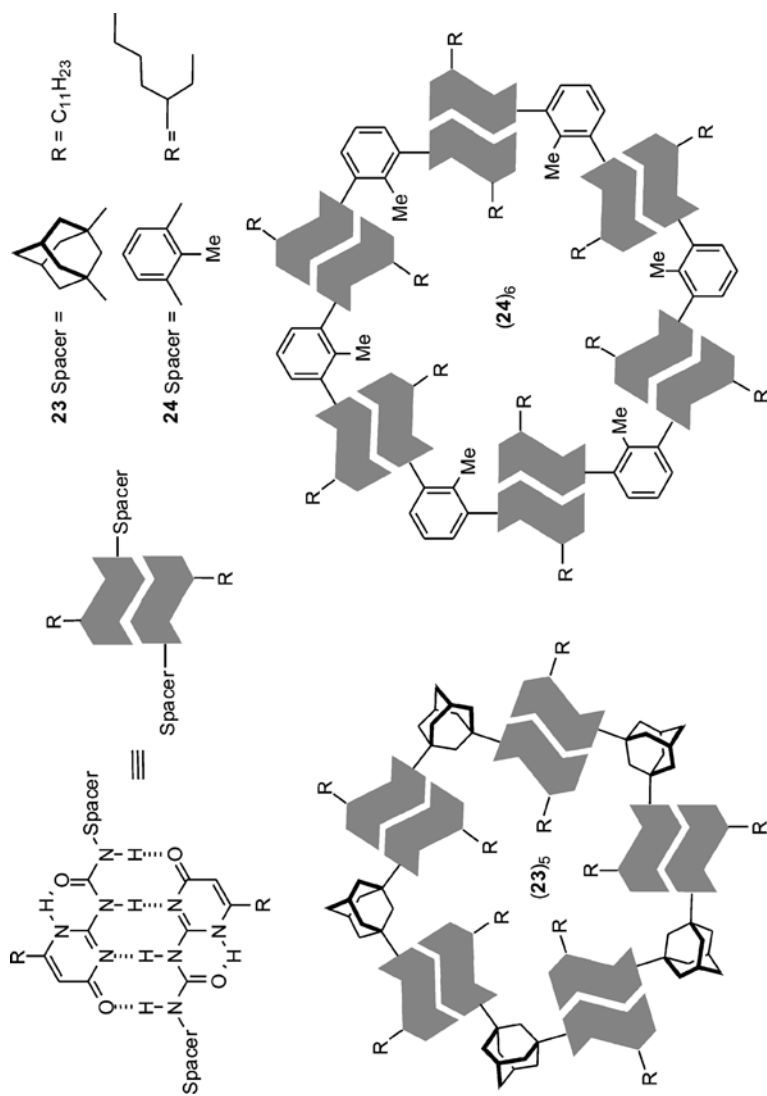
Figure 3.10 Structure of 1,3-adamantane and 2-methyl-1,3-phenylene bis-UPy compounds **23** and **24** and schematic representation of the pentameric (**23**)$_5$ and hexameric (**24**)$_6$ assemblies [33].

It is therefore not surprising that bis-UPy scaffolds have been employed to form not only polymeric materials but also extremely stable cyclic dimers [32] and macrocycles. The flexibility and shape of the linker between the two UPy subunits is a key in determining the size of the resulting dominant cyclic aggregate [33]. For example, the use of a 1,3-adamantyl spacer promotes formation of pentagonal rosettes $(23)_5$, whereas 1,3-phenylene gives rise to hexagonal rosettes $(24)_6$ (Figure 3.10).

Compounds **23** and **24** are soluble in chloroform, dichloromethane, benzene, or toluene, but almost insoluble in methanol at 30 °C. Remarkably, the viscosity of their highly concentrated (>50 mM) solutions in chloroform did not differ markedly from that of chloroform itself. Solutions of comparable concentration containing two UPy's linked through flexible alkyl spacers are, however, very viscous, showing that in chloroform the architecture of **23** and **24** is indeed quite different from a random coil polymer [28]. The aggregates were studied by a number of complementary techniques, such as VPO, GPC, and electrospray ionization mass spectrometry (ESI-MS). A high-intensity signal corresponding to the hexamer was observed in the ESI-MS spectrum of **24** [in THF/HCOOH (1/0.05 v/v)], showing that it forms macrocycles even in the presence of HCOOH. Signals for pentamers, tetramers, and other aggregates, were also present in the spectrum. For **23**, the values obtained by VPO and GPC at high concentrations (>40 mM) fully agree with those calculated for the proposed pentameric structure.

Diffusion-ordered ^{1}H NMR spectroscopy (DOSY) experiments were performed on solutions of **24** in CDCl$_3$ at different concentrations. Two concentration regimes were distinguished, suggesting that, above 10 mM, hexamers of **24** aggregate into higher-molecular-weight structures. The overall shapes of the cyclic aggregates are hard to estimate accurately, as the inner R groups are much too large to be accommodated inside flat rosettes. Furthermore, the need to avoid eclipsed conformations around the adamantane linker in **23**, as well as the presence of an inner methyl group in **24**, clearly point to non-planar, tubular, or bowl-shaped conformations, respectively (Figure 3.11).

$(23)_5$ $(24)_6$
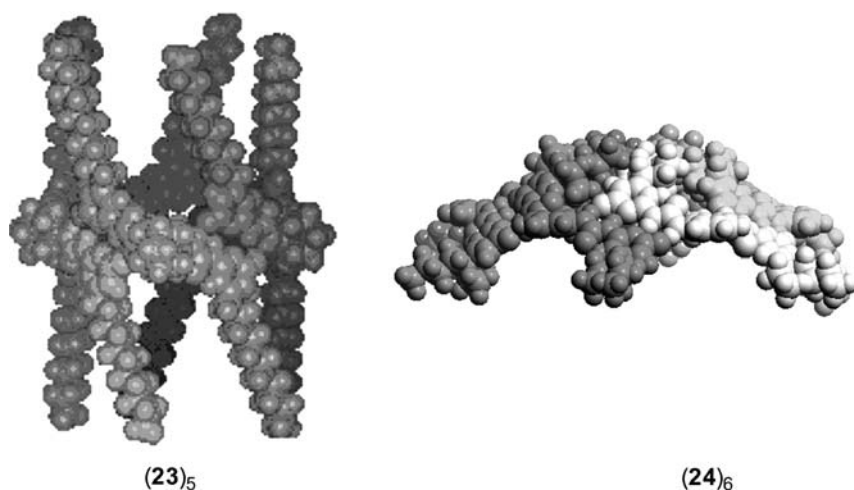
Figure 3.11 Front view representations of energy-minimized pentameric $(23)_5$ and hexameric $(24)_6$ assemblies.
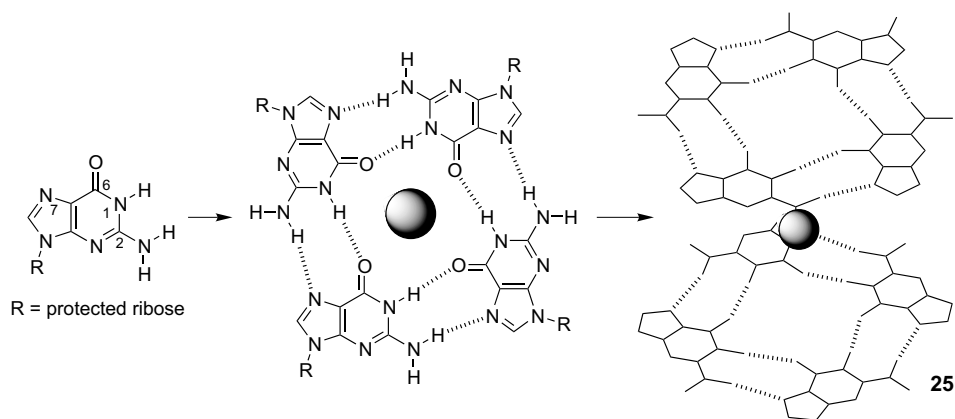
Figure 3.12 Hierarchical organization in the templated self-assembly of the G-quartets.

Macrocycles built from hydrogen bonds are not exclusive to synthetic systems. Nature offers a number of interesting examples. For instance, the G-quartet, a hydrogen-bonded macrocycle formed by cation-templated assembly of guanosine, first identified in 1962 by Gellert *et al.* [34], is not only a biologically relevant DNA motif, but also a perfect example of Nature's way to achieve rosettes. In the G-quartet, just two AD-DA hydrogen-bonded pairs are employed, linking the Hoogsteen and the Watson-Crick edges of guanine. The remaining carbonyl acceptor of the Watson-Crick edge is not involved in hydrogen bonding, such as in the typical G-C base pairs, but coordinates to a central metal instead, favoring cyclization and stacking of the quartets into higher-order aggregates (octamers or more complex quadruplexes) (**25**, Figure 3.12) [35].
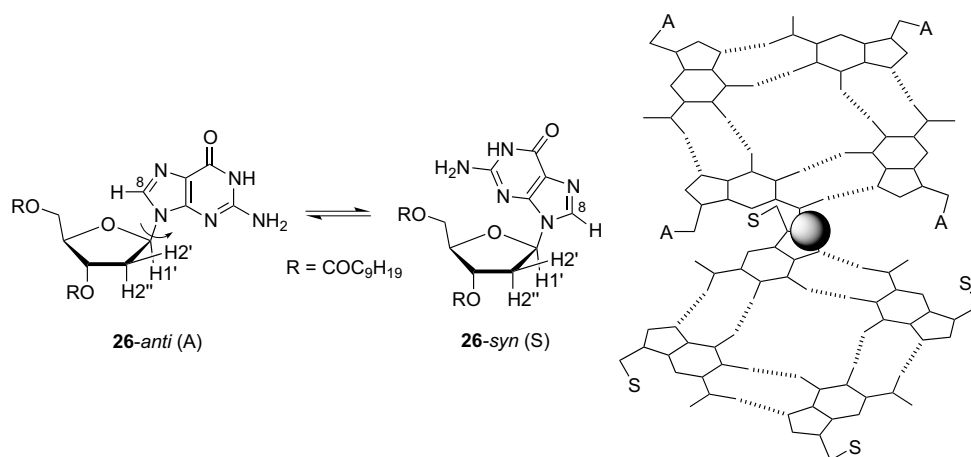
Figure 3.13 Self-sorting of *syn-anti* conformations about the glycosidic bonds in Gottarelli's octamer.
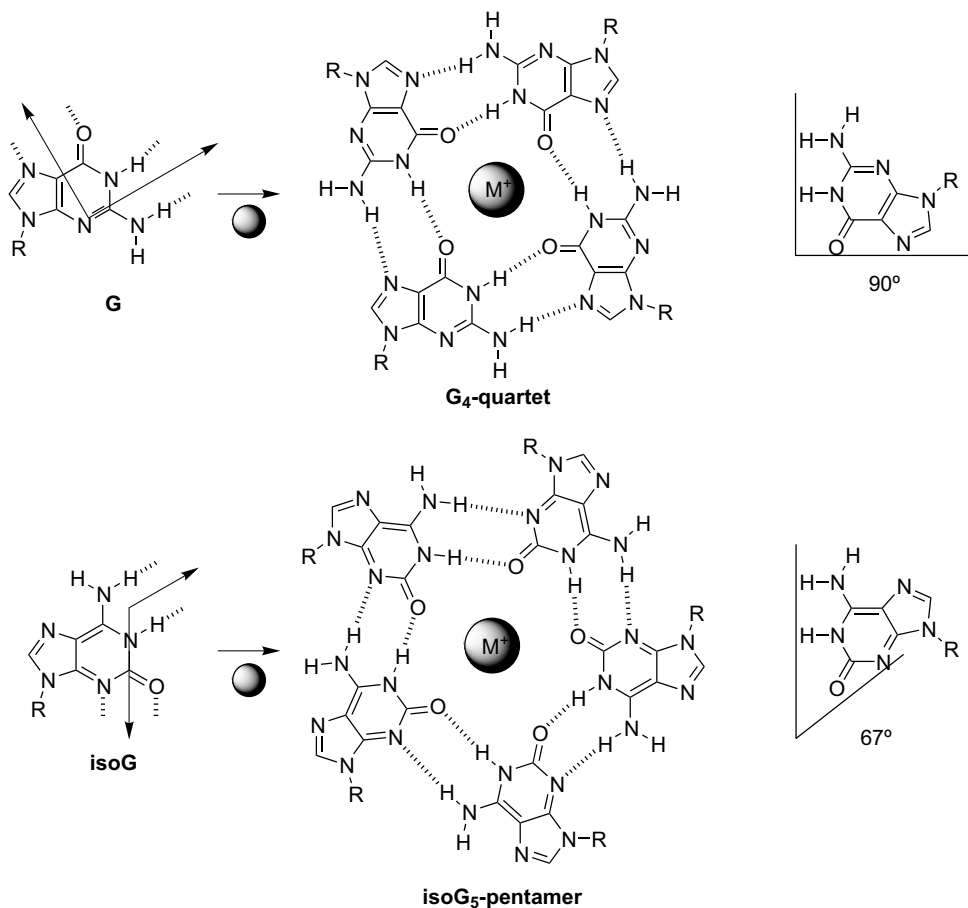
Figure 3.14 Relative orientation of hydrogen-bonding edges (van der Waals angle) to give G_4-quartets and isoG$_5$-pentamers.

Stacking of quartets, like in DNA double helices, prevents water from competing with the hydrogen bonding network, and is thus essential in order to allow self-assembly in water. Unlike G-quartets, most of the synthetic rosettes inspired by this natural scaffold are lipophilic and were designed to form macrocycles in organic solvents. In 1995, Gottarelli *et al.* reported the self-assembly of 3′,5′-didecanoyl-2′-dG (**26**) in chloroform [36]. Depending on conditions, **26** can extract K^+ picrate from water into chloroform to give either a discrete octamer, $(26)_8 \cdot K^+$, or a polymer, $[(26)_4]_n \cdot (K^+)_m$. Only one stereoisomer was detected by NMR. In one G-quartet, all dG units have a *syn-* conformation about the glycosidic bond, while the other tetramer is in an "all-anti" conformation (Figure 3.13) [37].

Most remarkably, whereas metal-templated guanine self-assembly favors tetramers (G-quartets), iso-guanine tends to form cyclic pentameric arrays in the presence of a suitable metal, such as Cs^+ [38]. The angle between the two
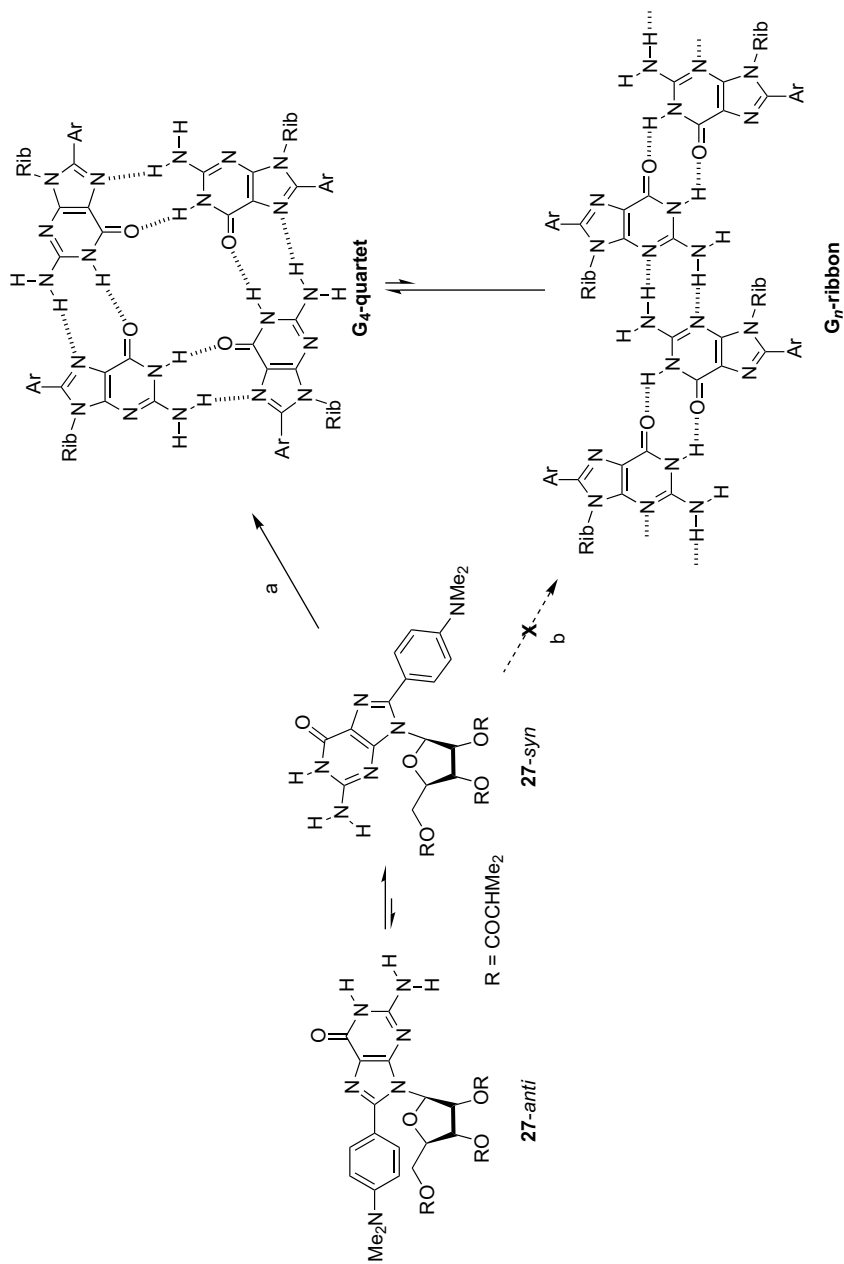
Scheme 3.7 Conformational constraints in **27** promote formation of quartets without metal templating.

hydrogen-bonding edges is 90° for guanine and 67° for iso-guanine (Figure 3.14). This has also been observed even with iso-G enriched strands of DNA [39].

A general rule for self-assembly into G-quartets is the presence of a templating metal to stabilize the resulting macrocycle. However, an "empty" G-quartet can be obtained by careful design promoting preorganization (i.e. conformational control) and preventing aggregation into ribbon-like, undesired aggregates. Sessler *et al.* have reported that guanine derivative **27** forms stable cyclic quartets both in the solid state and in solution in the absence of any stabilizing cation (Scheme 3.7, path a) [40]. Ribbon structures usually arise from participation of the nitrogen at position 3 as hydrogen acceptor (Scheme 3.7, path b). This is not possible in **27** because of the steric hindrance caused by the sugar moiety, whereas the bulky aryl substituent at position 2 forces a *syn* conformation about the glycosidic bond, locking the structure into the correct conformation for cycle formation.

An important difference between macrocyclic structures based on covalent bonding and those based on hydrogen bonds is that the latter are highly stable thermodynamically but by no means as kinetically inert as their covalent counterparts. Consequently, it has been possible to study the exchange process between molecular components of distinct cyclic aggregates. Dissociation rates of hydrogen-bonded aggregates that are not affected by mechanical constraints (steric imprisonment) are solely dependent on the number of hydrogen bonds that are broken in the dissociation process. For example, the stability constant of a dimeric assembly stabilized by two hydrogen bonds in a DA-AD array can be estimated to be around $30\,M^{-1}$. Assuming that the second-order complexation rate is close to diffusion control, that is, $k_{on} = 1 \times 10^8\,s^{-1}\,M^{-1}$ for an association constant $K_a = k_{on}/k_{off} = 30\,M^{-1}$, the first order decomplexation rate constant could be estimated as $k_{off} = 3.3 \times 10^6\,s^{-1}$. This value implies that dissociation is too fast for the ^1H NMR timescale. For association constants around $10^6\,M^{-1}$ or higher the dissociation rate becomes either on the ^1H NMR timescale or even slower ($k_{off} < 100\,s^{-1}$). Rate constants close to $20\,s^{-1}$ ($\Delta G^{\neq} = 15.7\,kcal\,mol^{-1}$) have been calculated in $CDCl_3$ at 20 °C for the dissociation of the barbituric units from assemblies of the type $\mathbf{14_3 \cdot 15_3}$ (Figure 3.4) [16]. This exchange process corresponds to the cleavage of six hydrogen bonds in the multimolecular assembly $\mathbf{14_3 \cdot 15_3}$, and, as mentioned previously, it takes place without complete disruption of the aggregate.

The exchange rates of the components of cyclic and acyclic hydrogen-bonded complexes are highly sensitive to the polarity and hydrogen-bonding capabilities of the solvent. The exchange of dimelamine units (cleavage of 12 hydrogen bonds) corresponding to two different homomeric assemblies of the type $\mathbf{14_3 \cdot 15_3}$, detected by the formation of heteromeric assemblies, occurs within seconds in $CDCl_3$, even at −50 °C, while it takes hours at 25 °C to reach the thermodynamic equilibrium in toluene. Likewise, a rate constant of $7 \times 10^{-5}\,s^{-1}$ has been reported for the dissociation of the dimelamine fragment **14** in the assembly formed with *n*-butyl cyanuric acid at 70 °C in benzene-d_6 [17].

Increasing the number of hydrogen bonds and reducing the number of components is a strategy to construct robust self-assembled macrocycles, both

thermodynamically and kinetically. The data discussed previously shows how dissociation rates of components pertaining to assemblies held together by multiple hydrogen bonds decrease as the number of hydrogen bonds and the strength of the interaction increases [41]. Thus, one may expect that such hydrogen bond-induced self-assembly processes become kinetically controlled. This is a well-known phenomenon for covalent synthesis and even for self-assembly processes induced by metal-ligand coordination [42]. One leading example is provided by Reinhoudt's double rosettes, where components can be exchanged in a controllable way once the rosette has been formed [16].

3.3
Strategies to Build up Supramolecular Cavities and Capsules Based on Hydrogen Bonds

Molecular cavities have been intensively studied over the last decades by supramolecular chemists, since they can be used for molecular recognition, catalysis, or transport processes across membranes. Bowl-shaped molecules such as calixarenes (**28**), resorcinarenes (**29**), or cyclotriveratrylene (CTV, **30**) derivatives constitute useful building blocks for cavities since their shapes and sizes can be controlled by covalent synthesis to a remarkable degree (Figure 3.15). The inherent flexibility of calixarenes and resorcinarenes can be limited either by substitution or by bridging, respectively.

Bridged resorcinarenes are known as cavitands (such as **31** or **32**). However, cavitand **32** is not yet fully preorganized as it can give two main conformers, namely a cylindrical vessel or the open kite (Figure 3.16).

The vase conformation can be stabilized by a seam of eight intramolecular amide hydrogen bonds forming a macrocyclic ring (compound **33**) that surrounds the open
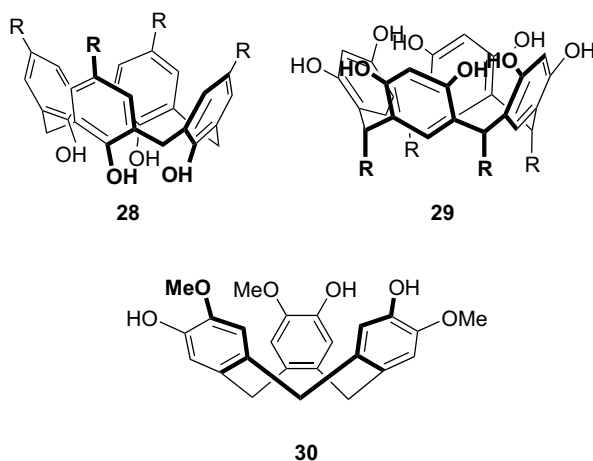
Figure 3.15 Representative examples of bowl-shaped cyclic oligomers of phenols.

31

Vase (C_{4v}) Kite (C_{2v})

32 R = $C_{11}H_{23}$; X = NO_2
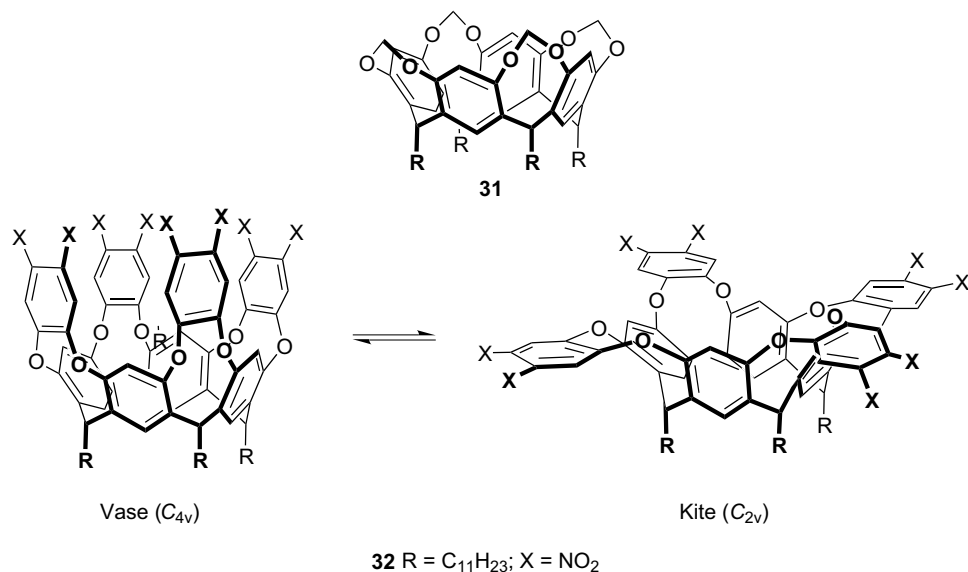
Figure 3.16 Cavitands as examples of preorganized macrocycles (a substantial conformational flexibility remains in **32**).

portal [43]. The head-to-tail cyclic array of hydrogen-bonded amides results in two cyclo-enantiomers, with clockwise and counterclockwise orientation (Figure 3.17). Because of the cyclo-enantiomerism, the C(O)CH$_2$ protons of **33** become diastereotopic. Thus, the ^{1}H NMR spectrum in various non-polar solvents shows two N-H resonances shifted far downfield. The chemical shifts of these signals are concentration independent, but their temperature coefficients ($\Delta\delta/\Delta T$) confirm that one of the hydrogen bonds in **33** is less sensitive to temperature and is shielded from external solvent, while the other is somewhat more exposed. The two N-H signals coalesce in toluene-d_8 at $T_c \approx 87\,^\circ$C.

Most often, the hydrogen-bonding edges of concave surfaces have been used for self-assembly into hollow capsules. Pioneering work was related to the use of the curvature of glycoluril to build up cavities endowed with hydrogen bonding edges at the concave and convex inner sides, and outer ends that are complementary and promote formation of pseudo-spherical cavities such as **34** (tennis ball) or **35** (soft ball) (Figure 3.18) when in the presence of suitable guests [44].

The subject has been extensively studied by Rebek and coworkers, who have written a substantial number of reviews covering different aspects of the topic [45]. Because of this, we do not intend to describe here in detail the different systems that have been developed, but focus instead on some of the dynamic aspects. Possible applications of these systems include molecular containers, enantioselective receptors, catalysts, drug-delivery devices, separation tools or simply unusual
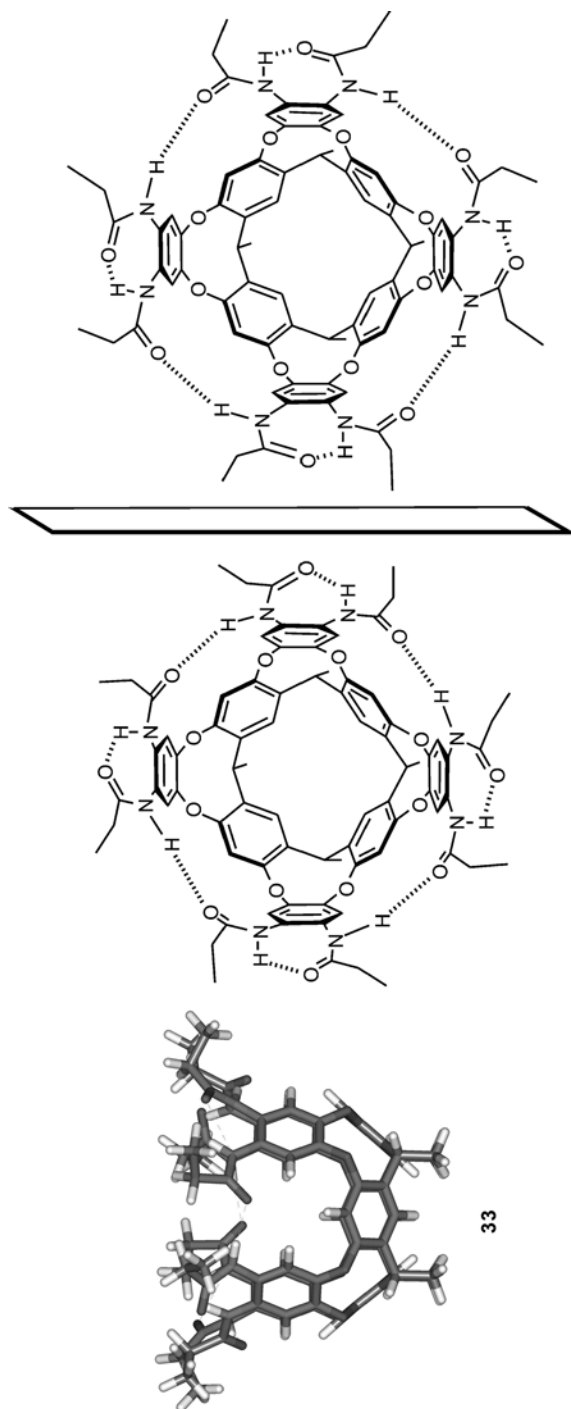
Figure 3.17 Cyclic array of hydrogen-bonded amides resulting in cyclo-enantiomerism.
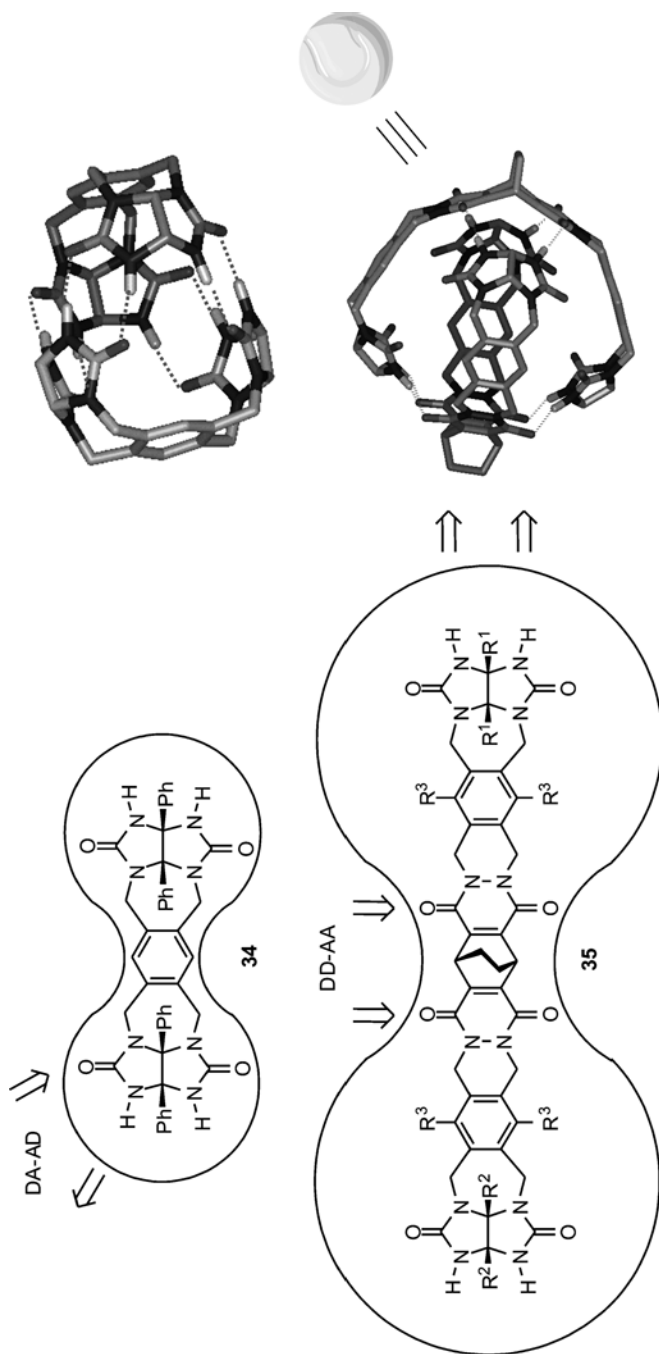
Figure 3.18 Glycoluril receptors **34** and **35** ($R^1 = R^2 = CO_2$-*i*-pentyl, $R^3 = H$) self-assemble into tennis-ball and soft-ball dimers, respectively.
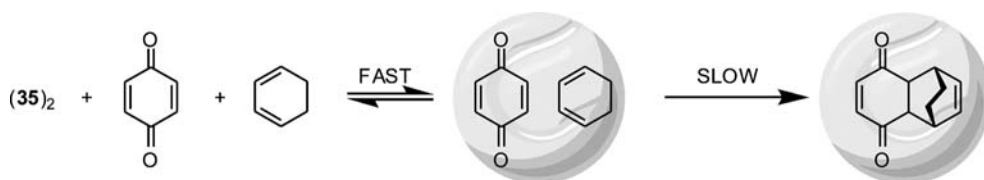
Scheme 3.8 A Diels-Alder reaction is accelerated in a tennis-ball like hydrogen bonded capsule (**35**)$_2$ (R^1 = R^2 = 4-*n*-heptylphenyl, R^3 = OH). True catalysis is prevented by product inhibition.

closed spaces where the encapsulated guests can display emerging properties or unexpected behavior.

In contrast to capsules based on covalent bonds (such as Cram's carcerands) [46], whose portals are usually too small to allow fast exchange of guests, hydrogen bonded self-assembly is beneficial for encapsulation, as it is reversible. For large capsules or multicomponent assemblies (see below), the guests can access the cavities by partial disruption of the hydrogen bonding array (opening of host's "flaps") or by separation of one of the components. Smaller dimeric capsules in general, however, require full dissociation of the two components. The process is relatively slow, on the order of seconds, although in extreme cases it can take from milliseconds to hours.

Despite some early successful reports, there are concerns about the practical use of self-assembled vessels for catalysis by encapsulation, especially for reactions that are inherently faster than the opening-closing events. For instance, a Diels-Alder reaction can be accelerated in the presence of the "soft-ball" capsule **35** (Scheme 3.8), although product inhibition forces the use of large amounts of capsule in the reaction mixture [47].
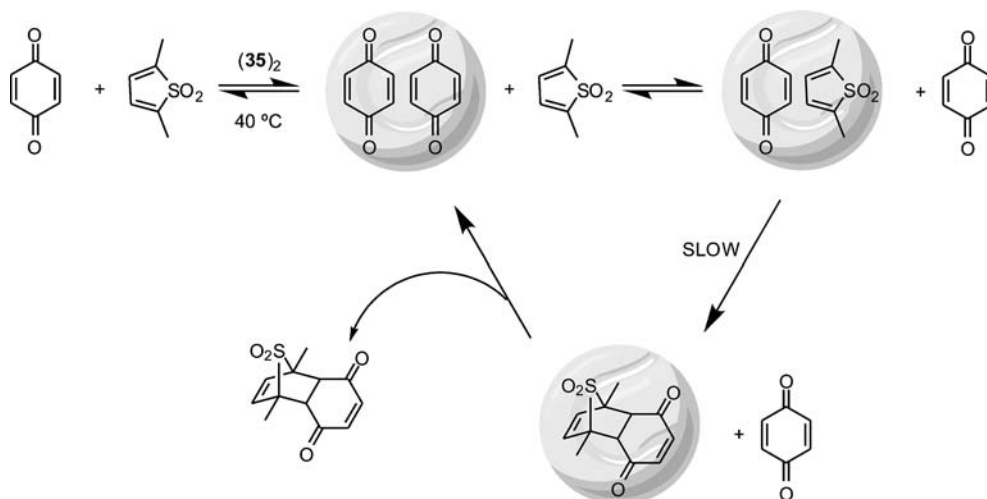
Scheme 3.9 Hydrogen-bonded dimeric capsule (**35**)$_2$ (R^1 = R^2 = 4-*n*-heptylphenyl, R^3 = OH) catalyzes a Diels-Alder reaction.

37

$R = C_{11}H_{23}$

36

(36)₂
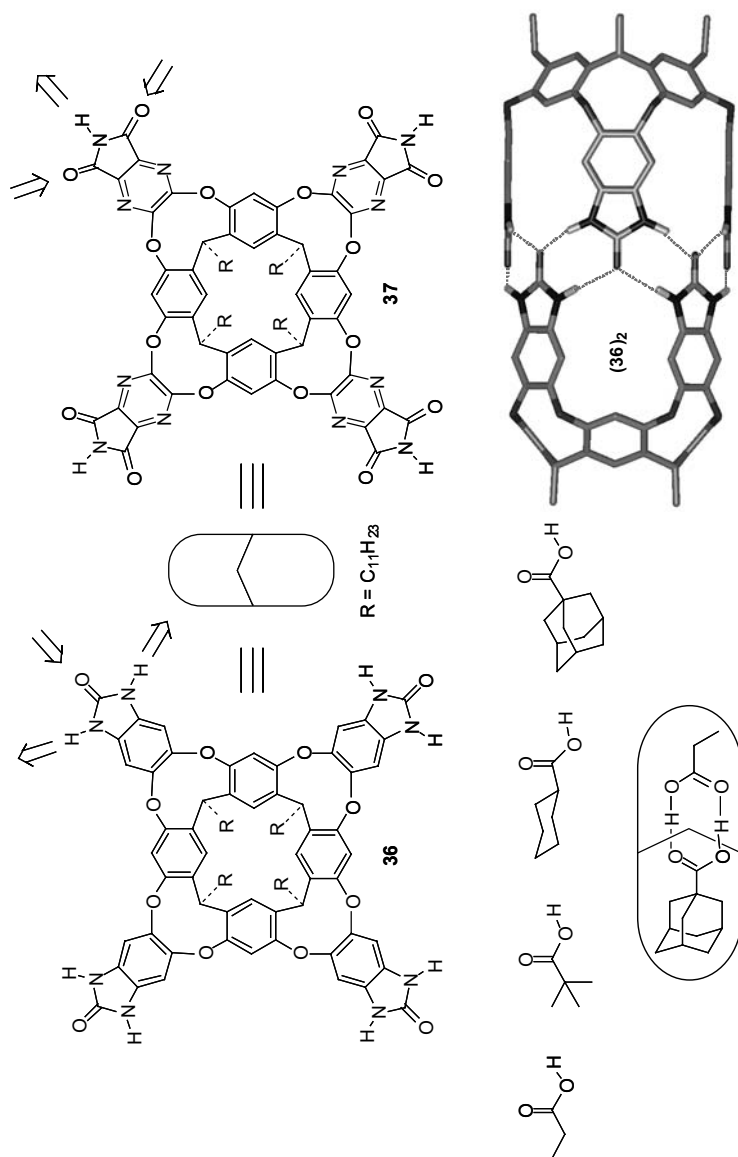
Figure 3.19 Cylindrical capsules from imides and ureas at the bridges of cavitands.

38   **39**
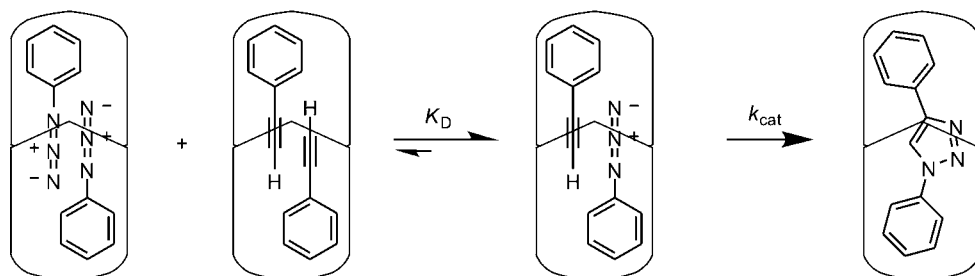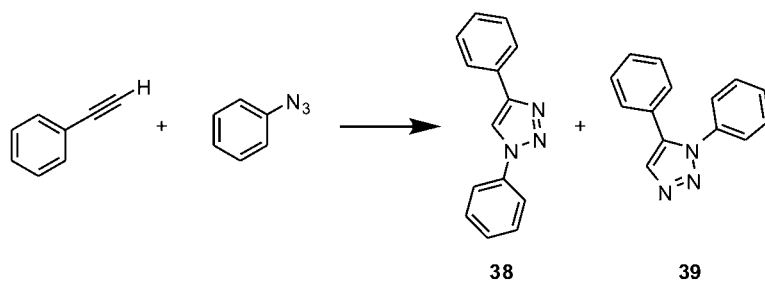
Scheme 3.10 Closed spaces inside a capsule impose restrictions in the orientation of reaction partners in a 1,3-dipolar cycloaddition.

For the more favorable case depicted in Scheme 3.9, where the Diels-Alder adduct is bound less tightly than the reactants, true catalysis and some turnover was observed [48]. In both cases, however, productive capsules (i.e. filled with diene and dienophile components) have to compete additionally with non-productive ones (filled with two dienes or two dienophiles).

The problem of correctly filling the capsules with only productive partners has been addressed by cylindrical capsules, such as $(36)_2$ [49] or $(37)_2$ [50], which can simultaneously hold one large and one small guest, but not two large (not enough room) or two small (too much void space left) ones. For instance, $(36)_2$ accommodates pair-wise carboxylic acid dimers (Figure 3.19) [49].

In addition, cylindrical shapes offer the possibility to favor the alignment of reactants in a specific way, not favored outside of a confined space. Thus, the 1,3-dipolar cycloaddition between an alkyne and an azide (Scheme 3.10) yields mainly triazole adduct **38** in the presence of $(37)_2$, whereas a mixture of regioisomers **38** and **39** are obtained in its absence [51].

Chirality can be introduced in capsules by substitution. Examples of chiral recognition inside the cavities are scarce as introduction of asymmetry in the periphery does not translate inside the cavity. Thus, introduction of different substituents at both side glycolurils in tennis balls and soft balls, such as in **35** ($R^1 = p$-$C_6H_4OC_6H_{15}$, $R^2 = CO_2$-i-pentyl, $R^3 = H$), removes one of the two symmetry planes

40 R^1 = C$_6$H$_4$-*p*-C$_7$H$_{15}$ **41** R^2 = SO$_2$C$_6$H$_4$-*p*-CH$_3$ R = C$_{10}$H$_{21}$
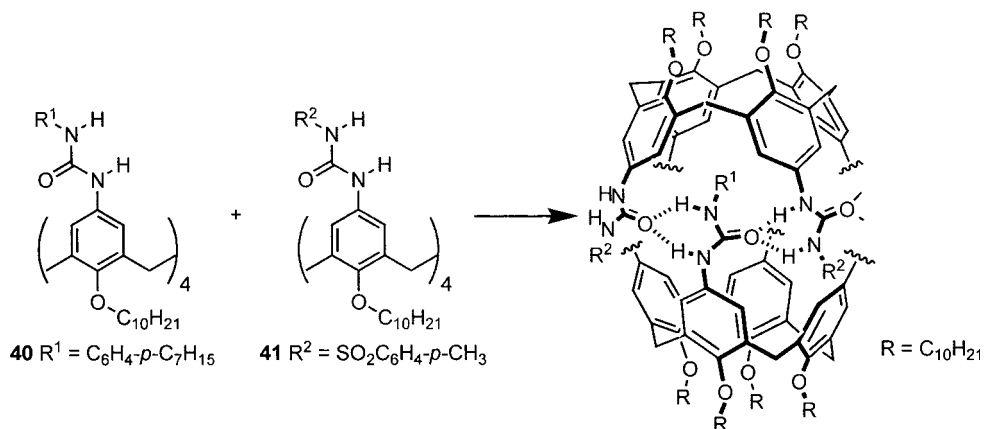
Scheme 3.11 Chirality in a heterodimeric ureidocalix[4]arene capsule, induced by the orientation of the cyclic array of hydrogen bonds.

of the monomer and leaves the dimer with a C_2 axis of symmetry [52]. Similarly, well known urea-urea hydrogen-bonding patterns have been independently studied by Rebek [45c,53] and Böhmer [54], using calix[4]arenes containing ureas at their wider rims. Heterodimers arising from a mixture of calix[4]arene ureas **40** and **41** are thus chiral (Scheme 3.11).

42 R = 4-*n*-heptylphenyl

Achiral Monomer   Enantiomeric Dimeric Capsules
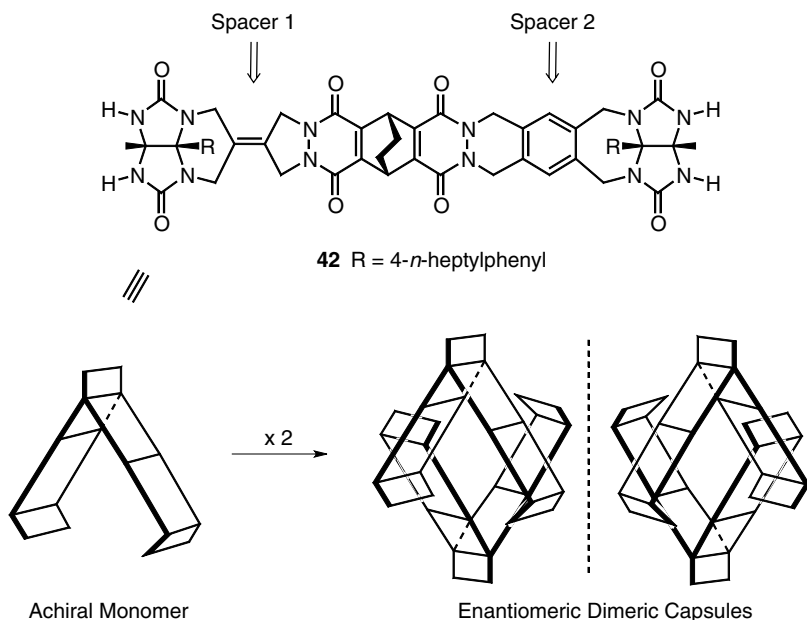
Scheme 3.12 Chirality generated by dimerization of an achiral monomer with two different spacers.

None of these dissymmetric capsules display enantioselectivity for chiral substrates. On the contrary, more distorted scaffolds, such as those resulting from use of different spacers in a soft ball (compound **42** in Scheme 3.12) yield enantiomeric capsules that can discriminate chiral guests, with a modest diastereomeric excess (up to 35% for the most favorable cases) [55].

When an enantiopure chiral guest is added to a racemic softball mixture, the initial 1:1 kinetic distribution of diastereoisomeric filled capsules slowly turns into a thermodynamic distribution favoring one diastereoisomer, on the timescale of capsule dissociation ($t_{1/2} = 19$ h). If an excess of the less favored enantiomer is added rapidly, a distribution favoring this unstable complex shows up quickly, and then the thermodynamic mixture is slowly reached again upon standing. This "memory effect" (one capsule retains its chirality even when its "shaping" guest template is removed) indicates also that complete dissociation of the capsule is unlikely for the exchange, and a "flap-opening" mechanism operates instead [56].

Exchange in cylindrical capsules, such as $(37)_2$, has also been studied by Rebek and coworkers. The lifetime of the capsule is ca. 0.5 s, and up to three guests can be accommodated inside, depending on their sizes and the solvent employed. Even for larger single guests, such as 4,4′-dimethylbiphenyl, exchange may occur without dissociation of the capsule and without formation of a completely vacant capsule. Most remarkably, *n*-alkanes that are much longer than the capsule can be accommodated, *n*-tetradecane being the longest guest allowing encapsulation. To achieve this, the alkane must coil into a chiral helical conformation. Detailed NMR studies show that the helix rapidly racemizes inside the capsule without fully unwinding, which suggests that racemization proceeds through propagation of short-range uncoiling [57].

Exchange processes in ureidocalix[4]arenes (i.e. **40** or **41**) have also been studied in detail. In each monomer of these aggregates (which require a guest the size of benzene to properly form), ureas are oriented in opposite directions (*P* or *M*), and the direction of rotation of the cyclic array is slow at the NMR timescale. The capsule is therefore a "meso" form. Exchange of benzene guests in these calixarene dimers occurs by simultaneous dissociation coupled with rotation of the ureas (racemization) [58]. For cationic guests, like tetraethylammonium, the bulkier substrate forces the capsule to expand to some extent relative to benzene. This weakens some hydrogen bonds (which is compensated by cation-π host-guest interactions), and favors rotation of the ureas to racemize without fully disrupting the dimeric assembly [59].

Wider ureidocalixarenes, such as calix[5]- or calix[6]arenes, cannot dimerize since there is no space between the ureas to allow interpenetration with the set of ureas provided by the second monomer, but calix[6]arene **43**, with just three unsubstituted ureas at alternate rings, forms quite stable dimers [60]. Interestingly, addition of increasing amounts DMSO to a 1:1 mixture of a triureidocalix[6]arene and tetra-ureidocalix[4]arene capsules in chloroform causes disruption of the calix[4]arene capsule (containing 8 ureas) prior to the calix[6]arene ones (endowed with a seam of just 6 ureas), a fact that can be explained by the better arrangement of the hydrogen bonding arrays in the latter (Scheme 3.13).

The flexibility and mutability of hydrogen bonds, as compared to covalent bonds, make self-assembled capsules unlikely to display good selectivities for closely related
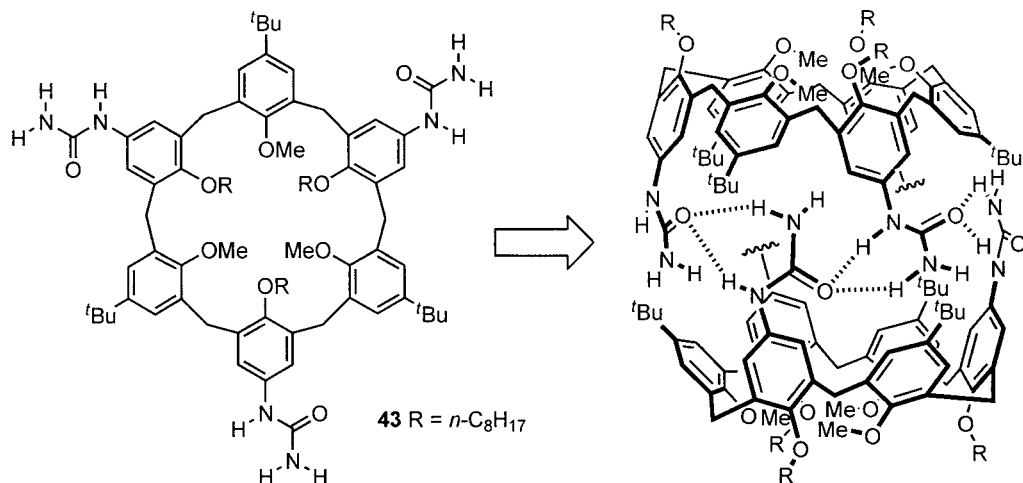
Scheme 3.13 Dimeric capsule formation in a triureidocalix[6]arene.

guests. A remarkable exception has recently been found in our laboratory for the encapsulation of fullerenes inside capsule $(44)_2$ built up from two CTV scaffolds endowed with three UPy hydrogen-bonding arrays [61]. This large capsule was specifically designed to encapsulate fullerenes, and indeed both C_{60} and C_{70} were readily complexed by $(44)_2$, with binding constants in the order of 10^3 and $10^4\,M^{-1}$, respectively. The selectivity for C_{70} allows for an expeditious method, not relying on chromatography, to efficiently extract this valuable material from carbon soot or from fullerite, which was attributed to the slightly different shape of each respective fullerene. Whereas C_{60} is roughly spherical, like a soccer ball, C_{70} is thinner and slightly elongated, resembling a rugby ball. The hydrogen-bond patterns of the UPy dimeric quadruple bond arrays are closer to the ideal planarity in the C_{70} complex (Figure 3.20).

Examples of enclosing the space with aggregates composed of more than two molecular components and simply stabilized by hydrogen bonds are scarce in the literature [62]. Cyclic sulfonamides (such as **45**) feature a self-complementary hydrogen bonding pattern of glycolurils (Scheme 3.14). Under the appropriate conditions, sulfonamides and glycolurils like to form heteromeric hydrogen-bonding aggregates, as we have previously seen demonstrated by the heterodimeric ureidocalix[4]arene dimeric capsules. Curved monomer **46** [62], containing both groups, is thus programmed to self-assemble in a head-to-tail manner, establishing hydrogen bonds between the best two partners. The final result is the assembly of a rare tetramolecular capsule $(46)_4$, induced by encapsulation of guests of appropriate size and functionality, such as adamantane (Figure 3.21).

Adamantane (**47**), however, only offers weak van der Waals interactions to the inner concave surface of the host assembly. This interaction, together with the enthalpic gains provided by the formation of 16 hydrogen bonds, is enough to overcome the entropy penalty for bringing together four monomers and one guest.
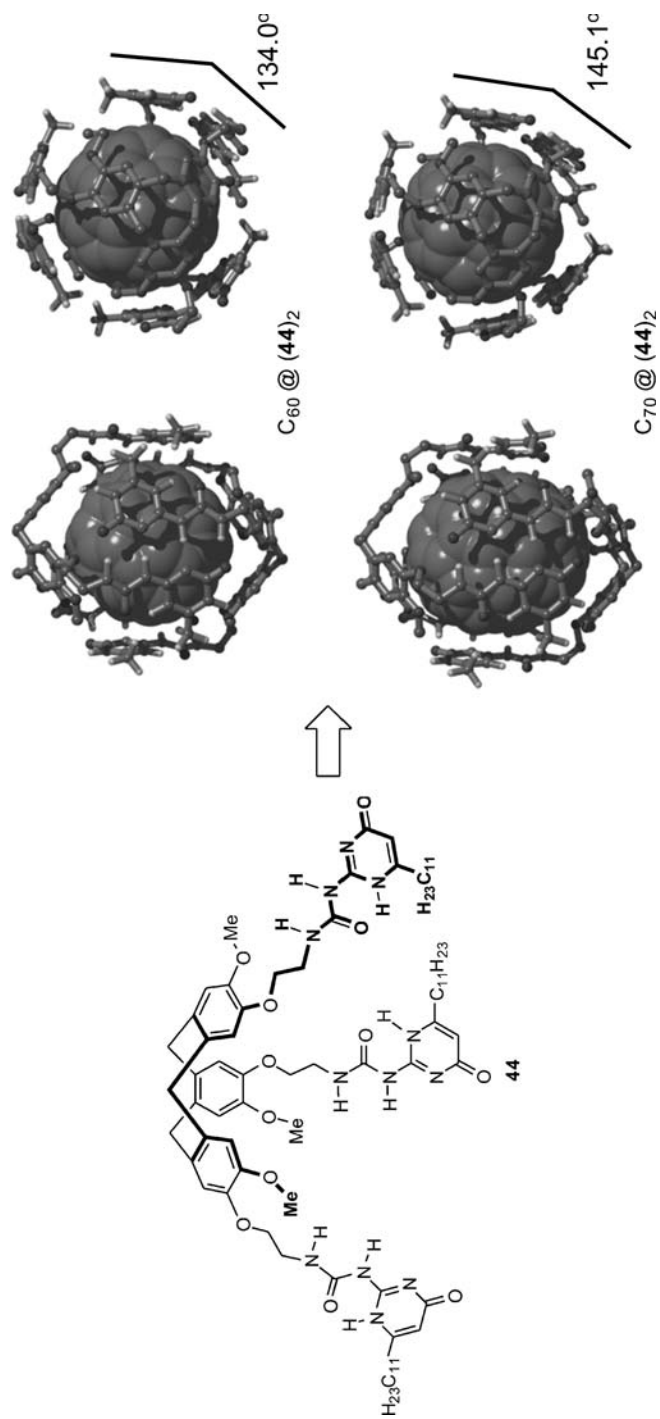
Figure 3.20 Dihedral angles closer to planarity between UPy binding subunits account for selective extraction of C_{70} with cyclotriveratrylene-based capsule $(44)_2$.
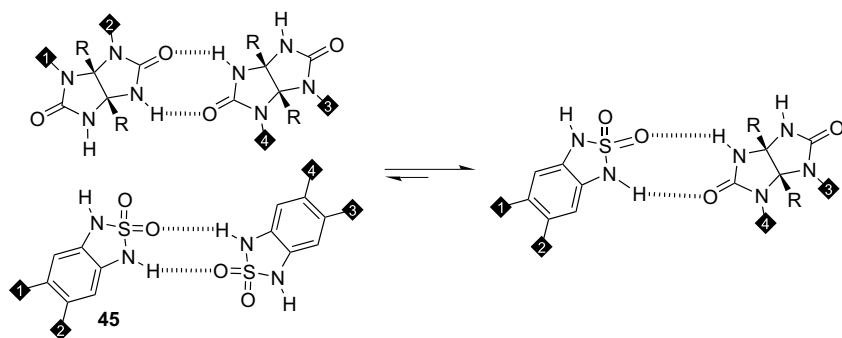
Scheme 3.14 Heterodimers formed between sulfonamides
(R = 4-*n*-heptylphenyl) and glycolurils.

Adamantane-2,6-dione (**48**) further stabilizes the tetrameric assembly by the presence of hydrogen-bonding acceptor groups (C=O) in the guest molecules through the formation of bifurcated hydrogen bonds with the glycoluril N—H groups of the capsule (Figure 3.22).

Dimeric self-assemblies based on resorcinarene cavitands have already been mentioned. However, resorcin[4]arene itself (**49a**) was the subject of the first report of a self-assembly process, directed simply by hydrogen bonds, capable of yielding a giant hexameric capsule. Thus, in 1997 Atwood and MacGillivray showed that **49a** crystallized into a chiral spherical molecular assembly [62b]. Six monomers (**49a**) assembled together, with eight structural water molecules occupying the corners of the assembly, to form a supramolecular hexameric structure that conforms to a snub cube (Figure 3.23). The capsule is held together by a complex pattern of 60 OH···H hydrogen bonds, 24 of which are intramolecular and help to stabilize the crown-like conformation of each resorcinarene component. Consequently, the six monomers and the eight water molecules are held together by 36 intermolecular hydrogen bonds (HB/$(N-1)$ = 2.8). The enclosed space in the cavity of the hexamer (**49a**)$_6$ is about 1403 Å^3 [63]. As expected, the solvent molecules present inside the cavity of (**49a**)$_6$, in the solid state, were too disordered to be located. Authors showed preliminary supporting evidence that the hexameric structure was also maintained in solution.
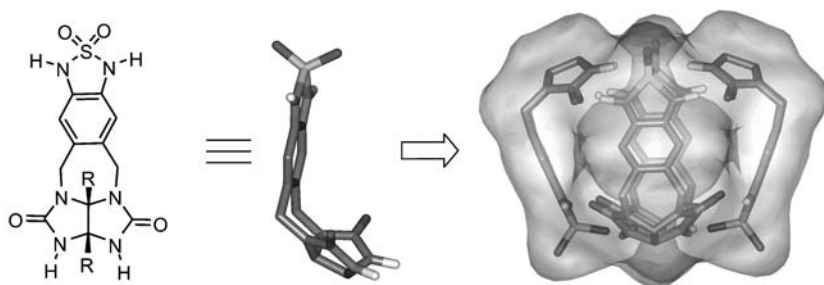
46 R = 4-*n*-heptylphenyl

Figure 3.21 A glycoluril with a sulfonamide self-assembles into a tetramer.

47@(46)₄

48@(46)₄
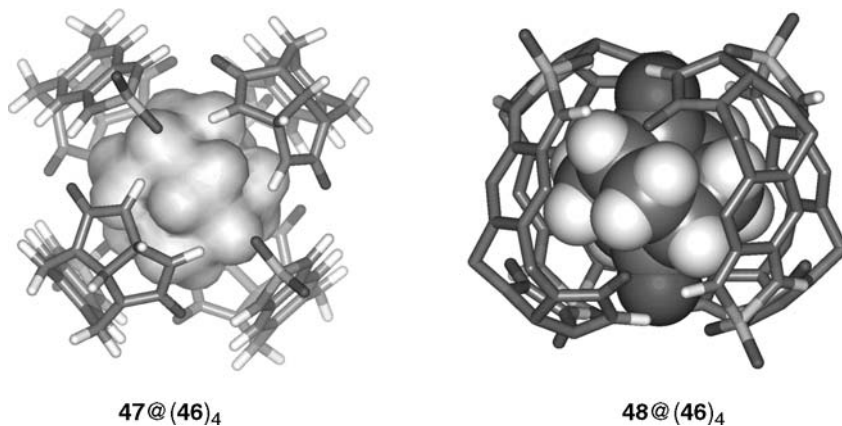
Figure 3.22 Encapsulation of adamantane (left) and adamantane-2,6-dione (right).

49a R^1 = Me, R^2 = H
49b R^1 = $C_{11}H_{23}$, R^2 = H
50a R^1 = Pr, R^2 = OH
50b R^1 = C_6H_{13}, R^2 = OH
50c R^1 = i-C_4H_9, R^2 = OH

(49a)₆
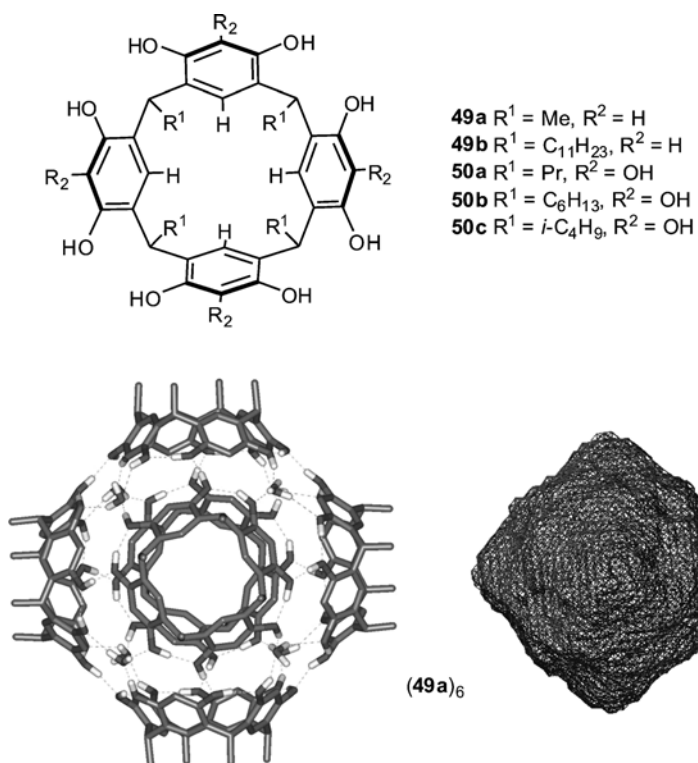
Figure 3.23 The resorcinarene octahedral self-assembled hexamer (left) and the volume of the enclosed cavity (right).

Crystal structures for several of the corresponding pyrogallol[4]arenes **50** (Figure 3.23) have been solved. These also form hexameric capsules, which now contain an array of 72 hydrogen bonds (48 are intramolecular and 24 intermolecular, HB/$(N-1) = 4$) and have no structural water molecules [64]. The increase in the I_{Tm} HB/$(N-1)$ value agrees very well with the fact that nanocapsules based on pyrogallol **50a** are more stable in polar media than those derived from resorcinarene **49a**.

A decade ago Aoyama *et al.* described the formation of a simple 1:1 open complex of resorcinarene **50b** with dicarboxylic acids in CDCl$_3$ and, subsequently, with ribose, terpenes and even steroids [65]. Convincing evidence from laboratories worldwide indicate that resorcinarenes **49** also assemble in water-saturated organic solvents as a hexamer [66]. These hexameric assemblies are observed in the encapsulation of a wide variety of guests in solution. However, the pyrogallol[4]arene hexamer does not require water to be stabilized and assembles in dry halogenated solvents as well. Addition of certain neutral [67] and positively charged [68] guests leads to an upfield shifted signals for the encapsulated guest's protons in the ^{1}H NMR spectra. The protons of the host experience do not exhibit significant changes in chemical shift. The exchange of the "free" and "encapsulated" guest is slow on the NMR timescale, as indicated by the appearance of two sets of resonances. Most guests occupy only about 55% of the available volume [69]. Interestingly, many guests within hexameric capsules show packing coefficients (PC) similar to those in solution, viz. ca. 0.5 [PC = volume of the guest(s)/volume of the cavity ($\sim$1400 Å^3)] [69].

Recently, Schalley and coworkers have presented evidence for the hexameric capsular structure, even in the gas phase after ionization [70]. The molecular structure of ruthenium complex **51**$^{2+}$ is congruent with the size, shape, and symmetry of the cavity of the hexameric host (**49a**)$_6$. Molecular modeling studies show an almost ideal fitting of **51**$^{2+}$ inside the cavity. The periphery of each pyridine ring on the guest cation is directed toward each end of the six resorcinarene monomers. Although the guest is only pseudo octahedral and deviates somewhat from a perfect octahedral geometry, it nevertheless matches well enough the structure of the hexameric capsular host. The
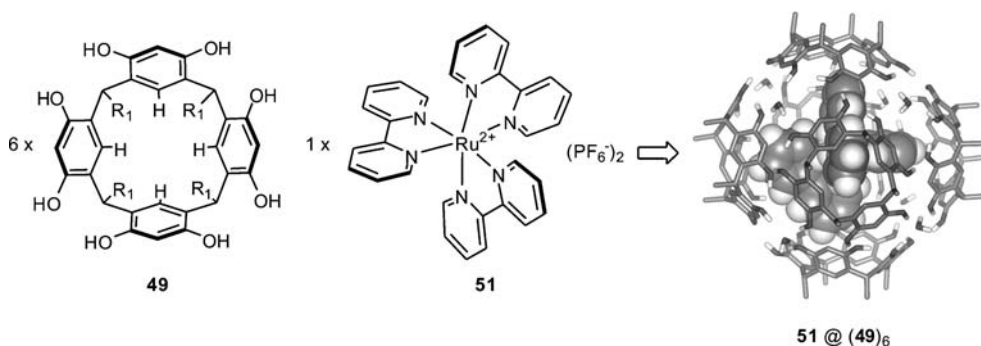
Figure 3.24 Ruthenium complex **51** is encapsulated in the hexameric self-assembly of resorcinarene **49**.

52
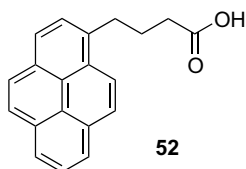
Figure 3.25 Pyrene butyric acid, a fluorescent guest to study interactions inside a capsule.

ESI mass spectra after the addition of **49** (or **50**) to **51**(PF$_6$)$_2$ show the hexameric clusters **51**@(**49**)$_6$ and **51**@(**50**)$_6$ as the dominating signals (Figure 3.24). These ions were irradiated in an infrared multiphoton dissociation experiment (IRMPD) with IR radiation from a CO$_2$ laser at different time intervals. The observed fragmentation behavior was exactly that expected for the hexameric capsule.

To further explore the environment inside such hexameric hosts, Atwood and coworkers performed structural characterization and spectrofluorometric studies of the capsule-bound fluorescent probe molecule pyrene butyric acid (PBA) **52** [71]. Single-crystal X-ray diffraction studies on **52**@(**50b**)$_6$ show not only that encapsulated guests interact with the host walls in the solid state, but also that the π surfaces of the guest molecules are well separated from one another within the capsule. The spectroscopic studies in solution corroborated this finding and revealed an average of 1.5 molecules of **52** per capsule. The assembly remains intact over four weeks in the solution phase, suggesting that the carboxylic acid groups and the polyaromatic nature of **52** do not destabilize the overall supramolecular assembly.

Resorcinarene platforms have also been developed in the generation of multi-component capsules stabilized by hydrogen bonds. In this sense, Kobayashi *et al.* have constructed a methylene-bridged resorcinarene scaffold functionalized with four carboxylic acids (**53**) [72]. 2-Aminopyrimidine is used as a wedged-shaped hydrogen-bonding bridge to form two hydrogen bonds with each of two carboxylic acids on neighboring molecules (Figure 3.26).

53
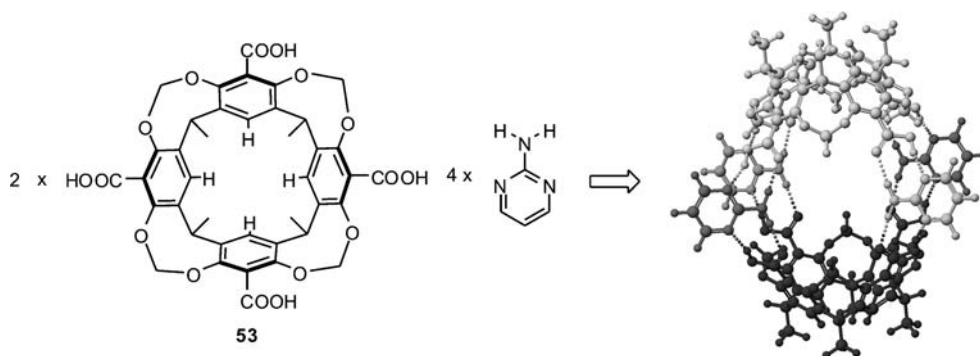
Figure 3.26 Two cavitands containing four carboxylic acids dimerize assisted by 2-aminopyrimidine hydrogen-bonded connectors.
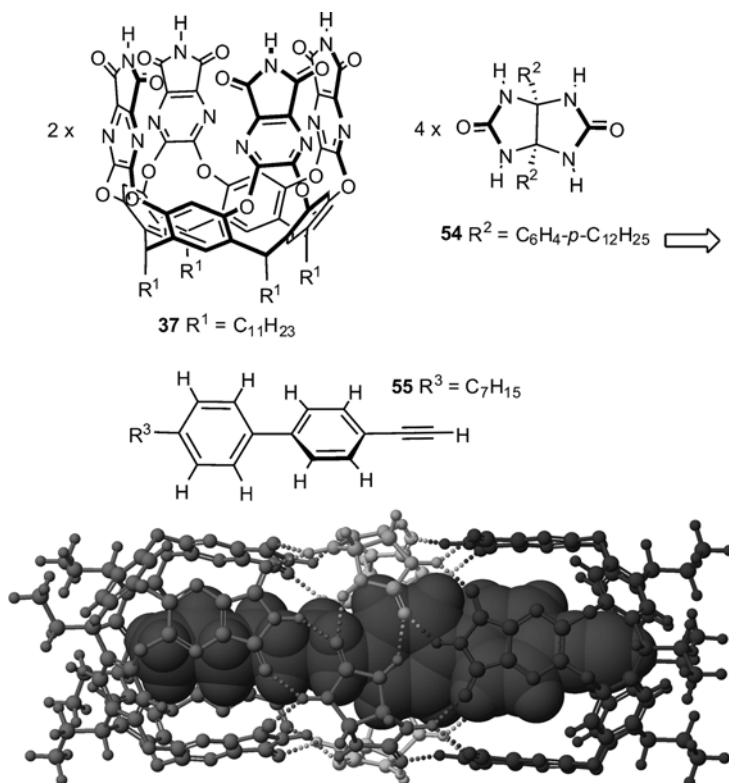
Figure 3.27 An expanded, six-component capsule is formed by addition of glycoluril **54** to cavitand **37**, which would otherwise form a dimeric (**37**)$_2$ capsule.

Rebek and Ajami have recently reported the reversible expansion of the dimeric capsule (**37**)$_2$ with four glycouril spacers (**54**), increasing the cavity's volume by ∼200 Å^3 and its length by ∼7 Å [73]. The expanded capsule self-assembles from six molecular components and is stabilized by 32 intermolecular hydrogen bonds. The expanded capsule is capable of encapsulating normal alkanes up to $C_{21}H_{44}$ and other guests of similar length, such as the biphenyl-alkyne derivative **55** shown in Figure 3.27.

3.4
Summary and Outlook

The non-covalent synthesis of discrete macrocyclic and macrooligocyclic structures using multiple hydrogen-bonding interactions has now become a reality. The supramolecular approach outlined here represents an attractive and effective alternative to traditional stepwise covalent synthesis. Use of multiple hydrogen bonds to organize molecular components into supramolecular nanostructures has

revolutionized the way in which chemists approach the construction of complex cyclic structures. The examples discussed in this chapter take place under thermo-dynamic control. This means that the products must be evaluated in terms of thermodynamic minima in equilibrating mixtures. As a consequence, they reflect a balance between enthalpy and entropy. We have presented and discussed several principles that can be used to influence the association of the components toward cyclic aggregates and to predict their relative stabilities.

The stability of a cyclic multimolecular aggregate stabilized by intermolecular interactions is not simply a consequence of $\Delta G°$, since this thermodynamic variable does not take into account the effect of the concentration (entropy) on the extent of the aggregation. The concepts derived from the study of simple model systems of macrocyclic structures stabilized by hydrogen bonds could be used to rationalize the association of more complex biological aggregates.

In addition, the construction of cyclic aggregates stabilized by hydrogen bonds paved the way for the study of reversible molecular encapsulation and the nature of intimate molecular relationships isolated from the bulk solvent, as well as the effects that molecular confinement in nanoscopic spaces has chemi-cal reactivity.

3.5
Experimental: Selected Procedures

3.5.1
Solid State Formation of the Hexameric Capsule Derived from Pyrogallol[4]arene (50c) [74]

Compound **50c** was obtained in ca. 25% yield as a precipitate from the acid-catalyzed condensation of pyrogallol and isovaleraldehyde. No evidence of any hexamer was found in the solid material. To convert this material into the hexamer $(50c)_6$, the original precipitate can be dissolved in Et_2O, acetone, or methanol, with a few drops of nitrobenzene or o-dinitrobenzene, followed by crystallization upon slow evapora-tion. The hexamer may also be obtained by thermal treatment of the initial precipi-tate or the initial filtrate. The product in the initial filtrate may be converted into hexamer by extraction in Et_2O, followed by evaporation to dryness with subsequent dissolution in methanol. The methanol solution is then heated to 120–150 °C for at least 12 h. Methanol may be removed under vacuum to yield a red-brown solid. Colorless hexameric spherical capsules are obtained from this solid utilizing the crystallization procedure described for the initial precipitate.

3.5.2
Crystals of the Host-Guest Arrangement of 52@(50b)$_6$

A hot, saturated HPLC grade acetonitrile solution containing pyrene butyric acid (**52**, 2 equivalents) was added to a hot, saturated HPLC grade acetonitrile solution

containing *C*-hexylpyrogallol[4]arene (**50b**) to give a pale yellow solution. The solution was sonicated for 10–15 min, re-heated, and allowed to cool slowly. The sample vial was capped and allowed to stand overnight, after which time the solution had darkened to a brown colour. Slow evaporation and concomitant concentration of this solution over a two to three week period afforded the growth of pale single crystals suitable for X-ray diffraction studies. The crystals were filtered off and used in the spectrofluorometric studies as required.

Acknowledgments

Abbreviations

EM	effective molarity
NMR	nuclear magnetic resonance
CA	cyanuric acid
M	melamine
DMSO	dimethylsulfoxide
A	acceptor
D	donor
VPO	vapor pressure osmometry
GPC	gel permeation chromatography
G	guanine
C	cytosine
TDP	tridodecyloxyphenyl
UV	ultraviolet
CD	circular dichroism
TEM	transmission electron microscopy
Upy	2-ureido-4-pyrimidinone
ESI	electrospray ionization
MS	mass spectrometry
THF	tetrahydrofuran
DOSY	diffusion ordered spectroscopy
CTV	cyclotriveratrylene
PC	packing coefficients
IRMPD	infrared multiphoton dissociation
PBA	pyrene butyric acid
HPLC	high performance liquid chromatography

References

1 (a) Ercolani, G. (2003) *J. Am. Chem. Soc.*, **125**, 16097–16103; (b) Ercolani, G. (2003) *J. Phys. Chem. B*, **107**, 5052–5057.

2 Hunter, C.A. (2004) *Angew. Chem.*, **116**, 5424–5439; *Angew. Chem. Int. Ed.*, **43**, 5310–5324.

3 (a) Jeong, K.S., Tjivikua, T. and Rebek, J., Jr (1990) *J. Am. Chem. Soc.*, **112**, 3215–3217; (b) Sartorius, J. and Schneider, H.-J. (1996) *Chem. Eur. J.*, **2**, 1446–1452.

4 Jorgensen, W.L. and Pranata, J. (1990) *J. Am. Chem. Soc.*, **112**, 2008–2010.

5 Ercolani, G., (ed. E. Alessio) (2006) *Noncovalent Multiporphyrin Assemblies*, Springer, Berlin.

6 Zimmerman, S.C. and Duerr, B.F. (1992) *J. Org. Chem.*, **57**, 2215–2217.

7 Ducharme, Y. and Wuest, J.D. (1988) *J. Org. Chem.*, **53**, 5787–5789.

8 Seto, C.T. and Whitesides, G. (1993) *J. Am. Chem. Soc.*, **115**, 905–916.

9 Whitesides, G.M., Simanek, E.E., Mathias, J.P., Seto, C.T., Chin, D., Mammen, M. and Gordon, D.M. (1995) *Acc. Chem. Res.*, **28**, 37–44.

10 Mammen, M., Simanek, E.E. and Whitesides, G.M. (1996) *J. Am. Chem. Soc.*, **118**, 12614–12623.

11 Experimental entropy measurements include contributions from desolvation and changes in internal structure: (a) Kyogoku, Y., Lord, R.C. and Rich, A. (1969) *Biochim. Biophys. Acta*, **179**, 10–17; (b) Searle, M.S. and Williams, D. H. (1992) *J. Am. Chem. Soc.*, **114**, 10690–10697.

12 A theoretical estimate of the entropy of association for the 6-particle aggregate reported by Whitesides *et al.* is in the order of $50\,\mathrm{kcal\,mol^{-1}}$: Mammen, M., Shakhnovich, E.I., Deutch, J.M. and Whitesides, G.M. (1998) *J. Org. Chem.*, **63**, 3821–3830.

13 Cram, D.J. (1986) *Angew. Chem.*, **98**, 1041–1060; *Angew. Chem. Int. Ed. Engl.*, **25**, 1039–1057.

14 Mathias, J.P., Simanek, E.E., Zerkowski, J.A., Seto, C.T. and Whitesides, G.M. (1994) *J. Am. Chem. Soc.*, **116**, 4316–4325.

15 (a) Chi, X., Guerin, A.J., Haycock, R.A., Hunter, C.A. and Sarson, L.D. (1995) *J. Chem. Soc. Chem. Commun.*, 2563–2565; (b) For a complete theoretical treatment of self-assembly macrocyclizations under thermodynamic control see also: Ercolani, G. (1998) *J. Phys. Chem. B*, **102**, 5699–5703.

16 For a review, see: Prins, L.J., Reinhoudt, D.N. and Timmerman, P. (2001) *Angew. Chem.*, **113**, 2446–2492; *Angew. Chem. Int. Ed.*, **40**, 2382–2426.

17 Prins, L.J., De Jong, F., Timmerman, P. and Reinhoudt, D.N. (2000) *Nature*, **408**, 181–184.

18 (a) Prins, L.J., Huskens, J., de Jong, F., Timmerman, P. and Reinhoudt, D.N. (1999) *Nature*, **398**, 498–502; (b) Prins, L. J., Hulst, R., Timmerman, P. and Reinhoudt, D.N. (2002) *Chem. Eur. J.*, **8**, 2288–2301; (c) Prins, L.J., Verhage, J.J., de Jong, F., Timmerman, P. and Reinhoudt, D.N. (2002) *Chem. Eur. J.*, **8**, 2302–2313.

19 (a) Yashima, E., Maeda, K. and Okamoto, Y. (1999) *Nature*, **399**, 449–451; (b) Furusho, Y., Kimura, T., Mizuno, Y. and Aida, T. (1997) *J. Am. Chem. Soc.*, **119**, 5267–5268.

20 (a) Marsh, A., Nolen, E.G., Gardinier, K. M. and Lehn, J.-M. (1994) *Tetrahedron Lett.*, **35**, 397–400; (b) Marsh, A., Silvestri, M. and Lehn, J.-M. (1996) *Chem. Commun.*, 1527–1528.

21 (a) Mascal, M., Hext, N.M., Warmuth, R., Moore, M.H. and Turkenburg, J.P. (1996) *Angew. Chem.*, **108**, 2348–2350; *Angew. Chem. Int. Ed. Engl.*, **35**, 2204–2206; (b) Mascal, M., Hext, N.M., Warmuth, R., Arnall-Culliford, J.R., Moore, M.H. and Turkenburg, J.P. (1999) *J. Org. Chem.*, **64**, 8479–8484.

22 Shao, X.-B., Jiang, X.-K., Zhu, S.-Z. and Li, Z.-T. (2004) *Tetrahedron*, **60**, 9155–9162.

23 Yagai, S., Nakajima, T., Karatsu, T., Saitow, K. and Kitamura, A. (2004) *J. Am. Chem. Soc.*, **126**, 11500–11508.

24 Fenniri, H., Mathivanan, P., Vidale, K.L., Sherman, D.M., Hallenga, K., Wood, K.V. and Stowell, J.G. (2001) *J. Am. Chem. Soc.*, **123**, 3854–3855.

25 (a) Sijbesma, R.P., Beijer, F.H., Brunsveld, L., Folmer, B.J.B., Hirschberg, J.H.K.K., Lange, R.F.M., Lowe, J.K.L. and Meijer, E.W. (1997) *Science*, **278**, 1601–1604; (b) Beijer, F.H., Sijbesma, R.P., Kooijman, H., Spek, A.L. and Meijer, E.W. (1998) *J. Am. Chem. Soc.*, **120**, 6761–6769; (c) Hirschberg, J.H.K.K., Brunsveld, L., Ramzi, A., Vekemans, J.A.J.M., Sijbesma, R.P. and Meijer, E.W. (2000) *Nature*, **407**, 167–170; (d) Brunsveld, L., Vekemans, J.A.J.M., Hirschberg, J.H.K.K., Sijbesma, R.P. and Meijer, E.W. (2002) *Proc. Natl. Acad. Sci. U.S.A.*, **99**, 4977–4982; (e) Ligthart, G.B.W.L., Ohkawa, H., Sijbesma, R.P. and Meijer, E.W. (2005) *J. Am. Chem. Soc.*, **127**, 810–811.

26 For similar motifs based on other heterocyclic systems, see for instance: (a) Zimmerman, S.C., Zeng, F., Reichert, D.E.C. and Kolotuchin, S.V. (1996) *Science*, **271**, 1095–1098; (b) Kolotuchin, S.V. and Zimmerman, S.C. (1998) *J. Am. Chem. Soc.*, **120**, 9092–9093; (c) Corbin, P.S., Lawless, L.J., Li, Z., Ma, Y., Witmer, M.J. and Zimmerman, S.C. (2002) *Proc. Natl. Acad. Sci. U.S.A.*, **99**, 5099–5104; (d) Lüning, U., Kühl, C. and Uphoff, A. (2002) *Eur. J. Org. Chem.*, 4063–4070; (e) Brammer, S., Lüning, U. and Kühl, C. (2002) *Eur. J. Org. Chem.*, 4054–4062.

27 Pranata, J., Wierschke, S.G. and Jorgensen, W.L. (1991) *J. Am. Chem. Soc.*, **113**, 2810–2819.

28 Folmer, B.J.B., Sijbesma, R.P., Versteegen, R.M., van der Rijt, J.A.J. and Meijer, E.W. (2000) *Adv. Mater.*, **12**, 874–878.

29 (a) Rispens, M.T., Sánchez, L., Knol, J. and Hummelen, J.C. (2001) *Chem. Commun.*, 161–162; (b) González, J.J., González, S., Priego, E.M., Luo, C., Guldi, D.M., de Mendoza, J. and Martín, N. (2001) *Chem. Commun.*, 163–164.

30 Hahn, U., González, J.J., Huerta, E., Segura, M., Eckert, J.-F., Cardinali, F., de Mendoza, J. and Nierengarten, J.-F. (2005) *Chem. Eur. J.*, **11**, 6666–6672.

31 See, for instance: Rispens, M.T., Sánchez, L., Beckers, E.H.A., Van Hal, P.A., Schenning, A.P.H.J., El-ghayouri, A., Peeters, E., Meijer, E.W., Janssen, R.A.J. and Hummelen, J.C. (2003) *Synth. Metals*, **135-136**, 801–803, and references therein.

32 Folmer, B.J.B., Sijbesma, R.P., Kooijman, H., Spek, A.L. and Meijer, E.W. (1999) *J. Am. Chem. Soc.*, **121**, 9001–9007.

33 Keizer, H.M., González, J.J., Segura, M., Prados, P., Sijbesma, R.P., Meijer, E.W. and de Mendoza, J. (2005) *Chem. Eur. J.*, **11**, 4602–4608.

34 Gellert, M., Lipsett, M.N. and Davies, D.R. (1962) *Proc. Natl. Acad. Sci. USA*, **48**, 2013–2018.

35 For an excellent recent review on G-quartets, see: Davis, J.F. (2004) *Angew. Chem.*, **116**, 684–716; *Angew. Chem. Int. Ed.*, **43**, 668–698.

36 Gottarelli, G., Masiero, S. and Spada, G.P. (1995) *J. Chem. Soc. Chem. Commun.*, 2555–2557.

37 Marlow, A.L., Mezzina, E., Spada, G.P., Masiero, S., Davis, J.T. and Gottarelli, G. (1999) *J. Org. Chem.*, **64**, 5116–5123.

38 (a) Cai, M., Marlow, A.L., Fettinger, J.C., Fabris, D., Haverlock, T.J., Moyer, B.A. and Davis, J.T. (2000) *Angew. Chem.*, **112**, 1339–1341; *Angew. Chem. Int. Ed.*, **39**, 1283–1285; (b) Shi, X., Fettinger, J.C., Cai, M. and Davis, J.T. (2000) *Angew. Chem.*, **112**, 3254–3257; *Angew. Chem. Int. Ed.*, **39**, 3124–3127.

39 Chaput, J.C. and Switzer, C. (1999) *Proc. Natl. Acad. Sci. USA*, **96**, 10614–10619.

40 Sessler, J.L., Sathiosatham, M., Doerr, K., Lynch, V. and Abboud, K.A. (2000) *Angew. Chem.*, **112**, 1356–1359; *Angew. Chem. Int. Ed.*, **39**, 1300–1303.

41 A binding strength of $K_a = 2 \times 10^7 \, \mathrm{M}^{-1}$ is reported for a triple hydrogen bonding array AAA-DDD: Djurdjevic, S., Leigh, D.A., McNab, H., Parsons, S., Teobaldi, G. and Zerbetto, F. (2007) *J. Am. Chem. Soc.*, **129**, 476–477.

42 Hasenknopf, B., Lehn, J.-M., Boumediene, N., Leize, E. and Van Dorsselaer, A. (1998) *Angew. Chem.*, **110**, 3458–3460; *Angew. Chem. Int. Ed.*, **37**, 3265–3268.

43 (a) Rudkevich, D.M., Hilmersson, G. and Rebek, J., Jr (1997) *J. Am. Chem. Soc.*, **119**, 9911–9912; (b) Rudkevich, D.M., Hilmersson, G. and Rebek, J., Jr (1998) *J. Am. Chem. Soc.*, **120**, 12216–12225.

44 (a) Wyler, R., de Mendoza, J. and Rebek, J., Jr (1993) *Angew. Chem.*, **105**, 1820–1821; *Angew. Chem. Int. Ed. Engl.*, **32**, 1699–1701; (b) Meissner, R.S., Rebek, J., Jr and de Mendoza, J. (1995) *Science*, **270**, 1485–1488.

45 See for instance: (a) Morgan Conn, M. and Rebek, J., Jr (1997) *Chem. Rev.*, **97**, 1647–1668; (b) Rudkevich, D.M. and Rebek, J., Jr (1999) *Eur. J. Org. Chem.*, 1991–2005; (c) Rebek, J., Jr (2000) *Chem. Commun.*, 637–643; (d) Hof, F., Craig, S.L., Nuckolls, C. and Rebek, J., Jr (2002) *Angew. Chem.*, **114**, 1556–1578; *Angew. Chem. Int. Ed.*, **41**, 1488–1508; (e) Palmer, L.C. and Rebek, J., Jr (2004) *Org. Biomol. Chem.*, **2**, 3051–3059; (f) Rebek, J., Jr (2005) *Angew. Chem.*, **117**, 2104–2115; *Angew. Chem,. Int. Ed.*, **44**, 2068–2078; (g) Biros, S.M. and Rebek, J., Jr (2007) *Chem. Soc. Rev.*, **36**, 93–104.

46 (a) Morán, J.R., Karbach, S. and Cram, D.J. (1982) *J. Am. Chem. Soc.*, **104**, 5826–5828; (b) Sherman, J.C., Knobler, C.C. and Cram, D.J. (1991) *J. Am. Chem. Soc.*, **113**, 2194–2204.

47 Kang, J. and Rebek, J., Jr (1997) *Nature*, **385**, 50–52.

48 Kang, J., Santamaría, J., Hilmersson, G. and Rebek, J., Jr (1998) *J. Am. Chem. Soc.*, **120**, 7389–7390.

49 Ebbing, M.H.K., Villa, M.J., Valpuesta, J.M., Prados, P. and de Mendoza, J. (2002) *Proc. Natl. Acad. Sci. U.S.A.*, **99**, 4962–4966.

50 Heinz, T., Rudkevich, D.M. and Rebek, J., Jr (1998) *Nature*, **394**, 764–766.

51 Chen, J. and Rebek, J., Jr (2002) *Org. Lett.*, **4**, 327–329.

52 Tokunaga, Y. and Rebek, J., Jr (1998) *J. Am. Chem. Soc.*, **120**, 66–69.

53 (a) Shimidzu, K. and Rebek, J., Jr (1995) *Proc. Natl. Acad. Sci. U.S.A.*, **92**, 12403–12407; (b) Hamann, B., Shimizu, K.D. and Rebek, J., Jr (1996) *Angew. Chem.*, **108**, 1425–1427; *Angew. Chem. Int. Ed. Engl.*, **35**, 1326–1329.

54 (a) Mogck, O., Böhmer, V. and Vogt, W. (1996) *Tetrahedron*, **52**, 8489–8496; (b) Mogck, O., Paulus, E.F., Böhmer, V., Thondorf, I. and Vogt, W.J. (1996) *Chem. Commun.*, 2533–2534.

55 Rivera, J.M., Martín, T. and Rebek, J., Jr (1998) *J. Am. Chem. Soc.*, **120**, 819–820; (b) Rivera, J.M., Martín, T. and Rebek, J., Jr (1998) *Science*, **279**, 1021–1023.

56 Rivera, J.M., Craig, S.L., Martín, T. and Rebek, J., Jr (2000) *Angew. Chem.*, **112**, 2214–2216; *Angew. Chem. Int. Ed.*, **39**, 2130–2132.

57 Scarso, A., Trembleau, L. and Rebek, J., Jr (2004) *J. Am. Chem. Soc.*, **126**, 13512–13518.

58 Mogck, O., Pons, M., Böhmer, V. and Vogt, W. (1997) *J. Am. Chem. Soc.*, **119**, 5706–5712.

59 Vysotsky, M.O., Pop, A., Broda, F., Thondorf, I. and Böhmer, V. (2001) *Chem. Eur. J.*, **7**, 4403–4410.

60 González, J.J., Ferdani, R., Albertini, E., Blasco, J.M., Arduini, A., Pochini, A., Prados, P. and de Mendoza, J. (2000) *Chem. Eur. J.*, **6**, 73–80.

61 Huerta, E., Metselaar, G.A., Fragoso, A., Santos, E., Bo, C. and de Mendoza, J.

(2007) *Angew. Chem.*, **119**, 206–209; *Angew. Chem. Int. Ed.*, **46**, 202–205.

62 (a) Martín, T., Obst, U. and Rebek, J., Jr (1998) *Science*, **281**, 1842–1845; (b) MacGillivray, L.R. and Atwood, J.L. (1997) *Nature*, **389**, 469–472.

63 DeepView/Swiss-PdbViewer, v. 3.7.: http://www.expasy.org./spdv.

64 (a) Gerkensmeier, T., Iwanek, W., Agena, C., Fröhlich, R., Kotila, S., Näther, C. and Mattay, J. (1999) *Eur. J. Org. Chem.*, **1999**, 2257–2262; (b) Cave, G.W.V., Antesberger, J., Barbour, L.J., McKinlay, R.M. and Atwood, J.L. (2004) *Angew. Chem.*, **116**, 5375–5378; *Angew. Chem. Int. Ed.*, **43**, 5263–5266.

65 Aoyama, Y., Tanaka, Y., Toi, H. and Ogoshi, H. (1988) *J. Am. Chem. Soc.*, **110**, 634–635.

66 (a) Wilson, C.F., Eastman, M.P. and Hartzell, C.J. (1997) *J. Phys. Chem. B*, **101**, 9309–9313; (b) Avram, L. and Cohen, Y. (2002) *J. Am. Chem. Soc.*, **124**, 15148–15149; (c) Shivanyuk, A. and Rebek, J., Jr (2003) *J. Am. Chem. Soc.*, **125**, 3432–3433; (d) Evan-Salem, T., Baruch, I., Avram, L., Cohen, Y., Palmer, L.C. and Rebek, J., Jr (2006)

Proc. Natl. Acad. Sci. U.S.A., **103**, 12296–12300.

67 Shivanyuk, A. and Rebek, J., Jr (2001) *Chem. Commun.*, 2424–2425.

68 (a) Shivanyuk, A. and Rebek, J., Jr (2001) *Proc. Natl. Acad. Sci. U.S.A.*, **98**, 7662–7665; (b) Philip, I. and Kaifer, A. (2005) *J. Org. Chem.*, **70**, 1558–1564.

69 Mecozzi, S. and Rebek, J., Jr (1998) *Chem. Eur. J.*, **4**, 1016–1022.

70 Beyeh, N.K., Kogej, M., Åhman, A., Rissanen, K. and Schalley, C.A. (2006) *Angew. Chem.*, **118**, 5339–5342; *Angew. Chem. Int. Ed.*, **45**, 5214–5218.

71 Dalgarno, S.J., Tucker, S.A., Bassil, D.B. and Atwood, J.L. (2005) *Science*, **309**, 2037–2039.

72 Kobayashi, K., Shirasaka, T., Horn, E., Furukawa, N., Yamaguchi, K. and Sakamoto, S. (2000) *Chem. Commun.*, 41–42.

73 (a) Ajami, D. and Rebek, J., Jr (2006) *J. Am. Chem. Soc.*, **128**, 5314–5315; (b) Ajami, D. and Rebek, J., Jr (2006) *J. Am. Chem. Soc.*, **128**, 15038–15039.

74 Atwood, J.L., Barbour, L.J. and Jerga, A. (2001) *Chem. Commun.*, 2376–2377.

4
Cucurbit[n]urils

Wei-Hao Huang, Simin Liu, and Lyle Isaacs

4.1
Introduction

This chapter focuses on the synthetic and supramolecular chemistry of the cucurbit[n]uril (CB[n]; n = number of glycoluril units) family of macrocycles. Our research in this area, which began in 1998 at the University of Maryland, has been largely driven by our efforts to understand the mechanism of CB[n] formation. The chapter is therefore organized around that theme and is illustrated by subsequently developed applications of the CB[n] family.

4.1.1
Synthesis and Structure of Cucurbit[6]uril and Decamethylcucurbit[5]uril

The cucurbituril story begins in 1905, when Behrend described the condensation of glycoluril (**1a**) with two equivalents of formaldehyde (Scheme 4.1) under aqueous acidic conditions (HCl, 100 °C) [1]. The substance formed during this reaction – referred to as Behrend's polymer in the literature – was insoluble in all common solvents but could be recrystallized from hot H_2SO_4, which yielded a well-defined substance. Although Behrend was not able to structurally characterize this substance, he did demonstrate that it forms complexes with a wide variety of species including $KMnO_4$, $AgNO_3$, and methylene blue. It was not until 1981 that Mock reported that the product of Behrend's reaction was the macrocyclic hexameric cucurbit[6]uril comprising six equivalents of glycoluril and 12 equivalents of formaldehyde [2]. During the course of this remarkable reaction, six rings and 24 bonds are formed with complete control over the disposition of the glycoluril methine C–H groups which point outward from the central cavity. It would be nearly 10 years later that Stoddart reported that the condensation of dimethylglycoluril (**1b**) with formaldehyde (two equivalents) under similar conditions yielded the first cucurbituril derivative – macrocyclic pentameric $Me_{10}CB[5]$ (Scheme 4.1) [3]. These two early
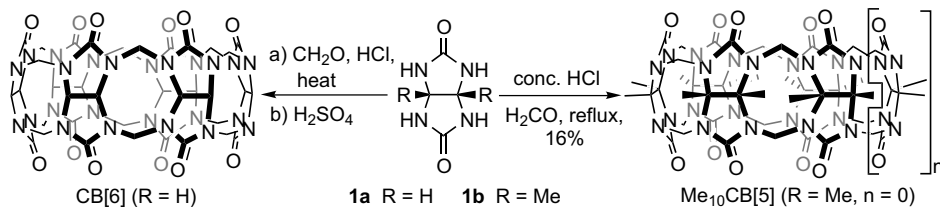
**Scheme 4.1** Synthesis of CB[6] and Me$_{10}$CB[5].

members of the cucurbit[n]uril family provided us, and several other groups, with numerous questions [4–6]:

1. What is the scope of glycoluril derivatives that can be used in the CB[n]-forming reaction?
2. Why does the CB[n]-forming reaction deliver hexameric CB[6] but pentameric Me$_{10}$CB[5]?
3. What factors are responsible for the remarkably high yield (82%) obtained for CB[6]?
4. What is the mechanism of CB[n] formation?

4.1.2
Molecular Recognition Properties of Cucurbit[6]uril

Throughout the 1980s, Mock published a series of pioneering papers that demonstrated that CB[6] has remarkable abilities as a molecular container in aqueous solution [2,7–9]. For example, he showed that pentanediamine (**2**) and hexanediamine (**3**) bind to CB[6] as their ammonium salts with values of $K_a > 10^6 \, M^{-1}$ in 40% aq. HCO$_2$H. Even more remarkable was the fact that compounds with shorter or longer spacer groups between the ammonium centers [e.g., butanediamine (**4**) or heptanediamine (**5**)] bind significantly more weakly ($K_a \approx 10^4$–$10^5 \, M^{-1}$). This high affinity and selectivity can be ascribed to the juxtaposition of three distinct binding regions: (a) two symmetry equivalent ureidyl–carbonyl lined portals that have a pronounced negative electrostatic potential and interact with cations (e.g., H$^+$, M$^+$, or RNH$_3^+$) by ion-dipole interactions and/or hydrogen bonds, and (b) a central hydrophobic cavity that has a slightly negative electrostatic potential which preferentially interacts with hydrophobic guests (Scheme 4.2). The high selectivity observed for **2** and **3** over **4** and **5** is due to the good match between the H$_3$N•••NH$_3$ separation on the guest and the C=O•••O=C separation on the host. CB[6] is also quite selective based on size and shape. For example, CB[6] binds nicely to *p*-methylaniline (**6**) but completely rejects the meta-isomer (**7**). Similarly, CB[6] readily encapsulates **8** which has a volume of 86 Å^3 but rejects the similarly sized **9** (89 Å^3). Lastly, polyammonium species like spermine (**10**) achieve very high affinity in their binding with CB[6] ($K_a = 1.3 \times 10^7 \, M^{-1}$) [8]. These high-affinity and highly selective binding events were utilized by Mock to achieve a 10^4-fold rate enhancement of a dipolar cycloaddition within the cavity [10] and in the construction of a molecular
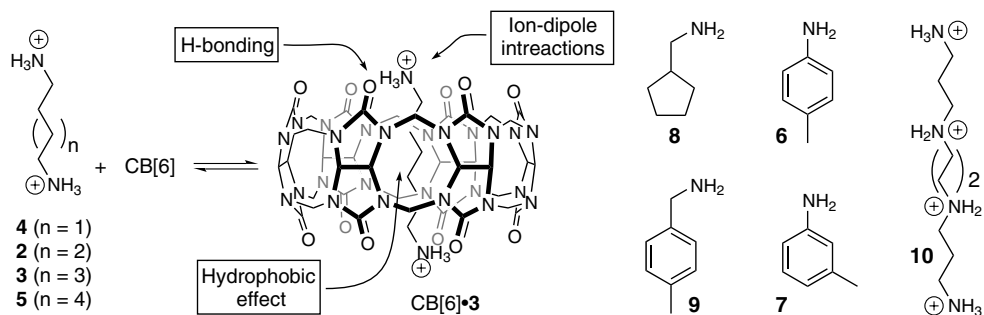
Scheme 4.2 Molecular recognition properties of CB[6].

shuttle based on changes in pH [11]. In the discussion above and in the remainder of this chapter we describe and depict the guests in the form (e.g., amine or ammonium) that was added to the aqueous solution; in nearly all cases it is the cationic ammonium form that actually binds to CB[n]. These examples convinced us that the supramolecular chemistry of CB[6], its derivatives, and it analogs would be especially well suited for the preparation of molecular machines and biomimetic systems. In 1998, therefore, we embarked on a journey to understand the mechanism of CB[6] formation, since we were confident that this would lead to the preparation of new members of the cucurbituril family with exciting new properties.

4.2
New Members of the Cucurbit[n]uril Family

This section describes the preparation of CB[n] homologs ($n = 5, 7, 8, 10$). We begin the discussion with a mechanistic hypothesis for CB[n] formation advanced by the Day and Isaacs groups [5,12].

4.2.1
Proposed Mechanism of Cucurbit[n]uril Formation

Although the CB[n]-forming reaction is remarkably complex, we sketched out a rough mechanism in 1998 and supplemented it along the way as new information became available [4,5,13,14]. Scheme 4.3 depicts our current understanding of the mechanism of CB[n] formation. Initially, glycoluril (**1a**) reacts with formaldehyde to yield methylene-bridged glycoluril dimers (**11C** and **11S**). These two compounds are diastereomers that differ in the relative orientation of the H-atoms on the convex face of the molecule. In CB[6], however, all of the methine C–H groups project outward from the center of the macrocycle similarly to **11C**. Key questions that we wished to address, therefore, were: (a) Are compounds with **11S**-type stereochemistry formed? (b) Are **11S** and **11C** in equilibrium with each other? and (c) What is the mechanism of the **11S** to **11C** interconversion? These methylene-bridged
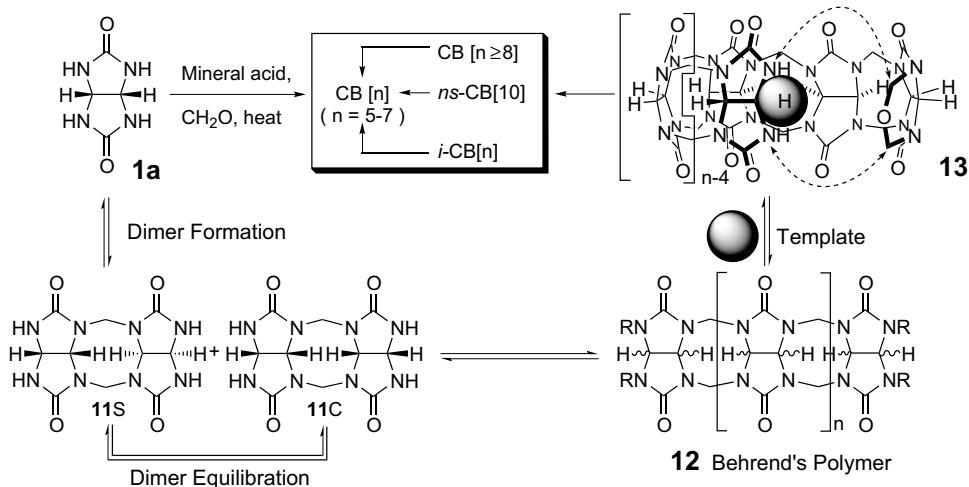
Scheme 4.3 Proposed mechanism of CB[n] formation (*i*-CB[n], inverted cucurbit[n]uril; *ns*-CB[10], bis-nor-seco-cucurbit[10]uril).

glycoluril dimers can then undergo further oligomerization to yield methylene-bridged glycoluril oligomers (e.g., trimer – decamer) as a mixture of S-shaped and C-shaped diastereomers (**12**). This mixture of oligomers has been referred to in the literature as Behrend's polymer. The mixture of oligomers can then undergo S- to C-shaped isomerization, perhaps under the influence of a templating group to yield the all C-shaped oligomer (**13**). The ends of oligomer **13** then react with one another to enter the CB[n] manifold as a mixture of CB[n] (n = 5, 6, 7, 8, 10). Through product resubmission experiments, Anthony Day demonstrated that CB[8] undergoes ring contraction to yield CB[5]–CB[7] whereas the smaller CB[n] homologs (CB[5]–CB[7]) are stable to the reaction conditions [12].

4.2.2
Synthesis and Structure of Cucurbit[n]uril Homologs (n = 5, 7, 8, 10)

The isolation of CB[n] homologs (CB[5], CB[7], and CB[8]) by the groups of Kim and Day around the turn of the millennium represented a major breakthrough in the cucurbituril field [12,15]. Figure 4.1 shows top views of CB[5]–CB[8] (drawn to scale) which illustrate the circular shape of the cavity and the gradual progression to larger cavity volumes [15,16]. In particular, the larger homologs CB[7] (279 Å^3) and CB[8] (479 Å^3) with their larger cavities which parallel those of β- and γ-cyclodextrin promise to greatly expand the range of applications to which CB[n] can be applied.

4.2.2.1 Reaction Conducted Under Milder Conditions
To access the unknown cucurbituril homologs, Kim and Day performed the CB[n]-forming reactions under milder conditions (100 °C, conc. HCl; 75 °C, 9M H$_2$SO$_4$) [12,15]. Although CB[6] is still the major component of the reaction mixture, the
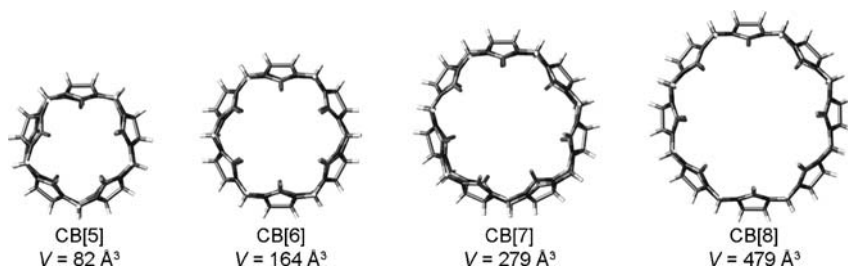
Figure 4.1 Molecular models of CB[5]–CB[8] and their calculated cavity volumes.

CB[n] homologs (CB[5], CB[7], CB[8], and CB[10]•CB[5]) can be readily isolated on the 10–100 g scale by straightforward – but time consuming – washing and recrystallization procedures that are detailed in Section 4.8.2. To date, CB[9] has not been isolated in pure form, although it has been detected as a minor component of the CB[n]-forming reaction mixture by mass spectrometry and ^{13}C NMR spectroscopy [12,15].

4.2.2.2 CB[5] Can be Released from CB[10]•CB[5] to Yield Free Cucurbit[10]uril

In addition to CB[5]–CB[8], Day and coworkers were also able to isolate CB[10] as its CB[10]•CB[5] complex (Scheme 4.4) [12,17]. Day and coworkers also demonstrated that added ^{13}C-labeled CB[5] undergoes chemical exchange with unlabeled CB[5] in the CB[10]•CB[5] complex. This observation suggested that it should be possible to remove CB[5] and isolate free CB[10] in its uncomplexed form. From our 1 kilogram scale CB[n]-forming reaction (Section 4.8.2) we were lucky enough to isolate a significant quantity of CB[10]•CB[5] and decided to try and remove CB[5]. We
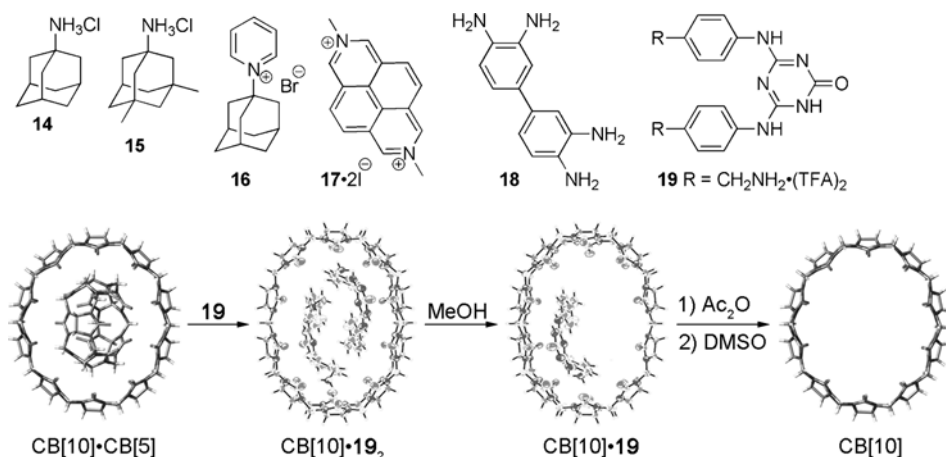
Scheme 4.4 Sequence used to remove CB[5] from CB[10]•CB[5]. The structures of CB[10]•CB[5] [17] and CB[10]•**19**$_2$ [18] are based on the X-ray crystal structures, whereas those for CB[10]•**19** and CB[10] are purely schematic representations.

discovered that some of the guests commonly used (e.g., **14–18**) to complex to the larger CB[n] ($n = 7, 8$) are capable of partially displacing CB[5] from the CB[10]•CB[5] complex. In CB[n]-binding studies, the free amines are commonly used when buffered D_2O is the solvent, whereas the more soluble hydrochloride salts are employed when applications demand the use of D_2O. Unfortunately, in many cases, all of the components (CB[5], excess guest, and CB[10]•guest) remained in solution, which complicated the isolation of the CB[10]•guest complex. We discovered that addition of excess guest **19** to CB[10]•CB[5] results in the formation of the soluble CB[10]•**19**$_2$ complex and precipitation of the (CB[5]•**19**)$_n$ supramolecular polymer (Scheme 4.4) [18]. The pure CB[10]•**19**$_2$ complex is isolated by filtration and rotary evaporation. Removal of the less strongly bound second equivalent of **19** occurs readily by washing with MeOH, which yields CB[10]•**19**. The final equivalent of **19** can be removed by heating with acetic anhydride, which transforms the ammonium groups into acetamides, followed by washing (DMSO, MeOH, H_2O). Uncomplexed CB[10] has a cavity volume of approximately 870 Å^3 and is poorly soluble in water and mildly acidic solution. Fortunately, its complexes have good solubility in D_2O, which allowed us to study its molecular recognition properties (Section 4.3.5).
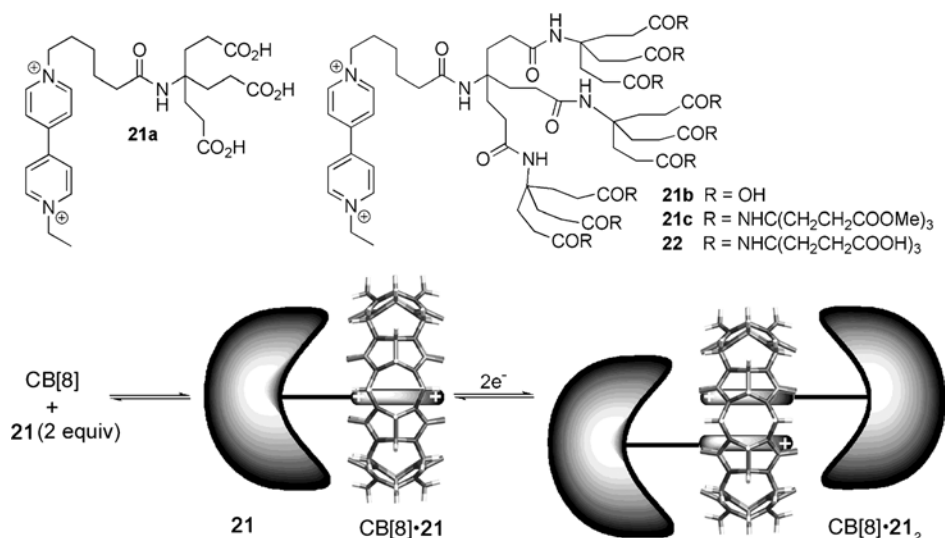
4.3
Applications of Members of the Cucurbit[n]uril Family

The early work of Mock on the recognition properties of CB[6] established that this macrocycle was amongst the tightest binding and most selective synthetic hosts in aqueous solution [2,7–9]. Subsequent work from our group demonstrated that the high affinity and selectivity translates to *individual* host-guest complexes of CB[7] and CB[8]. Even more impressively, the selectivity of a single guest toward CB[6], CB[7], and CB[8] can be remarkably large ($>10^4$) [19]. These, and related observations [20,21], suggested to us and others that CB[n] would function as smart components in a variety of applications that are described in this section.

4.3.1
Preparation of Molecular Switches

Compounds that function as molecular switches exist in two stable forms and can be reversibly switched between those two forms by application of a given stimulus (e.g., pH change, electrochemical, photochemical, or chemical). A particularly interesting molecular switch based on the triaminofluorene compound **20** was reported by Kim in 2000 (Scheme 4.5) [22]. When CB[6] is added to **20**$^{3+}$ in pH 1.0 solution, rotaxane CB[6]•**20**$^{3+}$ is formed where the CB[6] bead resides on the longer hexylene spacer in order to maximize both ion-dipole interactions and hydrophobic binding. In this form, the anilinium *N*-atom is protonated and the fluorene chromophore is highly fluorescent. When the pH is raised (8.0), however, the anilinium *N*-atom is deprotonated and the CB[6] macrocycle slides over to the butylene spacer to maintain two ion-dipole interactions while sacrificing some hydrophobic driving force. In this

CB[6]•**20**$^{3+}$ (Yellow, fluorescent)   CB[6]•**20**$^{2+}$ (Violet, non-fluorescent)

Scheme 4.5 A pH-responsive molecular switch that signals by color and fluorescence changes.

new complex (CB[6]•**20**$^{2+}$), the aniline *N*-atom is conjugated to the fluorene ring and the complex has a violet color; the *N*-atom also quenches the fluorescence output of the system. Upon lowering the pH, the CB[6] bead again switches back to the original location. Thus, CB[6] acts as a pH-controlled molecular switch with both UV/Vis and fluorescent output.

4.3.2
Self-Assembled Dendrimers

The ability of members of the CB[n] family to bind tightly to their guests has been used by the groups of Kaifer [23,24] and Kim [25] to modify the properties of dendrons containing guests at their focal points and to bring two or more dendrons together to create a self-assembled dendrimer. For example, Kaifer synthesized 1st, 2nd, and 3rd generation Newkome-type dendrons **21a–21c** containing viologen units at the focal point (Scheme 4.6) [23]. UV/Vis titrations allowed Kaifer to demonstrate that the association constant for the formation of the binary complex CB[8]•**21** decreases as the generation of the dendrimer increases. The electrochemical behavior was even more interesting. Upon reduction the viologen is transformed from its dicationic to its monocationic form, which subsequently induces dimerization inside CB[8] yielding ternary complex CB[8]•**21**$_2$ as evidenced by changes in the UV/Vis spectrum. Interestingly, CB[8]•**22** did not form CB[8]•**22** upon reduction, presumably because of unfavorable electrostatic interactions. The dramatic change in size of the ternary complex was also determined by measurement of its diffusion constant by pulsed field gradient NMR techniques. No dimerization is observed in the absence of CB[8]. This beautiful example demonstrates proof-of-concept for redox-switchable dendrimer self-assembly.

4.3.3
Preparation of Molecular Machines

The Kim group has capitalized on the ability of CB[8] to simultaneously bind two aromatic rings in the construction of a variety of molecular machines [26,27]. A

Scheme 4.6 Electrochemical control of dendrimer assembly.

recent and particularly elegant example is the construction of a molecular loop lock (Scheme 4.7) [27]. They found that the interaction of CB[8] with 23^{3+} leads to the folded conformation of CB[8]•23^{3+} (Scheme 4.7), which benefits from intramolecular charge transfer interaction between the electron-rich naphthalene and electron-poor viologen units. The addition of one equivalent of methylviologen (24^{2+}) does not result in a change in conformation of CB[8]•23^{3+}, presumably because 24^{2+} binds less strongly than the intramolecularly held viologen unit. Very interestingly, however, upon reduction of the solution of the mixture of CB[8]•23^{3+} and 24^{2+} with $Na_2S_2O_4$, the equilibrium shifts toward the unfolded ternary complex CB[8]•23^{2+}•24^{+}. This ternary complex benefits from the enhanced π-π interactions, as evidenced by the appearance of new bands at 368, 550, and 890 nm in the UV/Vis spectrum of the viologen radical-cation dimer. The system is fully reversible between the CB[8]•23^{2+}•24^{+} and CB[8]•23^{3+} states by exposing the system to molecular
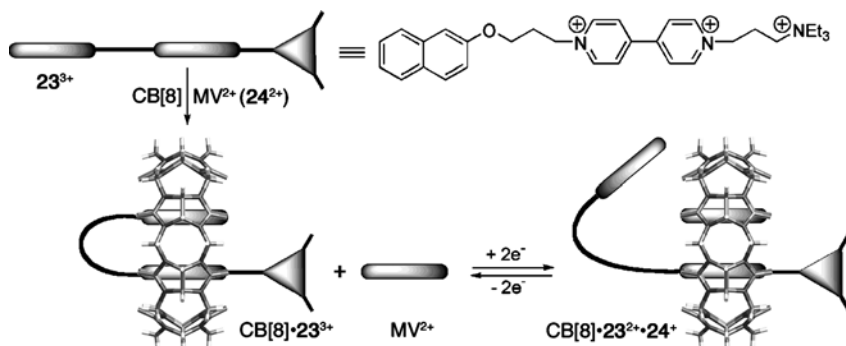
**Scheme 4.7** A molecular loop lock that responds to chemical and redox stimuli.

oxygen (O_2). This system may be regarded as a safeguarded molecular loop lock in that it requires not only the addition of **24**$^{2+}$, but also the application of a redox stimulus ($Na_2S_2O_4$ or O_2) to open or close the lock.

4.3.4
Preparation of Complex Self-Sorting Systems

Mock has shown that CB[6] undergoes tight and selective binding with cationic guest molecules in aqueous solution [8]. Our investigations of complex (e.g., 12-component) self-sorting mixtures which utilized CB[6] and CB[8] as components suggested that the binding strengths (K_a) and selectivities might be even higher than previously appreciated [20]. To provide quantitative evidence for this hunch, we measured the binding constants for CB[6], CB[7], and CB[8] toward a variety of guests by ^{1}H NMR competition experiments [19]. We found that values of K_a ranged between 10^2–10^{12} M^{-1} and moreover that selectivities could be exceedingly large ($>10^3$) in response to small structural changes. For example, CB[8] binds **19** 3250-fold tighter than CB[7] and induces a folding process at the same time (Scheme 4.8). Similarly, CB[7] binds **14** 5150-fold tighter than CB[8] because of an excellent size, shape, and electrostatic match between host and guest.

In addition to the high affinity and selectivity, members of the CB[n] family can exhibit unusual dynamics of complex association and dissociation [9,21,28]. We used the high binding affinities, high selectivities, and unusual dynamics to construct a system that undergoes well-defined transitions from free components, to one set of aggregates under kinetic control, to a second set of aggregates under thermodynamic control (Scheme 4.9). For example, when a solution of CB[6] and CB[7] is mixed
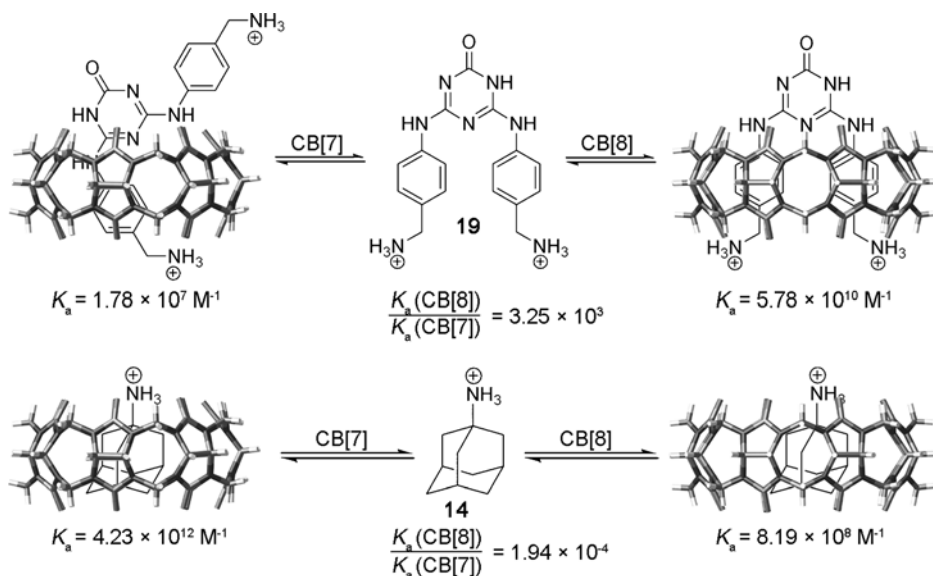

Scheme 4.8 High-selectivity binding within CB[n].
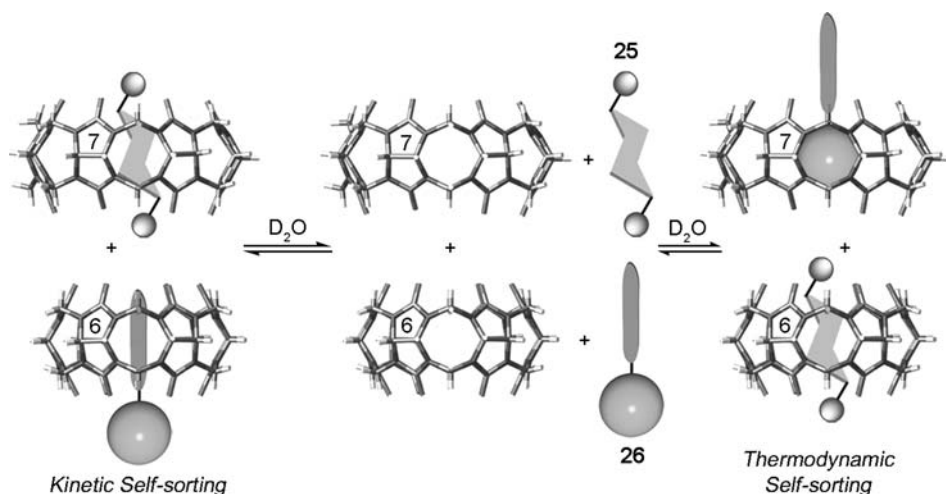
Scheme 4.9 Kinetic versus thermodynamic self-sorting using two-faced guests.

with a second solution containing guests **25** and **26** the components initially associate to form CB[6]•**26** and CB[7]•**25**. In this process, **25** undergoes fast kinetically controlled association with CB[7] in preference to CB[6] to form CB[7]•**25**. Subsequently, **26** – which we refer to as a two-faced guest since it contains two binding epitopes – uses its slimmer alkylammonium binding epitope to associate with CB[6]. This kinetically controlled self-sorting state comprising CB[6]•**26** and CB[7]•**25** slowly transforms over the course of 56 days into the thermodynamic self-sorting state comprising CB[6]•**25** and CB[7]•**26**.
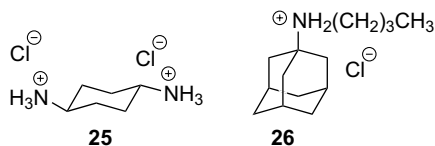
### 4.3.5
Allosteric Control of the Conformation of a Calix[4]arene Inside CB[10]

After we synthesized CB[10] we wanted to investigate its abilities as a host molecule. We found that CB[10] forms host-guest complexes with many of the guests typically used with the smaller members of the CB[n] family (e.g., ammonium salts of alkyl and arylamines, adamantanes, viologens, and ferrocene derivatives like **14–19**).

We discovered that CB[10] was also capable of forming a complex with cationic calix[4]arene **27**, which itself usually functions as a host molecule in aqueous solution (Scheme 4.10) [18]. Interestingly, when **27** is incorporated inside CB[10], two sets of resonances are observed which were in slow exchange on the NMR
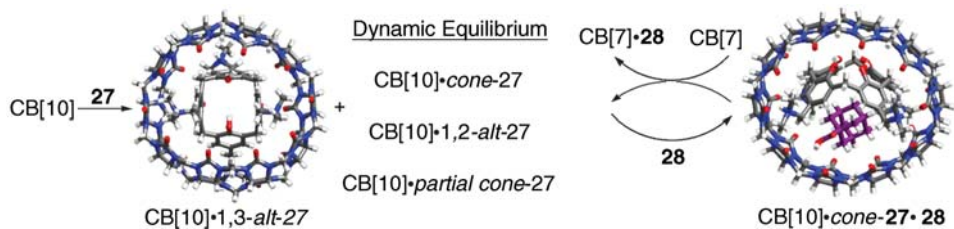
**Scheme 4.10** Allosteric control of the macromolecular conformation inside CB[10].

time scale. The major set of resonances corresponds to the CB[10]•1,3-*alt*-**27** conformer, whereas the minor set of resonances corresponds to a dynamic equilibrium between CB[10]•1,2-*alt*-**27**, CB[10]•*partial cone*-**27**, and CB[10]•*cone*-**27** conformations. Scheme 4.10 shows the MMFF calculated geometry of the CB[10]•1,3-*alt*-**27** conformation, which shows a good match between the circular shape of 1,3-*alt*-**27** and the cavity of CB[10]. We wondered whether it would be possible to stabilize one of the other three conformers of the macromolecular CB[10]•**27** complex by the addition of a guest molecule. After some experimentation, we found that adamantane carboxylic acid **28** is capable of shifting the equilibrium toward the CB[10]•*cone*-**27**•**28** complex. In this ternary complex, the calixarene **27** assumes the *cone*-conformation in order to maximize non-covalent interactions with **28**. The *cone*-**27**•**28** complex in turn binds within CB[10]. In the MMFF-computed conformation of CB[10]•*cone*-**27**•**28**, we once again saw a good match between the overall size, shape, and electrostatic complementarity between the cone-**27**•**28** complex and the cavity of CB[10]. To complete the cycle of allosteric control of conformation within CB[10], we added CB[7], which binds tightly to **28** forming CB[7]•**28** and switches the conformation of calix[4]arene **27** back to the original mixture of CB[10]•**27** conformers. This result demonstrated that CB[10] has great potential in controlling the conformation of non-natural macromolecular complexes.
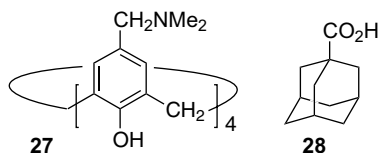
4.3.6
As a Carrier of Anti-Cancer Agents

One of the potential uses of any molecular container compound is in the formulation of active pharmaceutical agents. Accordingly, the groups of Kim [29] and Day [30] have demonstrated the ability of CB[7] and CB[8] to modify the properties of Pt-based anti-cancer agents (Scheme 4.11). For example, Kim's group reported that CB[7] forms a 1:1 complex with oxaliplatin (CB[7]•**29**). They found that encapsulation of the drug
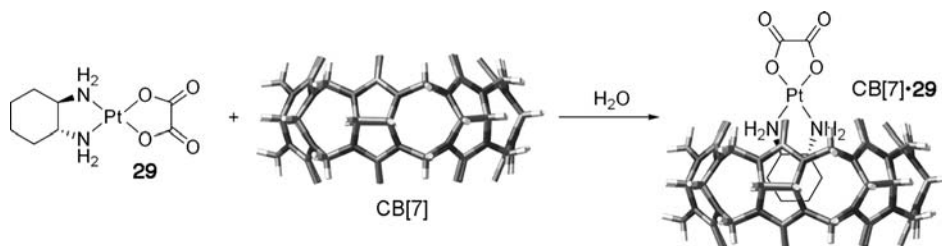
Scheme 4.11 Complexation of oxaliplatin **29** within CB[7].

within CB[7] resulted in a dramatic increase in its lifetime (e.g., 6 h versus >1 year). Furthermore, CB[7]•**29** showed markedly decreased reactivity toward L-methionine as a protein model relative to its reactivity toward guanosine as a DNA model. This result suggested that encapsulation of **29** within CB[7] may reduce unwanted side effects caused by protein binding of the drug.

4.4
Experimental Support for the Proposed Mechanism of CB[n] Formation

Although none of the applications of the CB[n] family described in Section 4.3 were known in 1998 when we began our work in the area, they provide post-facto support for our assertion that a firm knowledge of the mechanism of CB[n] formation would be important. This section describes our work with S- and C-shaped methylene-bridged glycoluril dimers that provided insight into the early steps of the mechanism of CB[n] formation.

4.4.1
S-shaped and C-shaped Methylene-bridged Glycoluril Dimers

The high level of complexity of the CB[n]-forming reaction led us to initially study S-shaped and C-shaped methylene-bridged glycoluril dimers (**11C** and **11S**, Scheme 4.3). This section details the lessons learned from those model studies.

4.4.1.1 Synthesis of Methylene-bridged Glycoluril Dimers
Although we wanted to study methylene-bridged glycoluril dimers **11C** and **11S**, we were mindful of the fact that the presence of four free ureidyl NH groups and the absence of solubilizing groups on the convex face of the glycoluril skeleton might lead to poor solubility characteristics. Thus, in accord with the precedent of the Nolte and Rebek groups, we decided to target compounds whose NH-groups were "protected" by o-xylylene groups and that contain solubilizing substituents on their convex face [31]. Although we have investigated this reaction in detail, the bare essence of the process is presented in Scheme 4.12. In brief, we discovered three pathways to methylene-bridged glycoluril dimers that each occured in refluxing dichloroethane containing p-toluenesulfonic acid with azeotropic removal of water.
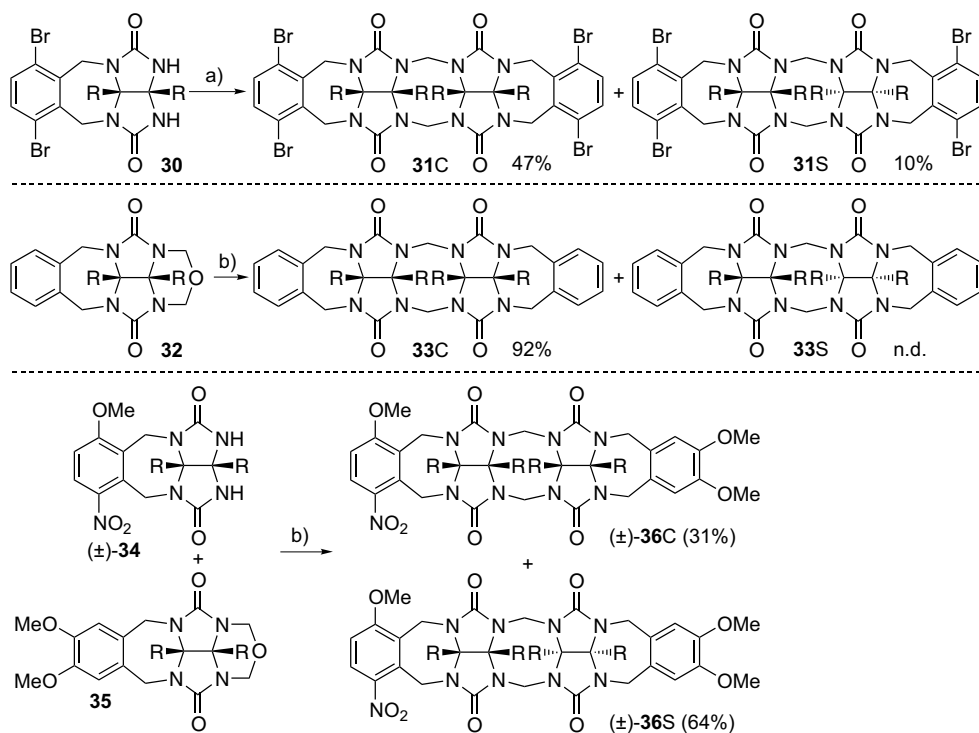
Scheme 4.12 Synthesis of S- and C-shaped methylene-bridged glycoluril dimers. R = CO$_2$Et. Conditions: (a) PTSA, (CH$_2$O)$_n$, ClCH$_2$CH$_2$Cl, reflux; (b) PTSA, ClCH$_2$CH$_2$Cl, reflux (n.d. = not detected).

The first method involves the homodimerization of glycoluril NH-compounds (e.g., **30**) with CH$_2$O and delivers both **31**C and **31**S. The second involves the homodimerization of glycoluril cyclic ethers (e.g., **32**), which occurs with formal extrusion of formaldehyde and selectively delivers **33**C (**33**S not detected). The third involves heterodimerization of a glycoluril NH-compound [e.g., (±)-**34**] with a glycoluril cyclic ether (e.g., **35**), which delivers a mixture of (±)-**36**C and (±)-**36**S. In this example of heterodimerization, the unsymmetrical substitution on the aromatic ring renders (±)-**34**, (±)-**36**C, and (±)-**36**S chiral and racemic. All three reactions occur in good to high yield and generally deliver the C-shaped diastereomers selectively. All three reactions are tolerant of substitution on the convex face of the glycoluril units (e.g., R = Ph, (CH$_2$)$_4$, CO$_2$Et, CO$_2$H, imide) and substitution on the *o*-xylylene rings (e.g., OMe, CH$_3$, Br, NO$_2$, F). Interestingly, the heterodimerization reaction allows the selective preparation of C-shaped methylene-bridged glycoluril dimers (e.g., **36**C) containing differentially functionalized aromatic rings. These three methods not only allow us to prepare a wide variety of methylene-bridged glycoluril dimers for studies of self-assembly; they also suggest methods for

the tailor-made synthesis of partially substituted CB[n] from appropriate glycoluril building blocks (Section 4.4.2).

4.4.1.2 S- to C-shaped Isomerization of Methylene-bridged Glycoluril Dimers

In our synthesis of methylene-bridged glycoluril dimers (Section 4.1), we were somewhat surprised that only very small amounts of the S-shaped diastereomers were observed in most cases. To determine whether this diastereoselectivity was due to thermodynamic or kinetic preferences we isolated diastereomerically pure samples of six C-shaped and S-shaped compounds and separately resubmitted them to the reaction conditions. Scheme 4.13 shows the separate isomerization of **37**C and **37**S. We found that both the C-shaped and S-shaped forms delivered an equilibrium mixture of S-and C-shaped forms in which the C-shaped form predominates (∼95:5) for a variety of compounds. This result established that the C-shaped form is thermodynamically more stable than the S-shaped form by ∼2 kcal mol^{-1} and provided a rationale for the high yield observed in the formation of CB[6], which presumably required all C-shaped oligomers. To delve deeper into the origin of this thermodynamic preference we performed the equilibration of **37**C and **37**S in a variety of solvents (e.g., CHCl$_3$, CCl$_4$, C$_6$F$_6$, THF, CH$_3$CN, ClCH$_2$CH$_2$Cl, CH$_3$NO$_2$, MeOCH$_2$CH$_2$OMe). The C-shaped to S-shaped ratio remained high (>90:10) across this series, which indicated that solvation was not a key factor determining the thermodynamic preference for the C-shaped form. We also ruled out the possibility that PTSA acted as a template by selectively engaging in π-π interactions with the cavity of the C-shaped form. Currently, we believe that the C-shaped form is more stable because of the conformational preference of the newly formed 8-membered ring for the crown conformation [32].

4.4.1.3 Mechanism of S- to C-shaped Isomerization

The selective heterodimerization of glycoluril NH-compounds and glycoluril cyclic ethers (Section 4.4.1.1) and the general preference for the C-shaped diastereomers suggested that the mechanism of S-shaped to C-shaped equilibrium might proceed by an intramolecular rather than an intermolecular process under anhydrous acidic
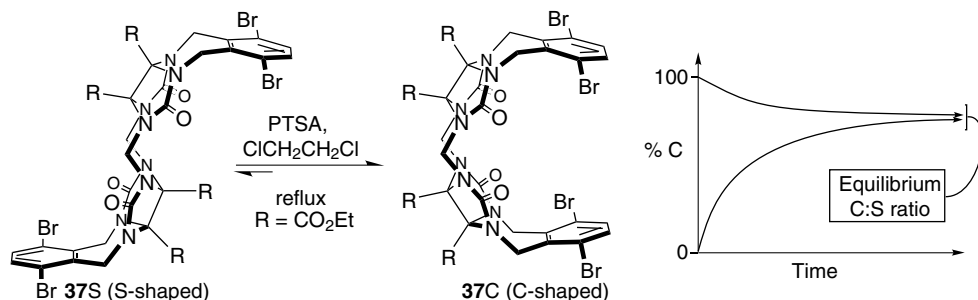
Scheme 4.13 Equilibration of **37**C and **37**S.
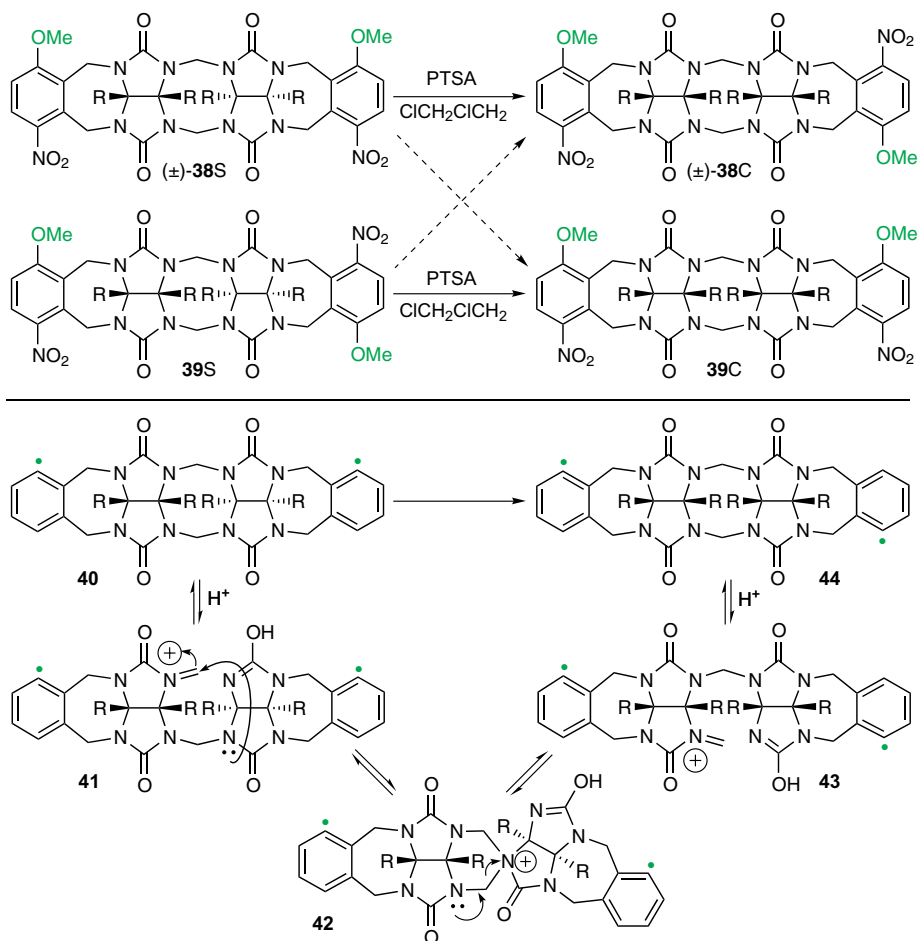
Scheme 4.14 Mechanism of diastereoselective intramolecular isomerization of S- to C-shaped compounds.

conditions (e.g., PTSA, ClCH$_2$CH$_2$Cl, reflux). To test this hypothesis, we designed a "double-labeling" experiment that utilized (±)-**38** and **39** (Scheme 4.14). In the equilibration of chiral but racemic (±)-**38**S, for example, one might expect to obtain either (±)-**38**C or **39**, or potentially a mixture of both [5]. Similarly, the equilibration of **39**S might deliver either (±)-**38**C or **39**, or both. In the experiment, we observe that (±)-**38**S cleanly delivers the chiral but racemic (±)-**38**C whereas the achiral meso compound **39**S cleanly delivers the achiral meso compound **39**C. This result indicates that the transformation of S- to C-shaped methylene-bridged glycoluril dimers is an *intramolecular process* under *anhydrous acidic conditions* that proceeds via retention of configuration of the two glycoluril "halves". Scheme 4.14 also shows a proposed mechanism that tracks the position of the labels (green dots). Initially, **40**

undergoes protonation and ring opening to yield iminium ion **41**. Iminium ion **41** can undergo ring closure by nucleophilic attack of the glycoluril *N*-atom to yield spirocyclic intermediate **42**, which can fragment in the opposite direction to yield iminium ion **43**. Subsequent ring closure of **43** followed by deprotonation gives **44**, which rationalizes the experimental results.

4.4.1.4 Implications for the Synthesis of Cucurbit[n]uril Analogs and Derivatives

The results presented in Sections 4.4.1.1–4.4.1.3 provide insight into the mechanism of CB[n] formation. For example, the isolation of the S-shaped diastereomers provides strong evidence that both **11**S and **11**C form in the initial stages of the CB[n]-forming reaction. The strong preference for the C-shaped diastereomers (>90:10) provides a rationale for the high yield obtained in the synthesis of CB[6] [33]. A simple calculation suggests that in a worst case scenario 53% (0.9^6) of the linear glycoluril hexamers would exist as the all C-shaped diastereomer required to form CB[6]. In addition, the intramolecular nature of the S-shaped to C-shaped equilibration suggests that the length of the growing methylene-bridged glycoluril oligomer chain (**13**, Scheme 4.3) determines the size (e.g., n) of the CB[n] formed. When considered together with highly selective heterodimerization reactions, these results further suggest that the pattern of substituents on the surface of the growing methylene-bridged glycoluril oligomer will be preserved in the CB[n] derivatives that are formed. As a specific example, we predicted that heating a combination of **1a** and bis(cyclic ether) **45a** under anhydrous acidic conditions (e.g., PTSA or MeSO₃H) would deliver the hexa-substituted CB[6] derivative **46a** (Scheme 4.15) [5]. Although this reaction did not yield the desired product **46a** (R = CO₂Et) because of substituent effects, the predictions made above were subsequently borne out in the synthesis of CB[n] derivatives (e.g., **46b**, R = Me) and CB[n] analogs (Sections 4.4.2 and 4.4.3).

4.4.2
Building-Block Approach to Cucurbit[n]uril Analogs

We hypothesized that the reaction depicted in Scheme 4.15 did not proceed smoothly in practice because the CO₂Et-groups on the convex face of the glycoluril reduce its reactivity (sterically and electronically) relative to the unsubstituted glycoluril **1a**. To

1a	**45a** R = CO₂Et	**46a** (EtO₂C)₆CB[6]
	45b R = Me	**46b** Me₆CB[6]
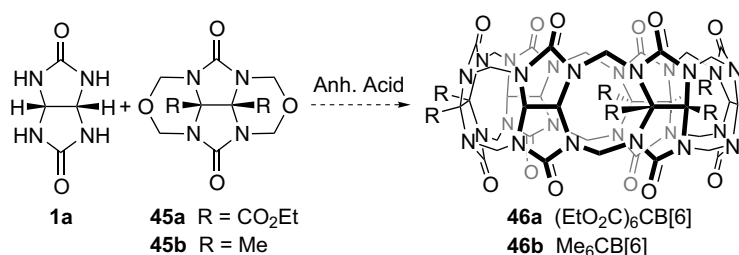
**Scheme 4.15** Predicted synthesis of CB[n] derivatives.
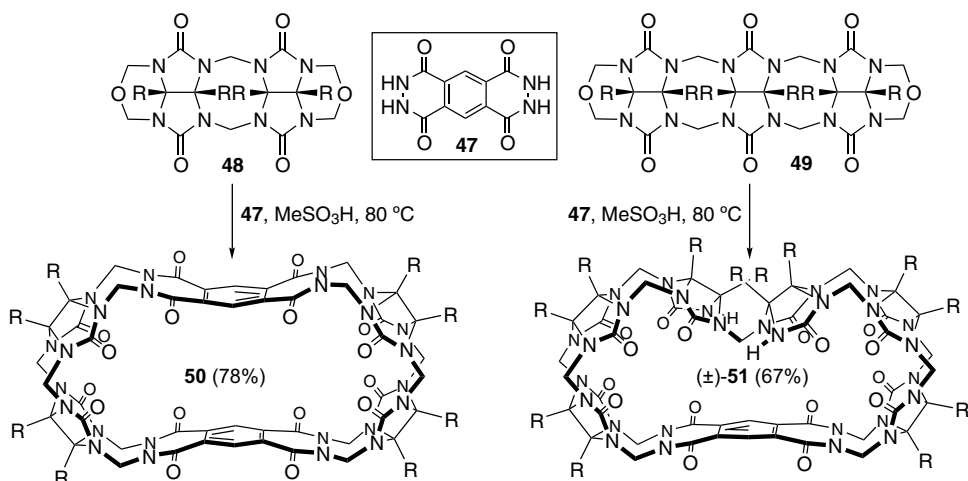
Scheme 4.16 Synthesis of CB[n] analogs. R = CO$_2$Et.

circumvent this issue we decided to search for a glycoluril analog that might participate efficiently in heterodimerization reactions with compounds like **45** to yield CB[n] analogs. With a little bit of luck we discovered that phthalhydrazides are superior nucleophiles – presumably because of the α-effect – that undergo selective hetero-dimerization with glycoluril cyclic ethers under anhydrous acidic conditions [34–36]. Specifically, bis(phthalhydrazide) **47** was found to undergo separate macrocyclization with dimeric **48** and trimeric **49** to yield CB[n] analogs (**50** and (±)-**51**) in remarkably high yield (Scheme 4.16). These macrocycles incorporate the UV/Vis, fluorescent, and electrochemically active bis(phthalhydrazide) walls, and the carboxylic acid version of **50** can be used as a fluorescent sensor in aqueous solution [36]. Compound (±)-**51** was particularly intriguing since the presence of two free ureidyl NH-groups and the twisted connection between the tips of the two glycoluril trimer building blocks **49** imparts C_2-symmetry to the macrocycle and renders (±)-**51** chiral and racemic. Compound (±)-**51** is the only chiral member of the CB[n] family known to date.

4.4.3
Building-Block Approach to Cucurbit[n]uril Derivatives

Concurrent with the synthesis of the CB[n] analogs, the groups of Day and Tao were also pursuing a building-block approach toward CB[n] derivatives [37,38]. For example, Day was able to isolate Me$_6$CB[6] (**46b**) from the reaction of **1a** and **45b** using aqueous acidic reaction conditions (Scheme 4.15). An elegant example of a building-block approach toward CB[n] derivatives was realized by reacting the unsubstituted methylene-bridged glycoluril dimer **52** with cyclic ether **45b**, which delivered the tetra-substituted CB[6] derivative Me$_4$CB[6] in 30% yield (Scheme 4.17). Quite interestingly, Me$_4$CB[6] has an ellipsoidal shape which binds aromatic compounds with a common orientation of the long axes of both host and guest [38].
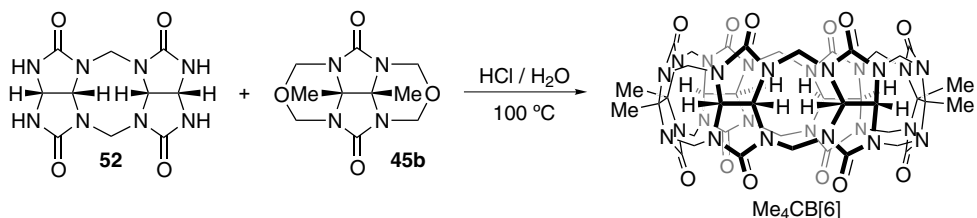
Scheme 4.17 Synthesis of Me₄CB[6].

4.4.4
Identification and Isolation of Inverted Cucurbit[n]urils (n = 6, 7)

The preferred – but not exclusive – formation of C-shaped methylene-bridged glycoluril dimers provided a rationale for the observed high yields in CB[n]-forming reactions. Conversely, those same experiments can also be interpreted as suggesting the possibility of diastereomeric CB[n]. Such diastereomeric CB[n], in which one or more pairs of glycoluril H-atoms point into the central CB[n] cavity, are referred to as inverted CB[n] (*i*-CB[n]). The first members of the *i*-CB[n] family were discovered by the groups of Isaacs and Kim and investigated jointly (Scheme 4.18) [13]. *i*-CB[6] and *i*-CB[7] are formed in small amounts in the CB[n]-forming reaction and can be detected in the ¹H NMR spectrum of the mixture by diagnostic resonances for the inverted H-atoms (∼5 ppm, see below). Pure *i*-CB[6] and *i*-CB[7] could be isolated in low yield (2.0 and 0.4%) by a combination of fractional recrystallization and gel permeation chromatography. Scheme 4.18 also shows the X-ray crystal structures of *i*-CB[6] and *i*-CB[7] and their electrostatic potential energy surfaces. The
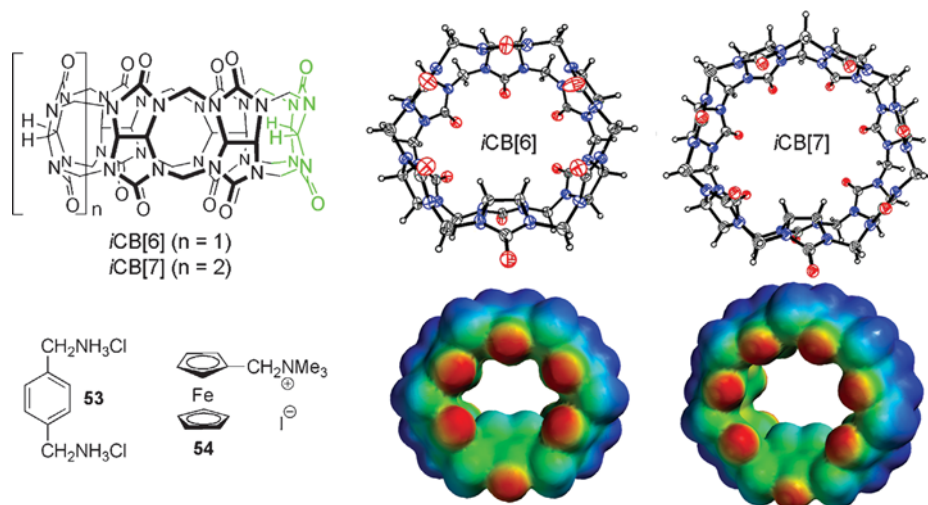
Scheme 4.18 Chemical structures, X-ray crystal structures, and electrostatic potential maps for *i*-CB[6] and *i*-CB[7].

consequences of the inverted glycoluril ring are reduced cavity volumes, flattened ellipsoidal-shaped cavities, more positive intra-cavity electrostatic potentials, and more open C=O lined portals. In accord with these considerations, *i*-CB[6] and *i*-CB[7] preferentially bind ellipsoidal and electrostatically negative aromatic guests like *p*-xylylene diamine (**53**) and ferrocene derivative **54**. Overall, the inverted glycoluril modulates the guest binding affinity and rates of dissociation in a way that might be useful in the creation of functional CB[n]-based systems.

4.5
Direct Functionalization of Cucurbit[n]urils

One of the major challenges in CB[n] chemistry is the poor solubility of CB[n] in neutral water and far worse solubility in organic solvents. A potential solution to this problem that has been pursued by several groups involves the preparation of CB[n] derivatives or analogs that contain solubility-enhancing functional groups on the convex face of the macrocycle. This strategy is easier to propose than to execute, and the sections above detail some of the challenges of using glycoluril derivatives in CB[n]-forming reactions. Perhaps the most onerous issue to be addressed in such a route is the modification of the separation scheme for each new CB[n] derivative. An alternative approach to the preparation of CB[n] derivatives is the direct functionalization of pure, unfunctionalized CB[n].

4.5.1
Perhydroxylation and Further Derivatization of CB[5]–CB[8]

Kim and coworkers addressed a major issue in CB[n] chemistry with their discovery of a method for direct functionalization [39]. They found that heating CB[5], CB[6], CB[7], or CB[8] with $K_2S_2O_8$ in water resulted in the perhydroxylation of CB[n] ($n = 5$–8) yielding $(HO)_{2n}CB[n]$ in modest to low yield (Scheme 4.19). Furthermore, the $(HO)_{2n}CB[n]$ had excellent solubility in DMSO and DMF, which allowed for subsequent functionalization. For example, $(HO)_{2n}CB[n]$ ($n = 5$, 6) underwent re-action with NaH and allyl bromide in DMSO to yield $(H_2C=CHCH_2O)_{2n}CB[n]$ in good yields. $(H_2C=CHCH_2O)_{2n}CB[n]$ ($n = 5$, 6) undergo photochemical addition

CB[n] $\xrightarrow{\text{a)}}$ (HO)$_{2n}$CB[n]

(HO)$_{10}$CB[5] (42%)
(HO)$_{12}$CB[6] (45%)
(HO)$_{14}$CB[7] (5%)
(HO)$_{16}$CB[8] (4%)

R$_{2n}$CB[n]

$n = 6$ R = OH

$n = 5, 6$ R = OCH$_2$CH=CH$_2$

$n = 5, 6$ R = O(CH$_2$)$_3$S(CH$_2$)$_7$CH$_3$

$n = 6$ R = O(CH$_2$)$_3$S(CH$_2$CH$_2$O)$_3$CH$_3$

b)
c)
d)
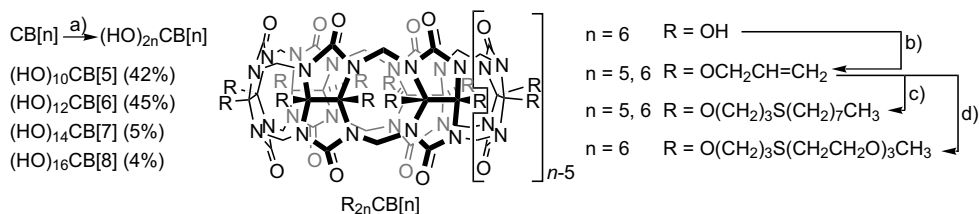
Scheme 4.19 Direct functionalization of CB[n]. Conditions: (a) $K_2S_2O_8$, H_2O, 85°C; (b) NaH, DMSO, allyl bromide; (c) $CH_3(CH_2)_7SH$, hν; (d) PEG-thiol, hν.

of thiols (e.g., $CH_3(CH_2)_7SH$ or $CH_3[O(CH_2)_2]_3SH$) to yield the highly lipophilic $\{CH_3(CH_2)_7S(CH_2)_3\}_{2n}CB[n]$ and $\{CH_3[O(CH_2)_2]_3S(CH_2)_3\}_{2n}CB[n]$.

4.5.2
Multivalent Binding of Sugar-Decorated Vesicles to Lectins

The study of vesicles is an area of wide interest largely because of their potential use in the areas of drug and gene delivery, biomimetic systems, and in the preparation of nanostructured materials. Kim's group discovered that the amphiphilic CB[6] derivative $\{CH_3[O(CH_2)_2]_3S(CH_2)_3\}_{2n}CB[6]$ formed vesicles of 170 ± 50 nm diameter as evidenced by transmission electron microscopy (**55**, Scheme 4.20) [40]. When they were prepared in a solution containing sulforhodamine G and purified by gel permeation chromatography, the vesicles showed bright fluorescence, which demonstrates their low permeability. The efficient non-covalent derivatization of the exterior of vesicles **55** was possible simply by the addition of the spermine-fluorescein conjugate **56** to yield **55•56$_n$**. Conjugate **56** was bound strongly to the cavities of the CB[6] derivatives on the surface of the vesicles by the hydrophobic effect and ion-dipole interactions as evidenced by ^1H NMR spectroscopy and confocal microscopy. This vesicle scaffold could also be used for the multivalent display of α-mannose groups tagged with a spermine tail. These α-mannose-derived vesicles were capable of aggregating concanavalin A by biospecific interactions between the sugar and the lectin. The potential for the introduction of multiple tags onto a single vesicle suggested a route toward the targeted delivery of pharmaceutical agents.

4.5.3
Cucurbit[n]uril-based Artificial Ion Channels

One of the major issues that has faced the development of applications of the CB[n] family – which has partially faded with Kim's direct functionalization route – is poor solubility in organic solvents. To improve the solubility in organic solvents and in
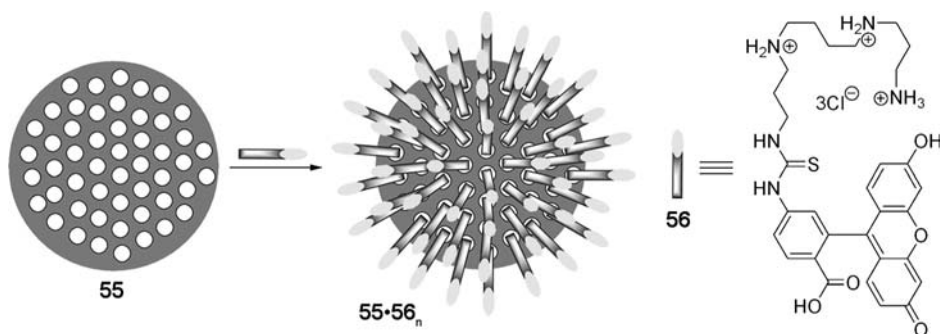
Scheme 4.20 Decoration of supramolecular vesicles with fluorescent labels.
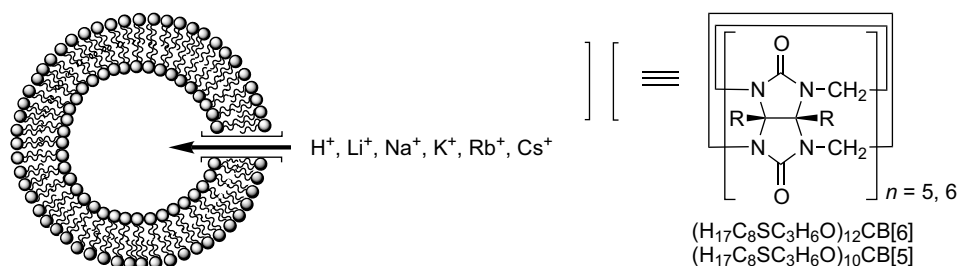
Scheme 4.21 Preparation of artificial ion-channels with CB[5] and CB[6] derivatives.

lipid membranes, Kim and coworkers attached long alkyl chains to the outside of CB[5] and CB[6] as described above [39]. They found that $\{CH_3(CH_2)_7S(CH_2)_3\}_{2n}$ CB[n] ($n = 5$, 6) could be incorporated into large unilamellar vesicles (LUVs) comprising egg yolk L-α-phosphatidyl-choline (EYPC), cholesterol, and dicetyl phosphate (Scheme 4.21) [41]. The flux of protons and alkali metal cations across the membrane could be quantified by following the fluorescence intensity (I_{460}/I_{403}) of 8-hydroxypyrene-1,3,6-trisulfonate (HPTS), which functions as a pH-sensitive dye. Interestingly, the order of transport activity across LUVs containing $\{CH_3(CH_2)_7S(CH_2)_3\}_{2n}CB[n]$ was $Li^+ > Cs^+ \approx Rb^+ > K^+ > Na^+$, which is opposite to the binding affinity of CB[6] toward alkali metal cations. Somewhat surprisingly, planar bilayer conductance measurements show that the ion transport occurs by a channel rather than a carrier mechanism. The ion-channel properties of $\{CH_3(CH_2)_7S(CH_2)_3\}_{12}CB[6]$ could be switched off by the addition of acetylcholine (Me$_3$NCH$_2$CH$_2$OAc, **57**) which binds in the cavity of the CB[6] derivative. The CB[6] derivative $\{CH_3(CH_2)_7S(CH_2)_3\}_{2n}CB[n]$ permits remarkably fast transport of Cs^+ across the membrane (~ 5 pA $\approx 3 \times 10^7$ ions s^{-1}), which is comparable to that observed for gramicidin. By using synthetic chemistry to tailor the structure and solubility of CB[n] and its derivatives, it is possible to expand the range of applications to which the CB[n] family can be applied!

4.6
Nor-Seco-Cucurbit[10]uril

Our model studies using the methylene-bridged glycoluril dimers allowed us to shed light on the initial steps in the CB[n]-forming reaction (see Section 4.4). For example, we provided evidence that both C-shaped and S-shaped compounds were formed initially, determined that the C-shaped forms are more stable than the S-shaped forms by approximately 2 kcal mol^{-1}, and showed that the S-shaped to C-shaped isomerization reaction is an intramolecular process. To get information about the latter stages of the CB[n]-forming reaction – the elongation to trimer, tetramer, pentamer, hexamer, and longer oligomers and their subsequent macrocyclization reactions – we decided to decrease the number of equivalents of CH$_2$O used in the

reaction. We hypothesized that reducing the number of equivalents of CH_2O would increase the stability of partially formed CB[n] macrocycles and thereby provide information on plausible intermediates in the CB[n]-forming reaction.

4.6.1
Detection and Isolation of Nor-Seco-Cucurbit[10]uril

When we reacted glycoluril (one equiv) with formaldehyde (1.67 equiv) in conc. HCl at 50 °C we observed the formation of a precipitate after three days (Figure 4.2). The precipitate (*ns*-CB[10]) was isolated by centrifugation and purified by washing with 1:1 H_2O:HCl and MeOH. Characterization of this compound by spectroscopic means alone proved challenging; luckily, we were able to obtain crystals of *ns*-CB[10] as its *ns*-CB[10]•**58**₂ complex. Figure 4.2 shows a cross-eyed stereoview of the structure of *ns*-CB[10]•**58**₂ in the crystal. Several features of structure are noteworthy: (a) the lack of two CH_2-groups, which reveals the presence of four free ureidyl NH groups (similarly to (±)-**51**), (b) the presence of two symmetry-equivalent cavities, and (c) the lack of vertical registration of the two cavities. The isolation of *ns*-CB[10] provides evidence for the existence of pentamer fragments in the CB[n]-forming reaction and further insight into the condensation pathways that are possible between methylene-bridged glycoluril oligomers [14].

4.6.2
Molecular Recognition Properties of Nor-Seco-Cucurbit[10]uril

After we isolated *ns*-CB[10] we decided to study its molecular recognition behavior. Initially, we sought to define the functional group preferences of *ns*-CB[10] and its
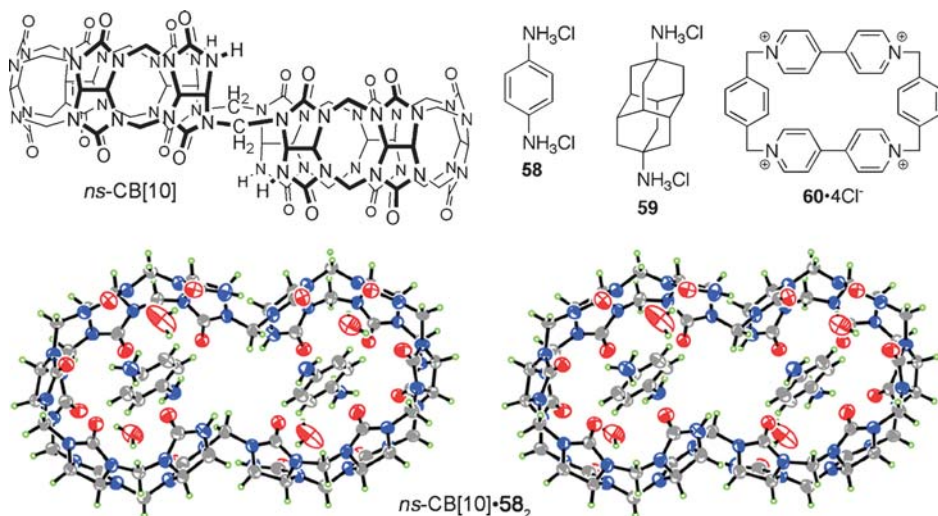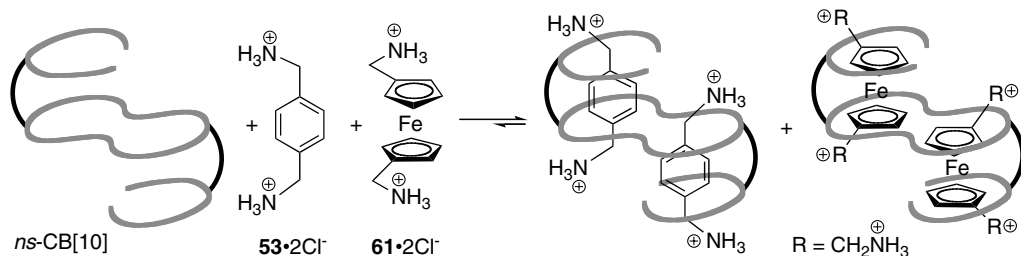

Figure 4.2 Chemical structure of *ns*-CB[10], some of its guests, and cross-eyed stereoview of the X-ray crystal structure of *ns*-CB[10]•**58**₂.

Scheme 4.22 Homotropic allostery inside *ns*-CB[10].

effective cavity size. We found that *ns*-CB[10] is capable of binding with a wide range of cationic guests that typically interact with CB[n] (e.g., **3**, **14–18**, **25**, **53**, **54**, **58**, **59**) as well as dyes, peptides, lipids, and electrochemically active substances. In these cases, *ns*-CB[10] forms ternary – rather than binary – complexes with these guests (i.e., *ns*-CB[10]•Guest$_2$) with 1:2 host:guest stoichiometry. Larger guests (**19** and **60**) fill both cavities simultaneously with formation of binary complexes (e.g., *ns*-CB[10]• Guest). The wide range of sizes of guests that form ternary complexes with *ns*-CB[10] suggests a high level of structural responsiveness of this host. Indeed, molecular modeling (MMFF) showed that the central non-bonded $CH_2 \cdots CH_2$ distance changes from 5.50 Å (*ns*-CB[10]•**53**$_2$) to 9.27 Å (*ns*-CB[10]•**61**$_2$) as the size of the guest increases [14]. The overall cavity volume undergoes a concomitant increase from 450 Å^3 to 740 Å^3 as the guest changes from **53** to **61** (Scheme 4.22). We wondered whether the responsiveness of the host to the size and shape of the guest would result in an allosteric response. To test for the presence of a guest-induced homotropic allostery, we combined *ns*-CB[10] with mixtures of guests composed of one small (e.g., **53** or **3**) and one large (e.g., **61** or **59**) guest (Scheme 4.22). In such cases, we observed exclusive formation of *ns*-CB[10]•**53**$_2$ and *ns*-CB[10]•**61**$_2$, with no evidence of the cross-over hetero-ternary complex *ns*-CB[10]•**53**•**61**. In contrast, when mixtures of similarly sized guests (e.g., **59** and **61**) were used, a mixture of homomeric and heteromeric ternary complexes was formed. This result demonstrates that *ns*-CB[10] is capable of distinguishing between molecules with modest to large differences in size.

4.7
Summary and Conclusions

The first synthesis of CB[6] by Behrend in 1905, its structural elucidation by Mock and coworkers in 1981, and subsequent studies by Mock and coworkers throughout the 1980s demonstrated the significant potential of CB[6] in studies of molecular recognition in aqueous acidic solution. The field has taken rapid steps forward since 2000 with the discovery of the CB[n] homologs CB[5], CB[7], and CB[8] by the groups of Kim and Day, whose cavity volumes span and exceed those available with α-, β-, and γ-cyclodextrin. For example, the smaller CB[5] readily encapsulates gases [42],

whereas the larger CB[n] homologs encapsulate species with significant biological and chemical potential (e.g., anticancer agents, dyes, peptides, viologens, and ferrocenes).

When we began our work in this area in 1998 we decided to tackle the issue of preparing CB[n] derivatives that contained solubilizing groups on the exterior of the macrocycle that would extend the range of applications to which CB[n] could be applied. This chapter has described the mechanistic approach, pursued by our group, that initially targeted the preparation of methylene-bridged glycoluril dimers as the fundamental building blocks of the CB[n] family. These model studies allowed us to provide evidence for some of the key early steps in the CB[n] formation mechanism, namely: (a) the presence of both S- and C-shaped diastereomers, (b) the presence of a thermodynamic driving force in favor of the C-shaped form ($\sim$2 kcal mol^{-1}), and (c) the intramolecular nature of the S- to C-shaped equilibrium under anhydrous acidic conditions.

These observations led us to propose a building-block strategy toward the preparation of CB[n] compounds [4,5] which was subsequently demonstrated experimentally in the synthesis of CB[n] derivatives and analogs [34,37,38]. Kim's synthetic advance in developing the direct per-hydroxylation of CB[5]–CB[8] allowed his group to prepare a wide range of per-functionalized CB[5] and CB[6] derivatives and to use them in new applications such as synthetic ion-channels and supramolecular vesicles [39–41].

More recently, in collaboration with Kim's group, we isolated inverted cucurbiturils (*i*-CB[6] and *i*-CB[7]), which are kinetic intermediates along the pathway toward CB[n], whose transformation into CB[5], CB[6], and CB[7] was demonstrated by product resubmission experiments [13]. These key experiments provided evidence on the fate of some of the final intermediates along the mechanistic pathway toward CB[n] and stimulated us to further probe the latter stages of the mechanism of CB[n] formation. Our key realization was that CB[n]-forming reaction mixtures containing a deficiency of formaldehyde would be unable to proceed to completion and therefore deliver intermediates as final products. Based on this idea, we were able to isolate *ns*-CB[10], which is formally derived from CB[10] by the removal of two CH_2 groups with subsequent bond reorganization. *ns*-CB[10] has displayed recognition properties including those reminiscent of biological systems such as the stabilization of ternary complexes and homotropic allostery based on guest size.

If the CB[n] family is to supplant the cyclodextrins as the platform of choice for basic and applied studies of molecular recognition, then a series of additional developments must take place, many of which involve the development of new synthetic procedures. First, improved methods for the separation of crude CB[n] mixture on the laboratory (i.e., up to 1 kg) to industrial (i.e., tonnes) scale must be developed. Alternatively, synthetic procedures that selectively target a specific CB[n] (e.g., CB[8] or CB[10]) would be tremendously valuable. Second, the development of high-yielding methods of functionalizing pre-formed CB[n] – particularly for CB[7], CB[8], and CB[10] – would have a dramatic impact on the field. Third, a deficiency of the CB[n] family relative to the cyclodextrins is that they are inherently achiral, which

renders chiral recognition inside CB[n] challenging. Our group and Inoue's group have recently shown that chiral recognition inside CB[n] can be achieved by "assembled enantioselection", where a chiral binary complex can be transformed into a diastereomerically enriched ternary complex by interaction with a chiral but racemic guest [18,43]. Fourth, to date a small number of studies have targeted the development of CB[n] for electronic applications [44]. Fifth, for applications involving humans (e.g., drug delivery, foodstuff additives, perfume additives, etc.) it will be necessary to demonstrate that CB[n] compounds are not toxic and that they are properly excreted from the body. Given the high chemical stability of CB[n] it seems unlikely that CB[n] will be metabolized *in vivo*. Lastly, it seems likely that CB[n] will be equal or superior to the cyclodextrins in the numerous application areas that have been demonstrated, and much future work will be directed accordingly.

4.8
Experimental: Selected Procedures

This experimental section describes several key procedures encountered during the synthesis of members of the CB [n] family.

4.8.1
Synthesis of Glycolurils

An excellent review by Petersen describes the preparation of numerous glycolurils [45]. In general, the formation of glycolurils occurs by the condensation of urea and its derivatives with 1,2-diketones under acidic conditions. Two specific examples are presented below which use either aqueous or anhydrous acidic conditions.

Synthesis of Glycoluril 1a A modification of the literature procedure was used [33]. To a solution of urea (600 g, 10 mol) in water (1 L) was added a 40% aq. solution of glyoxal (500 g, 3.45 mol) and conc. HCl (86 mL). The resulting solution was heated at ~85–90 °C until a heavy precipitate was formed. The reaction mixture was allowed to cool to room temperature and filtered. The filter cake was washed with copious amounts of water (2 L) followed by acetone to remove residual water. The resulting white solid (397.5 g, 81%) was dried under high vacuum. ^{1}H NMR (DMSO, 400 MHz): 7.11 (s, 4H), 5.20 (s, 2H).

Synthesis of Glycoluril 1b A modification of the literature procedures was used [46]. A mixture of benzil (21.0 g, 0.10 mol) and urea (12.1 g, 0.20 mol) in benzene (380 mL) was treated with TFA (20 mL) which resulted in a homogeneous mixture. The reaction mixture was then heated overnight at reflux with azeotropic removal of water. After cooling to room temperature, the white precipitate was isolated by filtration, washed with EtOH, and dried under high vacuum yielding **1b** as a white solid (22.8 g, 78%). ^{1}H NMR (DMSO, 400 MHz): 7.70 (s, 4H), 7.05-6.95 (m, 10H).

4.8.2
Synthesis and Separation of Cucurbit[n]urils

Although the synthesis and separation procedures given below may appear straight-forward, there are numerous details which affect the outcome of the CB[n]-forming reaction (e.g., rate of stirring, physical state and degree of physical mixing of the starting materials, homogeneity of the solution, etc.) and the efficiency of the separation procedure (e.g., HCl content in the crude solid). Therefore, each of the major laboratories involved in CB[n] chemistry has developed its own modifications of the basic procedures published by Day and Kim [12,15]. We present here the procedures used by our group at the University of Maryland.

Synthesis of CB[n] and *i*-CB[n]   Powdered glycoluril (795 g, 5.59 mol) and powdered paraformaldehyde (354 g, 11.2 mol) were mixed thoroughly. An ice-cold concentrated HCl solution (100 mL) was added gradually while stirring with a large glass rod. The reactants were transformed into a brick-like material, stirring was no longer possible, and the reaction became highly exothermic. An additional portion of ice-cold concentrated HCl (1030 mL) was added gradually. The heterogenous mixture was heated to 80 °C over 2.5 h and maintained at that temperature for an additional 2.5 h, at which point the solid had dissolved. The homogeneous red solution was heated to 100 °C for 14 h. After cooling to room temperature, the purification process was begun.

Monitoring of the Purification Process   It is possible to monitor the purification process by ^{1}H NMR using 20% DCl as the solvent. In this solvent CB[5]–CB[8], CB[10]•CB[5], and *i*-CB[6] show diagnostic resonances for the high-field
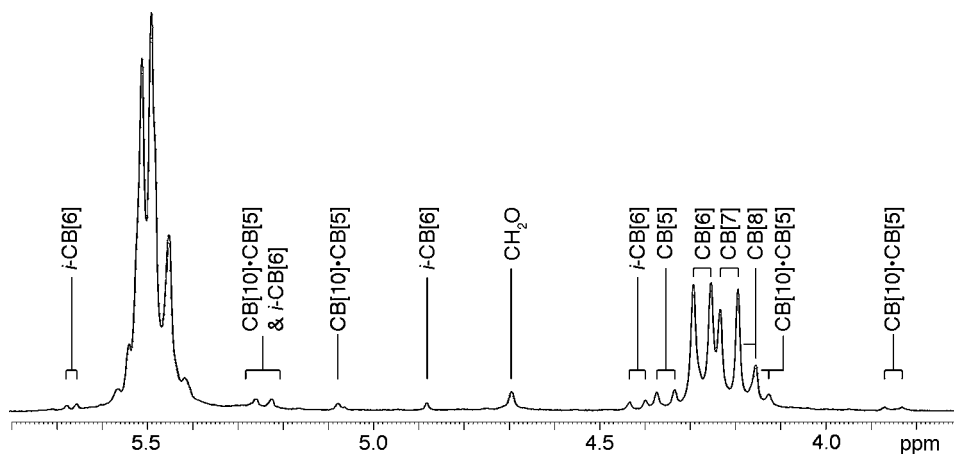
Figure 4.3 ^{1}H NMR spectrum (400 MHz, 20% DCl, RT) of the crude CB[n] reaction mixture.

diastereotopic CH_2-group (4.5–4.1 ppm). Figure 4.3 shows a representative ^1H NMR spectrum of the crude CB[n]-forming reaction mixture.

Purification of CB[5], CB[6], CB[7], CB[8], CB[10]•CB[5], and *i*-CB[6] The reaction mixture, which contained a large amount of solid, was evaporated to a minimum volume (∼600 mL). This slurry was poured into water (2.5 L). The solid was collected by filtration (Crop 1 contains CB[6], CB[7], CB[8], some *i*-CB[6], and some CB[10]• CB[5]). The filtrate was evaporated to about 600 mL and then slowly poured into a mixture of MeOH (3 L) and water (200 mL) with vigorous stirring. After stirring overnight, the precipitate was isolated by filtration (Crop 2 contains mainly CB[7] and CB[5] and smaller amounts of CB[6]).

Subsequent Purification The separation of each component (CB[5], CB[6], CB[7], CB[8], CB[10]•CB[5], and *i*-CB[6]) from Crop 1 and Crop 2 takes advantage of their differential solubility in HCl solutions of different concentration. For example, CB[5] and CB[7] have moderate solubility in water but other CB[n] compounds are nearly insoluble in pure water. The crude solids are stirred in a beaker with large volumes of water (2 L) repeatedly to isolate a solution consisting of mainly CB[5] and CB[7]. After concentration to 200 mL, the solution is poured into MeOH (1.5 L) and the solid isolated by filtration. Separation of CB[5] from CB[7] is based on its moderate solubility (about 33 mg mL^{-1}) in 50% aq. MeOH solution (v/v). The solubility of CB[7] is less than 4 mg mL^{-1} in this solution. Accordingly, the solid mixture of CB[5] and CB[7] is repeatedly stirred in a large beaker with 50% aq. MeOH to dissolve the CB[5] and leave the CB[7] as a solid. The solution of CB[5] is concentrated (not to dryness), which yields crystalline CB[5] (8% overall yield). Diffusion of acetone into an aq. soln. of CB[7] is used to obtain CB[7] as a crystalline solid (25% overall yield). The solid material from which CB[5] and CB[7] has been removed is subsequently processed to yield CB[6], *i*-CB[6], CB[8], and CB[10]•CB[5]. In 3 M HCl, CB[6], *i*-CB [6], and CB[10]•CB[5] have appreciable solubility, whereas CB[8] is substantially less soluble. By stirring the crude mixture of CB[6], CB[8], CB[10]•CB[5], and *i*-CB[6], with 3 M HCl in a large beaker it is possible to isolate CB[8] as an insoluble solid. CB [8] can then be recrystallized from warm conc. HCl to yield a crystalline solid (10% overall yield). The solution of CB[6], *i*-CB[6], and CB[10]•CB[5] in 3 M HCl is concentrated by rotary evaporation resulting in precipitation of CB[6]. The CB[n] compounds remaining in solution are precipitated by pouring the aq. soln. into MeOH. The solid obtained, which still contains CB[6], *i*-CB[6], and CB[10]•CB[5], can be separated by repeated fractional crystallization from HCl solutions of different concentrations. For example, CB[10]•CB[5] can be obtained by crystallization of the mixture from conc. HCl (2% overall yield). In samples that contain a large amount of *i*-CB[6], the CB[6] impurity can be removed by dissolving the mixture in 20% HCl, adding the calculated amount of hexanediamine, and diluting 10-fold with water. *i*-CB[6] is obtained as an insoluble precipitate (2% overall yield). CB[6] is obtained from multiple fractions and can be recrystallized from concentrated HCl (50% overall yield). The synthesis and purification procedure described above takes approximately 6 weeks.

4.8.3
Synthesis of Nor-Seco-Cucurbit[10]uril [14]

A mixture of glycoluril (1.42 g, 9.99 mmol), paraformaldehyde (0.50 g, 16.69 mmol), and conc. HCl (4 mL) was heated at 50 °C for 3 days. The resulting precipitate was separated by centrifugation to yield a crude solid (300 mg). This was dried under high vacuum for 10 min, washed with HCl:H_2O (1:1, v/v), washed with MeOH to remove HCl, and dried under high vacuum overnight to yield *ns*-CB[10] (238 mg, 0.145 mmol, 15%) as a white solid. ^1H NMR (400 MHz, 20% DCl): 5.47 (m, 28H), 5.40 (s, 4H), 5.33 (d, $J = 4.0$, 4H), 4.60 (s, 4H), 4.20 (m, 16H).

Abbreviations

aq.	aqueous
CB[n]	cucurbit[n]uril
Conc.	concentrated
d	doublet
DMF	dimethylformamide
DMSO	dimethylsulfoxide
equiv	equivalents
EYPC	egg yolk L-α-phosphatidyl-choline
HPTS	8-hydroxypyrene-1,3,6-trisulfonate
hν	light
i-CB[n]	inverted cucurbit[n]uril
J	coupling constant (Hz)
K_a	equilibrium association constant
LUVs	large unilamellar vesicles
m	multiplet
MMFF	Merck molecular force field
MV	methyl viologen
n.d.	not detected
NMR	nuclear magnetic resonance

ns-CB[10]   bis-nor-seco-cucurbit[10]uril
PTSA   *p*-toluenesulfonic acid
s   singlet
TFA   trifluoroacetic acid
v/v   volume to volume ratio

References

1 Behrend, R., Meyer, E. and Rusche, F. (1905) *Liebigs Ann. Chem.*, **339**, 1–37.

2 Freeman, W.A., Mock, W.L. and Shih, N.-Y. (1981) *J. Am. Chem. Soc.*, **103**, 7367–7368.

3 Flinn, A., Hough, G.C., Stoddart, J.F. and Williams, D.J. (1992) *Angew. Chem.*, **104**, 1550–1552; *Angew. Chem., Int. Ed. Engl.*, **31**, 1475–1477.

4 Wu, A., Chakraborty, A., Witt, D., Lagona, J., Damkaci, F., Ofori, M.A., Chiles, J.K., Fettinger, J.C. and Isaacs, L. (2002) *J. Org. Chem.*, **67**, 5817–5830.

5 Chakraborty, A., Wu, A., Witt, D., Lagona, J., Fettinger, J.C. and Isaacs, L. (2002) *J. Am. Chem. Soc.*, **124**, 8297–8306.

6 Witt, D., Lagona, J., Damkaci, F., Fettinger, J.C. and Isaacs, L. (2000) *Org. Lett.*, **2**, 755–758.

7 Mock, W.L. and Shih, N.-Y. (1983) *J. Org. Chem.*, **48**, 3618–3619; *J. Am. Chem. Soc.*, **110**, 4706–4710.

8 Mock, W.L. and Shih, N.-Y. (1986) *J. Org. Chem.*, **51**, 4440–4446.

9 Mock, W.L. and Shih, N.-Y. (1989) *J. Am. Chem. Soc.*, **111**, 2697–2699.

10 Mock, W.L., Irra, T.A., Wepsiec, J.P. and Manimaran, T.L. (1983) *J. Org. Chem.*, **48**, 3619–3620; Mock, W.L., Irra, T.A., Wepsiec, J.P. and Adhya, M. (1989) *J. Org. Chem.*, **54**, 5302–5308.

11 Mock, W.L. and Pierpont, J. (1990) *J. Chem. Soc. Chem. Commun.*, 1509–1511.

12 Day, A., Arnold, A.P., Blanch, R.J. and Snushall, B. (2001) *J. Org. Chem.*, **66**, 8094–8100.

13 Isaacs, L., Park, S.-K., Liu, S., Ko, Y.H., Selvapalam, N., Kim, Y., Kim, H., Zavalij, P.Y., Kim, G.-H., Lee, H.-S. and Kim, K. (2005) *J. Am. Chem. Soc.*, **127**, 18000–18001.

14 Huang, W.-H., Liu, S., Zavalij, P.Y. and Isaacs, L. (2006) *J. Am. Chem. Soc.*, **128**, 14744–14745.

15 Kim, J., Jung, I.-S., Kim, S.-Y., Lee, E., Kang, J.-K., Sakamoto, S., Yamaguchi, K. and Kim, K. (2000) *J. Am. Chem. Soc.*, **122**, 540–541.

16 Lee, J.W., Samal, S., Selvapalam, N., Kim, H.-J. and Kim, K. (2003) *Acc. Chem. Res.*, **36**, 621–630.

17 Day, A.I., Blanch, R.J., Arnold, A.P., Lorenzo, S., Lewis, G.R. and Dance, I. (2002) *Angew. Chem.*, **114**, 285–287; *Angew. Chem., Int. Ed.*, **41**, 275–277.

18 Liu, S., Zavalij, P.Y. and Isaacs, L. (2005) *J. Am. Chem. Soc.*, **127**, 16798–16799.

19 Liu, S., Ruspic, C., Mukhopadhyay, P., Chakrabarti, S., Zavalij, P.Y. and Isaacs, L. (2005) *J. Am. Chem. Soc.*, **127**, 15959–15967.

20 Mukhopadhyay, P., Wu, A. and Isaacs, L. (2004) *J. Org. Chem.*, **69**, 6157–6164.

21 Mukhopadhyay, P., Zavalij, P.Y. and Isaacs, L. (2006) *J. Am. Chem. Soc.*, **128**, 14093–14102.

22 Jun, S.I., Lee, J.W., Sakamoto, S., Yamaguchi, K. and Kim, K. (2000) *Tetrahedron Lett.*, **41**, 471–475.

23 Moon, K., Grindstaff, J., Sobransingh, D. and Kaifer, A.E. (2004) *Angew. Chem.*, **116**, 5612–5615; *Angew. Chem., Int. Ed.*, **43**, 5496–5499.

24 Ong, W. and Kaifer, A.E. (2003) *Angew. Chem.*, **115**, 2214–2217; *Angew. Chem., Int. Ed.*, **42**, 2164–2167.

25 Lim, Y.-B., Kim, T., Lee, J.W., Kim, S.-M., Kim, H.-J., Kim, K. and Park, J.-S. (2002)

Bioconjugate Chem., **13**, 1181–1185; Lee, J.W., Ko, Y.H., Park, S.-H., Yamaguchi, K. and Kim, K. (2001) *Angew. Chem.*, **113**, 768–771; *Angew. Chem., Int. Ed.*, **40**, 746–749.

26 Jeon, W.S., Ziganshina, A.Y., Lee, J.W., Ko, Y.H., Kang, J.-K., Lee, C. and Kim, K. (2003) *Angew. Chem.*, **115**, 4231–4234; *Angew. Chem., Int. Ed.*, **42**, 4097–4100; Ko, Y.H., Kim, K., Kang, J.-K., Chun, H., Lee, J.W., Sakamoto, S., Yamaguchi, K., Fettinger, J.C. and Kim, K. (2004) *J. Am. Chem. Soc.*, **126**, 1932–1933.

27 Jeon, W.S., Kim, E., Ko, Y.H., Hwang, I., Lee, J.W., Kim, S.-Y., Kim, H.-J. and Kim, K. (2005) *Angew. Chem.*, **117**, 89–93; *Angew. Chem., Int. Ed.*, **44**, 87–91.

28 Marquez, C. and Nau, W.M. (2001) *Angew. Chem.*, **113**, 3248–3253; *Angew. Chem., Int. Ed.*, **40**, 3155–3160.

29 Jeon, Y.J., Kim, S.-Y., Ko, Y.H., Sakamoto, S., Yamaguchi, K. and Kim, K. (2005) *Org. Biomol. Chem.*, **3**, 2122–2125.

30 Wheate, N.J., Day, A.I., Blanch, R.J., Arnold, A.P., Cullinane, C. and Collins, J.G. (2004) *Chem. Commun.*, 1424–1425; Wheate, N.J., Buck, D.P., Day, A.I. and Collins, J.G. (2006) *Dalton Trans.*, 451–458.

31 Rowan, A.E., Elemans, J.A.A.W. and Nolte, R.J.M. (1999) *Acc. Chem. Res.*, **32**, 995–1006; Rebek, J. Jr. (1999) *Acc. Chem. Res.*, **32**, 278–286.

32 Eliel, E.L. and Wilen, S.H. (1994) *Stereochemistry of Organic Compounds*, J. Wiley and Sons, New York.

33 Buschmann, H.-J., Fink, H. and Schollmeyer, E. (1997) "Preparation of cucurbituril" Ger. Offen. [Germany]: DE 19603377 [*Chem. Abstr. 1997*, *127*, 205599].

34 Lagona, J., Fettinger, J.C. and Isaacs, L. (2003) *Org. Lett.*, **5**, 3745–3747.

35 Lagona, J., Fettinger, J.C. and Isaacs, L. (2005) *J. Org. Chem.*, **70**, 10381–10392.

36 Lagona, J., Wagner, B.D. and Isaacs, L. (2006) *J. Org. Chem.*, **71**, 1181–1190.

37 Day, A.I., Arnold, A.P. and Blanch, R.J. (2003) *Molecules*, **8**, 74–84.

38 Zhao, Y., Xue, S., Zhu, Q., Tao, Z., Zhang, J., Wei, Z., Long, L., Hu, M., Xiao, H. and Day, A. I. (2004) *Chin. Science Bull.*, **49**, 1111–1116.

39 Jon, S.Y., Selvapalam, N., Oh, D.H., Kang, J.-K., Kim, S.-Y., Jeon, Y.J., Lee, J.W. and Kim, K. (2003) *J. Am. Chem. Soc.*, **125**, 10186–10187.

40 Lee, H.-K., Park, K.M., Jeon, Y.J., Kim, D., Oh, D.H., Kim, H.S., Park, C.K. and Kim, K. (2005) *J. Am. Chem. Soc.*, **127**, 5006–5007.

41 Jeon, Y.J., Kim, H., Jon, S., Selvapalam, N., Oh, D.H., Seo, I., Park, C.-S., Jung, S.R., Koh, D.-S. and Kim, K. (2004) *J. Am. Chem. Soc.*, **126**, 15944–15945.

42 Rudkevich, D.M. (2004) *Angew. Chem.*, **116**, 568–581; *Angew. Chem., Int. Ed.*, **43**, 558–571.

43 Rekharsky, M.V., Yamamura, H., Inoue, C., Kawai, M., Osaka, I., Arakawa, R., Shiba, K., Sato, A., Ko, Y.H., Selvapalam, N., Kim, K. and Inoue, Y. (2006) *J. Am. Chem. Soc.*, **128**, 14871–14880.

44 Ling, Y. and Kaifer, A.E. (2006) *Chem. Mater.*, **18**, 5944–5949.

45 Petersen, H. (1973) *Synthesis*, 243–292.

46 Butler, A.R. and Leitch, E. (1980) *J. Chem. Soc. Perkin Trans. 2*, 103–105.

5

Tetra-urea Calix[4]arenes – From Dimeric Capsules to Novel Catenanes and Rotaxanes

Ganna Podoprygorina and Volker Böhmer

5.1
### Introduction

The preparation of topologically interesting molecules and supramolecular structures such as catenanes, knots [1], or Möbius strips [2] is primarily an intellectual challenge, although more and more applications [3] have been proposed during the last decade(s). The synthesis of structures consisting of interlocked rings usually requires the formation of cyclic molecules from linear precursors while they are penetrating already existing rings. Similarly to the macroscopic example (the fabrication of a chain [Latin: catena]), an efficient synthesis of catenanes[1] requires a perfect prearrangement of the respective building blocks. On the molecular level, such a preorganization can be achieved by an appropriate covalent linkage which has to be cleaved after the intended ring-closure reaction(s). However, the desired mutual arrangement of the precursors can also be obtained via reversible links, such as coordination to metal cations, hydrogen bonding, or interactions of the donor-acceptor type. This has the advantage that wrong connections can be corrected during the assembly process. The rapid progress in the synthesis of topologically more and more demanding molecules and complex structures in reasonable yields, for which Borromean rings [4] represent an impressive example, is therefore strongly connected with the development of supramolecular chemistry in general [5].

The first rational synthesis of a [2]catenane was reported by Schill and Lüttringhaus [6], who successfully used a covalent attachment to a template. This "covalent approach" was recently applied by Godt and coworkers for the preparation of a series of [2]catenanes consisting of really large and thus mutually "mobile" chain rings ("non-rusty catenanes") [7]. In this case a prefabricated macrocycle and a precursor for the second ring were linked via a carbonate group. The oxidative coupling of the alkyne residues formed the second cycle, which has to be threaded through the first one (Scheme 5.1). Hydrolysis of the carbonate linkage disconnected the two rings, producing a [2]catenane.

---

[1] Similar considerations hold for the topologically trivial rotaxanes.
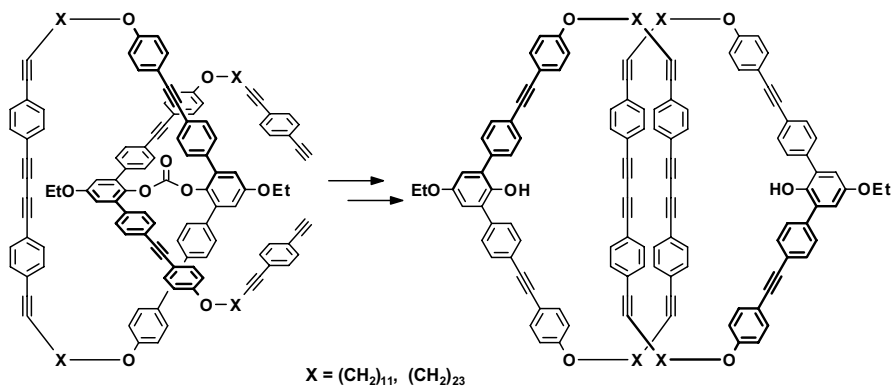
Scheme 5.1 Covalent prearrangement in the synthesis of [2]catenanes consisting of large, mobile rings. The structure of the first ring should not allow an *exo* orientation of the carbonate link.

Various catenanes [8], rotaxanes [8], and even trefoil knots [9] were synthesized in high yields using the coordination of suitably functionalized precursors as ligands around metal ions. The tetrahedral organization of phenanthroline derivatives by copper(I) was the first [10] and still remains [11] one of the most frequently used motifs. The synthesis of a bis[2]catenane [12] in which a large ring formed by metathesis reaction is threaded through two rings of an "eight-shaped" bis-macrocycle (Scheme 5.2) is a recent example.

Metal cations with an octahedral coordination sphere have also been utilized as templates for the directed synthesis of various interlocked structures [13], including Borromean rings [4,14]. Terpyridyl or 2,6-diiminopyridine derivatives (Scheme 5.3) self-organize into complexes in the presence of metal cations, providing an arrangement of the attached functional groups X suitable for their selective ring-closure to [2]catenanes. The same catenanes consisting of diiminopyridine rings can be also prepared from the corresponding diamines and 2,6-pyridine dialdehyde [13b]. In this case, reversible Schiff base formation favors the thermodynamically stable species and leads finally to those products which complete the octahedral coordination sphere of the templating cation.
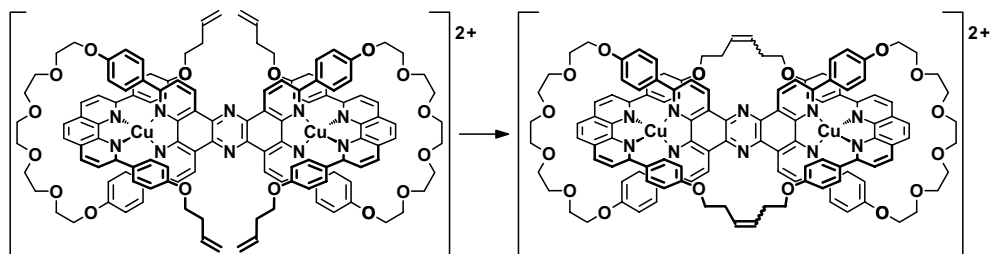
Scheme 5.2 Synthesis of a bis[2]catenane templated by two copper (I) ions. The starting complex is the only species which enables a complete interaction of all phenanthroline sites with Cu(I).
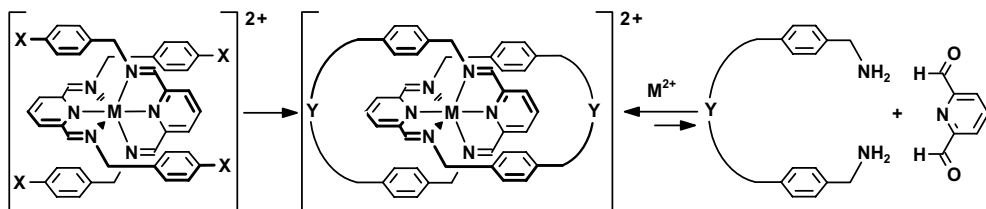
Scheme 5.3 Synthesis of [2]catenanes by coordination of 2,6-disubstituted pyridine ligands to cations $M^{2+} = Mn^{2+}$, Fe^{2+}, Co^{2+}, Ni^{2+}, Cu^{2+}, Zn^{2+}, Cd^{2+}, Hg^{2+}. Diimines are kept by the template in an orthogonal arrangement which leads to a selective ring closure. X symbolizes various reactive groups used for the covalent connection of the preorganized building blocks by an appropriate spacer Y.

Anions have also been used as templates in the synthesis of catenanes and rotaxanes, as recently described by Beer and coworkers [15]. They used the self-assembly of diamides, known as anion receptor molecules, around a chloride anion to produce, for example, [2]- and [3]catenanes by olefin metathesis [16] (Scheme 5.4). In this special example, the template effect was increased by hydrogen bonding between the *N*-methyl group to the crown ether chain and by π-π stacking interactions.

However, preorganization by reversible interactions via hydrogen bonds does not necessarily need a further template such as an anion. Direct intermolecular hydrogen bonds between derivatives of isophthalic acid and 2,6-pyridine diacid were used to synthesize a series of new catenanes [17,18], rotaxanes [18c,19], and trefoil knots [20]. The interaction of dibenzylammonium cations and dibenzo[24]crown[8] [21] led to the preparation of rotaxanes by the attachment of stoppers to the thread ends (Scheme 5.5) [22], or similarly by clipping of the crown ether chain wrapped around the ammonium dumbbell [23]. Recently, several novel catenanes were synthesized via the macrocyclic connection of three ammonium cations threaded through three crown ether rings attached to a triptycene core [24].

Numerous interlocked structures [25], including a [5]catenane (olympiadane) [26], were built using the self-organization of crown ether derivatives containing
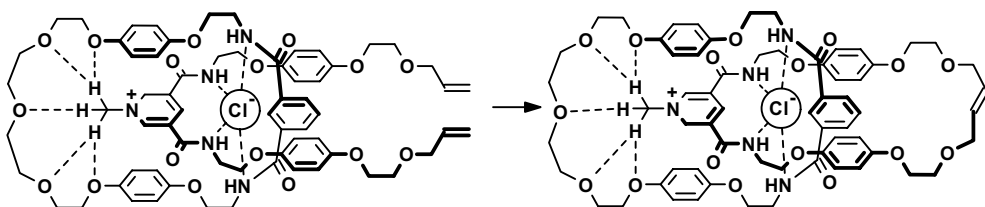
Scheme 5.4 Synthesis of a [2]catenane by self-organization of amides around a chloride anion as the template. The pseudorotaxane formed between the linear and the cyclic amides is held together additionally by various hydrogen bonds and π-π interactions.
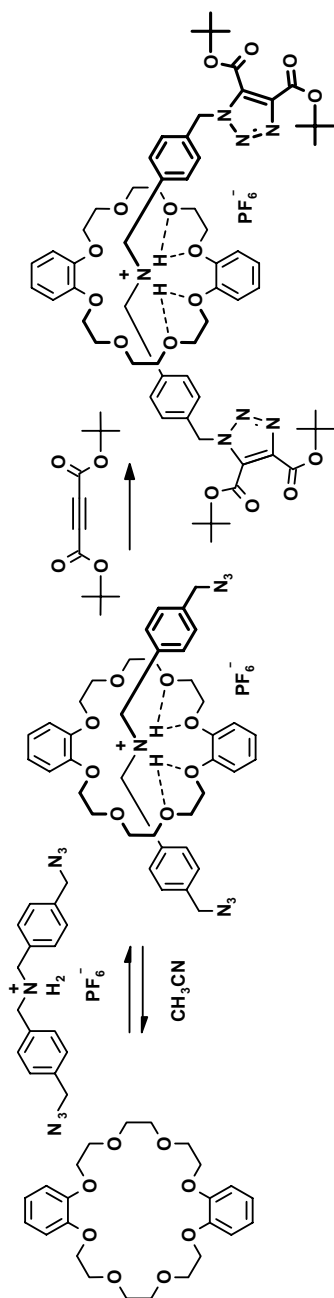
Scheme 5.5 A pseudorotaxane is formed by hydrogen bonding between benzylic protons and the -NH₂- protons of the ammonium cation with the oxygens of a crown ether. The introduction of bulky residues to appropriately functionalized thread ends produces a rotaxane, while catenanes are accessible by a cyclic connection of the ends.
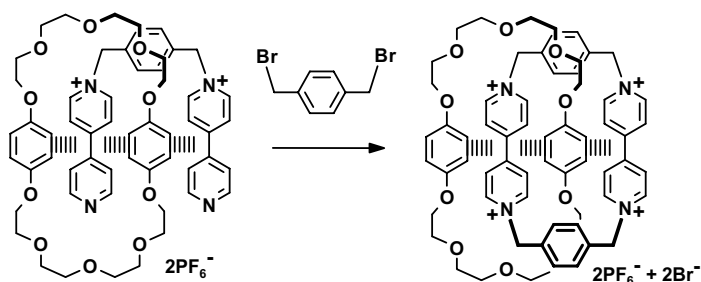
Scheme 5.6 The general principle for the synthesis of catenanes (or rotaxanes) based on cyclobis(paraquat-*p*-phenylene) and crown ethers containing hydroquinone units. The dipyridyl units are alternately stacked with two hydroquinones because of π-π interactions which direct the ring-closure toward the formation of a catenane.

hydroquinone (or similar π-electron-donating) units and bis(paraquat-*p*-phenylene) (Scheme 5.6) or its analogs. In this case, π-π interactions between a hydroquinone donor and a bipyridyl acceptor unit, enhanced by hydrogen bonding between the benzylic protons and the crown ether oxygens, are responsible for the preorganization.

As a general principle, effective syntheses of interlocked molecules are based on the supramolecular preorganization of the starting cyclic and linear components. These (more or less) stable intermediate assemblies are referred to as pseudorotaxanes [27]. Depending upon the functionalization, the same pseudorotaxane can be a precursor for catenanes (by ring-closure) and for rotaxanes (by appropriate stoppering). Pseudorotaxanes or rotaxanes can be also obtained via clipping, the cyclization of a chain assembled around a linear or dumbbell shaped molecule correspondingly. These possibilities are schematically summarized in Scheme 5.7.
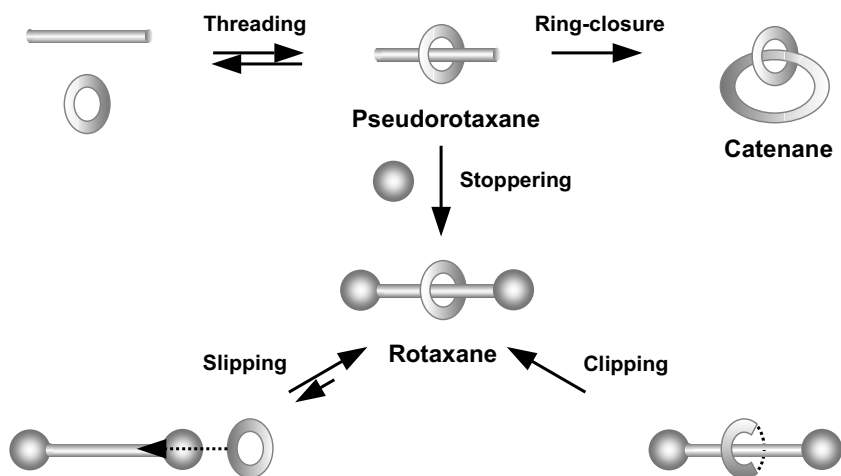
Scheme 5.7 Pathways leading to the formation of rotaxanes or catenanes.

Hydrogen-bonded dimers of tetra-urea calix[4]arenes offer a unique, unprecedented preorganization [28]. Before we describe how this can be used for the "rational" construction of molecules with novel topologies, it is reasonable to discuss the properties of such dimeric capsules and the conditions under which they exist.

5.2
Basics of Tetra-urea Calix[4]arenes

5.2.1
Synthesis

Starting from *tert*-butylcalix[4]arene [29], the preparation of a typical tetra-urea derivative usually requires four steps (Scheme 5.8):

a. Exhaustive *O*-alkylation to fix the cone conformation;
b. Substitution of *t*-butyl groups by *ipso*-nitration;
c. Reduction of the nitro groups;
d. Acylation by an appropriate isocyanate.

The isocyanate can be replaced by the corresponding activated urethane (as a milder reagent), and this activation can also involve the *p*-amino functions of the calix[4]arene (step e) and their subsequent reaction with a suitable amine (step f). Multigram quantities of simple tetra-urea calix[4]arenes are easily available in this way.

Selective substitution by different urea groups is easily accomplished using protection-deprotection strategies. Mono-, 1,2-di-, and tri-Boc derivatives are available in gram quantities [30], which allows the preparation of AAAB- and AABB-type
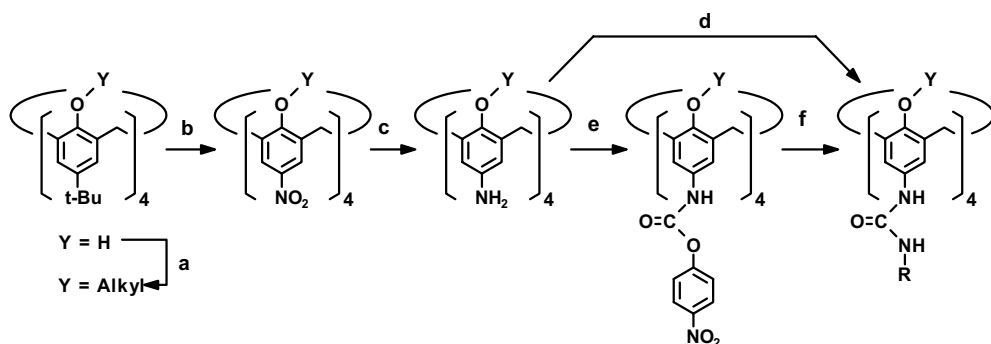
Scheme 5.8 Synthesis of tetra-urea calix[4]arenes. (a) Alkylating reagents, NaH, DMF, rt; (b) HNO_3/HOAc, CH_2Cl_2, rt; (c) H_2, Raney-Ni, toluene, rt; (d) R-NCO, rt; (e) *p*-nitrophenyl chloroformate; (f) $R-NH_2$, rt.
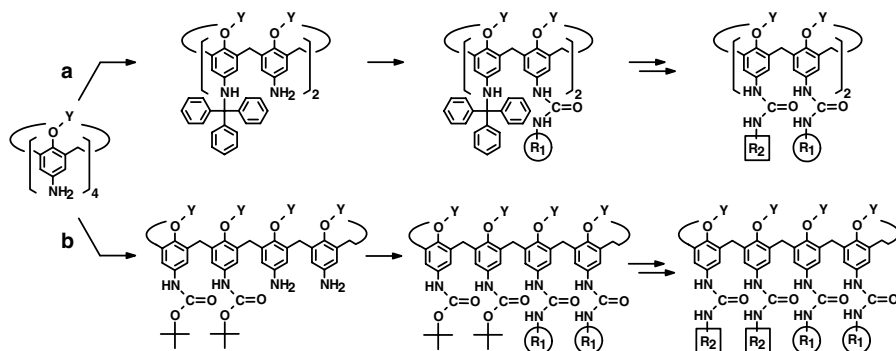
Scheme 5.9 Synthesis of tetra-urea calix[4]arenes bearing two
different urea residues in the sequence ABAB (a) and AABB (b),
using the protection of amino functions by trityl- or Boc-groups.
$(Y = C_5H_{11})$.

tetra-ureas.[2] The ABAB-type is now also readily accessible, using the protection of
distal (opposite) amino groups by alkylation with tritylchloride [31]. Examples of
these syntheses are shown in Scheme 5.9.

5.2.2
Dimeric Capsules

As first described by Shimizu and Rebek Jr. [32], tetra-urea calix[4]arenes form
dimeric capsules in aprotic, apolar solvents such as chloroform, cyclohexane, or
benzene, while they exist as single molecules in polar solvents such as acetone,
DMSO, pyridine, or ethanol [33]. This was first deduced from the ^{1}H NMR spectra
(compare Figure 5.1a,b) which show for the dimers a strong downfield shift for one
of the two NH-signals, indicating strong hydrogen bonds, and a splitting of the
singlet of the aromatic protons of the calix[4]arene skeleton into two *m*-coupled
doublets, indicating a change in symmetry from C_{4v} to C_4.

The structure of the capsule, proposed initially on the basis of these NMR-data,
was completely confirmed by the first single crystal X-ray structure (Figure 5.2) [34].
The two calix[4]arenes are connected via their wide rims by a seam of intermolecular
hydrogen bonds alternatingly involving the urea residues of both calixarenes. The
directionality of this hydrogen bonded belt is the reason for the inequivalence of the
two aromatic protons of a given phenolic unit mentioned above.

The internal volume of the capsule (190–200 Å^3) cannot be empty, and the inclu-
sion of a suitable guest (often the solvent) is a necessary condition for the dimer-
ization. Various organic molecules (for example, (1R)-(+)-nopinone, (1R)-(+)-cam-
phor, [32b,c]) have been included in the cavity [35], and the upfield shifts of their ^{1}H
NMR signals provide an independent proof of the formation of dimeric capsules,

---

2) **A** and **B** just characterize different phenolic units, where the difference may be due to the ether residues
Y or to the urea residues R or both.
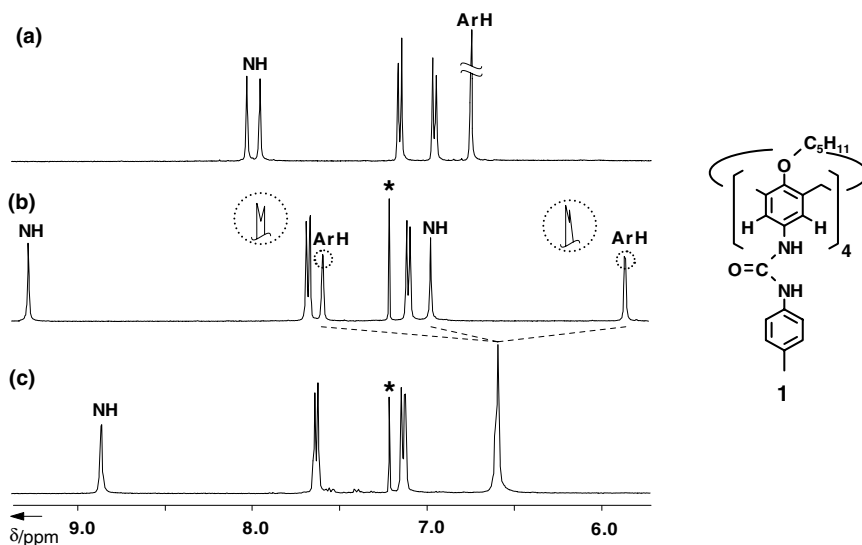
Figure 5.1 Sections of ^{1}H NMR spectra (400 MHz, 25 °C) of tetra-urea **1**: (a) in DMSO-d_6 (monomers); (b) in CDCl$_3$ (dimeric capsules **1**·CDCl$_3$·**1**); (c) in CDCl$_3$ in the presence of Et$_4$N$^+$·BF$_4^-$ (dimeric capsules [**1**·Et$_4$N$^+$·**1**]BF$_4^-$). The solvent signal is marked by an asterisk.

although these guests are usually not found by X-ray diffraction because of their disorder.

Organic cations are especially good guests, since their inclusion is favored by cation-π interactions with the aromatic walls. This enables the encapsulation to be studied by mass spectrometry also [36]. If cations such as tetraethylammonium or cobaltocenium are included [37], the directionality of the hydrogen-bonded belt
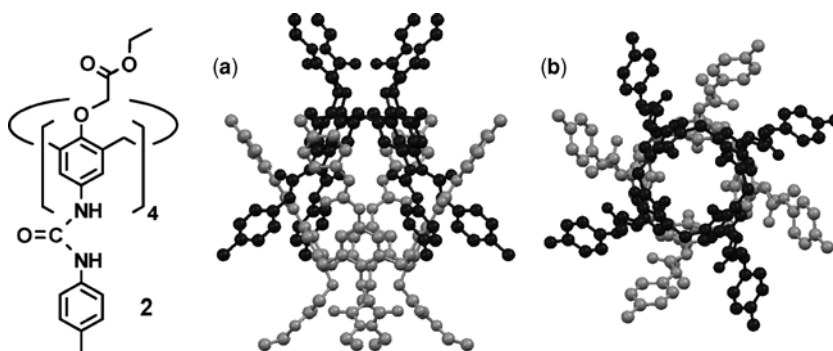
Figure 5.2 Molecular structure of a tetra-urea dimer **2**·**2** determined by X-ray analysis [34]. (a) Side view; (b) top view. Alkyl residues (in b), hydrogen atoms, and solvent molecules are omitted for clarity.

changes rapidly on the NMR-time scale. The typical *m*-coupled doublets for the aromatic protons, usually observed even at elevated temperatures, collapse into a singlet (Figure 5.1c). Neutral molecules of similar size (tetraethylsilane, ferrocene) are not accepted as guest, which demonstrates the importance of cation-π interactions for the stability of the whole assembly. Up to now, a dimer with tetraethylammonium is the only example where the guest was located in the X-ray structure [38].

5.2.3
Heterodimers

A dimeric capsule can also be formed by two different tetra-urea molecules, and in aprotic solvents a mixture of two tetra-urea derivatives usually contains not only the two homodimers but also the heterodimer in a more or less statistical ratio. This formation of heterodimers is an additional proof of the dimerization [39], which is also valid when other indications (e.g. *m*-coupled doublets for aryl protons) fail. As an example, sections of the spectra of tetra-tolylurea (**1**), tetra-hexylurea (**3**), and of a mixture of the two are shown in Figure 5.3a–c [37a].

However, the statistical formation of heterodimers is not the rule. Examples are known where *no* heterodimers are formed, e.g. between **1** and tetra-ureas derived from a rigid bis-crown-3 [40] (see Section 7). Further examples will be shown in the next sections. In such cases, the solution of the two tetra-urea calix[4]arenes contains exclusively the two homodimers.
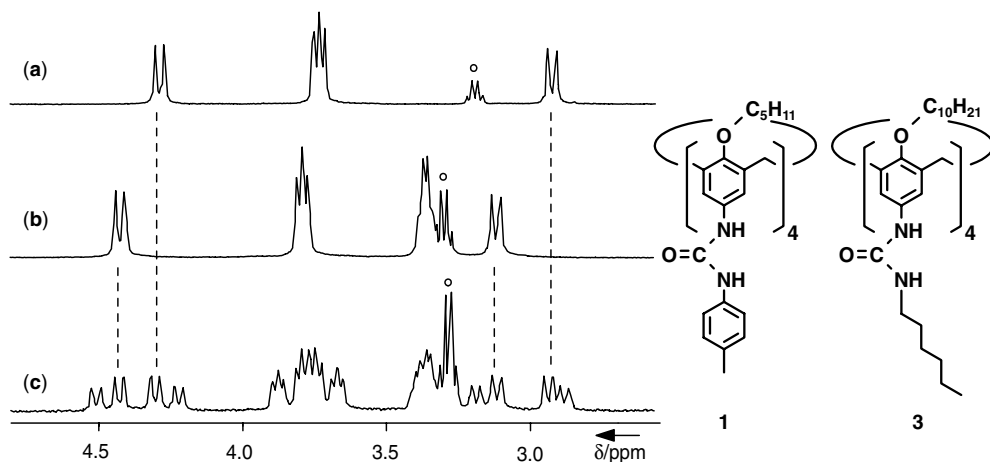
Figure 5.3 Sections of ^{1}H NMR spectra (CDCl$_3$, 400 MHz, 25 °C) of tetra-urea dimers with tetraethylammonium as guest: (a) [**1**·Et$_4$N$^+$·**1**]BF$_4^-$; (b) [**3**·Et$_4$N$^+$·**3**]BF$_4^-$; (c) 1:1 mixture of [**1**·Et$_4$N$^+$·**1**]BF$_4^-$, and [**3**·Et$_4$N$^+$·**3**]BF$_4^-$. In addition to the signals for the two homodimers (a, b), the mixture (c) contains a double set of signals for the two parts of the heterodimer. The signals of free Et$_4$N$^+$ are marked by a circle.
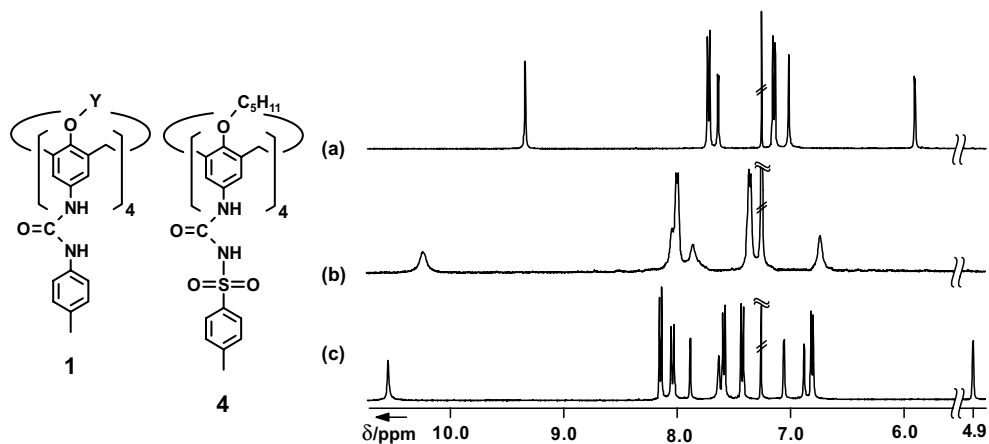
Figure 5.4 Representative sections of the ^{1}H NMR-Spectra
(CDCl$_3$, 400 MHz, 25 °C) of (a) tetra-tolylurea (**1**) (Y = C$_5$H$_{11}$),
(b) tetra-tosylurea (**4**), and (c) a 1:1 mixture of **1** and **4**.

On the other hand, there are examples of *exclusive* heterodimerization. Both tetra-aryl- and tetra-tosylureas readily form homodimers when they are dissolved alone in an apolar solvent. However, heterodimers are the only detectable species in a solution containing both compounds in a 1:1 ratio. An example of this selective hetero-dimerization [41] is demonstrated by the NMR-spectra in Figure 5.4. Only when one of these tetra-ureas is present in excess can signals for its homodimer be seen by NMR. This early observation by Rebek and Castellano [42] is especially important for the template syntheses described below. Other examples of exclusive formation of heterodimers will be discussed later.

5.2.4
Symmetry Properties

^{1}H NMR spectra still represent the main source of information for more sophisticated dimeric assemblies also. To understand these, it is useful to discuss some symmetry properties of hetero- and homodimers first, which are the basis for their characterization by ^{1}H NMR. Figure 5.5 summarizes the main examples.

A homodimer of a tetra-urea calix[4]arene consisting of identical phenolic units **A** is composed of two enantiomers with C_4-symmetry, which results in overall S_8-symmetry. Consequently, a heterodimer with a second calixarene consisting of four units **B** must be chiral, but this chirality is due only to the directionality of the hydrogen-bonded belt or (in other words) to the orientation of the carbonyl groups [42,43]. Rotation around the (four) aryl-NH bonds leads to the opposite enantiomer (conformational chirality).

A single calixarene consisting of two different phenolic units **A** and **B** in alternating order **ABAB** is (time averaged) C_{2v}-symmetric. Consequently, its homodimer is chiral (D_2-symmetry) without the directionality of the hydrogen-bonded belt, just by

Homodimer   **Heterodimer**

Homodimers

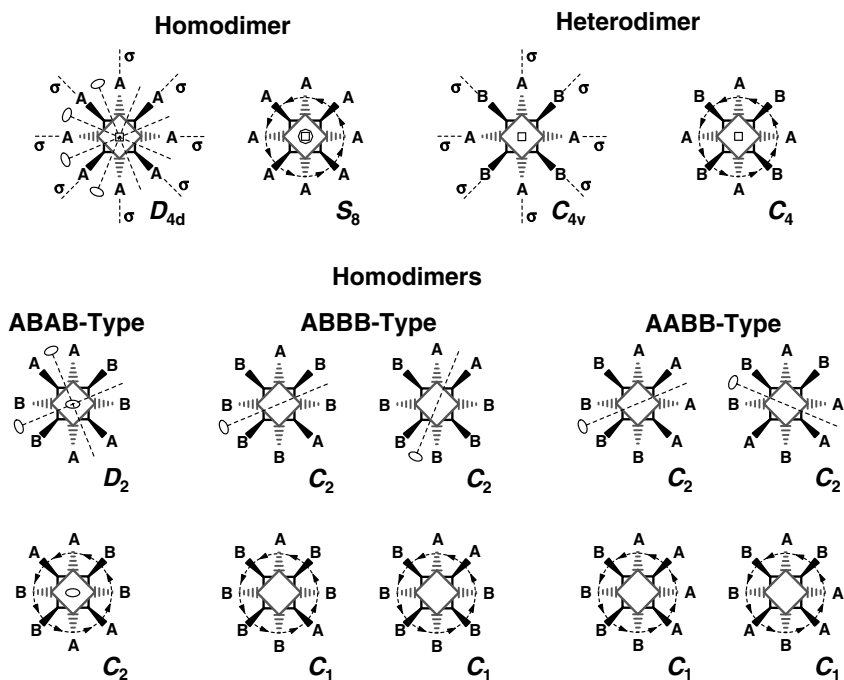**ABAB-Type**   **ABBB-Type**   **AABB-Type**

Figure 5.5 Survey of the symmetry properties for selected types of homo- and heterodimers of tetra-urea calix[4]arenes, represented by squares with the phenolic units (**A**, **B**) on the corners. Symmetry elements and symmetry classes (with and without directionality of the hydrogen bonds, shown by arrows) are indicated.

the mutual arrangement of the two non-chiral calix[4]arenes (supramolecular chirality) [44]. The directionality of the hydrogen bonds does not create new stereoisomers; it just reduces the symmetry from D_2 to C_2. For tetra-urea calix[4]arenes of the **AABB-** and **ABBB-**types, two regioisomeric dimers are possible, which both have C_2- or C_1-symmetry, respectively.

5.3
Preorganization in Dimers of Tetra-urea Calix[4]arenes

5.3.1
General Considerations

The inclusion of guests is not the only interesting aspect of the dimers formed by tetra-urea calixarenes. Numerous other self-assembled capsules are known, larger in volume, different in shape, and able to include more than one guest molecule, and various aspects of guest inclusion have been extensively studied [45].
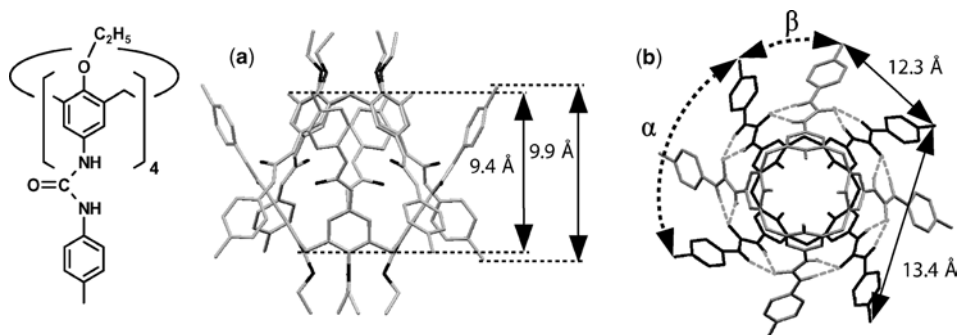
Figure 5.6 Hydrogen-bonded dimer of a tetra-tolylurea calix[4] arene. Stick models based on molecular modeling (a) and X-ray structures (b), illustrating possible intra- and intermolecular connections (α- and β-connections).

The dimerization also brings the eight residues attached to the urea groups into a unique mutual position. This means that the residues are *preorganized* for controlled reactions between them, for instance, for their intramolecular connection.

As illustrated in Figure 5.6 for a tetra-tolylurea (as an example), the two calix[4]-arenes forming the dimer are turned by 45° around their common fourfold axis. The tolyl residues attached to the urea groups point in opposite directions. Based on MD-simulations, the distance between adjacent tolyl methyl groups in the same calix-arene is slightly larger (13.4 Å) than the distance to the adjacent methyl groups in the other calixarene (12.3 Å).

In spite of the similar distance (13.4 Å vs. 12.3 Å), the different orientation of the urea residues of the two calixarenes could allow a selective connection of functional groups attached to the same calixarene. In the following we will name such a reaction "α-connection" to distiguish it from a "β-connection" taking place between functional groups belonging to different calixarenes.

5.3.2
First Attempts

The olefin metathesis between alkenyl groups has been frequently used in recent years to stabilize molecules (e.g., dendrimers [46]) or molecular assemblies [47] by additional covalent connectivities [48] and to synthesize macrocycles or more demanding structures like multiple catenanes [24]. Therefore, this reaction was chosen for the connection of alkenyl residues attached to a calix[4]arene via the urea residues. To avoid complications by cis/trans isomerism around the newly formed double bond, the crude reaction mixture was always hydrogenated before working up (Scheme 5.10).

In a first attempt, we tried to connect the alkenyl residues attached to the urea groups within a homodimer of **5**. A mixture of three products was obtained and separated chromatographically. Mass spectrometry revealed the expected molecular mass, while their symmetry, indicated for instance by the number of low-field NH signals

$$2 \, \text{\large\char"2307}\text{O-(CH}_2)_m\text{-CH=CH}_2 \longrightarrow \text{\large\char"2307}\text{O-(CH}_2)_m\text{-CH=CH-(CH}_2)_m\text{-O}\text{\large\char"2307} + \text{CH}_2\text{=CH}_2$$

$$\xrightarrow{\text{H}_2} \text{\large\char"2307}\text{O-(CH}_2)_n\text{-O}\text{\large\char"2307} \qquad \boxed{n = 2 \cdot m + 2}$$
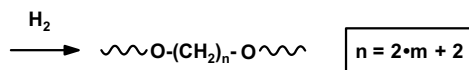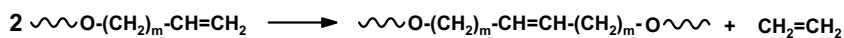
Scheme 5.10 Connection of pendant alkenyl residues by olefin metathesis, followed by exhaustive hydrogenation of the newly formed double bonds.
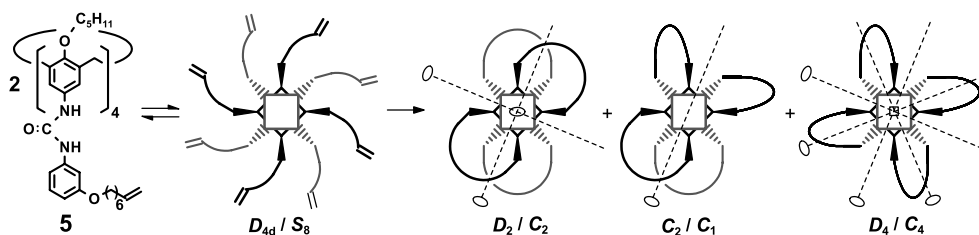
Scheme 5.11 Reaction products obtained by intramolecular olefin metathesis of the hydrogen bonded dimer **5·5**, identified by ^{1}H NMR and ESI-MS spectra.

in ^{1}H NMR spectra, led to their identification. While the starting homodimer shows only one NH signal (at ~10 ppm), four signals with equal intensity correspond to the envisaged bis[2]catenane formed by four α-connections. A doubly bridged [2]catenane (eight NH signals) is formed by two α- and two β-connections and a tetra-bridged capsule (two NH signals) by four β-connections [49] (Scheme 5.11). Considering the distances discussed above (Figure 5.6), this outcome is not entirely surprising.

To obtain selectively a single, well-defined product, it is obviously not sufficient to arrange the reacting groups in an appropriate mutual position. A "perfect" preorganization also demands the separation of those functional groups which should not be involved in the reaction. For an intramolecular connection between reactive functions attached to the urea residues, this preorganization is possible in heterodimers with a non-reactive tetra-urea calix[4]arene.

5.4
Multimacrocycles

5.4.1
Template Synthesis of Multimacrocyclic Calix[4]arenes

The intramolecular connection of two functional groups attached to the wide rim of calix[4]arene can be achieved under high-dilution conditions [50]. If the number of functional groups increases, a selective connection becomes more and more difficult, as illustrated in Figure 5.7. For methyl ethers, the situation is even more complicated by the presence of several conformations.
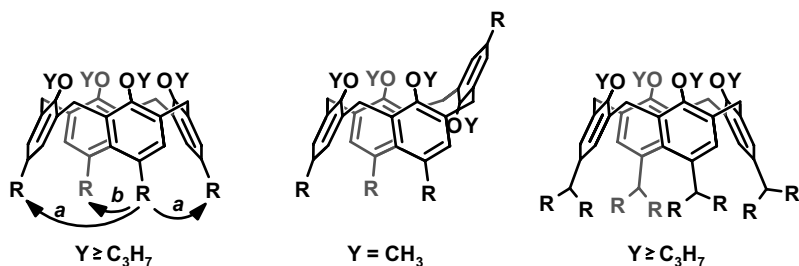
Figure 5.7 Possible side reactions and complications for the controlled intramolecular connection of functional groups R attached to the wide rim of a calix[4]arene.

Usual high-dilution conditions will not prevent a connection of opposite groups in **5**, and the controlled connection of eight alkenyl groups in **6** seems impossible (see Figure 5.8). In heterodimers with tetra-tosylurea **4** (Figure 5.4), however, the alkenyl residues are arranged in a way, which allows their interaction with the immediate neighbors only.[3] Furthermore, the template **4** induces the *cone*-conformation for tetramethylethers of type **5** or **6**, while tetramethoxy calix[4]arenes usually prefer the *partial cone* conformation.

In practice it is reasonable to use the non-reactive compound in the heterodimer, the tetra-tosylurea **4**, in a small excess, to exclude the undesired formation of homodimers **5·5** or **6·6**. After metathesis, the dimer is decomposed by a hydrogen-bond breaking solvent (usually THF), and the crude product is usually hydrogenated directly, to avoid complications by cis-trans isomerism. The whole reaction sequence is schematically summarized in Scheme 5.12. Bis- and tetraloop calix[4]-arenes **8** and **9** were easily prepared in high yields (70–95%) [51,52] for residues Y = methyl, pentyl, and dodecyl, and loop sizes of $n = 2 \cdot m + 2 = 8$, 10, 14, and 20.[4]

Several aspects show the generality of this approach:

a. The structure of the chains may be varied, using various different tetra-urea derivatives. Up to now, we have realized combinations of oligomethylene with oligoethyleneoxy chains [53].

b. As shown in Scheme 5.12, there is also a rational possibility of converting an AABB-type tetra-urea **7** into a trisloop compound **10**, possibly with different length of the connecting chain(s) [54]. Even in this case, the yield of pure **10** is surprisingly high (70–75%), although one undesired connection is possible between the two monoalkenyl urea residues.

c. Tetraloop compounds with different size and structure of the loops (characterized by X, Y, Z) are accessible; e.g. AAAB-type

---

[3] A transcavity contact should be possible only for very long chains.

[4] Up to $m = 11$, leading to $n = 20$ there was no indication of a reaction between two alkenyl groups attached to the same phenyl ring.
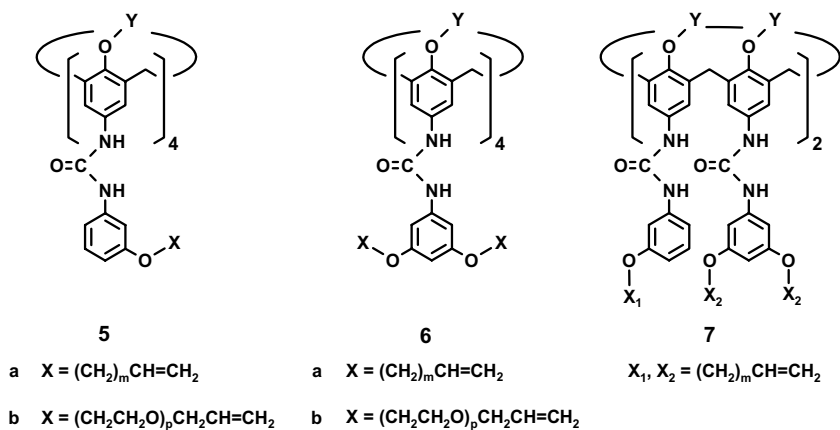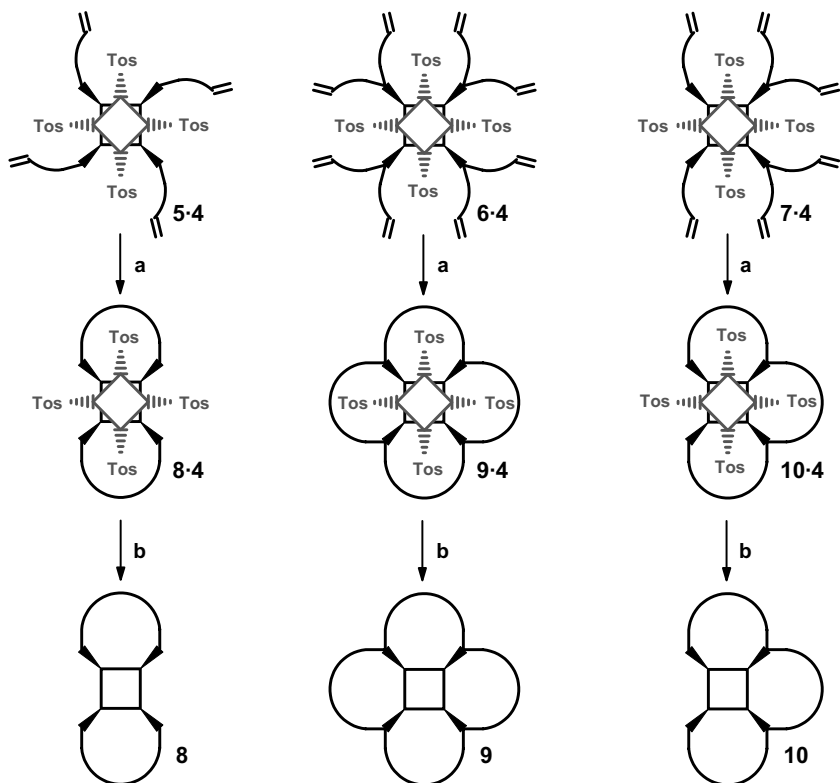
Figure 5.8 Formula survey of tetra-urea calix[4]arenes used as precursors for bis-, tris-, and tetraloop tetra-ureas (Y = alkyl).

Scheme 5.12 Selective synthesis of bis-, tris-, and tetraloop tetra-urea calix[4]arenes: (a) metathesis and subsequent hydrogenation, (b) decomposition of the heterodimer (a pseudorotaxane) and isolation of the multiloop calixarene.
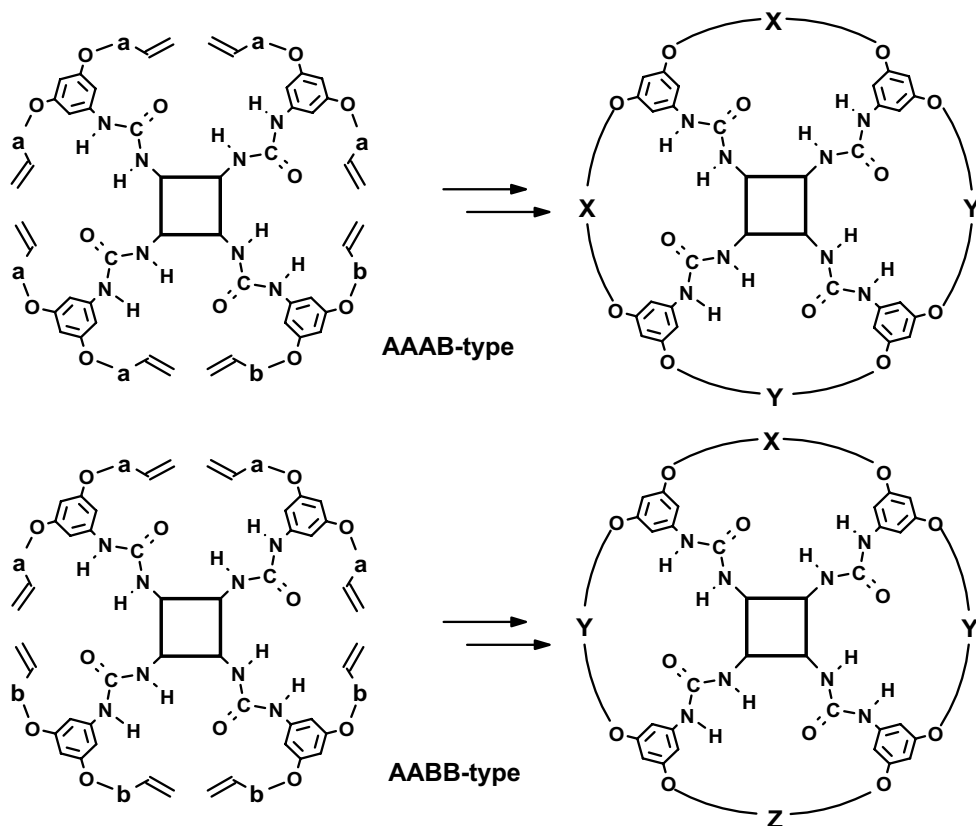
Figure 5.9 Approaches to tetraloop compounds with different size and structure of the loops via heterodimerization with tetra-tosylurea **4** followed by olefin metathesis and hydrogenation. X = a-(CH$_2$)$_2$-a; Y = a-(CH$_2$)$_2$-b; Z = b-(CH$_2$)$_2$-b.

ureas (compare Figure 5.5) lead to two different loops with the sequence XXYY, while the AABB-type gives three different loops with the sequence XYZY (see examples in Figure 5.9).

d. Finally, the reaction forming the macrocycle is not restricted to olefin metathesis. In principle, all reactions which proceed under conditions where the hydrogen bonded dimers exist should be suitable. (For an example, see Section 5.5)

The structure of bis- to tetraloop compounds is clearly proved by their ESI mass spectra (which usually show the molecular ion with high abundance) and by their ^{1}H NMR spectra in hydrogen bond breaking solvents, where they exist as mono-meric species. Examples of symmetrical bis- and tetraloop compounds are shown in Figure 5.10b,c. They demonstrate simultaneously that the molecules are kept in the
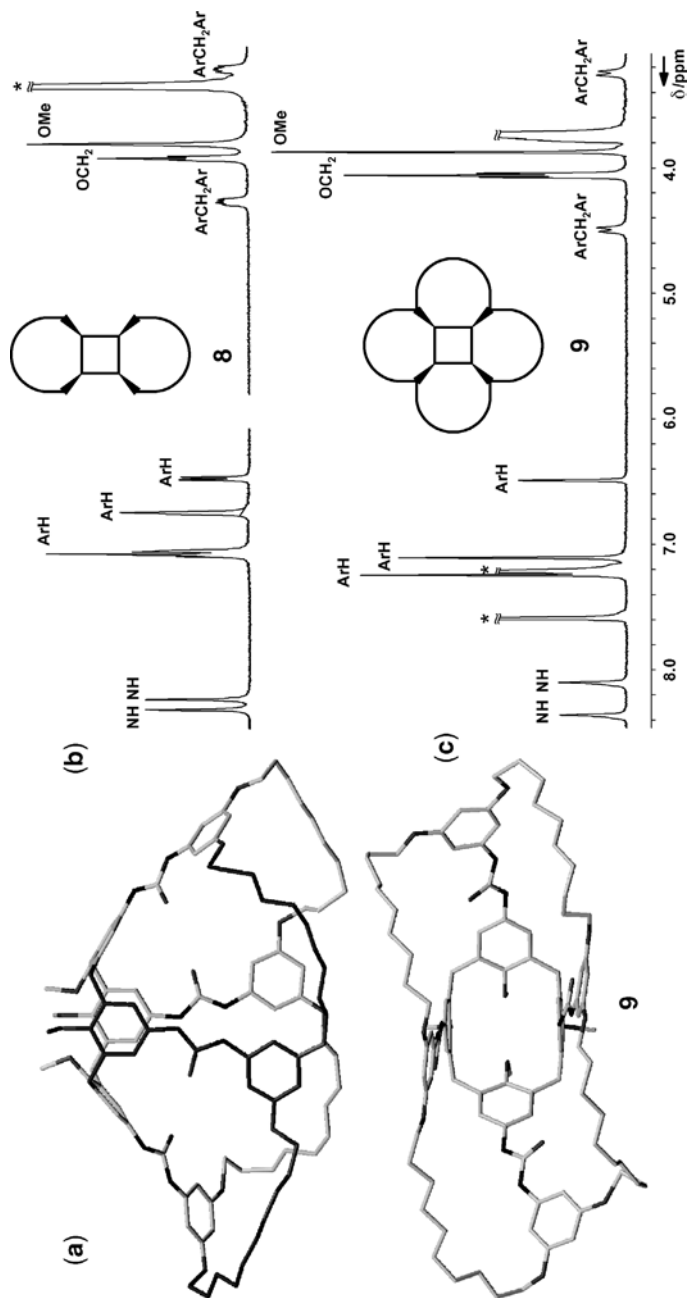
Figure 5.10 Molecular conformation of a tetraloop calix[4]arene **9** (Y=Me,n=10) in the crystalline state (a). ^{1}H NMR spectra (400 MHz) of a bisloop compound **8** (Y=Me,n=10) in DMSO-d$_6$ (H$_2$O peak is marked by asterisk) at 25 °C (b) and of a tetraloop compound **9** (Y=Me,n=14) in pyridine-d$_6$ (marked by asterisks) at 100 °C (c). A hydrogen bond-breaking solvent and elevated temperature are necessary to obtain a well-resolved spectrum of the monomeric molecule.

cone conformation, although tetramethylethers usually prefer the *partial cone* conformation. It may be assumed that a conformational interconversion becomes possible again for longer connecting chains. Indications are found already for bisloop compounds with $n = 20$ [53].

^{1}H NMR spectra in apolar solvents are less informative. Broad unresolved signals indicate the presence of undefined species. Obviously, the multicyclic structure does not allow the formation of regular dimers, which would lead to an unfavorable overlap of the loops, but the interaction via the urea functions creates "irregular" aggregates. This inability to form hydrogen-bonded homodimers can be exploited in further reactions, e.g., for the construction of multiple catenanes (see Section 5.5).

A single-crystal X-ray structure for a tetraloop compound shows the molecules (not unexpectedly) in a pinched cone conformation (see Figure 5.10a), although the time-averaged conformation deduced from the ^{1}H NMR-spectra is C_{4v}-symmetrical (Figure 5.10b).

5.4.2
Double Template Synthesis of Giant Macrocycles

Tetraloop compounds **9** contain a huge macrocycle (formed by fourfold metathesis), which is covalently connected to the calix[4]arene skeleton via four urea linkages. Cleavage of these connections is easily possible in boiling acetic acid (Scheme 5.13). Thus, flexible, macrocyclic molecules **11** are available in 50–75% yield [53], which would be difficult to obtain by non-templated macrocyclization reactions under high-dilution conditions.

The four *N*-(3,5-dioxyphenyl)acetamide fragments of the macrocyle **11** may be connected not only by oligomethylene chains of various lengths (up to now $n \leq 20$, corresponding to a total ring size of ≤ 100 atoms). Various other structural elements can be incorporated, and connecting chains may also be different in size and
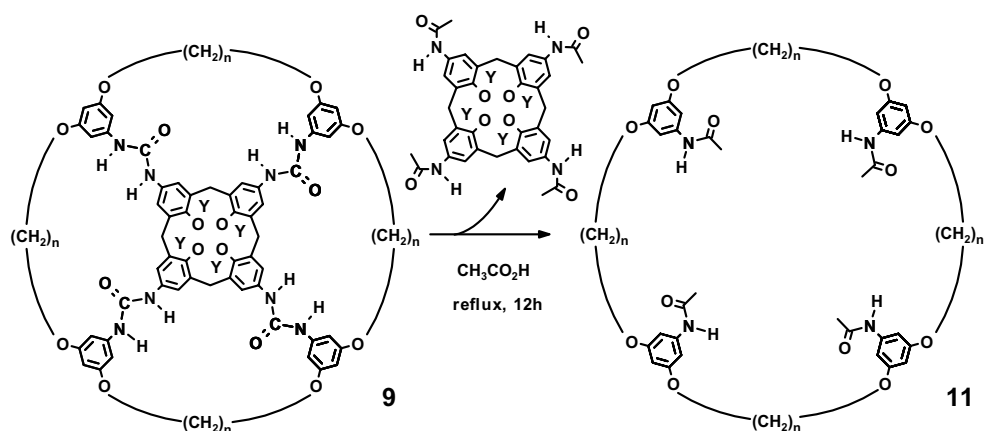
Scheme 5.13 Release of a macrocyclic molecule **11** by cleavage of the urea groups.
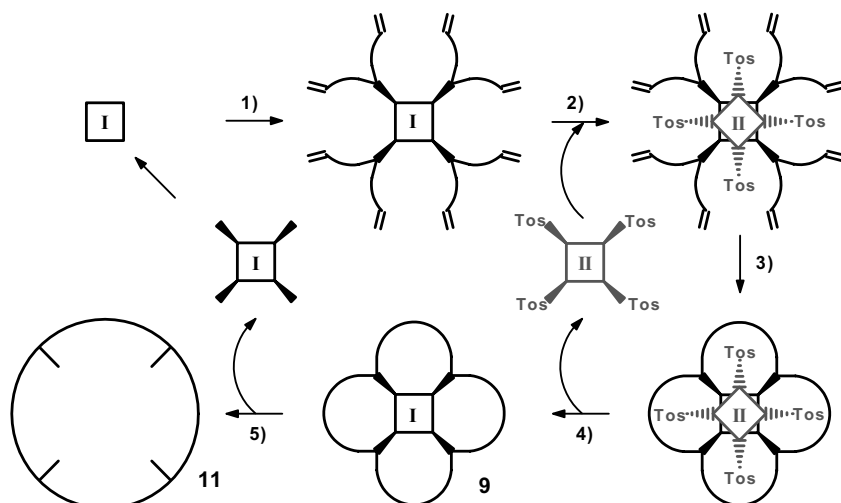
Scheme 5.14 Reaction sequence (schematic) for the synthesis of huge macrocycles using a calix[4]arene twice as template. The single steps are discussed in the text.

structure. From these possibilities, macrocycles containing ethyleneoxide segments have been realized so far [53].

The total reaction sequence, in which a macrocycle is formed in a well-defined way by the connection of four reactive, bifunctional fragments, involves two calix[4] arenes as template, as schematically shown in Scheme 5.14 and described below:

1. First a tetraamino calix[4]arene (template I) is used to attach four α,ω-bisethylene fragments via urea groups. Thus, the number (four) and, as indicated above, eventually the sequence of the fragments to be connected, is determined.

2. A second calix[4]arene, the tetra-tosylurea (template II) is used to bring the reactive groups into the correct position for their connection.

3. Metathesis, followed by hydrogenation, converts the heterodimer into a pseudorotaxane.

4. After the reaction, a hydrogen bond breaking solvent liberates template II, which can be used again.

5. Finally, the urea links are cleaved to isolate the target product (the macrocycle) and template I (as tetraacetamide), which can in principle be used again. (In practice it is easier to prepare the tetraamino calix[4]arene according to Scheme 5.8.)

It should be possible to synthesize still larger and more sophisticated macrocyclic molecules in a similar manner.

5.5
Multiple Catenanes Based on Calix[4]arenes

5.5.1
General Considerations

The inability of bis-, tris-, or tetraloop compounds to form homodimers and the general tendency of tetra-urea calix[4]arenes to dimerize can be further exploited for the synthesis of mechanically interlocked molecules. A 1:1 mixture of tetra-ureas **5** or **6** with bis- or tetraloop compounds **8** or **9** (in practice the non-reactive loop component is added in a small excess) contains *exclusively* heterodimers (e.g., **5·8**, **5·9**, or **6·9**), since this is the *only* possibility, to have all the urea functions involved in the favorable hydrogen-bonded belt.[5] Again this is easily evidenced by the complete absence of peaks for the homodimer **5·5**, or **6·6** in the ^{1}H NMR spectra (for an example see Figure 5.11).

Like in heterodimers with tetra-tosylurea (**4**), the alkenyl groups of **5** and **6** are prearranged in these heterodimers with **8** or **9** in a way which allows only one well-defined connection by metathesis reaction. The only difference is that this now leads
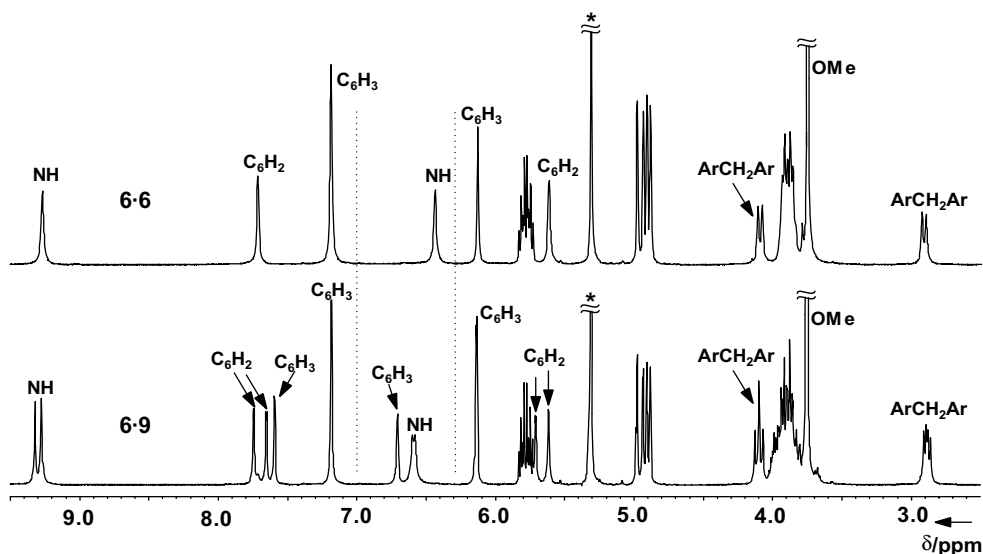
Figure 5.11 ^{1}H NMR (400 MHz, 25 °C) spectroscopic evidence for the exclusive formation of heterodimers in a stoichiometric mixture of **6** (Y=Me,n=6) and **9** (Y=Me,n=14) in CD$_2$Cl$_2$ (marked by asterisk). Mainly the region between 6.3 and 7.0 ppm shows that no signals for the homodimer **6·6** are present.

[5] A similar principle was used in the Cu(I) templated synthesis of various catenanes (see Sauvage and coworkers in Refs. [9–11]).
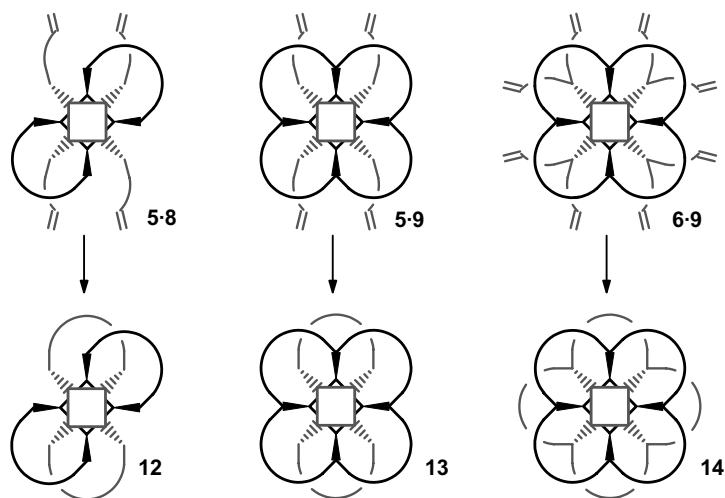
Scheme 5.15 Controlled syntheses of bis[2]catenanes **12**,
bis[3]catenanes **13** and cyclo [8]catenanes **14**.

to catenated ring structures. Thus, it is not entirely surprising that bis[2]catenanes **12**
(from **5·8**), bis[3]catenanes **13** (from **5·9** or **6·8**) and cyclic [8]catenanes **14** (from **6·9**) are
formed in excellent yields of 50–97% (isolated and purified product), as schematically
represented in Scheme 5.15 [55]. The formation of eight interlocked ring-systems in
one step and in a yield of up to 90% is a particularly striking example of the effect of
preorganization.

Based on all experience, it is justified to predict, that the combination of trisloop
compounds with bis- or tetraloop compounds to give the respective catenanes will
also proceed selectively with high yield (Scheme 5.16), since only one heterodimer is
possible in all these cases. Only the combination of a trisloop compound **10** with its
alkenyl precursor **7** may lead to two regioisomeric dimers.

5.5.2
Bis[2]catenanes

The synthesis of bis[2]catenanes outlined in Scheme 5.15 allows not only the prepa-
ration of compounds with identical loops (**12a**). The rings attached to the second
bisloop calix[4]arene may be also different from those of the first calix[4]arene (**12b**)
[55]. Two regioisomeric bis[2]catenanes are possible, where the two rings attached to
a given calix[4]arene are different (Figure 5.12) The isomer **12c** can be selectively
synthesized from a bisalkenyl urea, where the other two urea functions are con-
nected to a loop, while the third regioisomer **12d** would be not so easily available.

The rational synthesis of **12c** is shown in Scheme 5.17. The starting monoloop
di-urea **15** is prepared in the conventional way analogous to Scheme 5.9 by macro-
cyclization of the di-Boc derivative with an activated bisurethane under dilution
conditions, followed by deprotection and acylation [50]. Although **15** belongs to the
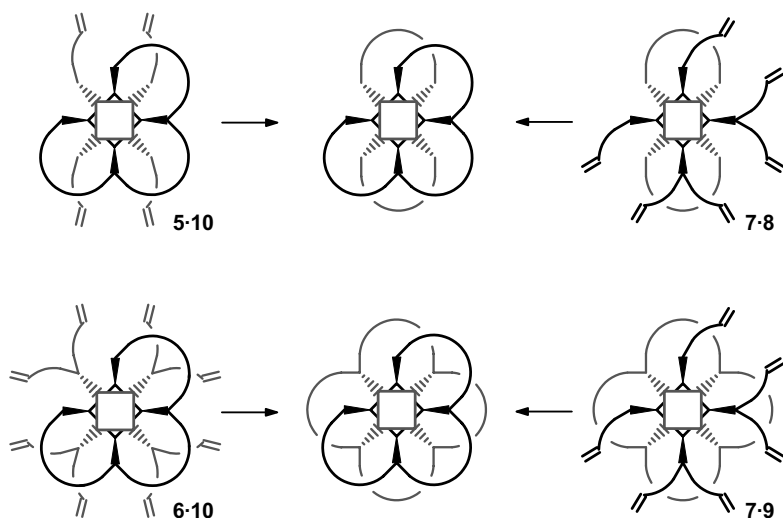
Scheme 5.16 Possible synthetic pathways to calix[4]arene-based multiple catenanes involving trisloop derivatives.
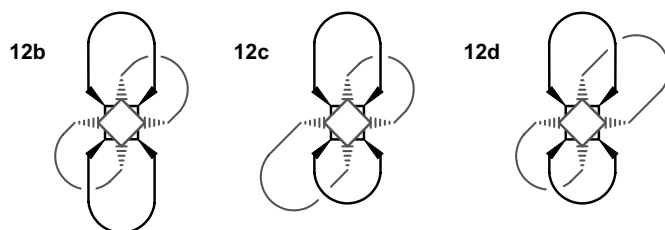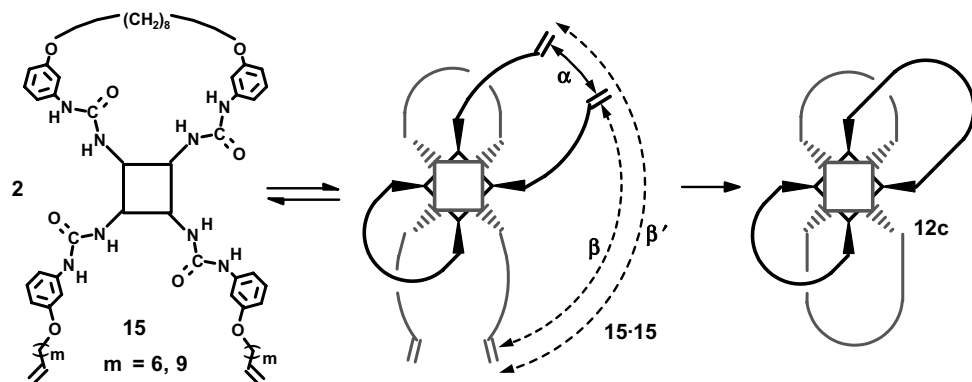

Figure 5.12 Regioisomeric bis[2]catenanes with pairwise different rings.

Scheme 5.17 Synthesis of bis[2]catenanes of type **12c**. Instead of the desired α-connections between alkenyl residues belonging to the same calixarene molecule, a β-connection between the two molecules of the dimer **15·15** is also possible. This would leave two remote alkenyl groups for a potential β′-connection.

AABB-type it forms only *one* regioisomeric dimer **15·15**, since the two macro-rings do not overlap for steric reasons. In dimer **15·15**, there is still one possibility for the undesired connection between (adjacent) alkenyl residues belonging to different calixarenes (β-connection), which may be the reason for the lower yield of ∼50%. For longer chains also a connection of remote alkenyl groups (β'-connection) cannot be excluded (see Section 5.5.3).

All bis[2]catenanes are chiral. Figure 5.13 illustrates their symmetry properties. ^{1}H NMR spectra are in agreement with the predicted symmetry, although for a C_1-symmetric species, such as **12c**, or a mixture of two diastereomeric C_2-symmetrical compounds of type **12b** a complete resolution of all peaks is usually not possible.

The optical resolution was achieved in most cases on an analytical scale by chromatography [52] (see the example in Figure 5.14) using chiral stationary phases of the Chiralcel OD or Chiralpak AD-H type. The separation factors vary between close to 1 and 2.36.

In two cases, it was possible to confirm the structure by single-crystal X-ray analysis, although the atoms of the interlocking chains are usually strongly disordered. Figure 5.15 shows one example. The crystal was grown from chloroform/methanol, a hydrogen bond breaking mixture, and the dimeric capsule is completely opened. The whole assembly is connected only by the interlocked rings. This disrupted capsule suggests that a guest exchange should be easily possible in bis[2]catenanes already for rings with n = 10.
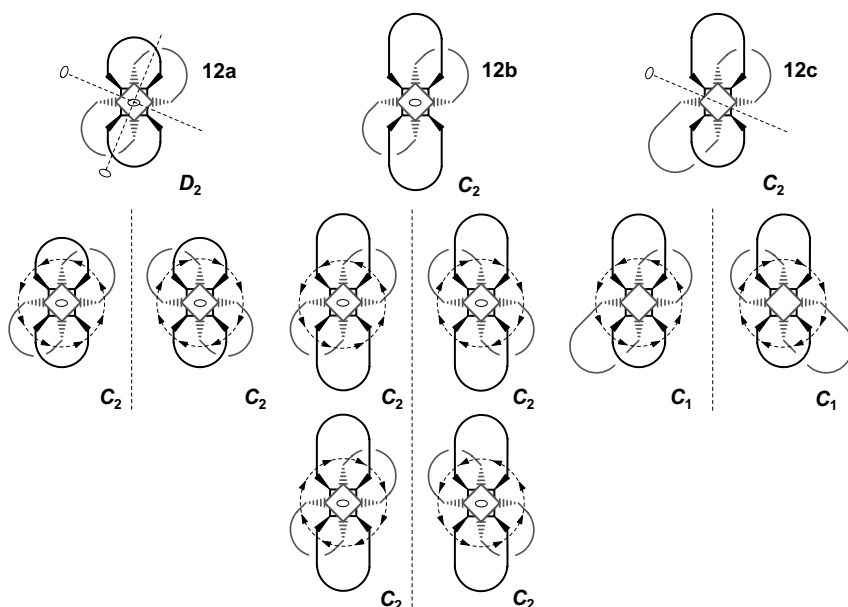

Figure 5.13 Symmetry properties of bis[2]catenanes with identical (**12a**) and different rings (**12b** and **12c**).
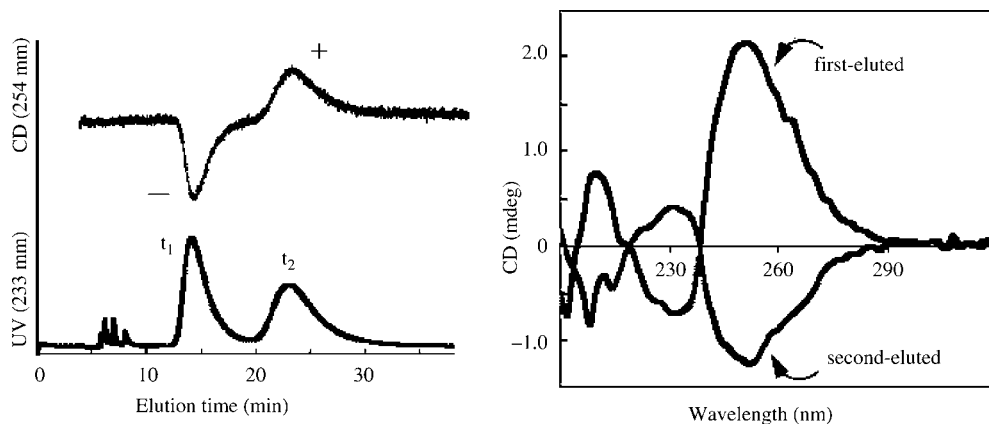
Figure 5.14 Example of the chromatographic resolution of **12a**.
Column: Chiralcel OD, eluent: hexane/ethanol (90/10, v/v), CD-
spectra of both fractions: hexane/ethanol (90/10, v/v), cell
length: 25 mm.

5.5.3
Towards Novel Topologies

When the synthesis outlined in Scheme 5.17 was applied to larger loops (e.g.,
n = 20), the purification of the product became more difficult or even impossible.
While the samples showed the expected ESI mass spectrum, a satisfactory purifica-
tion from a chromatographically similar compound was not possible, and the ^{1}H
NMR spectrum was not entirely in agreement with the expected structure. This led
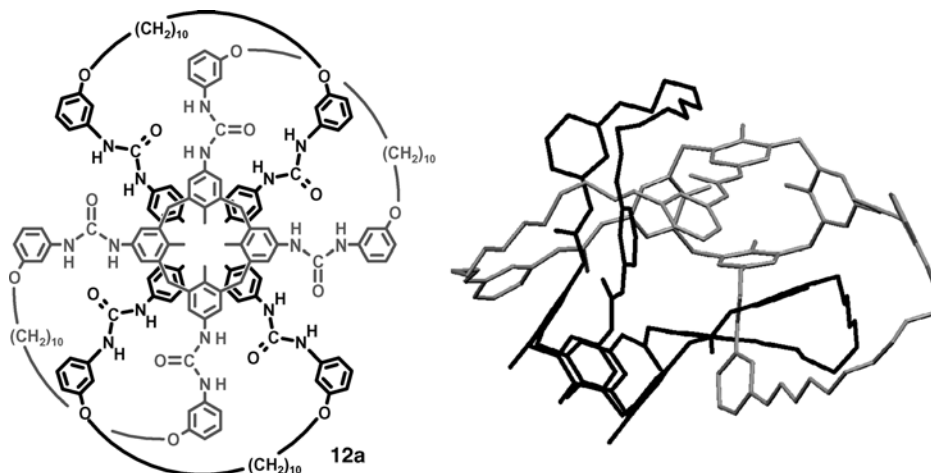
Figure 5.15 Molecular structure of **12a** as determined by X-ray
analysis (Y = pentyl, n = 10). Ether residues, solvent, and
H-atoms are omitted for clarity.
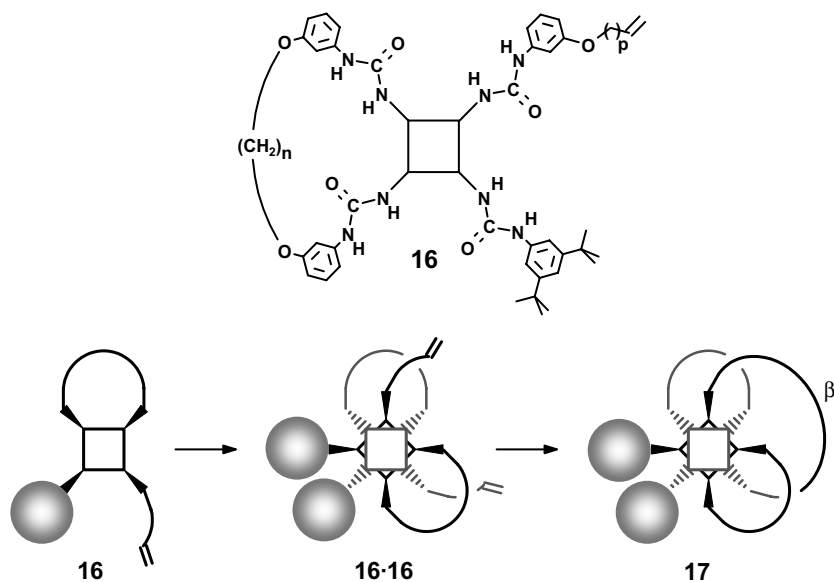
Scheme 5.18 Probing the possibility of a β'-connection: Dimerization and metathesis reaction of tetra-urea **16** (n = 8, 10; p = 9).

to the idea that an isomeric compound was formed by a combination of a β- and a β'-connection.

Molecular models suggest that such a β'-connection between remote alkenyl residues in a dimer is possible. To check whether it really occurs under the conditions of the metathesis reaction, we synthesized the monoloop tetra-urea compounds **16**, in which one of the non-cyclic urea residues is substituted by a bulky group which cannot penetrate the loop (Scheme 5.18). (The synthesis is analogous to that of **15**, introducing in the final two steps the bulky residue first.).

Formally compound **16** belongs to the **AABC**-type of tetra-ureas (compare Section 5.3.2) for which numerous regioisomeric dimers are possible. However, these substituents at the urea residues ensure that selectively only *one* dimer is formed, in which no overlap of the loops occurs and no penetration of the loop by the bulky group takes place. ^{1}H NMR spectra are in agreement with the formation of a single C_2-symmetrical dimer, which is necessarily composed of the same enantiomer of **16**.

In fact, after metathesis and hydrogenation a single reaction product is isolated in 40–55% yield, which cannot be split in its calix[4]arenes by hydrogen bond breaking solvents [56]. Although the structure for several single crystals could not be solved, the ^{1}H NMR and ESI mass spectra serve as an unambiguous structural proof.

The topology of these molecules becomes more evident by the "transformations" shown in Figure 5.16. The representation reached after some simplifications, which
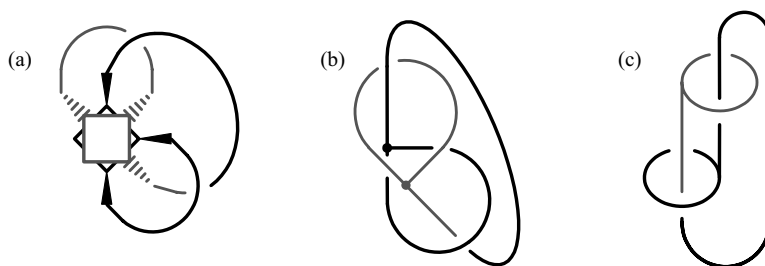
Figure 5.16 Illustration of the topology of **17** by stepwise simplification: (a) omission of non-cyclic urea arms; (b) graphical reduction of each calixarene to a branching point; (c) optical rearrangement of the graph.

do not change the topology, shows, that there are structural elements of catenanes and rotaxanes (and even some similarities to knots).[6]

5.5.4
Bis[3]catenanes and Cyclic [8]Catenanes

In contrast to bis[2]catenanes **12**, which are topologically chiral, bis[3]catenanes **13** and cyclic [8]catenanes **14** prepared via metathesis and subsequent hydrogenation are usually not chiral. For identical loops, their symmetry (without and with the directionality of the hydrogen-bonded belt) is C_{2v}/C_2 and D_{4d}/S_8, respectively. This is reflected by their NMR-spectra (for an example, see Figure 5.17).

The structure of **14** (n = 14) was unambiguously proved by single-crystal X-ray analysis (Figure 5.18). The space-filling representation suggests a more or less
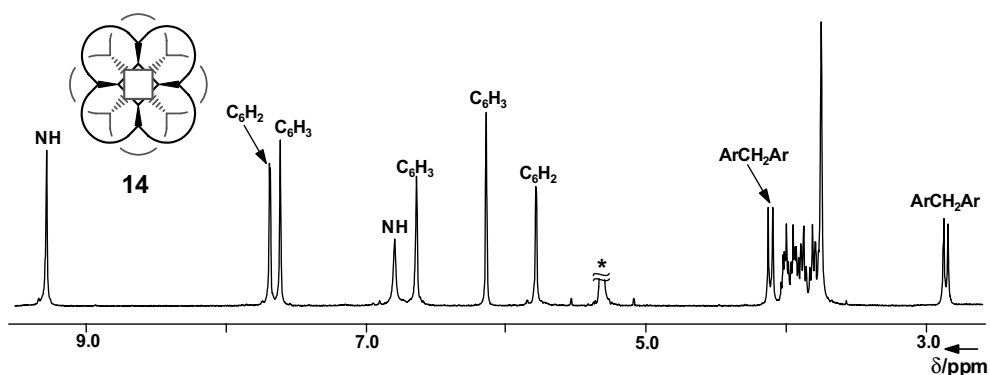
Figure 5.17 ^{1}H NMR spectrum (400 MHz, 25 °C) of a cyclic [8]catenane of type **14** (Y = methyl, n = 14) in CD$_2$Cl$_2$ (marked by asterisk) reflecting S_8-symmetry of the molecule (compare Fig. 5.1b).

---

6) For a similar rotaxane, see Ref. [3].

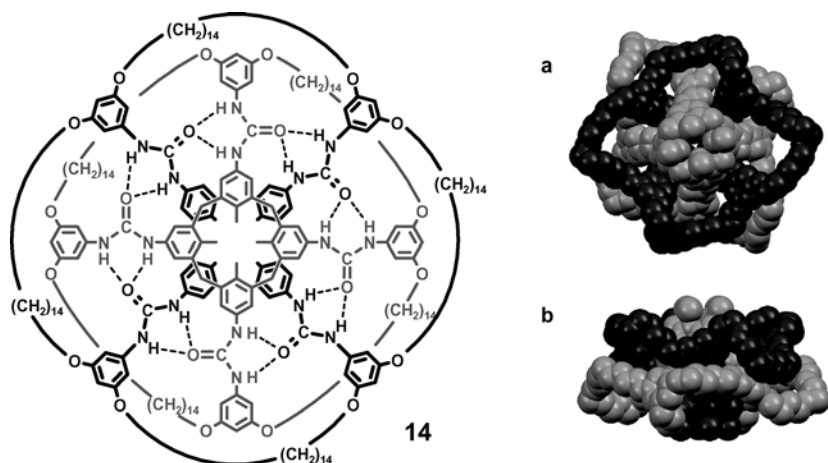**Figure 5.18** Molecular shape of the cyclic [8]catenane **14** (Y = methyl, $n = 14$) in the crystalline state, showing the interlocking of eight rings. Space-filling representation seen along the S_8-axis (a) and perpendicular to it (b). Alkyl residues and hydrogen atoms are omitted for clarity.

complete shielding of the included guest. However, it was shown by ESI mass spectra that, for the examples studied so far, an exchange of the guest is still possible. A solution of **13** or **14** in a 1:1:0.4 mixture of 1,4-difluorobenzene, dichloromethane, and methanol showed a strong peak corresponding to the doubly charged species of the respective catenane **13** or $\mathbf{14} + 2Na^+ + C_6H_4F_2$. Since 1,4-difluorobenzene was neither present during the synthesis nor during work-up, its inclusion during the MS-experiments with the catenanes remains the only reasonable explanation.

As discussed before, the strategy to synthesize catenanes is not necessarily restricted to olefin metathesis as the ring closing reaction. Any reaction which can be carried out under conditions where the hydrogen-bonded dimers exist should be appropriate. A first example was realized by the formation of anhydride linkages with dicyclohexylcarbodiimide as the reagent in benzene as the solvent [57], as schematically illustrated in Scheme 5.19.
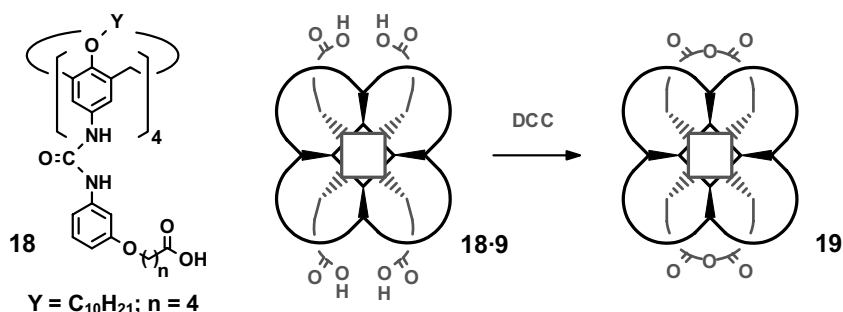
Scheme 5.19 Synthesis of a bis[3]catenane **19** with two cyclic anhydride structures.
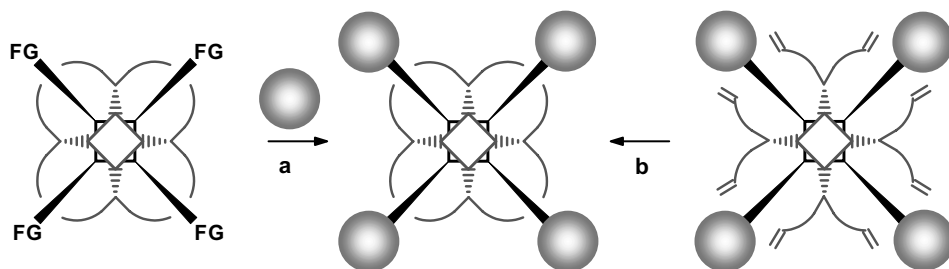
Scheme 5.20 Two possibilities to synthesize tetra[2]rotaxanes (schematic): (a) by stoppering (FG represents a suitable functional group) or (b) by clipping (ring closure by metathesis).

5.6
Multiple Rotaxanes

The preorganization of functional groups attached to the urea residues could also be used for the synthesis of multiple rotaxanes. Schematically, this is shown for tetra[2] rotaxanes in Scheme 5.20. Bis[2]rotaxanes will be available analogously, using a bisloop compound **8** instead of the tetraloop compound **9**.

In principle there are two possible pathways:

- Bulky residues can be attached to the urea groups of a tetra-urea under conditions where it forms a heterodimer (a pseudorotaxane) with a bis-, tris-, or tetraloop tetra-urea. Often this strategy is called "stoppering" (see Scheme 5.7), because stoppers are attached to the axles.
- Multiple ring-closure reactions between adjacent urea functions of a suitably functionalized tetra-urea in a heterodimer with a second tetra-urea bearing bulky groups can also create the structural elements of a rotaxane. This strategy is usually called "clipping" (see Scheme 5.7).

To realize the first possibility, the tetra-ureas **20** bearing maleic imide functions at all four urea arms were synthesized. These dienophiles react with anthracene derivatives, here 1,4,5,8-tetrapentoxyanthracene **21**, in a Diels-Alder cycloaddition (Scheme 5.21).

Tetra-ureas **20** form homodimers in solvents such as $CDCl_3$ or C_6D_6, but they are completely converted to heterodimers upon addition of an equimolar amount of a tetra-loop compound **9**. When a 5–10% excess of the anthracene derivative **21** was applied, a quantitative conversion was obtained in refluxing toluene after 72 h (as judged by NMR), and the tetra[2]rotaxane **22** was isolated in 40–50% yield.

The rotaxane structure of **22** can be demonstrated by ESI-MS or MALDI-TOF-MS. It remains intact in THF-d_8, a solvent in which the tetra-urea dimers usually dissociate. However, an upfield shift of the NH-signals in ^{1}H NMR indicates that the
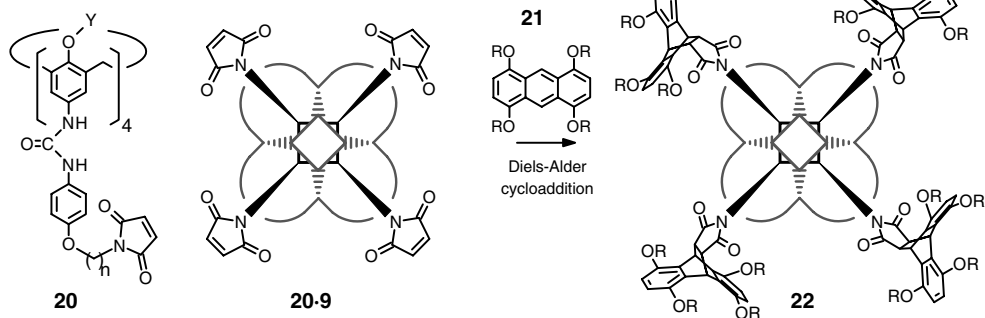
Scheme 5.21 Formation of tetra[2]rotaxanes **22** (n = 8, 10;
Y = R = C$_5$H$_{11}$) by stoppering. Introduction of bulky stopper
residues by Diels-Alder cycloaddition.

hydrogen-bonded belt is weakened and that the urea functions are partly solvated by
THF [58].

The synthesis of fourfold [2]rotaxanes by clipping requires the efficient formation of
heterodimers between a tetra-urea substituted by bulky stopper groups and an octaalk-
enyl urea **6**. We initially hoped that the steric crowding in homodimers of a tetra-
tritylphenylurea calix[4]arene would be sufficient to shift the equilibrium toward the
heterodimers in a mixture with **6**. However, the distribution of the dimers was close to
the statistical ratio and the desired rotaxane could be obtained in only 5% yield [59].

On the other hand, when smaller rings were synthesized according to the tem-
plate reaction discussed in Section 4 (Scheme 5.12), it became difficult to split the
tetraloop calix[4]arene **9** from the tetra-tosylurea **4** used as template. For n = 6, a
splitting was eventually completely impossible. This follows for instance from the
fact that the guest (here CH$_2$Cl$_2$), necessarily included when the heterodimeric
capsule is formed, is not released under hydrogen bond breaking conditions. Thus,
the molecules **23** represent the first examples of fourfold [2]rotaxanes which were
obtained by a clipping reaction [60].

In spite of having grown several single crystals, it was not possible to solve the
structure of **23**. To illustrate the shape of the rotaxane, Figure 5.19 shows an energy-
minimized structure obtained by MD simulation. It is evident that the tetrahedral
arrangement of the substituents around the sulfur atoms (N-S-C angle ca. 109°)
prevents a slipping of the loops.

It is not surprising that the stability of **23** depends on the size of the loops. For
n = 8, slow dissociation occurs in THF (estimated half-life 10–20 days), while im-
mediate decomposition occurs in DMSO or pyridine. For n = 6, however, no disso-
ciation was observed after several weeks. An exchange of the included guest(s) is
possible also for the intact rotaxane. For n = 8, ethyl acetate (included during the
chromatographic isolation) is exchanged against the solvent THF-d$_8$ in a first-order
reaction ($\tau_{1/2} = 32$ min). For n = 6, only one of two included dichloromethane
molecules is lost ($\tau_{1/2} \approx 12$ days). This inclusion of two guest molecules in a dimeric
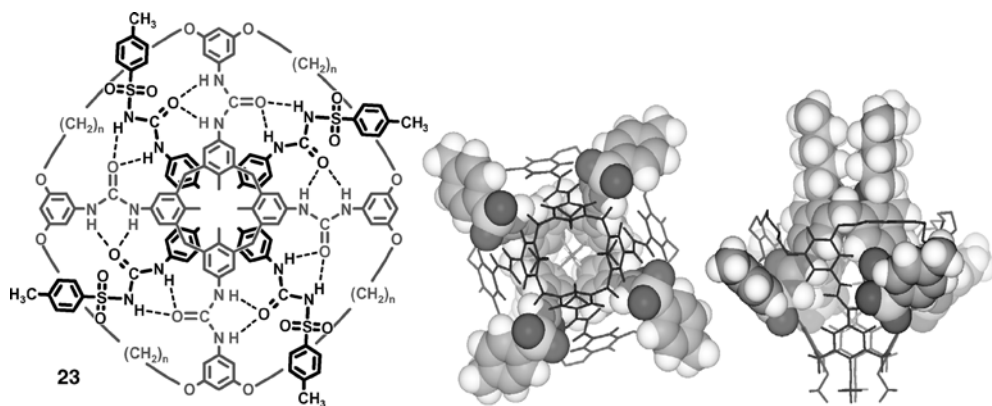capsule of the tetra-urea type was for the first time unambiguously proved by

Figure 5.19 Molecular shape of rotaxane **23** ($n = 6$), a hetero-dimeric assembly of a tetraloop tetra-urea **9** (stick representation) and tetra-tosylurea **4** (space filling), based on MD simulations. Ether groups ($OY = OC_5H_{11}$,) are omitted in the formula.

ESI-MS. Obviously heterodimers of tetra-arylureas, e.g., tolylurea (**1**), with **4** have a larger internal volume than homodimers **1·1** (260–270 Å^3 vs. 190–200 Å^3, based on MD simulations) [61] because of differences in the hydrogen-bonding pattern [62].

5.7
Self-sorting and Formation of Larger Assemblies

The covalent connection of two tetra-urea calix[4]arenes via their narrow rims leads to molecules which are *bifunctional* with respect to their ability to form dimeric capsules. This was used by Rebek and Castellano to form self-assembled "polycaps", including also alternating structures based on the heterodimerization of aryl- and tosylureas [42,63]. The idea was later extended to switchable polymers [64]. We recently able to show that the covalent connection of two tetra-urea calix[4]arenes via a rigid spacer between urea functions also leads to molecules **24**, which can form polymeric assemblies (Scheme 5.22) [57,65].

As shown in Section 5.5, bisloop or tetraloop tetra-ureas (**8**, **9**) do not form homodimers, while monoloop compounds (e.g., **15**) form selectively only one homodimer. These selectivities may be summarized as follows:

1. Tetra-urea molecules in which adjacent urea functions are covalently connected form only those dimers in which no overlapping of the loops occurs.
2. If urea functions with bulky substituents are present, only those dimers can be formed in which the bulky residues need not thread through a loop.

With the kind and size of loops studied so far, no exception to the first rule was found, while the situation is less clear for the second rule. The threading of a larger
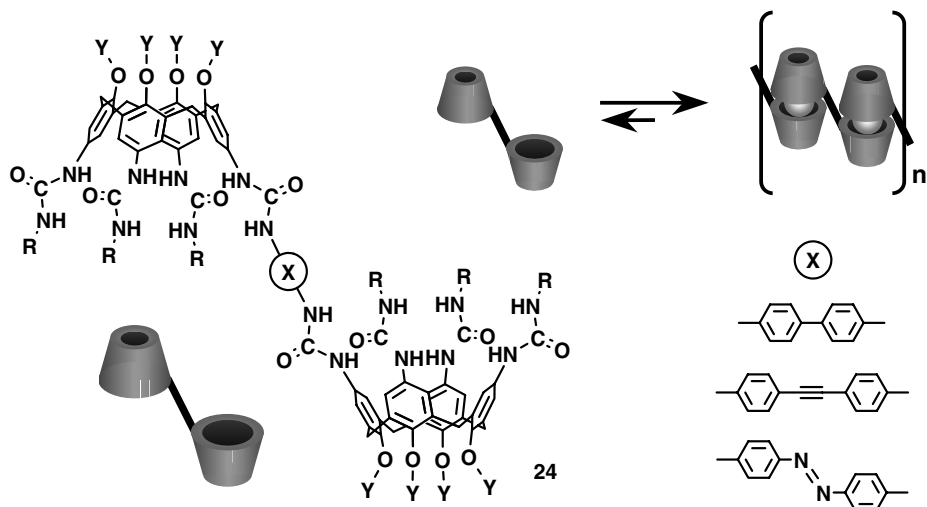
Scheme 5.22 Tetra-urea calix[4]arenes **24** connected via a rigid spacer **X** between their urea functions, and schematic representation of their self-organization.

urea residue may be sometimes a kinetic problem, depending also on the reaction conditions (solvent, temperature, etc.). In combination with the tendency to form dimeric capsules in apolar solvents, these rules describe a self-sorting process, illustrated in Scheme 5.23 by one example. The principle has already been used for the synthesis of multicatenanes (Section 5.5) and the synthesis of rotaxanes by stoppering (Section 6).

Such a self-sorting process can also lead to the formation of structurally well-defined assemblies of the dendrimer type [66]. We have demonstrated this in a first example, using the dimerization of tri-ureas **26** derived from triphenylmethanes [67]. It has been shown that this dimerization is independent of the dimerization of tetra-urea calix[4]arenes. It is neither disturbed by tetra-ureas nor does it disturb their dimerization. In addition, Figure 5.20 even shows that the dimerization of rigidified tetra-ureas **25** also occurs independently [68].

Therefore, we connected the tri-urea **27** with three tetra-ureas **28**, via covalent linkers, to a building block **A**. In apolar solvents molecules **A** alone would form crosslinked polymers via dimeric substructures formed by the tri- and tetra-ureas. Together with the building block **B**, a tetra-tosylurea substituted by four phthalimido alkylether residues, this polyassociation is prevented by the formation of hetero-dimers between tetra-aryl- and tetra-tosylureas. A solution of **A** and **B** in the ratio 2 : 6 therefore contains exclusively the dendritic assembly shown in Figure 5.21, as proved by light scattering and DOSY NMR spectroscopy [69].

The self-assembled dendrimer carries 24 phthalimide groups (= protected amino groups) on its surface, which can be replaced also by other groups (e.g., dyes). Even larger structures should be available, using the whole spectrum of selectivities indicated above.
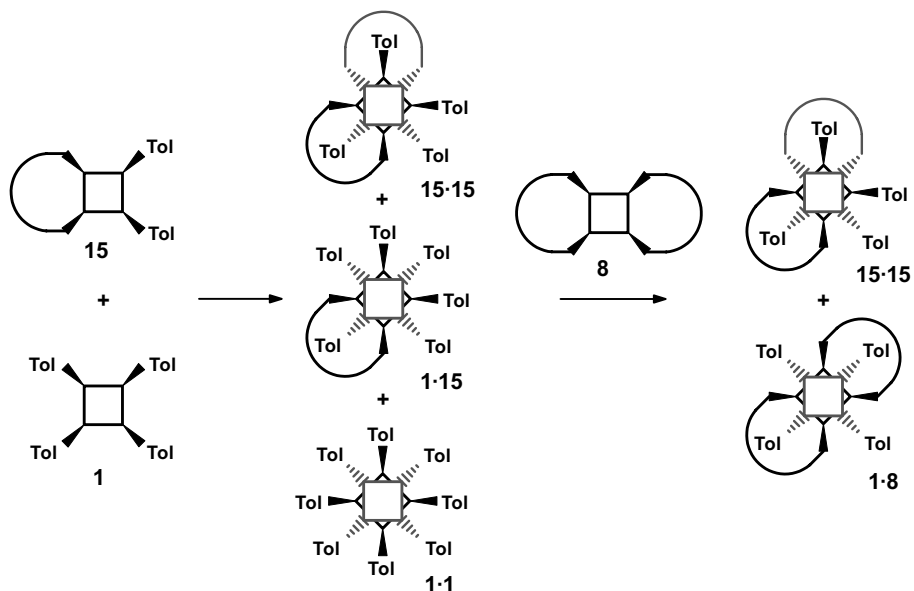
Scheme 5.23 Self-sorting of open (**1**), monoloop (**15** with tolyl urea residues), and bisloop (**8**) tetra-ureas. The addition of bisloop compound **8** converts the mixture of three dimers **1·1**, **1·15**, and **15·15** into a mixture of only two dimers, **1·8** and **15·15**, the only possibility to have all tetra-ureas assembled in a dimer.
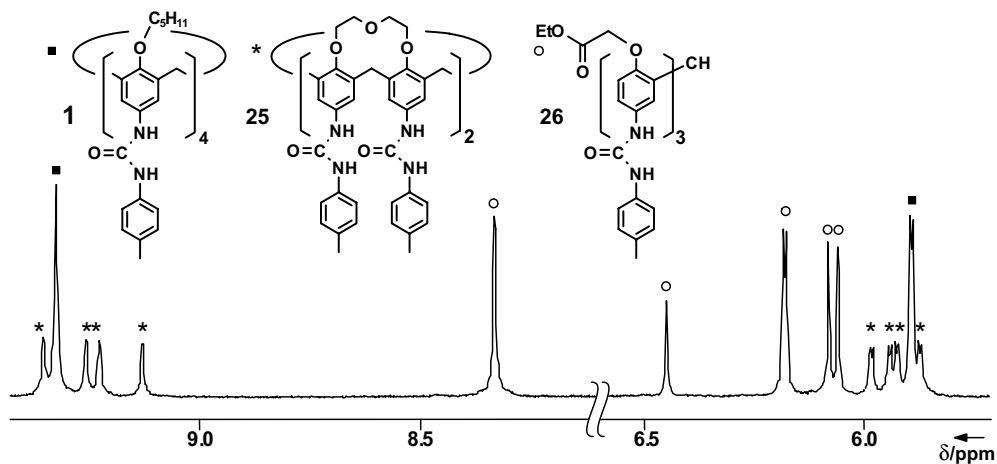

Figure 5.20 Partial ^{1}H NMR spectrum (400 MHz, CDCl$_3$, 25 °C) of a mixture of tetra-ureas **1** and **25** and tri-urea **26** showing only signals of the three homodimers. This proves the independent dimerization of the three different tri/tetra-urea molecules.
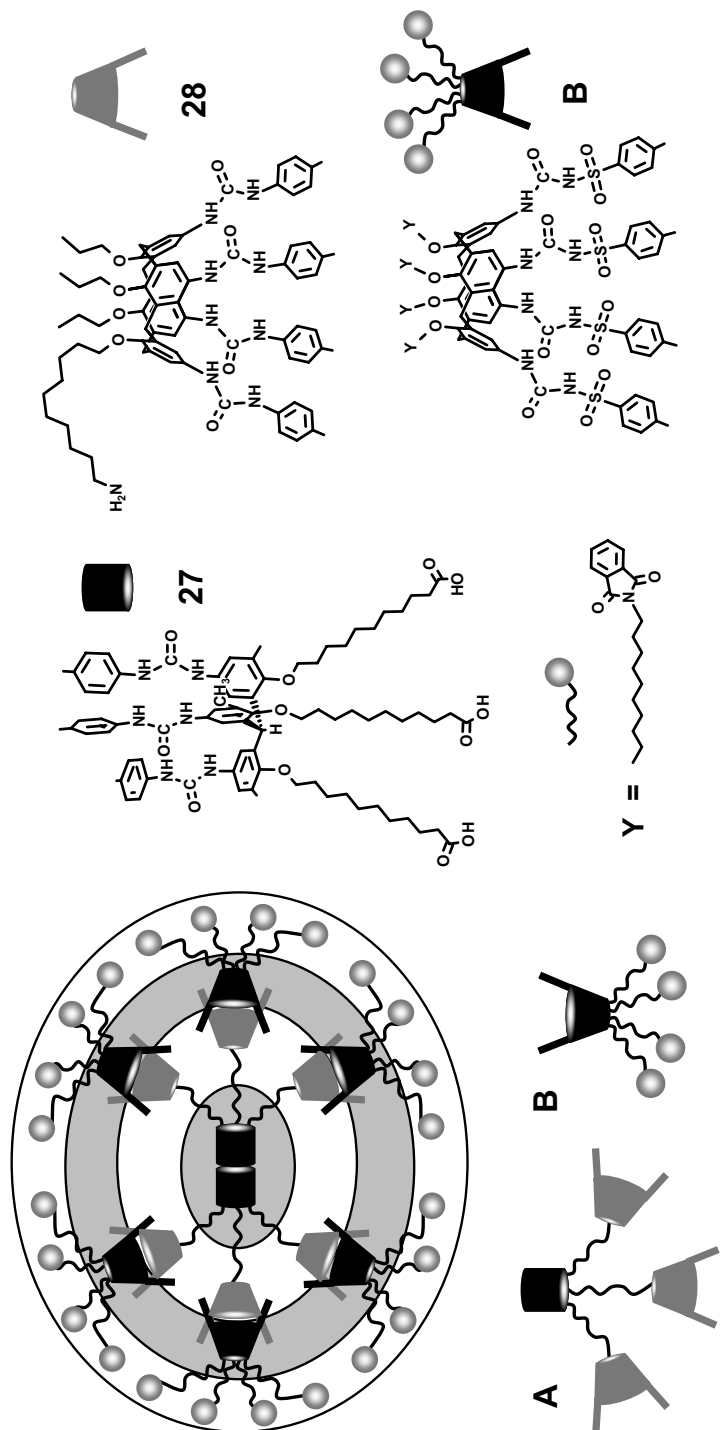
Figure 5.21 Self-assembly of two building blocks **A** and six building blocks **B** to a structurally uniform dendrimer.

5.8
Conclusions and Outlook

The principal idea of this present essay was to show how the unique preorganization of functional groups in self-assembled dimers of tetra-urea calix[4]arenes can be used to prepare novel multi-rotaxanes and -catenanes or topologically even more complex molecules and supramolecular structures. We will conclude by summarizing some related studies in which calixarenes were used in a different way as building blocks for the construction of such structures or assemblies.

As early as 1993, Gutsche and Kanamathareddy found that calix[6]arenes in which opposite oxygens are connected by a *p*-xylylene ether bridge have the tendency to assume a conformation which they dubbed "self-anchored rotaxane" [70,71]. However, the use of a calix[6]arene as a wheel for [2]rotaxanes did not occur before 2000 [72]. Their synthesis is based on the stability of pseudorotaxanes formed by 1,3,5-triphenylureidocalix[6]arenes and dialkylviologen cations as an axle [73], which allows the introduction of stoppers by esterification of the hydroxyl end groups of the axle (reflux with diphenyl acetyl chloride in toluene for 72 h). Since the threading of an asymmetrical dipyridinium axle occurs exclusively from the wide rim [74], it was even possible to prepare constitutionally isomeric rotaxanes, using two different stoppers [75]. In view of these examples, it is astonishing that the larger calix[8]arene was not yet used as a macrocyclic component in rotaxanes or catenanes. Calix[4]arenes have been used, however, as stoppers in rotaxanes [76], where they can contribute to the binding of guests [77].

Examples of the incorporation of calixarenes into [2]catenanes are rare. They are not based on the calixarene as such as a macrocycle, but as a fragment for the construction of a cyclobis(paraquat-*p*-phenylene) [78,79]. Thus, with bis-*p*-phenylene-[34]crown-10 as the second ring (Figure 5.22a) a [2]catenane is prepared, as described at the beginning of this chapter, using donor-acceptor interactions for the necessary preorganization.

The construction principle has recently been inverted, incorporating one of the phenolic units of a calix[4]arene in the crown ether ring (Figure 5.22b) [80].
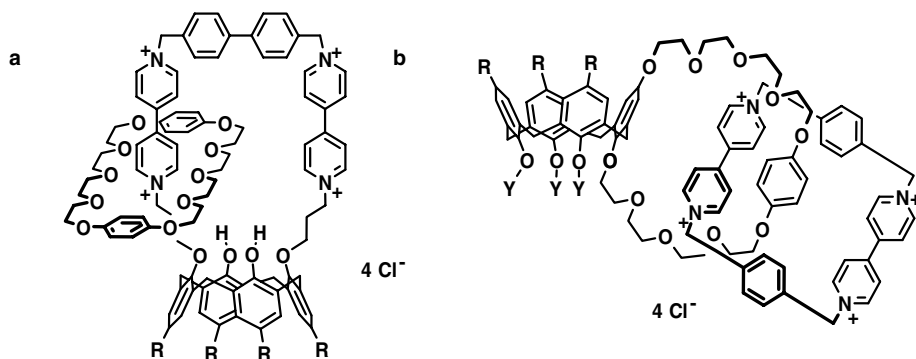

Figure 5.22 Examples of [2]catenanes based on the principle outlined in Scheme 5.6.

While these examples again demonstrate the unlimited possibilities for the chemical modification of calixarenes [81], the preorganization obtained by the dimerization of tetra-urea derivatives opens the door to the construction of molecules or molecular assemblies with entirely novel topologies.

5.9
Experimental: Selected Procedures

5.9.1
Synthesis of Tetra-urea 5 (Y = C$_5$H$_{11}$; m = 9) [52]

A solution of tetraamino calix[4]arene (0.363 g, 0.474 mmol), 4-nitrophenyl-*N*-(3-(10-undecenyloxy)phenyl)carbamate (1.0 g, 2.37 mmol), and triethylamine (0.343 mL, 2.37 mmol) in DMF (20 mL) was stirred for two days at room temperature. The reaction mixture was diluted by dichloromethane (250 mL), and a solution of K$_2$CO$_3$ (1 M, 150 mL) was added. The mixture was stirred for 1 h at room temperature, and the organic layer was washed with a solution of K$_2$CO$_3$ (0.3 M, 3 times 150 mL). After drying over MgSO$_4$, the solvent was evaporated, and the desired tetra-urea was purified by column chromatography (silica gel, THF/hexane, 1:6). Reprecipitation from methanol/dichloromethane gave the desired tetra-urea **5** (Y = C$_5$H$_{11}$; m = 9) (0.617 g, 68% yield) as a colorless powder.

5.9.2
Synthesis of Bisloop Tetra-urea 8 (Y = C$_5$H$_{11}$; n = 20) [52]

A mixture of tetra-tosylurea **4** (0.233 g, 0.150 mmol) and tetra-urea **5** (Y = C$_5$H$_{11}$; m = 9) (0.250 g, 0.131 mmol) in benzene (265 mL) was heated under reflux for 5–10 min. During this time a clear solution was usually formed. After cooling to room temperature the complete formation of the heterodimer was checked by ^{1}H NMR (benzene-d_6). The reaction mixture was purged with nitrogen for 30 min, and a solution of the Grubbs' catalyst (0.022 g, 0.0261 mmol) in benzene (3 mL) was added in one portion. After two days of stirring at 20 °C, triethylamine (1.5 mL) was added to destroy the catalyst and the complex with tetra-tosylurea **4**. After 1 h, the solvent was evaporated and the residue redissolved in THF (20 mL). Hydrogenation of the crude product obtained by evaporation was carried out in THF (20 mL) with hydrogen (normal pressure) in the presence of platinum dioxide (83% Pt, 0.0266 g, 0.117 mmol). The solvent was evaporated, and the residue was passed through a column (silica gel, THF/hexane, 1:2). Reprecipitation from THF/hexane gave the desired product **8** (Y = C$_5$H$_{11}$; n = 20) (0.203 g, 84% yield) as a colorless powder.

5.9.3
Synthesis of Bis[2]catenane 12 (Y = C$_5$H$_{11}$; n = 20) [52]

A mixture of tetra-urea **5** (Y = C$_5$H$_{11}$; m = 9) (0.050 g, 0.0261 mmol) and bisloop compound **8** (Y = C$_5$H$_{11}$; n = 20) (0.0510 g, 0.0274 mmol) in benzene (60 mL) was

heated under reflux until a clear solution was formed, which usually required 10–60 min. After cooling to room temperature, the formation of the heterodimer was checked by ^{1}H NMR (benzene-d_6). The reaction mixture was purged with nitrogen for 30 min, and a solution of Grubbs' catalyst (0.0043 g, 0.005 mmol) in benzene (5 mL) was added in one portion. After stirring at 20 °C for 48 h, triethylamine (1 mL) was added and the mixture was stirred for 1 h. The solvent was evaporated, and the residue was dissolved in THF (20 mL) and hydrogenated for 2 h using platinum dioxide (83% Pt, 0.0053 g, 0.0235 mmol) as catalyst. The crude product obtained by evaporation was passed through a column (silica gel, THF/hexane, 1:2). Recrystallization from chloroform/methanol gave the bis[2]catenane **12** (0.0854 g, 88% yield) as a colorless powder.

5.9.4
Synthesis of Tetra-urea 6a (Y = C$_5$H$_{11}$; m = 6) [53,55]

A solution of 3,5-di-(7-octenyloxy)benzoic acid (1.47 g, 3.92 mmol), diphenylphosphorylazide (1.19 ml, 4.31 mmol), and triethylamine (0.436 ml, 4.31 mmol) in toluene (79 ml) was stirred for 2 h at 55 °C. Tetraamino calix[4]arene (0.500 g, 0.654 mmol) was added, and the mixture was stirred for 2 h at 85 °C. Then the solvent was evaporated, and the residue was triturated with methanol. The crude product thus obtained was purified by column chromatography (silica gel, ethyl acetate/hexane, 1:20) followed by reprecipitation from methanol/dichloromethane, which gave the desired tetra-urea **6** (Y = C$_5$H$_{11}$; m = 6) (0.714 g, 48% yield) as a colorless powder.

5.9.5
Synthesis of Tetraloop Tetra-urea 9 (Y = C$_5$H$_{11}$; n = 14) [53,55]

Tetra-tosylurea **4** (0.311 g, 0.200 mmol) and tetra-urea **6** (Y = C$_5$H$_{11}$; m = 6) (0.300 g, 0.133 mmol) were dissolved in dichloromethane (540 mL). The solution was stirred under nitrogen for 4 h at 55 °C. The reaction mixture was purged with nitrogen for 30 min, a solution of Grubbs' catalyst (0.0440 g, 0.0533 mmol) in dichloromethane (5 mL) was added, and the stirring was continued for 48 h at room temperature. Then triethylamine (2 mL) was added, and the solution was stirred for 1 h to destroy the catalyst and the complex with tetra-tosylurea **4**. After evaporation at 60 °C, the residue was dissolved in dichloromethane (5 mL), and passed through a column (silica gel, THF/hexane, 1:2) to remove the catalyst and tetra-tosylurea rests. The crude product was hydrogenated in THF (25 mL) for 24 h (room temperature, normal pressure) using platinum dioxide (83% Pt, 0.0545 g; 0.240 mmol) as catalyst. The residue obtained by evaporation was purified by column chromatography (silica gel, THF/hexane, 1:2). After reprecipitation from chloroform/methanol the desired tetraloop calix[4]arene **9** (Y = C$_5$H$_{11}$; n = 14) (0.267 g, 93% yield) was finally obtained as a colorless powder.

5.9.6
Synthesis of [8]Catenane 14 (Y = C$_5$H$_{11}$; n = 14) [55]

A solution of tetraloop compound **9** (Y = C$_5$H$_{11}$; n = 14) (0.0500 g, 0.0233 mmol) and **6** (Y = C$_5$H$_{11}$; m = 6) (0.0499 g, 0.0222 mmol) in freshly distilled and degassed dichloromethane (90 mL) was stirred at room temperature for 48 h; the complete formation of the heterodimer was verified by ^{1}H NMR. When the signals of the homodimer **6** had disappeared, the reaction mixture was purged with nitrogen for 30 min, and a solution of Grubbs' catalyst (0.007 g, 0.0088 mmol) in dichloromethane (5 mL) was added. After stirring for 48 h, triethylamine (0.5 mL) was added and the solution was stirred for 1 h and evaporated. The residue was dissolved in dichloromethane (5 mL) and passed through a column (silica gel, THF/hexane, 1:12). The solvent was evaporated, the crude product was dissolved in THF (20 mL), platinum dioxide (83% Pt, 0.009 g, 0.0399 mmol) was added to the solution, and the reaction mixture was stirred vigorously under a hydrogen atmosphere for 6 h at room temperature. The final purification by column chromatography (silica gel, THF/hexane, 1:12) followed by recrystallization from chloroform/hexane gave the octacatenane **14** (Y = C$_5$H$_{11}$; n = 14) (0.0394 g, 41% yield) as a colorless crystalline powder.

Abbreviations

Ar	aryl
Boc	*tert*-butyloxycarbonyl
CD	circular dichroism
CMPO	carbamoylmethylphosphine oxide
DMF	*N,N′*-dimethylformamide
DMSO	dimethyl sulfoxide
DOSY	diffusion-ordered spectrometry
ESI-MS	electrospray ionization mass spectrometry
Et	ethyl
Grubbs' catalyst	bis-(tricyclohexylphosphine)benzylidine ruthenium(IV) dichloride
MALDI-TOF-MS	matrix assisted laser desorption ionization – time of flight mass spectrometry
MD	molecular dynamics
Me	methyl
MS	mass spectrometry
NMR	nuclear magnetic resonance
THF	tetrahydrofuran
Tol	tolyl
Tos	tosyl
UV	ultraviolet

References

1 Sauvage, J.-P. and Dietrich-Buchecker, C. (1999) *Molecular Catenanes, Rotaxanes and Knots*, Wiley-VCH, Weinheim.

2 Adjami, D., Hess, K., Köhler, F., Näther, C., Oeckler, O., Simon, A., Yamamoto, C., Okamoto, Y. and Herges, R. (2006) *Chem. Eur. J.*, **12**, 5434–5445.

3 (a) Steuerman, D.W., Tseng, H.-R., Peters, A.J., Flood, A.H., Jeppesen, J.O., Nielsen, K.A., Stoddart, J.F. and Heath, J.R. (2004) *Angew. Chem.*, **116**, 6648–6653; *Angew. Chem. Int. Ed.*, **43**, 6486–6491; (b) Sauvage, J.-P. (2005) *Chem. Commun.*, 1507–1510; (c) Kay, E. R., Leigh, D.A. and Zerbetto, F. (2007) *Angew. Chem.*, **119**, 72–196; *Angew. Chem. Int. Ed.*, **46**, 72–191.

4 For the first synthesis see: Chichak, K.S., Cantrill, S.J., Pease, A.R., Chiu, S.-H., Cave, G.W.V., Atwood, J.L. and Stoddart, J.F. (2004) *Science*, **304**, 1308–1312.

5 Philp, D. and Stoddart, J.F. (1996) *Angew. Chem.*, **108**, 1242–1286; *Angew. Chem. Int. Ed. Engl.*, **35**, 1154–1196.

6 Schill, G. and Lüttringhaus, A. (1964) *Angew. Chem.*, **76**, 567–568; *Angew. Chem. Int. Ed.*, **3**, 546–547.

7 (a) Ünsal, Ö. and Godt, A. (1999) *Chem. Eur. J.*, **5**, 1728–1733; (b) Duda, S. and Godt, A. (2003) *Eur. J. Org. Chem.*, 3412–3420.

8 (a) Chambron, J.-C., Sauvage, J.-P., Mislow, K., De Cian, A. and Fischer, J. (2001) *Chem. Eur. J.*, **7**, 4085–4096; (b) Flamigni, L., Talarico, A.M., Chambron, J.-C., Heitz, V., Linke, M., Fujita, N. and Sauvage, J.-P. (2004) *Chem. Eur. J.*, **10**, 2689–2699.

9 (a) Dietrich-Buchecker, C.O. and Sauvage, J.-P. (1989) *Angew. Chem.*, **101**, 192–194; (1989) *Angew. Chem. Int. Ed. Engl.*, **28**, 189–192; (b) Dietrich-Buchecker, C.O., Rapenne, G. and Sauvage, J.-P. (1997) *Chem. Commun.*, 2053–2054.

10 (a) Dietrich-Buchecker, C.O., Sauvage, J.-P. and Kintzinger, J.P. (1983) *Tetrahedron Lett.*, **46**, 5095–5098; (b) Dietrich-Buchecker, C.O., Sauvage, J.-P. and Kern, J.M. (1984) *J. Am. Chem. Soc.*, **106**, 3043–3045.

11 For a recent example see: Bäuerle, P., Ammann, M., Wilde, M., Götz G., Mena-Osteritz, E., Rang, A. and Schalley, C.A. (2007) *Angew. Chem.*, **119**, 367–372; *Angew. Chem. Int. Ed.*, **46**, 363–368.

12 Frey, J., Kraus, T., Heitz, V. and Sauvage, J.-P. (2005) *Chem. Commun.*, 5310–5312.

13 (a) Sauvage, J.-P. and Ward, M. (1991) *Inorg. Chem.*, **30**, 3869–3874; (b) Leigh, D.A., Lusby, P.J., Teat, S.J., Wilson, A.J. and Wong, J.K.Y. (2001) *Angew. Chem.*, **113**, 1586–1591; *Angew. Chem. Int. Ed.*, **40**, 1538–1543; (c) Fuller, A.M., Leigh, D. A., Lusby, P.J., Oswald, I.D.H., Parsons, S. and Walker, D.B. (2004) *Angew. Chem.*, **116**, 4004–4008; *Angew. Chem. Int. Ed.*, **43**, 3914–3918.

14 (a) Cantrill, S.J., Chichak, K.S., Peters, A. J. and Stoddart, J.F. (2005) *Acc. Chem. Res.*, **38**, 1–9; (b) Pentecost, C.D., Peters, A.J., Chichak, K.S., Cave, G.W.V., Cantrill, S.J. and Stoddart, J.F. (2006) *Angew. Chem.*, **118**, 4205–4210; *Angew. Chem. Int. Ed.*, **45**, 4099–4104.

15 (a) Beer, P.D., Sambrook, M.R. and Curiel, D. (2006) *Chem. Commun.*, **20**, 2105–2117; (b) Sambrook, M.R., Beer, P. D., Lankshear, M.D., Ludlow, R.F. and Wisner, J.A. (2006) *Org. Biomol. Chem.*, **4**, 1529–1538.

16 Sambrook, M.R., Beer, P.D., Wisner, J. A., Paul, R.L. and Cowley, A.R. (2004) *J. Am. Chem. Soc.*, **126**, 15364–15365.

17 (a) Hunter, C.A. (1992) *J. Am. Chem. Soc.*, **114**, 5303–5311; (b) Vögtle, F., Meier, S. and Hoss, R. (1992) *Angew. Chem.*, **104**, 1628–1631; *Angew. Chem., Int. Ed. Engl.*, **31**, 1619–1622; (c) Brodesser, G., Güther, R., Hoss, R., Meier, S., Ottens-Hildebrandt, S.,

Schmitz, J. and Vögtle, F. (1993) *Pure Appl. Chem.*, **65**, 2325–2328; (d) Carver, F.J., Hunter, C.A. and Shannon, R.J. (1994) *J. Chem. Soc., Chem. Commun.*, 1277–1280.

18 (a) Leigh, D.A., Moody, K., Smart, J.P., Watson, K.J. and Slawin, A.M.Z. (1996) *Angew. Chem.*, **108**, 321–326; *Angew. Chem. Int. Ed. Engl.*, **35**, 306–310; (b) Kidd, T.J., Leigh, D.A. and Wilson, A.J. (1999) *J. Am. Chem. Soc.*, **121**, 1599–1600; (c) Vögtle, F., Dunnwald, T. and Schmidt, T. (1996) *Acc. Chem. Res.*, **29**, 451–460.

19 (a) Vögtle, F., Jäger, R., Händel, M., Ottens-Hildebrandt, S. and Schmidt, W. (1996) *Synthesis*, 353–356; (b) Asakawa, M., Brancato, G., Fanti, M., Leigh, D.A., Shimizu, T., Slawin, A.M.Z., Wong, J.K. Y., Zerbetto, F. and Zhang, S. (2002) *J. Am. Chem. Soc.*, **124**, 2939–2950.

20 (a) Safarowsky, O., Nieger, M., Fröhlich, R. and Vögtle, F. (2000) *Angew. Chem.*, **112**, 1699–1701; *Angew. Chem. Int. Ed.*, **39**, 1616–1618; (b) Lukin, O., Müller, W. M., Müller, U., Kaufmann, A., Schmidt, C., Leszczynski, J. and Vögtle, F. (2003) *Chem. Eur. J.*, **9**, 3507–3517; (c) Passaniti, P., Ceroni, P., Balzani, V., Lukin, O., Yoneva, A. and Vögtle, F. (2006) *Chem. Eur. J.*, **12**, 5685–5690.

21 (a) Ashton, P.R., Chrystal, E.J.T., Glink, P.T., Menzer, S., Schiavo, C., Stoddart, J. F., Tasker, P.A. and Williams, D.J. (1995) *Angew. Chem.*, **107**, 2001–2004; *Angew. Chem. Int. Ed. Engl.*, **34**, 1869–1871; (b) Ashton, P.R., Campbell, P.J., Chrystal, E.J.T., Glink, P.T., Menzer, S., Philp, D., Spencer, N., Stoddart, J.F., Tasker, P.A. and Williams, D.J. (1995) *Angew. Chem.*, **107**, 1997–2001; *Angew. Chem. Int. Ed. Engl.*, **34**, 1865–1869.

22 (a) Ashton, P.R., Glink, P.T., Stoddart, J. F., Tasker, P.A., White, A.J.P. and Williams, D.J. (1996) *Chem. Eur. J.*, **2**, 729–736; (b) Horn, M., Ihringer, J., Glink, P.T. and Stoddart, J.F. (2003) *Chem. Eur. J.*, **9**, 4046–4054; (c) Williams, A.R., Northrop, B.H., Chang, T.,

Stoddart, J.F., White, A.J.P. and Williams, D.J. (2006) *Angew. Chem.*, **118**, 6817–6821; *Angew. Chem. Int. Ed.*, **45**, 6665–6669.

23 (a) Badjić, J.D., Cantrill, S.J., Grubbs, R. H., Guidry, E.N., Orenes, R. and Stoddart, J.F. (2004) *Angew. Chem.*, **116**, 3335–3340; *Angew. Chem. Int. Ed.*, **43**, 3273–3278.

24 (a) Zhu, X.-Z. and Chen, C.-F. (2006) *Chem. Eur. J.*, **12**, 5603–5609; (b) Zhu, X.-Z. and Chen, C.-F. (2005) *J. Am. Chem. Soc.*, **127**, 13158–13159.

25 (a) Ashton, P.R., Goodnow, T.T., Kaifer, A.E., Reddington, M.V., Slawin, A.M.Z., Spencer, N., Stoddart, J.F., Vicent, C. and Williams, D.J. (1989) *Angew. Chem.*, **101**, 1404–1408; *Angew. Chem. Int. Ed. Engl.*, **28**, 1396–1399; (b) Vögtle, F., Müller, W. M., Müller, U., Bauer, M. and Rissanen, K. (1993) *Angew. Chem.*, **105**, 1356–1358; *Angew. Chem. Int. Ed. Engl.*, **32**, 1295–1297; (c) Gunter, M.J., Hockless, D.C.R., Johnston, M.R., Skelton, B.W. and White, A.H. (1994) *J. Am. Chem. Soc.*, **116**, 4810–4823; (d) Li, Z.-T. and Becher, J. (1996) *Chem. Commun.*, 639–640; (e) Ashton, P.R., Ballardini, R., Balzani, V., Bělohradský, M., Gandolfi, M.T., Philp, D., Prodi, L., Raymo, F.M., Reddington, M.V., Spencer, N., Stoddart, J.F., Venturi, M. and Williams, D.J. (1996) *J. Am. Chem. Soc.*, **118**, 4931–4951; (f) Hamilton, D.G., Sanders, J.K.M., Davies, J.E., Clegg, W. and Teat, S.J. (1997) *Chem. Commun.*, 897–898; (g) Try, A.C., Harding, M.M., Hamilton, D.G. and Sanders, J.K.M. (1998) *Chem. Commun.*, 723–724.

26 (a) Amabilino, D.B., Ashton, P.R., Reder, A.S., Spencer, N. and Stoddart, J.F. (1994) *Angew. Chem.*, **106**, 1316–1319; *Angew. Chem. Int. Ed. Engl.*, **33**, 1286–1290; (b) Amabilino, D.B., Ashton, P.R., Boyd, S.E., Lee, J.Y., Menzer, S., Stoddart, J.F. and Williams, D.J. (1997) *Angew. Chem.*, **109**, 2160–2162; *Angew. Chem. Int. Ed. Engl.*, **36**, 2070–2072.

27 Ashton, P.R., Philp, D., Spencer, N. and Stoddart, J.F. (1991) *J. Chem. Soc. Chem. Commun.*, 1677–1679.

28 Bogdan, A., Rudzevich, Y., Vysotsky, M. O. and Böhmer, V. (2006) *Chem. Commun.*, 2941–2952.

29 Gutsche, C.D. and Iqbal, M. (1990) *Org. Synth.*, **68**, 234–237.

30 Saadioui, M., Shivanyuk, A., Böhmer, V. and Vogt, W. (1999) *J. Org. Chem.*, **64**, 3774–3777.

31 Rudzevich, Y., Rudzevich, V., Schollmeyer, D. and Böhmer, V. (2007) Org. Lett. **9**, 957–960.

32 (a) Shimizu, K.D. and Rebek, J. Jr (1995) *Proc. Natl. Acad. Sci. U.S.A.*, **92**, 12403–12407; (b) Hamann, B.C., Shimizu, K.D. and Rebek, J. Jr (1996) *Angew. Chem.*, **108**, 1425–1427; *Angew. Chem. Int. Ed.*, **35**, 1326–1329; (c) Castellano, R.K., Kim, B.H. and Rebek, J. Jr (1997) *J. Am. Chem. Soc.*, **119**, 12671–12672.

33 A similar dimerization was recently observed for thiocalix[4]arenes substituted by four CMPO-residues. (a) Kasyan, O., Kalchenko, V., Bolte, M. and Böhmer, V. (2006) *Chem. Commun.*, 1932–1934; (b) Rudzevich, V., Kasyan, O., Kalchenko, V., Bolte, M., Schollmeyer, D. and Böhmer, V. unpublished.

34 Mogck, O., Paulus, E.F., Böhmer, V., Thondorf, I. and Vogt, W. (1996) *Chem. Commun.*, 2533–2534.

35 Broda, F., Vysotsky, M.O., Böhmer, V. and Thondorf, I. (2006) *Org. Biomol. Chem.*, **4**, 2424–2432.

36 Schalley, C.A., Castellano, R.K., Brody, M.S., Rudkevich, D.M., Siuzdak, G. and Rebek, J. Jr (1999) *J. Am. Chem. Soc.*, **121**, 4568–4579.

37 (a) Vysotsky, M.O., Pop, A., Broda, F., Thondorf, I. and Böhmer, V. (2001) *Chem. Eur. J.*, **7**, 4403–4410; (b) Frish, L., Vysotsky, M.O., Böhmer, V. and Cohen, Y. (2003) *Org. Biomol. Chem.*, **1**, 2011–2014.

38 Thondorf, I., Broda, F., Rissanen, K., Vysotsky, M. and Böhmer, V. (2002) *J. Chem. Soc. Perkin Trans.*, **2**, 1796–1800.

39 Mogck, O., Böhmer, V. and Vogt, W. (1996) *Tetrahedron*, **52**, 8489–8496.

40 Vysotsky, M.O., Mogck, O., Rudzevich, Y., Shivanyuk, A., Böhmer, V., Brody, M. S., Cho, Y.L., Rudkevich, D.M. and Rebek, J. Jr (2004) *J. Org. Chem.*, **69**, 6115–6120.

41 For self-assembled monolayers of heterodimers with 3, see: Xu, S., Podoprygorina, G., Böhmer, V., Ding, Z., Rooney, D., Rangan, C. and Mittler, S. (2007) *Org. Biomol. Chem.*, **5**, 558–568.

42 Castellano, R.K. and Rebek, J. Jr (1998) *J. Am. Chem. Soc.*, **120**, 3657–3663.

43 Castellano, R.K., Nuckolls, C. and Rebek, J. Jr (1999) *J. Am. Chem. Soc.*, **121**, 11156–11163.

44 Pop, A., Vysotsky, M.O., Saadioui, M. and Böhmer, V. (2003) *Chem. Commun.*, 1124–1125.

45 (a) Warmuth, R. and Yoon, J. (2001) *Acc. Chem. Res.*, **34**, 95–105; (b) Rebek, J. Jr (2005) *Angew. Chem.*, **117**, 2104–2115; *Angew. Chem. Int. Ed.*, **44**, 2068–2078; (c) Dalgarno, S.J., Bassil, D.B., Tucker, S. A. and Atwood, J.L. (2006) *Angew. Chem.*, **118**, 7177–7180; *Angew. Chem. Int. Ed.*, **45**, 7019–7022; (d) Ajami, D., Schramm, M.P., Volonterio, A. and Rebek, J. Jr (2007) *Angew. Chem.*, **119**, 246–248; *Angew. Chem. Int. Ed.*, **46**, 242–244.

46 (a) Wendland, M.S. and Zimmerman, S. C. (1999) *J. Am. Chem. Soc.*, **121**, 1389–1390; (b) Zimmerman, S.C., Wendland, M.S., Rakow, N.A., Zharov, I. and Suslick, K.S. (2002) *Nature*, **418**, 399–403; (c) Beil, J.B., Lemcoff, N.G. and Zimmerman, S.C. (2004) *J. Am. Chem. Soc.*, **126**, 13576–13577.

47 (a) Clark, T.D., Kobayashi, K. and Ghadiri, M.R. (1999) *Chem. Eur. J.*, **5**, 782–792; (b) Prins, L.J., Jolliffe, K.A., Hulst, R., Timmerman, P. and Reinhoudt, D.N. (2000) *J. Am. Chem. Soc.*, **122**, 3617–3627; (c) Jin, W., Fukushima, T., Kosaka, A., Niki, M., Ishii, N. and Aida, T. (2005) *J. Am. Chem. Soc.*, **127**, 8284–8285.

48 For examples involving calixarene derivatives, see: Pitarch, M., McKee, V., Nieuwenhuyzen, M. and McKervey, M. A. (1998) *J. Org. Chem.*, **63**, 946–951.

49 Vysotsky, M.O., Bolte, M., Thondorf, I. and Böhmer, V. (2003) *Chem. Eur. J.*, **9**, 3375–3382.

50 Bogdan, A., Vysotsky, M.O., Ikai, T., Okamoto, Y. and Böhmer, V. (2004) *Chem. Eur. J.*, **10**, 3324–3330.

51 Vysotsky, M.O., Bogdan, A., Wang, L. and Böhmer, V. (2004) *Chem. Commun.*, 1268–1269.

52 Molokanova, O., Bogdan, A., Vysotsky, M.O., Bolte, M., Ikai, T., Okamoto, Y. and Böhmer, V. (2007) *Chem. Eur. J.* **13**, 6157–6170.

53 Cao, Y., Wang, L., Bolte, M., Vysotsky, M.O. and Böhmer, V. (2005) *Chem. Commun.*, 3132–3134.

54 Cao, Y., Rudzevich, Y., Rudzevich, V. and Böhmer, V. unpublished.

55 Wang, L., Vysotsky, M.O., Bogdan, A., Bolte, M. and Böhmer, V., (2004) *Science*, **304**, 1312–1314.

56 Bogdan, A. and Böhmer, V. unpublished.

57 Podoprygorina, G. and Böhmer, V. unpublished.

58 Gaeta, C., Vysotsky, M.O., Bogdan, A. and Böhmer, V. (2005) *J. Am. Chem. Soc.*, **127**, 13136–13137.

59 Vysotsky, M.O. and Böhmer, V. unpublished.

60 Molokanova, O., Vysotsky, M.O., Cao, Y., Thondorf, I. and Böhmer, V. (2006) *Angew. Chem.*, **118**, 8220–8224; *Angew. Chem. Int. Ed.*, **45**, 8051–8055.

61 Thondorf, I., Rudzevich, Y., Rudzevich, V. and Böhmer, V. (2007) *Org. Biomol. Chem.* **5**, 2775–2782.

62 Compare also: Rudzevich, Y., Rudzevich, V., Schollmeyer, D., Thondorf, I. and Böhmer, V. (2006) *Org. Biomol. Chem.*, **4**, 3938–3944.

63 (a) Castellano, R.K., Rudkevich, D.M. and Rebek, J. Jr (1997) *Proc. Natl. Acad. Sci. U.S.A.*, **94**, 7132–7137; (b) Castellano, R.K., Clark, R., Craig, S.L., Nuckolls, C. and Rebek, J. Jr (2000)

Proc. Natl. Acad. Sci. U.S.A., **97**, 12418–12421.

64 (a) Xu, H., Stampp, S.P. and Rudkevich, D.M. (2003) *Org. Lett.*, **5**, 4583–4586; (b) Xu, H., Hampe, E.M. and Rudkevich, D.M. (2003) *Chem. Commun.*, 2828–2829.

65 For an "intramolecular" dimerization of a molecule with a flexible hexamethylene spacer see: Brody, M.S., Schalley, C.A., Rudkevich, D.M. and Rebek, J. Jr (1999) *Angew. Chem.*, **111**, 1738–1742; *Angew. Chem. Int. Ed.*, **38**, 1640–1644.

66 For self-assembled dendrimers which are uniform in size but not necessarily in structure see: Franz, A., Bauer, W. and Hirsch, A. (2005) *Angew. Chem.*, **117**, 1588–1592; *Angew. Chem. Int. Ed.*, **44**, 1564–1567.

67 Rudzevich, Y., Rudzevich, V., Schollmeyer, D., Thondorf, I. and Böhmer, V. (2005) *Org. Lett.*, **7**, 613–616 See also Ref. [68].

68 Rudzevich, Y., Vysotsky, M.O., Böhmer, V., Brody, M.S., Rebek, J., Jr, Broda, F. and Thondorf, I. (2004) *Org. Biomol. Chem.*, **2**, 3080–3084.

69 Rudzevich, Y., Rudzevich, V., Moon, C., Schnell, I., Fischer, K. and Böhmer, V. (2005) *J. Am. Chem. Soc.*, **127**, 14168–14169.

70 Kanamathareddy, S. and Gutsche, C.D. (1993) *J. Am. Chem. Soc.*, **115**, 6572–6579.

71 A "self-threaded rotaxane" was also observed as a (by) product, when two homooxacalix[3]arenes were covalently connected to a molecular capsule via three *p*-xylylenediamide linkers: Zhong, Z., Ikeda, A. and Shinkai, S. (1999)

J. Am. Chem. Soc., **121**, 11906–11907.

72 Arduini, A., Ferdani, R., Pochini, A., Secchi, A. and Ugozzoli, F. (2000) *Angew. Chem.*, **112**, 3595–3597; *Angew. Chem. Int. Ed.*, **39**, 3453–3456.

73 Credi, A., Dumas, S., Silvi, S., Venturi, M., Arduini, A., Pochini, A. and Secchi, A. (2004) *J. Org. Chem.*, **69**, 5881–5887.

74 Arduini, A., Calzavacca, F., Pochini, A. and Secchi, A. (2003) *Chem. Eur. J.*, **9**, 793–799.

75 Arduini, A., Ciesa, F., Fragassi, M., Pochini, A. and Secchi, A. (2005) *Angew. Chem.*, **117**, 282–285; *Angew. Chem. Int. Ed.*, **44**, 278–281.

76 Fischer, C., Nieger, M., Mogck, O., Böhmer, V., Ungaro, R. and Vögtle, F. (1998) *Eur. J. Org. Chem.*, 155–161.

77 Smukste, I., House, B.E. and Smithrud, D.B. (2003) *J. Org. Chem.*, **68**, 2559–2571.

78 Li, Z.-T., Ji, G.-Z., Zhao, C.-X., Yuan, S.-D., Ding, H., Huang, C., Du, A.-L. and Wei, M. (1999) *J. Org. Chem.*, **64**, 3572–3584.

79 For an analogous example including a rigid, chiral calix[4]arene like building block see: Okada, Y., Miao, Z., Akiba, M. and Nishimura, J. (2006) *Tetrahedron Lett.*, **47**, 2699–2702.

80 Lu, L.-G., Li, G.-K., Peng, X.-X., Chen, C.-F. and Huang, Z.-T. (2006) *Tetrahedron Lett.*, **47**, 6021–6025.

81 Böhmer, V. (1995) *Angew. Chem.*, **107**, 785–818; *Angew. Chem. Int. Ed. Engl.*, **34**, 713–745.

6
Shape-Persistent Macrocycles Based on Acetylenic Scaffolding

Amber L. Sadowy and Rik R. Tykwinski

6.1
Introduction

Historically, one might argue that the synthesis of many shape-persistent macrocycles (SPMs) was initiated through a combination of their enticing symmetrical structures and the synthetic challenge they posed. More recently, however, SPMs have found an important role as functional components in supramolecular chemistry. In comparison to flexible macrocycles, SPMs have been designed to exhibit fewer degrees of conformational flexibility, which greatly facilitates their assembly into highly organized supramolecular systems. From the onset, acetylenic building blocks have played a defining role in the construction of SPMs, and, most recently, the evolution of modern metal-catalyzed coupling reactions to form sp-sp^2 and sp-sp carbon bonds has greatly advanced this field. Furthermore, SPMs based on acetylenic carbon scaffolding are particularly well suited to applications in supramolecular chemistry, given their synthetic accessibility, rigid or semi-rigid configuration, and lack of steric impedance about the acetylenic units.

The *synthesis* of acetylenic SPMs has been reviewed on a number of occasions, typically with a focus on a particular structural motif, and those molecules based on an arylene ethynylene framework have received the lion's share of the attention [1–13]. Likewise, the *use* of acetylenic SPMs in functional systems has also been reviewed, but, again, typically with respect to a particular molecular design [5,14–16]. In view of previous literature in this area, the goal of this particular chapter will be to integrate the two aspects. First, a general summary of synthetic strategies commonly used for the synthesis of acetylenic SPMs will be described. Second, the implementation of SPMs as building blocks in supramolecular chemistry will be presented, with an emphasis on the synthetic aspects as possible. The function of SPMs has been broadly divided into three sections: (a) SPMs used as components of supramolecular assemblies, (b) SPMs used in host–guest systems, and (c) aggregation/adsorption of SPMs, including solution state aggregation, liquid crystallinity, and surface adsorption. Clearly, the substantial breadth of research that has been conducted in the area of acetylenic SPMs prevents a comprehensive description of this in the confines of a

single chapter. Thus, examples have been chosen to highlight the diversity of recent synthetic achievements, as well as the application of SPMs in particular areas of supramolecular chemistry.

6.1.1
SPM Synthesis through Intermolecular Reactions

One of the most straightforward routes to the synthesis of acetylenic SPMs is the one-step $nA \rightarrow A_n$ approach, in which a suitable precursor is subjected to conditions that effect cyclooligomerization (Figure 6.1A). While often biased to selectively produce a desired cyclic oligomer, other macrocycles are often formed, which can lead to a tedious separation step. As with many macrocyclizations, the success of this strategy benefits from highly dilute conditions that favor the kinetic formation of cyclic products (first-order ring-closing reaction) over acyclic oligomers (second-order reaction). To circumvent the need for extraordinary amounts of solvent to achieve high dilution, many reactions are done under pseudo-high dilution, where one or more of the reactants is added slowly to the reaction mixture. The $nA \rightarrow A_n$ approach is often used for the synthesis of butadiynyl-based macrocycles, in which oxidative acetylenic homocoupling can be relied on for efficient bond formation. This is demonstrated in the synthesis of expanded radialenes (1) to which mesogenic side groups have been appended, as reported by Diederich and coworkers (Scheme 6.1A) [17]. In this case, trimer, tetramer, and pentamer macrocycles were observed with tetramer as the dominant product.

There are a number of variants of oxidative acetylenic homocoupling from which to choose, all based on adaptation of Glaser's original report [18,19]. Hay (e.g., CuCl, TMEDA, O_2, CH_2Cl_2) [20], Eglinton ($CuSO_4$ or $[Cu(OAc)_2]$, py) [21,22], and Breslow (CuCl, $CuCl_2$, oxygen-free pyridine) [23] conditions are the most commonly encountered. More recently, the use of Pd(II) as a co-catalyst in the presence of Cu(I) and O_2 (or an external oxidant such as chloroacetone or I_2) has emerged as an alternative to the traditional Cu(I)/Cu(II) homocoupling-based methods [24], as shown, for example, in the synthesis of TTF-based [18]annulenes 2 and 3 by Iyoda and coworkers (Scheme 6.1B) [25]. There seems, unfortunately, to be no real consensus as to how to predict which homocoupling protocol stands the best chance of success for a particular target, although it has been shown that reagent solubility, for example, can dictate the success of one method over another [26].

The most recent method developed for the $nA \rightarrow A_n$ approach relies on dynamic covalent bond formation using a metathesis reaction. In this case, reactions are typically under thermodynamic control, providing the potential for increased selectivity in product formation. The initial examples using alkyne metathesis toward the formation of SPMs were reported by Adams, Bunz, and coworkers using the precatalyst $[Mo(CO)_6]$ [27,28], but rather low yields of the desired products (4) limited general applicability (Scheme 6.2). Recent efforts by Moore and coworkers using a Mo(VI)-alkylidyne catalyst, however, have refined this process such that precipitation-driven reactions now provide moderate to excellent results (see Scheme 6.24) [29].
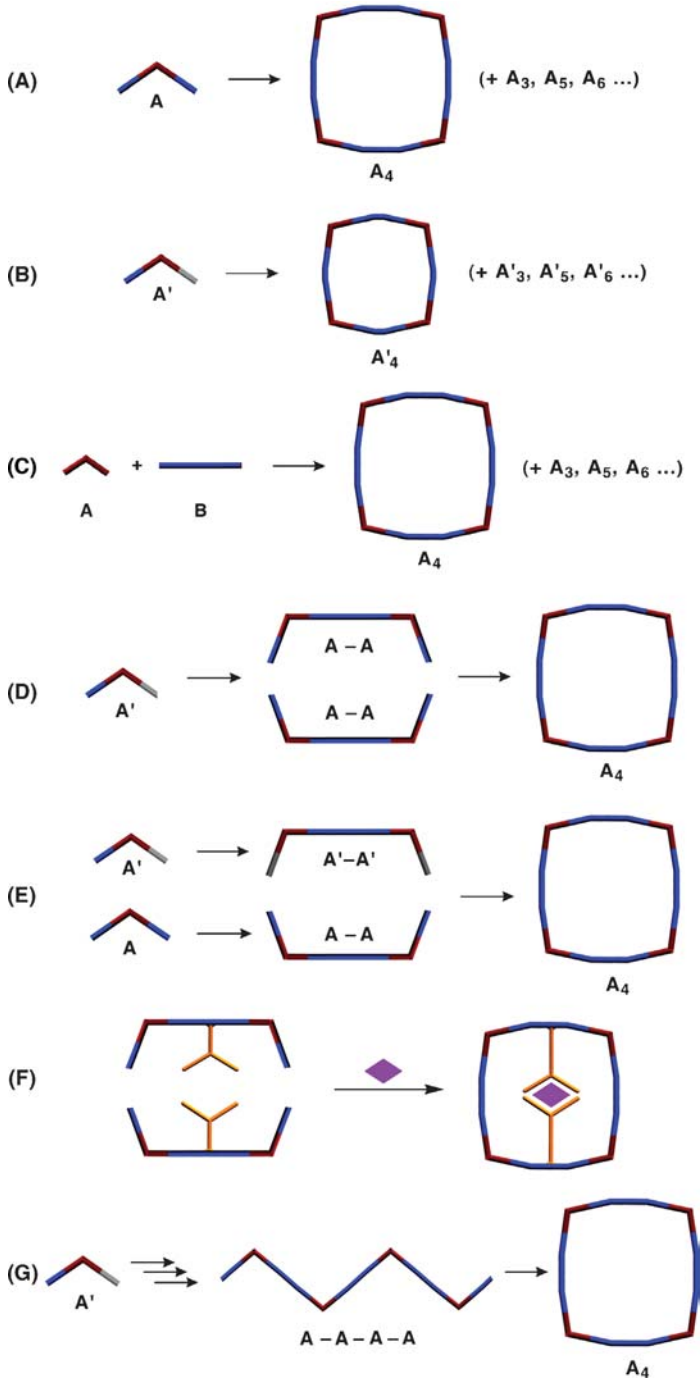
Figure 6.1 Schematic description of synthetic strategies for macrocycle formation.

A)

B)
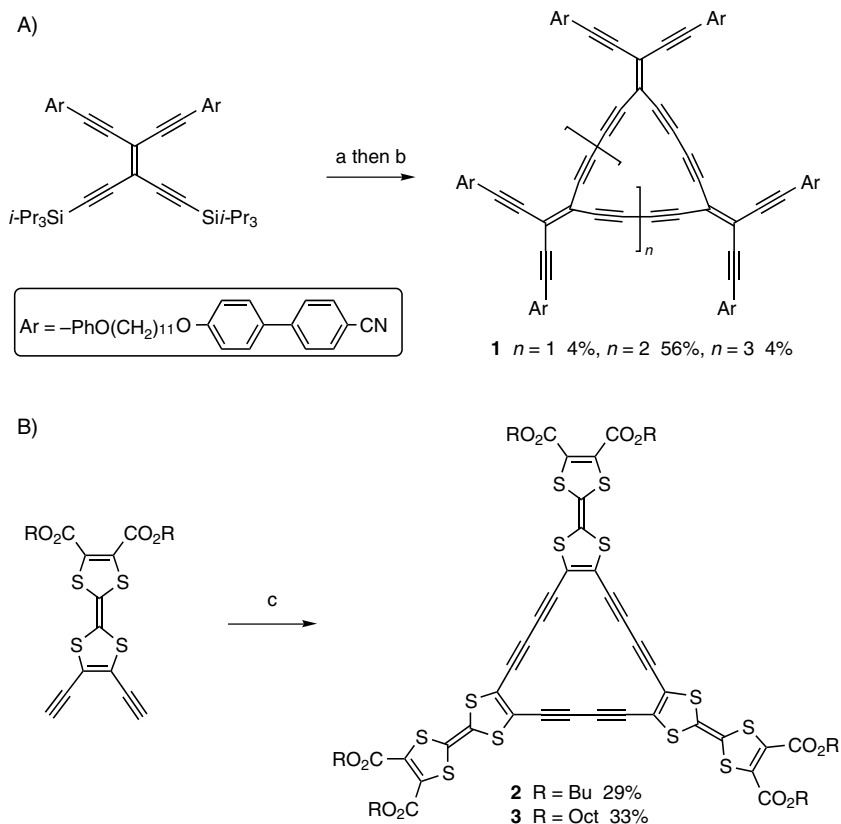
Scheme 6.1 (A) Synthesis of radialenes **1** by oxidative acetylenic homocoupling [17], and (B) Synthesis of TTF based [18]annulenes **2** and **3** by Pd-mediated homocoupling [25]. Reagents and conditions: (a) TBAF, THF; (b) [Cu(OAc)$_2$], O$_2$, py/PhH; (c) CuI, [PdCl$_2$(PPh$_3$)$_2$], Et$_3$N.

The $\mathbf{nA} \rightarrow \mathbf{A_n}$ approach to macrocycle assembly can also derive from an unsymmetrical, bifunctional precursor (Figure 6.1B) and often proceeds using a metal-catalyzed cross-coupling reaction. This approach was used by Eglinton and coworkers to synthesize the trimeric SPM **5** via a Castro–Stephens coupling starting with the preformed Cu-acetylide **6** (Scheme 6.3) [30]. The same product was later synthesized in improved yield by Linstrumelle and coworkers using a Pd-catalyzed Sonogashira coupling, a sequence starting with the *in situ* removal of acetone from **7** under basic conditions to provide the terminal alkyne [31].

A variation of the one-pot approach that has, perhaps, been underdeveloped to date involves the use of multiple components (**A** and **B**), where the geometry of the reactants is designed to provide selectivity toward one macrocyclic product, $\mathbf{nA} + \mathbf{nB} \rightarrow \mathbf{A_n}$ (Figure 6.1C). For example, Iyoda and coworkers exploited this approach to form selectively the cyclic trimer **8** based on the combination of a
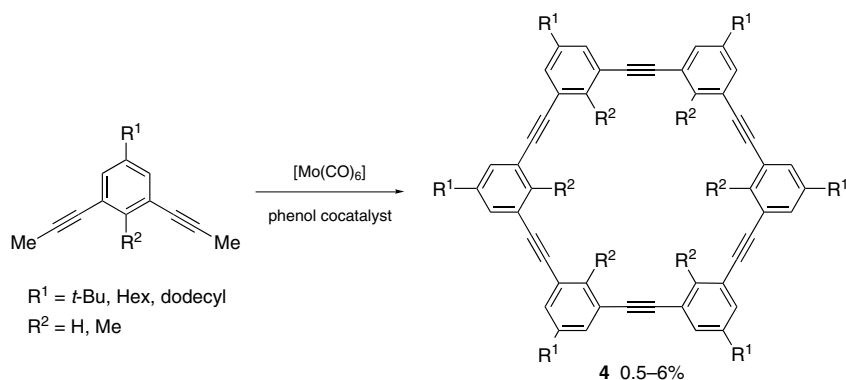
Scheme 6.2 SPM formation by alkyne metathesis [27].
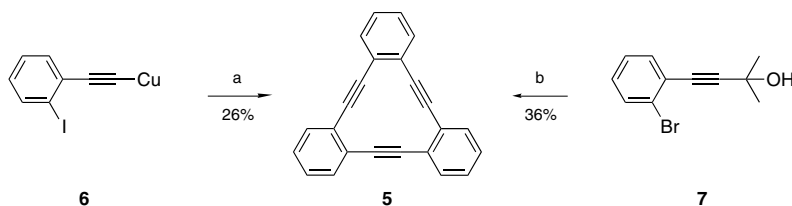
Scheme 6.3 Formation of SPM **5** from unsymmetrical precursors **6** or **7**. Reagents and conditions: (a) py, heat [30]; (b) NaOH, [Pd(PPh$_3$)$_4$], CuI, PhH, BTAC, 85 °C [31].

linear acetylene linker and 3,4-diiodothiophene corner piece **9** (Scheme 6.4) [32]. Considering that six new carbon-carbon bonds are in formed in this reaction, the overall yield represents an impressive 85% yield for each cross-coupling event.

A major drawback of the one-pot, one-step approach is the often encountered lack of selectivity toward forming a single cyclic oligomer, coupled with a potential lack of control over which oligomer is formed preferentially. To help to overcome this difficulty, oligomeric fragments of the desired target are often assembled (Figures 6.1D and 6.1E) and then combined together in the final step, helping to maximize product formation (e.g., 2(A–A) → A$_4$ or A–A + A′–A′ → A$_4$). Once again, the ring forming-step may be a homocoupling event, as in Figure 6.1D (typically via
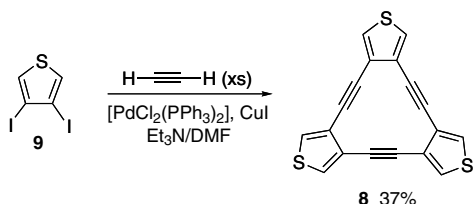
Scheme 6.4 Formation of SPM **9** via a one-pot, two-component reaction [32].

A)

B)
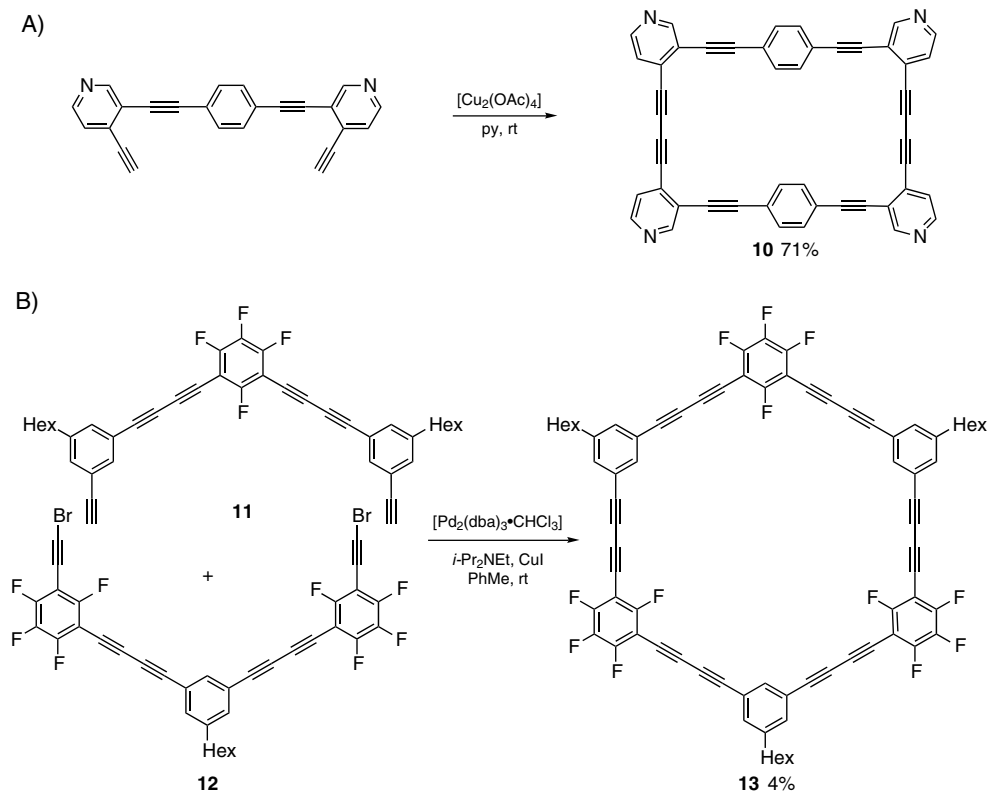
Scheme 6.5 Intermolecular cyclization of preformed oligomeric segments by (A) Eglinton homocoupling to form **10** [33] and (B) Cadiot–Chodkiewicz heterocoupling to form **13** [34].

oxidative acetylenic homocoupling) or the combination of two complementary pieces, as in Figure 6.1E (e.g., via a Sonogashira, Cadiot–Chodkiewicz, or metathesis reaction). Baxter's formation of the pyridine-containing macrocycle **10** using the Eglinton reaction provides an example of the former (Scheme 6.5A: see also Figure 6.3) [33], while Mayor and Shu's use of a Pd-catalyzed Cadiot–Chodkiewicz reaction to combine the two halves (**11** and **12**) of macrocycle **13** demonstrates the latter (Scheme 6.5B, see also Scheme 6.23) [34]. The synthesis of these two SPMs provides a salient example of how synthetic yields in macrocycle formation can vary widely, even with the use of a similar strategy.

6.1.2
SPM Synthesis through Intramolecular Reactions

A further improvement on the concept of using preassembled oligomers exploits the involvement of a template (covalent or noncovalent) to "entropically trap" the pieces
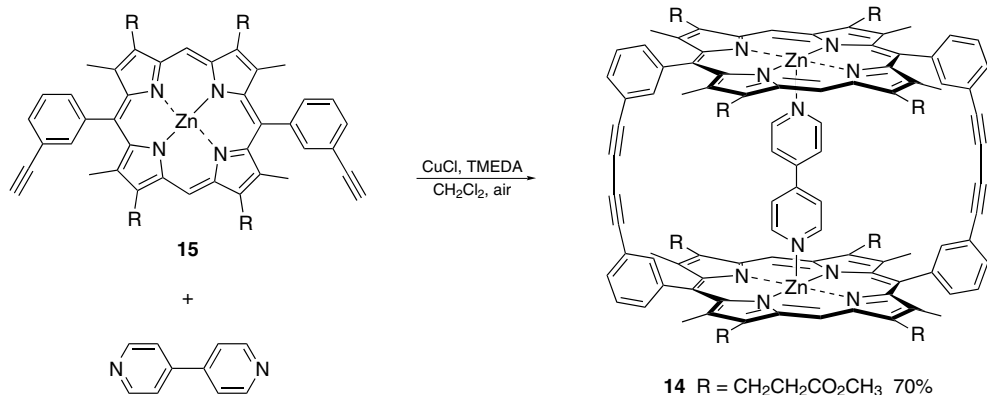
Scheme 6.6 Templated, selective formation of porphyrin "dimer" **14** [41].

in a synthetically favorable position (Figure 6.1F) [35–40]. Templation then nominally results in an intramolecular ring-closure reaction (albeit in the case where weaker non-covalent interactions template the fragments together, the definition of intramolecular may not rigorously apply). The concept of templated formation of shape-persistent macrocycles was originally introduced by Sanders and coworkers toward synthesis of porphyrin "dimer" **14** shown in Scheme 6.6, templated by 4,4′-bipyridine [40–43]. In the absence of the 4,4′-bipyridine template, cyclization of **15** under analogous conditions led to a mixture of di- and trimeric macrocycles in reduced yield. In addition, catenation (see Schemes 6.15 and 6.16), metal templation with Pt and Cu (see Schemes 6.16 and 6.20), quadrupolar interactions of aryl and perfluoroaryl groups (see Schemes 6.22 and 6.23) and covalent tethering (see Scheme 6.27) have also been successfully used in the context of templated macrocycle formation.

To achieve more precise control over a cyclization process, it is often desirable to reduce the cyclization to a single, intramolecular bond-forming reaction, as shown in Figure 6.1G. This approach necessitates the stepwise assembly of an acyclic oligomer lacking only this crucial ring-forming bond. While the synthesis of the requisite precursor can be tedious and time consuming relative to a one-pot cyclo-oligomerization, the intramolecular nature of the cyclization event ensures the highest selectivity toward formation of a single cyclic product. The route can also result in an increased product yield, although yields can remain frustratingly low even with this method. With respect to acetylenic macrocycles, two common approaches will be used to demonstrate. The first involves the use of triazenes as a masking group for aryl iodides, a transformation introduced by Moore and coworkers in 1991 [44]. As reported by Yoshida and coworkers, the two "halves" **16** and **17** were assembled separately and then connected through a Sonogashira reaction to give acyclic "octamer" **18** (Scheme 6.7) [45]. Three subsequent steps then gave the SPM **19**: (1) reaction of the aryltriazene **18** with I_2 to give the aryl iodide (MeI can also be used [44]), (2) removal of the trimethylsilyl group to provide the terminal alkyne, and (3) ring closure under Sonogashira conditions.
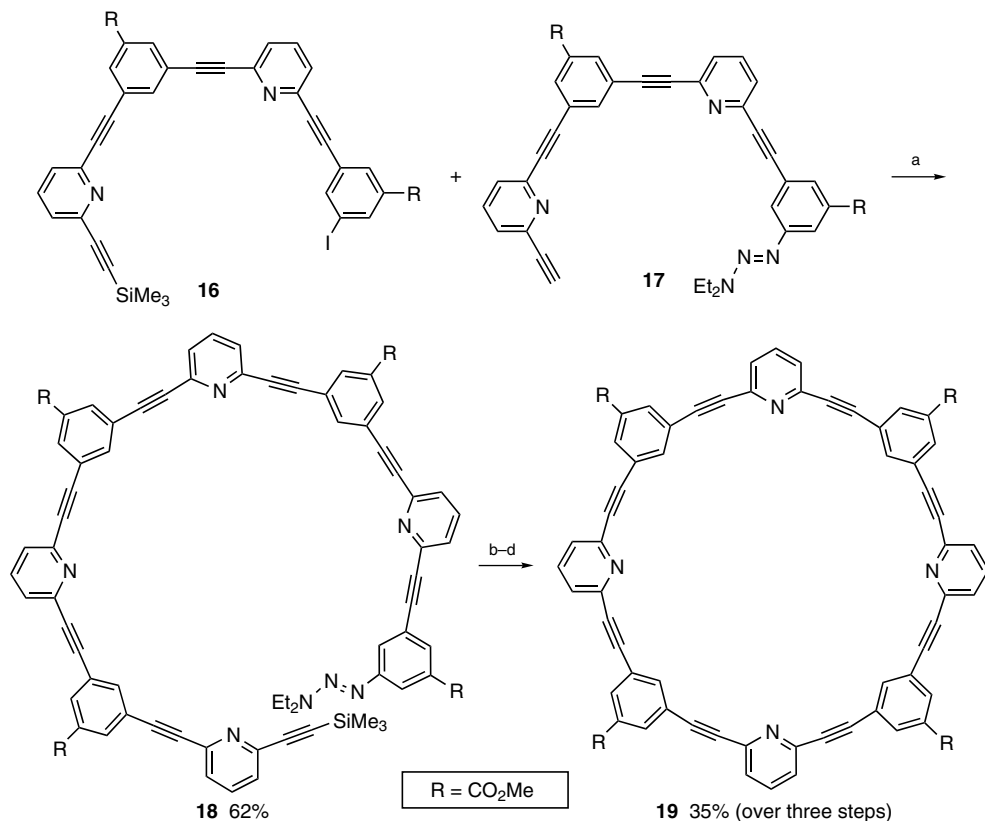
Scheme 6.7 Stepwise formation of SPM **19** using an aryltriazene as a masking group for an aryl iodide [45]. Reagents and conditions: (a) [PdCl$_2$(PPh$_3$)$_2$], CuI, Et$_3$N/THF (1:1); (b) I$_2$, ClCH$_2$CH$_2$Cl, 80 °C; (c) KOH, MeOH, CHCl$_3$; (d) [PdCl$_2$(PPh$_3$)$_2$], CuI, Et$_3$N/THF (1:1).

A second common technique relies on the use of orthogonal alkyne protecting groups, based on the ability to selectively remove a trimethylsilyl (or triethylsilyl) group in the presence of a triisopropylsilyl group (TMS, TES, and TIPS, respectively). The synthesis of tetramer **20** by Tobe and coworkers demonstrates this approach (Scheme 6.8) [46]. Starting with **21**, selective removal of the TMS group with K$_2$CO$_3$/MeOH generated the terminal alkyne, which was used without isolation in a Sonogashira reaction with **22**, and this was followed by a second Sonogashira reaction with TMS-acetylene to give **23**. Removal of the TMS group and oxidative homocoupling gave the macrocycle precursor **24**. Finally, the TIPS groups were removed with TBAF, and a homocoupling reaction gave the desired product **20**. While providing low yield (10%), the preassembly of **24** helped to ensure preferential formation of the desired cyclic tetramer.

In a comparison of Cu- versus Pd-homocoupling reactions, Haley and coworkers demonstrated a connection between the selectivity of the ring forming event, the
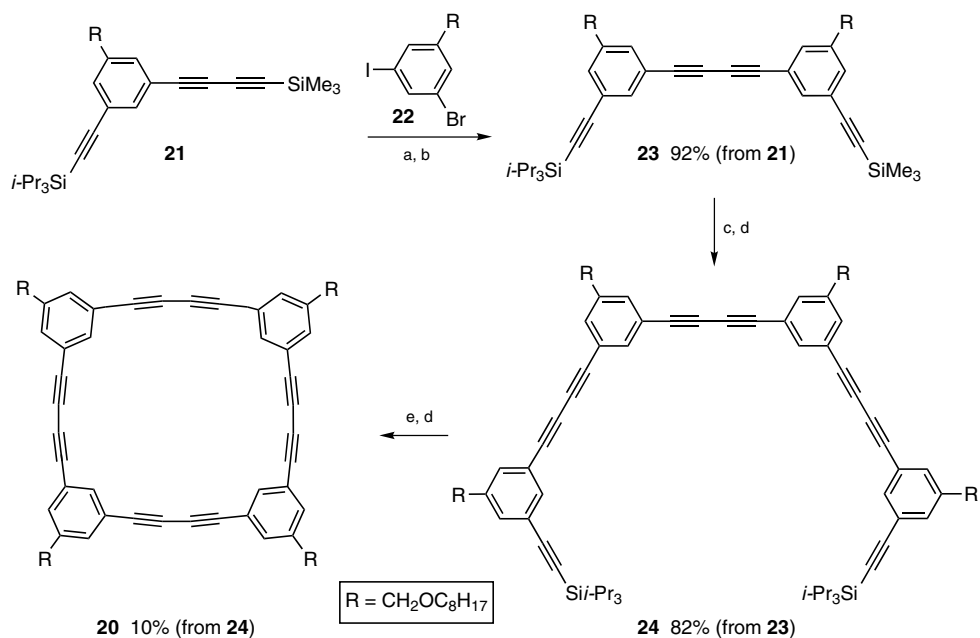
Scheme 6.8 Intramolecular ring closure to provide macrocycle
20 [46]. Reagents and conditions: (a) K₂CO₃, THF, MeOH, rt,
then [Pd₂(dba)₃•CHCl₃], CuI, PPh₃, Et₃N, **22**, 50 °C; (b)
[Pd₂(dba)₃•CHCl₃], PPh₃, CuI, Et₃N, TMSA, 75 °C; (c) K₂CO₃,
THF, MeOH, rt; (d) [Cu(OAc)₂], py, rt; (e) TBAF, THF, rt.

catalyst used, and the ring strain present in the transition state of the bond-forming
step [47,48]. The selectivity is demonstrated in the formation of bis[15]- and bis[14]
annulenes (**25**,**26** and **27**,**28**) shown in Scheme 6.9, several derivatives of which were
explored for self-association (see Figure 6.4). Briefly, it was shown that intramolecu-
lar homocoupling of **29** or **30** under Eglinton conditions gave preferentially the bis
[15]annulenes **25** and **26**. This selectivity was ascribed to the nature of the dimeric
Cu-acetylide intermediate, which, prior to reductive elimination, is commonly as-
sumed to adopt a pseudo-*trans*-configuration (Scheme 6.9, inset a). Molecular
modeling showed that such an intermediate geometrically favors the formation of
the less strained [15]annulenes over the more strained [14]annulenes. Conversely,
use of Pd-catalyzed homocoupling conditions with **29** or **30** results in selective
formation of the bis[14]annulenes **27** and **28**. In this case, the *cis*-configuration
of the Pd-diacetylide intermediate, prior to reductive elimination, is presumably
enforced by the chelating bidentate dppe ligand (Scheme 6.9, inset b), and this factor
ultimately leads exclusively to formation of the more strained products **27** and **28**.

Finally, it is worth noting that the formation of acetylenic SPMs on solid support
has also been attempted, although to date success has been limited [49]. Recent
advances in the formation of acyclic oligomers by Moore and coworkers, however,
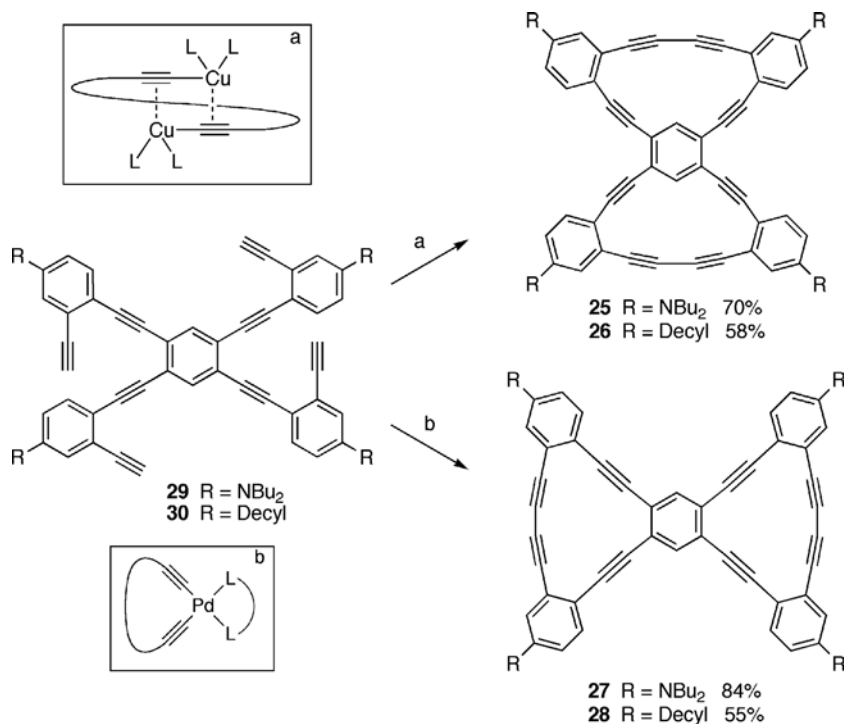
Scheme 6.9 Selective homocoupling based on Cu- or Pd-catalysis, by Haley and coworkers, in the formation of [15]annulenes **25** and **26** and [14]annulenes **27** and **28** [47]. Reagents and conditions: (a) [Cu(OAc)$_2$], py, 60 °C; (b) [PdCl$_2$(dppe)], CuI, I$_2$, THF, *i*-Pr$_2$NH, 50 °C.

suggest that this is a technique that could ultimately lend itself to selective SPM formation, as well as more facile purification [50].

6.2
Supramolecular SPMs

The use of shape-persistent macrocycles in supramolecular chemistry has been limited only by the imagination of those working in this vast area of science. In many cases, a specific component is engineered into the SPM framework to govern directed supramolecular assembly processes, often through metal ion complexation. In other cases, the SPM has been designed with a specific size and/or configuration so that it can act as a host for a guest ion or molecule. Alternatively, intermolecular interactions between the macrocycles result in aggregation that facilitates ordering of the system in the solution state, as liquid crystals, or on surfaces. Salient examples that illustrate some of these design concepts will be discussed below.

6.2.1
SPMs as Components in Supramolecular Assemblies

The placement of a particular functional group into the skeleton of a SPM provides rigid molecules capable of predictable self-assembly in supramolecular systems. To this end, Tykwinski and coworkers have synthesized cross-conjugated macrocycles with exocyclic pyridine donor sites to function as analogs to 4,4′-bipyridine (Scheme 6.10) [51]. For example, 3,5-diethynylpyridine was cross-coupled to vinyl triflate **31** using [Pd(PPh$_3$)$_4$], resulting in the macrocycle precursor **32**. Subsequent desilylation and oxidative homocoupling under high dilution (0.5 mM) using Hay conditions in CH$_2$Cl$_2$ gave SPM **33** in 52% yield.

The ability of **33** to function as a component in self-assembly reactions was established through reaction with the Ru-porphyrin **34** carried out in CH$_2$Cl$_2$ at room temperature and leading to the desired metal complex **35** (Scheme 6.11) [51][1]. While ^{1}H NMR spectroscopy showed quantitative formation of complex **35**, the isolated yield based on precipitation was only 60%, suggesting weak association between the SPM and the Ru-porphyrins. X-ray crystallographic analysis of **35** subsequently showed that unfavorable steric interactions between the phenyl rings of **35** and the pendent porphyrins were the likely origin of this weak association. The metal-directed, self-assembly of **33** with [Pt(OTf)$_2$(PEt$_3$)$_2$] gave dimeric assembly **36** [52]. X-ray crystallographic analysis of **36** showed that the macrocyclic ligand **33** had assumed a boat conformation through complexation to Pt (Scheme 6.11, inset). This conformation results in the solid-state formation of bidirectional channels, that incorporate eight molecules of the crystallization solvent ClCH$_2$CH$_2$Cl per unit cell.
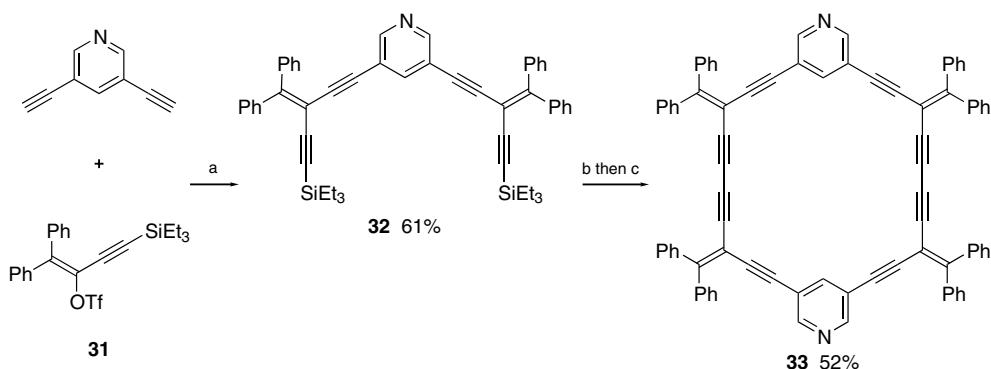
Scheme 6.10 Synthesis of macrocyclic ligand **33** [51]. Reagents and conditions: (a) [Pd(PPh$_3$)$_4$], CuI, Et$_2$NH, THF, 55 °C; (b) TBAF, THF, rt; (c) CuI, TMEDA, O$_2$, CH$_2$Cl$_2$, rt.

[1]) A similar SPM based on isopropylidene subunits gave the analogous complex **35** (see Ref. [51]).
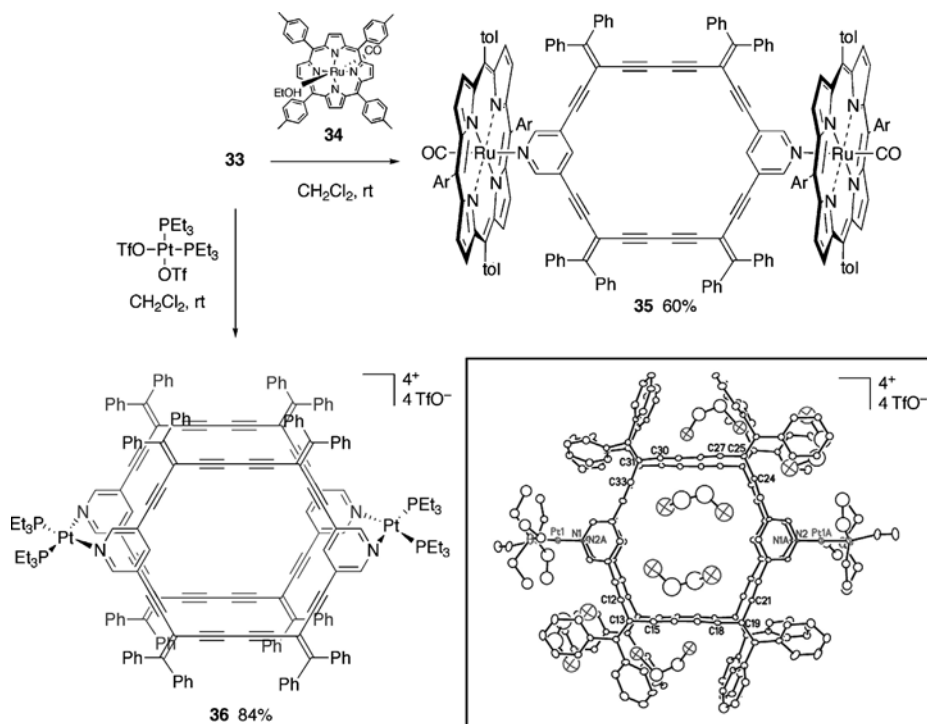
Scheme 6.11 Self-assembly of SPM **33** using an Ru-porphyrin **34** and [Pt(OTf)$_2$(PEt$_3$)$_2$], resulting in supramolecular complexes **35** [51] and **36** [52]. Inset: solid-state structure of **36** as determined by X-ray crystallography.

The possible use of this material as a porous solid was later evaluated using hyperpolarized ^{129}Xe NMR spectroscopy, which demonstrated the permanent porosity of the material even after the removal of the co-crystallized solvent [53].

Lees and Sun have synthesized similar macrocyclic ligands, with *meta*-substituted benzene ring linkers using Sonogashira and Hay reactions (Scheme 6.12) [54]. The reaction of dibromide **37** with terminal diyne **38** led solely to the formation of macrocycle **39**, which was purified easily by recrystallization from CH$_2$Cl$_2$. In a manner similar to that described by Tykwinski (vide supra), oxidative homocoupling of **38** gave the nearly insoluble SPM **40** in only 32% yield, along with oligomeric products. The Re(I) supramolecular transition metal complexes **41** and **42** were then prepared by refluxing **39** or **40** with the Re(I) diamine complex in THF. Both the SPMs (**39** and **40**) and their metal complexes (**41** and **42**) showed strong fluorescence in solution.

The SPMs **43** and **44** with opposing 2,2′-bipyridine donor sites for metal complexation were prepared by Schlüter and coworkers using a Sonogashira reaction to effect
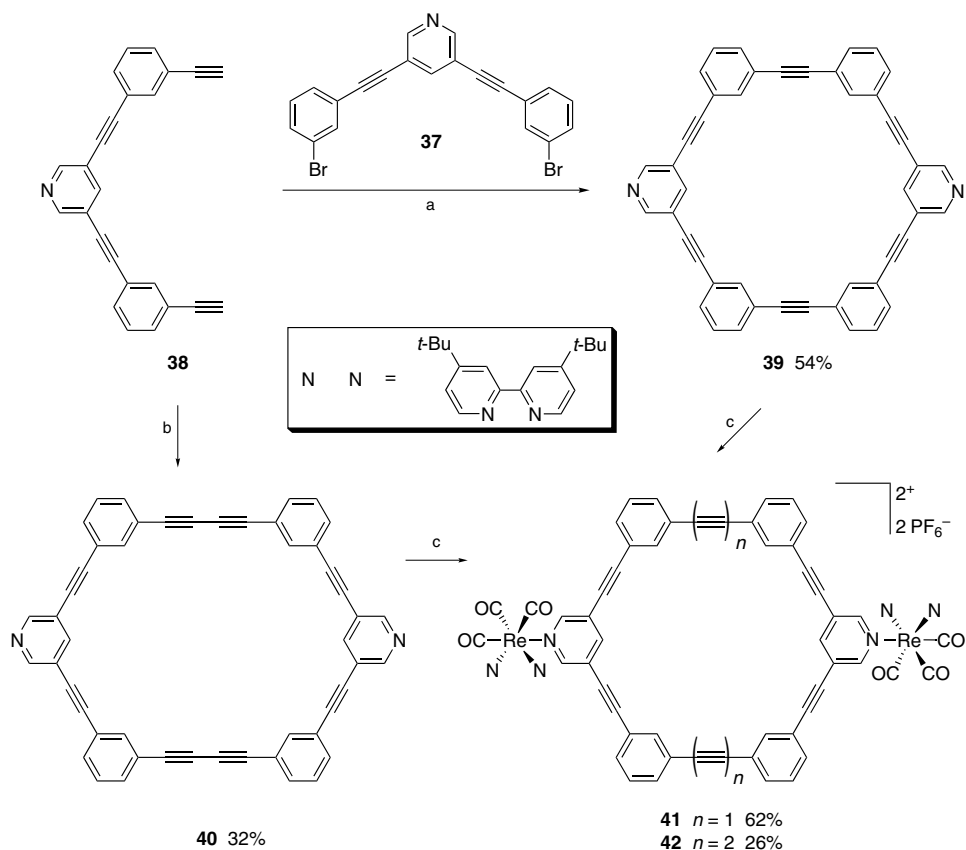
Scheme 6.12 Synthesis of SPMs **39** and **40** and formation of their metal complexes **41** and **42** [54]. Reagents and conditions: (a) [PdCl$_2$(PPh$_3$)$_2$], CuI, *i*-Pr$_2$NH, 70 °C, 16 h; (b) CuCl, py, O$_2$, rt, 30 h; (c) [(CH$_3$CN)Re(CO)$_3$(4,4′-*t*-Bu$_2$bipy)](PF$_6$), THF, 60 °C.

ring closure (ring closing bonds indicated[2] in Scheme 6.13A) [55,56]. While SPM **43** was formed in a reasonable yield of 28%, macrocycle **44** was inexplicably isolated in a much lower yield (14%) and could not be obtained pure. This disparity in yield for structurally similar macrocycles highlights an example of the unanticipated challenges that often face macrocycle assembly [57]. X-ray crystallographic analysis of **43** and **44** showed that the SPMs are layered in the solid state, resulting in "channels" that contain both co-crystallized solvent molecules and portions of the flexible side chains. The bipyridine group can rotate freely, allowing for either *exo*- or *endo*-cyclic metal ion complexation. When either **43** or **44** was reacted with [RuCl$_2$(bipy)$_2$], however, only assemblies **45** and **46** formed, with *exo*-cyclic complexed ruthenium.

---

2) This same convention will be used periodically throughout the chapter to show the final ring closing bond.

A)

43 R^1 = CH$_2$OHex, R^2 = H
44 R^1 = CH$_2$OTHP, R^2 = CH$_2$OHex

Sonogashira coupling here

[RuCl$_2$(bipy)$_2$]

45 R^1 = CH$_2$OHex, R^2 = H   55%
46 R^1 = CH$_2$OTHP, R^2 = CH$_2$OHex 80%

B)

47 R = OHex

48 R = OHex
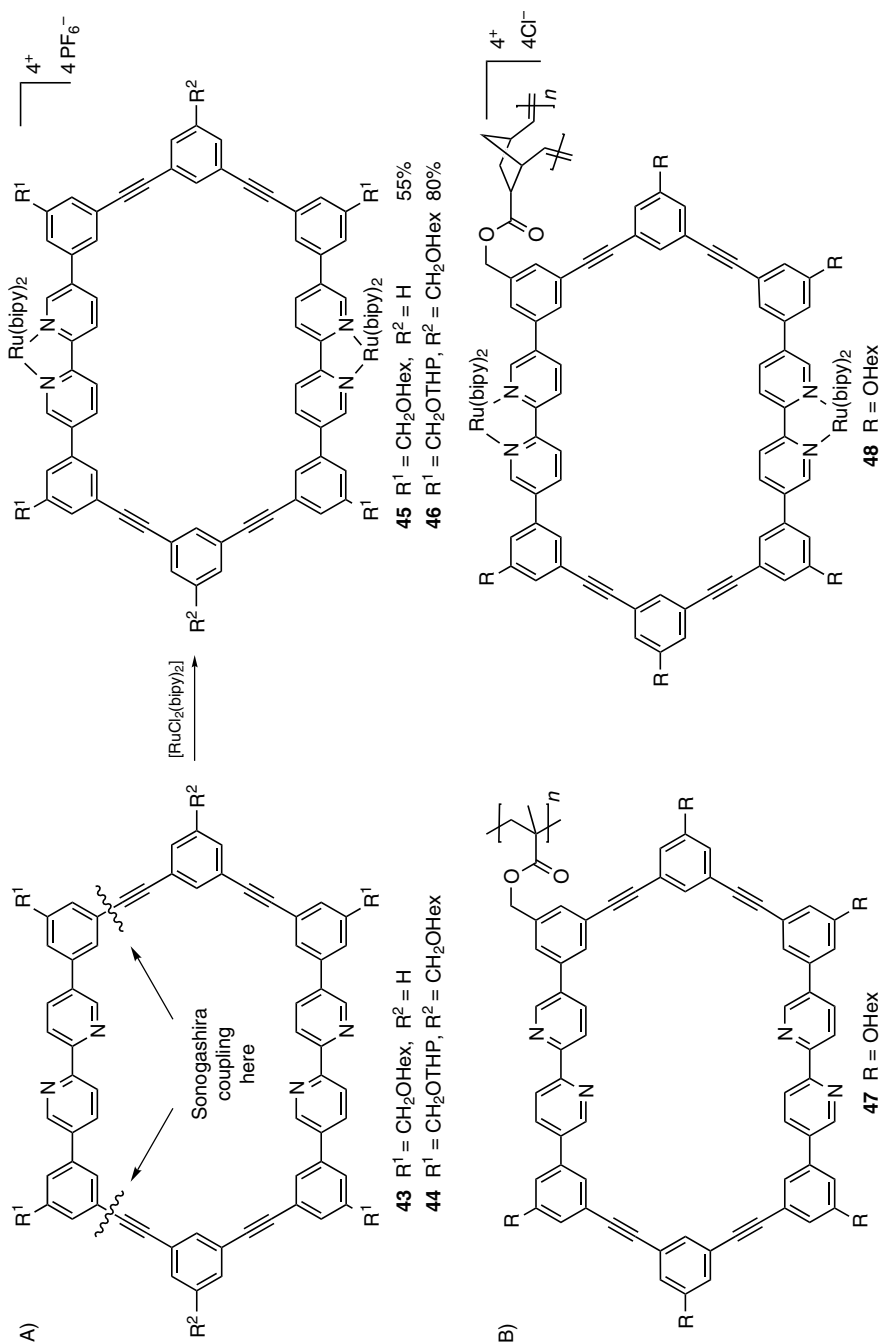
Scheme 6.13 (A) SPMs **43** and **44** with opposing bipyridine donor sites and synthesis of their metal complexes **45** and **46** [55], and (B) Polymers **47** and **48** formed via free-radical polymerization and ROMP, respectively [56].

This same group has reported one of the most detailed discussions of optimizing the synthesis of SPMs, using the basic macrocyclic structure found in **43** and **44**. The aim was to reduce the number of steps, increase yields, and replace Stille reactions with the more efficient and non-toxic Suzuki reactions [58]. The ultimate goal was to convert SPM monomers (not shown) into polymer **47** via free-radical polymerization and into polymer **48** through ring-opening metathesis polymerization (ROMP) using the Grubbs II catalyst (Scheme 6.13B). In the latter case, the "protected" Ru-complex of the macrocyclic monomer was required for the success of the ROMP reaction.

Schmittel and coworkers envisioned the SPM **49** (containing phenanthroline units with *exo*-cyclic binding sites) as the key building block to form supramolecular complexes **50** and **51** (Scheme 6.14) [59]. Macrocycle **49** was obtained in 16% yield through a Sonogashira reaction [60], and simply dissolving **49** with either components **52** or **53** in the presence of $[Cu(MeCN)_4]PF_6$ in CH_2Cl_2 at room temperature gave quantitative self-assembly to the phenanthroline nanoboxes **50a** or **50b**. The authors relied on the use of steric and electronic effects from bulky aryl substituents at one end of the phenanthroline ligand **52** or **53** to thermodynamically and kinetically direct coordination toward the desired heteroleptic Cu(I) complexes [61]. Although X-ray crystallographic analysis could not be done for boxes **50a** and **50b**, spectroscopic analysis and MM+ calculations suggested an internal volume of >5000 Å^3. The self-assembly reaction of **49** with $AgPF_6$ gave the analogous supramolecular structures **51a** and **51b**. Conversion of the Ag(I) complexes **51a** or **51b** to the Cu(I) complexes **50a** or **50b**, respectively, could be accomplished through the addition of CuI to a solution of the former at room temperature. Regeneration of the Ag(I) nanoboxes **51a** and **51b** from **50a** or **50b** could then be achieved through the addition of excess AgCN. SPM **49** was also used for the formation of a supramolecular nanobasket (not shown) [62].

Macrocycles with acetylenic subunits have been used a great deal in the formation of catenanes, and much of this work is detailed in Chapter 10 by Wisner and Blight. Two pertinent examples will, however, be described here. Using the preorganization concept pioneered by Sauvage and Dietrich–Buchecker [63], Godt and Ünsal have reported the synthesis of a [2]catenane with 87-membered, non-interacting rings (Scheme 6.15) [64]. Synthesis of the [2]catenane began with the formation of **54**, in which the two "halves" of the catenane are connected by a covalent carbonate template. Subsequent to desilylation, the terminal diyne **55** was subjected to acetylenic homocoupling under Breslow conditions and gave a mixture of the intended precatenane **56** and the non-catenated dimer (not shown) in a 2.6:1 ratio (90% combined yield). This mixture was subjected to carbonate cleavage with TBAF in THF, liberating the free [2]catenane in 63% yield (not shown). This synthesis was highly efficient, purification was simple, and large-scale reactions could be performed easily.

Bäuerle and coworkers have synthesized a "π-conjugated" catenane, utilizing Cu(I) templation and a newly developed method for acetylenic homocoupling based on the reductive elimination of platinum to generate the desired C–C bond formation (Scheme 6.16) [65,66]. The C-shaped **57** was first preorganized around Cu(I), resulting in the homoleptic bis-phenanthroline complex **58**. After removal

50a M = Cu(I), R₁ = H, R₂ = Me   100%
50b M = Cu(I), R₁ = Me, R₂ = Br   100%

51a M = Ag(I), R₁ = H,   R₂ = Me   100%
51b M = Ag(I), R₁ = Me, R₂ = Br   100%

52 R¹ = H, R² = Me
53 R¹ = Me, R² = Br

Sonogashira coupling here

49

a or b
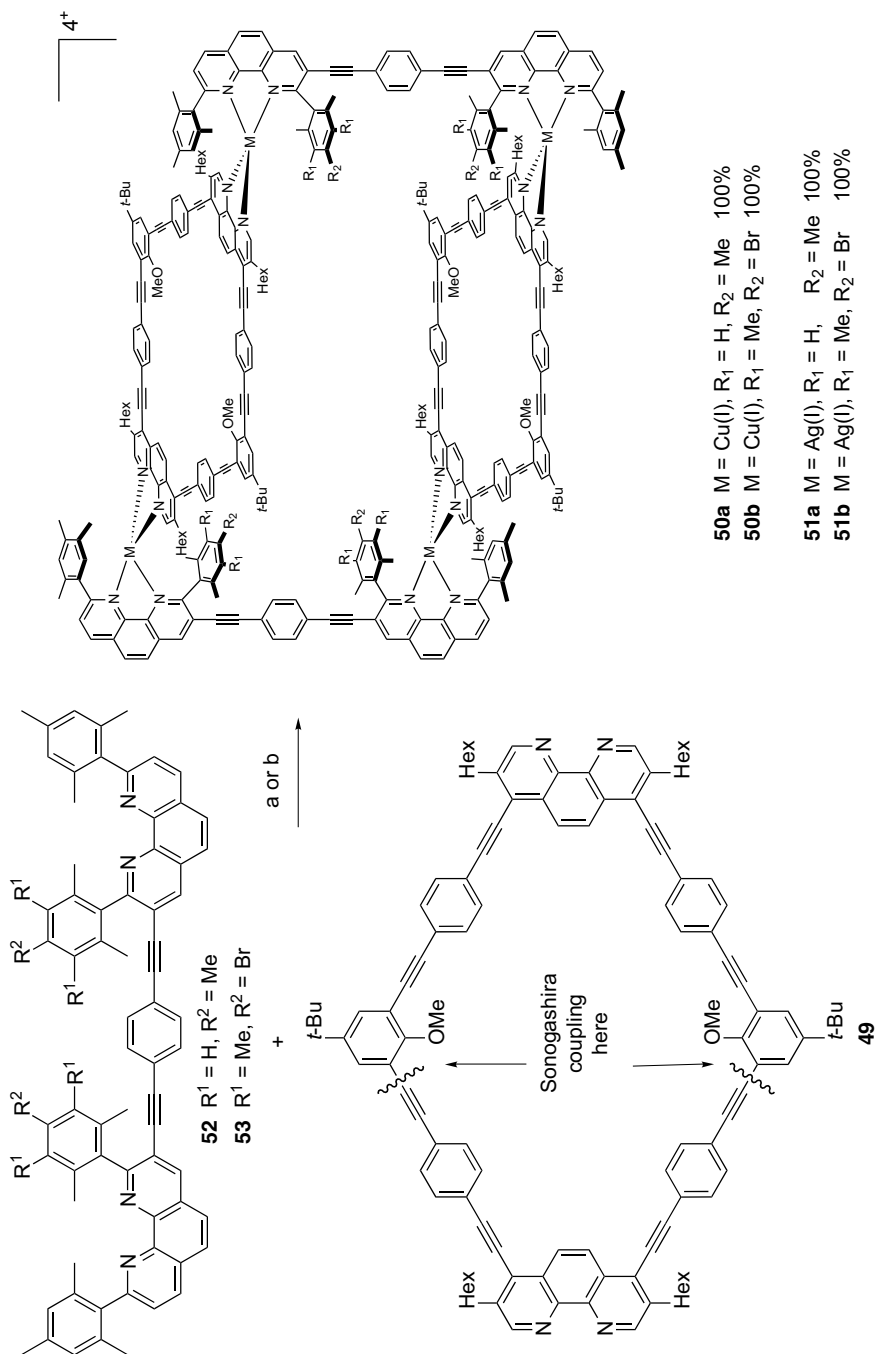
Scheme 6.14 Synthesis of nanoboxes **50** and **51** using metallosupramolecular assembly [59]. Reagents and conditions: (a) [Cu(MeCN)₄]PF₆, CH₂Cl₂, rt; (b) AgPF₆, CH₂Cl₂, rt.
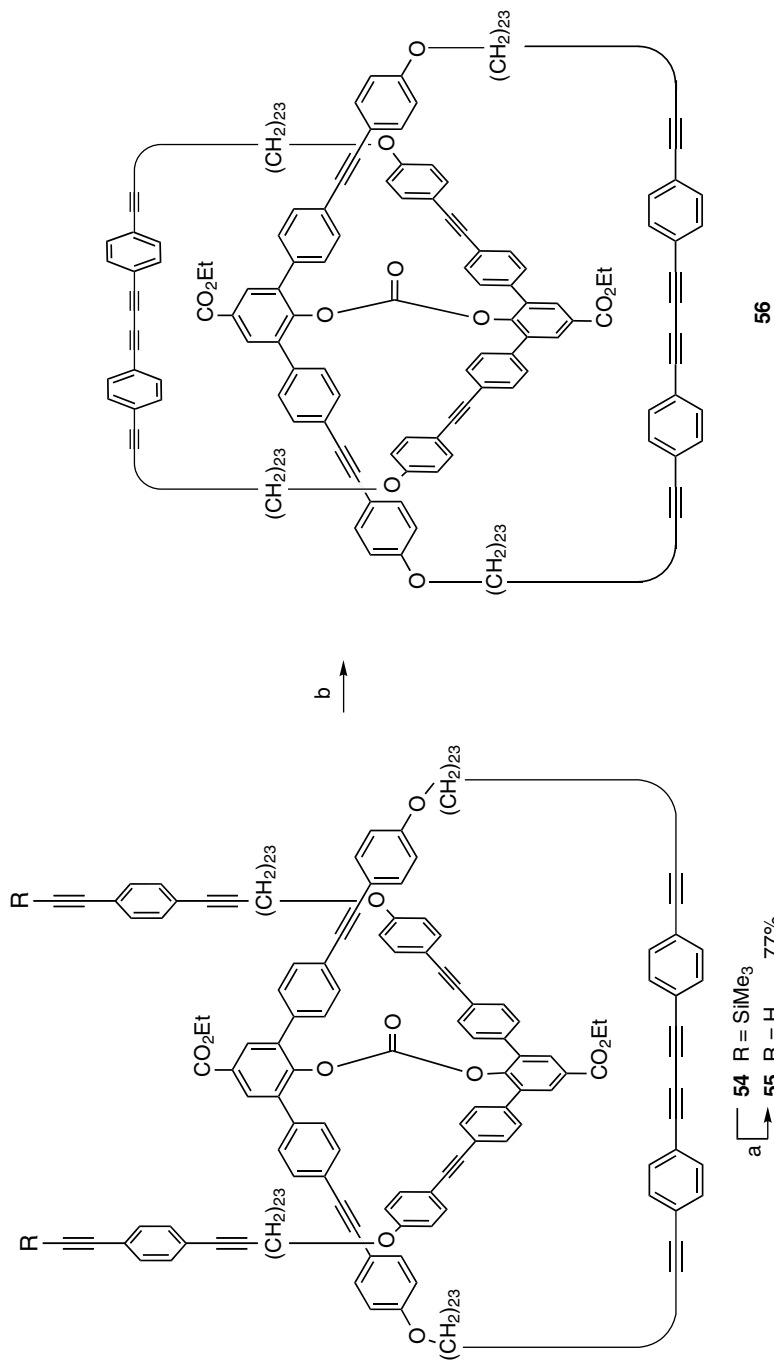
Scheme 6.15 Synthesis of precatenane **56** by carbonate-templated oxidative dimerization [64]. Reagents and conditions: (a) KOH, EtOH, THF; (b) CuCl, CuCl₂, py, rt.
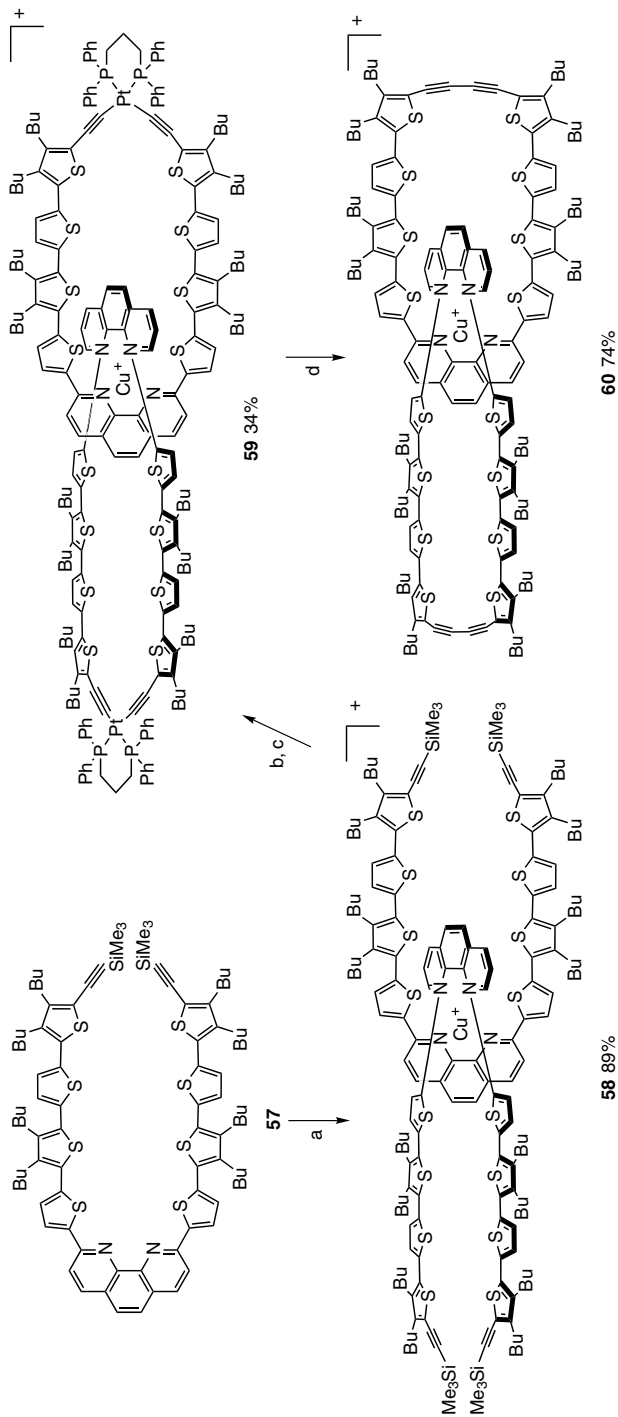
Scheme 6.16 Synthesis of conjugated Cu(I) catenate **60** using metal templation and Pt reductive elimination [65]. Reagents and conditions: (a) [Cu(CH$_3$CN)$_4$]BF$_4$; (b) CsF; (c) *cis*-[PtCl$_2$(dppp)], rt, Et$_3$N, PhMe, 60 h; (d) I$_2$, THF.
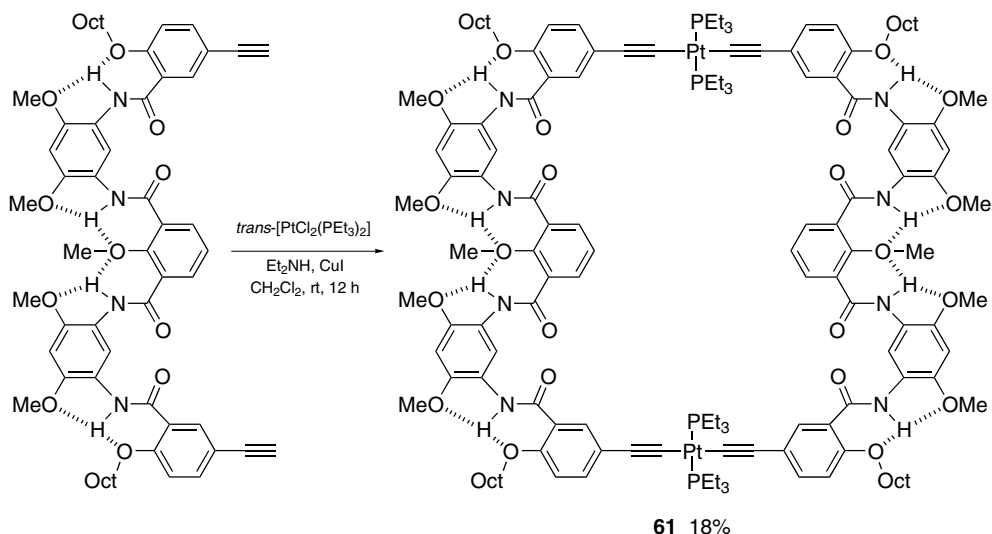
Scheme 6.17 Synthesis of rigid hydrogen-bonded SPM **61** [68].

of the four TMS groups with CsF, macrocyclization with *cis*-[PtCl$_2$(dppp)] led to the catenate **59**. The Pt-corners were reductively eliminated with I$_2$ in THF, leading to catenate **60**. Decomplexation with KCN gave the Cu-free "π-conjugated oligothiophene-based" catenane in good yield (not shown). It is worth noting that in smaller interlocked π-conjugated catenanes synthesized by this same group, Cu(I) demetalation was impossible, and therefore the Cu-free catenanes were not isolated [67].

In an interesting application of Pt-acetylide chemistry, Li and coworkers have used a preorganization concept to facilitate the self-assembly of SPM **61** (Scheme 6.17). The planar zig-zag precursor is stabilized through repeated, intra-molecular three-center hydrogen bonding, and its rigid structure presents both acetylene groups aligned on the same side of the molecule. With this orientation, the formation of **61** in the presence of *trans*-[PtCl$_2$(PEt$_3$)$_2$] and CuI should have been greatly favored, but the authors report an unexpectedly low yield of 18% for the cyclization step [68].

6.2.2
SPMs in Host–Guest Systems

The ability to selectively functionalize SPMs, coupled with their preorganized nature, makes them quite useful as molecular hosts for a wide variety of guests. One of the first examples capitalizing on this concept came from Diederich and coworkers, who synthesized a family of chiral binaphthyl-derived hosts including triangular, square, and rectangular derivatives (for example **62–67**, Figure 6.2) via a one pot (**nA → A$_n$**) Hay reaction. They subsequently studied the molecular recognition of
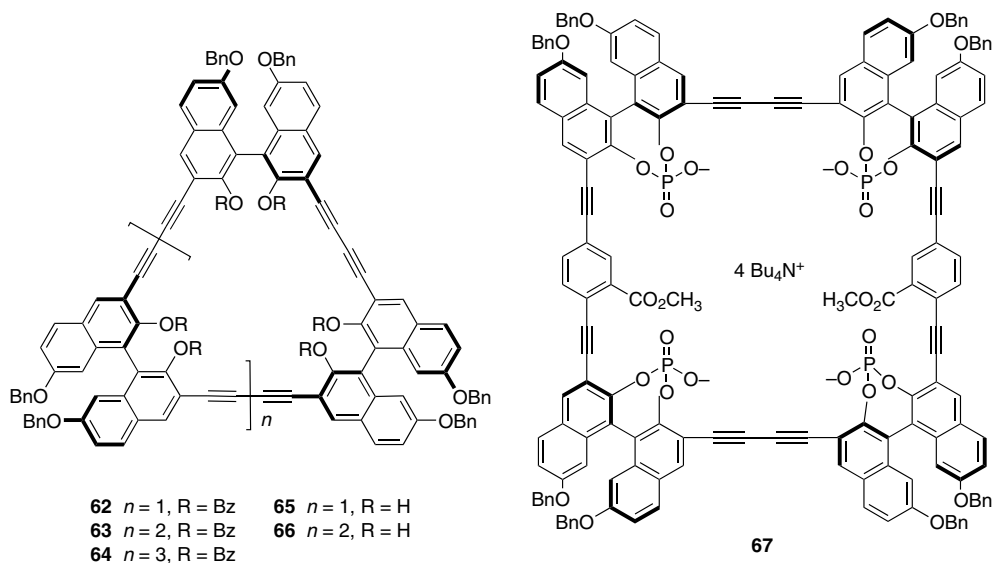
Figure 6.2 Examples of Diederich's saccharide receptors **62–66** [71,72] and disaccharide receptor **67** [69,70] based on *R*-binaphthol.

these SPMs with carbohydrates. The smaller SPM **65** was capable of selective carbohydrate recognition with several glucopyranosides, with modest enantioselectivity observed in some cases. Later generations of SPMs built on this same concept incorporated larger carbon scaffolds and modified receptor sites such as phosphate ester **67** shown below, a molecule that bonded selectively to disaccharides [69–72].

Kawase, Oda, and coworkers have synthesized a unique series of belt-shaped paraphenylacetylene macrocycles **68–71** (Scheme 6.18A) and studied their host-guest supramolecular chemistry. The precursor polyenes **72–75** were synthesized using a modified McMurry reaction, and a subsequent bromination/dehydrobromination sequence with *t*-BuOK gave the desired SPMs **68–71**. A 4:1 mixture of **72/74** gave the corresponding mixture of SPMs **68** and **70**, which could be separated by GPC, while pure samples of **73** and **75** could be obtained to provide **69** and **71** directly [73,74]. Using the same bromination/dehydrobromination procedure, SPMs **76–78** were synthesized with 1,4- or 2,6-naphthylene units, respectively, at opposing positions (Scheme 6.18B).

SPMs **68** and **76** have a diameter of 1.31 nm, which is suitable for inclusion of C_{60}, while that of **78** (1.41 nm) is nearly perfect for inclusion of C_{70} [75].[3] The $78 \supset C_{60}$ and $78 \supset C_{70}$ complexes are extremely stable, with association constants K_a of

---

3) Association constants (K_a), were determined by absorption spectroscopy and Stern–Völmer constants (K_{SV}) by fluorescence spectroscopy.
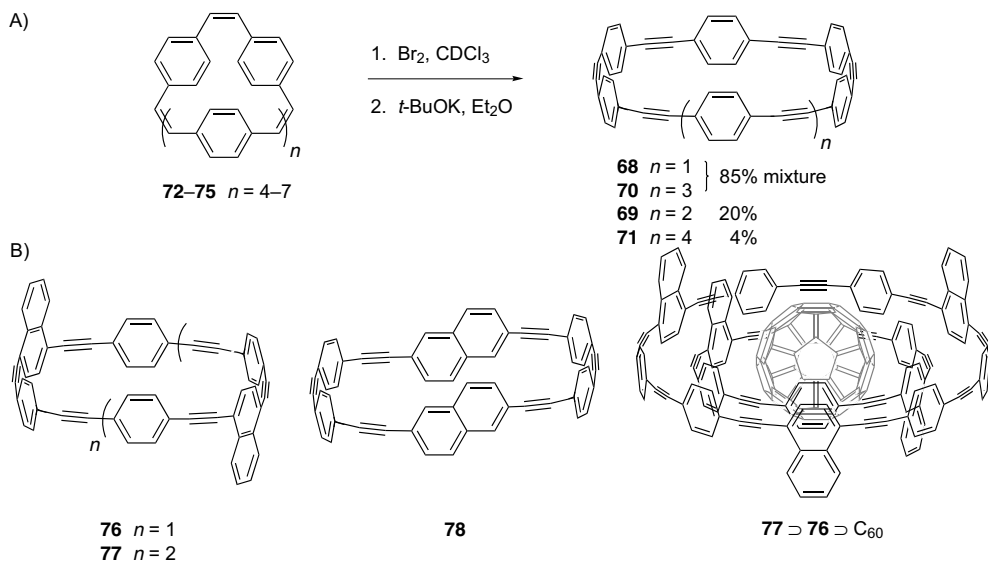
Scheme 6.18 (A) Synthesis of paraphenylacetylene SPMs 68–71 through bromination/dehydrobromination [74] and (B) molecular structure of SPMs 76–78 [75] and onion complex 77 ⊃ 76 ⊃ C$_{60}$ [76].

roughly 1×10^5 and 1×10^6 dm^3 mol^{-1} and Stern–Völmer constants K_{SV} of 2.6×10^5 and 4.3×10^6 dm^3 mol^{-1}, respectively. Using competitive complexation experiments, the selectivity of 78 for C$_{70}$ vs. C$_{60}$ was determined to be >10:1 [75]. Multicomponent onion-type complexes were then prepared, with two SPMs encompassing a single fullerene molecule, such as 77 ⊃ 76 ⊃ C$_{60}$ and 71 ⊃ 68 ⊃ C$_{60}$ (Scheme 6.18B) [76]. Initially, it was thought that charge-transfer interactions were the main driving force for fullerene-nanoring complexation. Recent studies have, however, shown that electrostatic and van der Waals energies are more significant than charge-transfer energies, and electrostatic interactions are now considered the most likely driving force for the observed complexation [77].

The binding of metal ions is a common use of SPMs in supramolecular chemistry. Toward this goal, Baxter has synthesized multiple *ortho*-fused arylene-ethynylene SPMs using either Hay or Eglinton reactions (Figure 6.3). Macrocycle 79 was formed using Hay conditions, and molecular modeling studies suggested the 2,2′-bipyridine rings are in a cisoid conformation. This places all four nitrogen lone pair electrons oriented toward the interior cavity, promoting the coordination of metal ions of a comparable size. UV–vis and fluorescence spectroscopy showed that 79 responded to only four of the 22 metal cations tested: Co(II), Ni(II), Cu(II) and Zn(II). Furthermore, the signal output was dependent on the metal cation, making 79 a possible multisubstrate, multiple readout ion sensor [78]. Macrocycles 80 and 81 were the first reported 2,2′-bipyridyl twistophanes with a 6,6′-connection, and the synthetic
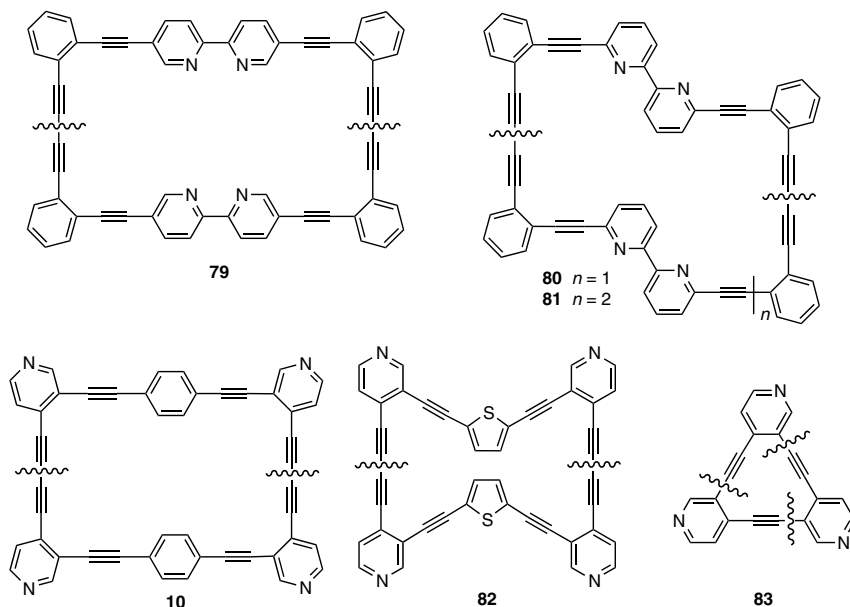
Figure 6.3 Baxter's *ortho*-fused SPMs **10** and **79–83** used for metal ion binding [33,78–81].

yield of SPM **80** was marginally higher under Hay (13%) than Breslow conditions (9%). SPM **80** acted as a fluorescence-quenching sensor for Cu(II) and Ag(I), while **81** functioned as a sensor only for Cu(II) [79]. Baxter synthesized SPM **10** in 71% yield using Eglinton conditions [33], and the coordination preference of **10** for metal ions was determined as Pd(II) > Co(II) ≈ Ni(II) ≈ Ag(I) > Fe(II) ≈ Hg(II). SPM **82** was synthesized in good yield (46%) using Eglinton conditions and was reported as the first SPM combining thienyl (electron donor) and pyridyl (electron acceptor) units. Metal-binding studies showed that **82** binds preferentially to metal cations in roughly the same order as **10**: Pd(II) >> Ni(II) > Co(II) > Ag(I) > Hg(II) [80]. Finally, Baxter and Dali-Youcef used the Castro–Stephens reaction for cyclotrimerization to **83**, formed in only 5% yield. This unexpectedly low yield was attributed to the linear and/or cross-linked nature of the cuprate intermediate, making formation of the final bond unfavorable. Nevertheless, macrocycle **83** was found to be a highly selective fluorescence-quenching sensor for Pd(II) [81].

Using the Sonogashira reaction, Yoshida and coworkers have reported the stepwise synthesis of SPM **84**, which was then converted to its butyl ester **85** (Scheme 6.19) [82]. X-ray crystallographic analysis confirmed that **85** had a completely planar structure, with acetylenic bond angles of 168.7 and 171.0°. The macrocycle shows unusually intense fluorescence ($\lambda_{em} = 355$ nm, $\Phi = 0.18$, CH_2Cl_2), and the emission maximum shifted dramatically to 433 nm ($\Phi = 0.41$) upon the addition of $SbCl_5$. Based on the ^{1}H NMR and UV–vis spectroscopic analyses, the luminophor was predicted to be the 1:1 complex **86**. Interestingly, no other metal investigated showed any effect on the fluorescence, making **85** a potentially useful ion sensor for toxic Sb(V).
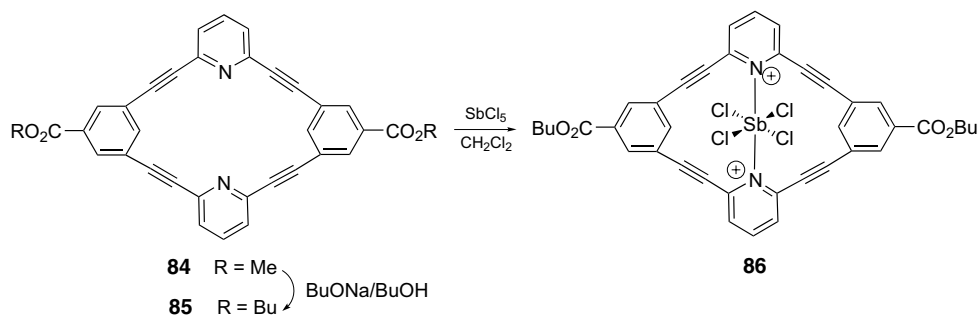
Scheme 6.19 SPMs **84–85** and a complex with Sb(V) **(86)** [82].

Fallis and Heuft have used a metal-templated synthesis to form the helical 1,10-phenanthroline-capped metal-complexed SPMs **87** and **88** (Scheme 6.20) and their demetalated analogs (not shown). The addition of [Cu(OAc)$_2$] (0.5 equiv) to a solution of **89** in pyridine and diethyl ether templated the formation of intermediate **90**. Following the addition of excess [Cu(OAc)$_2$] (5.5 equiv), the Cu(I)-complexed SPM **87** was isolated in an excellent yield of 84%. Treatment of **87** with aqueous KCN then provided the Cu-free SPM in 70% yield (not shown). The N,N-dibutylamine substituted analog **88** was formed in an analogous manner and taken on directly to the Cu-free SPM (39%) in a one-pot procedure. It was shown by variable temperature ^{13}C NMR spectroscopy that the helical Cu(I) complex **88** had a barrier to racemization of 4 kcal mol^{-1} higher than that of the Cu-free analog [83].

MacLachlan and coworkers have formed large SPMs **91–93** using a simple, one-pot, template-free, [3 + 3] Schiff-base condensation procedure (Scheme 6.21). The yields of the macrocycles were 40–68%, and no evidence of acyclic oligomer or polymer formation was observed. This is presumably due to the reversibility of the imine condensation, which allows the most thermodynamically stable product to
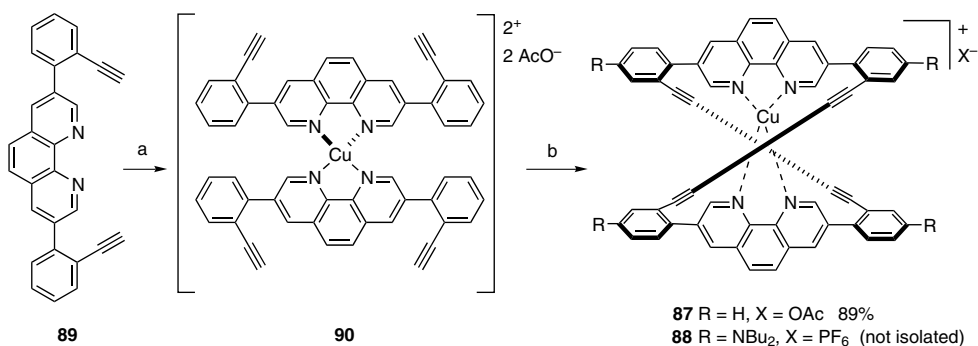
Scheme 6.20 Templated, one-pot synthesis of helical 1,10-phenanthroline SPMs [83]. Reagents and conditions: (a) [Cu(OAc)$_2$] (0.5 equiv), Et$_2$O/py, 2 h; (b) [Cu(OAc)$_2$] (5.5 equiv), Et$_2$O/py.
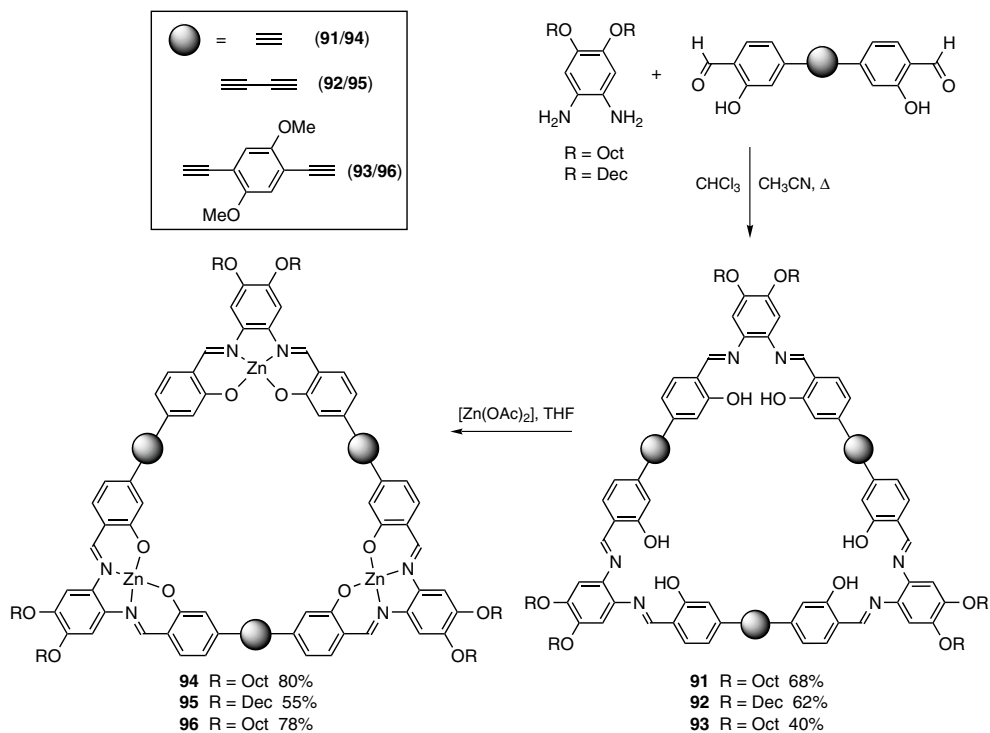
Scheme 6.21 Synthesis of Schiff-base SPMs **91–93** and their complexation with Zn(II) [84].

ultimately form, in this case the [3 + 3] macrocycles. These SPMs bind to a number of metal ions, but coordination to Zn(II) proved to be the most interesting. Pristine **91–93** are weakly fluorescent in THF ($\Phi = 0.13$–0.15), but complexation with Zn in THF at reflux to form **94–96** drastically increases the emission quantum yield ($\Phi = 0.86$–0.92). This enhanced luminescence is attributed to formation of a more rigid macrocycle after the binding of Zn(II) to the three host sites. The emission spectra of **94–96** are almost identical, and it was therefore suggested that the luminescence is localized to the site of metal complexation with little or no electronic coupling through the conjugated backbone of the molecule [84]. Strong solution-state aggregation was later reported for **94** (as well as a branched alkyl derivative, not shown) based on intermoledular Zn· · ·O interactions between the molecules [85].

6.2.3
Aggregation and Surface Chemistry of SPMs

The organization of SPMs into well-defined structures has been one of the most common goals, leading toward their application to supramolecular chemistry. The typically flat conjugated skeleton of acetylenic SPMs facilitates intermolecular self-association, and a number of other secondary bonding interactions can be used to augment the aggregation process. Incorporation of long pendent alkyl chains about

the disc-like structure of SPMs can lead to columnar, discotic liquid crystals (LC), as well as the ability to form highly ordered monolayers on surfaces such as HOPG. The role of SPMs in such applications is described in this section.

6.2.3.1 Aggregation of SPMs

Marsella and coworkers have reported SPM formation based on quadrupole enhanced self-assembly in solution (Scheme 6.22A) [86]. While solid-state packing based on aryl–perfluoroaryl interactions (Ar_H–Ar_F) is a well-established supramolecular motif [87,88], it was unique to see these electrostatic interactions manifested in a *solution-state* cyclization formation of **97–99** and then **100** and **101**. Using Sonogashira conditions in THF and pseudo-high dilution conditions to reduce polymer formation, a mixture of terminal diynes **102** and **103** and diiodides **104** or **105** were reacted. Macrocycles **97–99** were formed in yields of 12, 10 and 30%, respectively, and the higher yield of **99** was taken as evidence of the ability of Ar_H–Ar_F electrostatic interactions to template the cyclization. The generality of this outcome was explored through the competitive coupling of diiodides **104** and **105** with terminal diyne **106** under the same conditions (Scheme 6.22B). An enhanced yield was again observed for the Ar_H–Ar_F SPM **100** (26%) in comparison to that of the Ar_H–Ar_H SPM **101** (10%). A stepwise cross coupling was proposed, in which equilibrium was established between a folded and an open intermediate. When both Ar_H and Ar_F were present, the folded intermediate facilitated cyclization.
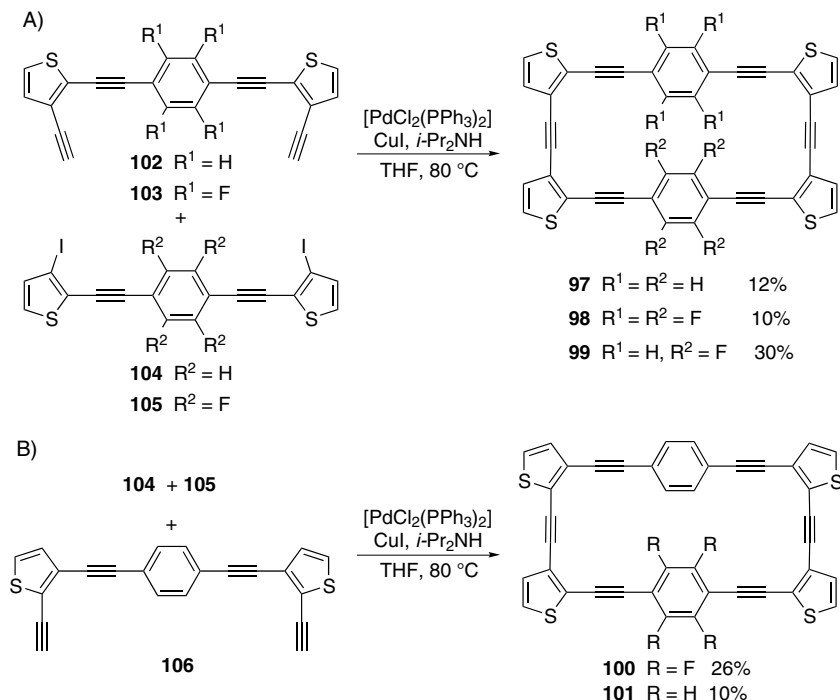
Scheme 6.22 Synthesis of SPMs **97–101** [86].

SPM **13** was designed by Shu and Mayor to foster intermolecular aggregation based on Ar_H–Ar_F interactions and was synthesized via two different routes [34]. The first strategy coupled two halves of the macrocycle using a modified Cadiot–Chodkiewicz reaction, yielding 4% of macrocycle **13** after a difficult purification process (see Scheme 6.5B). The second strategy coupled dibromide **107** with diyne **108** under the same Cadiot–Chodkiewicz conditions, affording **13** in 7% yield after GPC purification (Scheme 6.23). While the overall yield of the second strategy was slightly lower than that of the first, product isolation in this case was much easier and more efficient, making synthesis through the pentamer **107** preferred. MALDI-TOF MS of **13** identified signals consistent with aggregation, and a study of concentration dependence using ^{1}H NMR spectroscopy showed a consistent upfield shift in the proton signals of the benzene moiety, indicative of face-to-face aggregation due to π–π stacking [89–95]. The size of these aggregates was not, however, determined.

Tobe and coworkers have synthesized butadiyne-bridged SPMs **109–112** via an intramolecular Eglinton reaction to effect ring closure in yields of 27–50% (Figure 6.4) [89,93,96]. Aggregation studies between electron-poor SPMs **111–112** and electron-rich SPMs **109–110** show results that are in many ways analogous to those arising from Ar_F–Ar_H quadrupole–quadrupole interactions as described above. Since this interaction requires mutual overlap of the aromatic rings, it is not unexpected to find that SPMs with more interaction sites formed heteroaggregates more readily (i.e., **110** and **112** vs. **109** and **111**). Pyridinophanes **111** and **112** also efficiently serve as a host for the tropylium cation, forming 1:1 and 2:1 complexes.

Haley and coworkers have explored aggregation of isomeric SPMs with charge distribution biased by strong electron donors and acceptors. For example, [15]- and [14]annulenes **113–116** all form dimers in a range of solvents, but the [15]annulenes
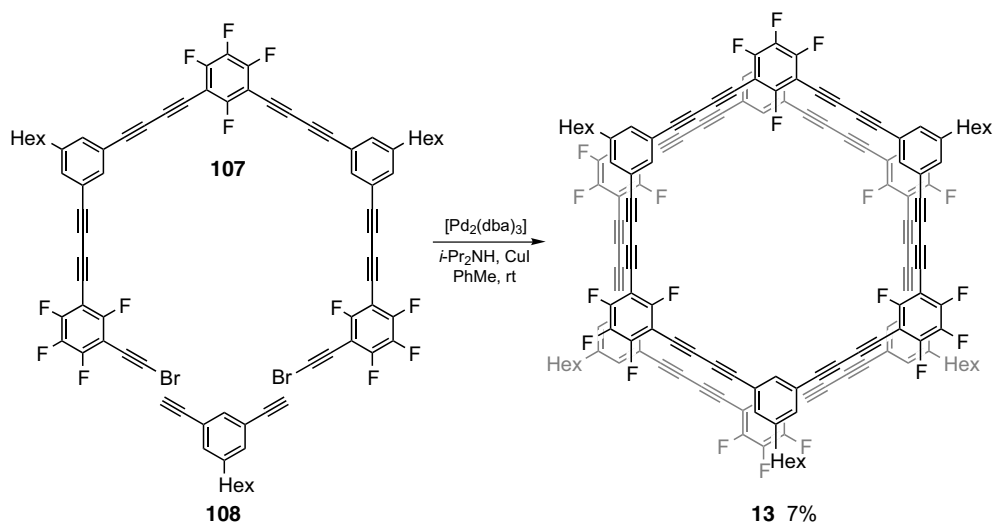
Scheme 6.23 Synthesis of SPM **13** by a Pd-catalyzed Cadiot–Chodkiewicz reaction [34].

109 X = CH, *n* = 1
110 X = CH, *n* = 3
111 X = N, *n* = 1
112 X = N, *n* = 3

113 R^1 = NBu$_2$, R^2 = NO$_2$
114 R^1 = NO$_2$, R^2 = NBu$_2$

115 R^1 = NBu$_2$, R^2 = NO$_2$
116 R^1 = NO$_2$, R^2 = NBu$_2$
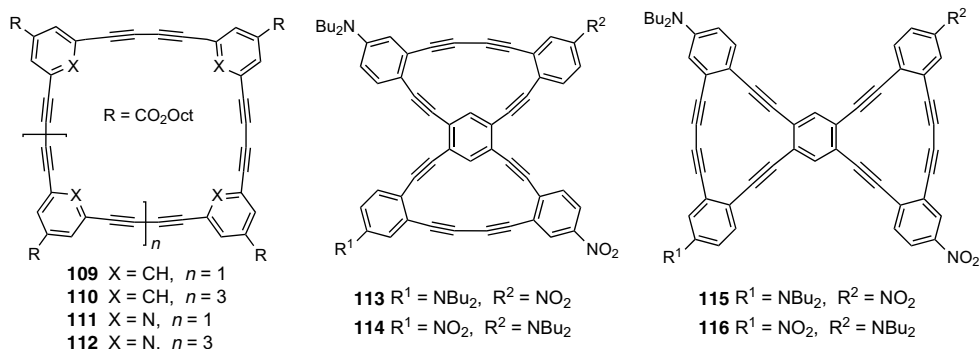
Figure 6.4 SPMs **109**–**112** synthesized by Tobe and coworkers [96] and SPMs **113**–**116** synthesized by Haley and coworkers [48].

113 and **114** consistently show association constants about one order of magnitude higher than those of the analogous [14]annulenes **115** or **116** [48].

Tetrathiafulvalene (TTF) based [18]annulenes **117** and **118** (Figure 6.5) have been synthesized via cyclooligomerization (see Scheme 6.1B), while the [12]annulene **119** was formed under Sonogashira conditions using a terminal diyne and a diiodide (not shown) [25]. All three SPMs show strong self-aggregation in benzene and toluene, but not in CDCl$_3$, CD$_2$Cl$_2$ and THF-d_8. STM measurements have been carried out on samples of **117** and **118** deposited from dilute CH$_2$Cl$_2$ solutions onto an Au(1 1 1) surface and show that **117** and **118** have similar dimensions of about 2.2 nm long and 0.2–0.25 nm high.

Helicene-based SPM (*M,M,M*)-**120**, as well as all other possible stereoisomers, have been synthesized by Yamaguchi and coworkers using a Sonogashira reaction of the corresponding diiodide and terminal diyne (Figure 6.6) [92]. Self-aggregation of these SPMs was evident in concentration dependence ^{1}H NMR spectroscopic studies in CDCl$_3$ (0.1 and 10 mM). Dimer formation (even in benzene) was observed

117 R = CO$_2$Bu
118 R = CO$_2$Oct

119 R = CO$_2$Bu
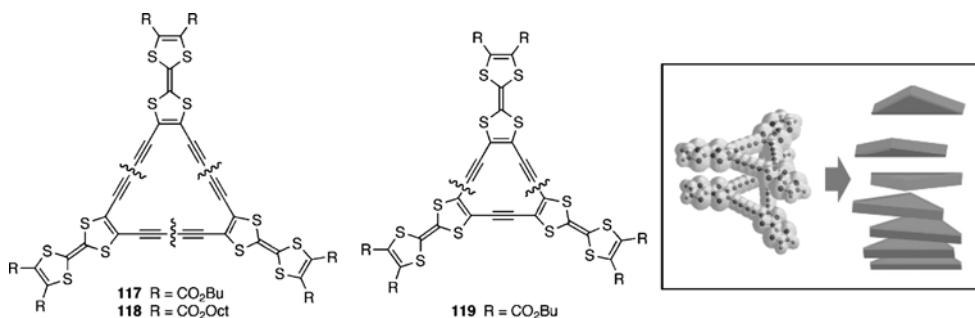
Figure 6.5 TTF[18]annulenes **117** and **118** and TTF[12]annulene **119** synthesized by Iyoda and coworkers [25]. Inset: schematic representation of their self-assembly. Reprinted with permission from *Org. Lett.* **2006**, *8*, 1917–1920. Copyright 2006 American Chemical Society.
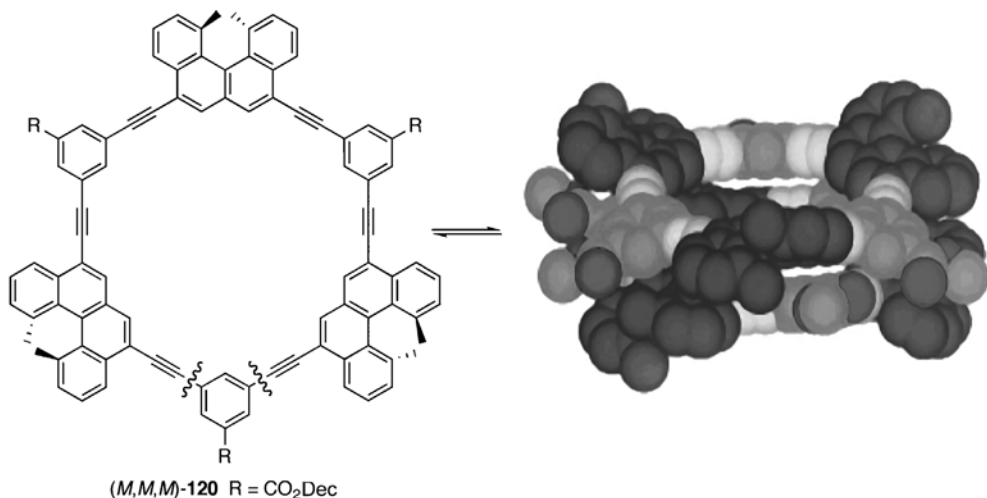
Figure 6.6 SPM (*M*,*M*,*M*)-**120** and the structure of the dimer
from Amber* calculations [92]. Reprinted with permission from
Org. Lett. **2001**, *3*, 1097–1099. Copyright 2001 American
Chemical Society.

by vapor pressure osmometry (VPO), but higher aggregation was not. The dimerization appeared to depend substantially on the configuration of the helicene units: (*M*,*M*,*M*)-**120** and (*M*,*M*,*M*)-**120** > (*M*,*P*,*M*)-**120** and (*M*,*P*,*M*)-**120** > (*M*,*M*,*M*)-**120** and (*P*,*P*,*P*)-**120** > (*M*,*P*,*M*)-**120** and (*P*,*M*,*P*)-**120**.

It was later shown that an amine derivative of (*M*,*M*,*M*)-**120** could be oxidatively dimerized using MnO$_2$ in toluene to provide azo-linked *cis*- and *trans*-(*M*,*M*,*M*)/(*M*,*M*,*M*)-**121**, respectively (Figure 6.7) [97]. These isomers were easily separated by GPC and their stereochemistry was determined by UV–vis spectroscopy. Isomerization was not observed for the isomers upon heating or irradiation. VPO studies in CHCl$_3$ indicated that *trans*-(*M*,*M*,*M*)/(*M*,*M*,*M*)-**121** was monomeric below 0.01 mM and dimeric above 2 mM. On the other hand, *cis*-(*M*,*M*,*M*)/(*M*,*M*,*M*)-**121** was a trimeric aggregate below 1 mM and polymeric above 1 mM. These observations were explained based on the conformation of the isomers, as depicted in Figure 6.7. Intramolecular or bimolecular aggregates are not possible for *cis*-(*M*,*M*,*M*)/(*M*,*M*,*M*)-**121** because of the rigidity of the azo group at 120°; therefore two *cis* molecules cannot exist in the same plane. These findings provided a new motif for selective self-assembly of bimolecular π-π interactions of helicenes.

Höger and coworkers have recently observed that the free-base derivative of pyridinium SPM **122** (Figure 6.8) shows only weak aggregation in solution, forming tubular structures [98]. Once the pyridyl groups were alkylated to form the cationic species **122**, however, well-defined dimers were formed, even at very low concentrations. This behavior was explained through a conformational locking of the SPM into a boat conformation that directs the pyridinium groups toward the center of the dimer to accommodate the bromide ions. Ultimately, this hinders any further aggregation from either the top or bottom of the system.
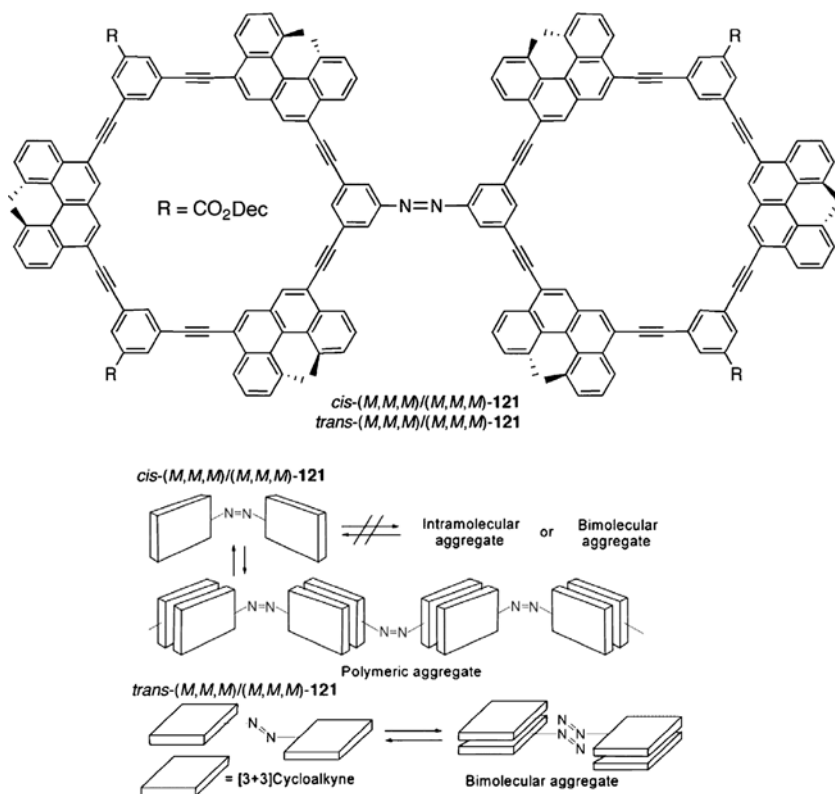
Figure 6.7 Structure of *cis*- and *trans*-(*M,M,M*)/(*M,M,M*)-**121** (top) and schematic description of their aggregation behavior (bottom) [97]. Reprinted with permission from *J. Am. Chem. Soc.* **2003**, *125*, 9268–9269. Copyright 2003 American Chemical Society.

Alkyne metathesis reactions have emerged as an efficient and effective means of forming macrocycles, as described in detail by Prunet *et al*. in Chapter 2 of this book. In the case of acetylenic SPMs, Adams, Bunz, and coworkers were the first to employ alkyne metathesis (see Scheme 6.2). Moore and coworkers have subsequently refined this strategy, capitalizing on the selective formation of the thermodynamically favored product under equilibrium control using precipitation-driven alkyne metathesis [99]. These reactions were typically high yielding, and could be scaled up to provide gram quantities of the desired SPM. For example, reaction of **123** using EtC≡Mo[NAr(*t*-Bu)]₃ as a catalyst in the presence of *p*-nitrophenol gave **124** in 81% isolated yield on a milligram reaction scale and an amazing 77% yield on a gram scale (Scheme 6.24) [29,100]. SPM **124** was shown to form aggregates in solution, especially in polar solvents such as acetone [101]. An analogous metathesis reaction gave tetrameric carbazole-based SPM **125** in 84% yield as the sole product. This SPM self-assembled into nanofibrils using the sol-gel method, driven by the favorable
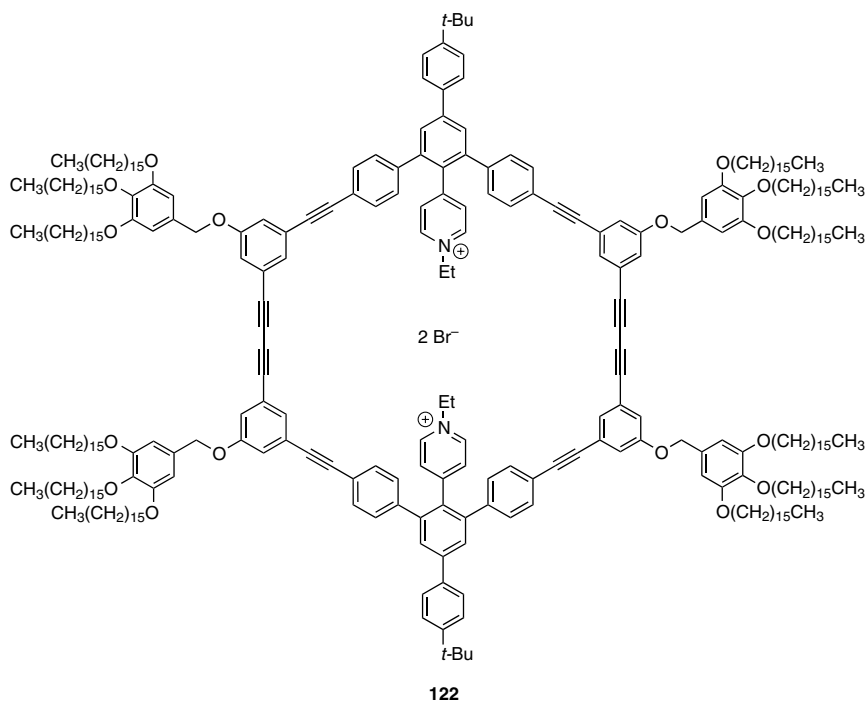
Figure 6.8 Cationic SPM **122** [98].

π-π-stacking of the planar macrocycles and hydrophobic interactions between the alkyl side chains [102]. The related SPM **126** also aggregated to give nanofibrils that, when fabricated into thin films, could be used in the detection of explosives (e.g., TNT) based on fluorescence quenching [103].

Moore and Zhao have also reported the use of imine metathesis for the synthesis of SPM **127** in almost quantitative yield from **128** and **129** (Scheme 6.25) [104]. It had previously been shown that SPM **127** aggregates into columnar assemblies in acetonitrile [105], a phenomenon driven by the solvophobically favored aromatic stacking. It was thus proposed that, once **127** was formed under the metathesis reaction conditions, it was stabilized by the free energy gained from the intermolecular aggregation. This makes aggregates the thermodynamically most stable species and shifts the metathesis equilibrium in favor of cyclization. This "aggregation driven" formation of macrocycles presents a powerful new strategy for high-yield formation of SPMs. The same group also reported the quantitative formation of SPM **127** via a simple condensation of an amine and an aldehyde to introduce the imine bond [106].

In contrast to the work just described, in which aggregation facilitates product formation, aggregation can also lead to the demise of SPMs as a result of intermolecular close contacts that lead to polymerization. For example, Tobe and coworkers
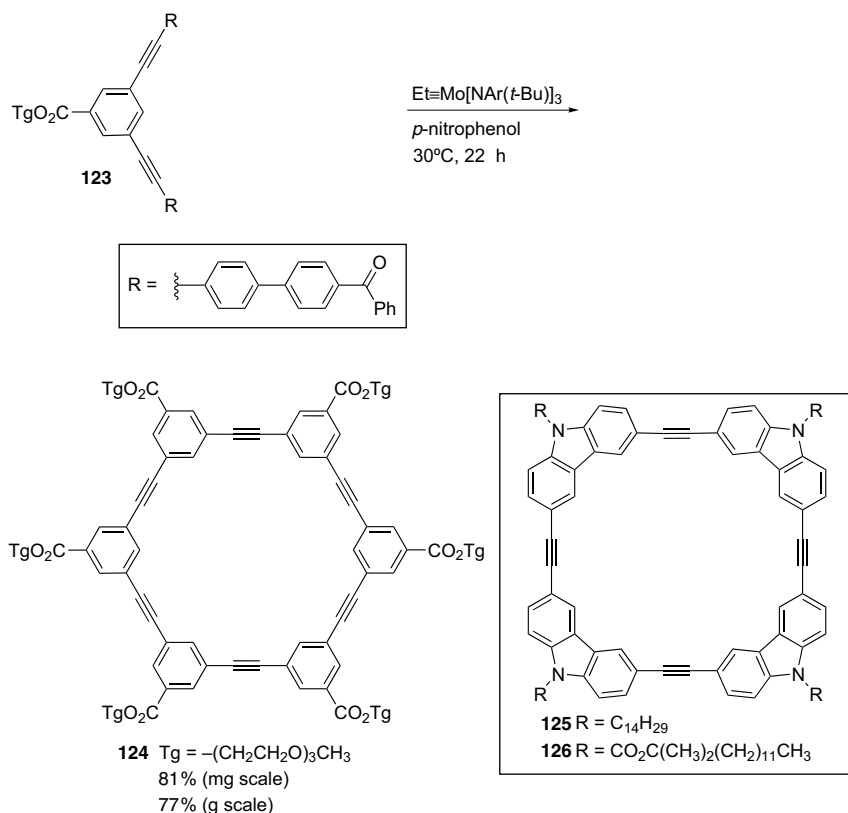
Scheme 6.24 Synthesis of SPM **124** by alkyne metathesis [29,100]. Inset: molecular structures of SPMs **125** and **126** [102,103].

have described the unusual spontaneous polymerization of hexameric SPM **130** at room temperature, while the tetramer (**131**) and octamer (**132**) were quite stable (Figure 6.9) [46]. Thus, in cases where the isolation of an SPM with butadiynyl groups proves challenging, it is wise to consider both whether the SPM was formed and whether it was stable.

6.2.3.2 Liquid-Crystalline SPMs

The formation of liquid crystals (LC) from suitably functionalized acetylenic SPMs has often been the motivation for their synthesis. A number of groups have sought to capitalize on the planar or nearly planar disk-like geometry of SPMs to promote the formation one-dimensional columnar stacks based on a combination of π–π stacking, van der Waals, dipole, and hydrophobic interactions. For example, Heiney, Moore, and coworkers have reported the high-resolution X-ray diffraction analysis (XRD) of a tubular, discotic LC based on SPM **133**, which has been synthesized via a Sonogashira reaction [106]. These studies reveal an unanticipated distortion and
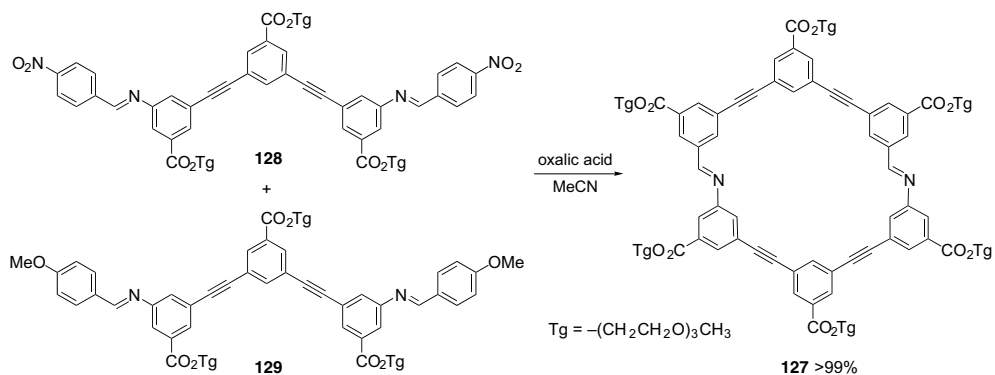
Scheme 6.25 Synthesis of **127** by imine metathesis [104].

doubling of an underlying hexagonal lattice with $b \approx 2a$, as shown in Figure 6.10, suggesting that the unit cell must contain two crystallographically inequivalent molecules A and B. To determine the degree to which ions could be integrated into the columnar structure, SPM **133** was doped with AgOTf (1, 2, or 4 wt.%) and examined via powder XRD. At 4%, columnar order is essentially destroyed, but at 1 and 2%, order is maintained, and there is strong evidence that the silver and triflate ions are located in the center of the channels, offering a potential anisotropic LC ionic conductor.

Tew and coworkers have reported *ortho*-phenylene ethynylene SPMs **134–136** with discotic LC properties (Figure 6.11) [107]. All attempts at the formation of **134–136** through the metathesis approach were discouraging; **136** could not be synthesized, while **134** and **135** were formed as mixtures. Ultimately, an intramolecular Sonogashira reaction was used. X-ray diffraction shows that symmetric **134** and **135**

131 *n* = 1; **130** *n* = 3; **132** *n* = 5
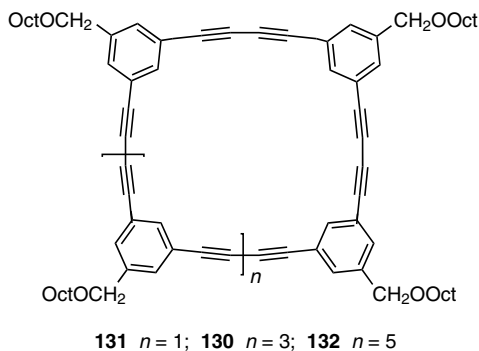
Figure 6.9 Tetramer **131**, hexamer **130** and octamer **132** SPMs synthesized by Tobe and coworkers [46].

133
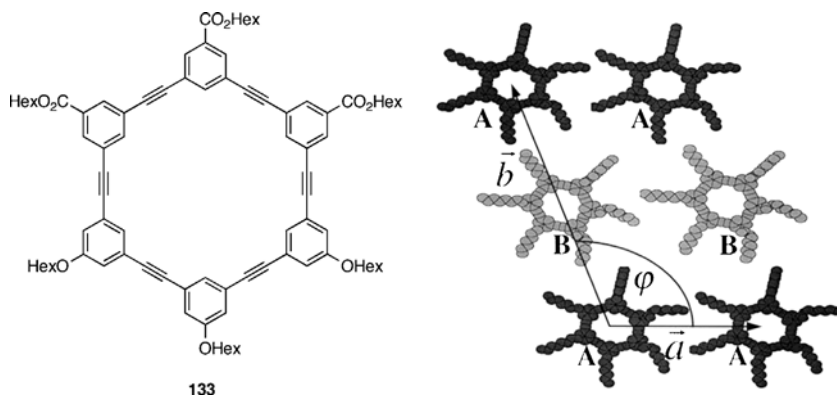
Figure 6.10 Liquid-crystalline SPM **133** and its molecular arrangement in the unit cell [106]. Reprinted with permission from O. Y. Mindyuk, M. R. Stetzer, P. A. Heiney, J. C. Nelson, J. S. Moore, *Adv. Mater.* **1998**, *10*, 1363–1366.

self-assemble into highly ordered columnar structures, while asymmetric macrocycle **136** is less ordered. The most significant difference between the *meta*-phenylene ethynylene SPMs reported by Moore (e.g., **133**) and **134–136** is the size of the central cavity, which is ca. 8 Å for **133** (H to H) compared to 2.4 Å for **134** [108]. Since columnar assembly is thought to be inhibited by large internal voids, the small cavity size of **134–136** favors self-assembly.

As described above, the common design of a discotic LC integrates the (semi)rigid core of an SPM with flexible side chains about the periphery. An interesting twist of this concept was introduced by Höger and coworkers: Would a LC material arise from an SPM with flexible side groups that fill the *inside* of the macrocycle? SPM **137** was synthesized to probe the idea of an *inverted LC*, using an acetylenic homocoupling reaction to combine the two halves (Figure 6.12) [109]. X-ray crystallography shows that the alkyl chains are arranged within the macrocyclic framework, and the compound forms a mesophase at 185 °C that becomes isotropic at 207 °C. The long alkyl chains of **137** occupy an adaptable position on the SPM core, however, that could place them either inside or outside the cavity in the LC. It is thus unclear whether **137** represented a true inverted LC. SPMs **138–142** have subsequently been
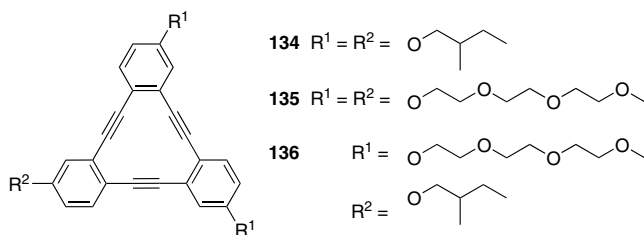
Figure 6.11 *Ortho*-phenylene ethynylene SPMs **134–136** synthesized by Tew and coworkers [107].
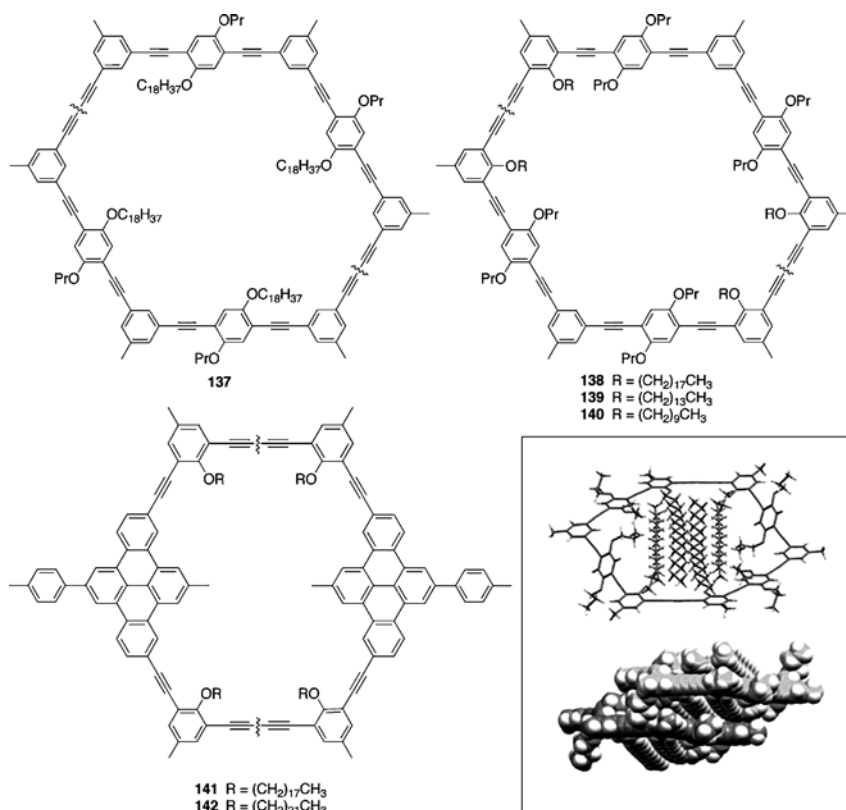
Figure 6.12 Macrocycles **137**–**142** exhibit inverted discotic liquid crystalline properties. Inset: crystal structure of **138** [110]. Reprinted with permission from S. Höger, X. H. Cheng, A.-D. Ramminger, V. Enkelmann, A. Rapp, M. Mondeshki, I. Schnell, *Angew. Chem. Int. Ed.* **2005**, *44*, 2801–2805.

synthesized by an analogous sequence and also show thermotropic mesophases [110,111]. Given that the long alkyl chains in this case are constrained directionally into the interior of the SPM, as shown crystallographically for **138** (Figure 6.12, inset), the formation of inverted LCs is established. Preliminary guidelines toward the formation of inverted LCs have arisen from this study. First, there must be alkyl substituents that have the potential to fill the internal void, and second, SPMs must not contain bulky extraannular substituents that cause the molecules to become interlocked [110].

6.2.3.3 Adsorption of SPMs on Surfaces

With the recent surge in surface analysis techniques, the characterization of surface-adsorbed SPMs has blossomed. This is particularly true for the use of scanning tunneling microscopy (STM), where the conjugated core of the SPM is expected to show a higher tunneling efficiency than nonconjugated portions (e.g.,
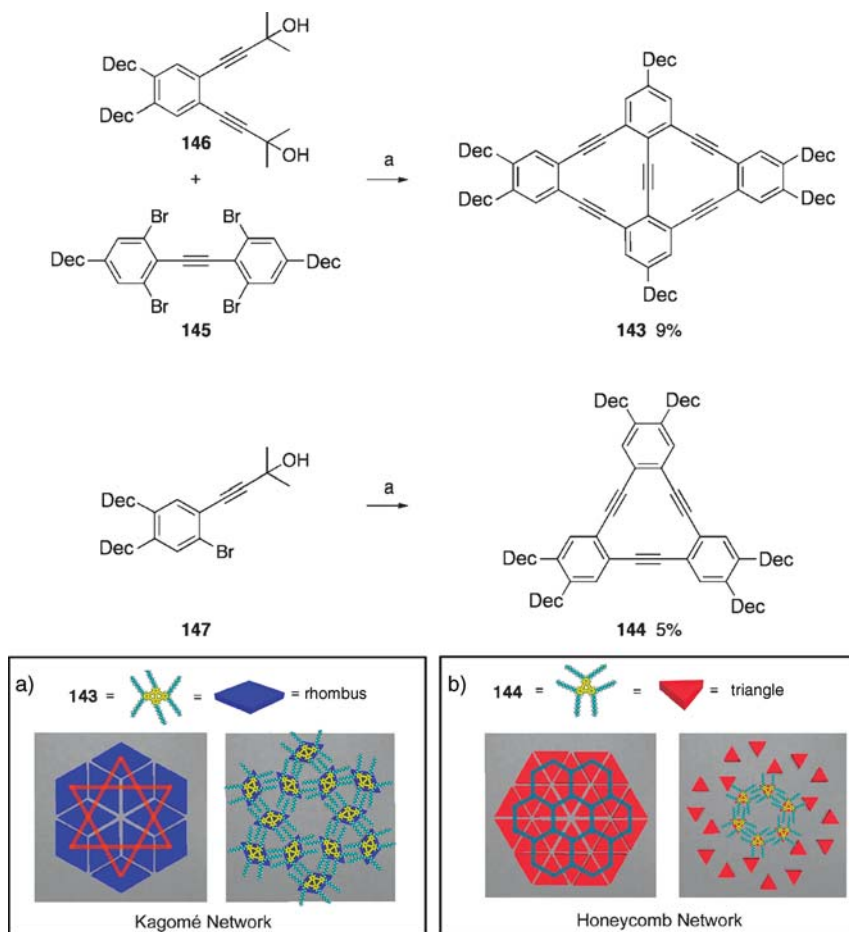
Scheme 6.26 Synthesis of macrocycles **143** and **144** [114]. Reagents and conditions: (a) [Pd(PPh₃)₄], CuI, PPh₃, KOH, PhH, CH₃N[(CH₂)₇CH₃]₃Cl, reflux. Insets: a) Schematic representation of the dense packing of *ideal* rhombic plates (left) and of networks of **143** (right); b) Schematic representation of the dense packing of *ideal* triangular plates (left) and networks of **144** (right) [115].

pendent alkyl groups), facilitating analysis [112]. Since the same intermolecular forces that provide for solution state aggregation and/or LC formation can also be exploited to organize SPMs onto surfaces, it is perhaps not surprising that structural motifs for surface-adsorbed SPMs are often similar to those described in Sections 6.2.3.1 and 6.2.3.2.

Tobe and coworkers have synthesized SPMs **143** and **144** using the *in situ* deprotection Pd(0)-catalyzed cross-coupling protocol developed by Linstrumelle (Scheme 6.26) [31,113]. The cyclization of tetrabromotolan **145** with diethynylbenzene **146** in the presence of the phase-transfer catalyst CH₃N[(CH₂)₇CH₃]₃Cl

afforded **143** in 9% yield, while the same protocol with **147** gave **144** in 5% yield [114]. It was demonstrated that **143** and **144** formed specific topologies at the liquid/solid interface (TCB/HOPG), designated as a Kagomé lattice for **143** (Scheme 6.26, inset a) and a honeycomb structure for **144** (Scheme 6.26, inset b) [115]. The rarely observed Kagomé lattice is very interesting because of its relevance in the field of spin-frustrated magnetic materials. Only a handful of 3D crystals have shown this lattice packing, and **143** is the first 2D network to be reported with this motif. Whereas the rhomboid-shaped SPM **143** shows a corner-sharing hexagonal packing pattern, triangular **144** has side-sharing hexagonal packing. For both SPMs, the alkyl chains run almost perpendicular to the sides of the SPM framework, and each core thus obeys the symmetry aspects of its respective network.

Höger and coworkers have used SPMs **148**–**151** to establish that the size of a rigid macrocycle should be balanced against the presence of flexible extra- and intraannular groups that decorate the core periphery (Scheme 6.27) [116,117]. SPMs with both ester (**148** and **149**) and carboxylic acid (**150**) groups form well-ordered, structured monolayers on an HOPG surface (Scheme 6.27, inset a), whereas those containing intraannular thiol groups (**151**) form self-assembled monolayers on Au(1 1 1) (Scheme 6.27, inset b). The ring-closing step to **148**–**151** relied on acetylenic homocoupling of the two halves of the macrocycle, which typically provided only moderate yields. In an effort to increase the quantity of these macrocycles available for study, the covalent template approach has been applied, converting **152** to **153** and **154** in excellent yields over the three steps [118]. Unlike **148**–**151**, however, attempts to melt the template-bound SPMs **153** and **154** into a LC phase were unsuccessful. The lack of LC behavior was attributed to the presence of the biphenylene bridge, which is longer than the diameter of the macrocycle, and therefore results in a non-planar conformation. Efforts then turned to the adsorption of **153** and **154** onto the surface of HOPG. STM has established that the SPMs are planarized on the HOPG surface and that the biphenylene bridge is also adsorbed onto the surface. Modeling studies have been used to show that in the absence of the solid support, the molecules prefer a nonplanar conformation and only become planar when adsorbed.

STM has also been used to characterize SPM **155** (Figure 6.13A) and **155**/C_{60}, after assembling highly ordered arrays from 1,2,4-trichlorobenzene (TCB) onto a HOPG surface [119]. Monolayers of pure **155** exhibit perfect ordering over a relatively large area, but only two alkyl chains for each extraannular side group are observed. The STM image of the ordered array of **155**/C_{60} at high resolution (Figure 6.13B–C) displays well-ordered bright spots, vastly different from the STM images of pure **155**. The C_{60} molecules are not sequestered inside of the macrocycle, but are located at the sides of the macrocycle near the bithiophene units. This observation indicates that the driving force for the supramolecular assembly is the donor–acceptor interaction between the C_{60} and bithiophene groups rather than C_{60} and the uncovered HOPG surface inside macrocycle **155**.

The synthesis of SPMs **156** and **157** (Figure 6.13D) has been reported by Bäuerle and coworkers [120]. Characterization of **156** and **157** by STM at the solution/HOPG interface shows that both SPMs self-assemble to form well-ordered, stable hexagonal
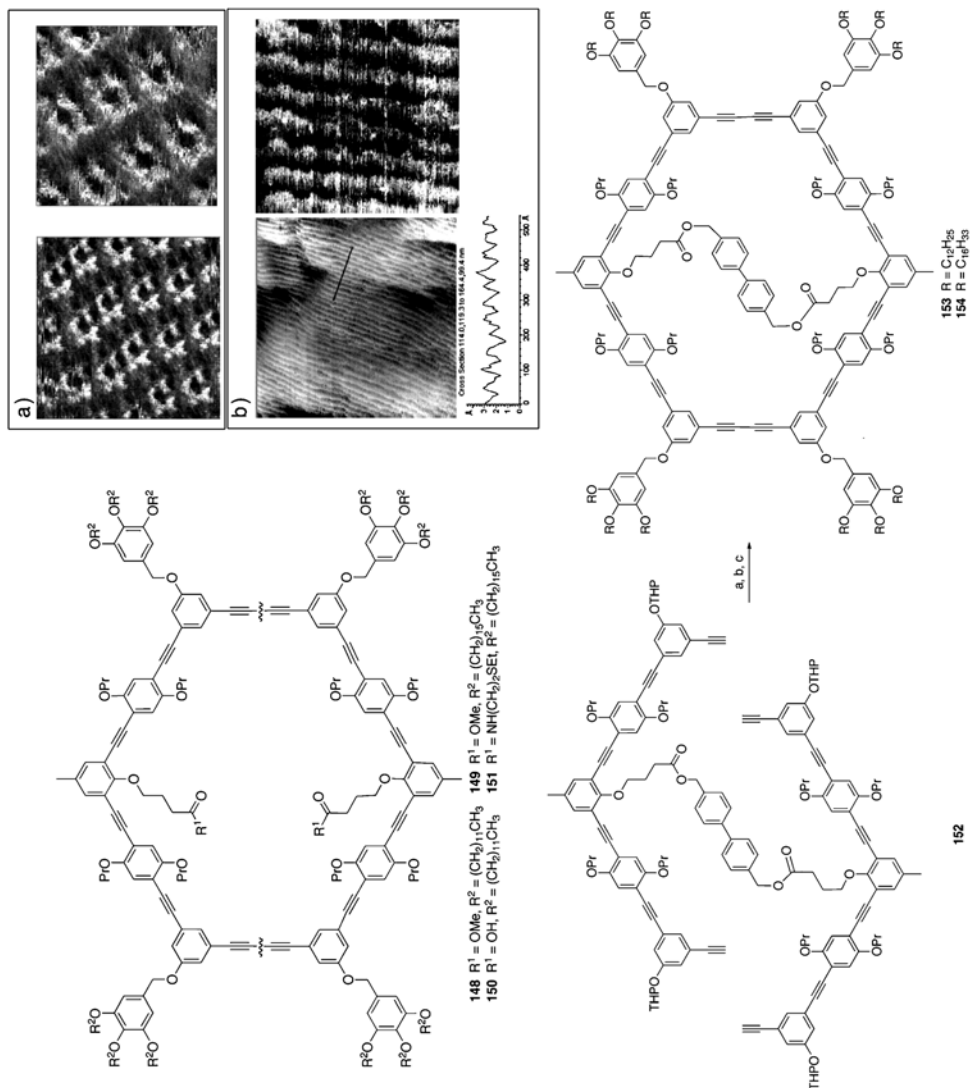
Scheme 6.27 Structure of SPMs **148**–**151** [116,117] and templated synthesis of **153** and **154** [118]. Reagents and conditions: (a) CuCl, CuCl$_2$, py, 81%; (b) *p*-TsOH, MeOH, CHCl$_3$, 99%; (c) ClCH$_2$Ph(OR)$_3$, K$_2$CO$_3$, DMF, 59% (**153**) and 72% (**154**). Inset a) STM images of **148** at the liquid/solid (1-phenyloctane/HOPG) interface, 17.7×17.7 nm^2 (left) and 12.7×12.7 nm^2 (right); Reprinted with permission from *J. Am. Chem. Soc.* **2004**, *126*, 214–222. Copyright 2004 American

Chemical Society. Inset b) STM images of SAMs of **151** on Au(111) at the air-substrate interface, 200×200 nm^2 and z-profile taken along the black line showing a row width of 5 ± 0.4 nm (left). The same SAMs at higher magnification at the vacuum-substrate interface, 40×40 nm^2 (right); Reprinted with permission from *Langmuir* **2004**, *20*, 2781–2784. Copyright 2004 American Chemical Society.
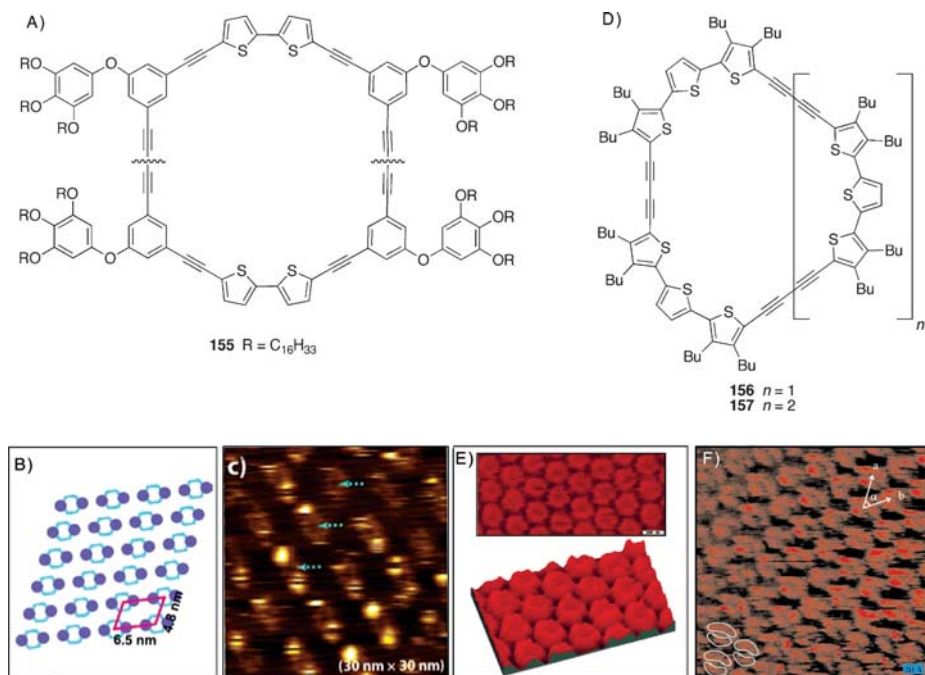
Figure 6.13 (A) SPM **155** [119]; (B) A proposed structural model for **155**/C$_{60}$ on HOPG; (C) A high-resolution STM image (30×30 nm^2) of an ordered array with **155**/C$_{60}$ on HOPG showing the adsorption site of C$_{60}$ on the macrocycle **155**. Both images reprinted with permission from *J. Am. Chem. Soc.* **2006**, *128*, 4218–4219. Copyright 2006 American Chemical Society; (D) Oligothiophene SPMs **156** and **157** [120]; (E) Short-range ordering at solution/HOPG interface of SPM **156** from top view and 3D side view; (F) Short-range ordering at the solution/HOPG interface for SPM **157** [121]; Both images reprinted with permission from E. Mena-Osteritz, P. Bäuerle, *Adv. Mater.* **2001**, *13*, 243–246.

arrays [121]. The STM image of **156** shows the unique "donut-like" molecular shape of macrocycle **156** from a top and 3D side view (Figure 6.13E). The images agree with the semiempirical calculations that predict a "spider-like" conformation for the SPM, with the butyl side chains bent downwards. The STM image of **157** displays a cycle divided into two halves (Figure 6.13F). This substructure corresponds to the electron density distribution of the HOMO–1 for **157**, where one nodal plane results in two "C-shaped" pieces of the macrocycle. The cyclic structure and highly ordered self-assembly of these molecules lend themselves to the possible formation of channels or nanotubes.

Schlüter and coworkers have synthesized a number of macrocycles (**158–159**) with either one or two (opposing) terpyridine groups (Figure 6.14), and they provide an excellent comparison of the synthetic efficiency of routes used for their formation [57]. The peripheries of the macrocycles have been decorated with different flexible side chains, and physical properties were assessed as a function of the nature and number of these. It is interesting to note that while all SPMs with one terpyridine

159

n = 0, 1
m = 0, 1
R^1 = CH$_2$OHex
R^2 = CH$_2$OHex,CH$_2$OTHP
R^3 = H, Hex

158

n = 0, 1
R^1 = CH$_2$OHex, OHex
R^2 = CH$_2$OHex, OHex, CH$_2$OTHP
R^3 = OHex, H
R^4 = H, Hex
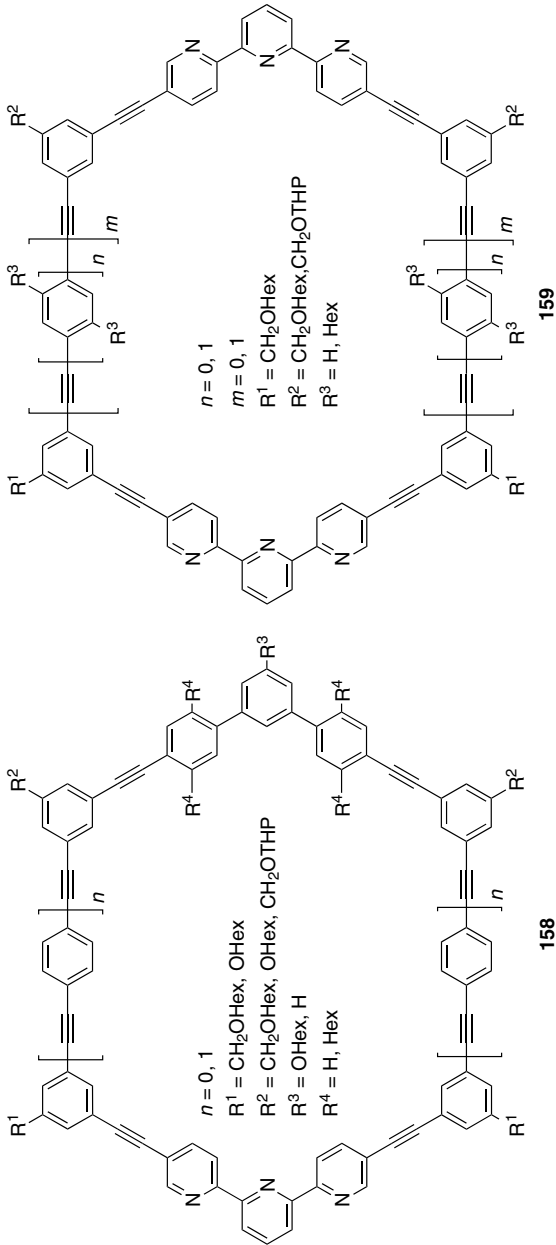
Figure 6.14 SPMs **158** and **159** synthesized by Schlüter and coworkers [57].

group (**158**) are nicely crystalline, those with two are not. X-ray crystallographic characterization of three derivatives provides insight into the packing effects of the various pendent alkyl chains as well as the propensity to adsorb onto the surface of HOPG. For one derivative of **158** ($n = 0$, $R^1 = R^2 =$ OHex, $R^3 =$ H, $R^4 =$ Hex), an ordered, albeit loosely packed, molecular arrangement was observed by STM on the HOPG surface. Crystallographic analysis shows that the SPM is not planar, however, a fact that likely makes surface adsorption entropically "expensive", and this has thus limited the resolution of their analysis.

6.3
Conclusions

Whether by more traditional means such as acetylenic homocoupling or by more modern metathesis reactions, the synthesis of SPMs for use in supramolecular chemistry continues to evolve at an ever-increasing pace. Modern metal-mediated coupling techniques have helped to improve many ring-forming reactions, but it has been the imagination of the chemists involved that has been the most significant advance. Once considered only as structural curiosities, acetylenic SPMs have now evolved into building blocks for an incredible range of functional materials. The synthesis of acetylenic SPMs and their applications to supramolecular chemistry will no doubt continue to challenge and fascinate the chemists who cannot resist their allure.

6.4
Experimental: Selected Procedures

6.4.1
SPM 13: Pd-Catalyzed Cadiot–Chodkiewicz Conditions

A stirred solution of [Pd_2(dba)$_3$•CHCl$_3$] (0.03 g, 0.03 mmol) and CuI (0.015 g, 0.078 mmol) in dry toluene (700 mL) and dry i-Pr$_2$EtN (3 mL) was deoxygenated by bubbling with N$_2$. Over a 10 h period a solution of **11** (61.4 mg, 0.10 mmol) and **12** (75 mg, 0.10 mmol) in dry toluene (120 mL) was added dropwise under an N$_2$ atmosphere. After stirring for 4 d, the solvents were removed under reduced pressure, and the residue was dissolved in toluene (15 mL), filtered, and purified by SEC and column chromatography (SiO$_2$, toluene) to provide **13** (5.1 mg, 4.2%) as a brown solid [34].

6.4.2
SPM 19: Use of Aryltriazene as a Masking Group for Aryl Iodides

Aryltriazene deprotection occurred in a sealable flask charged with the starting material **18**, I$_2$ (1.2 equiv), and ClCH$_2$CH$_2$Cl. The solution was degassed, back-filled with Ar, sealed, and stirred at 80 °C for 12 h. After cooling, the reaction mixture was washed three times with 10% aqueous Na$_2$S$_2$O$_3$, dried over MgSO$_4$, and

concentrated *in vacuo*. The residue was purified by column chromatography on SiO_2 ($CHCl_3$:EtOAc) to give the aryl iodide product. Subsequently, TMS-acetylene deprotection proceeded by dissolving the aryl iodide in an approximate 10:1 mixture of $CHCl_3$ and MeOH with 2 M aqueous KOH (10 equiv). The reaction mixture was stirred at room temperature and monitored by TLC until reaction was complete. It was then carefully washed with water, and the organic fractions were dried over $MgSO_4$ and evaporated. Column chromatography on SiO_2 ($CHCl_3$:EtOAc) yielded the terminal alkyne product. The cyclization step was done in dry Et_3N and THF (2:1) with [$PdCl_2(PPh_3)_2$] (0.1 equiv) and CuI (0.05 equiv) in a Schlenk flask that had been evacuated and back-filled with Ar three times. While this mixture was stirred under Ar at 75 °C, a solution of the terminal acetylene/aryl iodide in dry THF was added to the flask by a syringe pump at a rate of 8 mL/h. After this addition, the reaction mixture was stirred at the same temperature for 2 h, and the solvent was then removed with a rotary evaporator. The product was purified by column chromatography on SiO_2 ($CHCl_3$:EtOAc and/or PhH:EtOAc) followed by recrystallization from $CHCl_3$ to yield **19** (5%) [45].

6.4.3
SPM 20: Eglinton Conditions

To a solution of [$Cu(OAc)_2$] (546 mg, 3.00 mmol) in 200 mL of py/PhH (3:2) was added dropwise a solution of desilylated **24** (320 mg, 300 µmol) in 100 mL of the same solvent mixture over 24 h in the dark (using a Hershberg dropping funnel). After stirring at room temperature for an additional 3 h, the solvent was removed *in vacuo,* the green residue was passed through a short plug of SiO_2, and the solvent was removed to afford crude products. The residue was purified by flash chromatography followed by preparative HPLC, which afforded SPM **20** as a white solid (32.0 mg, 10%) [46].

6.4.4
SPM 33: Hay Conditions

Compound **32** (82 mg, 0.12 mmol) was desilylated by treatment with TBAF in THF at room temperature for 30 min. Following workup, the deprotected polyyne was oxidatively coupled in the presence of CuI (0.18 g, 0.92 mmol), TMEDA (0.35 mL. 2.3 mmol), and air in dry CH_2Cl_2 (220 mL) for 3 h at room temperature followed by 12 h at 4 °C. Following aqueous workup, the solvent was reduced by approximately 80%, resulting in the formation of a bright yellow precipitate. Isolation of the precipitate afforded **33** (29 mg, 51%) as a bright yellow solid [51].

6.4.5
Pre-Catenane 56: Breslow Conditions

Compound **55** (1.50 g, 0.52 mmol) dissolved in py (150 mL) was added to a suspension of CuCl (6.86 g, 69.2 mmol) and $CuCl_2$ (1.12 g, 8.30 mmol) in py (1 L) at room temperature over a period of 120 h via a syringe pump. After a stirring for an

additional 24 h, the py was distilled off, the residue was dissolved in CH_2Cl_2 and HCl (2N), and the organic phase was separated and washed with HCl (2N). The combined aqueous phases were extracted with CH_2Cl_2, the combined organic phases were then dried ($MgSO_4$), and the solvent was removed *in vacuo*. Column chromatography gave a mixture of the non-catenated dimer and precatenane **56** (1.35 g, 90%, 1:2.6) as a brownish solid [63].

6.4.6
SPM 91: Schiff-base Condensation Conditions

Under an N_2 atmosphere, the corresponding dialdehyde (0.106 g, 0.40 mmol) and 1,2-dioctyloxy-4,5-diaminobenzene (0.145 g, 0.40 mmol) were combined in a solution of degassed $CHCl_3$ (15 mL) and CH_3CN (5 mL), resulting in a cloudy orange solution. This mixture was heated to reflux (90 °C) for 24 h, giving a clear, red solution. Upon cooling, **91** precipitated as a red powder (0.16 g, 67%), which was isolated and washed with CH_3CN [84].

6.4.7
Large-scale Synthesis of SPM 124 via an Alkyne Metathesis

In an Ar-filled glove box, a solution of the molybdenum triamide catalyst (1.69 g, 2.54 mmol) and *p*-nitrophenol (1.06 g, 7.61 mmol) in CCl_4 (200 mL) was added to a solution of the monomer precursor **125** (21.0 g, 25.4 mmol) in CCl_4 (500 mL). The flask was sealed and removed from the glove box. The resulting mixture was stirred for 22 h at 30 °C. The precipitated by-product formed almost immediately upon warming to 30 °C. After filtration to remove the precipitate, the filtrate was concentrated *in vacuo* and the residue was purified by column chromatography (*i*-PrOH: CH_2Cl_2, 1:9). The product **124** was obtained cleanly as a yellow wax (5.68 g, 77%). The major impurity was cyclic pentamer with a ratio of hexamer to pentamer of 9:1 based upon ^1H NMR integration [29].

Acknowledgments

Symbols and Abbreviations

Ac	acetyl
AFM	atomic force microscopy
AIBN	azobis(isobutyronitrile)
AM1	Austin model 1

bipy	bipyridyl
Bn	benzyl
BTAC	benzyltriethylammonium chloride
Bz	benzoyl
Cy	cyclohexyl
dba	dibenzylideneacetone
DME	1,2-dimethoxyethane
DMF	*N,N′*-dimethylformamide
dppe	1,2-bis(diphenylphosphino)ethane
dppp	1,3-bis(diphenylphosphino)propane
GPC	gel permeation chromatography
HOMO	highest occupied molecular orbital
HOPG	highly oriented pyrolytic graphite
K_a	association constant
K_{SV}	Stern–Völmer constant
λ_{em}	wavelength of emission
LC	liquid crystal
MALDI-TOF	matrix-assisted laser desorption/ionization time-of-flight
NBS	*N*-bromosuccinimide
ORTEP	Oak Ridge thermal ellipsoid plot
OTf	trifluoromethanesulfonate
PCBM	[6,6]-phenyl-C_{61} butyric acid methyl ester
PhH	benzene
PhMe	toluene
py	pyridine
ROMP	ring-opening metathesis polymerization
Φ	quantum yield
SEC	size exclusion chromatography
SPM	shape-persistent macrocycle
STM	scanning tunneling microscopy
TBAF	tetrabutylammonium fluoride
TCB	1,2,4-trichlorobenzene
TES	triethylsilyl
THF	tetrahydrofuran
THP	tetrahydropyranyl
TIPS	triisopropylsilyl
TMEDA	*N,N,N′,N′*-tetramethylethylenediamine
TMS	trimethylsilyl
TMSA	trimethylsilylacetylene
tol	tolyl
Ts	tosyl (*p*-toluenesulfonyl)
TTF	tetrathiafulvalene
VPO	vapor pressure osmometry
XRD	X-ray diffraction

References

1 Zhang, W. and Moore, J.S. (2006) *Angew. Chem. Int. Ed.*, **45**, 4416–4439; *Angew. Chem.* **118**, 4524–4548.

2 Zhao, D. and Moore, J.S. (2003) *Chem. Commun.*, 807–818.

3 Young, J.K. and Moore, J.S. (1995) in *Modern Acetylene Chemistry* (eds. F. Diederich and P.J. Stang), Wiley-VCH, Weinheim, Chapter 12.

4 Höger, S. (2005) *Angew. Chem. Int. Ed.*, **44**, 3806–3808; *Angew. Chem.*, **117**, 3872–3875.

5 Höger, S. (2005) in *Acetylene Chemistry* (eds. F. Diederich , P.J. Stang and R.R. Tykwinski), Wiley-VCH, Weinheim, Chapter 10.

6 Jones, C.S., O'Connor, M.J. and Haley, M.M. (2005) in *Acetylene Chemistry* (eds. F. Diederich, P.J. Stang and R.R. Tykwinski), Wiley-VCH, Weinheim, Chapter 8.

7 Höger, S. (1999) *J. Polym. Sci., Part A: Polym. Chem.*, **37**, 2685–2698.

8 Tahara, K. and Tobe, Y. (2006) *Chem. Rev.*, **106**, 5274–5290.

9 Spitler, E.L., Johnson, C.A. and Haley, M.M. (2006) *Chem. Rev.*, **106**, 5344–5386.

10 Nielsen, M.B. and Diederich, F. (2005) *Chem. Rev.*, **105**, 1837–1867.

11 Marsden, J.A., Palmer, G.J. and Haley, M.M. (2003) *Eur. J. Org. Chem.*, 2355–2369.

12 Grave, C. and Schlüter, A.D. (2002) *Eur. J. Org. Chem.*, 3075–3098.

13 Gleiter, R. and Hopf, H. (eds.) (2004) *Modern Cyclophane Chemistry*, Wiley-VCH, Weinheim.

14 Cheng, X.H., Ju, X.P. and Hoeger, S. (2006) *Chin. J. Org. Chem.*, **26**, 733–743.

15 Höger, S. (2004) *Chem. Eur. J.*, **10**, 1320–1329.

16 Yamaguchi, Y. and Yoshida, Z. (2003) *Chem. Eur. J.*, **9**, 5430–5440.

17 Nielsen, M.B., Schreiber, M., Baek, Y.G., Seiler, P., Lecomte, S., Boudon, C., Tykwinski, R.R., Gisselbrecht, J.-P., Gramlich, V., Skinner, P.J., Bosshard, C., Günter, P., Gross, M. and Diederich, F. (2001) *Chem. Eur. J.*, **7**, 3263–3280.

18 Glaser, C. (1869) *Ber. Dtsch. Chem. Ges.*, **2**, 422–424.

19 For an excellent review, see: Siemsen, P., Livingston, R.C. and Diederich, F. (2005) *Angew. Chem. Int. Ed.*, **39**, 2632–2657; *Angew. Chem.*, **112**, 2740–2767.

20 Hay, A.S. (1962) *J. Org. Chem.*, **27**, 3320–3321.

21 Eglinton, G. and Galbraith, A.R. (1959) *J. Chem. Soc.*, 889–896.

22 Eglinton, G. and Galbraith, A.R. (1956) *Chem. Ind.*, 737–738.

23 O'Krongly, D., Denmeade, S.R., Chiang, M.Y. and Breslow, R. (1985) *J. Am. Chem. Soc.*, **107**, 5544–5545.

24 Rossi, R., Carpita, A. and Bigelli, C. (1985) *Tetrahedron Lett.*, **26**, 523–526.

25 Enozawa, H., Hasegawa, M., Takamatsu, D., Fukui, K. and Iyoda, M. (2006) *Org. Lett.*, **8**, 1917–1920.

26 Tobe, Y., Utsumi, N., Nagano, A., Sonoda, M. and Naemura, K. (2001) *Tetrahedron*, **57**, 8075–8083.

27 Ge, P.-H., Fu, W., Herrmann, W.A., Herdtweck, E., Campana, C., Adams, R.D. and Bunz, U.H.F. (2000) *Angew. Chem. Int. Ed.*, **39**, 3607–3610; *Angew. Chem.*, **112**, 3753–3756.

28 Pschirer, N.G., Fu, W., Adams, R.D. and Bunz, U.H.F. (2000) *Chem. Commun.*, 87–88.

29 Zhang, W. and Moore, J.S. (2004) *J. Am. Chem. Soc.*, **126**, 12796.

30 Campbell, I.D., Eglinton, G., Henderson, W. and Raphael, R.A. (1966) *J. Chem. Soc. Chem. Commun.*, 87–89.

31 Huynh, C. and Linstrumelle, G. (1988) *Tetrahedron*, **44**, 6337–6344.

32 Iyoda, M., Vorasingha, A., Kuwatani, Y. and Yoshida, M. (1998) *Tetrahedron Lett.*, **39**, 4701–4704.

33 Baxter, P.N.W. (2003) *Chem. Eur. J.*, **9**, 2531–2541.

34 Shu, L. and Mayor, M. (2006) *Chem. Commun.*, 4134–4136.

35 For an excellent recent example, see: Hoffmann, M., Wilson, C.J., Odell, B. and Anderson, H.L. (2007) *Angew. Chem. Int. Ed.*, **46**, 3122–3125; *Angew. Chem.*, **119**, 3183–3186.

36 Laughrey, Z.R. and Gibb, B.C. (2005) *Top. Curr. Chem.*, **249**, 67–125.

37 Dietrich-Buchecker, C., Colasson, B.X. and Sauvage, J.-P. (2005) *Top. Curr. Chem.*, **249**, 261–283.

38 Godt, A. (2004) *Eur. J. Org. Chem.*, 1639–1654.

39 Anderson, S. and Anderson, H.L. (2000) in *Templated Organic Synthesis* (eds. F. Diederich and P.J. Stang) Wiley-VCH, Weinheim, Chapter 1.

40 Anderson, S., Anderson, H.L. and Sanders, J.K.M. (1993) *Acc. Chem. Res.*, **26**, 469–475.

41 Anderson, H.L. and Sanders, J.K.M. (1990) *Angew. Chem. Int. Ed. Engl.*, **29**, 1400–1403; *Angew. Chem.*, **102**, 1478–1480.

42 Anderson, H.L. and Sanders, J.K.M. (1989) *J. Chem. Soc. Chem. Commun.*, 1714–1715.

43 Walter, C.J., Anderson, H.L. and Sanders, J.K.M. (1993) *J. Chem. Soc. Chem. Commun.*, 458–460.

44 Moore, J.S., Weinstein, E.J. and Wu, Z. (1991) *Tetrahedron Lett.*, **32**, 2465–2466.

45 Yamaguchi, Y., Kobayashi, S., Miyamura, S., Okamoto, Y., Wakamiya, T., Matsubara, Y. and Yoshida, Z. (2004) *Angew. Chem. Int. Ed.*, **43**, 366–369; *Angew. Chem.*, **116**, 370–373.

46 Nomoto, A., Sonoda, M., Yamaguchi, Y., Ichikawa, T., Hirose, K. and Tobe, Y. (2006) *J. Org. Chem.*, **71**, 401–404.

47 Marsden, J.A., Miller, J.J. and Haley, M.M. (2004) *Angew. Chem. Int. Ed.*, **43**, 1694–1697; *Angew. Chem.*, **116**, 1726–1729.

48 Marsden, J.A., Miller, J.J., Shirtcliff, L.D. and Haley, M.M. (2005) *J. Am. Chem. Soc.*, **127**, 2464–2476.

49 Shortell, D.B., Palmer, L.C. and Tour, J.M. (2001) *Tetrahedron*, **57**, 9055–9065.

50 Elliott, E.L., Ray, C.R., Kraft, S., Atkins, J.R. and Moore, J.S. (2006) *J. Org. Chem.*, **71**, 5282–5290.

51 Campbell, K., McDonald, R. and Tykwinski, R.R. (2002) *J. Org. Chem.*, **67**, 1133–1140.

52 Campbell, K., Kuehl, C.J., Ferguson, M.J., Stang, P.J. and Tykwinski, R.R. (2002) *J. Am. Chem. Soc.*, **124**, 7266–7267.

53 Campbell, K., Ooms, K.J., Wasylishen, R.E. and Tykwinski, R.R. (2005) *Org. Lett.*, **7**, 3397–3400.

54 Sun, S.-S. and Lees, A.J. (2001) *Organometallics*, **20**, 2353–2358.

55 Henze, O., Lentz, D., Schäfer, A., Franke, P. and Schlüter, A.D. (2002) *Chem. Eur. J.*, **8**, 357–365.

56 Henze, O., Lentz, D. and Schlüter, A.D. (2000) *Chem. Eur. J.*, **6**, 2362–2367.

57 Grave, C., Lentz, D., Schäfer, A., Samori, P., Rabe, J.P., Franke, P. and Schlüter, A.D. (2003) *J. Am. Chem. Soc.*, **125**, 6907–6918.

58 Opris, D.M., Franke, P. and Schlüter, A.D. (2005) *Eur. J. Org. Chem.*, 822–837.

59 Schmittel, M., Ammon, H., Kalsani, V., Wiegrefe, A. and Michel, C. (2002) *Chem. Commun.*, 2566–2567.

60 Schmittel, M. and Ammon, H. (1999) *Synlett*, 750–752.

61 Schmittel, M. and Ganz, A. (1997) *Chem. Commun.*, 999–1000.

62 Kalsani, V., Ammon, H., Jäckel, F., Rabe, J.P. and Schmittel, M. (2004) *Chem. Eur. J.*, **10**, 5481–5492.

63 Dietrich-Buchecker, C.O., Hemmert, C., Khémiss, A.-K. and Sauvage, J.-P. (1990) *J. Am. Chem. Soc.*, **112**, 8002–8008.

64 Ünsal, Ö. and Godt, A. (1999) *Chem. Eur. J.*, **5**, 1728–1733.

65 Bäuerle, P., Ammann, M., Wilde, M., Götz, G., Mena-Osteritz, E., Rang, A. and Schalley, C.A. (2007) *Angew. Chem. Int. Ed.*, **46**, 363–368; *Angew. Chem.*, **119**, 367–372.

66 For a review of Pt-acetylide macrocycles, see: Kaiser, A. and Bäuerle, P. *Top. Curr. Chem.*, **249**, 127–201.

67 Ammann, M., Rang, A., Schalley, C.A. and Bäuerle, P. (2006) *Eur. J. Org. Chem.*, 1940–1948.

68 Zhu, J., Wang, X.-Z., Chen, Y.-Q., Jiang, X.-K., Chen, X.-Z. and Li, Z.-T. (2004) *J. Org. Chem.*, **69**, 6221–6227.

69 Droz, A.S., Neidlein, U., Anderson, S., Seiler, P. and Diederich, F. (2001) *Helv. Chim. Acta*, **84**, 2243–2289.

70 Droz, A.S. and Diederich, F. (2000) *J. Chem. Soc. Perkin Trans.*, **1**, 4224–4226.

71 Bähr, A., Droz, A.S., Püntener, M., Neidlein, U., Anderson, S., Seiler, P. and Diederich, F. (1998) *Helv. Chim. Acta*, **81**, 1931–1963.

72 Anderson, S. Neidlein, U. Gramlich, V. and Diederich, F. (1995) *Angew. Chem. Int. Ed. Engl.*, **34**, 1596–1600; *Angew. Chem.*, **107**, 1722–1725.

73 Kawase, T., Darabi, H.R. and Oda, M. (1996) *Angew. Chem. Int. Ed. Engl.*, **35**, 2664–2666; *Angew. Chem.*, **108**, 2803–2805.

74 Kawase, T., Ueda, N., Tanaka, K., Seirai, Y. and Oda, M. (2001) *Tetrahedron Lett.*, **42**, 5509–5511.

75 Kawase, T., Tanaka, K., Seirai, Y., Shiono, N. and Oda, M. (2003) *Angew. Chem. Int. Ed.*, **42**, 5597–5600; *Angew. Chem.*, **115**, 5755–5758.

76 Kawase, T., Tanaka, K., Shiono, N., Seirai, Y. and Oda, M. (2004) *Angew. Chem. Int. Ed.*, **43**, 1722–1724; *Angew. Chem.*, **116**, 1754–1756.

77 Kawase, T. and Oda, M. (2006) *Pure Appl. Chem.*, **78**, 831–839.

78 Baxter, P.N.W. (2001) *J. Org. Chem.*, **66**, 4170–4179.

79 Baxter, P.N.W. (2002) *Chem. Eur. J.*, **8**, 5250–5264.

80 Baxter, P.N.W. (2004) *J. Org. Chem.*, **69**, 1813–1821.

81 Baxter, P.N.W. and Dali-Youcef, R. (2005) *J. Org. Chem.*, **70**, 4935–4953.

82 Kobayashi, S., Yamaguchi, Y., Wakamiya, T., Matsubara, Y., Sugimoto, K. and Yoshida, Z. (2003) *Tetrahedron Lett.*, **44**, 1469–1472.

83 Heuft, M.A. and Fallis, A.G. (2002) *Angew. Chem. Int. Ed.*, **41**, 4520–4523; *Angew. Chem.*, **114**, 4702–4705.

84 Ma, C., Lo, A., Abdolmaleki, A. and MacLachlan, M.J. (2004) *Org. Lett.*, **6**, 3841–3844.

85 Ma, C.T.L. and MacLachlan, M.J. (2005) *Angew. Chem. Int. Ed.*, **44**, 4178–4182; *Angew. Chem.*, **117**, 4250–4254.

86 Marsella, M.J., Wang, Z.-Q., Reid, R.J. and Yoon, K. (2001) *Org. Lett.*, **3**, 885–887.

87 Coates, G.W., Dunn, A.R., Henling, L.M., Dougherty, D.A. and Grubbs, R.H. (1997) *Angew. Chem. Int. Ed. Engl.*, **36**, 248–251; *Angew. Chem.*, **109**, 290–293.

88 Coates, G.W., Dunn, A.R., Henling, L.M., Ziller, J.W., Lobkovsky, E.B. and Grubbs, R.H. (1998) *J. Am. Chem. Soc.*, **120**, 3641–3649.

89 Tobe, Y., Utsumi, N., Kawabata, K., Nagano, A., Adachi, K., Araki, S., Sonoda, M., Hirose, K. and Naemura, K. (2002) *J. Am. Chem. Soc.*, **124**, 5350–5364.

90 Lin, C.-H. and Tour, J. (2002) *J. Org. Chem.*, **67**, 7761–7768.

91 Höger, S., Bonrad, K., Mourran, A., Beginn, U. and Möller, M. (2001) *J. Am. Chem. Soc.*, **123**, 5651–5659.

92 Nakamura, K., Okubo, H. and Yamaguchi, M. (2001) *Org. Lett.*, **3**, 1097–1099.

93 Tobe, Y., Utsumi, N., Nagano, A. and Naemura, K. (1998) *Angew. Chem. Int. Ed.*, **37**, 1285–1287; *Angew. Chem.*, **110**, 1347–1349.

94 Shetty, A.S., Zhang, J. and Moore, J.S. (1996) *J. Am. Chem. Soc.*, **118**, 1019–1027.

95 Zhang, J. and Moore, J.S. (1992) *J. Am. Chem. Soc.*, **114**, 9701–9702.

96 Tobe, Y., Nagano, A., Kawabata, K., Sonoda, M. and Naemura, K. (2000) *Org. Lett.*, **2**, 3265–3268.

97 Saiki, Y., Sugiura, H., Nakamura, K., Yamaguchi, M., Hoshi, T. and Anzai, J.

(2003) *J. Am. Chem. Soc.*, **125**, 9268–9269.

98 Klyatskaya, S., Dingenouts, N., Rosenauer, C., Müller, B. and Höger, S. (2006) *J. Am. Chem. Soc.*, **128**, 3150–3151.

99 Zhang, W., Brombosz, S.M., Mendoza, J.L. and Moore, J.S. (2005) *J. Org. Chem.*, **70**, 10198–10201.

100 Zhang, W. and Moore, J.S. (2005) *J. Am. Chem. Soc.*, **127**, 11863–11870.

101 Lahiri, S., Thompson, J.L. and Moore, J.S. (2000) *J. Am. Chem. Soc.*, **122**, 11315–11319.

102 Balakrishnan, K., Datar, A., Zhang, W., Yang, X., Naddo, T., Huang, J., Zuo, J., Yen, M., Moore, J.S. and Zang, L. (2006) *J. Am. Chem. Soc.*, **128**, 6576–6577.

103 Naddo, T., Che, Y., Zhang, W., Balakrishnan, K., Yang, X., Yen, M., Zhao, J., Moore, J.S. and Zang, L. (2007) *J. Am. Chem. Soc.*, **129**, 6978–6979.

104 Zhao, D. and Moore, J.S. (2003) *Macromolecules*, **36**, 2712–2720.

105 Zhao, D. and Moore, J.S. (2002) *J. Org. Chem.*, **67**, 3548–3554.

106 Mindyuk, O.Y., Stetzer, M.R., Heiney, P.A., Nelson, J.C. and Moore, J.S. (1998) *Adv. Mater.*, **10**, 1363–1366.

107 Seo, S.H., Jones, T.V., Seyler, H., Peters, J.O., Kim, T.H., Chang, J.Y. and Tew, G.N. (2006) *J. Am. Chem. Soc.*, **128**, 9264–9265.

108 Zhang, J. and Moore, J.S. (1994) *J. Am. Chem. Soc.*, **116**, 2655–2656.

109 Höger, S., Enkelmann, V., Bonrad, K. and Tschierske, C. (2000) *Angew. Chem. Int. Ed.*, **39**, 2268–2270; *Angew. Chem.*, **112**, 2355–2358.

110 Höger, S., Cheng, X.H., Ramminger, A.-D., Enkelmann, V., Rapp, A., Mondeshki, M. and Schnell, I. (2005) *Angew. Chem. Int. Ed.*, **44**, 2801–2805; *Angew. Chem.*, **117**, 2862–2866.

111 For a more detailed discussion of the LC and surface chemistry of SPMs such as **141–142**, see: Cheng, X., Ver Heyen, A., Mamdouh, W., Uji-i, H., De Schryver, F., Höger, S. and De Feyter, S. (2007) *Langmuir*, **23**, 1281–1286.

112 De Feyter, S., Gesquière, A., Abdel-Mottaleb, M.M., Grim, P.C.M., De Schryver, F.C., Meiners, C., Sieffert, M., Valiyaveettil, S. and Müllen, K. (2000) *Acc. Chem. Res.*, **33**, 520–531.

113 Ohkita, M., Ando, K., Suzuki, T. and Tsuji, T. (2000) *J. Org. Chem.*, **65**, 4385–4390.

114 Sonoda, M., Sakai, Y., Yoshimura, T., Tobe, Y. and Kamada, K. (2004) *Chem. Lett.*, **33**, 972–973.

115 Furukawa, S., Uji-i, H., Tahara, K., Ichikawa, T., Sonoda, M., De Schryver, F.C., Tobe, Y. and De Feyter, S. (2006) *J. Am. Chem. Soc.*, **128**, 3502–3503.

116 Fischer, M., Lieser, G., Rapp, A., Schnell, I., Mamdouh, W., De Feyter, S., De Schryver, F.C. and Höger, S. (2004) *J. Am. Chem. Soc.*, **126**, 214–222.

117 Borissov, D., Ziegler, A., Höger, S. and Freyland, W. (2004) *Langmuir*, **20**, 2781–2784.

118 Ziegler, A., Mamdouh, W., Ver Heyen, A., Surin, M., Uji-i, H., Abdel-Mottaleb, M.M.S., De Schryver, F.C., De Feyter, S., Lazzaroni, R. and Höger, S. (2005) *Chem. Mater.*, **17**, 5670–5683.

119 Pan, G.-B., Cheng, X.-H., Höger, S. and Freyland, W. (2006) *J. Am. Chem. Soc.*, **128**, 4218–4219.

120 Krömer, J., Rios-Carreras, I., Fuhrmann, G., Musch, C., Wunderlin, M., Debaerdemaeker, T., Mena-Osteritz, E. and Bäuerle, P. (2000) *Angew. Chem. Int. Ed.* **39**, 3481–3486; *Angew. Chem.*, **112**, 3623–3628.

121 Mena-Osteritz, E. and Bäuerle, P. (2001) *Adv. Mater.*, **13**, 243–246.

7

Supramolecular 3D Architectures by Metal-directed Assembly of Synthetic Macrocycles

Laura Pirondini and Enrico Dalcanale

7.1
Introduction

Synthetic macrocycles have played a major role in shaping the field of supramolecular chemistry. The study of their host-guest properties has been pivotal in defining and understanding non-covalent interactions, which constitute the heart of supramolecular chemistry. Afterwords, the mastering of such weak interactions has allowed the emergence of self-assembly as a new tool to generate complex and otherwise elusive molecular architectures. Calixarenes [1], cavitands [2], and cleft-type receptors [3] represent three-dimensional concave surfaces capable of binding complementary organic molecules and ions. Their association into larger assemblies has been pursued initially via covalent bonding, thanks to the seminal work of Cram (carcerands) [2] and Collet (cryptophanes) [4]. Their studies have triggered the interest of the chemical community in molecular containers and their peculiar inclusion properties. The drawback of the covalent approach, i.e. the need for multistep, time-consuming synthetic procedures, has been overcome by the introduction of self-assembly protocols, with H-bonding and metal coordination as the preferred options among non-covalent interactions [5]. The diversity of available objects in terms of size and shape has dramatically increased, thanks to the inherent modularity of the self-assembly approach. Metal-directed self-assembly in particular offers the following advantages [6]: (a) high directionality of the metal-ligand coordinative bonds leading to many possible coordination geometries, (b) great versatility due to diverse transition-metal complexes and to a broad spectrum of available multidentate ligands, (c) fine tuning of the kinetic lability of the complexes to different self-assembly conditions, and (d) control of the polarity and charge state of the resulting objects via formation of charged or neutral complexes.

The modulation of the metal-directed self-assembly protocols according to the above-mentioned guidelines introduces additional features for non-covalent molecular containers with respect to their covalent counterparts. Reversibility, selection,

and, above all, predictable and reproducible responses to external stimuli are the major ones.

Synthetic macrocycles are ideally suited for the self-assembly of 3D objects because they offer three-dimensional scaffolds amenable to multiple ligand functionalization. Type, number, and relative orientation of the ligands can be engineered according to the final object to be assembled. Also, the degree of rigidity of multidentate macrocyclic ligands can be finely tuned according to the requirements of the self-assembly protocol.

All potential applications of molecular containers revolve around a major issue: the compartmentalization of the included guests. Drug delivery [7], catalysis [8], storage [9], separation technology [10], and stabilization of reactive intermediates [11] are typical examples in which compartmentalization determines the function. For some applications envisioned, however, compartmentalization alone is not enough. In the case of drug delivery, for instance, the possibility of releasing a guest following external stimuli constitutes an essential feature. Needless to say, this additional feature is much more easily realized using non-covalent interactions [12].

Decisive factors to be considered in designing molecular containers are: (a) size of the inner cavity, which in most cases must be of nanoscale dimensions to accommodate either single nanoscale guests or multiple smaller molecules [13], (b) size and shape of the cavity portals, to govern the communication with the exterior, and (c) solubility in an aqueous environment, to take advantage of the hydrophobic effect in driving the inclusion of non-polar, neutral guests.

Another important sector where metal-directed self-assembly offers unparalleled advantages over covalent synthesis is the generation of 3D objects on surfaces. The main issue in this case is the quantitative, error-free generation of 3D architectures directly on surfaces, made possible by the thermodynamic control and reversibility of self-assembly. The transfer of single-output self-assembly protocols from solutions to surfaces provides a unique entry into highly organized, defect-free, hybrid inorganic-organic materials, which are in high demand for nanotechnology and molecular electronics [14].

In this chapter, we cover the metal-directed self-assembly of 3D architectures using macrocycles as molecular scaffolds. Particular emphasis will be given to the synthetic strategies leading to coordination cages and to multitopic macrocyclic receptors, as well as to their complexation properties.

7.2
Coordination Cages

The need for highly preorganized, multidentate ligands presenting concave surfaces has led some researchers to resort to calixarenes, resorcinarenes, and cavitands as sources of molecular scaffolds for the self-assembly of coordination cages. They have almost unlimited potential as molecular receptors and building blocks for higher architectures, and their inherent half-bowl-shaped structure is particularly advantageous in the design of molecular capsules. The topic is treated in terms of increasing complexity, expressed by the number of macrocyclic subunits connected together.
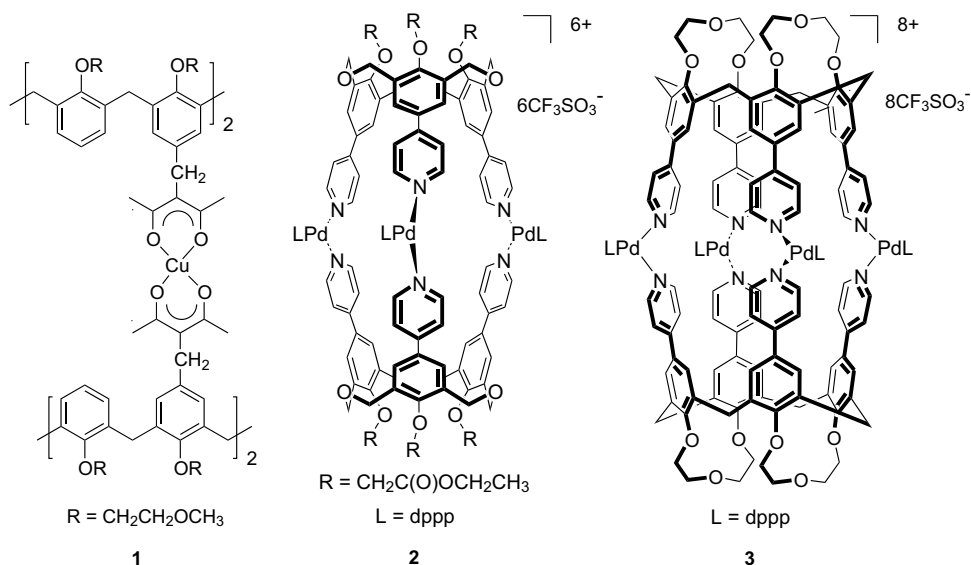
Figure 7.1 Calixarene-based dimeric capsules.

7.2.1
Dimeric Calixarene-based Coordination Cages

In the specific case of calixarenes, there are very few studies related to metal-mediated self-assembly into cage molecules. Early examples reported by Shinkai and coworkers include bis(acac)-calix[4]arene dimer (1) held together by Cu^{2+} cations [15] and the dimeric capsule 2 (Figure 7.1), in which two homooxacalix[3]arene units bearing 4-pyridyl groups are linked through coordination to Pd(II) metal complexes [16]. This study was particularly significant because it showed that capsule formation requires the favorable preorganization of the building blocks: only calixarenes in a cone conformation [$R = CH_2C(O)OC_2H_5$] yield a dimeric molecular capsule with D_{3h} symmetry, while conformational mobility ($R = CH_3$) switches off capsule formation. Other important prerequisites are Py-Pd(II)-Py angle close to 90°, a precise 2:3 calixarene/PdL_n concentration ratio, and an appropriate solvent choice. Further studies on cage 2 revealed that this capsule can specifically include [60]fullerene [17] with a K_{ass} of 39 M^{-1} at 30 °C. The kinetically stable capsule-fullerene complex was characterized by ^1H and ^{13}C NMR spectroscopy. Li^+-binding to the lower rims enhances the [60]fullerene inclusion ability of 2 by a factor of approximately 54, whereas Na^+-binding removes it entirely [18]. In 2001 Shinkai and coworkers reported the self-assembly of the coordination cage 3 composed of two *cone*-tetrapyridylcalix[4]arene bis-crown ligands linked through four *cis*-Pd(II) complex molecules [19]. The presence of the short crown linkages at the lower rim forces the calixarene into a rigid cone conformation, preventing entropically favorable intramolecular bonds. Again the rigidity and preorganization of the calixarene scaffold provides a prerequisite for capsule formation.

A different approach to the self-assembly of a supramolecular calix[4]arene capsule through metal-ligand interaction was described by Baldini *et al.* [20]. In this case, bis- and tetra-functionalization of the calixarene upper rim with metalloporphyrins gives subunits that dimerize in a face-to-face fashion when an appropriate bidentate ligand such as DABCO is added (Figure 7.2). The originality of this approach consists in the reversal of the metal-ligand relationship usually employed in the self-assembly of coordination cages: the metal centers are introduced on the calixarene, and bidentate ligands are used as linkers. The calix-bisporphirin **4** forms the intermolecular 2 : 2 sandwich complex **6** with 1 equivalent of DABCO, generating a large cavity capable of entrapping guests of appropriate dimensions. When more than 1 equiv of DABCO is added, the system enters a fast exchange regime, leading to the formation of the open **4**·(DABCO)$_2$ complex. The calix-tetraporphyrin **5**, on the other hand, forms four different complexes with DABCO, depending on the stoichiometry (1 : 1; 2 : 4; 1 : 3; 1 : 4). During the addition of DABCO, all four complexes are populated, giving both intramolecular and intermolecular **5**: DABCO sandwiches. The complicated equilibria between the complexes were studied using both UV-visible and ^{1}H NMR spectroscopy. At the precise **5**:DABCO ratio of 2 : 4, the major species is the dimeric cage **7**, but unfortunately it is not the only complex in solution. This example highlights the difficulty of driving the self-assembly equilibrium toward a single thermodynamic minimum. The presence of intramolecular complexes between porphyrin moieties on the same calix[4]arene is due to their residual conformational mobility.

Cotton *et al.* showed the assembly of a very stable coordination cage formed by linking two calixarene scaffolds functionalized with four carboxylic acid groups via bimetal units, (DaniF)$_2$Rh$_2$ [21]. This capsule permanently includes an NEt$_4^+$ cation and has a BF$_4^-$ counterion external to the cage, as shown by the X-ray crystal structure determination.

7.2.2
Cavitand-based Dimeric Coordination Cages

7.2.2.1 The Apical Functionalization Approach

Cavitand-based coordination cages are receiving increasing attention because of the versatility of the cavitand platforms in terms of synthetic modularity and molecular recognition properties. The vast majority of coordination cages of this class are dimeric, composed of two concave macrocycles facing each other, connected through metal centers. The introduction of the ligands at the upper rim of the resorcinarene skeleton has been obtained following two different strategies: (a) functionalization at the apical positions, and (b) introduction of the ligands as bridging units between the phenolic OHs. In this section we analyze examples of such cages assembled from cavitands bearing ligand moieties at the apical positions. In this way up to four ligands can be introduced at the upper rim of a single cavitand in a diverging spatial orientation. The first communication on cavitand-based coordination cages was reported by our group in 1997 [22]. Two tetracyano cavitands were connected through four Pd(II) or Pt(II) square-planar complexes. The self-assembly is quantitative, the cage forming immediately as the only product on simply mixing tetradentate cavitand ligands **8** with [M(dppp)(CF$_3$SO$_3$)$_2$] (M = Pd, Pt)
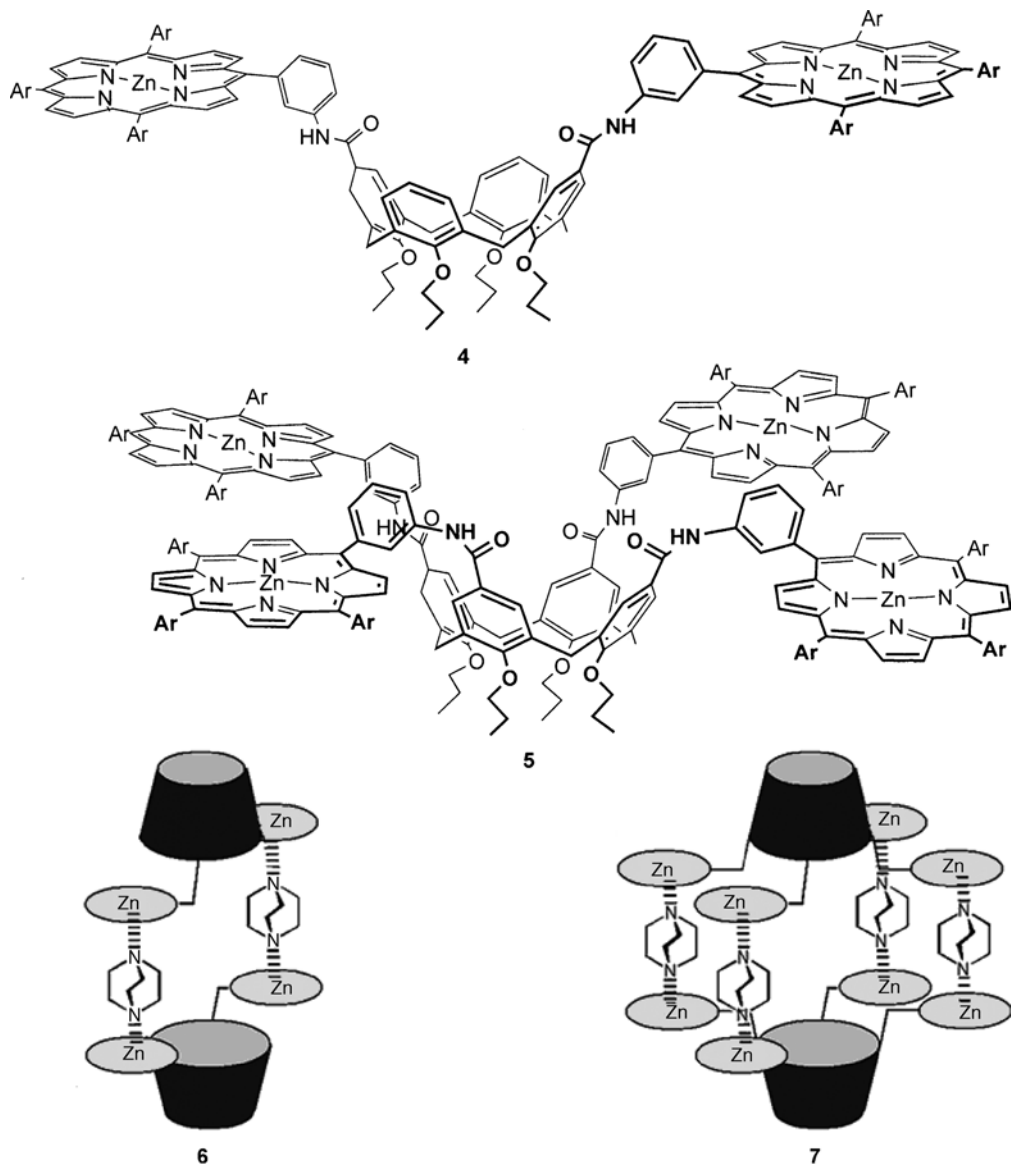
Figure 7.2 Calix-bisporphyrin and calix-tetraporphyrin and their sandwich complexes with DABCO (Ar = p-pentylphenyl).

in a 1 : 2 molar ratio at room temperature (Scheme 7.1). In the presence of excess cavitand, a mixture of cage and free cavitand is obtained; on the other hand if an excess of metal precursor is added, the reaction leads to the cage plus unchanged metal precursor. Control of the self-assembly process was achieved through metal-ligand exchange (Scheme 7.2). Addition of eight equivalents of a competing ligand

8a R = C_6H_{13}
8b R = $C_{11}H_{23}$
8c R = CH_2CH_2Ph
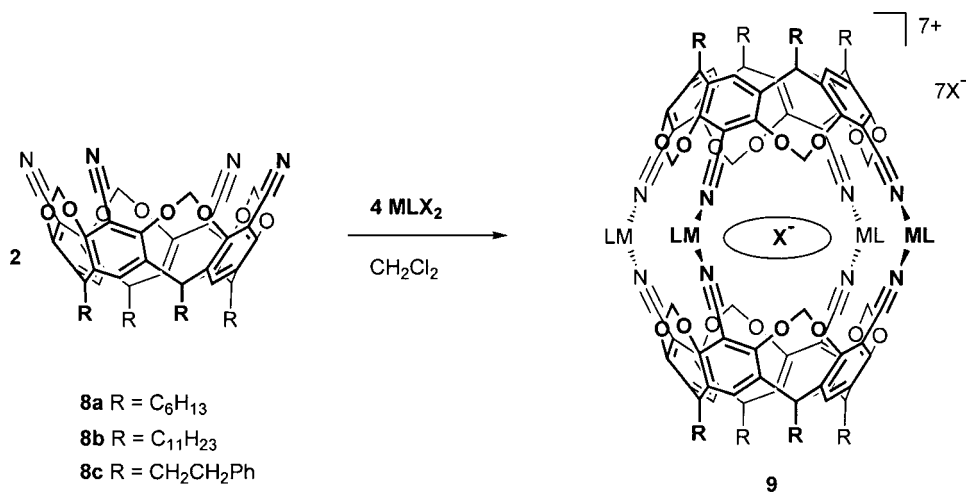
9a R=C_6H_{13}, M=Pd, L=dppp, X=CF_3SO_3

9b R=$C_{11}H_{23}$, M=Pd, L=dppp, X=CF_3SO_3

9c R=C_6H_{13}, M=Pt, L=dppp, X=CF_3SO_3

9d R=$C_{11}H_{23}$, M=Pt, L=dppp, X=CF_3SO_3

9e R=CH_2CH_2Ph, M=Pt, L=dppp, X=CF_3SO_3

9f R=$C_{11}H_{23}$, M=Pd, L=dppb, X=CF_3SO_3

9g R=$C_{11}H_{23}$, M=Pt, L=2 PEt_3, X=CF_3SO_3

9h R=$C_{11}H_{23}$, M=Pd, L=dppp, X=BF_4

9i R=$C_{11}H_{23}$, M=Pt, L=dppp, X=BF_4

9j R=$C_{11}H_{23}$, M=Pt, L=dppp, X=PF_6

9k R=$C_{11}H_{23}$, M=Pd, L=dppp, X=PF_6

Scheme 7.1 Self-assembly of Pd and Pt cage molecules **9a–k**.

+ $PtL(NEt_3)_2(CF_3SO_3)_2$

8b R = $C_{11}H_{23}$
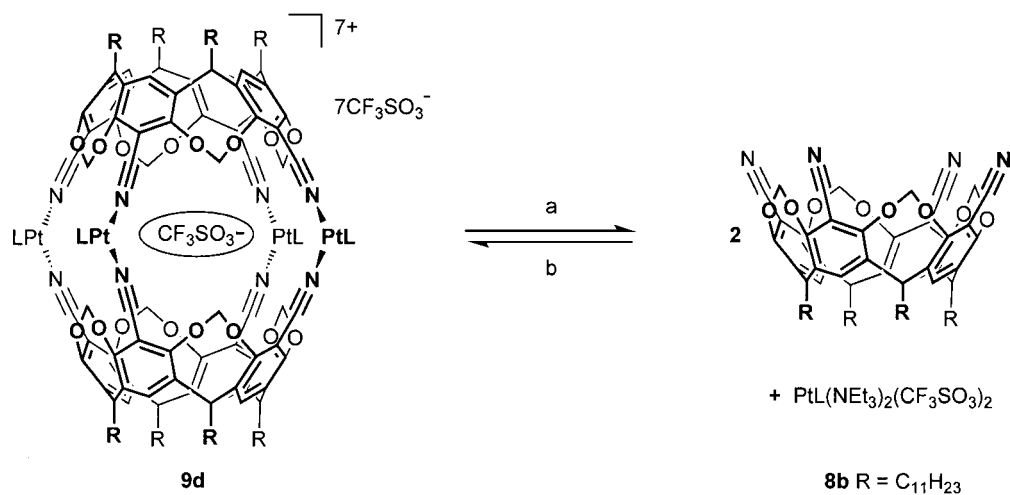
Scheme 7.2 Control of the self-assembly of cage **9d**. (a) 8 eq. NEt_3; (b) 8 eq. CF_3SO_3H. L = dppp.
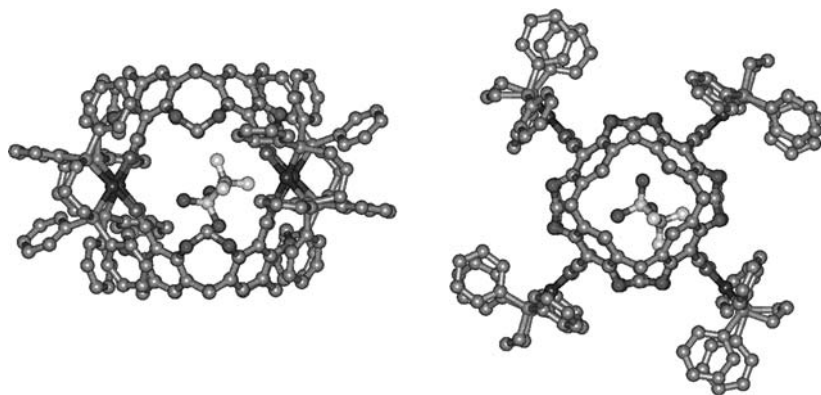
Figure 7.3 Side and top views of the molecular structure of **9d**. The eight undecyl feet are omitted. Reproduced with permission from Ref. [23].

such as NEt$_3$ to the preformed **9d** led to a complete and clean disassembly of the cage into its cavitand components and [Pt(dppp)(NEt$_3$)(CF$_3$SO$_3$)$_2$]. Subsequent addition of eight equivalents of trifluoromethanesulfonic acid restored the original Pt complex, which immediately and quantitatively reassembled the cage.

The presence of two signals in the ^{19}F NMR spectra in a 1:7 integral ratio indicates encapsulation of one of the eight trifluoromethanesulfonate counterions inside the cage. An X-ray crystal structure of **9d** (Figure 7.3) confirms the inclusion of a single, desolvated trifluoromethanesulfonate anion inside the cavity [23].

A more comprehensive study published in 2001 showed the self-assembly of a whole family of coordination cages **9a–k** [23]. The main factors controlling cage self-assembly (CSA) have been identified as (a) a P-M-P angle close to 90° between the chelating ligand and the metal precursor, (b) Pd and Pt as metal centers, (c) a weakly coordinated counterion in the precursor complex, and (d) preorganization of the tetradentate cavitand ligand. Regarding this last point, the influence of rigidity of the tetradentate cavitand ligand has been evaluated by introducing conformationally mobile ethylene bridges instead of the more rigid methylene ones. Table 7.1 reports the results of the self-assembly process between ethylene-bridged cavitands **10** and several metal precursors compared to the case of **8**. In the case of **10**, CSA is possible only with Pt complexes (Scheme 7.3), which provide sufficient coordinative strength toward nitriles to freeze the cavitand in the required cone conformation. Their Pd analogs fail to give CSA under the same conditions. Moreover, in all cases, the CSA is partial at 300 K and complete only above 350 K.

Calorimetric measurements on the formation of cages **9**, together with ^{1}H and ^{19}F NMR experiments, indicated that CSA is entropy driven, with the enthalpic cost of desolvating the molecular components, and particularly the encapsulated anion, compensated by the large entropic gain associated with the release of solvent molecules into the bulk. Desolvation is pivotal also in determining selectivity in anion encapsulation, together with cavity size. As proven in ESI-MS measurements, only in the case

Table 7.1 Influence of cavitand preorganization on CSA.

Entry	Metal Precursor	Cavitand 8b	Cavitand 10b
1	$Pd(dppp)(CF_3SO_3)_2$	CSA (**9b**)	No CSA
2	$Pd(dppp)(BF_4)_2$	CSA (**9h**)	No CSA
3	$Pd(dppp)(PF_6)_2$	CSA (**9k**)	No CSA
4	$Pd(dppb)(CF_3SO_3)_2$	CSA (**9f**)	No CSA
5	$Pt(dppp)(CF_3SO_3)_2$	CSA (**9d**)	CSA (**11b**)
6	$Pt(dppp)(BF_4)_2$	CSA (**9i**)	CSA (**11c**)
7	$Pt(dppp)(PF_6)_2$	CSA (**9j**)	CSA (**11d**)

of encapsulated BF_4^- is there enough room in the cavity for one molecule of solvent ($CHCl_3$ or acetone), while in the case of $CF_3SO_3^-$ and PF_6^- the anion is included alone. This explains the discrepancy between the observed ($BF_4^- \gg CF_3SO_3^- \gg PF_6^-$) and the expected ($CF_3SO_3^- > PF_6^- > BF_4^-$) selectivity in anion encapsulation. The predicted selectivity trend is dictated by the relative enthalpy of desolvation of the anions, but since in the case of BF_4^- one molecule of solvent is included, this trend is biased toward BF_4^- in the observed data.

Recently, dynamic and structural NMR studies have been carried out by Macchioni and coworkers in collaboration with our group [24]. The combined use of PGSE, NOE, and EXSY NMR techniques has helped determine the interionic structure, kinetic stability, and degree of anion encapsulation of coordination cages **9b,c,d** in solution. Both the interionic structure and kinetic stability are solvent dependent, while anion encapsulation is not. In chloroform, all counterions are positioned around the cationic cage and move with it in solution. Addition of a more polar solvent like nitromethane disrupts the ionic integrity, leaving only the included $CF_3SO_3^-$ plus one or two anions

10a R = C_6H_{13}
10b R = $C_{11}H_{23}$

11a R=C_6H_{13}, L=dppp, X=CF_3SO_3
11b R=$C_{11}H_{23}$, L=dppp, X=CF_3SO_3
11c R=$C_{11}H_{23}$, L=dppp, X=BF_4
11d R=$C_{11}H_{23}$, L=dppp, X=PF_6
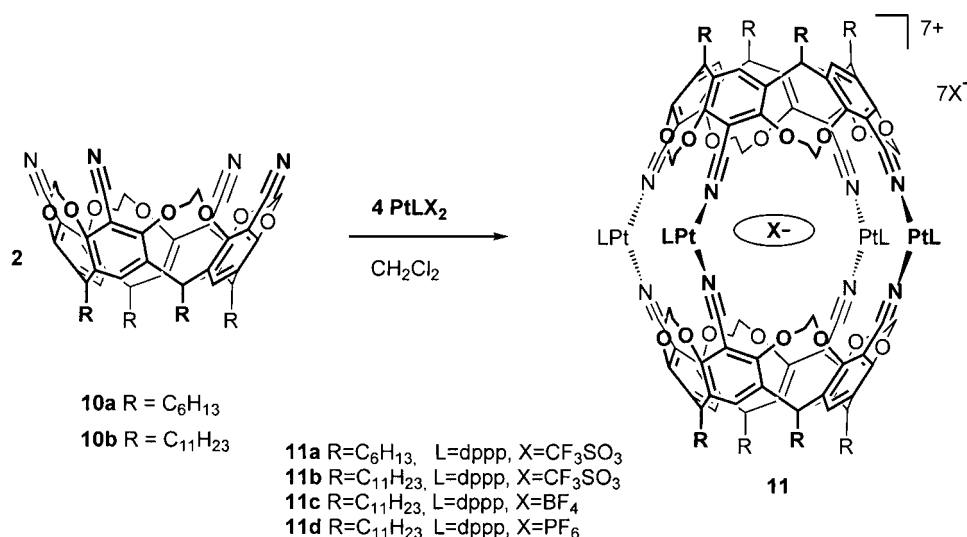
Scheme 7.3 Cage self-assembly using ethylene-bridged cavitands **10a,b**.

connected to the cage. On the other hand, anion encapsulation is quantitative, regardless of the polarity of the solvent. Concerning the kinetic stability of the cage, it can be tuned by changing the coordinating metal and the solvent. The rate constants for the formation/dissociation processes of the Pd cage **9b** are accelerated by more than one order of magnitude on passing from a low-polarity solvent such as chloroform-d ($k_{obs}(s^{-1}) = 0.30 \pm 0.04$) to a polar one, namely, nitromethane-d_3 ($k_{obs}(s^{-1}) = 5.2 \pm 0.8$). The exchange process is remarkably slower when Pt cage **9c** is considered, where the kinetically more inert Pt complex replaces the Pd one.

The quest for cages with internal cavities of nanoscopic dimensions able to encapsulate large guests led our group, in collaboration with de Mendoza's, to enlarge the size of the reacting ligands [25]. In particular, phenyl groups were chosen as spacers introduced in the apical position of the resorcinarene in order to extend the cavity size, while retaining the relative orientation of the cyano groups and the rigidity of the cavitand framework. Cavitands **12a,b** were synthesized from tetrakis-(bromophenyl)-cavitands through a reaction with CuCN. The corresponding cages **13a,b** were obtained in a quantitative yield by mixing **12a,b** with [Pt(dppp)(CF$_3$SO$_3$)$_2$] in a 1 : 2 molar ratio at room temperature (Scheme 7.4). In this case no permanent inclusion of the CF$_3$SO$_3^-$ counterions was observed by ^{19}F NMR even at low temperatures: rapid exchange with the external counterions occurs because of the
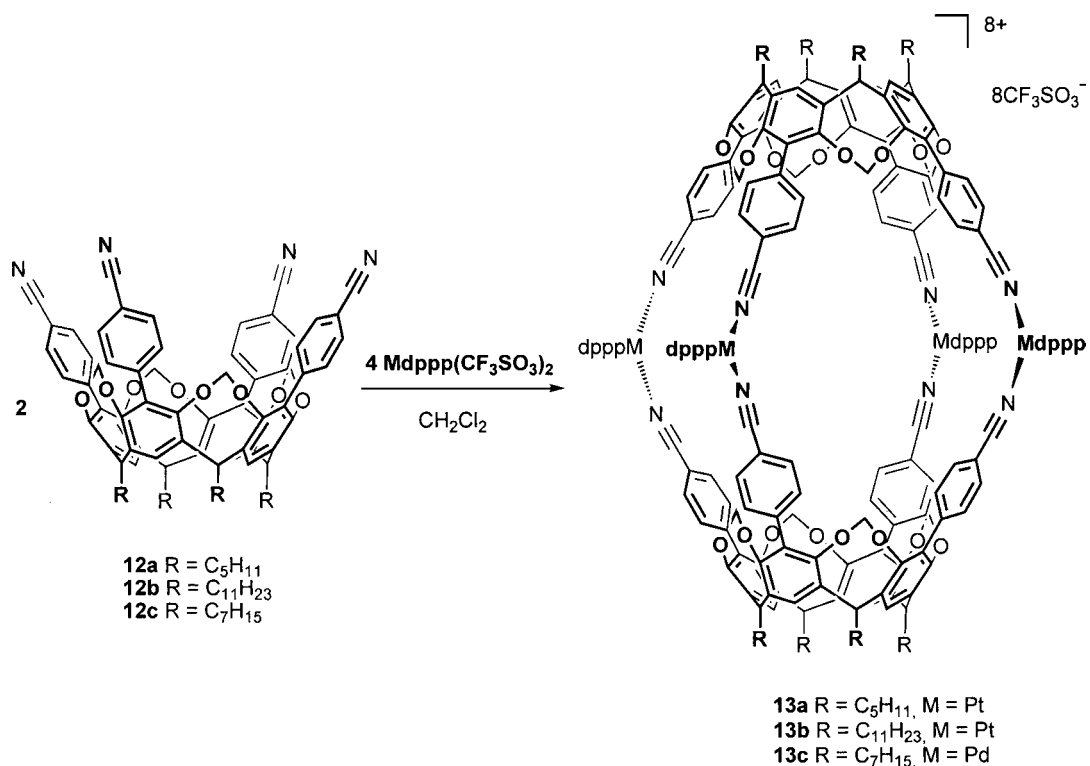
Scheme 7.4 Self-assembly of enlarged Pt and Pd cage molecules **13a–c**.

14   R = C$_7$H$_{15}$ **15**
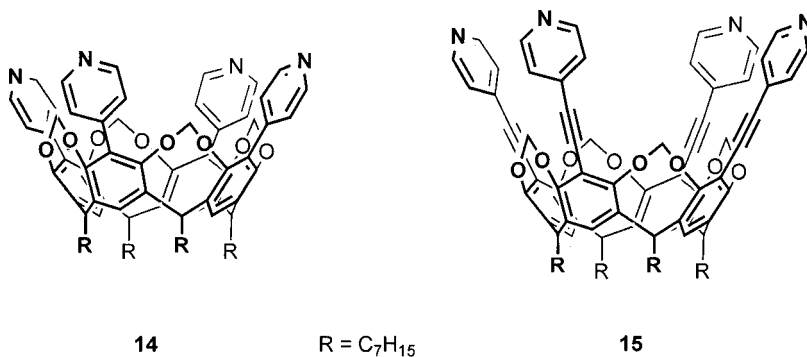
Figure 7.4 Cavitand ligands with four pyridyl (**14**) and
pyridylethynyl (**15**) substituents at the apical position.

large dimensions of the lateral portals. Enlarging the size of the cavitand ligand leads
to the self-assembly of nanosize coordination cages; the drawback is the concomitant
widening of the lateral portals, which prevents permanent inclusion of suitable
guests. The self-assembly of the corresponding Pd cage **13c** was attempted using
[Pd(dppp)(CF$_3$SO$_3$)$_2$] as a metal complex. The resultant product showed ^{1}H and ^{31}P
NMR spectra consistent with the corresponding cage formation; however, no con-
firmation came from MALDI-TOF or ESI-MS analyses. This different behavior is
because the CN-Pd bond is weaker than the CN-Pt bond.

A different synthetic procedure to introduce cyanophenyl groups at the apical
position (**12c**) was reported by Kobayashi *et al*. in 2004, together with the synthesis of
the two new tetradentate cavitand ligands **14** and **15** (Figure 7.4) [26].

A 2 : 4 mixture of **14** and [Pd(dppp)(CF$_3$SO$_3$)$_2$] led to the formation of various
aggregates which were not related to the expected coordination cage. This behav-
ior is mainly due to a hindered rotation of the pyridyl groups directly attached to
the apical positions. By introducing an ethynyl spacer, pyridylethynyl cavitand **15**
self-assembled into the corresponding cage **16** quantitatively through a concerted
process (Figure 7.5). The inability of cavitand **14** to form the corresponding
homocage has been exploited in a unique and very elegant way to exclusively
produce heterocages in solution. In fact, heterocage **17** was self-assembled as a
sole product by mixing **12c** : **14** : [Pd(dppp)(CF$_3$SO$_3$)$_2$] in a 1 : 1 : 4 molar ratio. On
the other hand a 1 : 1 : 4 mixture of **12c** : **15** : [Pd(dppp)(CF$_3$SO$_3$)$_2$] exclusively gave
the two homocages **13c** and **16** in a 1 : 1 ratio. The authors have therefore dem-
onstrated that by tuning the coordination ability of the cavitand ligands on the
basis of the kinetic stability of their metal complexes and their steric demand it is
possible to direct the self-assembly process towards either exclusively homo-or
heterocages.

Further studies on the kinetic and thermodynamic stabilities of Pd cages **13c**, **16**,
17, and the corresponding Pt cages have been reported by Kobayashi and coworkers
in a subsequent paper [27]. The stability of the cages increases in the order
13c < **17** < **16**.
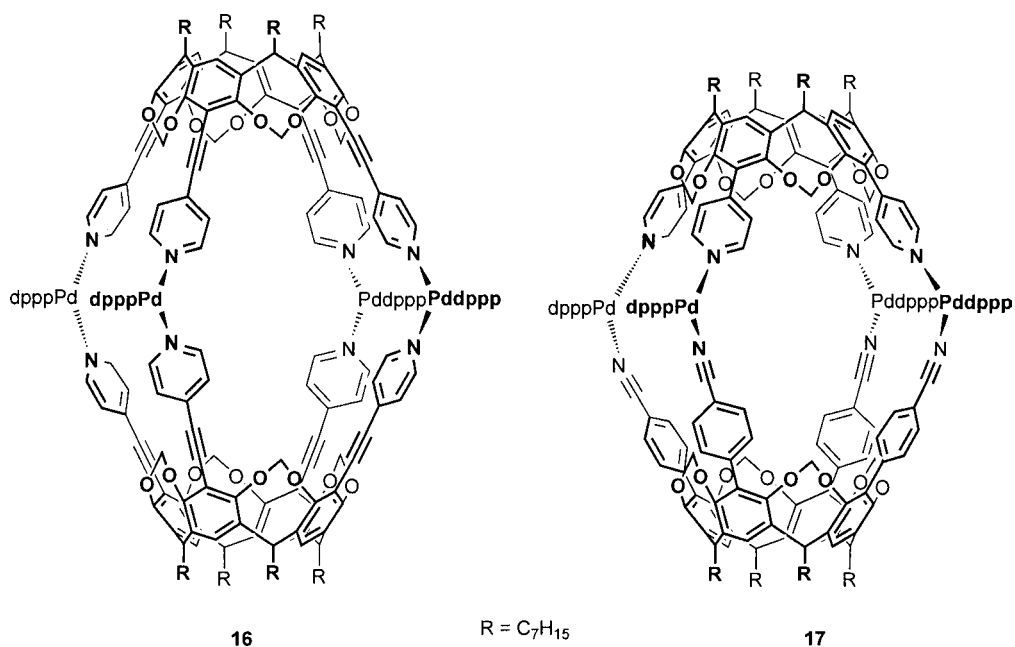
Figure 7.5 Homocage **16** and heterocage **17**.

A different approach to cage widening has been proposed by Sherburn, Stang, and coworkers [28]. Using large dinuclear Pt precursors like [2,9-(*trans*-Pt(PEt$_3$)$_2$NO$_3$)$_2$-phenanthrene] in connection with bis-4-pyridyl cavitands **18** and **19**, they assembled expanded coordination cages **20** and **21**, which have wide lateral portals (Scheme 7.5). This strategy offers a useful alternative to the often synthetically demanding introduction of long, rigid ligands on the cavitand upper rim. It also highlights one of the hallmarks of self-assembly: modularity.

Other examples of coordination cages prepared by self-assembly of cavitand derivatives were shown by Hong and coworkers starting from the more flexible tetradentate cavitands **22a–c** (Scheme 7.6) [29]. Also in this case, cages **23a–d** were instantly formed as the sole product by simply adding two equivalents of Pd or Pt square planar complexes to CH$_2$Cl$_2$, CHCl$_3$, or acetone solutions of the cavitand ligands. Positively charged *N*-methylpyridinium derivatives turned out to be encapsulated via cation-π interactions, the guest being entrapped in the forming capsule. In a subsequent report the authors have demonstrated how metal-induced self-assembly can be tuned by subtle changes in the solvent system [30]. A dynamic equilibrium between the interclipped capsule **23c,d** and the intraclipped bowl **24a,b** has been observed in nitromethane using [M(dppp)(CF$_3$SO$_3$)$_2$] (M = Pd, Pt) as metal precursors. This equilibrium is totally shifted toward the interclipped capsule in chloroform/methanol, while the intraclipped bowl forms exclusively in the aqueous phase using water-soluble complexes [Pd(en)(NO$_3$)$_2$] [31]. NMR studies clarify the thermodynamic parameters that control the dynamic equilibrium in nitromethane:

R = C$_7$H$_{15}$

18

19

20

21
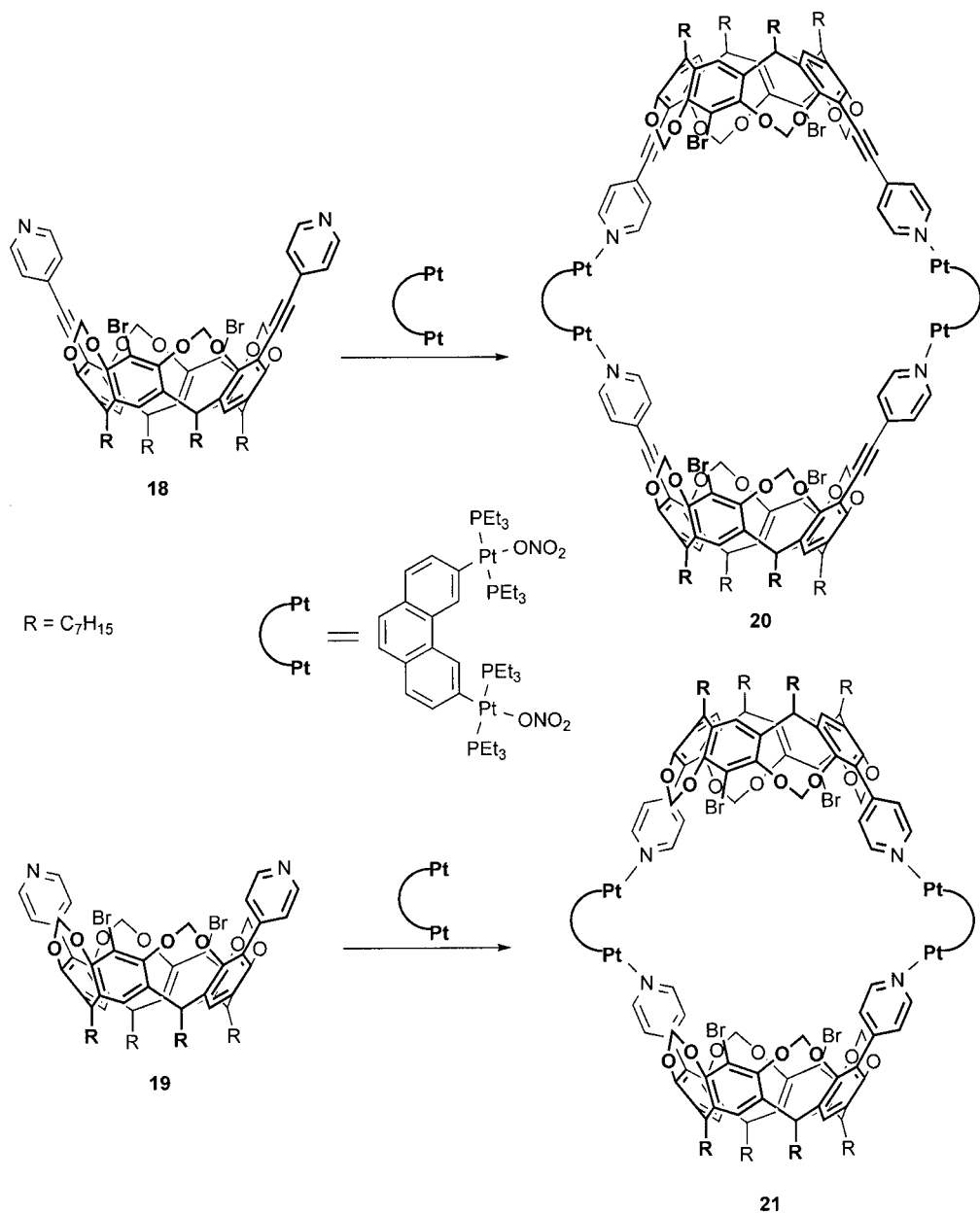
Scheme 7.5 Self-assembly of 2+2 coordination cages **20** and **21** using dinuclear metal precursors.
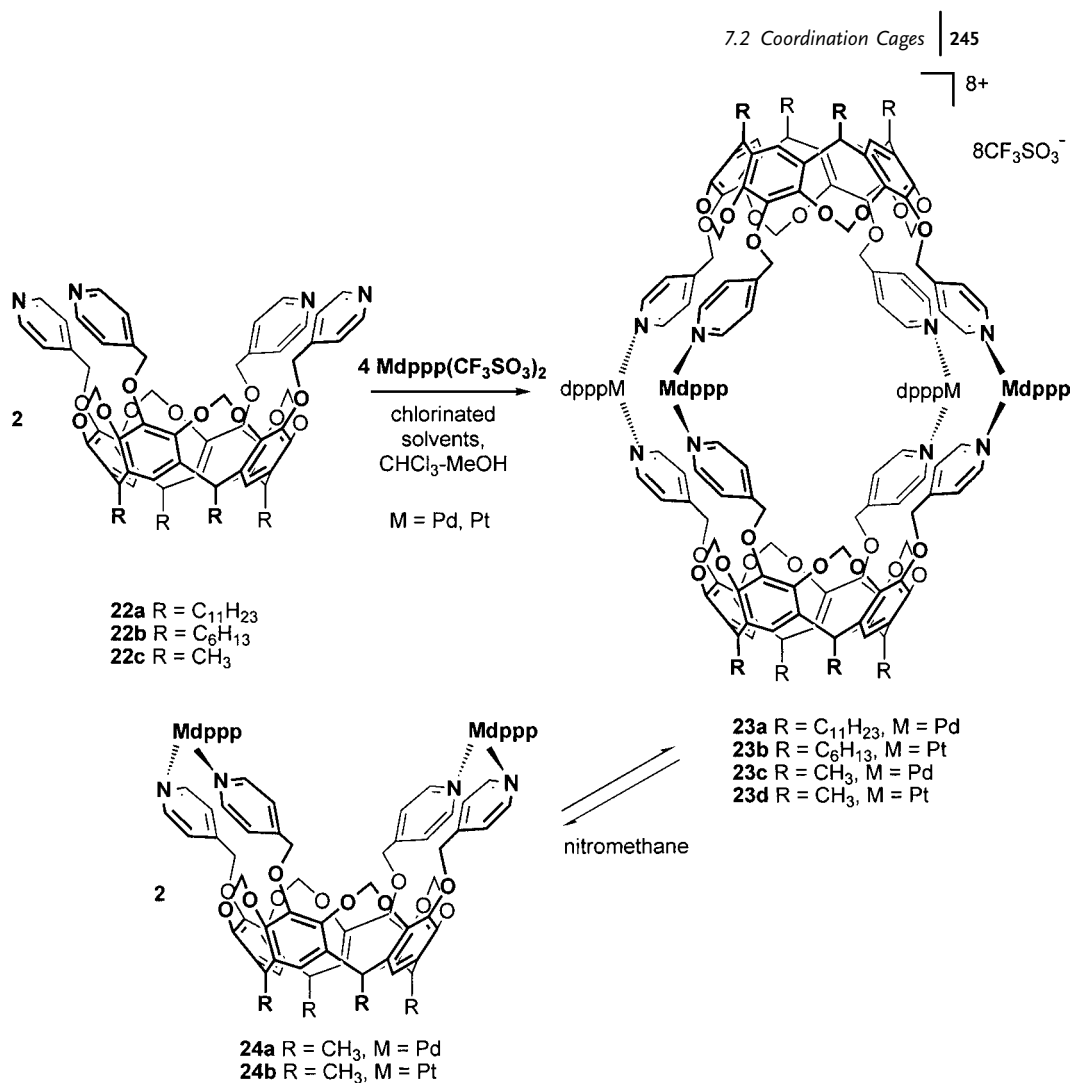
Scheme 7.6 Solvent-mediated self-assembly of coordination capsules **23a–d** and bowls **24a,b**.

the conversion from the capsule to the bowl is enthalpically disfavored, but entropically favored. The structure of the interclipped capsule **23d** was corroborated by means of X-ray crystallography.

Haino *et al.* synthesized the new octadentate cavitand **25** (Figure 7.6) bearing phenyl-bipyridine groups at the apical position [32]. Cavitand **25** forms a stable dimeric cage **26** via coordination to four Ag$^+$ metal centers. Each silver cation coordinates with two bipyridines in a tetrahedral fashion. The size and shape of the large three-dimensional cavity allows encapsulation of rigid guests such as biphenyls **27a,b** because of the presence of acidic protons on the guest, creating a CH/π interaction with the resorcinarene cavity. Moreover, when a 1 : 1 mixture of
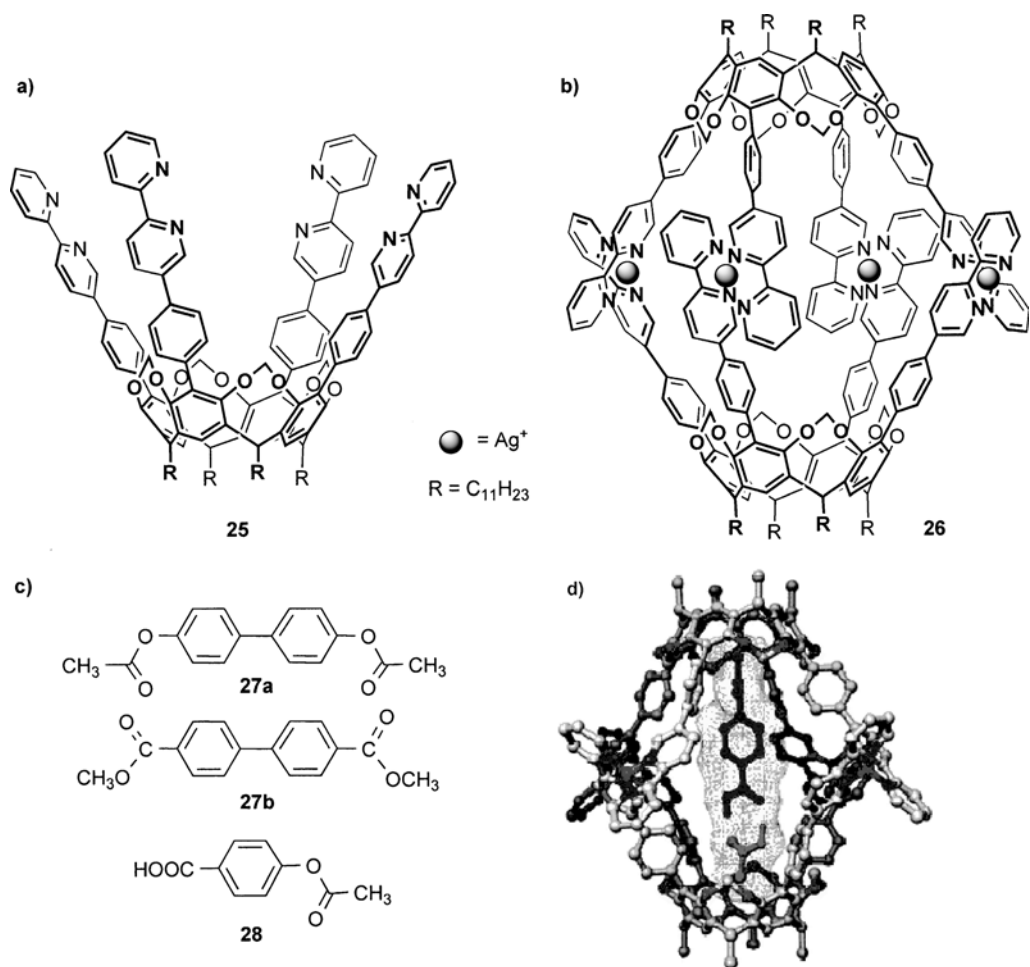
Figure 7.6 (a) octadentate bipyridine cavitand **25**; (b) the corresponding Ag⁺ cage **26**; (c) encapsulated guests **27a–b** and **28**; (d) optimized structure of the co-encapsulation complex of **26** with **28** and acetic acid. Reproduced with permission from Ref. [32].

acetic acid and **28** was added to the solution of the capsule, the uncommon co-encapsulation of the guests with surprising selectivity was observed, even in the presence of an equal amount of propionic acid. Out of several possible H-bonded pairs, only the one matching the overall length of the cavity was selected (see Figure 7.6 bottom right).

A subsequent detailed thermodynamic study on guest encapsulation within the above-mentioned capsule revealed that not only CH/π interactions between the methyl groups on the guest ends and the aromatic cavity, but also desolvation of the inner cavity, play a key role in guest encapsulation [33].
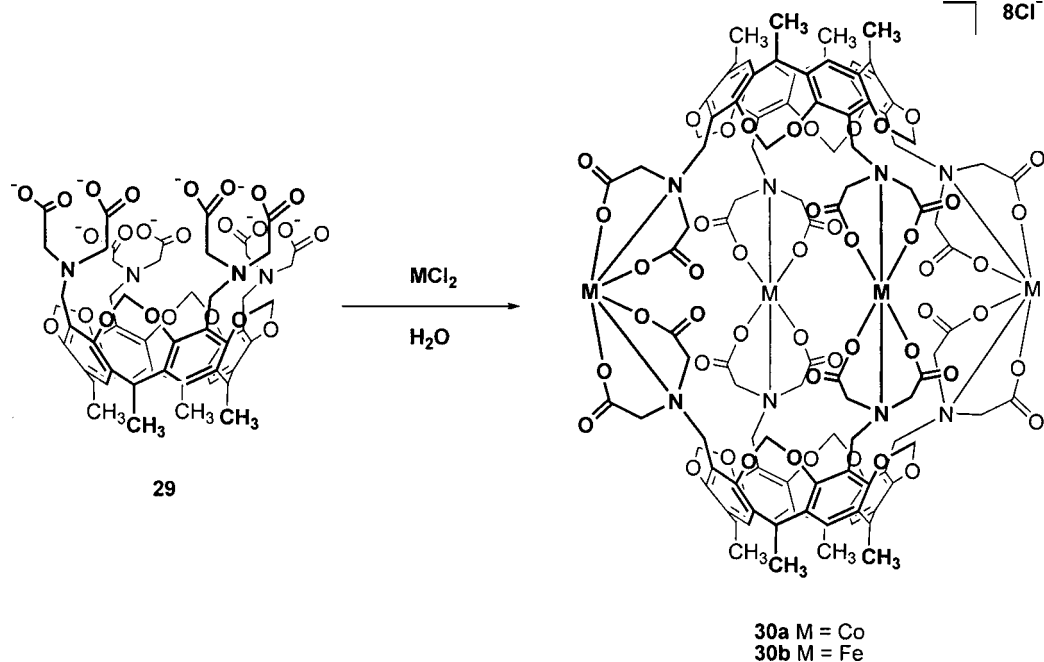
Scheme 7.7 Self-assembly of the octaanionic cages **30a,b**.

Harrison and coworkers introduced four iminodiacetate moieties as chelating ligands at the apical position of resorcinarene-based cavitands (**29** in Scheme 7.7). Treatment with CoCl$_2$ under basic conditions led to the formation of cage **30a**, with the four octahedrally coordinated Co(II) ions connecting two cavitand scaffolds [34]. Cage **30a**, which has been structurally characterized, presents two very interesting features: (a) it is water soluble and (b) the self-assembly process is pH-dependent: at pH values below 2 the carboxyl groups and amine nitrogen atoms are protonated and do not coordinate cobalt(II) ions, but upon addition of a base at pH 5, cage **30a** is formed. Taking advantage of the hydrophobic effect, these water-soluble cages are able to include several small liphophilic guests within the cage, such as aromatic molecules, alkanes, alkenes, and haloalkanes [35]. Because of the paramagnetic nature of **30a**, large upfield shifts in the proton resonances of the encapsulated guest are observed (30–40 ppm): the cage behaves as an NMR shift reagent for the included guest.

Calorimetric studies demonstrated that the most dominant factors in encapsulation selectivity are guest fit and polarity. In most cases, molecules with intermediate polarity are preferred to those that are either non-polar or very polar [36]. Using the same cavitand ligand, the corresponding Fe$_4$ cage **30b** has been prepared and structurally characterized [37]. The iron atoms in each complex exhibit a trigonal prismatic geometry. Also, cage **30b** is capable of encapsulating organic molecules, moving the chemical shifts of the guests upfield by 20–30 ppm. More recently, the same group described the preparation of a new cage using cavitands substituted

with bpa ligands and FeCl$_3$ in a 2:4 ratio [38]. For the first time the cage was characterized by sonic spray mass spectrometry (SSI MS), which allowed the observation of a monocharged ion peak. Thanks to the soft ionization coupled with its simple design, SSI MS provides a powerful tool to characterize such supramolecular cages.

7.2.2.2 Introduction of the Ligands as Bridging Units

Concerning the decoration of cavitands at the upper rim, an alternative strategy was described by Gibb and coworkers some years ago [39]. Using this approach in our group, a new series of cavitand ligands was synthesized bearing picolyl groups as bridges between the phenolic OH groups of the resorcinarene scaffold [40]. The synthesis of cavitands **31a,b**, was performed by bridging the corresponding resorcinarenes with 4-(α,α-dibromomethyl)pyridine. In this case, unlike the previously described cavitands bearing ligands at the apical positions, each picolyl bridge may assume two different orientations with respect to the cavity, pointing either inward (i) or outward (o) and thus leading to the formation of various isomers. Among these isomers, only the cavitand with four pyridines preorganized in a diverging spatial orientation, i.e. pointing outward from the cavity (oooo isomer), is suitable for cage self-assembly. The correct stereochemical assignment of the oooo isomer has been confirmed by the X-ray crystal structure of cavitand **31b** (Figure 7.7a). Moreover, it is possible to evaluate the α angle of the pyridyl ligands relative to the C_{4v} symmetry axis: the estimated value is 42°, close to the ideal value of 45° required for the formation of strainless square-planar complexes. The typical procedure for cage formation is shown in Scheme 7.8: cavitands **31a,b** and various metal precursors MLX$_2$ (M = Pd, Pt; L = dppp, en; X = CF$_3$SO$_3$, NO$_3$) were mixed in a 1:2 molar ratio at room temperature in solvents like CH$_2$Cl$_2$, CHCl$_3$, acetone, or DMSO, giving cages **32a-h** in quantitative yields. In all cases the ^{1}H NMR spectra showed the formation of a new set of signals, indicative of the presence of a single highly symmetric compound (D_{4h} symmetry). No permanent inclusion of trifluoromethanesulfonate counterions was detected by ^{19}F NMR. Additional proof of cage formation was obtained through ESI and MALDI-TOF mass spectrometry. The X-ray crystal structure of cage **32f** (Figure 7.7b) confirms the formation of four square-planar complexes [41]. The four large lateral portals (dimensions 12.3 Å × 10.8 Å), allow the entrance/exit of solvent molecules as well as anions, eliminating any possibility of permanent counterion inclusion in solution. In the solid state, one trifluoromethanesulfonate anion is included in the cavity, together with two disordered acetone molecules (not shown in Figure 7.7b). The internal volume of the cavity has been estimated as 840 Å^3.

Several encapsulation experiments with suitably sized guests such as adamantane, 1,2,4,5-tetramethylbenzene, anthracene, pyrene, sodium picrate, and fullerenes in various solvents were carried out. The complexation experiments, monitored by ^{1}H NMR, were performed at room temperature by forming capsule **32f** in the presence of excess guest. The only successful encapsulation experiment performed was the one using methano[60]fullerene derivatives bearing dimethyl and diethyl malonate addends. Evidence for inclusion complexation, provided by ^{1}H NMR, was confirmed by ESI-MS investigations, which showed the formation of 1:1
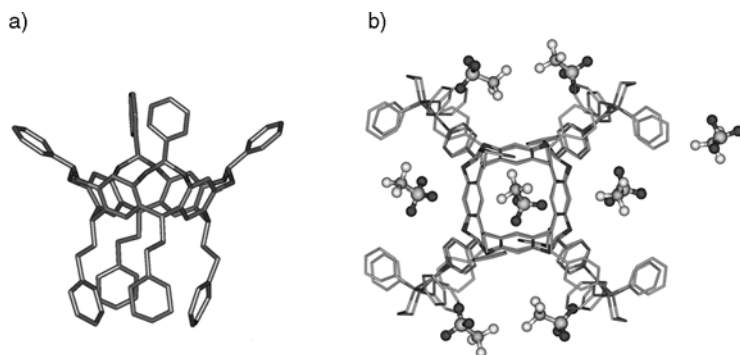
Figure 7.7 Molecular structure of (a) cavitand **31b** and (b) cage **32f**, top view as determined by X-ray crystallography. Reproduced with permission from Ref. [41b].

31a R = $C_{11}H_{23}$

31b R = CH_2CH_2Ph

32a-h
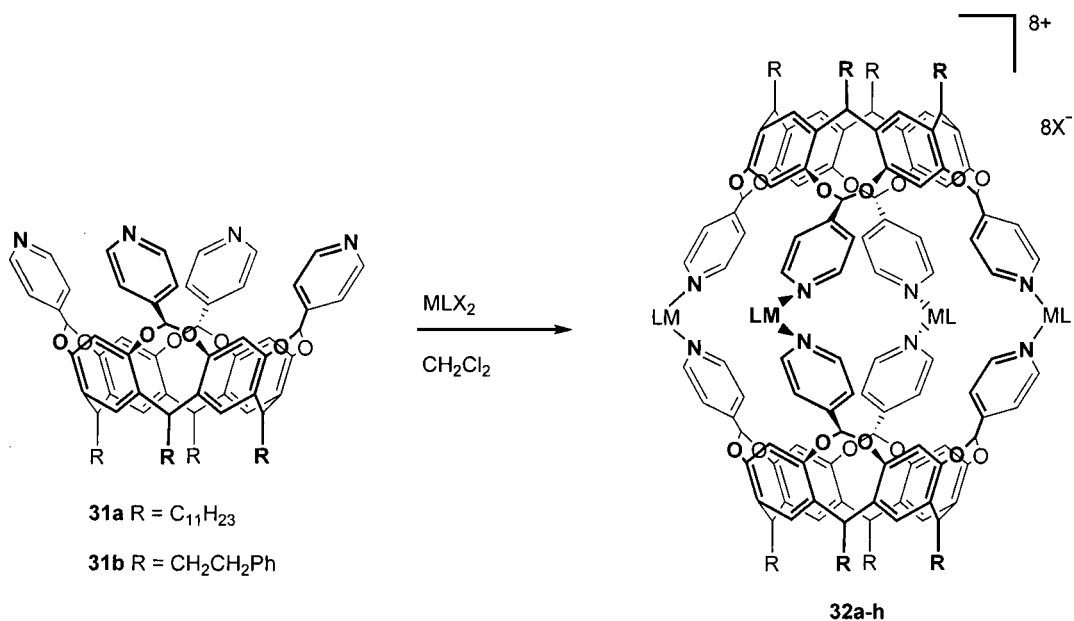
32a R=$C_{11}H_{23}$, M=Pt, L=dppp, X=CF_3SO_3

32b R=$C_{11}H_{23}$, M=Pd, L=dppp, X=CF_3SO_3

32c R=$C_{11}H_{23}$, M=Pd, L=en, X=CF_3SO_3

32d R=$C_{11}H_{23}$, M=Pd, L=en, X=NO_3

32e R=CH_2CH_2Ph, M=Pt, L=dppp, X=CF_3SO_3

32f R=CH_2CH_2Ph, M=Pd, L=dppp, X=CF_3SO_3

32g R=CH_2CH_2Ph, M=Pd, L=en, X=CF_3SO_3

32h R=CH_2CH_2Ph, M=Pd, L=en, X=NO_3

Scheme 7.8 Self-assembly of coordination cages **32a–h**.

fullerene-cage complexes. In collaboration with the group of Diederich and coworkers [41b], the association constant was experimentally determined to be approximately $150 M^{-1}$ at 298 K in CD_2Cl_2. The preference for fullerene inclusion is not related to specific host-guest interactions, but it is driven by dispersion forces and π-stacking contacts between the guest and the inner surface of the capsule.

An uncommon experiment of cage self-assembly in a liquid-liquid two-phase system has been described. Cavitand **31b** (1 equiv) dissolved in 1,1,2,2-tetrachloroethane was exposed to an aqueous solution of $Pd(en)(NO_3)_2$ (2.5 equiv) in a test tube. Immediately, a solid formed at the interface, which became more abundant over time. ^1H NMR analysis of the recovered solid indicated the formation of cage **32h** in pure form. A MALDI-TOF experiment performed directly on the solid sample confirmed the attribution. This last result is particularly interesting since liquid-liquid interfaces represent another potentially useful field of action for self-assembly protocols, which has barely been explored so far [42].

The kinetic stability of the Pt cages [43] has been assessed by ESI-MS. A ligand-exchange experiment was performed starting from two Pt-cages **32a** and **32e**, differing by the chains at the lower rim ($R = C_{11}H_{23}$ and CH_2CH_2Ph): both cages were separately analyzed by ESI-MS, showing $[M-2CF_3SO_3]^{2+}$, $[M-3CF_3SO_3]^{3+}$, and $[M-4CF_3SO_3]^{4+}$ ions. They were then mixed in a 1:1 molar ratio at room temperature, giving a spectrum resulting from the simple addition of the signals due to the two homocages. Upon heating the mixture, the ESI-MS spectrum exhibited a third set of peaks belonging to the heterocage in a statistical 1:2:1 ratio with the signals of the homocages. Another interesting finding is that the introduction of four methyl groups at the apical positions of cavitand **31** completely switches off the CSA process by hindered rotation of the pyridyl ligands, as in the case of cavitand **14**.

Our chosen strategy for enlarging the dimensions of the coordination cage lies in deepening the cavitand precursor cavity via introduction of a phenyl spacer between the methylene bridge and the pyridine ligand [44]. For the synthesis of the tetradentate cavitand ligands **33a,b**, 4-(α-α-dibromo)tolylpyridine was used as bridging reagent. In this case, only the desired oooo isomer formed for steric reasons. Following the above-mentioned procedure of cage formation, cages **34a–f** were obtained in quantitative yields by simply mixing **33a** or **33b** with MLX_2 complexes in a 1:2 ratio (Scheme 7.9).

The crystal structure of cage **34d** revealed the exact position of the eight trifluoromethanesulfonate counterions, which are all placed outside the cavity (Figure 7.8), near the metal centers, thanks to the increased distance between the adjacent Pt centers (close Pt-Pt distance = 14.7 Å). It is worth noting that anion inclusion in this class of cages is determined by the distance between the metal centers. When this distance is large enough to permit all counterions to sit close to the metal centers, no inclusion is observed in the solid state (compare Figure 7.7b with Figure 7.8). The new cages reach nanoscopic dimensions, and the estimated internal volume of the cavity is 1800 Å^3, more than twice that of the picolyl-bridged analogue **32**.

A competition experiment has been performed to test the self-recognition properties of cavitands **31b** and **33b** in the CSA process. After the addition of a

33a R = C$_{11}$H$_{23}$
33b R = C$_6$H$_{13}$
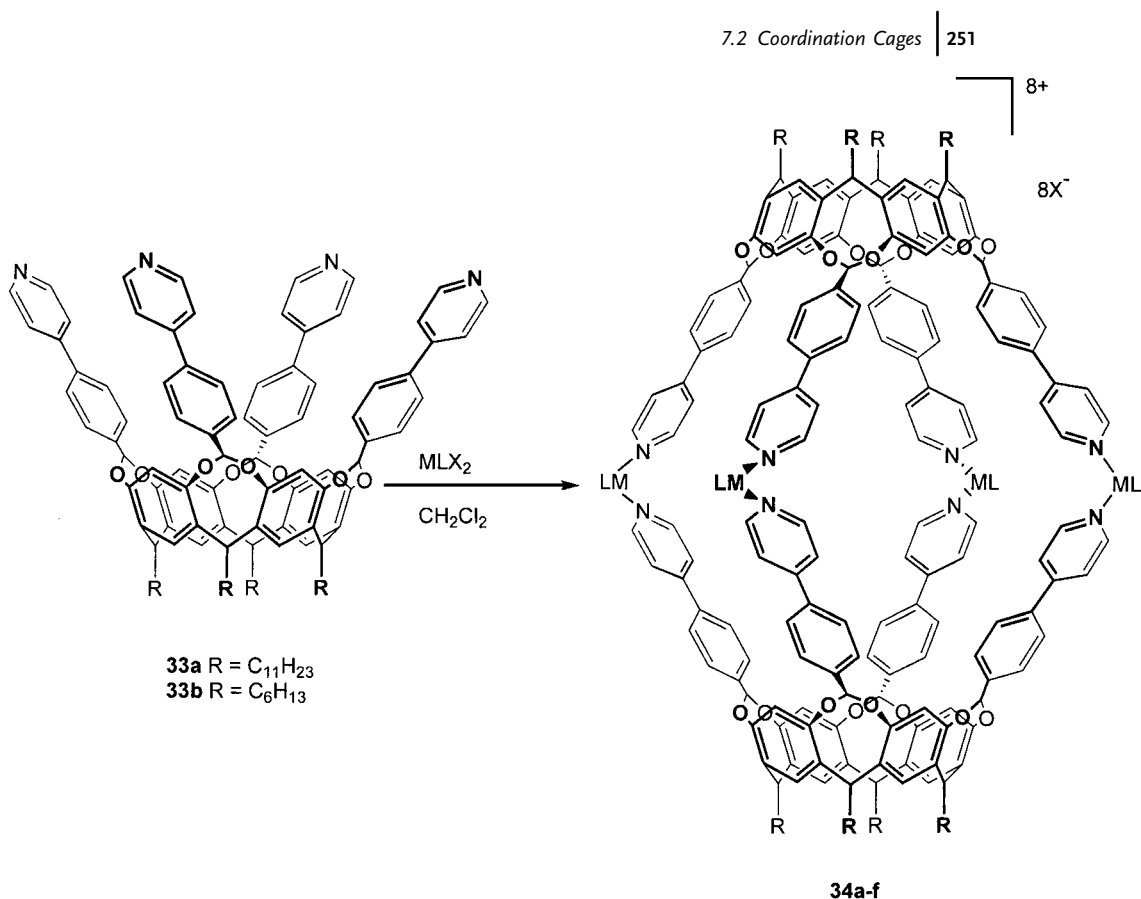
34a-f

34a R=C$_{11}$H$_{23}$, M=Pt, L=dppp, X=CF$_3$SO$_3$

34b R=C$_{11}$H$_{23}$, M=Pd, L=dppp, X=CF$_3$SO$_3$

34c R=C$_{11}$H$_{23}$, M=Pt, L=2(PEt$_3$), X=CF$_3$SO$_3$

34d R=C$_6$H$_{13}$, M=Pt, L=dppp, X=CF$_3$SO$_3$

34e R=C$_6$H$_{13}$, M=Pd, L=dppp, X=CF$_3$SO$_3$

34f R=C$_6$H$_{13}$, M=Pd, L=en, X=CF$_3$SO$_3$

Scheme 7.9 Self-assembly of nanosize coordination cages **34a–f**.

stoichiometric amount of [Pd(en)(CF$_3$SO$_3$)$_2$] to an equimolar mixture of **31b** and **33b**, only the signals belonging to the homocages **32g** and **34f** were detected. The mismatch between the biting angles of the two cavitands leads to complete self-recognition during cage self-assembly.

In a recent report we described the preparation of cavitand **35**, which bears only two tolylpyridyl moieties as bridging ligands in an **AC** distal position, and its self-assembly behavior with [Re(CO)$_5$Br], which undergoes cis ligand exchange exclusively (Scheme 7.10) [45]. In this case, the self-assembled *fac*-[Re(CO)$_3$**35**$_2$Br] cage **36** is neutral and kinetically stable at room temperature.
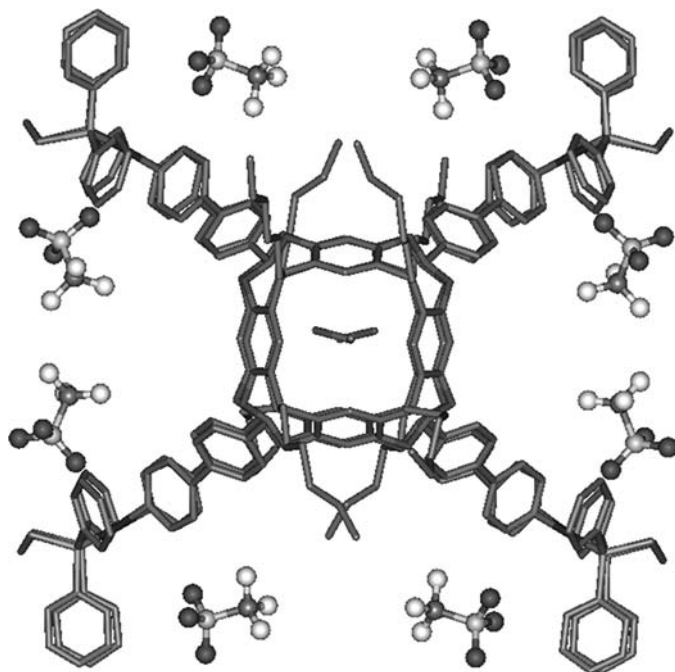
Figure 7.8 Top view of the molecular structure of **34d**. Reproduced with permission from Ref. [44].

In the examples reported so far, the ligand bridging units are oriented outward with respect to the cavity. Dutasta and coworkers reported a case where inward-facing P = S ligands bridging a resorcinarene skeleton form a coordination cage in the presence of Ag$^+$ cations [46]. A drawback is that the inner space of the cage is highly reduced by the presence of the sulfur atoms.

7.2.3
Trimeric, Tetrameric, and Hexameric Coordination Cages

One of the long-term goals of metal-directed self-assembly is the generation of coordination cages of nanoscale dimensions, capable of confining large objects within their inner space. To widen the inner space of coordination cages, three different strategies have been implemented so far:

1. introduction of rigid spacers between the ligand and the macrocycle (see **34** as an example)
2. use of dinuclear metal precursors (see **20** and **21** as examples)
3. assembly of more than two macrocyclic ligands. This last approach is covered in the present chapter.

Beer and coworkers were the first to report the metal-directed synthesis of trimeric and tetrameric coordination cages **37** and **38**, assembled from dithiocarba-
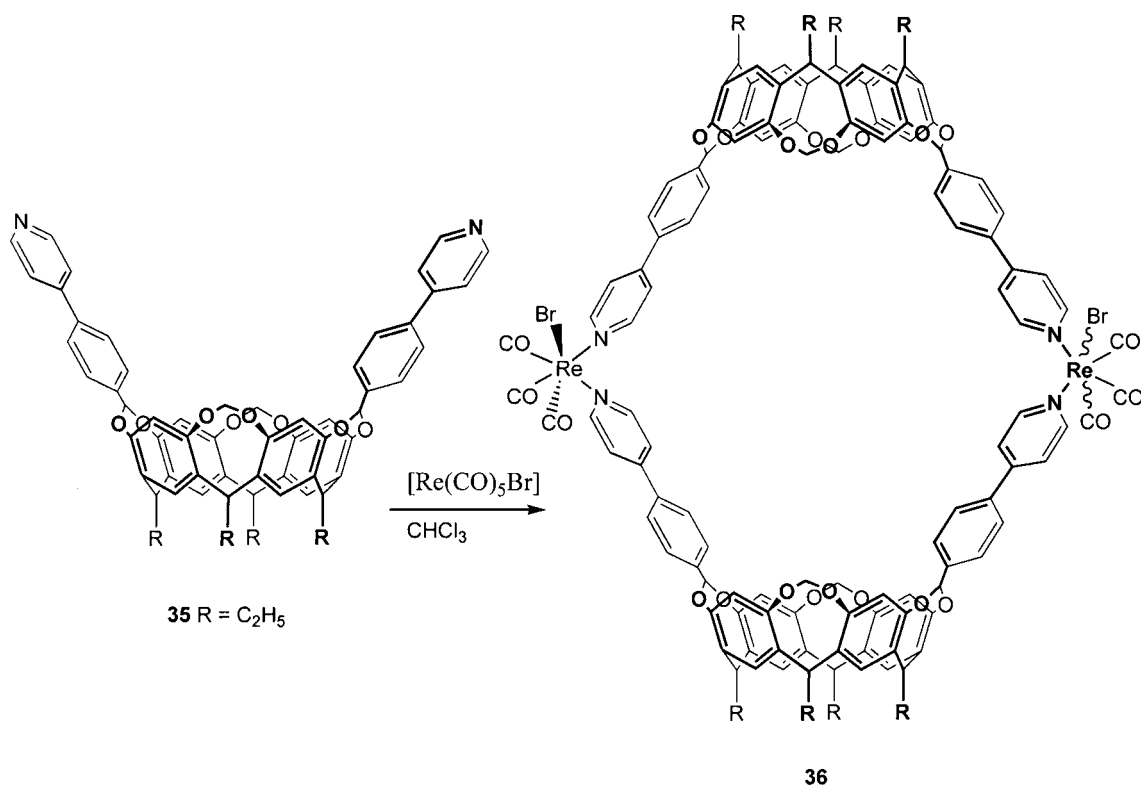
Scheme 7.10 Self-assembly of *fac*-[Re(CO)₃Br] **AC** dimeric cage. The relative orientation of the two Br on the Re metal centers has not been determined.

mate (dtc) functionalized cavitands and various metal ions (Figure 7.9) [47]. The coordination preference of the transition metal used dictates the assembly that is adopted. Using group 12 metals such as zinc(II) and cadmium(II), trimeric hexanuclear cavitand assemblies **37a–f** form. As shown by X-ray crystallographic studies, the three resorcinarene cups provide the corners for an equilateral molecular triangle with two zinc or cadmium ions positioned at the midpoints of each side. In this case the metal ions coordinate two bidentate dtc moieties and a pyridine molecule. Treatment of the same resorcinarene ligand with copper(II) acetate provided an intermediate copper(II) tetrameric octanuclear complex, whose X-ray crystal structural analysis reveals a flattened tetrahedron shape. Chemical oxidation produced the corresponding copper(III) complexes **38a–c**, where an X-ray structure determination displayed a similar tetrahedral arrangement of the cavitand connected to each other by eight copper(III) ions forming approximately square planar complexes. To obtain the analogous gold(III) octanuclear complex **38d**, a transmetalation reaction was undertaken on the corresponding copper (II) complex. Strong 1 : 1 complexes are formed between fullerenes (C₆₀ and C₇₀) and hexanuclear assemblies **37a,b,d,e**
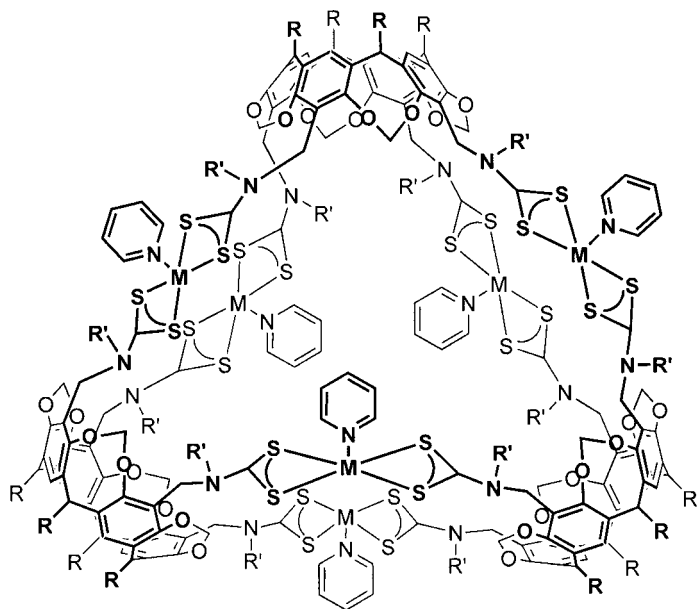
37a M = Cd, R = C_5H_{11}, R' = *n*-butyl
37b M = Cd, R = C_5H_{11}, R' = *n*-propyl
37c M = Cd, R = C_5H_{11}, R' = *n*-hexyl

37d M = Zn, R = C_5H_{11}, R' = *n*-butyl
37e M = Zn, R = C_5H_{11}, R' = *n*-propyl
37f M = Zn, R = C_5H_{11}, R' = *n*-hexyl
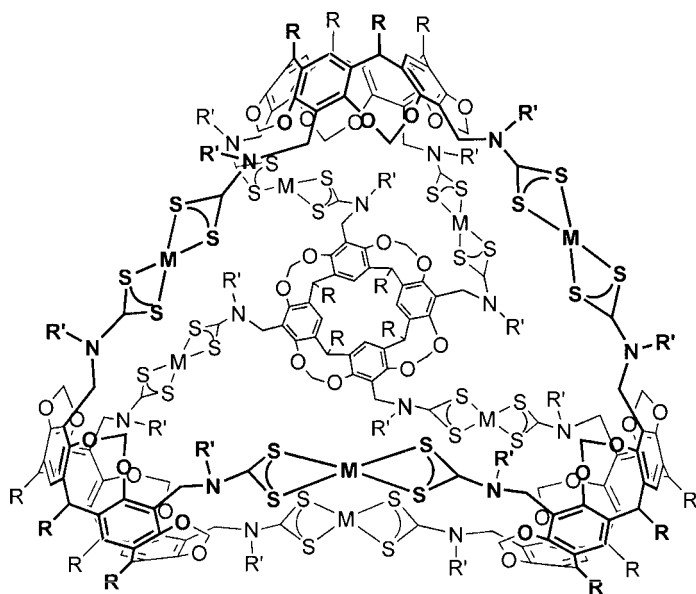
38a M = Cu, R = C_5H_{11}, R' = *n*-propyl
38b M = Cu, R = C_5H_{11}, R' = *n*-butyl
38c M = Cu, R = C_5H_{11}, R' = *n*-hexyl
38d M = Au, R = C_5H_{11}, R' = *n*-butyl

Figure 7.9 Trimeric and tetrameric polymetallic architectures **37a–f** and **38a–d**.

with log K_{ass} ranging from 3 to 6, determined via UV-visible spectroscopy. In particular, the cadmium hexanuclear architectures **37a–c** were found to be the superior host systems. ESI-MS provided evidence for the encapsulation of [60]fullerene by the copper(II) octanuclear assemblies. Structural data in conjunction with molecular modeling studies revealed that it is the lability of the copper(II) dithiocarbamate bond which allows guest encapsulation, since the entrance to the nanosized cavity is restricted by its relatively small portals. In both cases it is the electronic character of the dithiocarbamate sulfur donor atoms which, affected by the nature of the metal ion, determines the strength of the binding to the electron-deficient fullerene guest species.

Another example of trimeric polymetallic architectures has been described by Stang and coworkers starting from bispyridyl-cavitand ligands and linear bimetallic precursors such as 1,4-[bis((PEt$_3$)$_2$Pt(NO$_3$))$_2$-benzene] and [4,4′-bis((PEt$_3$)$_2$Pt(NO$_3$))$_2$-biphenyl] in a CD$_3$NO$_2$/D$_2$O two-phase solvent system (Figure 7.10) [28]. The four nanoscopic metallacyclic cavitand complexes **39a–d** were characterized by a combination of NMR analysis and ESI mass spectrometry. In particular, the ^{31}P and ^{1}H NMR spectra of these assemblies suggest highly symmetrical architectures on the NMR timescale.

Atwood and coworkers developed a different strategy. They used calix[4]arenes and pyrogallol[4]arenes [48] directly as multidentate ligands, avoiding further functionalization of the macrocycles. By simply deprotonating the sulfonic and phenolic OHs, they obtained the corresponding chelating ligands, capable of complexing metal ions.

They described the formation of nanometer-scale spheres and tubules assembling *p*-sulfonatocalix[4]arene building blocks by the addition of pyridine-*N*-oxide and lanthanide ions [49]. Crystallographic studies revealed how metal ion coordination and substrate recognition direct the formation of these assemblies. In particular, from a 2 : 2 : 1 aqueous solution of *p*-sulfonatocalix[4]arene sodium salt, pyridine-*N*-oxide and La(NO$_3$)$_3$·6H$_2$O, spherical supermolecules form that contain 12 calixarene anions placed at the vertices of an icosahedron (Figure 7.11a). On the other hand, mixing the three components in a 2 : 8 : 1 molar ratio, tubular assemblies form which show a chiral helical assembly along the length of the tube.

In another article, the same group reported the formation of a large neutral hexameric pseudo-spherical coordination capsule assembled from 6 pyrogallol[4]-arene ligands and 24 Cu(II) metal ions [50]. A single-crystal X-ray analysis shows that the centroids of the six pyrogallol[4]arene ligands reside on the vertices of a hypothetical octahedron and enclose a cavity of 1200 Å^3. Amazingly, this coordination capsule is structurally analogous to its hydrogen-bonded counterpart (Figure 7.11b, c). These hydrogen-bonded assemblies function as a supramolecular blueprint during metal ion addition, preserving the desired structural framework in response to the interchange between the hydrogen-bonded networks for metal coordination. After the insertion of 24 Cu(II) metal ions, a combination of 96 Cu-O coordination bonds and 24 intramolecular hydrogen bonds binds the framework together.

A different neutral hexameric coordination cage structure was assembled from six either C-propyl- or C-pentyl-pyrogallol[4]arene units and 12 Ga(III) ions [51]. In both cases the centroids of the macrocyclic ligand components reside on the vertices of a squeezed octahedron enclosing a space of approximately 1150 Å^3. Only a total of 20

$6+$

$6\ NO_3^-$

39a R = C_5H_{11}, n = 1, L = PEt_3
39b R = C_5H_{11}, n = 2, L = PEt_3

$6+$

$6\ NO_3^-$

39c R = C_5H_{11}, n = 1, L = PEt_3
39d R = C_5H_{11}, n = 2, L = PEt_3
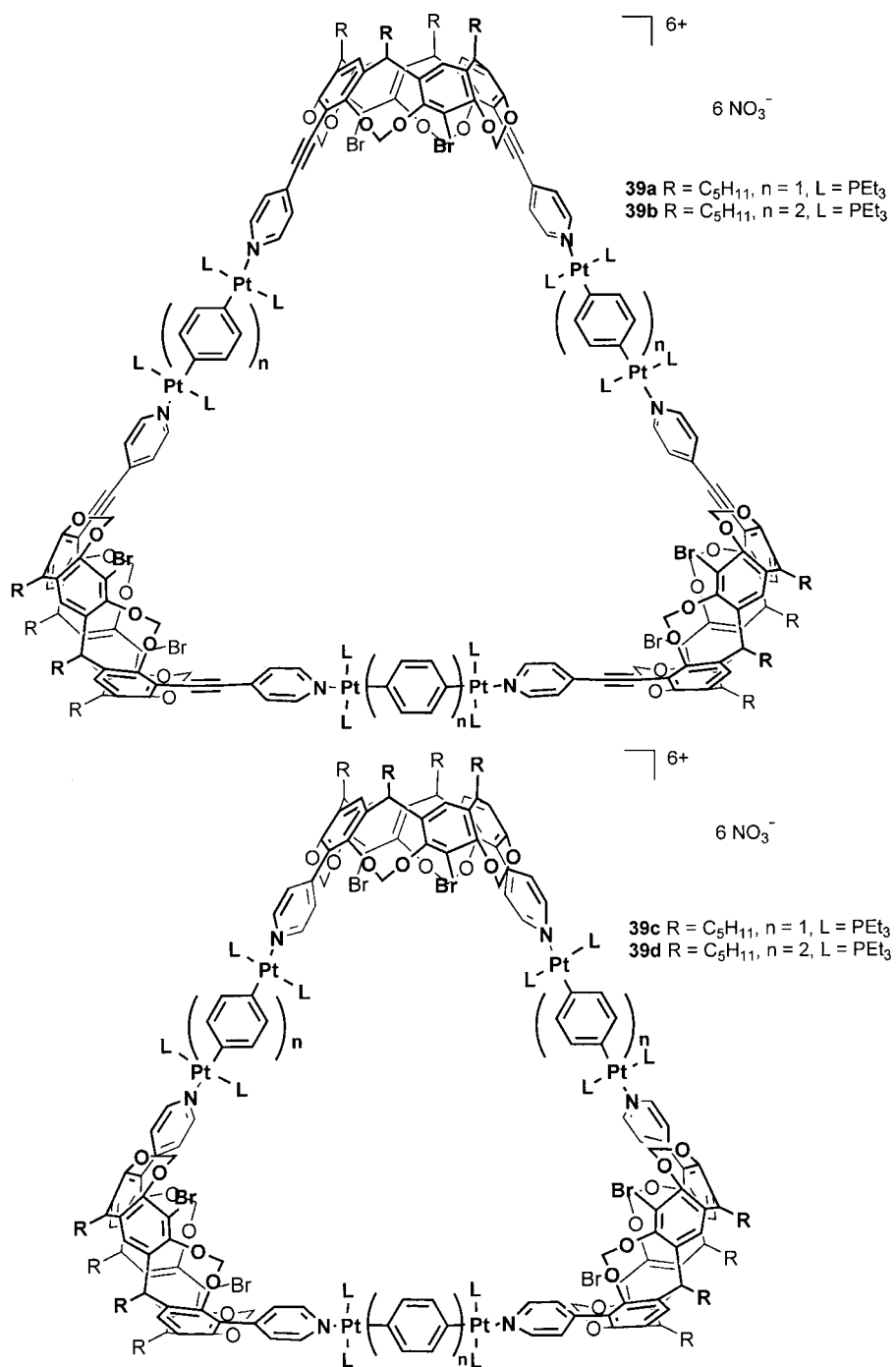
Figure 7.10 Trimeric assemblies of bispyridyl cavitand ligands **39a–d**.
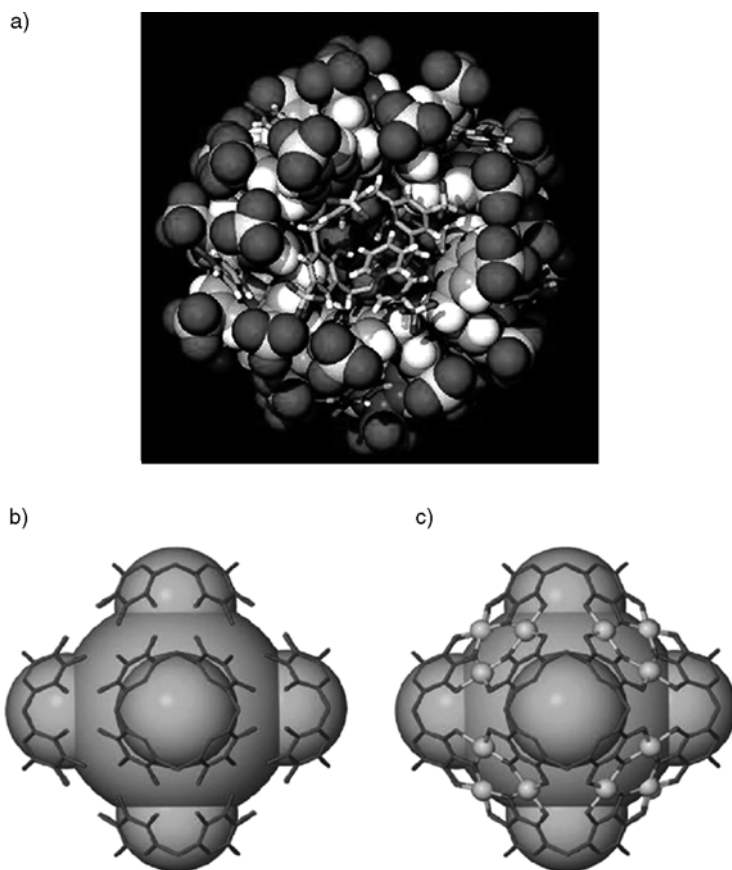
Figure 7.11 (a) Spherical assembly of sulfonatocalix[4]arene sodium salt; (b) hydrogen- and (c) metal-directed self-assembly of six pyrogallol[4]arenes. Reproduced with permission from Refs. [49,50].

intramolecular hydrogen bonds remain after insertion of gallium atoms which bind the framework together.

7.2.4
Self-assembly of Coordination Cages on Surfaces

The clean, precise, and reversible modification of surfaces represents an important opportunity to expand the application range of self-assembly. In particular, the thermodynamic control and reversibility of CSA can be exploited for the error-free generation of three-dimensional architectures directly on surfaces.

Our group, in collaboration with Reinhoudt and coworkers [52], has recently reported an intriguing example of the generation of coordination cages directly on surfaces by using self-assembled monolayers (SAMs) as molecular platforms. First,

41a M = Pd, R = C$_6$H$_{13}$, L = dppp
41b M = Pt, R = C$_6$H$_{13}$, L = dppp
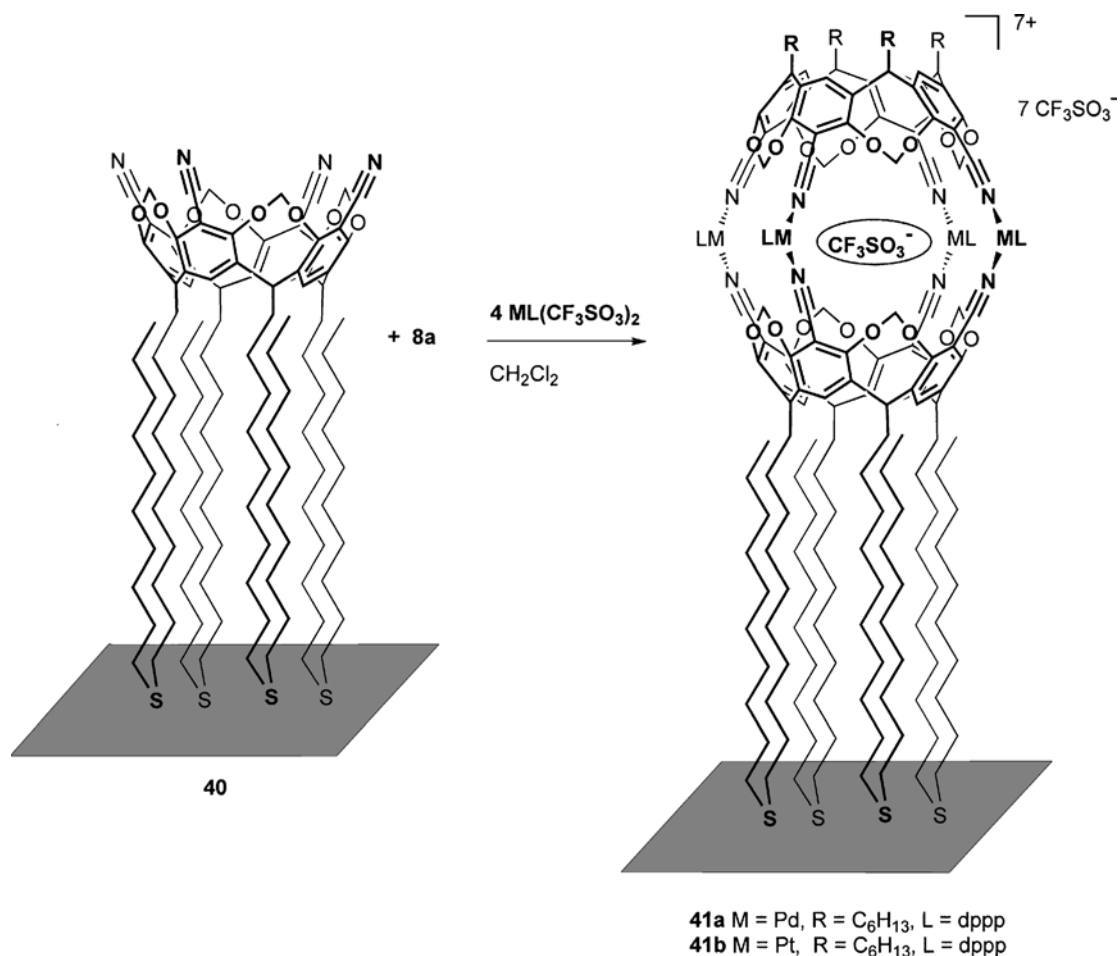
Scheme 7.11 Self-assembly leading to the formation of cages on gold.

monolayers of **40** were prepared by adsorption of the thioether chains on gold surfaces. The layers obtained were used to perform the metal-induced capping reactions directly on the SAMs through the addition of a solution of **8a** and [Pd(dppp)(CF$_3$SO$_3$)$_2$] (cage **41a**) in the first case or of **8a** and [Pt(dppp)(CF$_3$SO$_3$)$_2$] (cage **41b**) in the second case (Scheme 7.11). The formation of cages **41a,b** on SAMs was proved by contact-angle measurements, electrochemistry, X-ray photoelectron spectroscopy (XPS), and atomic force microscopy (AFM). A series of control experiments were performed in order to prove that the self-assembly of the cages occurs on the surface of the SAMs via metal coordination. Treatment of the SAM of **41a** with triethylamine shifted the equilibrium toward the formation of [Pd(dppp) (NEt$_3$)$_2$(CF$_3$SO$_3$)$_2$] plus uncomplexed cavitands. The complete disassembly of the cages on the SAM was shown by electrochemistry measurements. Formation of the
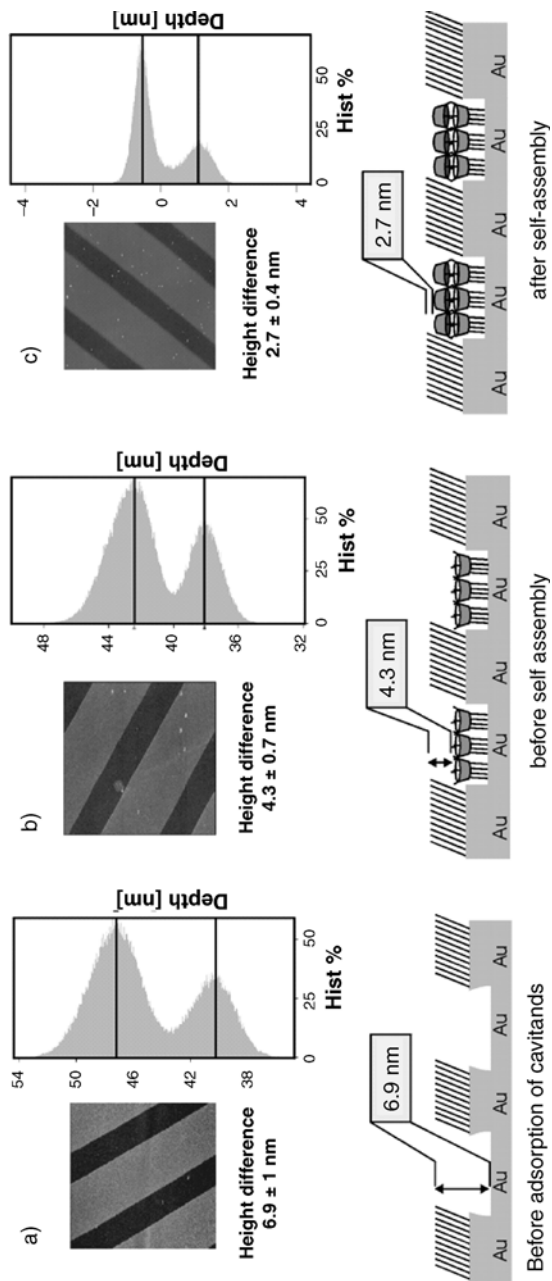
Figure 7.12 CSA on microcontact-printed surfaces. Reproduced with permission from Ref. [52].

42

43 R = R' = $C_{10}H_{20}SC_{10}H_{21}$
44 R = C_6H_{13}, R' = $C_{10}H_{20}SC_{10}H_{21}$
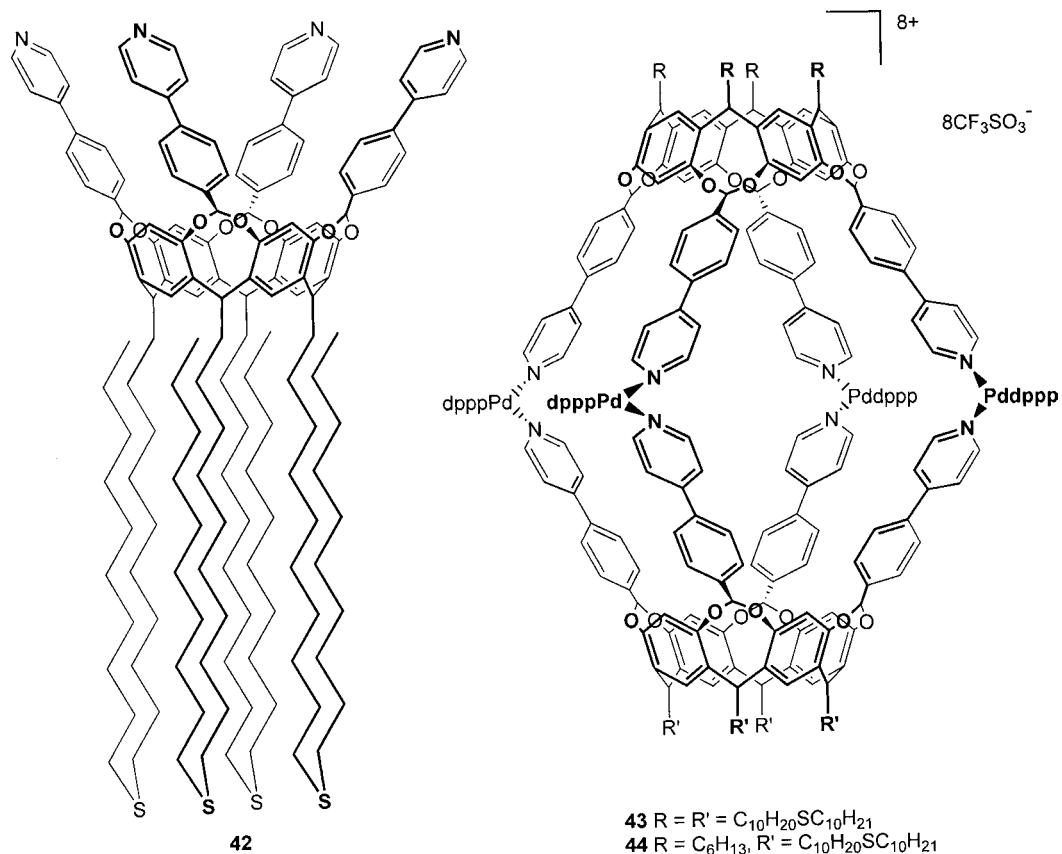
Figure 7.13 Thioether-functionalized cavitand ligand and the corresponding homocage **43** and heterocage **44**.

molecular cages was monitored directly by AFM. For this purpose, microcontact-printed templates were created using standard soft lithography methods [53]. These templates showed the presence of very regular features over large areas (Figure 7.12). Stripes with a lower height correspond to areas exposing bare gold, whilst stripes with a higher topographic profile are covered by the SAM of 11-mercaptoundecanol (Figure 7.12a). After deposition of a monolayer of cavitand **40** on the bare gold grooves, AFM was used to directly measure the differences in the height profile (Figure 7.12b). The height difference of 2.6 nm is consistent with the formation of a monolayer of **40**.

Self-assembly of the molecular cages on the printed layers was performed using the same procedure as for the full monolayers, leading to a total height difference of 4.2 nm from the bare gold grooves (Figure 7.12c), a value which is consistent with the calculated dimensions of the cage.

A different approach has been undertaken when highly ordered monolayers of cavitands do not form. This typically happens when the cross-sectional area of the
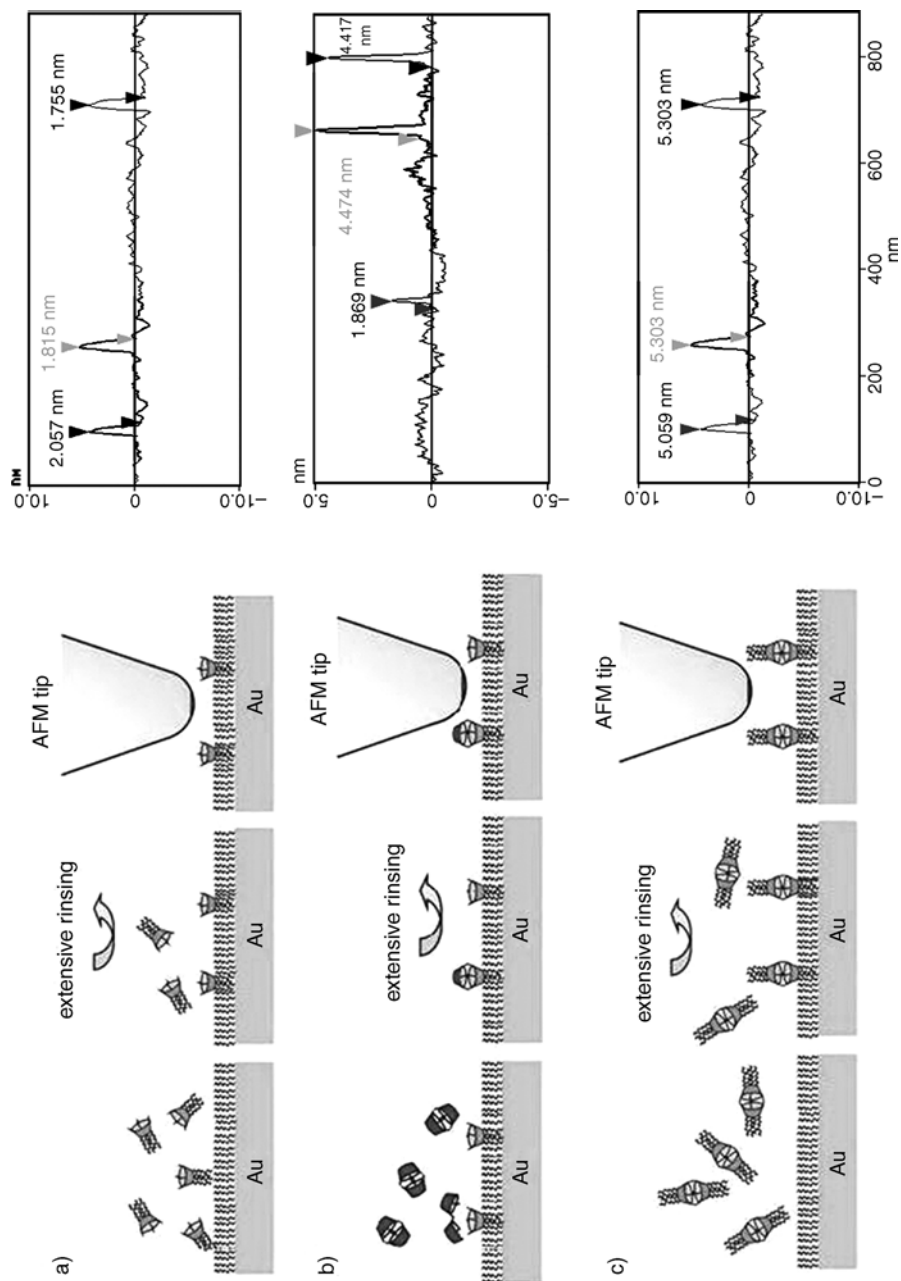
Figure 7.14 Schematic representation and AFM section analysis of a MU SAM with inserted cavitand **42** (a), heterocage **44** (b), and homocage **43** (c). Reproduced with permission from Ref. [54].
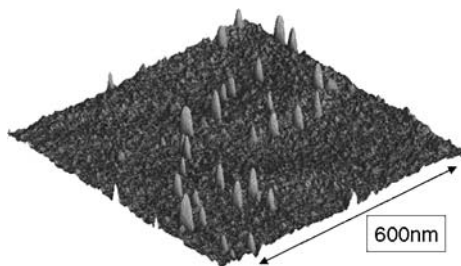
Figure 7.15 3D-AFM image of MU SAM with inserted homocage **43**.

cavitand head exceeds that of the underlying feet, as in the case of **42** (Figure 7.13) [54]. The CSA on disordered full SAMs of **42** do not work properly because of the interdigitation of the tolylpyridyl ligands. As an alternative, the insertion of cavitand **42** into a monolayer of 11-mercaptoundecanol (MU) was achieved by soaking SAMs of thiol in a 0.25-mM solution of **42** in dichloromethane. Extensive washing with large amounts of solvents guaranteed the removal of all physisorbed material. AFM experiments and profile analysis showed the presence of individual round entities which protrude from the flat by approximately 2 nm, which is the expected height difference between cavitand **42** and MU (Figure 7.14a). The next step was the assembly of the heterocage **44** by exposing the SAM of **42** in MU to a solution of cage **34e**, bearing hexyl tails at the lower rim. The formation of heterocage **44** on gold was thus obtained through ligand exchange. In this case, AFM analysis revealed the presence of two different protruding objects: (a) those with a height of about 4–5 nm, corresponding to the heterocage, and (b) those with a height of about 2 nm due to the presence of free cavitand ligands on gold (Figure 7.14b). The outcome of this analysis suggests that both uncapped cavitands and heterocages are present because the very dilute conditions employed do not allow a complete ligand exchange.

For the formation of coordination cages on gold, another strategy has been explored which leads to the insertion of preformed homocage **43** into a monolayer of MU. Homocage **43** has been directly inserted by soaking a clean MU SAM in a dichloromethane solution of the preformed cage for 1 h at room temperature (Figures 7.14c and 7.15). Extensive rinsing is necessary to ensure the removal of physisorbed material. AFM analysis showed the presence of objects protruding 5.1–5.3 nm from the MU SAM, in accordance with the expected protrusion length of the cages.

As in the previously described case of cyano-cages grafted on gold, a control experiment was carried out, consisting in the disassembly of cage **43** immobilized on gold. By exposing a gold substrate with inserted homocages to a solution of triethylamine, more than half of the cages were disassembled, as shown in the AFM analysis.

Another topic related to the self-assembly of coordination cages in the solid state has been described by Harrison and coworkers [55]. Octaanionic cages **30a** with four Ca^{2+} countercations form grids in the solid state and pack into porous materials resembling zeolites. The carboxylate groups on the four sides of cage **30a** can bind to more than one metal ion. In particular, the calcium ions coordinate with carboxylates from two
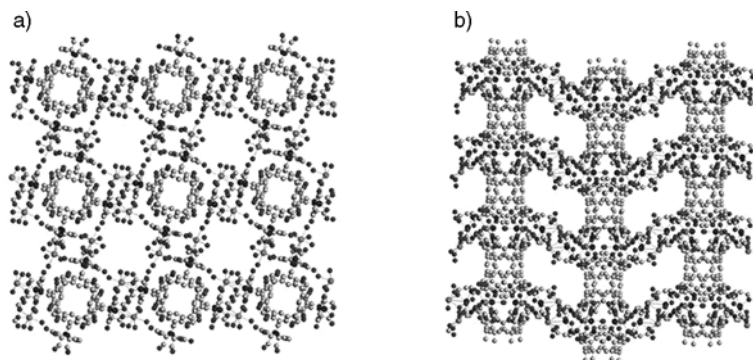
Figure 7.16 Structure of the Ca-assembled material: (a) top view and (b) side view. Reproduced with permission from Ref. [55b].

cages, creating a bridge between them. Thus, octaanionic **30a** arranges into sheets of cages linked together by Ca^{2+}. Voids are formed between neighboring cages, and water molecules bound to calcium ions surround them. Regarding the placement of the next layers, the cages of one layer are positioned above the cation bridges of another layer. The third layer lies directly over the first layer, creating an ABAB cage packing arrangement, and this results in the formation of rhombic pores of width 13 Å and length 21 Å. The channels connecting the pores lie between the layers (Figure 7.16). These pores and channels contain water, which can be removed by thermal desorption. In fact, when the temperature of the material is raised from 25 to 250°C, a total weight loss of 20% is observed, corresponding to a 40 : 1 water-to-cage molar ratio in the pristine material. After releasing water, this material is able to regain the amount of water that was lost by cooling in the presence of a stream of water vapor.

Moreover, pore and channel size and shape can be tuned by using different alkaline-earth cations (Mg^{2+}, Ca^{2+}, Sr^{2+}, Ba^{2+}) having different sizes and coordination numbers. The heat of water adsorption ranges from -46 to $-52 \, kJ \, mol^{-1}$, values similar to those of silica-containing zeolites. As recently reported, the properties of these materials can be further differentiated through the incorporation of transition (i.e. Co^{2+}) or alkaline cations (i.e. K^+) into the channels of barium-linked materials composed of metal-assembled cages.

7.2.5
Self-assembly of Multitopic Macrocyclic Complexes

While the design and formation of self-assembled coordination cages described in the previous sections have received much attention, the corresponding metal-directed self-assembly of open multitopic receptors has been almost neglected so far. One reason is related to the need for partially derivatized precursors, which are synthetically more demanding than the corresponding fully derivatized ones.

The first approach to the formation of a ditopic cavitand complex has been reported by Sorrell *et al.* [56]. They identified the tri-bridged resorcinarene as a

45a: M = Cu(II)

45b: M = Cu(II)
45c: M = Zn(II)
45d: M = Co(II)

45e: M = Ni(II)

45a
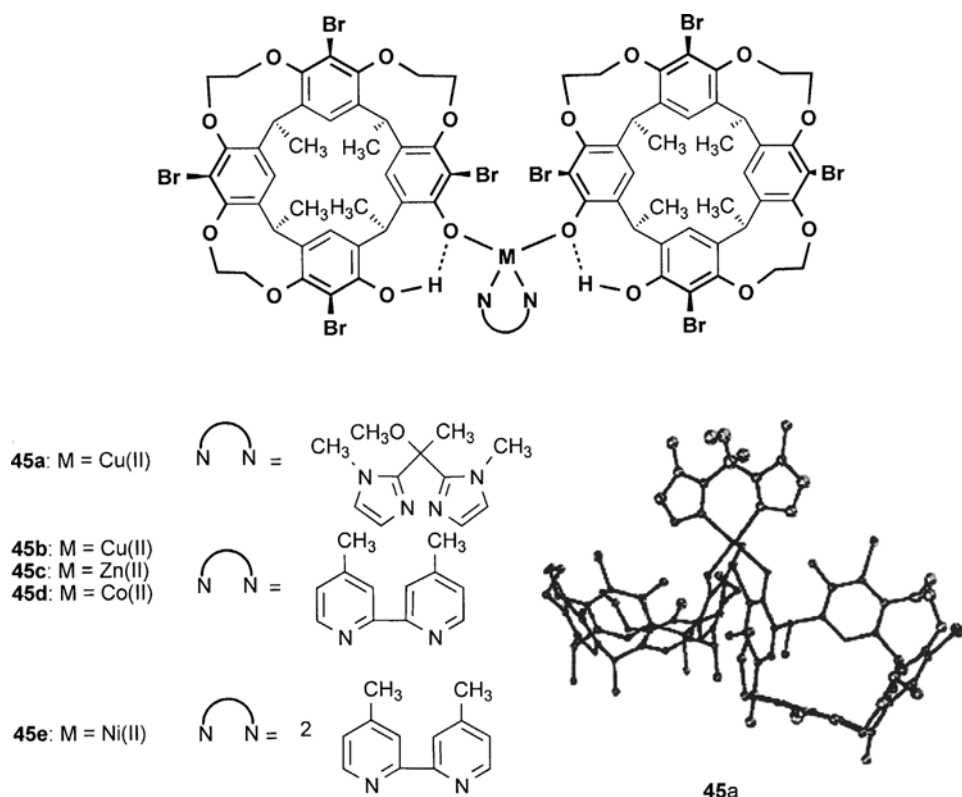
Figure 7.17 *Cis*-ditopic resorcinarene complexes **45a–e** and the molecular structure of complex **45a**. Reproduced with permission from Ref. [56].

46a: R= $C_{11}H_{23}$
46b: R= C_2H_5
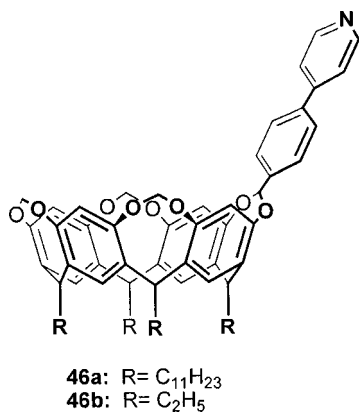
Figure 7.18 Tolylpyridyl monodentate cavitand ligand **46**.
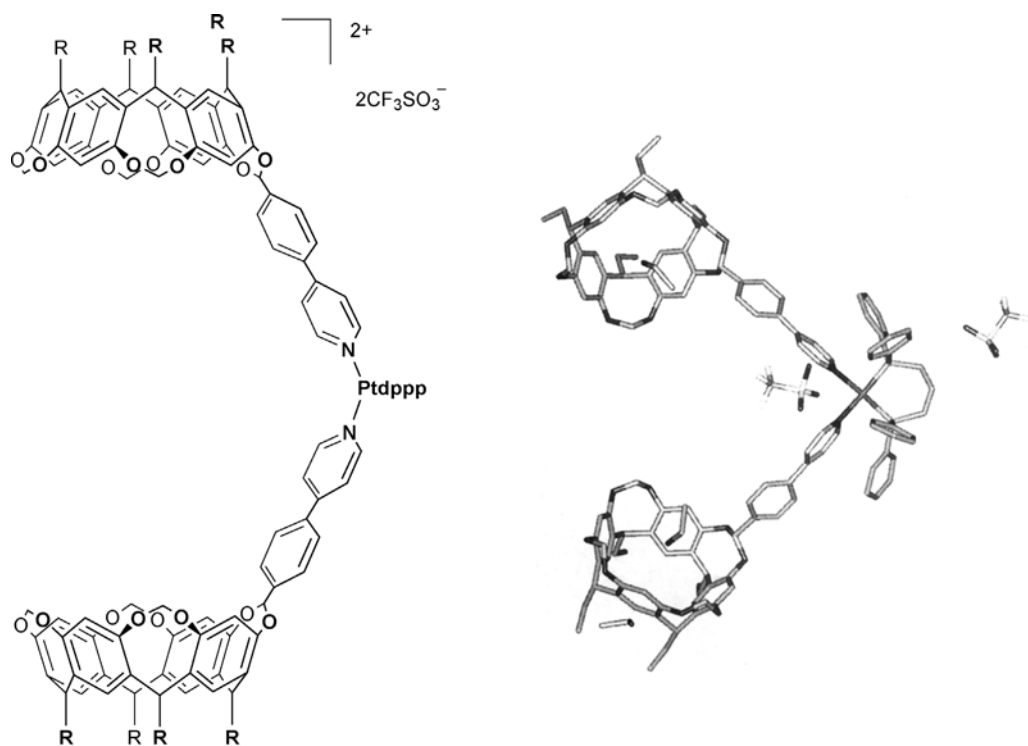
Figure 7.19 *Cis*-ditopic cavitand complex **47** and its crystal structure (side view). Reproduced with permission from Ref. [57].

suitable monodentate ligand in its monodeprotonated form. Two of these macrocyclic monodentate ligands have been linked using M(II) metal precursors having bipyridines or bisimidazoles as chelating ligands (Figure 7.17). In the case of copper complex **45a**, the crystal structure revealed that the two macrocycles are not facing each other, but rather lie side by side, ruling out any possibility of cooperative guest binding.

More recently our group has tackled this problem in a different way [57]. The starting point was again a tri-bridged resorcinarene, in which the last pair of free OHs has been used to introduce a single pyridine (not shown) or tolylpyridyl ligand (**46a,b** in Figure 7.18) as bridging unit. These monodentate cavitands are versatile ligands for the formation of ditopic and tetratopic complexes either charged or neutral. The formation of charged ditopic complexes with the two cavities facing each other is straightforward, employing the same metal precursors and conditions used in the CSA protocols (see for example complex **47** in Figure 7.19 where [Pt (dppp)(CF$_3$SO$_3$)$_2$] has been used).

48: R= C₂H₅
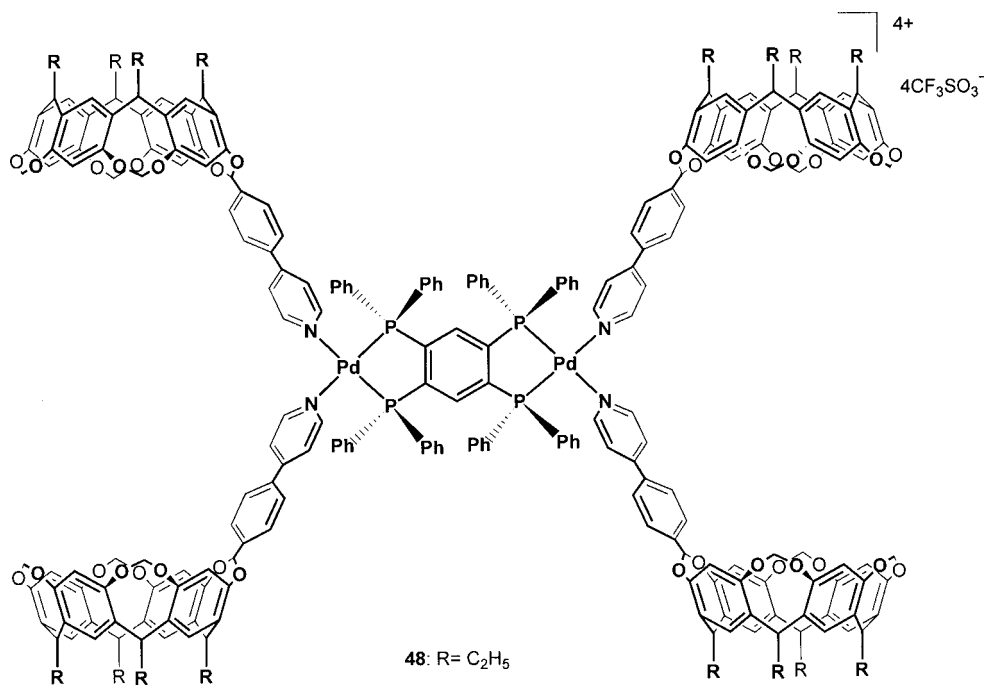
Figure 7.20 Tetratopic cavitand complex **48**.

49: R= C₂H₅
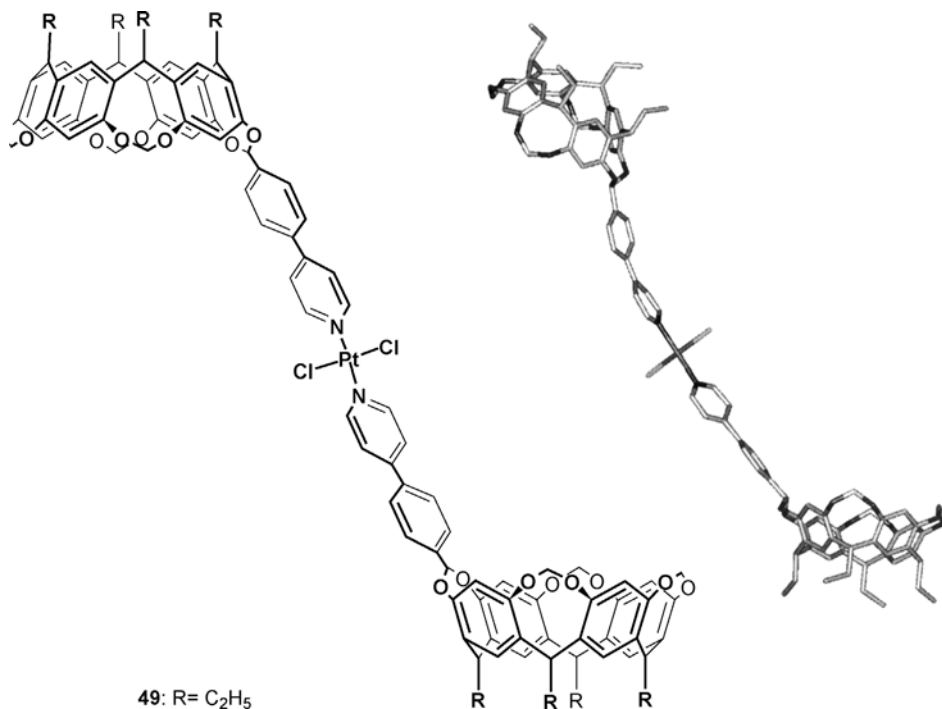
Figure 7.21 *Trans*-ditopic cavitand complex **49** and its molecular structure as determined by X-ray crystallography (side view). Reproduced with permission from Ref. [57].

R = C₂H₅
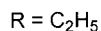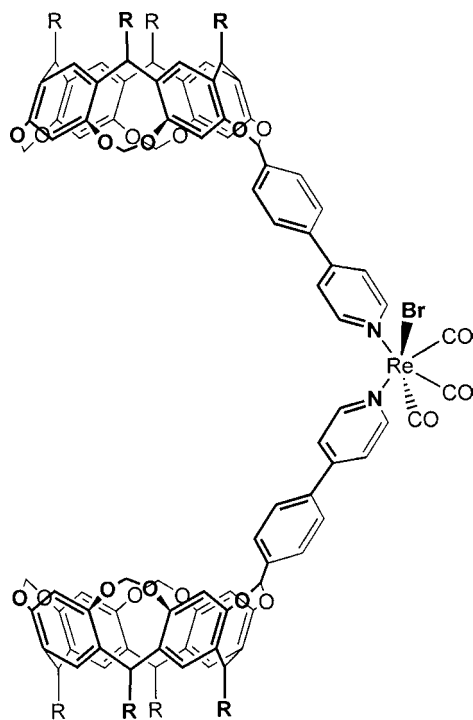
50

Figure 7.22 *Cis*-ditopic neutral cavitand complex **50**.

Using [Pd₂(tppb)(CF₃SO₃)₄] as a dinuclear metal precursor, the corresponding tetratopic complex **48** was assembled in quantitative yields (Figure 7.20). The only drawback of such complexes is related to their limited kinetic stability in solution, which can hamper their use as multitopic receptors, particularly for charged guests that increase the ionic strength of the medium.

We therefore turned our attention to the self-assembly of neutral complexes, which are kinetically stable in solution, starting from the same cavitand ligands [57]. The use of *cis*-[Pt(CH₃CN)₂Cl₂] and *cis*-[Pt(DMSO)₂Cl₂] as metal precursors led to the formation of the trans complex **49** in both cases (Figure 7.21). The unexpected stereochemistry of the final product is the result of the cis-to-trans isomerization of the intermediate monofunctionalized complexes.

To overcome this problem we switched to [Re(CO)₅Br] as the metal precursor, because it is one of the few octahedral complexes that undergoes an exclusive cis ligand exchange, because of the remarkable trans effect of the carbonyl ligands. The replacement of two equatorial *cis*-CO groups gave the desired neutral

52
Tetratopic complex
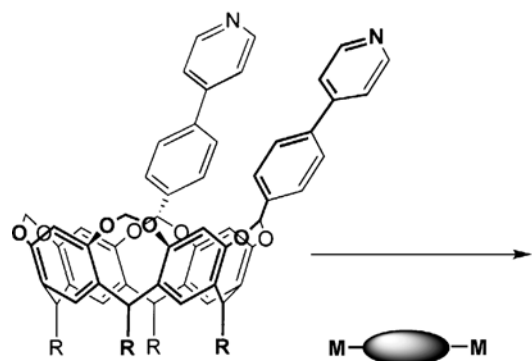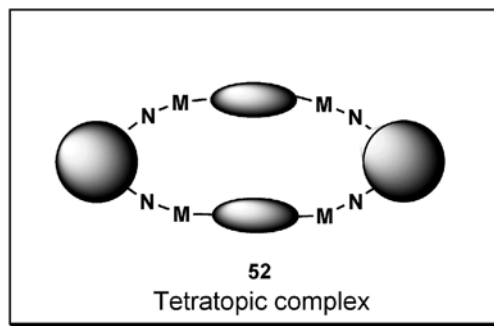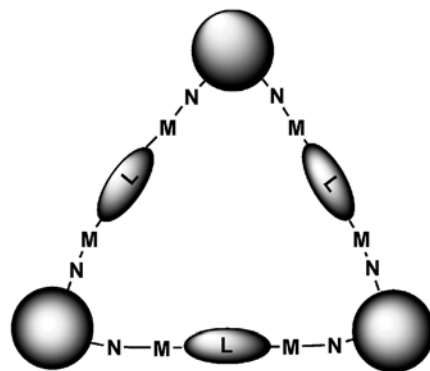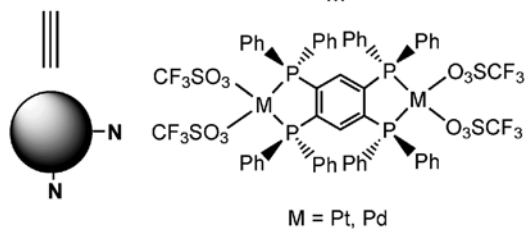
Hexatopic complex
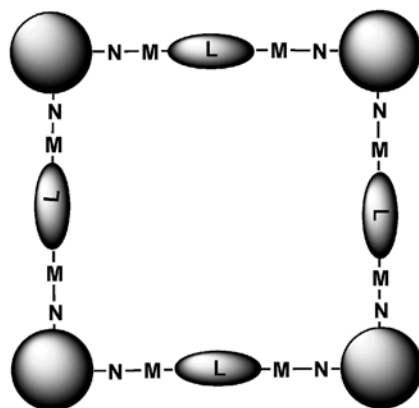
Octatopic complex

51: R = C₂H₅

M = Pt, Pd

Scheme 7.12 Self-assembly of tetratopic Pd/Pt complex **52** and the other two possible cyclic structures. In the top views sketched in the scheme each sphere corresponds to two cavitands, one over the other.
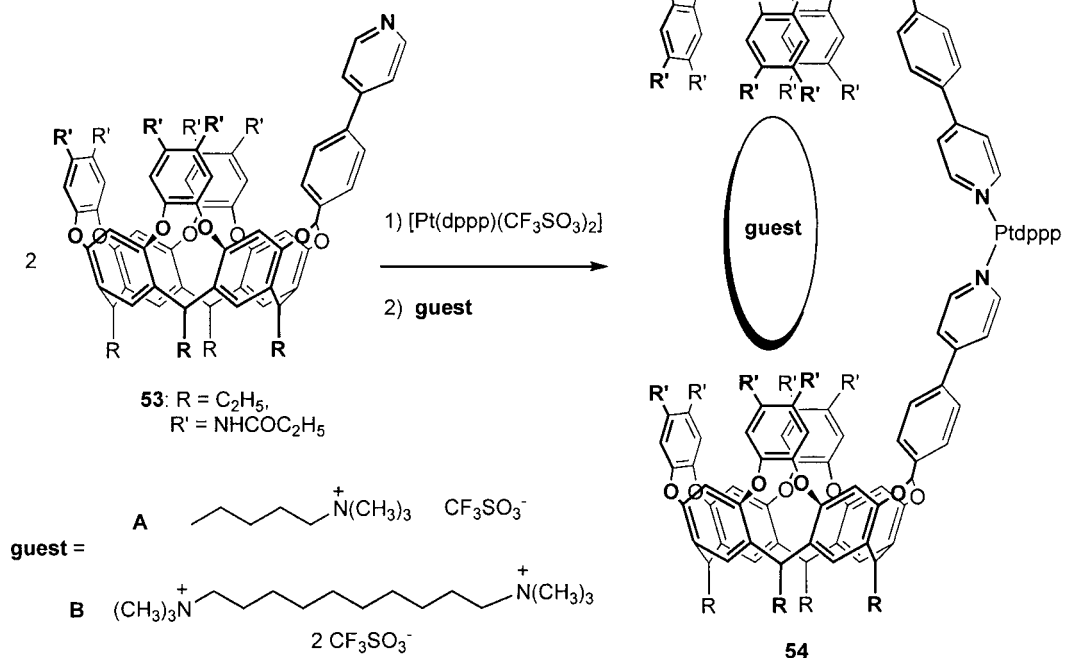
Scheme 7.13 Self-assembly of ditopic container **54** and inclusion of guests (alkylammonium salts).

fac-[(CO)₃**46b₂**Br] ditopic complex **50** (Figure 7.22). This last protocol was found to be the best one for the generation of kinetically inert, ditopic receptors.

In Section 7.2.2 the self-assembly of bidentate **AC** cavitand **35** using [Re(CO)₅Br] as the metal precursor to obtain the dimeric capsule **36** was described. The corresponding AB bidentate cavitand **51** has been reacted with dinuclear metal precursors [M₂(tppb)(CF₃SO₃)₄] (M = Pt, Pd) by mixing the two building blocks in a 2 : 1 ratio [45]. At this level of complexity, the self-assembly can lead to three possible cyclic structures (tetratopic, hexatopic, and octatopic cavitand complexes, Scheme 7.12). Out of them, only the entropically favored tetratopic complex **52** forms, as predicted by molecular modeling and demonstrated by PGSE NMR and ESI-MS experiments.

The potential of ditopic cavitand complexes to bind ditopic guests has been demonstrated by Rebek and coworkers using cavitand **53** as monodentate ligand (Scheme 7.13) [58]. Cavitand **53** combines the advantages of a deep vase-like cavity obtained through a network of hydrogen bonds and the presence of a tolylpyridyl group able to coordinate to the metal center. The ditopic complex **54** forms quanti-
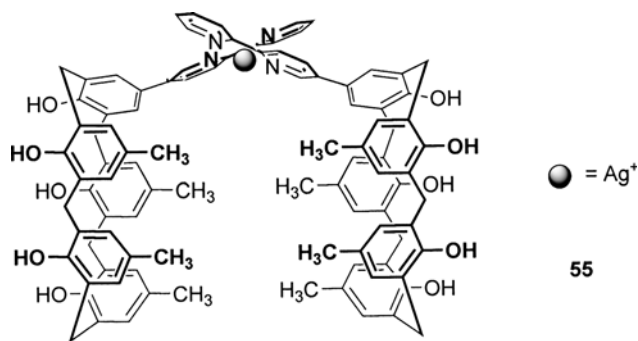
Figure 7.23 Calix[5]arene ditopic receptor **55**.

tatively by combining **53** and [Pt(dppp)(CF$_3$SO$_3$)$_2$] in a 2 : 1 ratio; it has nanoscale dimensions and is able to reversibly bind alkylammonium guests. The presence of two receptors facing each other has a twofold effect:

1. Reduction of the exchange rate of the alkyldiammonium guest **B** compared to the alkylammonium **A**
2. The inclusion of **B** takes place with a positive cooperative effect gained from the preorganization of the host **54**.

An interesting example of a self-assembled ditopic receptor (**55**) has been developed by Fukazawa and coworkers starting from two calix[5]arenes with bipyridine units at the upper rim (Figure 7.23) [59]. In a previous article, the same authors

56a: R = C$_{11}$H$_{23}$
56b: R = C$_5$H$_{11}$

57a: R = C$_{11}$H$_{23}$
57b: R = C$_5$H$_{11}$
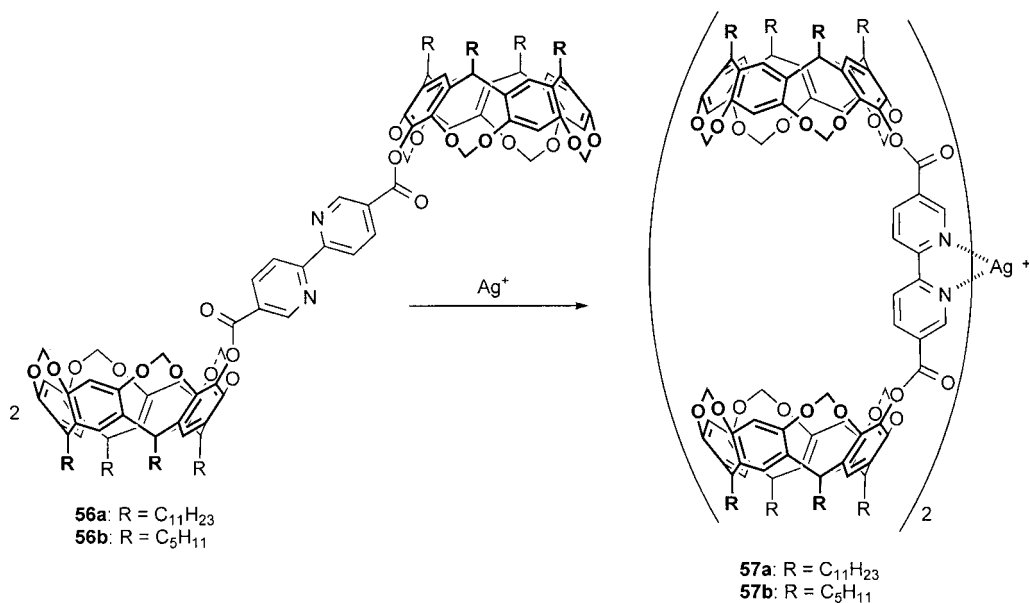
Figure 7.24 2,2′-bipyridine-bridged biscavitand **56** and its Ag$^+$ complex **57**.

reported that the covalent linking of two calix[5]arene units brings strong binding to C_{60} and C_{70} within the cavity formed by the two calixarene scaffolds [60]. Also, in this case, metal-directed self-assembly through the addition of 0.5 equivalents of Ag^+ leads to the formation of the ditopic receptor **55** capable of forming a 1 : 1 inclusion complex with fullerene molecules (C_{60} and C_{70}).

Examples of ditopic and tetratopic macrocycles have been described by Stang and coworkers by combining the calixarene chemistry with the metal-directed self-assembly of molecular squares [61]. In this case the calixarene units coordinate to the Pt through their $P(Ph)_2$ ligands at the lower rim and assume a diverging spatial orientation in the macrocycle. These calixarene metallamacrocycles are used in transport experiments to carry sulfonate salts from one aqueous phase into another through chloroform.

Allosteric behavior in a ditopic cavitand receptor has been induced via metal coordination [62]. Addition of Ag^+ ions to a solution of a 2,2′-bipyridine-bridged biscavitand **56** switches the molecule from an S-shaped to a C-shaped conformation with the two cavities facing each other. At the same time two bis-cavitand molecules are brought together to give an overall tetratopic complex **57** (Figure 7.24).

7.3
Conclusion

The stimulus behind the rapid development of molecular containers is their potential application as molecular devices. The metal-directed assembly of synthetic macrocycles represents a valuable tool for the generation of such container molecules avoiding the problems related to the synthesis of their purely organic counterparts, which often is time consuming and leads to the formation of kinetically distributed products. The results described in this chapter demonstrate the vast and almost unlimited possibilities of creating new molecular architectures constructed in simple self-assembly processes starting from calixarene and cavitand scaffolds. The final shape of the metal-directed nanoscopic structures is defined by two main factors: (a) the rational design of the macrocyclic building blocks through the correct orientation of their ligand groups, and (b) the accurate choice of the metal center and its coordination geometry. In this way the metal-directed self-assembly of the two components produces architectures having predefined and predictable shapes and sizes in quantitative yields under mild conditions.

Among the several challenges and opportunities looming ahead, in our opinion two are worth pursuing. One is the self-assembly of coordination cages endowed with molecular recognition properties determined by specific interactions and not by hydrophobic or shape-driven inclusion. This requires the decoration of the inner space of the coordination cages with suitable functional groups, which must be spatially organized and inert toward metal coordination. The other challenge concerns the extension of the self-assembly protocol to technologically interesting surfaces, like silicon, in order to build hybrid inorganic-organic structures featuring selective inclusion and other useful properties. The generation of such complex

organic architectures on silicon will be pivotal in developing new integrated devices presenting peculiar optical, magnetic, and sensing properties.

7.4
Experimental: Selected Procedures

7.4.1
Tetrapicolyl-bridged Cavitand 31a

(This synthetic approach has been applied for the synthesis of cavitand **31b** from the corresponding CH_2CH_2Ph-footed resorcinarene.)

   A mixture of undecyl-footed resorcinarene (0.707 g, 0.64 mmol), K_2CO_3 (1.06 g, 7.67 mmol), and 4-(dibromomethyl)pyridine [40] (1.61 g, 6.40 mmol) in 30 mL of dry *N,N*-dimethylacetamide (DMA) was stirred in a sealed tube at 80 °C for 15 h. The reaction mixture was then cooled, poured into a saturated Na_2CO_3 solution, and extracted with CH_2Cl_2. Removal of the CH_2Cl_2 gave a black solid that was purified in two steps: first by column chromatography (SiO_2, CH_2Cl_2/EtOH from 9 : 1 to 1 : 1), then on silica gel plates (CH_2Cl_2/EtOH 9 : 1) to give 90 mg (0.06 mmol) of cavitand **31a** (yield 10%).

7.4.2
Tetracyano Cavitand 40

(This synthetic approach has been applied for the synthesis of cavitands **8a–c** from the corresponding tetrabromo derivatives.)

   Cavitand **40** was prepared from the corresponding tetrabromo derivative [63]. A mixture of tetrabromo cavitand (1.8 g, 0.865 mmol) and of CuCN (0.767 g, 8.56 mmol) in NMP was refluxed for 24 h at 200 °C. After cooling, a mixture of $FeCl_3 \cdot 6H_2O$ (2.32 g, 8.58 mmol) and 1 N HCl (8.5 mL, 8.5 mmol) was added, and the rection mixture was heated to 75°C for 30 min. After cooling, the solvent was evaporated, and the residue was dissolved in dichloromethane and washed with NH_4Cl, brine, and H_2O, three times each respectively. The organic phase was dried with $MgSO_4$ and subsequently concentrated under reduced pressure. Purification was performed via column chromatography (SiO_2: hexane/ethyl acetate 7 : 1). After recrystallization from methanol, **40** (1.1 g, 0.588 mmol) was obtained as a white solid (yield 68%).

7.4.3
AC-dibridged Tolylpyridyl Cavitand 35

(This synthetic approach has been applied for the synthesis of AB-dibridged tolylpyridyl cavitand **51** from the corresponding AB-dimethylene-bridged resorcinarene.)

   4-(α,α-Dibromotolyl)pyridine (0.3 g, 0.92 mmol) and K_2CO_3 (0.35 g, 2.5 mmol) were added under nitrogen to a solution of the corresponding AC-dimethylene-bridged resorcinarene (0.19 g, 0.31 mmol) [45] in dry DMA (*N,N*-dimethylaceta-

mide, 15 mL). The mixture was stirred in a sealed tube at 80 °C for 16 h. The reaction was quenched by addition of 10 mL water, and the resulting mixture was extracted with 15 mL CH$_2$Cl$_2$. The organic layer was washed with water (3 × 15 mL), dried over Na$_2$SO$_4$, and evaporated. The material obtained was purified by column chromatography (SiO$_2$: hexane/acetone/EtOH 7 : 2 : 1) to give cavitand **35** (0.12 g, 0.13 mmol, *out-out* isomer) as a white solid (yield 42%).

7.4.4
fac-Br(CO)$_3$Re AC Ditopic Cavitand Complex 36

Cavitand **35** (41 mg, 4.29 × 10^{-2} mmol) was added to a solution of [Re(CO)$_5$Br] (14.0 mg, 3.43 × 10^{-2} mmol) in CHCl$_3$ and heated at reflux for 24 h. After solvent evaporation, the product was purified by column chromatography (SiO$_2$: CHCl$_3$/ethyl acetate 6 : 4) to give the *fac*-ditopic cavitand complex **36** (30 mg, 6.9 × 10^{-3} mmol, yield 40%).

7.4.5
Tetratopic Cavitand Complex 48

Tetratopic cavitand complex **48** was assembled by mixing cavitand **46b** with the dinuclear complex [Pd$_2$(tppb)(CF$_3$SO$_3$)$_4$] [57] in a 4 : 1 molar ratio at room temperature in 10 mL of a CHCl$_3$/CH$_3$NO$_2$/CH$_3$CN 7 : 2 : 1 mixture. After stirring for 15 min, the desired complex **48** was obtained in quantitative yield after removal of the solvent under vacuum.

Acknowledgments

Abbreviations

dppp	1,3-bis(diphenylphosphino)propane
dppb	1,4-bis(diphenylphosphino)butane
DABCO	1,4-diazabicyclo[2.2.2]octane
DaniF	*N,N′*-di-*p*-anisylformamidinate
CSA	cage self-assembly
en	ethylenediamine
bpa	bis(2-pyridylmethyl)amine
SSI MS	sonic spray mass spectrometry
dtc	dithiocarbamate

SAM   self-assembled monolayer
XPS   X-ray photoelectron spectroscopy
AFM   atomic force microscopy
MU   11-mercaptoundecanol
tppb   1,2,4,5-tetrakis(diphenylphosphino)benzene
oooo   out,out,out,out (the four ligands point outward)
DMSO   dimethyl sulfoxide
acac   acetylacetonate
py   pyridine
NMP   1-methyl-2-pyrrolidinone
DMA   *N,N*-dimethylacetamide
MALDI-TOF   matrix assisted laser desorption ionization-time-of-flight mass
             spectrometry
ESI   electrospray ionization mass spectrometry

References

1 Gutsche, C.D. (1989) *Calixarenes*, Royal Society of Chemistry, Cambridge.

2 Cram, D.J. and Cram, J.M. (1994) *Container Molecules and Their Guests*, Royal Society of Chemistry, London.

3 Rebek, J., Jr. (1990) *Angew. Chem.*, **102**, 261–272; *Angew. Chem. Int. Ed.*, **29**, 245–255.

4 Collet, A., (Eds. J.L. Atwood , J.E.D. Davis , D.D. MacNicol and F. Vögtle) (1996) *Comprehensive Supramolecular Chemistry, Vol. 2*, Pergamon, Oxford, pp.325–365.

5 (a) Conn, M.M. and Rebek, J., Jr. (1997) *Chem. Rev.*, **97**, 1647–1668. (b) for the use of ionic interactions in the self-assembly of molecular containers see: Corbellini, F., Fiammengo, R., Timmerman, P., Crego-Calama, M., Versluis, K., Heck, A.J.R., Luyten, I. and Reinhoudt, D.N. (2002) *J. Am. Chem. Soc.*, **124**, 6569–6575.

6 Leininger, S., Olenyuk, B. and Stang, P. J. (2000) *Chem. Rev.*, **100**, 853–908.

7 Gibb, C.L.D. and Gibb, B.C. (2004) *J. Am. Chem. Soc.*, **126**, 11408–11409.

8 For two selected examples see: (a) Chen, J., Körner, S., Craig, S.L., Rudkevich, D. M. and Rebek, J., Jr. (2002) *Nature*, **415**, 385–386. (b) Koblenz, T.S., Dekker, H.L., de Koster, C.G., van Leeuwen, P.W.N.M. and Reek, J.N.H. (2006) *Chem. Commun.*, 1700–1702.

9 Rudkevich, D.M. (2004) *Angew. Chem.*, **116**, 568–581. *Angew. Chem. Int. Ed.*, **43**, 558–571.

10 Hof, F., Craig, S.L., Nuckolls, C. and Rebek, J., Jr. (2002) *Angew. Chem.*, **114**, 1556–1578. *Angew. Chem. Int. Ed.*, **41**, 1489–1508.

11 Warmuth, R. (2001) *Eur. J. Org. Chem.*, 423–437.

12 For the few examples of controlled guest delivery from hemicarceplexes see: (a) Piatnitski, E.L. and Deshayes, K.D. (1998) *Angew. Chem.*, **110**, 1022–1024. (1998) *Angew. Chem. Int. Ed.*, **37**, 970–972. (b) Ro, S., Rowan, S.J., Pease, A.R., Cram, D.J. and Stoddart, J.F. (2000) *Org. Lett.*, **2**, 2411–2414.

13 Rudkevich, D.M. (2002) *Bull. Chem. Soc. Jpn.*, **75**, 393–413.

14 Service, R.F. (2002) *Science*, **295**, 2398–2399.

15 Fujimoto, K. and Shinkai, S. (1994) *Tetrahedron Lett.*, **35**, 2915–2918.

16 Ikeda, A., Yoshimura, M., Tani, F., Naruta, Y. and Shinkai, S. (1998) *Chem. Lett.*, 587–588.

17 Ikeda, A., Yoshimura, M., Udzu, H., Fukuhara, C. and Shinkai, S. (1999) *J. Am. Chem. Soc.*, **121**, 4296–4297.

18 Ikeda, A., Udzu, H., Yoshimura, M. and Shinkai, S. (2000) *Tetrahedron*, **56**, 1825–1832.

19 Zhong, Z., Ikeda, A., Ayabe, M., Shinkai, S., Sakamoto, S. and Yamaguchi, K. (2001) *J. Org. Chem.*, **66**, 1002–1008.

20 Baldini, L., Ballester, P., Casnati, A., Gomila, R.M., Hunter, C.A., Sansone, F. and Ungaro, R. (2003) *J. Am. Chem. Soc.*, **125**, 14181–14189.

21 Cotton, F.A., Lei, P., Lin, C., Murillo, C.A., Wang, X., Yu, S.-Y. and Zhang, Z.-X. (2004) *J. Am. Chem. Soc.*, **126**, 1518–1525.

22 Jacopozzi, P. and Dalcanale, E. (1997) *Angew. Chem.*, **109**, 665–667. *Angew. Chem. Int. Ed.*, **36**, 613–615.

23 Fochi, F., Jacopozzi, P., Wegelius, E., Rissanen, K., Cozzini, P., Marastoni, E., Fisicaro, E., Fokkens, R. and Dalcanale, E. (2001) *J. Am. Chem. Soc.*, **123**, 7539–7552.

24 Zuccaccia, D., Pirondini, L., Pinalli, R., Dalcanale, E. and Macchioni, A. (2005) *J. Am. Chem. Soc.*, **127**, 7025–7032.

25 Cuminetti, N., Ebbing, M.H.K., Prados, P., de Mendoza, J. and Dalcanale, E. (2001) *Tetrahedron Lett.*, **42**, 527–530.

26 Kobayashi, K., Yamada, Y., Yamanaka, M., Sei, Y. and Yamaguchi, K. (2004) *J. Am. Chem. Soc.*, **126**, 13896–13897.

27 Yamanaka, M., Yamada, Y., Sei, Y., Yamaguchi, K. and Kobayashi, K. (2006) *J. Am. Chem. Soc.*, **128**, 1531–1539.

28 Jude, H., Sinclair, D.J., Das, N., Sherburn, M.S. and Stang, P.J. (2006) *J. Org. Chem.*, **71**, 4155–4163.

29 Park, S.J. and Hong, J.-I. (2001) *Chem. Commun.*, 1554–1555.

30 Park, S.J., Shin, D.M., Sakamoto, S., Yamaguchi, K., Chung, Y.K., Lah, M.S. and Hong, J.-I. (2005) *Chem. Eur. J.*, **11**, 235–241.

31 Park, S.J., Shin, D.M., Sakamoto, S., Yamaguchi, K., Chung, Y.K., Lah, M.S. and Hong, J.-I. (2003) *Chem. Commun.*, 998–999.

32 Haino, T., Kobayashi, M., Chikaraishi, M. and Fukazawa, Y. (2005) *Chem. Commun.*, 2321–2323.

33 Haino, T., Kobayashi, M. and Fukazawa, Y. (2006) *Chem. Eur. J.*, **12**, 3310–3319.

34 Fox, O.D., Dalley, N.K. and Harrison, R.G. (1998) *J. Am. Chem. Soc.*, **120**, 7111–7112.

35 Fox, O.D., Leung, J.F.-Y., Hunter, J.M., Dalley, N.K. and Harrison, R.G. (2000) *Inorg. Chem.*, **39**, 783–790.

36 Harrison, R.G., Burrows, J.L. and Hansen, L.D. (2005) *Chem. Eur. J.*, **11**, 5881–5888.

37 Fox, O.D., Dalley, N.K. and Harrison, R.G. (1999) *Inorg. Chem.*, **38**, 5860–5863.

38 Gardner, J.S., Harrison, R.G., Lamb, J.D. and Dearden, D.V. (2006) *New J. Chem.*, **30**, 1276–1282.

39 Xi, H., Gibb, C.L.D., Stevens, E.D. and Gibb, B.C. (1998) *Chem. Commun.*, 1743–1744.

40 Pirondini, L., Bertolini, F., Cantadori, B., Ugozzoli, F., Massera, C. and Dalcanale, E. (2002) *Proc. Natl. Acad. Sci. U. S. A.*, **99**, 4911–4915.

41 (a) Pirondini, L. and Dalcanale, E. (2004) Dekker Encyclopedia of Nanoscience and Nanotechnology 3415–3430. (b) Pirondini, L., Bonifazi, D., Cantadori, B., Braiuca, P., Campagnolo, M., De Zorzi, R., Geremia, S., Diederich, F. and Dalcanale, E. (2006) *Tetrahedron*, **62**, 2008–2015.

42 Bowden, N., Terfort, A., Carbeck, J. and Whitesides, G.M. (1997) *Science*, **276**, 233–235.

43 Dynamic interconversion of similar square-planar Pd(II) complexes with pyridyl cycloveratrylenes has been shown by Shinkai *et al.* to occur at room temperature: Zhong, Z., Ikeda, A., Shinkai, S., Sakamoto, S. and Yamaguchi, K. (2001) *Org. Lett.*, **3**, 1085–1087.

44 Pinalli, R., Cristini, V., Sottili, V., Geremia, S., Campagnolo, M., Caneschi,

A. and Dalcalane, E. (2004) *J. Am. Chem. Soc.*, **126**, 6516–6517.

45 Menozzi, E., Busi, M., Massera, C., Ugozzoli, F., Zuccaccia, D., Macchioni, A. and Dalcanale, E. (2006) *J. Org. Chem.*, **71**, 2617–2624.

46 Bibal, B., Tinant, B., Declercq, J.-P. and Dutasta, J.-P. (2002) *Chem. Commun.*, 432–433.

47 (a) Fox, O.D., Drew, M.G.B. and Beer, P.D. (2000) *Angew. Chem.*, **112**, 139–144. *Angew. Chem. Int. Ed.*, **39**, 136–140. (b) Fox, O.D., Drew, M.G.B., Wilkinson, E.J.S. and Beer, P.D. (2000) *Chem. Commun.*, 391–392. (c) Fox, O.D., Cookson, J., Wilkinson, E.J.S., Drew, M.G.B., MacLean, E.J., Teat, S.J. and Beer, P.D. (2006) *J. Am. Chem. Soc.*, **128**, 6990–7002.

48 Cometti, G., Dalcanale, E., Du vosel, A. and Levelut, A.-M. (1990) *J. Chem. Soc. Chem. Commun.*, 163–165.

49 (a) Orr, G.W., Barbour, L.J. and Atwood, J.L. (1999) *Science*, **285**, 1049–1052. (b) Dalgarno, S.J., Atwood, J.L. and Raston, C.L. (2006) *Chem. Commun.*, 4567–4574.

50 McKinlay, R.M., Cave, G.W.V. and Atwood, J.L. (2005) *Proc. Natl. Acad. Sci. U. S. A.*, **102** (17), 5944–5948.

51 (a) McKinlay, R.M., Thallapally, P.K., Cave, G.W.V. and and Atwood, J.L., (2005) *Angew. Chem.*, **117**, 5879–5882; *Angew. Chem. Int. Ed.*, **44**, 5733–5736. (b) McKinlay, R.M., Thallapally, P.K. and Atwood, J.L. (2006) *Chem. Commun.*, 2956–2958.

52 Levi, S.A., Guatteri, P., van Veggel, F.C.J.M., Vancso, G.J., Dalcanale, E. and Reinhoudt, D.N. (2001) *Angew. Chem.*,

113, 1945–1948; *Angew. Chem. Int. Ed.*, **40**, 1892–1896.

53 Xia, Y. and Whitesides, G.M. (1998) *Angew. Chem.*, **110**, 568–594. *Angew. Chem. Int. Ed.*, **37**, 550–575, and references within.

54 Menozzi, E., Pinalli, R., Speets, E.A., Ravoo, B.J., Dalcanale, E. and Reinhoudt, D.N. (2004) *Chem. Eur. J.*, **10**, 2199–2206.

55 (a) Harrison, R.G., Dalley, N.K. and Nazarenko, A.Y. (2000) *Chem. Commun.*, 1387–1388. (b) Harrison, R.G., Fox, O.D., Meng, M.O., Dalley, N.K. and Barbour, L.J. (2002) *Inorg. Chem.*, **41**, 838–843. (c) Harrison, R.G., Burrows, J.L. and Dalley, N.K. (2003) *Inorg. Chim. Acta*, **351**, 399–403.

56 Sorrell, T.N., Pigge, F.C. and White, P.S. (1994) *Inorg. Chem.*, **33**, 632–635.

57 Menozzi, E., Busi, M., Ramingo, R., Campagnolo, M., Geremia, S. and Dalcanale, E. (2005) *Chem. Eur. J.*, **11**, 3136–3148.

58 Menozzi, E. and Rebek, J., Jr. (2005) *Chem. Commun.*, 5530–5532.

59 Haino, T., Araki, H., Yamanaka, Y. and Fukazawa, Y. (2001) *Tetrahedron Lett.*, **42**, 3203–3206.

60 Haino, T., Yanase, M. and Fukazawa, Y. (1998) *Angew. Chem.*, **110**, 1044–1046. (1998) *Angew. Chem. Int. Ed.*, **37**, 997–998.

61 Stang, P.J., Cao, D.H., Chen, K., Gray, G.M., Muddiman, D.C. and Smith, R.D. (1997) *J. Am. Chem. Soc.*, **119**, 5163–5168.

62 Lützen, A., Haß, O. and Bruhn, T. (2002) *Tetrahedron Lett.*, **43**, 1807–1811.

63 van Velzen, E.U.T. (1994) Ph.D thesis, University of Twente (The Netherlands).

8

New Properties and Reactions in Self-assembled M$_6$L$_4$ Coordination Cages

Makoto Fujita and Michito Yoshizawa

8.1
Introduction

In 1990, our group first reported the quantitative self-assembly of the Pd(II)-cornered square molecule **1** in water [1]. The molecular design of the square within which a transition metal's 90-degree coordination angle occupies every corner of the square has since been confirmed by a number of groups studying a variety of squares, e.g., organic soluble squares [2], luminescent squares [3], porphyrin squares [4], chiral squares [5], and crown or ferrocene-conjugated squares [6]. These molecules, called molecular squares, consist of transition metal corners linked together by linear organic ligands.
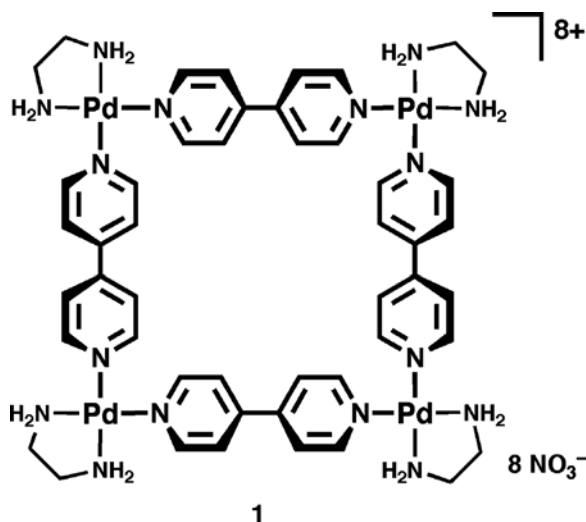
The extension of the basic two-dimensional design of the squares and related polygons into three-dimensional systems led us to explore the self-assembly of

metal-cornered polyhedra. In this way, the two-dimensional structure of Pd(II)-cornered square **1** was extended into an octahedral coordination cage **2** with composition M_6L_4 [7]. In this compound, the six vertices of an octahedron are occupied by cis end-capped Pd(II), whereas the eight triangular faces of the hypothetical octahedron are alternately occupied by four *exo*-tridentate triangular ligands. At each Pd(II) corner, the bite angle of the two pyridyl groups is approximately 90 degrees, causing almost no distortion in this cage framework. Hence, this compound is self-assembled quantitatively by mixing the metal and the ligand in water. Thanks to this facile synthetic procedure, compound **2** is now produced on a large scale as a commercial product.

2
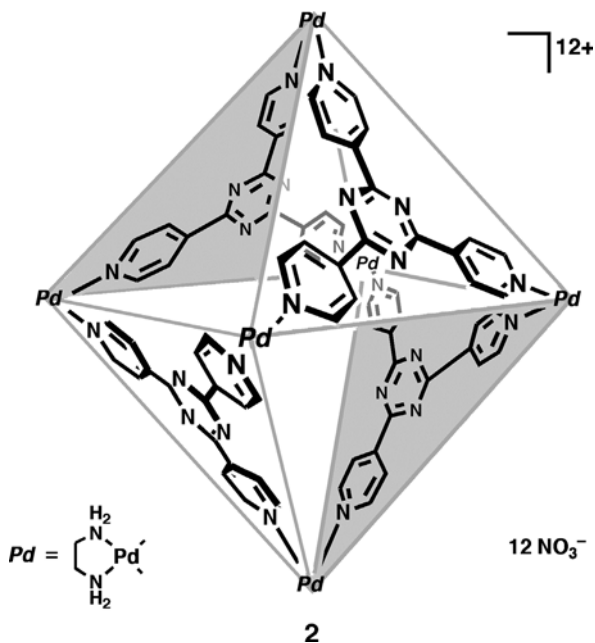
Metal-cornered cages with the same symmetry have subsequently been reported by many groups, and the self-assembly of polygons and polyhedra using di- or multidentate exotopic ligands and metal hinges is now recognized as a very efficient and versatile way for the production of large hollow coordination objects. In this article, a focus will be on the hollow complex **2** [7], which is one of the first examples of a self-assembled cage. The self-assembly of the cage and associated new phenomena (new properties and reactions in this cage) are discussed here.

8.2
Self-assembly of Hollow Complexes

Prior to our report on the self-assembly of M_6L_4 cage **2**, Saalfrank prepared intriguing M_4L_6 cages (**3**) aggregated from various metal ions (Mg²⁺, Mn²⁺, Fe²⁺, Co²⁺,

Ni^{2+}, and Zn^{2+}) and bridging ligands with binding sites at each end [8]. In these complexes, the shape is a tetrahedron, in which metals are located at each vertex, and the six ligands are on the edges of the tetrahedron. By inserting aromatic spacers into the ligand, the volume of the cage can be expanded [8]. However, the inclusion of organic guests into these complexes has not been reported; this could be attributed to the lack of an efficient driving force for inclusion of such guests in organic solvents.

3
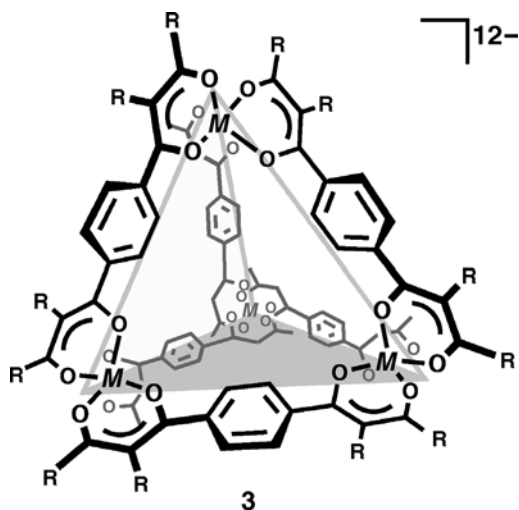
M_4L_6 cages (**4**) with the same symmetry were later reported by Raymond, these being anionic and able to accommodate cationic guests quite efficiently [9]. The use of this complex and related cages as molecular flasks has been actively developed by their group. In particular, intriguing chemical transformations within the cages have been reported [9].

4
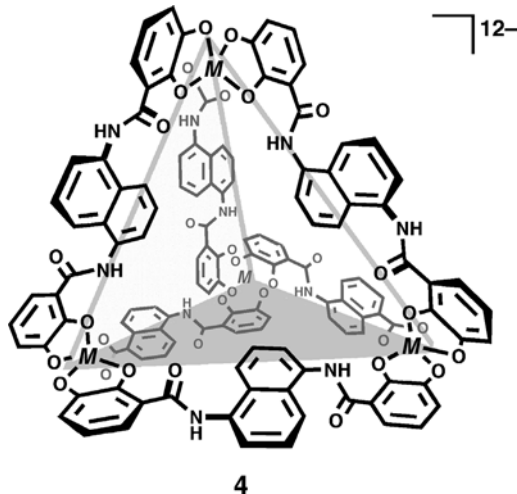
Representative self-assembled coordination cages reported so far (since Saalfrank's 1988 report) are summarized in Table 8.1 [10–15]. An M$_{12}$L$_{24}$ hollow complex reported recently is one of the largest frameworks defined by X-ray analysis [15g–i].

8.2.1
M$_6$L$_4$ Octahedral Complex

Of the various hollow complexes, the Pd(II)-cornered M$_6$L$_4$ octahedral complex **2** features the following characteristics rarely shown by other complexes:

1. Quantitatively assembled from commercially available reagents: 100 g scale synthetic procedure has been established and the cage complex **2** itself is now commercially available from Wako Pure Chemicals Industries Ltd. (Pd-Nanocage®).

2. Highly soluble in water because of the exposure of cationic Pd (II) units at the periphery of the complex.

3. Strongly binds large neutral organic guests through efficient hydrophobic interaction in water. Because of the electron-deficient nature of the ligand, charge transfer interaction also favors electron-rich guests.

4. Possesses an extraordinarily large cavity, with a diagonal Pd-Pd distance of 2.2 nm, capable of binding as many as four adamantane or carborane molecules [16].

5. Highly symmetric, with T_d symmetry, rendering the twelve pyridyl nuclei equivalent. Once guests are accommodated, however, the host symmetry is often reduced as it adapts to the included guest (or its aggregate). By analyzing the symmetry of the host, therefore, the guest geometry in the cage can be elucidated [17].

6. Mediates photo-induced electron transfer from the guest to the host because of the extremely electron-deficient triazine ring of the ligand, which is made electron-poor by three metal-coordinated pyridyl rings.
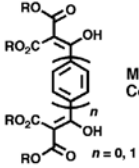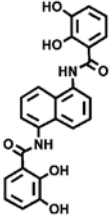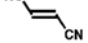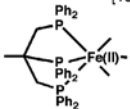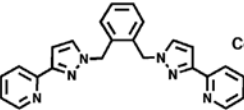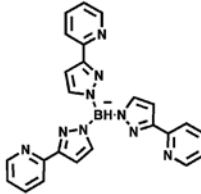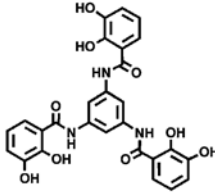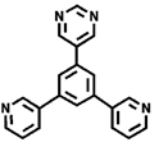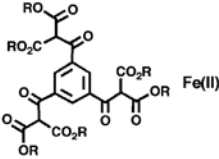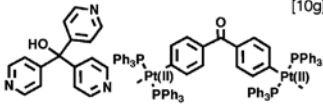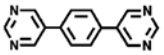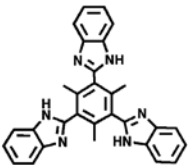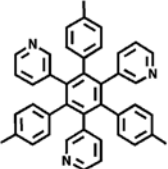
Based on these characteristics, cage **2** shows unique properties not demonstrated in previously known organic hosts such as crown ethers [18], cyclodextrins [19], calixarenes [20,21], calixresorcarenes [21], cucurbituril [22], and so on. The details of these properties are discussed in the following sections.

8.2.2
Large-scale Production of the M$_6$L$_4$ Complex

As already mentioned, complex **2** is easily prepared on a large scale and isolated in high purity. Normally, an ethylenediamine (en) group is placed on the Pd(II) centers as the *cis*-protective group. This protective group is often replaced by 2,2′-bipyridine

Table 8.1 Self-assembled hollow compounds composed of metals and multidentate ligands. Schematic drawings of the hollow frameworks and components (metals and ligands) are listed.

Ligand	Metal	Ligand	Metal

	Ligand	Metal		Ligand	Metal

[11a]

[11b]

[11c]

[11d]

[11e,f]

[11g]

[11h]

[11i]

[11j]

[11k]

[11l]

Ligand	Metal	Ligand	Metal

The structures are arranged in a grid. Reference codes and metal assignments:

[7,24] — M = Pd(II), Pt(II)

[12a,b] — M = Pd(II), Pt(II); X = CN, Py, C$_6$H$_4$CN

[12c,d] — M = Pd(II), Pt(II); Me$_3$P–Pt(II)

[12e,f] — Pd(II)

[12g] — Fe(II), Co(II), Cu(II)

[12h] — Ag(I)

[12i] — Mo, Mo (Ar)$_2$

[12j] — Pd(II)

[12k] — Ni(II)

[12l] — Pd(II), Pt(II)

Ligand	Metal	Ligand	Metal
	Pd(II) [12m]		Pd(II) [12n]
	Ga(III) [12o]		Ag(I) [12p]
	Mn(II), Fe(II), Co(II), Ni(II), Pd(II), Pt(II), Cu(II), Zn(II), Cd(II), Hg(II) [12q]		
		Pd(II) [13a]	Pd(II) [13b]
		Pd(II) [13c]	

	Ligand	Metal		Ligand	Metal	

Ligand	Metal		Ligand	Metal
		[14a]		[14b]
		[14c,d]		[14e]
		[14f]		[14g,h]
				M = Pd(II), Pt(II)
		[14i]		[14j]
	M = Pd(II), Pt(II)			
		[14k-m]		[14n]
	n = 1~3			
		[15a]		
	n = 1, 2			

or *N,N,N′,N′*-tetramethylethylenediamine because the complex crystallizes more easily, which is convenient for crystallographic analysis of various host-guest complexes [23]. The metal center, Pd(II), is often replaced by Pt(II) because the Pt(II) analogs are more robust than the Pd(II)-containing cage [24]. Because of the

Ligand	Metal	Ligand	Metal

[15b]

[15b]

[15c]

Cu(II)

[15d-f]

Cu(II)

[15g-i]

Pd(II)

n = 0, 1

[15j]

[15k]

Cu(II),
Co(II)

+
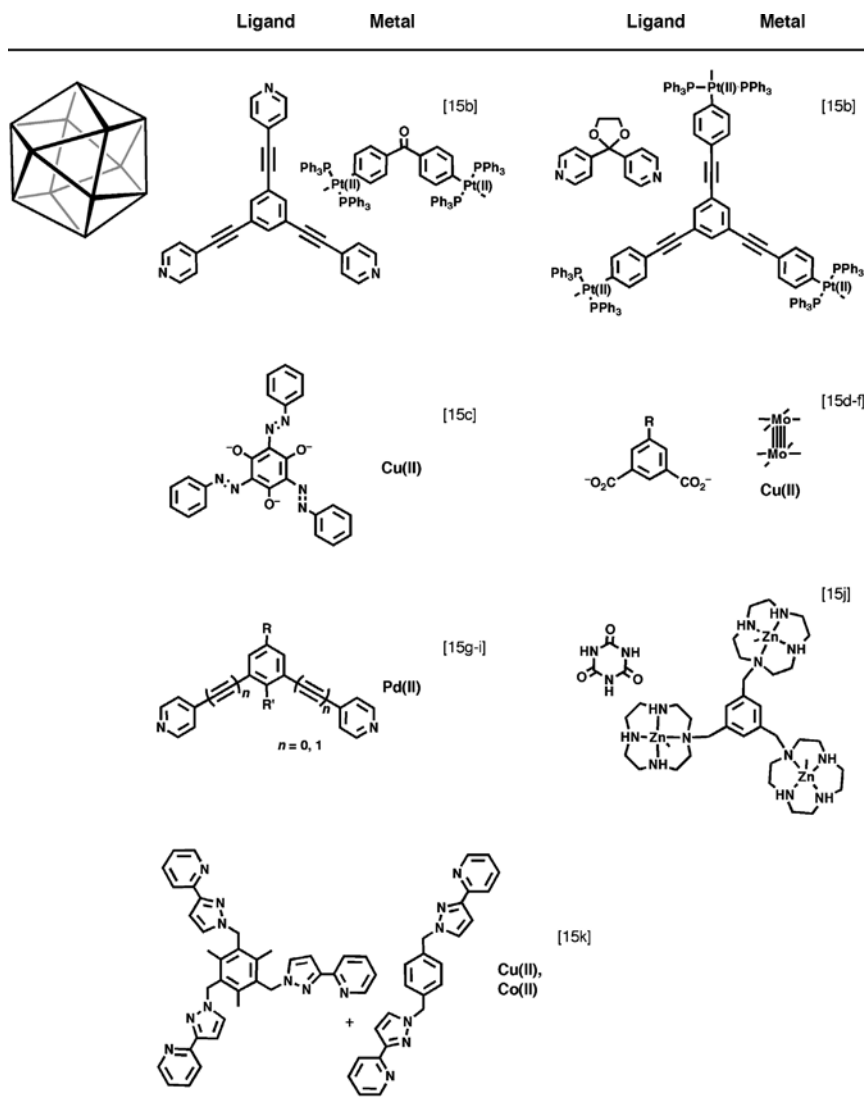
inertness of the Pt(II)-pyridine coordination bond, however, the Pt(II) cage requires the solution to be heated for a few weeks in the presence of a template to facilitate and complete the self-assembly. Although the synthesis is more tedious, once formed, the Pt(II) cage is more stable than the Pd(II) cages and it is tolerant of a relatively large pH range [24]. All the derivatives mentioned above are structurally defined by crystallographic analyses, which showed that all the cages have cavities of nearly the same shape and size, independent of the protective group (en, 2,2′-bpy, or tmen) or metal center [Pd(II) or Pt(II)].
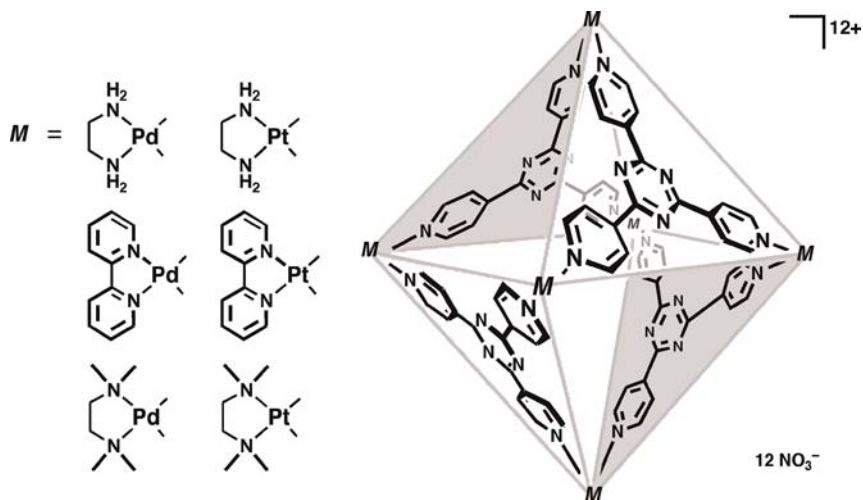
8.3
Inclusion Properties

8.3.1
Inclusion of Adamantane and Carborane

By suspending excess adamantane (**5a**) in the aqueous solution of **2**, the water-immiscible **5a** was gradually dissolved and included into the large hydrophobic cavity of **2**, forming the **2**·(**5a**)$_4$ inclusion complex [16]. When complex **2** was titrated with aqueous sodium adamantane carboxylate (**5b**), a 1:4 complex **2**·(**5b**)$_4$ was observed (Figure. 8.1a), irrespective of the amount of the guest. For example, **2**·(**5b**)$_4$ was formed in 25% yield, leaving 75% of empty cage **2** upon addition of one equivalent of **5b**. Similarly, **2**·(**5b**)$_4$ (50%) and the empty cage (50%) were independently observed upon the addition of two equivalents of **5b**. The chemical shifts of the 1:4 complex did not change at all during the titration, and no other host-guest complexes were observed [7]. These facts indicated that the **2**·(**5b**)$_4$ complex is much more stable than the intermediary **2**·(**5b**)$_n$ ($n = 1$–3) complexes, and a strong positive cooperative effect is present among the guests in the formation of the 1:4 complex.

The overwhelmingly dominant formation of 1:4 complexes was also observed for the reaction of **2** with 1- and 2-adamantanol [23]. Analysis of the upfield shift of the individual protons of these guests elucidated the guest geometry, in which the hydrophilic OH group extends out from the cavity of the cage. This geometry was, in fact, confirmed by X-ray crystallographic analysis (Figure 8.1b). *o*-Carborane, whose diameter (8 Å) is slightly larger than that of adamantane (7 Å), also formed
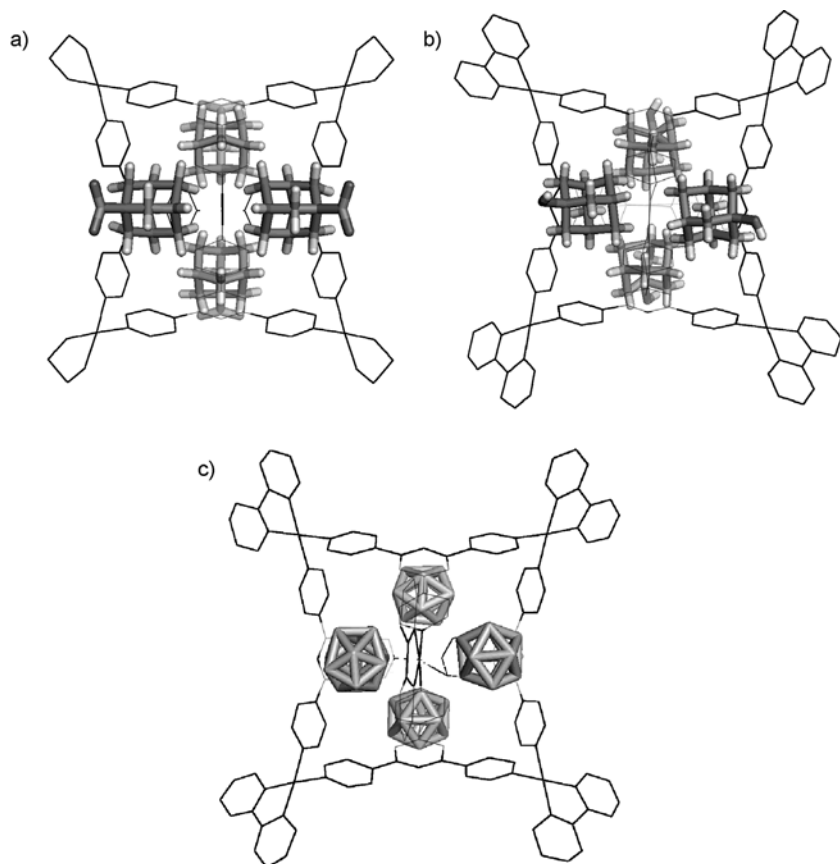
Figure 8.1 Crystal structures of (a) **2**·(**5b**)$_4$, (b) **2**·(1-adamanta-nol)$_4$, and (c) **2**·(o-carborane)$_4$.

a similar 1:4 complex, as confirmed by NMR spectroscopy and X-ray crystallographic analysis (Figure 8.1c) [23].

8.3.2
Inclusion Geometry

Cage **2** formed 1:2 complex with α-diketone **6** (Figure 8.2) [17]. The ^{1}H NMR of the 1:2 complex displayed twelve signals (with the same intensity) for the triazine ligand. Associated with 2D NMR measurements, it was confirmed that four triazine ligands involved in **2** were equivalent, yet the twelve protons on each ligand were all in-equivalent (Figure 8.2b). This observation indicates that the fixation of the included guests in the cage adopts S_4 symmetry. In fact, crystallographic analysis of the 1:2 complex shows that each α-diketone **6** adopts a twisted conformation (with a dihe-dral angle of ca. 80° between the two carbonyl groups) and an enantiomeric pair forms a meso aggregate with S_4 symmetry (Figure 8.3).
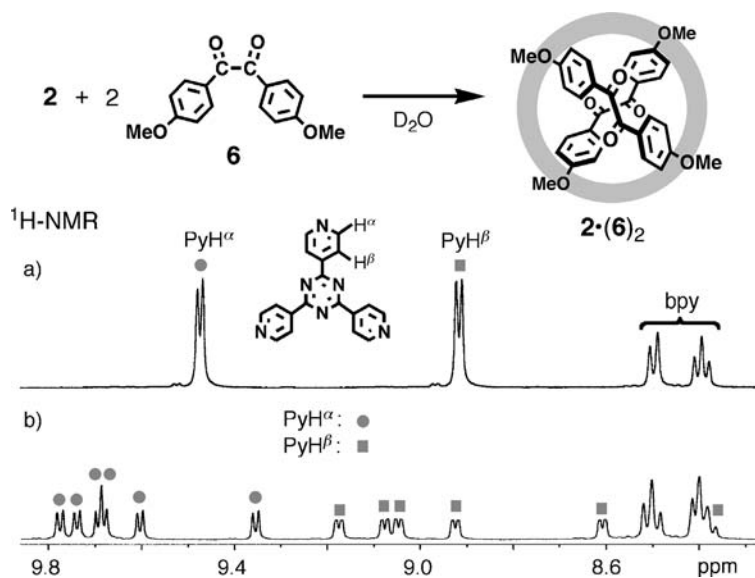
Figure 8.2 ^{1}H NMR spectra of the aromatic region of (a) cage **2** and (b) **2·(6)$_2$** complex in D$_2$O.
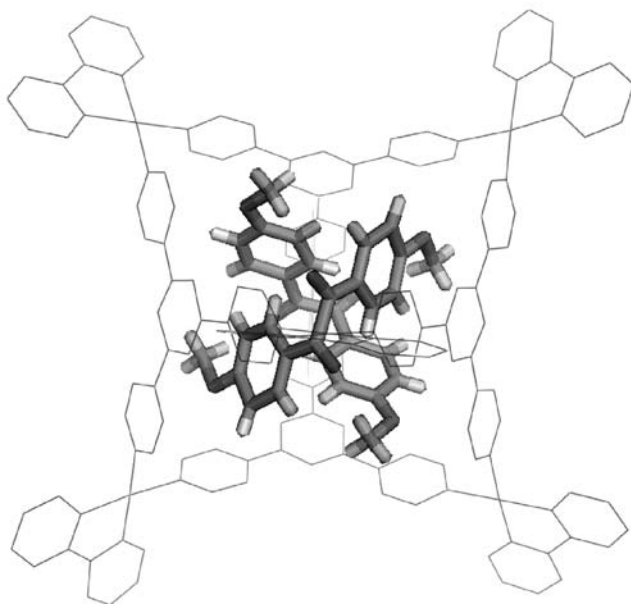
Figure 8.3 Crystal structure of the **2·(6)$_2$** complex.
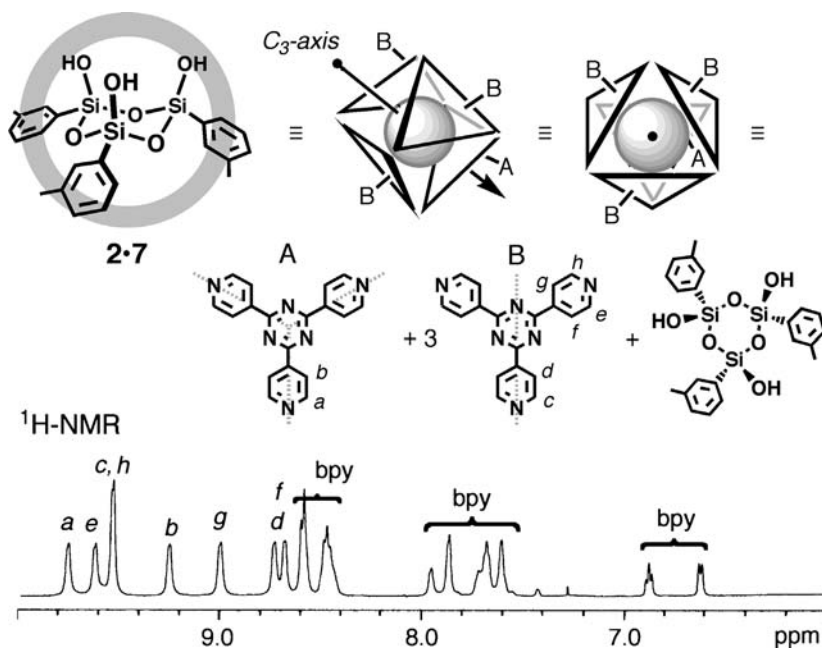
Figure 8.4 ^{1}H NMR spectrum of the aromatic region of cage **2·7** in D_2O.

In the ^{1}H NMR spectrum of cage **2** accommodating cyclic trisilanol **7**, eight signals were observed for the triazine ligand with the same integral ratio, indicating that the guest was fixed along a C_3 axis of the cage (Figure 8.4) [17]. The triazine ligand perpendicular to the C_3 axis showed two different types of protons (PyH_a and PyH_b). Thus, the free rotation of the *m*-tolyl group of **7** on the NMR time scale affords C_{3v} (rather than C_3) symmetry. In the solid state, the *m*-tolyl flipping is restricted and crystallographic analysis showed the inclusion of C_3 symmetric guest with three *m*-tolyl groups arrayed in the same direction (Figure 8.5) [17].

From these spectroscopic and crystallographic observations, it can be concluded that (a) the symmetry of the guest aggregation can be elucidated by the symmetry analysis of the host rather than that of the guests, and (b) there is a good correlation between the guest geometry in solution and that in the crystalline state, probably because the atmosphere in the cage is nearly independent of whether it is in solution or the crystalline state. Thus, the cavity of the cage is essentially isolated from outside environment.

8.3.3
Bimolecular Recognition

When two different guests ($\mathbf{G}_a$ and $\mathbf{G}_b$) are added to the solution of cage **2**, a heterotopic inclusion complex $\mathbf{2 \cdot G_a \cdot G_b}$ can be more stable than homotopic
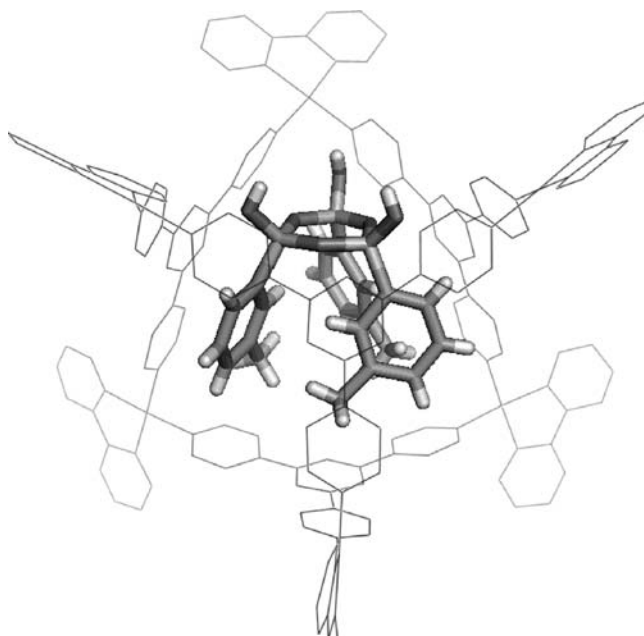
Figure 8.5 Crystal structure of cyclic trisilanol **7** within cage **2**.

complexes $2 \cdot (G_a)_2$ or $2 \cdot (G_b)_2$. If the first guest G_a is a planar aromatic compound, it stacks with a ligand of the cage, leaving a roughly spherical void in the cavity. Thus, a spherical guest G_b fits well. An interesting example of this is the pairwise selective recognition of perylene (**8**) and *cis*-decalin (**9**) [25]. These guests were unable to form homotopic inclusion complexes [$2 \cdot (8)_2$ or $2 \cdot (9)_2$] when they were individually combined with cage **2**. Nevertheless, when they were combined together and suspended in the aqueous solution of **2**, a stable heterotopic complex $2 \cdot 8 \cdot 9$ was formed in good yield, despite the absence of any special attractive forces between the guests **8** and **9**. Molecular modeling displayed a stable guest packing with C_{3v} symmetry (assuming free rotation of the guests along the C_3 axis), where the perylene molecule stacked on the triazine ligand and the remaining void is occupied by *cis*-decalin (Figure 8.6).

Although there are many reports on similar bimolecular recognition (or ternary complex formation), in most cases, attractive forces such as charge-transfer interactions are present between the two guests. In contrast, two guests have to be spatially paired in the cavity of **2** despite the absence of any strong affinity between the guests. In addition to the combination of perylene and *cis*-decalin, highly pairwise selectivities were observed for various combinations of two different guests (e.g., pyrene and *cis*-decalin, or pyrene and hexane), often by adjusting the steric demand of one substrate. The facile formation of the ternary complexes ($2 \cdot G_a \cdot G_b$) is an important issue for designing cavity-directed chemical reactions between two substrates, as discussed below.
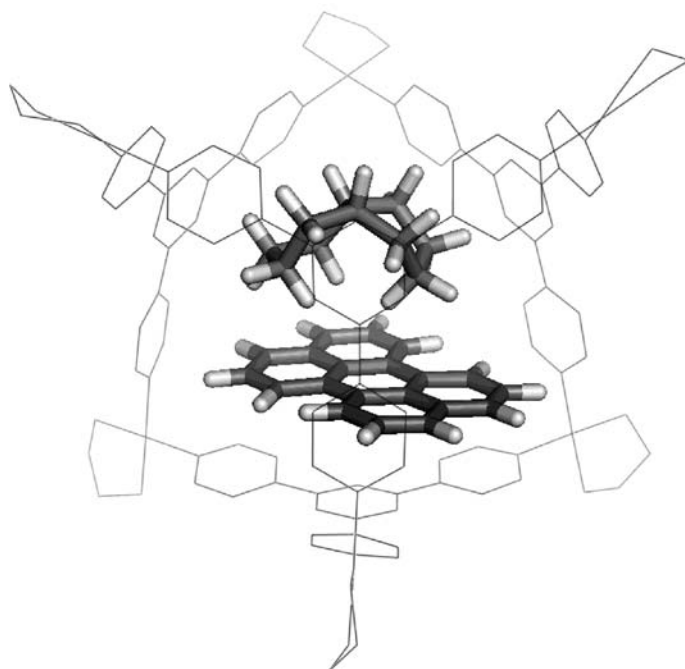
Figure 8.6 Molecular modeling of heterotopic inclusion complex **2·8·9**.

8.3.4
Recognition of Bulky Guests

Cage **2** possesses four portals whose dimensions are considerably smaller than that of the cage's cavity itself. Since Pd-N dissociation is a very slow process in comparison with the host-guest complexation, guest molecules should enter the cavity without breaking any bonds of the cage. Therefore, a guest which is larger than the host portal is expected to enter by expanding the portal framework with some energy barrier. A bulky guest, 1,3,5-tri(*t*-butyl)benzene (**10**), is not included in the cage at room temperature because of the high energy barrier. On heating the solution to 80 °C, however, this bulky guest was included in ca. 45% yield into the cavity via thermal slippage [23]. After the solution was cooled down to room temperature, the guest (**10**) was no longer able to escape from the cavity. In this way, the large guest was incarcerated (Figure 8.7).

Tetrabenzylsilane (**11**) has a number of conformational isomers in equilibrium. Interestingly, during the inclusion process of this large guest, symmetry-broken spectra were observed for intermediary species before obtaining a simple ^{1}H NMR spectrum, indicating the formation of the highly symmetric **2·11** complex, whose structure was confirmed by X-ray analysis (Figure 8.8) [23]. It is therefore reasonable
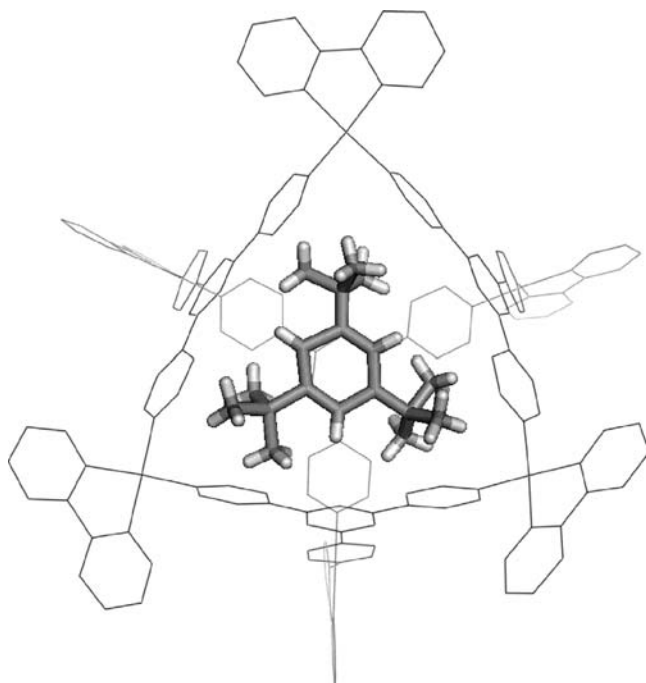
Figure 8.7 Crystal structure of 1,3,5-tri(*t*-butyl)benzene (**10**) within cage **2**.
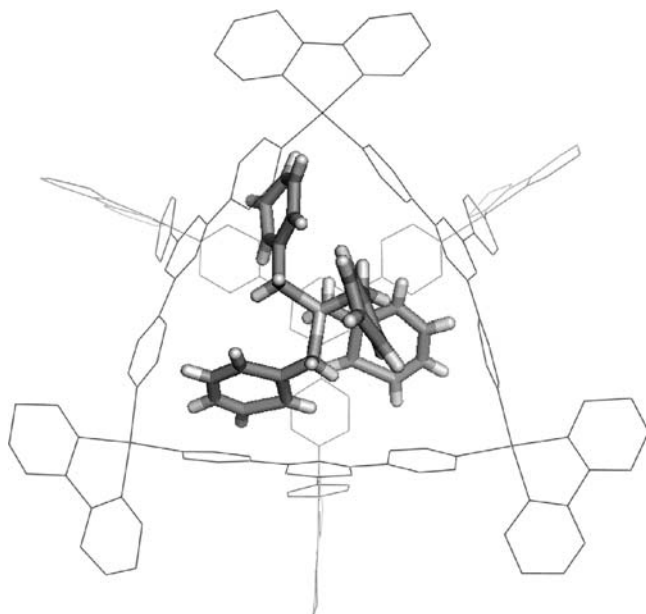
Figure 8.8 Crystal structure of tetrabenzylsilane (**11**) within cage **2**.

that structures including less than four benzyl groups of **11** exist as intermediates before the guest is finally trapped in the cavity of **2**.

8.3.5
The Recognition of Azobenzene and Stilbene

Since the cavity of cage **2** is surrounded by four ligands arrayed in S_4 symmetry, guest molecules or aggregates with S_4 symmetry interact efficiently with the cage. In the complexation with 4,4′-dimethylstilbene, the *cis* isomer was bound quite strongly to give quantitatively a 1:2 inclusion complex, whereas the *trans* isomer showed no interaction [26]. The preferential complexation of the *cis* isomer is explained by assuming the formation of a "tennis ball"-like aggregation with an S_4 symmetry from two *cis*-4,4′-dimethylstilbene molecules. In fact, this proposed aggregation was strongly suggested by molecular modeling study (Figure 8.9).

A similar *cis*-selective inclusion was observed for 4,4′-dimethylazobenzene. Although the *cis-trans* isomerization of azobenzene by UV irradiation is a well-known process, 100% conversion from *trans* to *cis* at a photostationary state is normally impossible. In the presence of cage **2**, however, only the *cis* isomer is trapped by the cage via the formation of the stable tennis-ball like S_4 dimer, pushing the *cis-trans* photo-equilibration overwhelmingly toward the *cis*-isomer [26].
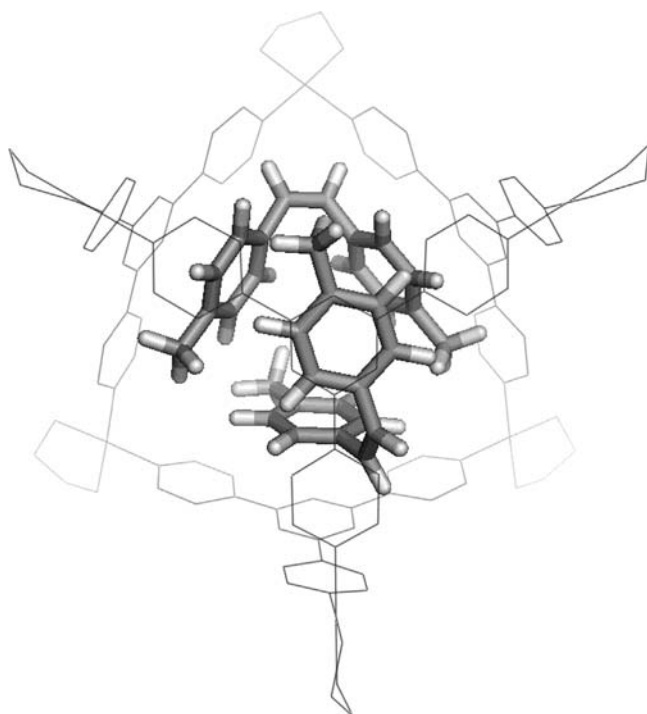
Figure 8.9 Optimized structure for the "tennis ball"-like aggregation of two 4,4′-dimethylstilbene molecules within **2**.

8.3.6
Molecular Ice

Among various potential guests for cage **2**, the simplest is a water molecule. The cavity of the cage is expected to be filled with water in aqueous solution when organic guests are absent. We wondered whether the included water molecules would behave as bulk water or adopt a more highly ordered state. On the surface of hydrophobic substances, water molecules are known to develop an ordered hydrogen-bonded network to neutralize their own high polarity. The origin of this hydrophobic interaction is considered to be the entropic advantage when the high-potential water molecules at the surface become free from the restrictions of the network upon contact with the hydrophobic species. Thus, in the hydrophobic cavity of the cage, endohedral clusterization (network formation) of water is expected. Crystallographic analysis was therefore carried out for the empty cage that had been crystallized from water. Interestingly, ten water molecules form an adamantane-like $(H_2O)_{10}$ cluster in the cavity of cage **2**, as expected (Figure 8.10) [27].

This cluster structure is the smallest unit of the 3D hydrogen-bonded network of naturally occurring I_c-type ice. If the ice structure is defined by the 3D network of water molecules, the $(H_2O)_{10}$ cluster in our cavity is regarded as "molecular ice". The
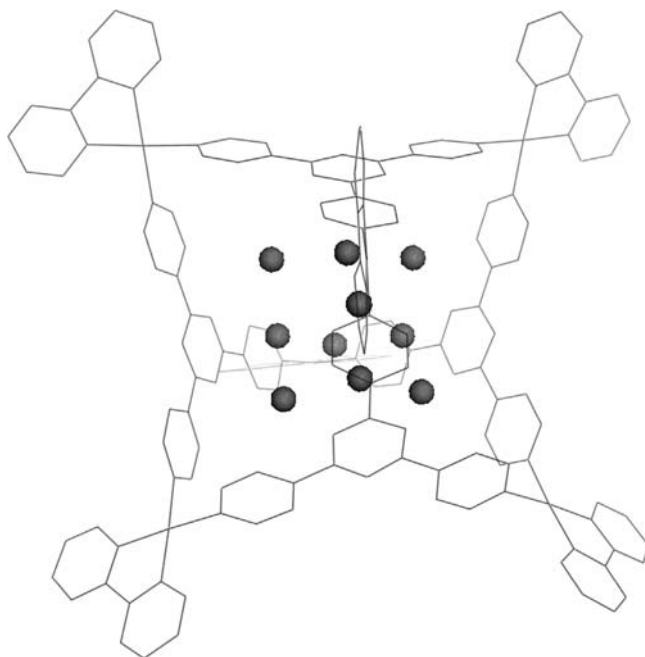
Figure 8.10 Crystal structure of an adamantane-like $(H_2O)_{10}$ cluster within cage **2**.
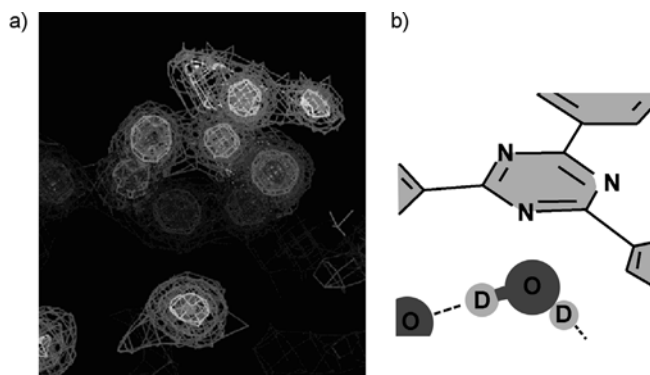
Figure 8.11 (a) Neutron diffraction analysis of a $(D_2O)_{10}$ cluster within cage **2**, and (b) the corresponding structural drawing.

crystallographic analysis showed that the cavity size is ideal for binding the molecular ice. As shown in Figure 8.10, the adamantane-like framework of the molecular ice has almost no distortion in the framework as compared with the unit of I_c-type ice; the molecular ice is only slightly compressed by the four ligands of the cage, making O • • • O • • O angles (108.8–122.3°) at the bridgehead of the adamantane framework slightly larger than that of I_c-type ice (109.5°). A question arises as to whether this molecular ice cluster is recognized via OH • • • π hydrogen bonding or HO: • • • π (n-π) interaction in the cage. The answer is not to be derived from X-ray crystallography, because hydrogen atoms were not located in the crystallographic analysis. Therefore, neutron diffraction was used to distinguish whether or not a hydrogen atom exists between the bridgehead water oxygen and the ligand. Single crystals of the cage were grown from D_2O solution. The neutron diffraction analysis of the molecular ice structure $(D_2O)_{10}$ in the cage clearly revealed the absence of deuterium nuclear density between the bridgehead oxygen and the ligand (Figure 8.11) [27]. This observation indicates that the bridgehead water is recognized by the ligands via HO: • • • π (n-π) interaction not OH • • • π hydrogen bonding. In contrast to a typical OH • • • π interaction, where an aromatic ring is an electron donor and hydrogen is an acceptor, the extremely electron-poor triazine ring seems to work as an electron acceptor to the lone pair of the oxygen of water. This reverse charge donation is probably the driving force for the formation of a stable molecular ice cluster.

8.3.7
Peptide Recognition

Recognition of a specific amino acid sequence from a protein or a specific tag peptide sequence is expected to lead to variety of medical and materials applications. Whereas the recognition of a single amino acid residue by synthetic hosts has been reported previously, the artificial recognition of a sequence of two or more amino acid residues has been quite limited. There are only a few reports on the
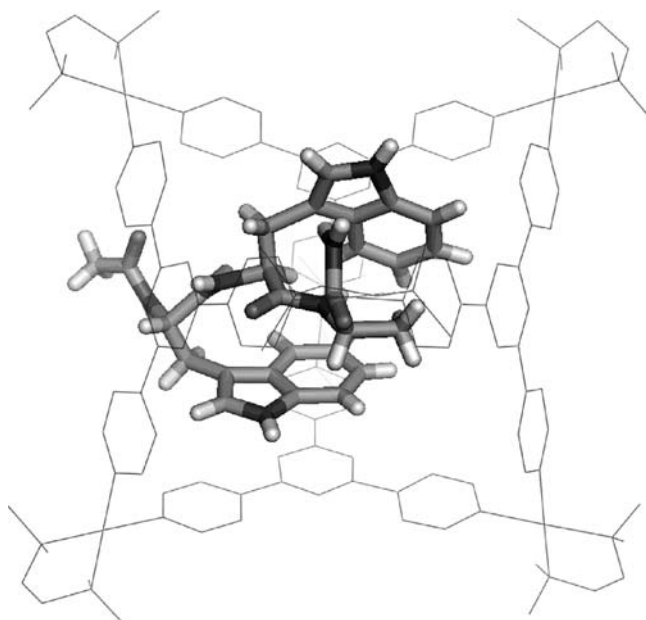
Figure 8.12 Crystal structure of cage **2** accommodating Ac-Trp-Trp-Ala-NH$_2$ (**12**).

sequence-selective recognition of peptides by synthetic hosts, where two amino acid receptors are simply connected to recognize dipeptides. Cage **2** is able to recognize an oligopeptide sequence because its binding pocket can accommodate up to three amino acid residues. Therefore, various oligopeptides were prepared and the interaction with **2** examined. The X-X-Ala tripeptides (where X denotes aromatic residue such as Phe, Tyr, Trp) were sequence-selectively bound by the cage [28]. The largest association constant was observed for Ac-Trp-Trp-Ala-NH$_2$ (**12**; $K_a > 10^6\,M^{-1}$), whose geometry in the cage was crystallographically analyzed (Figure 8.12). The crystal structure revealed that the indole rings of two Trp groups and the methyl group of Ala efficiently interacted with the cage via π-π and CH-π interactions, respectively. Even the Ala-Gly mutant, Ac-Trp-Trp-Gly-NH$_2$, showed a considerably smaller association constant ($K_a = 7.4 \times 10^4\,M^{-1}$), indicating the importance of cooperativity of the above three interactions. The sequence of the three residues was particularly important: Ac-Trp-Ala-Trp-NH$_2$ and Ac-Ala-Trp-Trp-NH$_2$, which have the same residues but different sequence, were poorly recognized. These results represent the first example of sequence-selective recognition of peptides by a single recognition site.

The crystal structure of **2·12** also revealed that the *N*-terminal of **12** contacts with the π-face of the ligand, whereas the *C*-terminal is directed toward the portal of the cage. Hence, as expected, oligopeptides extending the sequence at the *C*-terminal were also bound strongly, whereas those extending the sequence at the *N*-terminal were not.

8.4
New Physical Properties

Since the environment of the cavity presented by **2** is spatially and electronically
confined, physical properties of encapsulated molecules are expected to change to
some extent, or even dramatically. In this section, the variable properties of guests in
the cavity of cage **2** are discussed.

8.4.1
Redox Control of Ferrocene

The formation of a 1:4 complex **2·(13)₄** (**13**: ferrocene) was confirmed both by NMR
spectroscopy and crystallographic analysis (Figure 8.13) [29]. The oxidation potential
of ferrocene to ferrocenium ion [Fe(III)] in the cage was anodically shifted by 73 mV
as compared to that in water. Thus, the cationic cage **2** suppresses the oxidation of
ferrocene to ferrocenium ion.

8.4.2
Induction of Intermolecular Spin–spin Interaction

Cage **2** can bind two organic radical molecules such as 2-naphthyl nitronyl nitroxide
(**14**). Normally, the organic spin centers are protected by bulky substituents to enhance
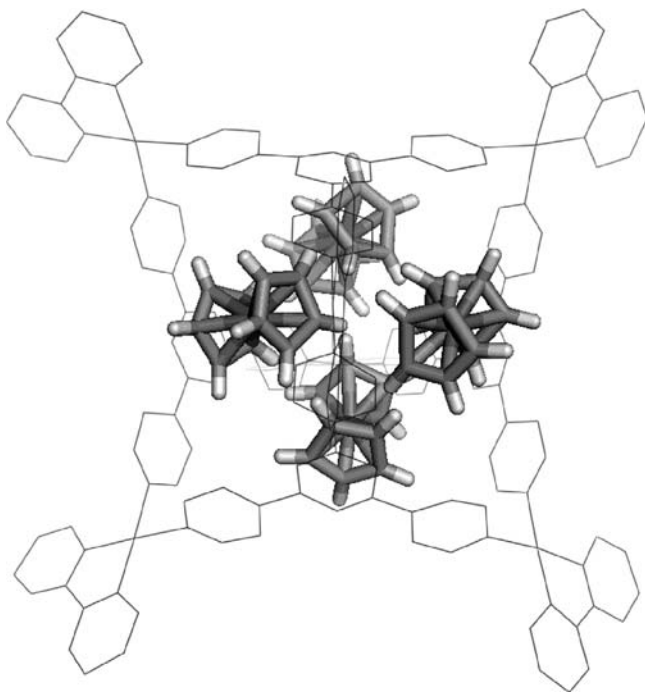
Figure 8.13 Crystal structure of **2·(13)₄** complex.

the kinetic stability of the radical. Because of the steric demand of the bulky sub-stituents, intermolecular spin-spin interaction can be difficult to observe for common organic radicals. As for the radical **14**, the intermolecular spin-spin interaction is not observed even in the solid state because of the offset packing of the molecules, which distances the radical centers from each other. However, when a solution of the 1:2 inclusion complex **2·(14)₂**, obtained by suspending solid **14** in the aqueous solution of **2**, was frozen at low temperatures and subjected to ESR study, new broad signals ascribable to the intermolecular spin-spin interaction of the included guests were clearly observed (Figure 8.14) [30]. The spin-spin interaction was unambiguously confirmed by the observation of $\Delta m_s = 2$ signal, which is attributed to the triplet state
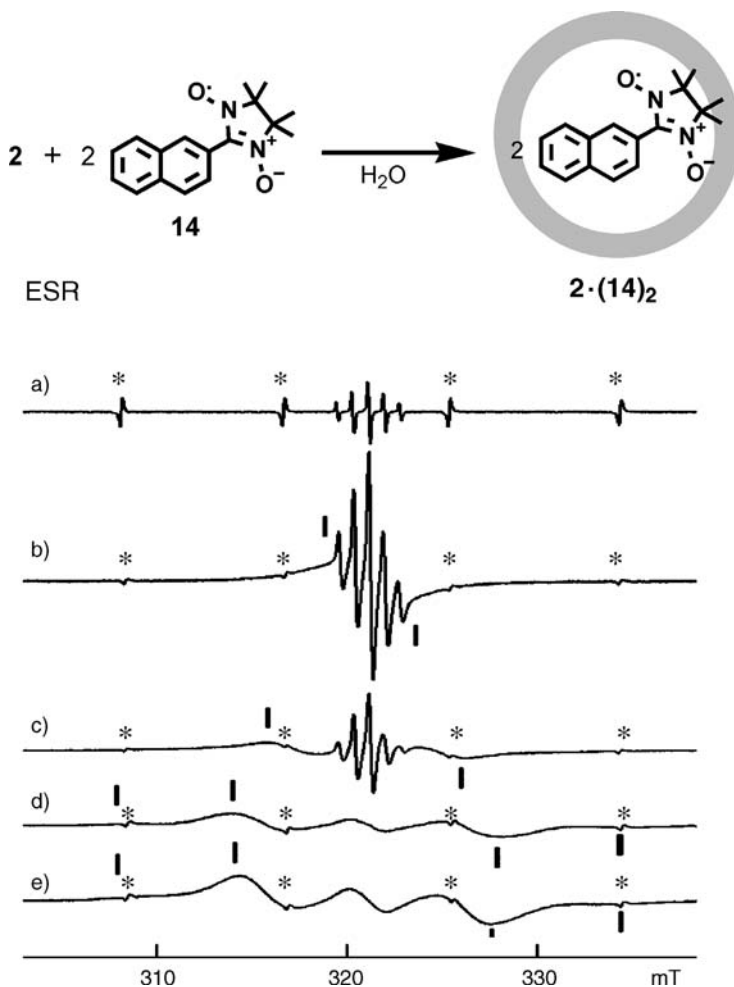
Figure 8.14 ESR spectra of (a) **14** at 293 K and **2·(14)₂** at (b) 363, (c) 293, (d) 273, and (e) 103 K.
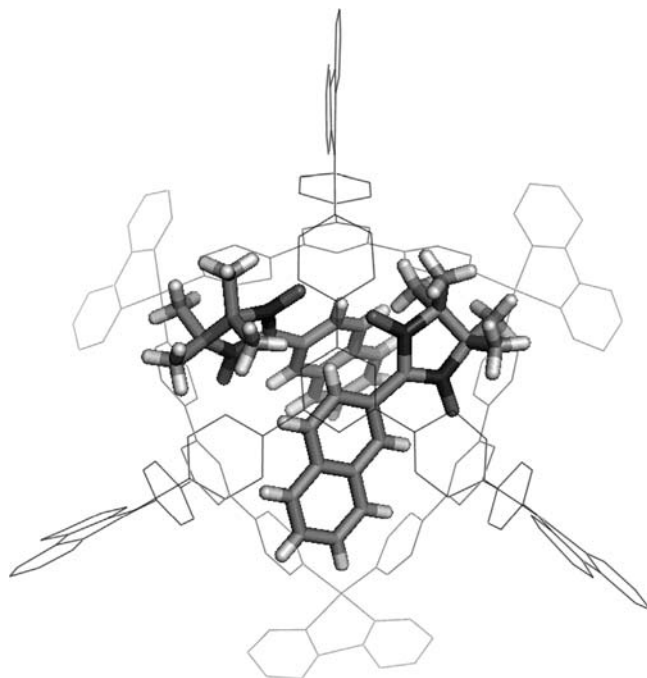
Figure 8.15 Crystal structure of **2**·(**14**)$_2$ complex.

of two interacting spins, at half the resonance magnetic field. The crystal structure (Figure 8.15) also confirmed the proximity of the two spin centers. The averaged spin-spin distance is ca. 5.8 Å, consistent with those estimated from the ESR spectrum according to the equation: $D' = 3/2(\mu_0 g\beta)/(4\pi r^3)$. For a series of organic radicals **14–17**, the interaction decrease in the order **14** > **15** > **16** > **17** [31]. Consistent with this observation, crystallographic studies revealed that the spin-spin distances increased in the same order.

15   **16**   **17**
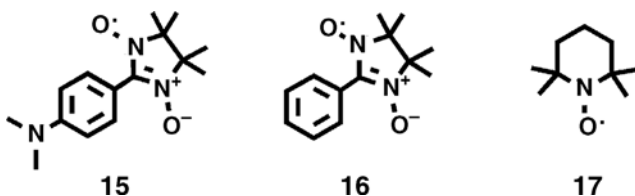
8.5
New Reactions

The cavity of cage **2** can normally accommodate two or more guest molecules. The proximity of reaction centers of two substrates confined in the cavity of the cage

reduces the entropy cost significantly and controls the orientation of the substrates, leading to a remarkable enhancement of reaction rates as well as the induction of high stereo- and regioselectivities. In addition, quite unusual reactions have been found because of the high binding ability and electron-deficient nature of the cage. Intriguing and sometimes unexpected reactions occurring in the cage structure of **2** are discussed in the following sections.

8.5.1
[2+2] Olefin Photodimerization

Upon irradiation of the cage accommodating two olefinic compounds, [2+2] photo-dimerization often takes place quite efficiently with high stereoselectivity. A well-studied substrate for the [2+2] photoaddition is acenaphthylene (**18**), which is known to react at the 1,2 position to give a mixture of *syn*- and *anti*-isomers, wherein the yields and the stereoselectvity are not excellent. This reaction was examined in cage **2**. First, we observed the quantitative formation of 1:2 host-guest complex [**2·(18)₂**] by suspending powdered **18** in an aqueous solution of **2**. Upon irradiation with a high-pressure mercury lamp, the reaction was complete within 30 min to give the *syn* [2+2] adduct **19** stereoselectively (Figure 8.16) [32]. In a similar way, the [2+2] photoaddition of 1-methylacenaphthylene was examined. In common organic solvents, this substrate does not afford the [2+2] dimer because of the steric demands of the methyl group at the 1-position. In cage **2**, however, the reaction took place smoothly to give only the *syn* and head-to-tail isomer (Figure 8.16) [32]. Thus, both stereo- and regioselectvies were perfectly controlled in the reaction of an otherwise unreactive substrate.
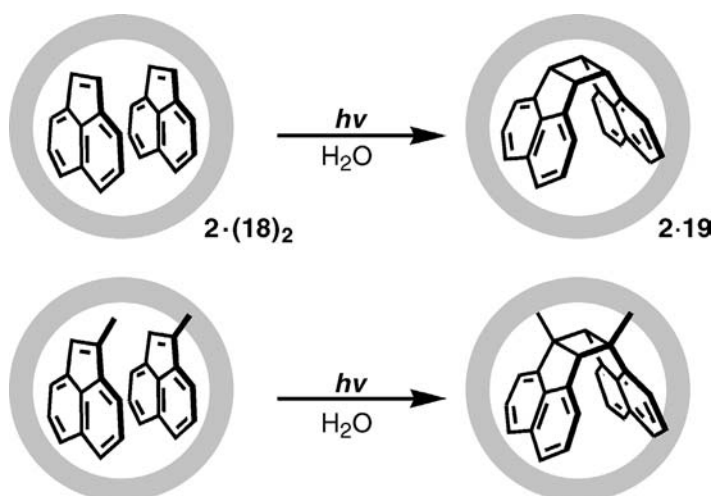
Figure 8.16 [2+2] Photodimerization of acenaphthylene (**18**) and 1-methylacenaphthylene within cage **2**.
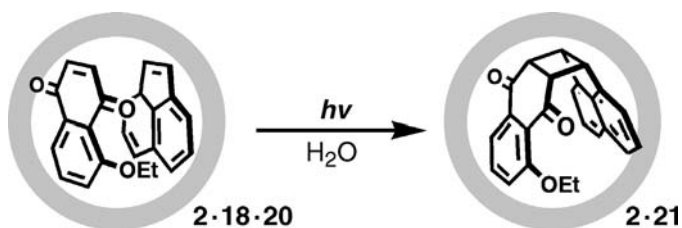
Figure 8.17 Pairwise-selective [2 + 2] photodimerization of acenaphthylene (**18**) and 5-ethoxy-1,4-naphthoquinone (**20**) within cage **2**.

8.5.2
Pairwise-selective Olefin Photodimerization

In common organic solvents, irradiation of a mixture of two olefins provides a mixture of homo- and hetero-dimers (and their regio- and stereoisomers) unless one of the substrates is used in large excess. By utilizing the large cavity of cage **2**, a cross dimer is often selectively formed from two different olefins. For example, by suspending two olefins **18** and 5-ethoxy-1,4-naphthoquinone (**20**) in an aqueous solution of **2**, the ternary complexes **2·18·20** was quantitatively formed. On irradiation, cross adduct **21** was formed in 92% yield with 100% *syn* stereoselectivity (Figure 8.17) [33].

8.5.3
Unusual [2+2] Photoaddition

In many cases, unusual [2+2] photoadditions have been observed, reactions that typically would never take place in common solvents under ordinary photoreaction conditions. Pyrene (**22**) was reacted with *N*-cyclohexylmaleimide (**23**) after forming a ternary complex **2·22·23** and being irradiated for 6 h to give the cross [2+2] adduct **24** in 77% yield based on **2** (Figure 8.18) [34]. The [2+2] photoaddition of maleimide **23** with fluoranthene (**25**), whose photoaddition has never been reported, is also intriguing. The LUMO orbital of **25** is not localized at a specific C=C bond, but rather equally delocalized over the molecule, making the reaction site unpredictable. When ternary complex **2·23·25** was irradiated (365 nm) in D_2O for 5 min at room temperature, a single product **26** was obtained that arises from via [2+2] photoaddition at the C_2=C_3 site of **25** (Figure 8.18) [34]. The high regioselectivity is presumably ascribed to the geometric control of the inclusion complex defined by the confined cavity of **2**.

8.5.4
Diels-Alder Reaction

In addition to [2+2] photoadditions, thermal [4+2] cycloadditions (Diels-Alder reactions) are also remarkably accelerated in the cavity of cage **2**. The reaction of
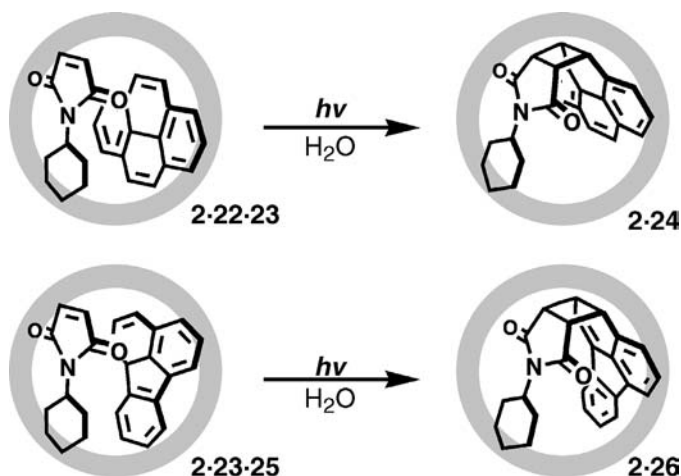
Figure 8.18 Unusual [2+2] photoadditions of maleimide (**23**) and pyrene (**22**) or fluoranthene (**25**) within cage **2**.

benzoquinone and 2,3-dimethyl-1,3-butadiene in the cage proceeds approximately 100 times faster than the analogous reaction in a common organic solvent or an aqueous suspension [35]. Surprisingly, some aromatic compounds which otherwise show no Diels-Alder reactivity participate in Diels-Alder reactions when they are co-enclathrated with a dienophile in the cage. For example, triphenylene (**27**) and maleimide **23** were pairwise selectively bound in the cavity in a moderate yield. Upon heating the solution, these two substrates underwent a Diels-Alder cycloaddition in which one of the benzene rings of **27** participated as a diene [34]. NMR spectroscopic analysis showed that the included triphenylene was quantitatively converted into the unusual adduct **28**, in an exo-selective fashion, without the formation of any by-products (Figure 8.19). In the reaction with perylene (**8**), the Diels-Alder adduct **29** was also formed in a high yield. Although this reaction proceeds to some extent in common organic solvents, the adduct is easily air-oxidized to reproduce the perylene aromaticity. In the cage, however, the adduct was protected from oxidation and the adduct **29** was observed as a stable product within **2** (Figure 8.19) [34].

Anthracene (**30**), a classical substrate for the Diels-Alder reaction, always reacts with dienophile at its 9,10-position because of the highest HOMO level at this position. To our surprise, the reaction of **30** with dienophile **23** proceeded at a terminal, rather than a central, benzene ring of **30** to give unusual adduct **31** with *exo*-selectivity (Figures 8.20 and 8.21) [36]. Molecular modeling predicted that, because of the steric demand of the *N*-cyclohexyl group, dienophile **23** is only allowed access to the terminal benzene ring, precluding the reaction at the central ring (Figure 8.21b).
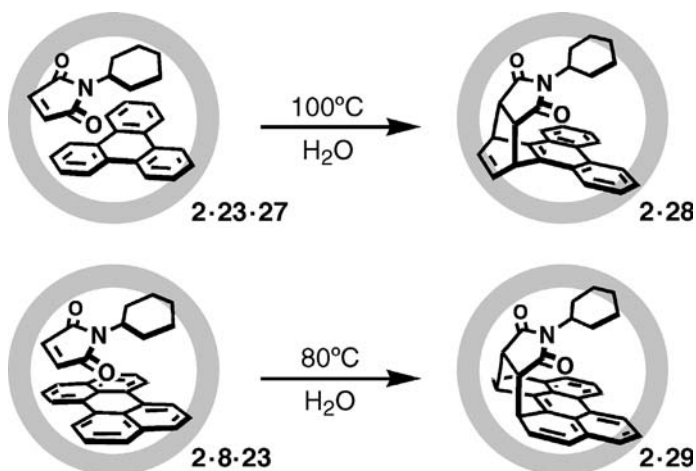
Figure 8.19 Diels-Alder reactions of maleimide (**23**) and triphenylene (**27**) or perylene (**8**) within cage **2**.
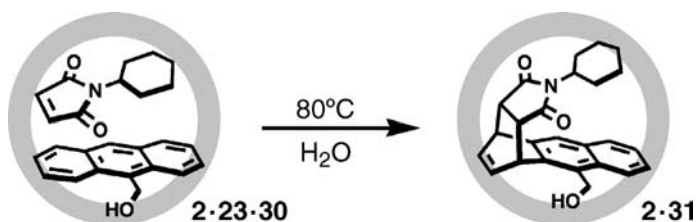
Figure 8.20 Diels-Alder reactions of maleimide (**23**) and anthracene (**30**) within cage **2**.
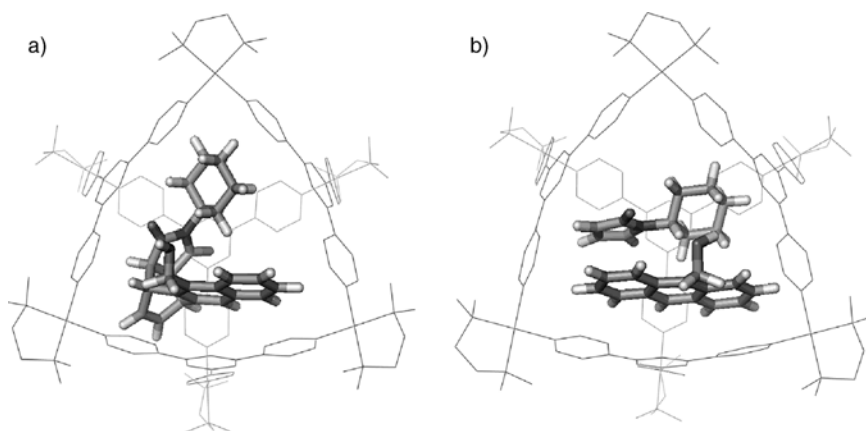
Figure 8.21 (a) Crystal structure of **2·31** complex (after Diels-Alder reaction) and (b) optimized structure of ternary complex **2·23·30** (before the reaction).

8.5.5
Alkane Oxidation

In the above photo and thermal cycloaddition reactions, the reaction pathway is restricted by the space of the cavity reducing the energy barrier of a specific pathway while enhancing the others. The cage itself, however, does not function electronically as a catalytic redox medium. In contrast, an alkane photo-oxidation takes place in the cage via the cage-mediated electron transfer. When the aqueous solution of 1:4 adamantane inclusion complex $2 \cdot (5a)_4$ was irradiated (>300 nm) under anaerobic conditions, the solution color turned blue, indicating the generation of radical species. Analysis of the substrate after irradiation indicated the formation of adamantan-1-ol (as a mixture with the corresponding peroxide) in 24% yield, suggesting that one out of four included guest molecules was oxidized (Figure 8.22) [37]. Electrochemical measurement showed a first one-electron reduction potential of the cage that was considerably low compared with the subsequent second through fourth reduction potentials. From these facts, the most probable pathway to promote the alkane oxidation includes (a) excitation of the triazine ligand with a low-lying LUMO, followed by (b) a one-electron transfer from the H−C bond at the bridgehead of adamantane to the ligand, (c) the resulting adamantane radical cation is immediately dissociated into adamantyl radical and proton, and (d) the adamantane radical is then immediately trapped by dissolved molecular oxygen or water (which was confirmed by experiments using $^{18}O_2$ and $H_2^{18}O$). Since the cage can accept only one electron, as suggested by electrochemical measurements, only one adamantane guest is oxidized (in 96% yield based on cage **2**). The crystal structure of $2 \cdot (5a)_4$ shows that the adamantane C−H bond and the triazine ligand are within van der Waals contact, presumably facilitating the unusual photo-induced alkane oxidation mediated by the electron-deficient cage [37]. Similar oxidations were also promoted with cycloalkanes to give the corresponding alcohols and ketones.

8.5.6
Wacker Oxidation

The Pd(II) hinge in cage **2** can also participate in a chemical transformation. The catalytic Wacker-type oxidation of olefins took place when 8-nonen-1-ol (**32**) was heated for 5 h at 80 °C in the presence of cage **2** (5 mol%), giving 9-hydroxynonan-2-one (**33**)
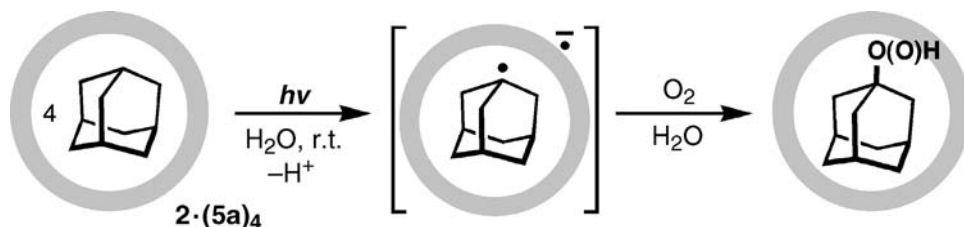
Figure 8.22 Photo-oxidation of adamantane (**5a**) within cage **2** via guest-host electron transfer.
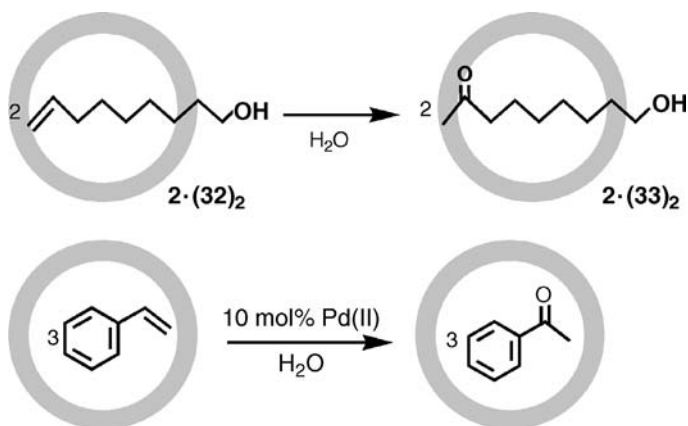
Figure 8.23 Catalytic Wacker oxidation of 8-nonen-1-ol (**32**) and styrene in the presence of cage **2**.

in 66% yield (Figure 8.23) [38]. The crystal structure of 1:2 nonan-1-ol (**34**) inclusion complex [**2**·(**34**)$_2$] revealed the proximity of the terminal carbon of **34** to the Pd(II) center (Figure 8.24), implying a similar placement of the olefin part of **32** with respect to the Pd(II) center, as found in the [**2**·(**32**)$_2$] complex. The Pd(0) species that would result from the Wacker-type oxidation is reoxidized into Pd(II) despite the absence of
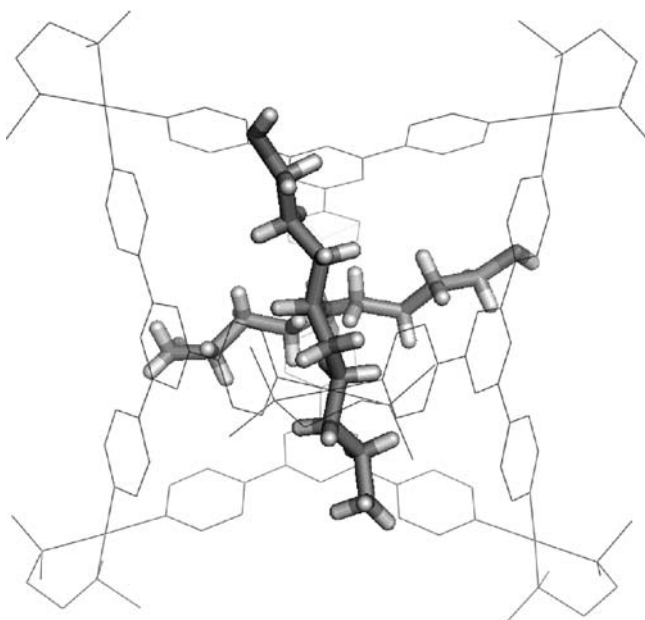
Figure 8.24 Crystal structure of **2**·(**34**)$_2$ complex.
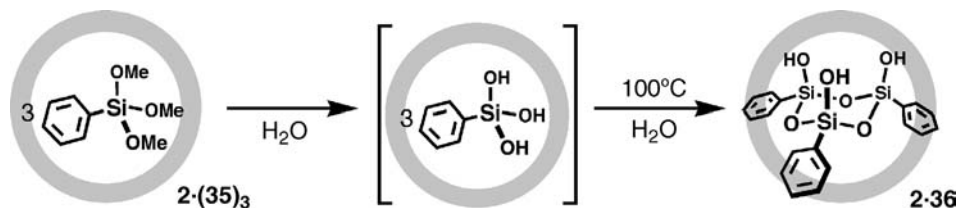
Figure 8.25 Sol-gel condensation of PhSi(OMe)$_3$ (**35**) within case **2** to give cyclic trimer **36**.

any reoxidant. It is likely that dissolved molecular oxygen in the aqueous solution is sufficient to promote the reoxidation of the Pd(0) species. Similar Wacker-type oxidation was also observed for other olefins such as styrene, but a slight excess of (en)Pd (NO$_3$)$_2$, the hinge component of cage **2**, is necessary to attain formation of acetophenone in high yield (Figure 8.23) [39]. A two-phase reaction can be proposed for the catalytic cycle. First, styrene (organic phase) is dissolved into the cavity of **2** in the aqueous phase, where the oxidation is promoted. Then, the more hydrophilic product, acetophenone, is replaced by unreacted styrene to promote the catalytic cycle.

8.5.7
Discrete Siloxane Synthesis

While all the reactions discussed above are organic transformations, we also examined inorganic transformations in the cage. Inorganic reactions often provide structurally infinite bulk materials. For example, hydrolysis and dehydration of trialkoxysilanes, well-known as sol-gel condensation, gives a three-dimensional Si−O network, providing an efficient low-temperature synthesis of functionalized silica gel. When the sol-gel condensation of PhSi(OMe)$_3$ (**35**) was carried out in the presence of cage **2**, the selective formation of the all-*cis* isomer of a cyclic trimer **36** was observed (Figure 8.25) [40,41]. In the common solution-state reaction, it is known that a stereoisomeric mixture of cyclic tetramers is predominantly formed, which is subsequently condensed into a 3D network because of the presence of reactive Si−OH groups. In the cavity of **2**, the cyclic trimer **36** is stabilized, and, despite the presence of the reactive Si−OH group, it is unreactive toward further polymerization even after several weeks in solution.

8.6
Conclusion

New chemistry – particularly, new reactions and properties – created by exploiting the confined cavity of self-assembled M$_6$L$_4$ coordination cages **2** is discussed in this chapter. Thanks to the large cavity and strong binding ability of the cage, as compared with many other known host compounds, this cage allows us to examine binding and chemical transformations that have previously been impossible. This

provides for the continual discovery of new reactions and properties within the confined cavity of cage **2** since its first synthesis in 1995. The chemistry of space promises creative research and will last forever. It is therefore our hope that this chapter will be welcomed by readers as an inspiring source for creative research.

8.7
Experimental: Synthesis of M$_6$L$_4$ Cage 2

In a 100-mL round-bottom flask, (en)Pd(NO$_3$)$_2$ (2.00 g, 6.88 mmol) and 2,4,6-tris-(4-pyridyl)-1,3,5-triazine (1.51 g, 4.83 mmol) were combined with H$_2$O (60 mL). When the suspended mixture was stirred at 100 °C for 3 h, a pale yellow solution was obtained. The resulting solution was filtered to remove excess triazine ligand. After removal of the solvent by evaporation under reduced pressure, **2** was obtained as a pale yellow powder in 93% yield (3.20 g, 1.07 mmol). ^{1}H NMR (500 MHz, D$_2$O, TMS as an external standard): δ 2.98 ppm (s, 24H, -CH_2-), 8.63 ppm (dd, $J = 6.8, 3.9$ Mz, 24H), 9.13 ppm (dd, $J = 6.8, 3.9$ Hz, 24H). ^{13}C NMR (125 MHz, D$_2$O, CHCl$_3$ as an external standard): δ 46.9 (CH), 125.5 (CH), 145.6 (C$_q$), 152.2 (CH), 169.8 (C$_q$).

Acknowledgments

Abbreviations

en	ethylenediamine
bpy	2,2′-bipyridine
tmen	*N,N,N′,N′*-tetramethylethylenediamine
Py	pyridyl

References

1 Fujita, M., Yazaki, J. and Ogura, K. (1990) *J. Am. Chem. Soc.*, **112**, 5645–5647.

2 Stang, P.J. and Cao, D.H. (1994) *J. Am. Chem. Soc.*, **116**, 4981–4982.

3 (a) Lahav, M., Gabai, R., Shipway, A.N. and Willner, I. (1999) *Chem. Commun.*, 1937–1938. (b) Bélanger, S., Hupp, J.T., Stern, C.L., Slone, R.V., Watson, D.F. and Carrell, T.G. (1999) *J. Am. Chem. Soc.*, **121**, 557–563. (c) Lau, V.C., Berben, L.A. and Long, J.R. (2002) *J. Am. Chem. Soc.*, **124**, 9042–9043.

4 (a) Drain, C.M. and Lehn, J.-M. (1994) *J. Chem. Soc. Chem. Commun.*, 2313–2315. (b) Stang, P.J., Fan, J. and Olenyuk, B. (1997) *Chem. Commun.*, 1453–1454.

5 Olenyuk, B., Whiteford, J.A. and Stang, P.J. (1996) *J. Am. Chem. Soc.*, **118**, 8221–8230.

6 (a) Stang, P.J., Olenyuk, B., Fan, J. and Arif, A.M. (1996) *Organometallics*, **15**, 904–908. (b) Stang, P.J., Cao, D.H., Chen, K., Gray, G.M., Muddiman, D.C. and Smith, R.D. (1997) *J. Am. Chem. Soc.*, **119**, 5163–5168.

7 Fujita, M., Oguro, D., Miyazawa, M., Oka, H., Yamaguchi, K. and Ogura, K. (1995) *Nature*, **378**, 469–471.

8 (a) Saalfrank, R.W., Stark, A., Peters, K. and von Schnering, H.G. (1988) *Angew. Chem. Int. Ed. Engl.*, **27**, 851–853; *Angew. Chem.*, **100**, 878–880., (b) Saalfrank, R.W., Stark, A., Bremer, M. and Hummel, H.-U. (1990) *Angew. Chem. Int. Ed. Engl.*, **29**, 311–314; *Angew. Chem.*, **102**, 292–295., (c) Saalfrank, R.W., Hörner, B., Stalke, D. and Salbeck, J. (1993) *Angew. Chem. Int. Ed. Engl.*, **32**, 1179–1182; *Angew. Chem.*, **105**, 1223–1225.

9 (a) Beissel, T., Powers, R.E. and Raymond, K.N. (1996) *Angew. Chem. Int. Ed. Engl.*, **35**, 1084–1086; *Angew. Chem.*, **108**, 1166–1168. (b) Caulder, D.L., Powers, R.E., Parac, T.N. and Raymond, K.N. (1998) *Angew. Chem. Int. Ed.*, **37**, 1840–1843; *Angew. Chem.*, **110**, 1940–1943. (c) Ziegler, M., Brumaghim, J.L. and Raymond, K.N. (2000) *Angew. Chem. Int. Ed.*, **39**, 4119–4121; *Angew. Chem.*, **112**, 4285–4287. (d) Fiedler, D., Bergman, R.G. and Raymond, K.N. (2004) *Angew. Chem. Int. Ed.*, **43**, 6748–6751; *Angew. Chem.*, **116**, 6916–6919. (e) Dong, V.M., Fiedler, D., Carl, B., Bergman, R.G. and Raymond, K.N. (2006) *J. Am. Chem. Soc.*, **128**, 14464–14465.

10 (a) Mann, S., Huttner, G., Zsolnai, L. and Heinze, K. (1996) *Angew. Chem. Int. Ed. Engl.*, **35**, 2808–2809; *Angew. Chem.*, **108**, 2983–2984. (b) Fleming, J.S., Mann, K.L. V., Carraz, C.-A., Psillakis, E., Jeffrey, J. C., McCleverty, J.A. and Ward, M.D. (1998) *Angew. Chem. Int. Ed.*, **37**, 1279–1281; *Angew. Chem.*, **110**, 1315–1318. (c) Amoroso, A.J., Jeffery, J. C., Jones, P.L., McCleverty, J.A., Thornton, P. and Ward, M.D. (1995) *Angew. Chem. Int. Ed. Engl.*, **34**, 1443–1446; *Angew. Chem.*, **107**, 1577–1580. (d) Brückner, C., Powers, R. E. and Raymond, K.N. (1998) *Angew. Chem. Int. Ed.*, **37**, 1837–1839; *Angew. Chem.*, **110**, 1937–1940. (e) Umemoto, K., Yamaguchi, K. and Fujita, M. (2000) *J. Am. Chem. Soc.*, **122**, 7150–7151. (f) Saalfrank, R.W., Glaser, H., Demleitner, B., Hampel, F., Chowdhry, M.M., Schünemann, V., Trautwein, A.X., Vaughan, G.B.M., Yeh, R., Davis, A.V. and Raymond, K.N. (2002) *Chem. Eur. J.*, **8**, 493–497.(g) Schweiger, M., Seidel, S. R., Schmitz, M. and Stang, P.J. (2000) *Org. Lett.*, **2**, 1255–1257. (h) Bourgeois, J.-P., Fujita, M., Kawano, M., Sakamoto, S. and Yamaguchi, K. (2003) *J. Am. Chem. Soc.*, **125**, 9260–9261. (i) Hiraoka, S., Yi, T., Shiro, M. and Shionoya, M. (2002) *J. Am. Chem. Soc.*, **124**, 14510–14511. (j) Hiraoka, S., Harano, K., Shiro, M. and Shionoya, M. (2005) *Angew. Chem. Int. Ed.*, **44**, 2727–2731; *Angew. Chem.*, **117**, 2787–2791.
(k) Albrecht, M., Janser, I., Meyer, S., Weis, P. and Fröhlich, R. (2003) *Chem. Commun.*, 2854–2855.

11 (a) Takeda, N., Umemoto, K., Yamaguchi, K. and Fujita, M. (1999) *Nature*, **398**, 794–796. (b) Umemoto, K., Tsukui, H., Kusukawa, T., Biradha, K. and Fujita, M. (2001) *Angew. Chem. Int. Ed.*, **40**, 2620–2622; *Angew. Chem.*, **113**, 2690–2692. (c) Ikeda, A., Yoshimura, M., Udzu, H., Fukuhara, C. and Shinkai, S. (1999) *J. Am. Chem. Soc.*, **121**, 4296–4297. (d) Müller, I.M. and Möller, D. (2005) *Angew. Chem. Int. Ed.*, **44**, 2969–2973; *Angew. Chem.*, **117**, 3029–3033.

(e) Fujita, M., Nagao, S. and Ogura, K. (1995) *J. Am. Chem. Soc.*, **117**, 1649–1650. (f) Hiraoka, S. and Fujita, M. (1999) *J. Am. Chem. Soc.*, **121**, 10239–10240. (g) Sun, X., Johnson, D. W., Caulder, D.L., Powers, R.E., Raymond, K.N. and Wong, E.H. (1999) *Angew. Chem. Int. Ed.*, **38**, 1303–1307; *Angew. Chem.*, **111**, 1386–1390. (h) Catalano, V.J., Bennett, B.L., Kar, H.M. and Noll, B.C. (1999) *J. Am. Chem. Soc.*, **121**, 10235–10236. (i) Claessens, C.G. and Torres, T. (2002) *J. Am. Chem. Soc.*, **124**, 14522–14523. (j) Su, C.-Y., Cai, Y.-P., Chen, C.-L., Lissner, F., Kang, B.-S. and Kaim, W. (2002) *Angew. Chem. Int. Ed.*, **41**, 3371–3375; *Angew. Chem.*, **114**, 3519–3523. (k) Su, C.-Y., Cai, Y.-P., Chen, C.-L., Smith, M.D., Kaim, W. and zur Loye, H.-C. (2003) *J. Am. Chem. Soc.*, **125**, 8595–8613. (l) Kumazawa, K., Yamanoi, Y., Yoshizawa, M., Kusukawa, T. and Fujita, M. (2004) *Angew. Chem. Int. Ed.*, **43**, 5936–5940; *Angew. Chem.*, **116**, 6062–6066.

12 (a) Jacopozzi, P. and Dalcanale, E. (1997) *Angew. Chem. Int. Ed. Engl.*, **36**, 613–615; *Angew. Chem.*, **109**, 665–667. (b) Kobayashi, K., Yamada, Y., Yamanaka, M., Sei, Y. and Yamaguchi, K. (2004) *J. Am. Chem. Soc.*, **126**, 13896–13897. (c) Stang, P.J., Olenyuk, B., Muddiman, D.C. and Smith, R.D. (1997) *Organometallics*, **16**, 3094–3096. (d) Schweiger, M., Yamamoto, T., Stang, P. J., Bläser, D. and Boese, R. (2005) *J. Org. Chem.*, **70**, 4861–4864. (e) Hartshorn, C. M. and Steel, P.J. (1997) *Chem. Commun.*, 541–542. (f) Liu, H.-K. and Tong, X. (2002) *Chem. Commun.*, 1316–1317. (g) Fox, O.D., Dalley, N.K. and Harrison, R.G. (1998) *J. Am. Chem. Soc.*, **120**, 7111–7112. (h) James, S.L., Mingos, D.M.P., White, A.J.P. and Williams, D.J. (1998) *Chem. Commun.*, 2323–2324. (i) Cotton, F.A., Daniels, L.M., Lin, C. and Murillo, C.A. (1999) *Chem. Commun.*, 841–842. (j) Ikeda, A., Ayabe, M., Shinkai, S., Sakamoto, S. and Yamaguchi, K. (2000) *Org. Lett.*, **2**, 3707–3710. (k) Hong, M., Zhao, Y., Su, W., Cao, R., Fujita, M., Zhou, Z. and Chan, A.S.C. (2000) *J. Am. Chem. Soc.*, **122**, 4819–4820. (l) Zhong, Z., Ikeda, A., Ayabe, M., Shinkai, S., Sakamoto, S. and Yamaguchi, K. (2001) *J. Org. Chem.*, **66**, 1002–1008. (m) Chand, D.K., Biradha, K., Fujita, M., Sakamoto, S. and Yamaguchi, K. (2002) *Chem. Commun.*, 2486–2487. (n) Müller, I.M., Spillmann, S., Franck, H. and Pietschnig, R. (2004) *Chem. Eur. J.*, **10**, 2207–2213. (o) McKinlay, R.M., Thallapally, P.K., Cave, G.W.V. and Atwood, J.L. (2005) *Angew. Chem. Int. Ed.*, **44**, 5733–5736; *Angew. Chem.*, **117**, 5879–5882. (p) Haino, T., Kobayashi, M., Chikaraishi, M. and Fukazawa, Y. (2005) *Chem. Commun.*, 2321–2323. (q) Hiraoka, S., Harano, K., Shiro, M., Ozawa, Y., Yasuda, N., Toriumi, K. and Shionoya, M. (2006) *Angew. Chem. Int. Ed.*, **45**, 6488–6491; *Angew. Chem.*, **118**, 6638–6641.

13 (a) McMorran, D.A. and Steel, P.J. (1998) *Angew. Chem. Int. Ed.*, **37**, 3295–3297; *Angew. Chem.*, **110**, 3495–3497. (b) Chand, D.K., Biradha, K. and Fujita, M. (2001) *Chem. Commun.*, 1652–1653. (c) Yue, N.L.S., Eisler, D.J., Jennings, M.C. and Puddephatt, R.J. (2004) *Inorg. Chem.*, **43**, 7671–7681. (d) Fujita, M., Yu, S.-Y., Kusukawa, T., Funaki, H., Ogura, K. and Yamaguchi, K. (1998) *Angew. Chem. Int. Ed.*, **37**, 2082–2085; *Angew. Chem.*, **110**, 2192–2196. (e) Schnebeck, R.-D., Freisinger, E. and Lippert, B. (1999) *Angew. Chem. Int. Ed.*, **38**, 168–171; *Angew. Chem.*, **111**, 235–238. (f) Yu, S.-Y., Huang, H., Liu, H.-B., Chen, Z.-N., Zhang, R. and Fujita, M. (2003) *Angew. Chem. Int. Ed.*, **42**, 686–690; *Angew. Chem.*, **115**, 710–714. (g) Baxter, P.N.W., Lehn, J.-M., Kneisel, B.O., Baum, G. and Fenske, D. (1999) *Chem. Eur. J.*, **5**, 113–120. (h) Garcia, A.M., Bassani, D.M., Lehn, J.-M., Baum, G. and Fenske, D. (1999)

Chem. Eur. J., **5**, 1234–1238.
(i) Fujita, N., Biradha, K., Fujita, M., Sakamoto, S. and Yamaguchi, K. (2001) *Angew. Chem. Int. Ed.*, **40**, 1718–1721; *Angew. Chem.*, **113**, 1768–1771; (j) Benkstein, K.D. and Hupp, J.T. (2000) *Mol. Cryst. Liq. Cryst.*, **342**, 151–158. (k) Sun, S.-S. and Lees, A.J. (2001) *Chem. Commun.*, 103–104. (l) Sommer, R.D., Rheingold, A.L., Goshe, A.J. and Bosnich, B. (2001) *J. Am. Chem. Soc.*, **123**, 3940–3952. (m) Kuehl, C.J., Yamamoto, T., Seidel, S.R. and Stang, P. J. (2002) *Org. Lett.*, **4**, 913–915. (n) Kumazawa, K., Biradha, K., Kusukawa, T., Okano, T. and Fujita, M. (2003) *Angew. Chem. Int. Ed.*, **42**, 3909–3913; *Angew. Chem.*, **115**, 4039–4043. (o) Yoshizawa, M., Nakagawa, J., Kumazawa, K., Nagao, M., Kawano, M., Ozeki, T. and Fujita, M. (2005) *Angew. Chem. Int. Ed.*, **44**, 1810–1813; *Angew. Chem.*, **117**, 1844–1847.
(p) Yoshizawa, M., Nagao, M., Kumazawa, K. and Fujita, M. (2005) *J. Organomet. Chem.*, **690**, 5383–5388.
(q) Yoshizawa, M., Ono, K., Kumazawa, K., Kato, T. and Fujita, M. (2005) *J. Am. Chem. Soc.*, **127**, 10800–10801. (r) Yoshizawa, M., Kumazawa, K. and Fujita, M. (2005) *J. Am. Chem. Soc.*, **127**, 13456–13457. (s) Mahmoudkhani, A.H., Côté, A.P. and Shimizu, G.K.H. (2004) *Chem. Commun.*, 2678–2679.

14 (a) Roche, S., Haslam, C., Adams, H., Heath, S.L. and Thomas, J.A. (1998) *Chem. Commun.*, 1681–1682.
(b) Heinrich, J.L., Berseth, P.A. and Long, J.R. (1998) *Chem. Commun.*, 1231–1232. (c) Klausmeyer, K.K., Rauchfuss, T. B. and Wilson, S.R. (1998) *Angew. Chem. Int. Ed.*, **37**, 1694–1696; (1998) *Angew. Chem.*, **110**, 1808–1810. (d) Klausmeyer, K.K., Wilson, S.R. and Rauchfuss, T.B. (1999) *J. Am. Chem. Soc.*, **121**, 2705–2711. (e) Johannessen, S.C. and Brisbois, R.G. (2001) *J. Am. Chem. Soc.*, **123**, 3818–3819. (f) Drain, C.M. and Lehn, J.-M. (1994) *J. Chem. Soc. Chem.*

Commun., 2313–2315. (g) Slone, R.V. and Hupp, J.T. (1997) *Inorg. Chem.*, **36**, 5422–5423. (h) Stang, P.J., Fan, J. and Olenyuk, B. (1997) *Chem. Commun.*, 1453–1454. (i) Würthner, F. and Sautter, A. (2000) *Chem. Commun.*, 445–446. (j) Yamanoi, Y., Sakamoto, Y., Kusukawa, T., Fujita, M., Sakamoto, S. and Yamaguchi, K. (2001) *J. Am. Chem. Soc.*, **123**, 980–981. (k) Aoyagi, M., Biradha, K. and Fujita, M. (1999) *J. Am. Chem. Soc.*, **121**, 7457–7458. (l) Aoyagi, M., Tashiro, S., Tominaga, M., Biradha, K. and Fujita, M. (2002) *Chem. Commun.*, 2036–2037. (m) Tominaga, M., Tashiro, S., Aoyagi, M. and Fujita, M. (2002) *Chem. Commun.*, 2038–2039. (n) Yamaguchi, T., Tashiro, S., Tominaga, M., Kawano, M., Ozeki, T. and Fujita, M. (2004) *J. Am. Chem. Soc.*, **126**, 10818–10819.

15 (a) Olenyuk, B., Levin, M.D., Whiteford, J.A., Shield, J.E. and Stang, P.J. (1999) *J. Am. Chem. Soc.*, **121**, 10434–10435.
(b) Olenyuk, B., Whiteford, J.A., Fechtenkötter, A. and Stang, P.J. (1999) *Nature*, **398**, 796–799. (c) Abrahams, B. F., Egan, S.J. and Robson, R. (1999) *J. Am. Chem. Soc.*, **121**, 3535–3536.
(d) Moulton, B., Lu, J., Mondal, A. and Zaworotko, M.J. (2001) *Chem. Commun.*, 863–864. (e) Eddaoudi, M., Kim, J., Wachter, J.B., Chae, H.K., O'Keeffe, M. and Yaghi, O.M. (2001) *J. Am. Chem. Soc.*, **123**, 4368–4369. (f) Ke, Y., Collins, D.J. and Zhou, H.-C. (2005) *Inorg. Chem.*, **44**, 4154–4156. (g) Tominaga, M., Suzuki, K., Kawano, M., Kusukawa, T., Ozeki, T., Sakamoto, S., Yamaguchi, K. and Fujita, M. (2004) *Angew. Chem. Int. Ed.*, **43**, 5621–5625; *Angew. Chem.*, **116**, 5739–5743. (h) Tominaga, M., Suzuki, K., Murase, T. and Fujita, M. (2005) *J. Am. Chem. Soc.*, **127**, 11950–11951. (i) Sato, S., Iida, J., Suzuki, K., Kawano, M., Ozeki, T. and Fujita, M. (2006) *Science*, **313**, 1273–1276. (j) Aoki, S., Shiro, M. and Kimura, E. (2002) *Chem. Eur. J.*, **8**, 929–939. (k) Argent, S.P., Adams, H., Riis-Johannessen, T., Jeffery, J.C., Harding, L.P.

and Ward, M.D. (2006) *J. Am. Chem. Soc.*, **128**, 72–73.

16 Kusukawa, T. and Fujita, M. (1998) *Angew. Chem. Int. Ed.*, **37**, 3142–3144; *Angew. Chem.*, **110**, 3327–3329.

17 Kusukawa, T., Yoshizawa, M. and Fujita, M. (2001) *Angew. Chem. Int. Ed.*, **40**, 1879–1884; *Angew. Chem.*, **113**, 1931–1936.

18 Gokel, G.W. (1991) *Crown Ethers and Cryptands*, Royal Society of Chemistry, Cambridge.

19 Szejtli, J. (1988) *Cyclodextrin Technology*, Kluwer Academic Publishers, Dordrecht.

20 Gutsche, C.D. (1989) *Calixarenes*, Royal Society of Chemistry, Cambridge.

21 Asfari, Z. Bohmer, V. Harrowfield, J. Vicens, J. and Saadiouli, M. (eds) (2001) *Calixarenes*, Kluwer Academic Publishers, Dordrecht.

22 Lagona, J., Mukhopadhyay, P., Chakrabarti, S. and Isaacs, L. (2005) *Angew. Chem. Int. Ed.*, **44**, 4844–4870; *Angew. Chem.*, **117**, 4922–4949.

23 Kusukawa, T. and Fujita, M. (2002) *J. Am. Chem. Soc.*, **124**, 13576–13582.

24 Ibukuro, F., Kusukawa, T. and Fujita, M. (1998) *J. Am. Chem. Soc.*, **120**, 8561–8562.

25 Yoshizawa, M., Tamura, M. and Fujita, M. (2004) *J. Am. Chem. Soc.*, **126**, 6846–6847.

26 Kusukawa, T. and Fujita, M. (1999) *J. Am. Chem. Soc.*, **121**, 1397–1398.

27 Yoshizawa, M., Kusukawa, T., Kawano, M., Ohhara, T., Tanaka, I., Kurihara, K., Niimura, N. and Fujita, M. (2005) *J. Am. Chem. Soc.*, **127**, 2798–2799.

28 Tashiro, S., Tominaga, M., Kawano, M., Therrien, B., Ozeki, T. and and Fujita, M. (2005) *J. Am. Chem. Soc.*, **127**, 4546–4547.

29 Sun, W.-Y., Kusukawa, T. and Fujita, M. (2002) *J. Am. Chem. Soc.*, **124**, 11570–11571.

30 Nakabayashi, K., Kawano, M., Yoshizawa, M., Ohkoshi, S. and Fujita, M. (2004) *J. Am. Chem. Soc.*, **126**, 16694–16695.

31 Nakabayashi, K., Kawano, M., Kato, T., Furukawa, K., Ohkoshi, S., Hozumi, T. and Fujita, M. (2007) *Chem. Asian J.*, **2**, 164–170.

32 (a) Yoshizawa, M., Takeyama, Y., Kusukawa, T. and Fujita, M. (2002) *Angew. Chem. Int. Ed.*, **41**, 1347–1349; *Angew. Chem.*, **114**, 1403–1405. (b) Takaoka, K., Kawano, M., Ozeki, T. and Fujita, M. (2006) *Chem. Commun.*, 1625–1627.

33 Yoshizawa, M., Takeyama, Y., Okano, T. and Fujita, M. (2003) *J. Am. Chem. Soc.*, **125**, 3243–3247.

34 Nishioka, Y., Yamaguchi, T., Yoshizawa, M. and Fujita, M. (2007) *J. Am. Chem. Soc.*, **129**, 2000–2001. .

35 Kusukawa, T., Nakai, T., Okano, T. and Fujita, M. (2003) *Chem. Lett.*, **32**, 284–285.

36 Yoshizawa, M., Tamura, M. and Fujita, M. (2006) *Science*, **312**, 251–254.

37 Yoshizawa, M., Miyagi, S., Kawano, M., Ishiguro, K. and Fujita, M. (2004) *J. Am. Chem. Soc.*, **126**, 9172–9173.

38 Ito, H., Kusukawa, T. and Fujita, M. (2000) *Chem. Lett.*, **29**, 598–599.

39 Yoshizawa, M., Sato, N. and Fujita, M. (2005) *Chem. Lett.*, **34**, 1392–1393.

40 Yoshizawa, M., Kusukawa, T., Fujita, M. and Yamaguchi, K. (2000) *J. Am. Chem. Soc.*, **122**, 6311–6312.

41 Yoshizawa, M., Kusukawa, T., Fujita, M., Sakamoto, S. and Yamaguchi, K. (2001) *J. Am. Chem. Soc.*, **123**, 10454–10459.

9
Anion-binding Macrocycles

Evgeny A. Katayev, Patricia J. Melfi, and Jonathan L. Sessler

9.1
Introduction

The synthesis and subsequent characterization of macrocyclic compounds is often accompanied by the observation of small species, such as cations, anions, or neutral molecules, encapsulated within the inner cavity of the macrocycle. Anions are particularly important in the context of such recognition because of the range of applications where macrocycles can be used as anion-binding systems, namely in analytical chemistry, biology, medicine, or environmental remediation [1]. The last decade has seen an explosion of interest in the area of anion binding, and it is becoming a common procedure to test new macrocyclic systems for the ability to bind anionic species [2]. Moreover, the range of anions studied has grown as the number of anion-binding agents has increased and their potential utility has come to be better appreciated [3–5]. Not surprisingly, the structures of the macrocyclic receptors in question have grown in their complexity; many of these are so-called hybrid systems that combine various "anion-binding units", each of which either provides a specific type of interaction with the anion (i.e. hydrogen bonding, electrostatic interactions, π-bonding, etc.) or plays a specific role in the recognition process [6]. This chapter is devoted to recent approaches to the design of such hybrid macrocyclic anion receptors.

   The first stage in the design of synthetic anion-binding receptors involves identifying and characterizing different potential binding motifs. The second stage then involves combining one or more of these motifs in such a way that the resulting receptor is appropriately tailored to the geometry of a given target anion. This tailoring, which in favorable cases provides good substrate-receptor compatibility, allows for the production of macrocyclic systems that, as a general rule, display enhanced affinity for anions relative to open-chain analogs or cyclic compounds that have not been appropriately optimized. The result, at least in principle, is receptors with very high affinities and selectivities for the targeted anionic analytes [2]. However, this idealized goal of substrate-receptor complementarity is rarely achieved,

especially in the case of non-spherical anions. For this reason, there is an ongoing search for both new binding motifs and improved design strategies that will allow these motifs to be exploited in promising ways. Over the past few years, a number of reviews has appeared that highlight the development of anion receptors based on widely used anion-binding motifs, including polyammoniums, which are generally considered to be the first well-defined anion receptor motifs [7–10], amides [11,12], guanidiniums [13,14], imidazoliums [15], steroids [16], pyrroles [17,18], and also metal-based systems [19,20]. While great success has been encountered using these classic single-motif approaches, a new generation of macrocyclic anion receptors has recently emerged in the literature, wherein a number of different motifs are combined together. These integrated macrocycles represent a novel class of hybrid organic compounds, in which the combination of different motifs is designed to stabilize a specific interaction between the host and the guest. On some level, therefore, the move toward hybrid anion receptors reflects an appreciation of Nature, wherein complex protein-based systems exploit multiple and generally distinct subunits and interactions to achieve exquisite anion-binding selectivity.

Scheme 9.1 summarizes the main directions in the development of hybrid macrocycles that are considered most promising in the context of the paired goals of achieving improved anion-binding efficiency and enhanced selectivity. These can be viewed in the context of three dominant themes: (a) functionalization of scaffolds, namely the introduction of additional binding motifs with the intent to "fine-tune" the binding properties of a particular receptor type or to introduce a signaling group for sensing anions [21,22]. (Note: In the context of this chapter, "scaffolds" will be defined as receptors with similar binding motifs.) (b) receptors for ion pairs – ditopic receptors capable of binding a cation and an anion simultaneously [1,2], and (c) the development of macrocyclic ligands containing different binding motifs for the specific binding of non-spherical anions [23]. Here, as a general rule, the geometry of the receptor and nature of its presumed non-isotropic interactions with the targeted guest play a crucial role in selective recognition. It is worth mentioning that these three directions overlap significantly. They also have connections to other broader themes in supramolecular chemistry. For example, anion-templated assembly, which touches on the emerging theme of dynamic combinatorial chemistry,
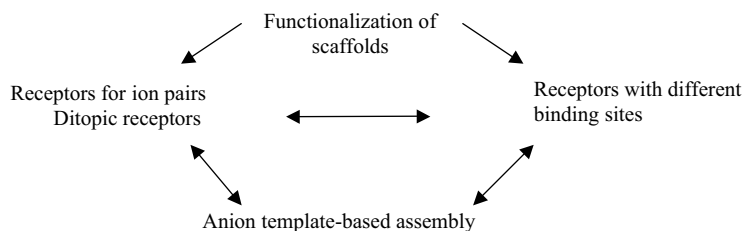
Scheme 9.1 Scheme showing the interplay between different synthetic approaches and the resulting elaborated receptors discussed in this chapter. For the sake of coherence and brevity, the focus is on so-called hybrid macrocyclic anion receptors as detailed further in the text.

represents an effective, albeit still infrequently employed, means of producing highly selective receptors. Given this, it is considered probable that the investigation of assemblies as well as template-based synthesis of known receptors can provide clues to the synthesis of an ideal receptor [2,24,25]. For instance, by using a template it is possible, at least in principle, to direct combinatorial libraries toward the production of highly selective receptors. Such strategies can also provide key insights into the binding properties of a given putative anion recognition motif. On the other hand, to be most informative, studies of this type should involve systems with more than one anion-binding motif, referred to as hybrid receptor systems in the context of this chapter.

This chapter consists of two main subchapters in accordance with Scheme 9.1. This scheme is meant to show in a simplified fashion how the generalized set of macrocyclic receptor systems containing more than one kind of binding motif, so-called hybrid receptors, can be organized according to desired function, namely recognition of more than one substrate (ion pair and ditopic receptors) or the binding of (primarily) a single set of guests (e.g., anions) using multiple recognition motifs (receptors with different binding sites). Needless to say, the dynamic nature of the generalized ion recognition field means there is some overlap between these two limiting categorizations. In fact, the same strategies (e.g., functionalization of known scaffolds and template-based assembly) are often used to obtain both classes of receptor, a point that is underscored in Scheme 9.1. Nonetheless, for the sake of coherence, this chapter is organized according to receptor type following the distinctions made by the authors of the original research publications being reviewed. Needless to say, the authors apologize in advance for any confusion this choice of organization might cause, as well as for any omissions to specific work as necessitated by the length considerations of this chapter.

9.2
Ditopic Receptors and Receptors for Ion Pairs

Since the properties of simple macrocyclic ligands, such as crown ethers, calixarenes, or cholapods, are well known, it is perhaps not surprising that many researchers have chosen to functionalize them with different anion-binding motifs with a view to generating ditopic receptors and receptors for ion pairs. In general, three basic strategies have been employed to effect such functionalization. The first involves appending one or more functional groups to the scaffold either to increase the affinity or to enhance the utility of the recognition process. Thus, in the broadest sense this approach includes the tethering of new binding motifs and the attachment of signaling groups that permit sensing applications. The second strategy involves the capping of the basic receptor core with an additional linker ("strap") so as to control the conformation, enforce a specific geometry, or provide additional binding motifs. Since the length of the "straps" can be adjusted, at least in principle, this strategy often permits a high degree of design optimization. The third strategy consists of linking two or more receptor systems, either open-chain or macrocyclic,

via appropriately chosen linkers so as to generate elaborated polytopic binding agents. Since the individual components in these latter systems need not be the same, considerable selectivity in tuning is possible. For this reason, this third strategy, along with the second, has often been exploited to generate ion pair receptors in addition to systems targeting just anionic (or cationic) substrates.

9.2.1
Crown Complexes

Bradley Smith and coworkers have developed a "strapped" diazacrown complex, **1** (Scheme 9.2), capable of extracting salts as contact ion pairs [26–30]. In initial work with this receptor, they demonstrated transport of KCl across a phospholipid bilayer membrane [27]. They then demonstrated the transport of an array of ion-pairs across a supported liquid membrane (SLM) [28]. This group noted that transport was more efficient using their ditopic system than with a corresponding set of paired anion and cation receptors under the same conditions. Under the interfacial conditions employed in these experiments, the anion transport selectivity was found to be $I^- > Br^- > Cl^-$ with K^+. However, when the conditions were altered, (i.e., from through-membrane transport to solid-liquid extraction), the selectivity was reversed. Specifically, under a solid-liquid transport scenario, extraction with lithium was reported to be 15 times more effective than with either K^+ or Na^+ when Cl^- was used as the counter ion and 11 times better when Br^- was employed as the counter ion [29]. The authors rationalized this reversal in terms of the higher solubility of the lithium salts, among other reasons. While initial characterization studies of this receptor were focused on metal cation extraction, the anions employed being limited to the halides, more recently Smith and coworkers have investigated oxoanions to good effect. In the context of these latter efforts, a series of crystal structures was compared. In a first set of comparisons, employing the KNO_3, $NaNO_3$, and $LiNO_3$ salts, an immediate correlation between the size of the cation and the inclusion of the anion within the macrobicycle was seen. The orientation of the NO_3^- was also
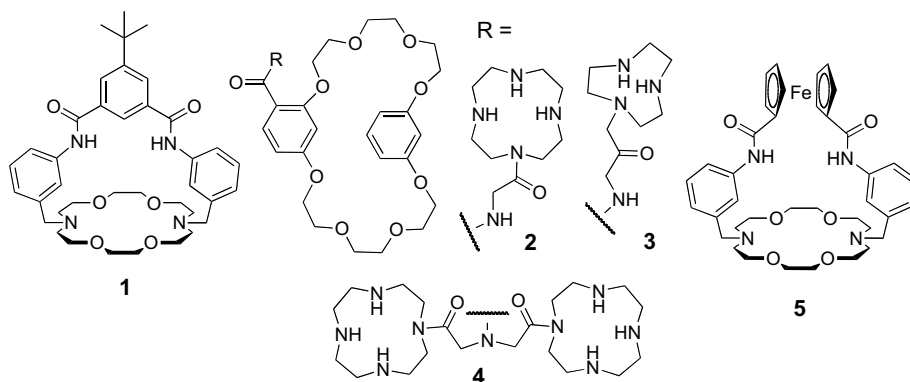
Scheme 9.2 Crown-based ditopic receptors.

observed to change, presumably allowing for better alignment of the amide NH protons with the lone pairs of an oxygen atom. Additionally, in all three instances, the amide NH protons were found to form hydrogen bonds with just one of the NO_3^- oxygen atoms; again, this could be rationalized in terms of the stronger hydrogen bond formed upon ideal alignment of the amide NH protons with the oxygen lone pairs. Similar asymmetry and hydrogen-bond formation were found in a complex formed from $NaNO_2$. In all but one instance (KNO_3), some degree of chelation with the counter cation was observed. NMR spectroscopic studies provided evidence for anistropic shielding, a feature that was attributed to the oxoanions. While the NH signals moved downfield upon the addition of NaCl, NaOAc, and KOAc, as would be expected for normal hydrogen bond-mediated anion recognition, this did not prove to be the case for NO_3^- or NO_2^-. Here, various effects, including an upfield shift in the pyrrolic NH proton signal, were seen in the case of the nitrate and nitrite salts. The authors attributed this behavior to the dual shielding and deshielding properties of NO_3^- and NO_2^- [30].

Gunning et al. have investigated the ability of a cyclene-dibenzacrown hybrid macrocycle to bind various substituted phosphates [31]. This system, which functions as an ion pair receptor, consists of a cyclene and dibenzo-24-crown-8 macrocycle joined by a glycine bridge. The zinc complex (Zn-$\mathbf{2}^{2+}$) was readily synthesized and subsequently reacted with either sodium or potassium phosphate salts. The ability to interact with inorganic phosphate and other substituted phosphates was investigated by ^1H NMR spectroscopy, UV-vis spectroscopy, and isothermal titration calorimetry (ITC). A Zn^{2+}-cyclene macrocycle was used in these studies as a control system. ITC experiments revealed 2:1 binding values with dihydrogen phosphate on the order of $4 \times 10^4 \, M^{-2}$ and $9 \times 10^4 \, M^{-2}$ (in the case where the counter cations were Na^+ and K^+, respectively). The stronger affinities observed for K^+ over Na^+ for receptor $Zn \cdot \mathbf{2}^{2+}$ led the authors to suggest that K^+ is bound by the crown and that the system is functioning as an ion pair receptor. In contrast, the use of K^+ or Na^+ salts was observed to have little effect compared to the "control" zinc complex, which displayed 1:1 binding constants of $1.6 \times 10^4 \, M^{-1}$ and $1.5 \times 10^4 \, M^{-1}$ for Na^+ and K^+, respectively. Association constants for the substituted phosphates, glycerophosphate monoanion, and 4-nitrophenylphosphate dianion were reported, but were found to be similar to those seen in the case of the control Zn^{2+}-cyclene system. The thermodynamic quantities ΔG, ΔH, and $-T\Delta S$ were also reported, and the authors noted that anion-binding with the Zn^{2+}-cyclene system was exothermic, whereas with the hybrid macrocycle, anion-binding was endothermic. The authors rationalized this dichotomy in terms of the suggestion that a pocket of water exists and that these solvent molecules are hydrogen-bonded to the free receptor system. Upon anion association, this pocket of water must be removed, requiring energy. Nonetheless, since the entropy of the overall system increases, increases in affinity are observed.

This work was later expanded to include a larger crown ether system functionalized with either the above-mentioned cyclene macrocycle (**2**), two cyclene macrocycles (**4**), or a triazacyclononane macrocycle (**3**) [32]. Unfortunately, the $Cu \cdot \mathbf{3}^{2+}$ complex did not display any appreciable affinity for the phosphate species (NaH_2PO_4, KH_2PO_4, sodium glycerophosphate, or disodium 4-nitrophenylphosphate).

The authors rationalized this finding on steric grounds, noting that the phosphate anion was a poor geometric complement to the presumed distorted five-coordinate copper complex. The Zn·4^{2+} complex was shown by UV-vis spectroscopic titrations to coordinate two phosphate anions. Unfortunately, a binding constant could not be determined by ITC. However, comparisons between the free receptors **2** and **4** could be made in the case of the substituted phosphate salts, sodium glycerophosphate and disodium 4-nitrophenyl phosphate. Both receptors formed 1:1 complexes with these anions; however, Zn·4^{2+} displayed association constants that were roughly three times greater than those seen in the case of Zn·2^{2+}. Intrigued by these results, Gunning investigated binding cooperativity in a similar system in which the cyclene was appended to a 19-benzocrown-6 [33]. Following a procedure first put forth by Jencks [34], positive or negative cooperativity of the host-guest system, defined by ΔG_s, was determined for the Na$^+$, K$^+$, and Li$^+$ dihydrogen phosphate salts. This was done by subtracting the ΔG observed when both the anion (A) and cation (C) were allowed to coordinate concurrently (ΔG_{AC}) from those ΔG determined for exclusive anion (ΔG_A) or cation binding (ΔG_C); in other words, $\Delta G_s = \Delta G_A + \Delta G_C - \Delta G_{AC}$, which is a definition that permits both positive and negative cooperativity (i.e., ΔG_s may be positive or negative).

While the perchlorate salts could be used directly for the analysis of cation binding, the low solubility of the tetrabutylammonium (TBA) dihydrogen phosphate complex required the use of a model system to obtain the baseline dihydrogen phosphate binding values. However, subject to such caveats, ΔG_s values of +0.83, +0.72, and +1.03 (all in kcal mol^{-1}) could be calculated for NaH$_2$PO$_4$, KH$_2$PO$_4$, and LiH$_2$PO$_4$, respectively. This system was thus claimed as one of the first examples in which *positive* ion pair cooperative binding was observed.

In a related series of investigations, Suksai, Tuntulani, and coworkers appended an amidoferrocene moiety to a diaza-18-crown-6 and probed the anion association constants in the presence of various alkali metal ions [35]. In an effort to assess the utility of this receptor as a potential heteroditopic receptor, they first determined the association constants for binding Na$^+$ and K$^+$ (studied as the perchlorate or hexafluorophosphate salts, respectively); this was done via ^{1}H NMR spectroscopic titrations carried out in 5% CD$_3$CN/CDCl$_3$. Separate studies of anion binding were carried out using the TBA salts of Cl$^-$, Br$^-$, and I$^-$ in the same solvent. However, a K_a value could only be determined in the case of Cl$^-$ (those for the Br$^-$ and I$^-$ salts proved to be too small). Based on these analyses and a comparison of the diaza-18-crown-6 as a reference receptor and the functionalized amidoferrocene receptor **5**, it was concluded that the chloride affinity *decreased* when a crown ether was appended onto the core ferrocene receptor. This behavior was rationalized in terms of the enhanced rigidity of the new receptor, which was considered likely to inhibit binding. Addition of TBA chloride to either the K$^+$ or Na$^+$ complex (previously formed through addition of either KPF$_6$ or NaClO$_4$) of the receptor produced no discernible change in the amide NH signals in the ^{1}H NMR spectrum up to one equivalent. In the presence of more than one equivalent of Cl$^-$, a significant shift in the NH signal was observed, which the authors attributed to formation of an ion pair that does not involve binding of the amide NH protons. Similar behavior was observed upon the

addition of TBABr to the K$^+$ complex. However, upon formation of the presumed Na-Br, Na-I, or K-I pairs, a significant downfield shift was seen for the amide NH proton signal in the ^{1}H NMR spectrum. Furthermore, in these cases, the anion-binding constants (which were previously too low to determine) were found to be greatly enhanced. For instance, the Na$^+$ complex displayed a binding constant of 16 000 M^{-1} for bromide anion, while the K-I and Na-I pairs displayed anion affinities of 39 and 93 M^{-1}, respectively. While the latter values are not extremely high, the fact that they are measurable is fully consistent with the proposal that positive cooperativity effects are contributing to ion pair binding in this heteroditopic system.

9.2.2
Calixarenes

Calixarenes and their derivatives (Scheme 9.3) are among the most widely used scaffolds in anion-binding chemistry. Strategies for their functionalization have been reviewed recently [36,37]. The popularity of calixarenes reflects to a large extent the ease with which the cores themselves can be modified as well as the fact that they
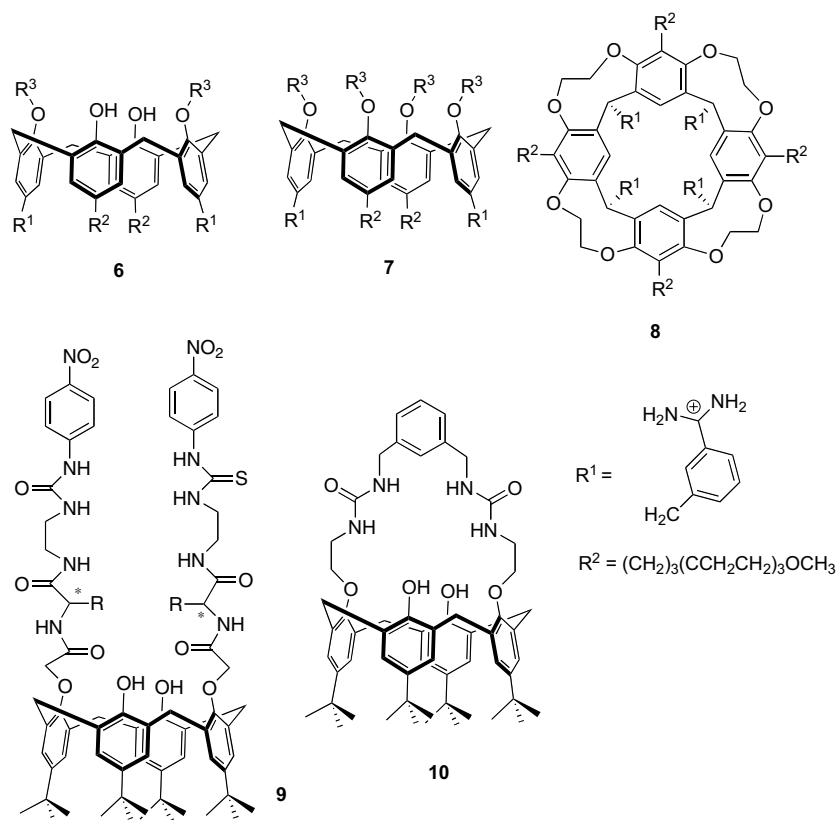
Scheme 9.3 Selected representatives of functionalized calixarenes.

possess well-defined upper and lower faces. The most common strategy for calix-arene functionalization involves appending additional binding motifs onto the macrocycle to give a product with general structure **6** or **7**. Such functionalizations are usually performed so as to provide either two or four groups on the calixarene skeleton. The resulting hybrid systems display binding selectivities that are quite varied. For instance, certain functionalized calixarenes bearing amido substituents on the upper rim displayed a preference for hydrogen sulfate anions ($K_a = $ ca. $10^5 \, M^{-1}$, in CDCl$_3$) [38], whereas others showed selectivity for carboxylate anions (K_a values up to $10^6 \, M^{-1}$) [39–43]. Examples of functionalized calixarenes bearing a charged scaffold, obtained by the use of amidinium [44,45] or imidazolium func-tionalizing groups [46], are also known in the literature [36] and have been seen to display affinities K_a up to 10^4–$10^5 \, M^{-1}$ in highly solvated solvents, such as DMSO, methanol, and water.

A tetraamidinium functionalized, bowl-type cavitand (receptor **8**) was developed by Diederich and Sebo [47]. This receptor was found to complex 1,3-dicarboxylate anions with good selectivity and a 1:2 binding stoichiometry both in CD$_3$OD and D$_2$O, as revealed by standard Job plot analysis. In contrast, various nucleotide phosphates were found to be bound with a 1:1 stoichiometry in D$_2$O. In the case of the adenosine phosphates, the association constants increased as a function of nucleotide charge [i.e., the affinity order (K_a, M^{-1}) was: cAMP (1400) < AMP (10 000) < ADP (48 700) < ATP (660 000) in pure D$_2$O]. This charged receptor (**8**) also showed moderate selectivity towards AMP ($K_a = 10 000 \, M^{-1}$) over other nucle-otide monophosphate anions, such as GMP ($K_a = 5200 \, M^{-1}$), CMP ($K_a = 3500 \, M^{-1}$), TMP ($K_a = 5900 \, M^{-1}$), and UMP ($K_a = 3800 \, M^{-1}$) in D$_2$O containing TRIS buffer (2.5 mM, pH 8.3).

The doubly functionalized calix[4]arene **9**, bearing two chiral "arms", was pre-pared recently [48]. This neutral system proved not only to be a good receptor for α-phenylglycine anions, it was also found to display good enantioselectivity towards the L-isomer $K_a(L)/K_a(D) = 4.76$. It was thus proposed by the authors, that this presumably preorganized receptor could function as a chromogenic sensor for nonracemic α-phenylglycine anions.

Another strategy for functionalizing calixarenes is to strap the macrocycles. Sev-eral systems bearing a diamido strap have been prepared and have shown a selec-tivity for acetate anions (e.g., receptor **10**; $K_a = 10^3 \, M^{-1}$ in CDCl$_3$) [49]. Similar selectivity preferences were observed for thiacalix[4]arene receptors functionalized with four ureido or thioureido units on the lower rim [50].

Appropriately strapped calixarenes have also been shown to complex anions and cations simultaneously. Such a system is the ditopic, calixarene-based receptor **11** (Scheme 9.4) reported by Tumcharern and coworkers [51]. Receptor **11**, in which the strap incorporates two different binding motifs (urea and amide), showed selectivity for the tetrahedral phenylphosphinate anion (PPhHO$_2$)$^-$ over simple Y-shaped anions, such as acetate. After initial screening studies, quantitative analyses were carried out using ^{1}H NMR spectroscopic methods. Specifically, titrations were carried out in CD$_3$CN using the TBA salts of three promising anions, namely acetate, phenylphosphinate, and diphenylphosphate. Standard analyses of the

15 R = H
16 R = (CH₂CH₂O)₃CH₂CH₂

$$15\ R = H$$
$$16\ R = (CH_2CH_2O)_3CH_2CH_2$$

14

13

12

11
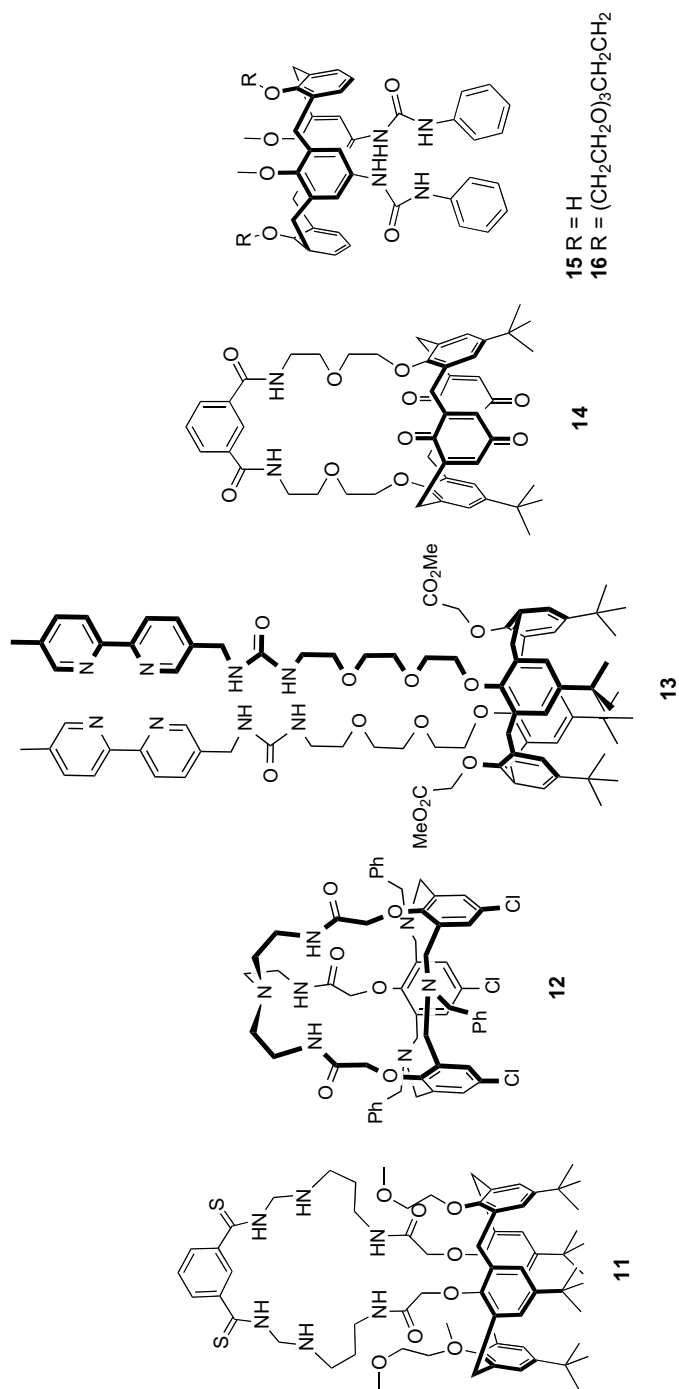
Scheme 9.4 Calixarene-based ditopic receptors.

anion-dependent changes in the thiourea NH proton signals led to calculated 1:1 binding constants of 11 000, 24 000, and 1800 M^{-1}, respectively, for these three anions. Separate titration-based studies were carried out to determine the binding constants for the complexation of the alkali metal cations Li^+, Na^+, and K^+ (studied as perchlorate salts). The resulting values led to the suggestion of a clear preference for the sodium cation, with K_a values of 760, 5500, and 970 M^{-1} determined for Li^+, Na^+, and K^+, respectively.

In a third experiment, acetate or diphenylphosphate anions (as their TBA salts) were added to the sodium salt of the receptor. No change in the ^1H NMR spectral features was observed upon the addition of acetate anions until 1 equivalent had been added. Based on this observation, the authors suggested that the Na^+ cation was sequestered out of the receptor, forming what was presumably a more stable ion-pair in solution. On the other hand, with diphenylphosphate, 1:1 binding is observed in the presence of Na^+, with the resulting K_a value (for anion complexation) being on the order of 2200 M^{-1}, a finding that could be interpreted in terms of effective ion pair recognition. Thus, the receptor **11**, in the absence of Na^+ cation, shows selectivity for acetate anions over diphenylphosphates, but in the presence of Na^+ this selectivity is reversed. Tumcharern and coworkers postulated that the phenoxy groups may interact favorably with the bound cation and that this could lead to the observed strong binding of the ion pair [51].

Cryptand **12** was synthesized through an amidation reaction in which a calix[3] arene was capped with a tren residue [52]. The anion-binding properties of this receptor, termed N_7-azacalix[3]cryptand, were studied in DMSO using UV-vis spectroscopy and the TBA salts of the test anions in question. On the basis of these studies, it was found that halide anions are generally bound more effectively than Y-shaped or trigonal planar anions; in fact, chloride displayed the highest constant for this system with a log K of 4.55 being derived from quantitative analyses. The other anions were bound in the following sequence: $Cl^- > Br^- > CH_3COO^- > F^- \approx I^- > PhCOO^- > NO_3^-$, with the value for perchlorate being too low to be determined. Interestingly, when this system was investigated as a potential ditopic receptor through the addition of Zn^{2+} (as the trifluoromethanesulfonate salt), the affinity for Cl^- was found to be *reduced*, while the association constants corresponding to the binding of the other halide anions were found to be enhanced. The authors reasoned that electrostatic interactions involving the bound anion and the zinc cation, while beneficial in the case F^-, I^-, and Br^-, are actually destabilizing in the case of chloride anion since the number of hydrogen bonds between the bound chloride anion and the receptor would be reduced. While there is currently no independent verification for this supposition, it nonetheless serves to highlight the fact that there are often several competing effects that serve to modulate the overall binding and selectivity process.

Recently, the effect of two proximate cations on anion-binding was investigated [53]. Toward this end, the basic calix[4]arene framework was functionalized on the lower rim with two methyl ester units and in two separate positions with two urea-linked bipyridine-functionalized polyether units to give **13**. This receptor was designed to allow for the coordination of "hard" metal cations via the ester groups, as

well as soft cations through the bipyridine units. It was further postulated that various targeted anions would bind to the urea moieties, while being encapsulated between the two co-bound metal cations.

Anion affinities for receptor **13** were calculated from ^{1}H NMR spectroscopic titrations carried out in CDCl$_3$/CD$_3$CN, and were found to be very low for the anion alone. Specifically, logK_a values were found to be 1.88 for NO$_3^-$ and 1.4 for CF$_3$SO$_3^-$, (studied as the corresponding TBA salts). However, in the presence of either sodium or silver cations (added as the tetrakis[3,5-bis(trifluoromethyl)phenyl] borate (TFPB) salts), the association constants increased dramatically. In the case of nitrate, the logK_a recorded for the **Ag$^+$•13** complex was 3.31, whereas that for the corresponding **Na$^+$•13** derivative was found to be 3.82. Finally, according to design expectations, the anion affinity constants for the binuclear metal complex, **Na$^+$•Ag$^+$•13**, were found to be considerably higher than those of the mono-cationic complexes; specifically, logK_a values of 5.07, 4.7, and 4.28 were derived for NO$_3^-$, CF$_3$SO$_3^-$, and BF$_4^-$, respectively.

The hybrid calix[4]arene **14**, in which calix[4]diquinone is functionalized with an isophthalamide strap [54], has been reported to act as a contact ion pair receptor. In this case, the neutral receptor does not display a discernible affinity for tetrabuty-lammonium chloride, as determined by ^{1}H NMR spectroscopic analyses carried out in CD$_3$CN. Similarly, only a moderate affinity for K$^+$ (as the PF$_6^-$ salt) was reported, with no evidence of complexation being observed in the case of Na$^+$ or NH$_4^+$ (as the Cl$^-$ salts), as judged by UV-vis spectroscopic titrations. However, the calculated association constants were found to be substantially enhanced when a cation was added to the receptor. In particular, the association constants (log K_a) for chloride anion-binding were found to be 3.79 in the presence of excess K$^+$ and above 4 in the case of Li$^+$, Na$^+$, and NH$_4^+$. According to the authors, such findings represent a rare example of cooperative binding being manifest in a system wherein essentially no affinity is seen for the individual free ions.

Tongraung, Chantarasiri, and Tuntulani have reported two calix[4]arenes **15** and **16**, one with urea appendages and a second with a crown "strap" in addition to the urea arms. These systems were found to bind tetrabutylammonium dihy-drogen phosphate with a $K_a \geq 200\,M^{-1}$ in DMSO-d_6. In line with the authors' expectations, the anion-binding affinities were then found to be enhanced upon the addition of sodium cation. For instance, in the presence of this cation, the association constant for calix[4]arene **16** increased to $K_a = 1030\,M^{-1}$ (as the PF$_6^-$ salt; DMSO-d_6 solution) [55].

9.2.3
Cholapods

Cholapods (Scheme 9.5) are receptors based on a steroid core that feature both electron-withdrawing substituents (to enhance anion-binding) and a C$_{20}$ side chain (to increase solubility in organic solvents). As might be expected, the rigid backbone present in cholapods makes them potentially ideal scaffolds in that they possess a fixed inner cavity as well as conformational rigidity [16,56,57]. However, only a few
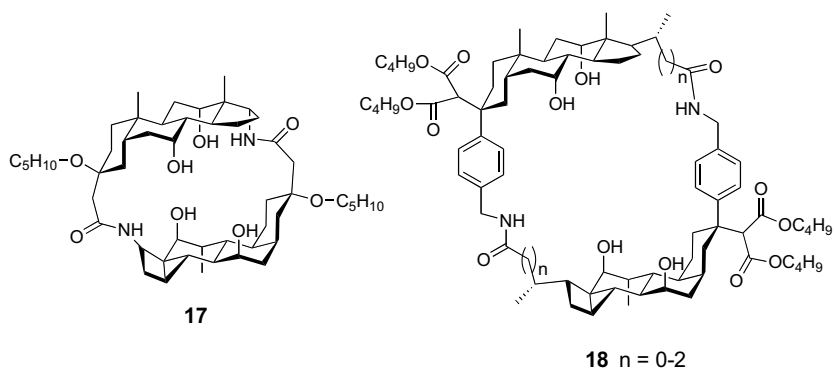
Scheme 9.5 Cholapod-based macrocyclic receptors.

hybrid macrocyclic receptors based on the cholapod paradigm have been reported in the literature, although recently Davis and coworkers reported a steroid-based cryptand **17**, which combines two types of functional groups – hydroxyl and amide. This system contains a relatively small cavity incorporated within a rigid framework that serves to preclude intramolecular hydrogen-bonding interactions and thus favors halide anion recognition [58]. In fact, anion-binding studies, performed using standard ^{1}H NMR spectroscopic titration methods in CDCl$_3$, revealed that receptor **17** is selective for fluoride anions over other halide anions ($K_a = 3220$, 990, and 250 M^{-1} for F$^-$, Cl$^-$, and Br$^-$, respectively; all studied as the corresponding TBA salts).

Although conceptually similar to **17** in terms of its 3-dimensional design, receptor **18**, with 1,4-phenylene spacer groups between two cholic acid subunits, was found to bind β-D-glucoside in CDCl$_3$, with $K_a = 10^3$ M^{-1} and a 1:1 binding stoichiometry, and to extract this key biomolecule efficiently from aqueous solutions into an organic phase [59]. This change in selectivity toward a larger, neutral substrate was rationalized in terms of the expanded system **18** being appropriately larger than its smaller congener **17**.

9.2.4
Pyrroles

Calix[4]pyrroles (Scheme 9.6) are another class of scaffold that has been extensively functionalized [18]. Although a range of modifications of this easy-to-make core have been carried out, most functionalized pyrrole-containing macrocycles can nonetheless be represented by the generalized structure **19**. As a rule of thumb, it is possible to effect functionalization on only one group (R^1 or R^2), on two opposite groups (R^1 and R^1), on all of the β-pyrrolic positions (R^3), or on one of the *meso* positions (R^1 and R^2). An example of the latter approach is embodied in the two kinds of so-called deep or extended cavity calix[4]pyrrole prepared to date [60–63]. In both cases, the size of the cavity was enhanced by appending bulky groups, namely substituted aryls [60–62] or steroid subunits [63], onto the four *meso* positions. The introduction of these
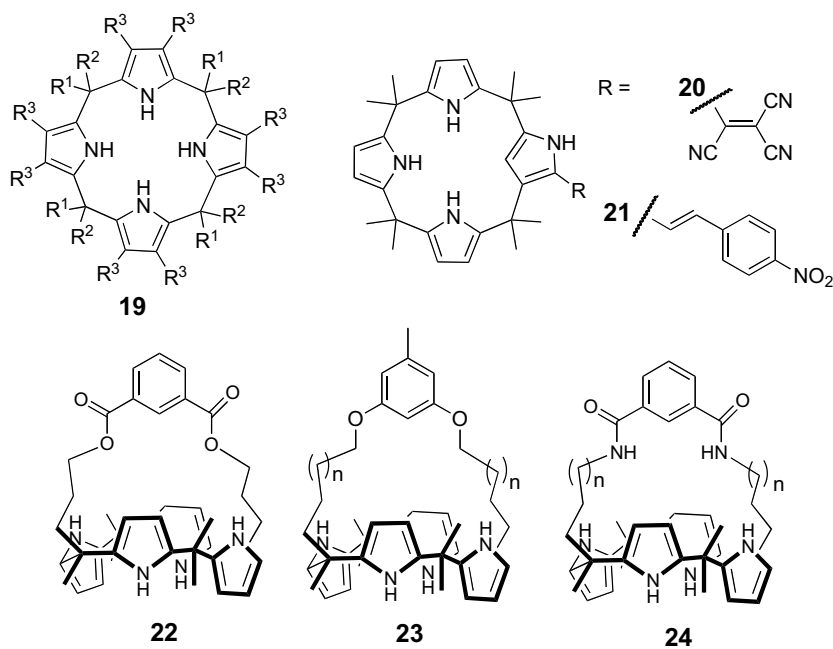
Scheme 9.6 Calix[4]pyrrole-based receptors.

or other substituents at the *meso* position of calix[4]pyrroles has been shown to increase the selectivity for various targeted anions [64]. Other systems, not necessarily involving *meso*-substitution, have allowed for the analytical determination of anions through the use of appended chromophores or fluorophores [65,66]. A different class of substituted calix[4]pyrroles bears nucleic acid base appendages that were designed to effect the cooperative recognition of a complementary mononucleotide substrate. The resulting systems have been studied as key components in ion-selective electrodes [67], as well as stationary phases in chromatographic separations [68].

A relatively new class of pyrrole-containing macrocycles are the N-confused calix[4]pyrroles (e.g., **20** and **21**) [69]. Compared to the traditional calix[4]pyrroles, these congeners display totally different binding modes. Such systems bind anions via three normal NH hydrogen bonding interactions, as well as through an unusual CH-anion contact. Additionally, the presence of the so-called inverted pyrrole does not permit the macrocycle to adopt readily the cone-like conformation usually observed in the case of calix[4]pyrrole-anion complexes. Inverted calix [4]pyrroles also allow for facile and selective chemical modifications of the receptor skeleton. This latter feature has been exploited to prepare the sensor systems **20** and **21**. Both of these show selectivity for acetate over chloride and dihydrogen phosphate anions; the K_a values for acetate, chloride, and dihydrogen phosphate are $>10^6$, 319, and $810\,000\,\text{M}^{-1}$, respectively, for **20**, and, likewise for the same anion set, 16 600, < 50, and $430\,\text{M}^{-1}$ for **21** (all systems studied in DMSO as their

tetrabutylammonium salts). The ratio of binding constants for the acetate anion over chloride is 50-fold for **20** and 28-fold for **21** [70]. These kinds of systems have also been employed in optical sensor arrays that exploit pattern recognition.

An interesting addition to the hybrid macrocyclic family is the strapped calix[4] pyrrole. The first example of strapped calix[4]pyrroles was system **22** reported by Lee and coworkers in 2002 [71]. More recently, calix[4]pyrroles have been strapped with *m*-resorcinol-derived diether straps of various lengths (**23**, where $n = 1–3$). This latter synthetic work was carried out in order to optimize the length of the strap for binding of halide anions [72] and to produce systems that could be compared effectively with simple calix[4]pyrrole (**19**, $R^1 = R^2 = CH_3$; $R^3 = H$) as well as the original ester-strapped calix[4]pyrrole **22**. From an analysis of the anion-binding properties, an interesting pattern of binding affinities was inferred. For instance, the use of a tight C-4 ether strap (system **23**, $n = 1$) was found to give rise to an extremely high chloride-binding affinity. By contrast, the use of a C-6 ether strap (**23**, $n = 3$) produced a system with an enhanced bromide-binding ability, at least relative to the parent macrocycle calix[4]pyrrole (**19**; $R^1 = R^2 = CH_3$; $R^3 = H$ and $R^1 = R^2 = CH_3$; $R^3 = F$).

In separate work, C_3 C_4 and C_5 amide *cis*-strapped calix[4]pyrroles (**24**, $n = 1, 2$, and 3) were synthesized, and their anion affinities were reported by Lee, Sessler, and coworkers [73]. While increased anion affinity was observed with the TBA salts of Cl^-, Br^- and I^- as compared to the unstrapped parent calix[4]pyrrole **19**, no anion-to-receptor size selectivity was found. This behavior led the authors to suggest that the anion binds outside the binding pocket. On the other hand, the fact that a dramatic increase in affinity was observed relative to simple calix[4]pyrrole indicates that, in the case of **24**, anion binding likely benefits from interactions involving both the amide and pyrrolic NH protons.

The expanded porphyrin sapphyrin **25** represents a different class of pyrrole-based macrocyclic anion receptors (Scheme 9.7). Sapphyrin is among the best studied of all expanded porphyrins and was actually the first pyrrolic receptor system in which anion recognition was observed [17]. As often happens in the discovery of new types of binding phenomena, the initial finding was serendipitous. Specifically, in an effort to obtain diffraction-grade single crystals, sapphyrin was crystallized as what was thought to be the bis-HPF_6 salt. However, the ensuing X-ray diffraction analysis and follow-up control studies revealed that the crystalline material contained a fluoride anion bound inside the inner cavity (as well as a PF_6^- anion not proximate to the sapphyrin core) [74]. Later, it was found that sapphyrin can efficiently bind not only fluoride [75], but also the chloride and phosphate anions [76,77]. Although actually antedating the work involving calix[4]pyrroles, it was likewise found that various functional groups could be appended to sapphyrin. The resulting systems were used for the enantioselective recognition of dicarboxylate anions [78], as well as receptors and solution-phase carriers for nucleotides [79,80] and nucleotide analogs [81,82].

In an attempt to generate hybrid macrocyclic carriers for di- and triphosphate species, various oligosapphyrins, e.g., **26** and **27**, were prepared. Among the resulting species, oligosapphyrin **27**, which remains multiply protonated at neutral pH, was found to be an effective carrier for nucleotide diphosphates [83].
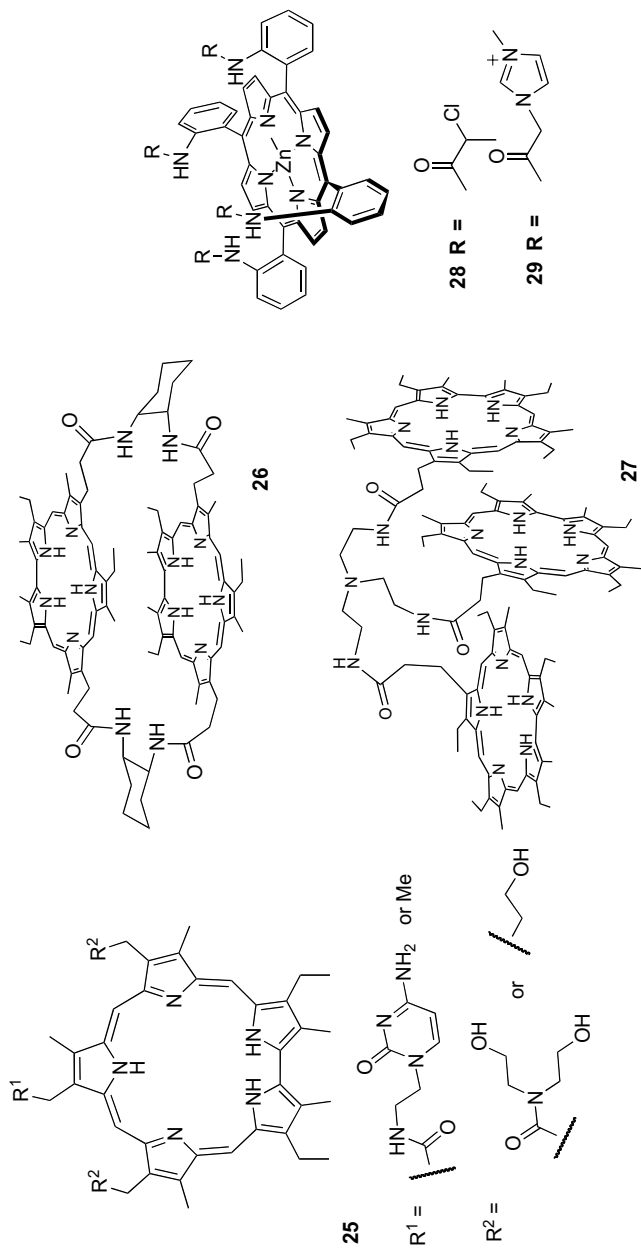
Scheme 9.7 Sapphyrin-based receptors.

Beer and coworkers have reported selectivity for sulfate anions using a zinc tetra-phenylporphyrin scaffold [84]. They synthesized two new receptors, **28** and **29**, via functionalization of the phenyl groups with either neutral amide moieties or proton-ated imidazolium linkages. A number of binding studies was performed: ^{1}H NMR titrations in DMSO-d$_6$, UV-visible titrations in DMSO and a water-DMSO mixture, electrochemical titrations in acetonitrile, and luminescence titrations in acetonitrile or DMSO. As a general rule, the tetra-imidazolium porphyrin **29** was found to be a better anion receptor than the neutral porphyrin **28**. Additionally, UV-vis titrations with receptor **29** revealed a strong preference for the TBA salt of hydrogen sulfate (log $K_a > 6$ M^{-1} in a 95:5 v/v DMSO: water mixture) when compared to the TBA salts of Cl$^-$ and H$_2$PO$_4^-$ (log K 4.2 and 4.8, respectively) or Br$^-$, I$^-$, ATP^{2-} and SO$_4^{2-}$ (spectral changes were too small to determine association constants).

9.2.5
Miscellaneous

Gong and Gibb have reported a pyridine-containing macrocycle, **30** (R = H), in which anion binding could be improved via an appropriate choice of counter cation (Scheme 9.8) [85]. Initial experiments with the TBA salts of various anions revealed relatively low binding affinities, with the K_a values (^{1}H NMR in CDCl$_3$) ranging from

30
R = H, CH$_3$OH, CH$_3$Ph

31
M = Cu(II), Ni(II)

32 = 1, 4 - phenylene
2,7- naphthalenediye

M = Cu(II), Ni(II), Zn(II)

2,7-naphthalenediye (**33**)
1,1'-biphenyl-3,3'- diyl (**34**)
1,1'-biphenyl-4,4'-diyl (**35**)
—CH$_2$—O—(p–phenylene)—O—CH$_2$—(**36**)

37

38
R = *t*-Bu, R' = *n*-C$_2$H$_{13}$
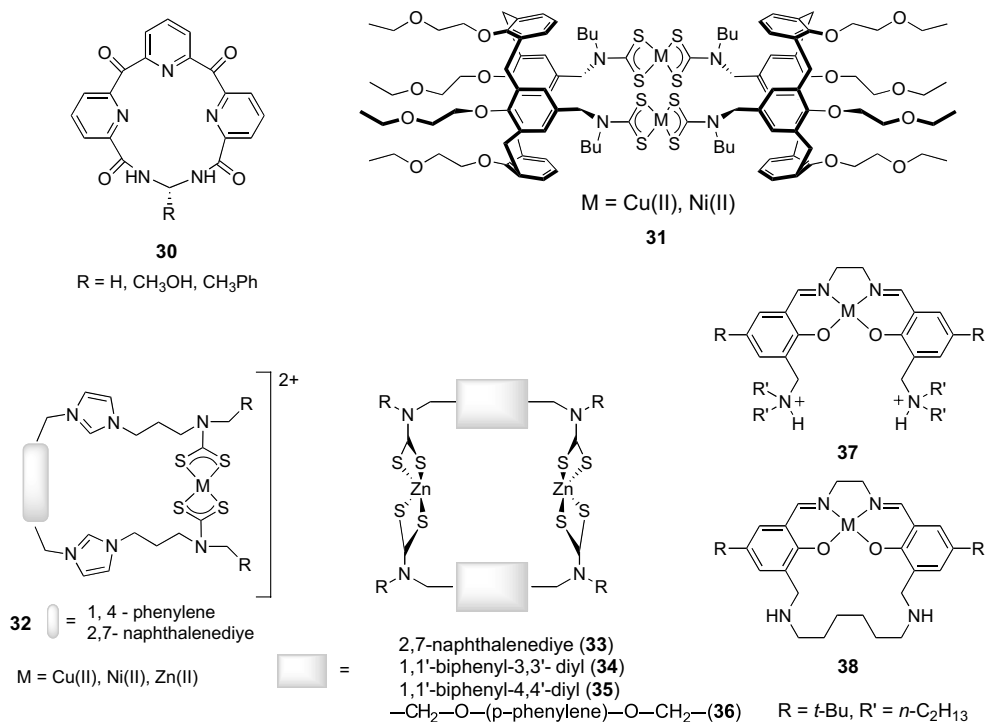
Scheme 9.8 Ditopic receptors.

110 (F$^-$) to 32 M^{-1} (I$^-$). However, when the counter cations were switched to L-phenylalanine methyl ester (H$_3$N$^+$CH(Bn)CO$_2$Me), these and other anion affinities were found to increase by an order of 10^3 M^{-1}. It should be noted, however, that the inherent anion selectivities remained the same with both counter cations, namely NO$_3^-$ > Cl$^-$ > CF$_3$CO$_2^-$ > Br$^-$ ≈ TsO$^-$ > I$^-$. *Ab initio* calculations supported the assumption that the binding of both the anion and the cation was cooperative.

Enantiomeric recognition was probed in this system via the synthetic "addition" of a phenyl or alcohol substituent onto the periphery of the macrocycle **30** (R = CH$_2$OH or CH$_2$Ph) [86]. While not the focus of the study, the effects of counter anions (NO$_3^-$, Cl$^-$, Br$^-$, TsO$^-$) were investigated with the phenyl-functionalized macrocycle. Association constants followed the same trend as the unfunctionalized macrocycle, and unfortunately the inherent enantiomeric selectivity could not be altered by using different anions. Such findings led the authors to conclude that although this macrocycle is capable of both enantiomeric and ditopic recognition, the two binding phenomena are not necessarily related.

Beer and coworkers have published a number of reports [87,88] investigating the use of the dithiocarbamate (*dtc*) motif in metal-directed self-assembly. While the majority of these reports have either been discussed elsewhere [89] or involved acyclic species and thus fall outside the scope of this Chapter, a few recent publications have been concerned with self-assembled macrocycles [89–91]. In one such paper, the Beer group describe calix[4]arenes functionalized on the upper or lower rims with the *dtc* ligand, as well as the use of the resulting dimeric structures **31**, formed from the addition of Cu^{2+}, Zn^{2+}, or Pd^{2+}, to sense anions electrochemically [91]. Toward this latter end, the Cu(II)/Cu(III) redox couple was monitored as a function of increasing anion concentration, with the degree of cathodic shift being considered a semi-quantitative indicator of anion binding. It was reported that, for equivalent concentrations, the dihydrogen phosphate, benzoate, fluoride, and acetate anions engendered much greater shifts than less charge-dense anions such as hydrogen sulfate or nitrate. Complex **32** was also prepared with differing aromatic spacer groups. While UV-vis titrations in acetonitrile showed little change, a cathodic shift of the Cu(II)/Cu(III) redox couple was observed upon addition of the TBA salt of dihydrogen phosphate or chloride in acetonitrile [92].

In a separate study reported by the Beer group, a similarly functionalized *dtc* ligand was appended to various aromatic cores, with five different macrocycles of differing sizes (e.g., **33–36**) then being synthesized through a metal-directed self-assembly technique using Zn^{2+} as the templating cation [90]. The host-guest interactions with 4,4-bipyridine, 1,4-diazabicyclo[2.2.2]octane (DABCO), pyrazine, and the TBA salts of terephthalate and isonicotinate were investigated by ^{1}H NMR spectroscopic titration methods in a mixture of CDCl$_3$ and DMSO-d$_6$. The authors found that the two anions, terephthalate and isonicotinate, formed strong 1:1 inclusion complexes with all of the receptors produced by this self-assembly process. Molecular modeling calculations provided relative Zn-Zn distances, leading to the conclusion that the terephthalate anion would fit well into receptors **33** and **34**. Strong binding was observed with receptors **34** and **36** (>10 000 M^{-1}), while receptors **33** and **35** displayed moderate binding constants (5000 and 8000 M^{-1},

respectively). The authors could not rationalize why these larger systems displayed equally strong association constants other than to propose that the flexible nature of the linkers, especially of receptor **36**, would allow for variations in the intermolecular Zn-Zn distance. The strongest association constant for isonicotinate was observed for receptor **35** (6500 M^{-1}), which contains a biphenyl spacer. Interestingly, control titrations showed no interaction with benzoate, stressing the importance of cooperative interactions with zinc in these systems.

Beer and coworkers have also reported a cryptand species formed again from the self-assembly of a *dtc* ligand with Co(IV) [93]. Addition of the TBA salt of H$_2$PO$_4^-$ to the resulting receptor in dichloromethane led to a significant cathodic shift as compared to what was seen for other anions, such as chloride, benzoate, or hydrogen sulfate [88]. Pyrrole-based *dtc* macrocycles and cryptands have also been synthesized using copper and nickel cations as the templating species. As a general rule, however, these systems failed to give interpretable results when titrated with H$_2$PO$_4^-$, Cl$^-$, Br$^-$, or I$^-$ as inferred from UV-vis spectroscopic titrations (in CH$_2$Cl$_2$/CH$_3$CN or CH$_3$Cl). However, reliable binding constants could be calculated in the case of a Ni-macrocycle with TBA-OAc (log K_a = 7.06) and a Cu^{2+}-cryptand with TBA-benzoate (log K_a = 5.73). Still, it is important to note that in the case of the Ni-macrocycle, the log$K$ values did not prove to be substantially higher than those obtained for the control species, nickel diethyldithiocarbamate [94].

Plieger *et al.* have recently reported a series of salen-based anion receptors that have been modified in an effort to improve sulfate extraction [95,96]. In earlier work, these researchers had reported that appending tertiary amine groups to a metalated salen scaffold (cf., e.g., receptor **37**) led to preferential sulfate binding and extraction over hydrogen sulfate [95]. They then investigated the effect of pre-organizing the anion-binding site by inserting a hexamethylene strap between the two amine groups (to give e.g., receptor **38**). While extraction studies led to the conclusion that sulfate binding had increased, it was reported that the sulfate was not encapsulated by the macrocycle; rather, a dimer was formed with two sulfate anions being complexed by two salen ligands. On this basis, it was rationalized that the hexamethylene strap was too small to allow for idealized sulfate anion encapsulation [96].

9.3
Receptors with Different Binding Sites

In this section, we discuss macrocyclic receptors prepared specifically with the aim of producing molecules with different binding motifs. Such systems, which will be considered mostly in the context of binding anions with multiple protonation sites (e.g., phosphates or sulfates) in solution, can be considered as a subset of the large class of compounds known as ditopic receptors.

The combination of amine-containing motifs with amides is a popular approach to the design of hybrid anion-binding agents. The resulting receptors contain two kinds of recognition motifs and, as a result, can act as both hydrogen-bond donors (amide NH protons) and hydrogen-bond acceptors (amine lone pairs). They can also

stabilize a bound anion through a Coulombic interaction involving a protonated (and hence charged) amine group, especially under acidic conditions. Taken together, these characteristics make amido-amine receptors promising for use in both water and organic phases.

One of the first hybrid amido-amine anion receptors was reported by Lehn in 1988 [97]. This system, the tricyclic receptor **39**, possesses three amide and three amine functionalities and was prepared through a coupling of a cyclophane bearing three appended aliphatic amine chains and 1,3,5-benzenetriacyl chloride. By using various aminoalkyl cyclophane derivatives, the size of the resulting cavity could be varied (i.e., $n = 1$–3 in structure **39**), with all three derivatives being shown by NMR spectroscopy to complex nitrate anions efficiently, although no quantitative binding data was provided.

More recently, a series of amido-amine macrocyclic receptors, **40-43**, was developed by Bowman-James et al. (Scheme 9.9). Because of the presence of both binding motifs, these receptors, like many of their congeners, were seen to bind dihydrogen
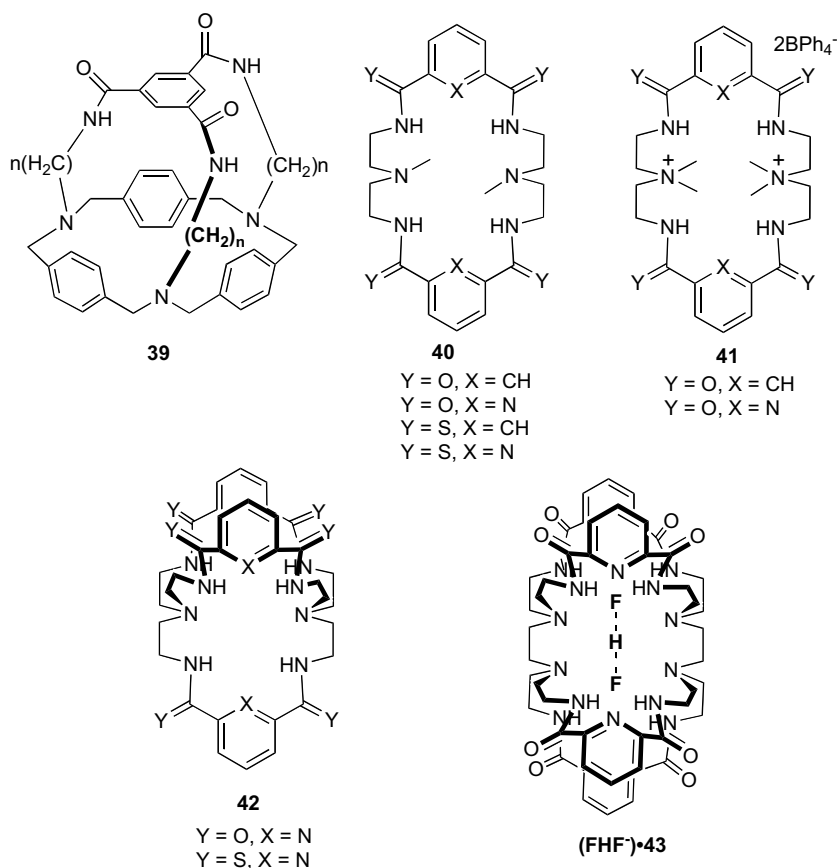
Scheme 9.9 Amido-amine type receptors.

phosphate and hydrogen sulfate anions well in DMSO-d_6 with observed K_a values up to 10^5 M^{-1}. These association constants were roughly 2 orders of magnitude greater than those seen for nitrate, chloride, or iodide in the same solvent, and roughly 4 orders of magnitude greater than the K_a values seen for perchlorate [98].

3-Dimensional analogs of the original amido-amine receptors (e.g., **42**) [99,100] were also reported by these same researchers and were put forward as part of an ongoing, rational effort to develop receptors for tetrahedral anions. A single-crystal X-ray diffraction structure of the complex **42**•H$_2$SO$_4$ revealed that sulfate anion binding in the solid state involves eight NH-derived hydrogen-bonding interactions, where two of the NH protons are situated on the amino motifs. In this system, the orientation of the amide protons is presumably pre-established in a favorable orientation as the result of hydrogen-bonding interactions involving the pyridine nitrogen lone pairs. Although increased affinity and selectivity for tetrahedral anionic substrates can be expected for appropriately designed 3-dimensional receptor systems as compared to the corresponding macrocyclic (and hence topographically planar) analogs, in the case of **42** the spherical halide anions, fluoride (log $K_a > 5$) and chloride (log $K_a > 3$), compete effectively with the targeted tetrahedral species, namely phosphate (log $K_a > 3$) and sulfate (log $K_a \geq 1.8$), at least in DMSO.

Bowman-James et al. have also described a new system **43** containing four amide-containing fragments connected through polyamine linkers. These tricyclic systems possess a unique complementary structure for ditopic anions such as the bifluoride anion FHF$^-$ [101]. In particular, receptor **43** was found to trap efficiently a bifluoride anion inside the macrocycle and to stabilize a complex with the molecular formula Bu$_4$N[**43**(FHF)]3H$_2$O. ^{1}H NMR spectroscopic titration studies of **43** provided support for the proposed selectivity; specifically, these studies revealed that the FHF$^-$ anion is bound with a K_a 5500 M^{-1} in DMSO-d_6, whereas the dihydrogen phosphate (K_a 740 M^{-1}), azide (K_a 340 M^{-1}), and acetate anions (K_a 100 M^{-1}) are bound far less well. Other anions such as the halides, hydrogen sulfate, nitrate, and perchloride did not show any propensity to bind to this host molecule.

An exciting class of amido-amine hybrid anion-binding systems was reported recently by Kubik et al. (Scheme 9.10) [102]. One of the first receptors of this type, **45**, is derived from L-proline and 6-aminopicolinic acid, and consists of two cyclopeptides bridged by a spacer group. The net result is a potentially ditopic binding system. Earlier studies of the simple cyclopeptide **44** showed that this latter monotopic analog forms a 2:1 complex with sulfate. Thus, it was reasoned that linking two subunits together, to provide systems such as **45-48**, would give rise to highly efficient systems that would bind sulfate with a 1:1 stoichiometry. In the case of the prototypical system **45**, the stability constants were measured in a 50% methanol/water solution using both ^{1}H NMR spectroscopic titrations and ITC analysis; the resulting K_a values were found to vary over the 10^2–10^5 M^{-1} range and to decrease in the following order (log K_a values in parentheses as determined by NMR/ITC measurements, respectively): SO$_4$$^{2-}$ (5.54/4.55) > I$^-$ (3.95/3.79) > Br$^-$ (3.72/3.45) > Cl$^-$ (2.85/2.85) > NO$_3$$^-$ (2.11/not determined). A good correlation between the NMR spectroscopic analyses and ITC measurements was observed. The advantage of the latter studies is that they allowed the associated thermodynamic
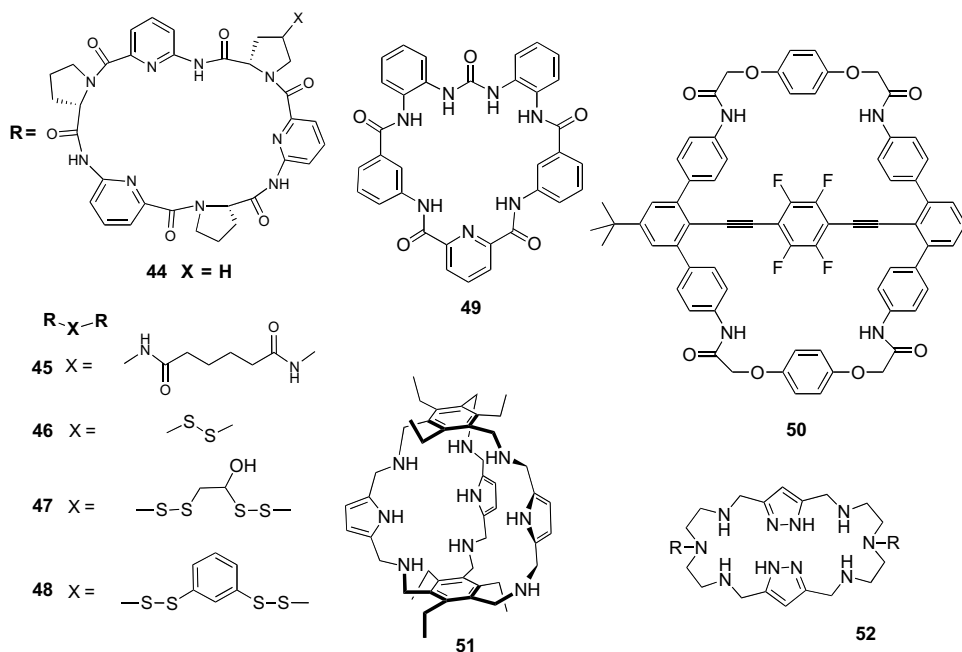
Scheme 9.10 Selected hybrid receptors.

parameters to be obtained. In particular, for the binding of sodium sulfate, ΔH was found to be $-15.0\,\text{kJ mol}^{-1}$ and $T\Delta S = 11.0\,\text{kJ mol}^{-1}$. In contrast, for sodium iodide, values of $\Delta H = -13.2\,\text{kJ mol}^{-1}$ and $T\Delta S = 8.4\,\text{kJ mol}^{-1}$ were measured.

A noteworthy finding emerging from these detailed studies was that the monotopic cyclopeptide **44** actually proved to be a more efficient receptor for sulfate anions than the ditopic system **45** (for **44**, $\Delta H = -19.3\,\text{kJ/mol}$ and $\log K_T = 6.48$ in 50% D_2O/CH_3OH, where $K_T = K_{a1} \cdot K_{a2}[M^{-2}]$). Furthermore, in contrast with the design expectations, microcalorimetric titrations (e.g., ITC analyses) revealed that sulfate is bound to receptor **45** with a 2:1 binding stoichiometry.

Needless to say, the finding that the simple macrocyclic control system **44** was a better receptor than **45** was an unexpected result. The authors attributed this finding to the low flexibility inherent in the ditopic receptor **45**. Hence, by choosing a more appropriate linkage, it should prove possible to enhance the binding affinity. Toward this end, the authors generated a dynamic combinatorial library (DCL); this was done by exposing dimer **44** to several thiols in the presence of oxygen and potassium sulfate using a 2:1 acetonitrile/water mixture as the solvent [103]. Under these conditions, amplification of the two bis(cyclopeptides) **47** and **48** was observed, supporting the conclusion that both systems bind sulfate strongly [104]. In agreement with this consideration, receptors **47** and **48** were indeed found to display an affinity for sulfate anion that was enhanced 10-fold relative to what was seen in the case of the first generation system **45**, at least in a 2:1 acetonitrile/water mixture.

Such intriguing findings provide support for the notion that the right spacer group can significantly increase the binding affinity of a given type of ditopic receptor.

Another interesting hybrid receptor, system **49**, was recently reported by Gale and coworkers [105]. Receptor **49** contains urea and amide motifs in an ideal geometry for binding carboxylates. It was shown by ^{1}H NMR spectroscopic titrations carried out in DMSO-d_6 that this receptor possesses high affinity for acetate ($K_a = 16\,500$ M^{-1}) and benzoate ($K_a = 6430$ M^{-1}) anions. It also displays a 100-fold selectivity for these carboxylate anions over dihydrogen phosphate ($K_a = 142$ M^{-1}) or chloride ($K_a = 194$ M^{-1}) anions. Analysis of the ^{1}H NMR spectroscopic binding data, particularly the chemical shift of each type of proton, led the authors to suggest that the receptor interacts with carboxylate anions differently from the way it interacts with either dihydrogen phosphate or chloride.

In the context of the above studies, it was found that receptor **49** was able to fix carbon dioxide from the atmosphere. This unexpected discovery was made during attempts to crystallize the receptor in the presence of tetrabutylammonium fluoride. The resulting single-crystal X-ray diffraction analysis revealed the presence of a carbonate anion coordinated by six hydrogen bonds in the cavity of the macrocycle, the formula of the resulting complex being $(49)_4[(C_4H_9)_4N^+]_9(CO_3{}^{2-})_4(F^-) \cdot 4H_2O$.

Shinkai and coworkers have reported that a combination of both allosteric and hydrogen-bonding interactions with anions was achieved by the bicyclic host **50** [106]. In this work, the host molecule, which consists of two bisamide-type subunits separated by a diethynyltetrafluorophenyl group, was designed to operate in a "turnstile" fashion. Specifically, the central spacer was expected to rotate upon binding of one guest molecule and to elicit the cooperative binding of a second guest molecule. This receptor system was observed to preferentially bind anions such as acetate, ($K_a = 144$ M^{-1}), dibenzyl phosphinate, ($K_a = 196$ M^{-1}) and chloride ($K_a = 110$ M^{-1}) in THF-d_8 DMSO-d_6, 5:1 v/v.

Pyrroles are good hydrogen-bond donors and, subject to appropriate caveats, are relatively insensitive to either protonation or deprotonation effects. Therefore, they have seen increasing use in the construction of highly efficient anion receptors [18], as well as more recently in the construction of hybrid receptors. An example of a pyrrole-containing hybrid receptor that was reported quite recently is compound **51** [107]. This was prepared by condensing 2,5-pyrroledialdehyde with 1,3,5-triethyl-2,4,6-trimethylaminobenzene followed immediately by the reduction of the imino bonds to the corresponding amines. This hybrid amino-pyrrole receptor displayed a unique ability to recognize specifically the β anomer of D-glucose ($K_a = 4.83 \times 10^4$ M^{-1}) and its corresponding alkyl glucosides with complete β/α-selectivity. It was also able to discriminate effectively the β-monosaccharides of the gluco-series from the α and β anomers of the galacto and manno series.

A somewhat analogous hybrid macrocycle was developed by Garcia-España and coworkers [108]. Specifically, these researchers reported a series of [2 + 2] dipodal systems (**52**) containing 1H-pyrazole rings and amino linkers. These receptors were found to complex L-glutamic acid efficiently in water [109]. The actual structures could be varied somewhat by changing the substituents on the amines (i.e. R = alkyl or benzyl), and the stability of the macrocycle-glutamic acid adduct was found to be

higher when R was benzyl. This result was rationalized in terms of the presence of stabilizing π-cation interactions.

Expanded porphyrins can also be considered a class of hybrid receptors. Despite the fact that these ligands were originally explored in the context of metal complexation [110], anion interactions were first observed for such systems in 1990, as noted in Section 9.2.4 above [74]. Cyclo[8]pyrrole (**53**), a recent addition to the expanded porphyrin family, contains both aminic and iminic nitrogen atoms in its core (Scheme 9.11). While analogous in some respects to the sapphyrins discussed earlier (cf. Section 9.2.4), it is discussed here in the context of hybrid receptors because it contains two types of binding motifs within its macrocyclic core, namely imino-like nitrogen atoms that can serve as hydrogen-bond acceptors (or donors after protonation) and pyrrole NH sites that are expected to act as strong hydrogen-bond donors. The combination of these two motifs in one macrocyclic cavity was shown to facilitate the complexation of sulfuric acid [111].
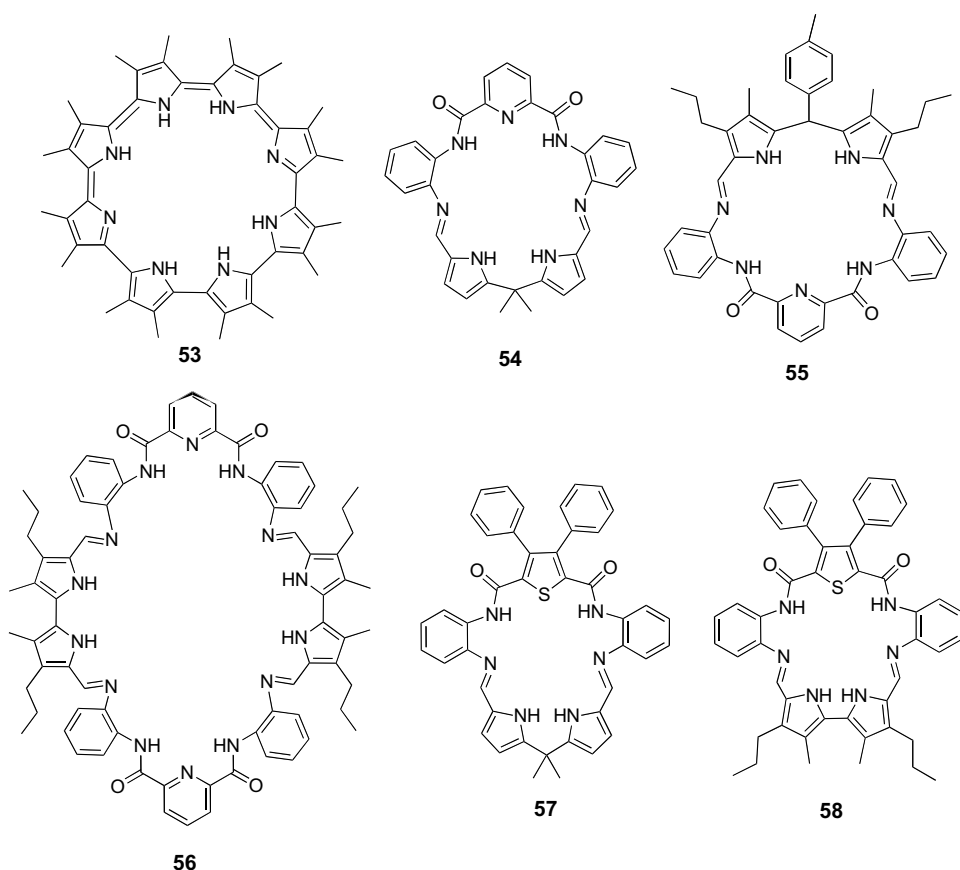
Scheme 9.11 Pyrrole-based hybrid receptors.

In an attempt to "tune" the anion-binding features of pyrrole-containing hybrid receptors so as to favor tetrahedral species, the authors' groups have recently introduced pyridine 2,6-diamido subunits into pyrrolic macrocycles through the use of simple-to-effect iminations [112]. The advantage of this latter approach lies in the combination of known anion recognition groups with an imine functionality that can provide additional anion recognition sites, either through protonation or via direct interaction with the acid form of an oxoanion (e.g., a P-OH proton). The first member of this potentially large series of compounds to be reported was receptor **54**, a system that was shown to possess a high affinity for both sulfate and dihydrogen phosphate (both studied as the corresponding TBA salts). Whereas the first of these anions was bound in a 1:1 fashion ($K_a = 64\,000\,M^{-1}$ in acetonitrile), dihydrogen phosphate was actually complexed in a stepwise fashion and with a 1:2 stoichiometry ($K_{a1} = 342\,000$ and $K_{a2} = 26\,000\,M^{-1}$ in acetonitrile). Moreover, this receptor displayed no appreciable affinity for nitrate, bromide, or perchlorate. This high inherent selectivity makes these systems of potential interest in the area of nuclear waste remediation, where the selective extraction of sulfate from nitrate-rich mixtures is considered beneficial [113].

With the goal of simplifying the binding stoichiometry and enhancing the sulfate-phosphate selectivity, a tolyl group was added to the meso-like position of the dipyrromethane fragment. This gave rise to receptor **55**, which was designed to be far more rigid than **54** because of a need to avoid potential steric interactions between the tolyl and methyl substituents on the pyrrolic 3-positions [114]. This structural "fine-tuning" produced a receptor with a selectivity for hydrogen sulfate anion ($K_a = 108\,000\,M^{-1}$) relative to dihydrogen phosphate ($K_a = 29\,000\,M^{-1}$) in acetonitrile. In analogy to what proved true for cyclo[8]pyrrole (**53**) (see above), hybrid system **55** was found to complex sulfuric acid in the solid state through a combination of two imino fragments that become protonated upon complexation, as well as through hydrogen bonds involving the pyrrole and amido motifs.

In the context of the above studies, it was discovered that the same kinds of building blocks, namely diformyl pyrrolic precursors and diamines, could be used to effect the combinatorial selection of macrocyclic Schiff base targets when an appropriate anion is used as a template [115]. For example, condensation between a diformyl bipyrrole and a diamine produces the [2 + 2] macrocycle **56** cleanly, but only when the reaction was carried out in the presence of the acid form of tetrahedral oxoanions. The use of other acids led to formation of a mixture of [n + n] macrocycles, where $n = 1$–4, as well as products presumed to be open-chain oligomers, as inferred from mass spectrometric analyses. In acetonitrile, receptor **56** displayed binding properties analogous to those of receptor **54**, with the exception that no evidence of chloride binding was seen. A particularly intriguing property of receptor **56** is that it undergoes rearrangement in acetonitrile to produce the corresponding [3 + 3] macrocycle (instead of the [2 + 2] congener) in the presence of TBA-HSO$_4$ or TBA-H$_2$PO$_4$ provided that the reaction mixture is allowed to sit for several days in the absence of stirring. Under conditions of greater agitation, the initial [2 + 2] macrocycle precipitated in the form of its anion complex salt. The molecular structure of the [3 + 3] product was confirmed via X-ray

diffraction analysis of the sulfuric acid salt; this analysis revealed, not surprisingly, that the bound anion is stabilized in part by hydrogen-bonding interactions involving all three bipyrrole fragments.

This group of anion receptors has been expanded by the replacement of the 2,6-diamidopyridine with 2,5-diamidothiophene (structures **57** and **58**) [116]. Condensation of bis(2-aminophenyl)-thiophene-2,5-dicarboxamide with either a diformyl dipyrromethane or diformyl bipyrrole led to the formation of macrocycles **57** and **58**, respectively. Binding constants for the TBA salts of AcO^-, Cl^-, Br^-, HSO_4^-, $H_2PO_4^-$, and NO_3^- were determined through UV-vis spectroscopic titrations carried out in dichloroethane, and were generally found to be on the order of 10^3–$10^4\,M^{-1}$. It was reported that the larger, more flexible receptor **57** displayed overall higher binding affinities when compared to **58**, a finding that was attributed to the flexibility of the receptor, enabling it to easily accommodate anions of different geometries. While still giving rise to K_a values below those of **57**, the more rigid receptor **58** did show increased binding affinities for the larger anions, namely bromide and hydrogen sulfate.

Binding of a complex anionic species with the help of hybrid macrocycles able to provide different interactions with the anion simultaneously was demonstrated in an elegant manner by Stoddart *et al.* They reported the organization of macrocycle via the anion-assisted assembly of large [5]- and [6]pseudorotaxanes from dibenzylammonium threads and polyether macrocycles. The resulting systems were found to be interwoven around a central hexafluorophosphate anion (Scheme 9.12, structure **59**) [117].

A similar strategy, also permitting the highly efficient synthesis of macrocyclic systems, was recently reported by Beer and coworkers [24]. This work, which involves a general anion templation strategy for the construction of a variety of interpenetrated and interlocked molecular structures, has led to the preparation of a series of [2]rotaxanes and [2]catenanes [118]. The resulting interlocked structures **60-62** feature a unique topology and a defined directionality within the hydrogen-bonding network; they also exhibit a high degree of selectivity for chloride.

The anion templated syntheses by Beer afforded receptors **60-62** by reacting the chloride salt of the starting pyridinium precursor with an appropriately chosen 1,3-diamidobenzene derivative. Based on ^{1}H NMR spectroscopic titrations carried out in acetone-d_6, the structure Cl^-•**60** was found to form with a 1:1 stoichiometry and with an association constant of $2400\,M^{-1}$.

It is important to appreciate that these ditopic macrocycles contain a polyether moiety on one side and present a diamido motif on the other. Addition of a charged pyridinium cation to the substrate-free form of these macrocycles then generates a highly efficient receptor for chloride, presumably as the result of both template-induced organization and electrostatic effects. The further incorporation of hydroquinone groups and polyether functionalities into the cyclic framework presumably contributes to the stabilization of the cationic pyridinium component within the final interpenetrated structure. Interestingly, while titration of the pyridinium cation building block alone revealed a preference for oxoanions, the final receptor-anion
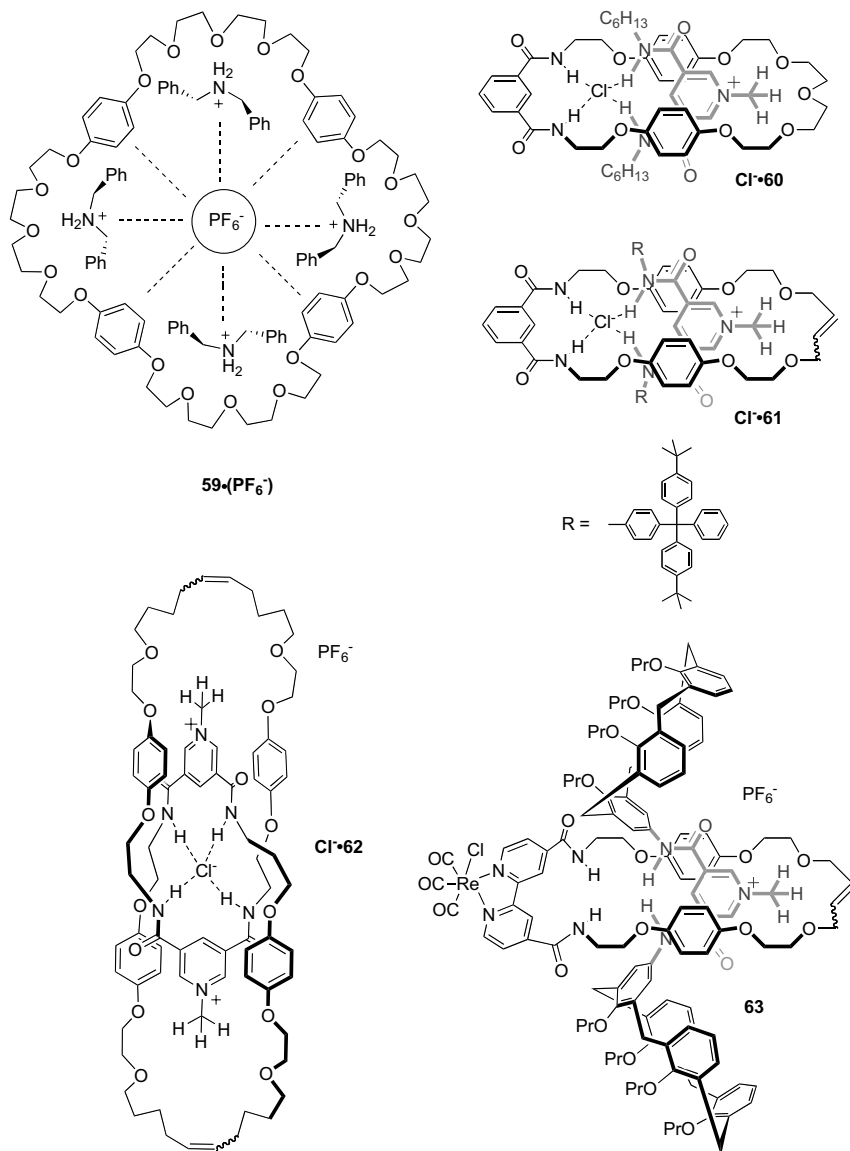
Scheme 9.12 [2]Rotaxane chloride-selective receptors.

complex $PF_6^-\bullet 61$ did not display any particular affinity for normal test oxoanions such as dihydrogen phosphate and acetate. However, it was found to bind chloride anions efficiently ($K_a = 1130\,M^{-1}$ in $CDCl_3$ CD_3OD 1:1).

More recently, Beer and his group developed a high-yielding anion-templated synthesis of the chloride-selective receptor **62**. This was done by carrying out two identical cyclizations of two macrocyclic rings in the presence of chloride anion,

which served as the templating agent [119]. Here, a key feature was the double ring-closing metathesis (RCM) reaction carried out under conditions where the components of the receptor were orthogonal to each other. This resulted in the formation of a [2]catenane product. Interestingly, the RCM reaction was found to depend critically on the relative concentration of the chloride anion. The resulting receptor was found to bind anions with an apparent 1:2 stoichiometry, a 20-fold selectivity for chloride compared to acetate being observed [K_{11} and K_{12} values (all M^{-1} and all in acetone-d_6) for chloride are 9420 and 160, for acetate 420 and 40, and for bromide 790 and 40 M^{-1}].

A new hybrid system **63**, selective for hydrogen sulfate, has also been synthesized with the aid of an anion-templating agent [118]. This receptor combines in one framework a vinyl-appended rhenium(I)bipyridyl fragment, a calix[4]arene, four amido fragments, and a pyridinium cation. Luminescent spectroscopy binding studies with chloride, nitrate, and hydrogen sulfate (studied as their hexafluorophosphate salts in acetone-d_6) revealed the ability of the [2]rotaxane **63** to operate as a sensor for hydrogen sulfate via a significant enhancement in the rhenium bipyridine metal to ligand charge transfer (MLCT) emission intensity. Under these conditions, hydrogen sulfate anions were bound strongly ($K_a > 10^6 M^{-1}$), with the binding constants for both chloride and nitrate anions also being rather high (e.g., on the order of $10^5 M^{-1}$) for these two species, respectively.

9.4
Conclusions

Hybrid macrocycles represent one of the current, cutting-edge approaches to the preparation of functioning anion receptors. While an almost infinite number of hybrid receptor systems is conceivable, within the anion recognition area the focus to date has been on two broad structural classes, namely ditopic receptors, including those for ion pairs, and functionalized systems containing more than one kind of anion-binding motif. The latter systems offer the possibility of bringing more than one key anion-binding motif to bear on a targeted anionic substrate and thus have the potential to display exceptionally high affinities and selectivities. Likewise, systems containing recognition sites for both anions and cations are of interest as receptors for zwitterions and salts. Thus, considered together, these hybrid receptor classes offer the prospect of binding a large range of species and of doing so with considerable selectivity and affinity. At present, this potential is only beginning to be realized. However, the large number of motifs that can be employed, considered in conjunction with the almost infinite number of potentially conceivable structural forms the resulting receptors could attain, means that the opportunities for further development are ample. Indeed, it is safe to predict that the day is not far off when, after the full power of modern theoretical calculations and combinatorial synthetic methods are harnessed, it should be possible to design rationally and synthesize expeditiously a hybrid receptor that is specifically "fine-tuned" for the binding and recognition of a specifically chosen anionic substrate.

9.5
Experimental: Selected Procedures

9.5.1
Macrocycle H$_2$SO$_4$•53

A 1-L round bottom flask was charged with a stir bar, dichloromethane (500 mL), and a solution of FeCl$_3$•6H$_2$O (2.7 g, 10 mmol) in 1-M sulfuric acid (100 mL). The resulting biphasic mixture was stirred at 300 rpm, while a solution of 3,4-dimethyl-bipyrrole (188 mg; 1 mmol) in dichloromethane (50 mL) was added slowly by syringe pump over a period of 9 h, with the needle injecting into the organic phase. After completion of the addition, the mixture was stirred for an additional 5 h. The phases were then separated, and the organic phase was dried over anhydrous sodium sulfate. After removal of the solids by filtration, the solvent was removed *in vacuo* to yield the crude product. The crude product was purified by column chromatography on silica gel using dichloromethane containing methanol (2–5%) as the eluent. The solid residue obtained in this way was recrystallized from dichloromethane/methanol to yield H$_2$SO$_4$•53 as a dark microcrystalline powder in 74% yield (155 mg; 0.185 mmol).

9.5.2
Macrocycle 55

Bis(2-aminophenyl)pyridine-2,6-dicarboxamide (200 mg, 0.576 mmol), 2,2′-(5-formyl-3-methyl-4-propyl-pyrrolyl)(*p*-tolyl)methane (232 mg, 0.665 mmol), and 2.2 equiv. of conc. H$_2$SO$_4$ were mixed in dry methanol (50 mL). The mixture was heated to reflux under Ar for 15 min. After cooling, the volatile components were removed under low pressure. The resulting solid was dissolved in CHCl$_3$ (10 mL) and layered with pentane (30 mL). The product, macrocycle **55**, was found to crystallize overnight in the form of its sulfate salt in 96% yield (454 mg; 0.558 mmol). The corresponding free base form was prepared using the same procedure as that described for H$_2$SO$_4$•55, with the exception that after heating to reflux in methanol for 15 min, an excess (20 equiv.) of triethylamine was added. The resulting mixture was then heated to reflux for an additional 5 min and allowed cool to room temperature with stirring for 30 min. The product was collected as a yellow precipitate in 96% yield (399 mg; 0.536 mmol).

Abbreviations

AcO$^-$	acetate anion ($CH_3CO_2^-$)
ADP	adenosine diphosphate
AMP	adenosine monophosphate
ATP	adenosine triphosphate
cAMP	cyclic adenosine monophosphate
cyclene	1,4,7,10-tetraazacyclododecane
DMSO	dimethyl sulfoxide
DCL	dynamic combinatorial library
dtc	dithiocarbamate
ITC	isothermal titration calorimetry
MLCT	metal to ligand charge transfer
salen	2:1 Schiff base formed from salicylic aldehyde and ethylene diamine, or their derivatives
RCM	ring-closing metathesis
TBA	tetrabutylammonium
tren	tris(2-aminoethyl)amine
TFPB	tetrakis[3,5-bis(trifluoromethyl)phenyl]borate
TsO$^-$	tosylate anion (*p*-CH$_3$-C$_6$H$_4$-SO$_3^-$)

References

1 Bianchi, A., Bowman-James, K. and Garcia-España, E. (1997) *Supramolecular Chemistry of Anions*, Wiley-VCH, New York.

2 Sessler, J.L., Gale, P.A. and Cho, W.-S. (2006) *Anion Receptor Chemistry*, in Monographs in Supramolecular Chemistry (ed.Stoddart, J.F.) Royal Society of Chemistry, Cambridge.

3 Gunnlaugsson, T., Glynn, M., Tocci, G.M., Kruger, P.E. and Pfeffer, F.M. (2006) *Coord. Chem. Rev.*, **250**, 3094–3117.

4 Nguyen, B.T. and Anslyn, E.V. (2006) *Coord. Chem. Rev.*, **250**, 3118–3127.

5 Martínez-Máñez, R. and Sancenón, F. (2006) *Coord. Chem. Rev.*, **250**, 3081–3093.

6 Gale, P.A. and Quesada, R. (2006) *Coord. Chem. Rev.*, **250**, 3219–3244.

7 Llinares, J.M., Powell, D. and Bowman-James, K. (2003) *Coord. Chem. Rev.*, **240**, 57–75.

8 Hosseini, M.W. (2003) *Coord. Chem. Rev.*, **240**, 157–166.

9 (a) Bowman-James, K. (2005) *Acc. Chem. Res.*, **38**, 671–676. (b) Kang, S.O., Begum, R.A. and Bowman-James, W. (2006) *Angew. Chem.*, **118**, 8048–8061; *Angew. Chem. Int. Ed.*, **45**, 7882–7894.

10 Wichmann, K., Antonioli, B., Söhnel, T., Wenzel, M., Gloe, K., Price, J.R., Lindoy, L.F., Blake, A.J. and Schröder, M. (2006) *Coord. Chem. Rev.*, **250**, 2987–3003.

11 Bondy, C.R. and Loeb, S.J. (2003) *Coord. Chem. Rev.*, **240**, 77–99.

12 Kang, S.O., Hossain, Md.A. and Bowman-James, K. (2006) *Coord. Chem. Rev.*, **250**, 3038–3052.

13 Best, M.D., Tobey, S.L. and Anslyn, E.V. (2003) *Coord. Chem. Rev.*, **240**, 3–15.

14 Schmuck, C. (2006) *Coord. Chem. Rev.*, **250**, 3053–3067.

15 Yoon, J., Kim, S.K., Singh, J. and Kim, K.S. (2006) *Chem. Soc. Rev.*, **35**, 355–360.

16 Davis, A.P. and Joos, J.-B. (2003) *Coord. Chem. Rev.*, **240**, 143–156.

17 Sessler, J.L. and Davis, J.M. (2001) *Acc. Chem. Res.*, **34**, 989–997.

18 Sessler, J.L., Camilolo, S. and Gale, P.A. (2003) *Coord. Chem. Rev.*, **240**, 17–55.

19 Beer, P.D. and Hays, E.J. (2003) *Coord. Chem. Rev.*, **240**, 167–189.

20 (a) Severin, K. (2006) *Chem. Commun.*, 3859–3867. (b) Severin, K. (2006) "*Synthetic Organometallic Hosts for Biologically Interesting Molecules*" in *Bioorganometallic Chemistry (Topics in Organometallic Chemistry)* (ed. Simonneaux, G.), Springer, Heidelberg, 123–142.

21 Martinez-Máñez, R. and Sancenón, F. (2003) *Chem. Rev.*, **103**, 4419–4476.

22 Callan, J.F., Prasanna de Silva, A. and Magri, D.C. (2005) *Tetrahedron*, **61**, 8551–8588.

23 Katayev, E.A., Ustynyuk, Y.A. and Sessler, J.L. (2006) *Coord. Chem. Rev.*, **250**, 3004–3037.

24 Lankshear, M.D. and Beer, P.D. (2006) *Coord. Chem. Rev.*, **250**, 3142–3160.

25 Gimeno, N. and Vilar, R. (2006) *Coord. Chem. Rev.*, **250**, 3161–3189.

26 (a) Mahoney, J.M., Beatty, A.M. and Smith, B.D. (2001) *J. Am. Chem. Soc.*, **123**, 5847–5848. (b) Mahoney, J.M., Davis, J.P., Beatty, A.M. and Smith, B.D. (2003) *J. Org. Chem.*, **68**, 9819–9820. (c) Mahoney, J.M., Marshall, R.A., Beatty, A.M., Smith, B.D., Camiolo, S. and Gale, P.A. (2001) *J. Supramol. Chem.*, **1**, 289–292.

27 Koulov, A.V., Mahoney, J.M., Beatty, A.M. and Smith, B.D. (2003) *Org. Biomol. Chem.*, **1**, 27–29.

28 Mahoney, J.M., Nawaratna, G.U., Beatty, A.M., Duggan, P.J. and Smith, B.D. (2004) *Inorg. Chem.*, **43**, 5902–5907.

29 Mahoney, J.M., Beatty, A.M. and Smith, B.D. (2004) *Inorg. Chem.*, **43**, 7617–7621.

30 Mahoney, J.M., Stucker, K.A., Jiang, H., Carmichael, I., Brinkmann, N.R.,

Beatty, A.M., Noll, B.C. and Smith, B.D. (2005) *J. Am. Chem. Soc.*, **127**, 2922–2928.

31 Gunning, P., Benniston, A.C. and Peacock, R.D. (2004) *Chem. Commun.*, 2226–2227.

32 Benniston, A.C., Gunning, P. and Peacock, R.D. (2005) *J. Org. Chem.*, **70**, 115–123.

33 Gunning, P.T. (2005) *Org. Biomol. Chem.*, **3**, 3877–3879.

34 Jencks, W.P. (1981) *Proc. Natl. Acad. Sci. U.S.A.*, **78**, 4046–4050.

35 Suksai, C., Leeladee, P., Jainuknan, D., Tuntulani, T., Muangsin, N., Chailapakul, O., Kongsaeree, P. and Pakavatchai, C. (2005) *Terahedron. Lett.*, **46**, 2765–2769.

36 Mathews, S.E. and Beer, P.D. (2005) *Supramol. Chem.*, **17**, 411–435.

37 Lhotak, P. (2005) "*Anion Receptors Based on Calixarenes*" in *Anion Sensing, (Topics in Current Chemistry)* (ed. Stibor, J.), Springer, Heidelberg, **255**, 65–95.

38 Morzherin, Y., Rudkevich, D.M., Verboom, W. and Reinhoudt, D.N. (1993) *J. Org.Chem.*, **58**, 7602–7605.

39 Cameron, B.R. and Loeb, S.J. (1997) *Chem. Commun.*, 573–574.

40 Sansone, F., Baldini, L., Casnati, A., Lazzarotto, M., Ugozzoli, F. and Ungaro, R. (2002) *Proc. Natl. Acad. Sci. U.S.A.*, **99**, 4842–4844.

41 Miao, R., Zheng, Q.-Y., Chen, C.-F. and Huang, Z.-T. (2005) *Tetrahedron Lett.*, **46**, 2155–2158.

42 Casnati, A., Pirondini, L., Pelizzi, N. and Ungaro, R. (2000) *Supramol. Chem.*, **12**, 53–65.

43 Casnati, A., Fochi, M., Minari, P., Pochini, A., Reggiani, M. and Ungaro, R. (1996) *Gazz. Chim. Ital.*, **126**, 99–102.

44 Gale, P.A. (1998) *Tetrahedron Lett.*, **39**, 3873–3876.

45 (a) Camiolo, S., Gale, P.A., Ogden, M.I., Skelton, B.W. and White, A.H. (2001) *J. Chem. Soc. Perkin Trans.*, **2**, 1294–1298. (b) Camiolo, S., Gale,

P.A., Light, M.E. and Hursthouse, M.B. (2001) *Supramol. Chem.*, **13**, 613–615.

46 Kim, S.K., Kang, B.-G., Koh, H.S., Yoon, Y.J., Jung, S.J., Jeong, B., Lee, K.-D. and Yoon, J. (2004) *Org. Lett.*, **6**, 4655–4658.

47 Sebo, L., Schweizer, B. and Diederich, F. (2000) *Helv. Chim. Acta*, **83**, 80–92.

48 Qing, G.-Y., He, Y.-B., Zhao, Y., Hu, C.-C., Liu, S.-Y. and Yang, X. (2006) *Eur. J. Org. Chem.*, 1574–1580.

49 Yang, Y.S., Ko, S.W., Song, I.H., Ryu, B.J. and Nam, K.C. (2003) *Bull. Korean Chem. Soc.*, **24**, 681–683.

50 Zlatuskova, P., Stibor, I., Tkadlecova, M. and Lhotak, P. (2004) *Tetrahedron*, **60**, 11383–11390.

51 Tumcharern, G., Tuntulani, T., Coles, S. J., Hursthouse, M.B. and Kilburn, J.D. (2003) *Org. Lett.*, **5**, 4971–4974.

52 Kaewtong, C., Fuangswasdi, S., Muangsin, N., Chaichit, N., Vicens, J. and Pulpoka, B. (2006) *Org. Lett.*, **8**, 1561–1564.

53 Nabeshima, T., Saiki, T., Iwabuchi, J. and Akine, S. (2005) *J. Am. Chem. Soc.*, **127**, 5507–5511.

54 Lankshear, M.D., Cowley, A.R. and Beer, P.D. (2006) *Chem. Commun.*, 612–614.

55 Tongraung, P., Chantarasiri, N. and Tuntulani, T. (2003) *Tetrahedron Lett.*, **44**, 29–32.

56 Sisson, A.L., Clare, J.P. and Davis, A.P. (2005) *Chem. Commun.*, 5263–5265.

57 Khatri, V.K., Upreti, S. and Pandey, P.S. (2006) *Org. Lett.*, **8**, 1755–1758.

58 Davis, A.P., Gilmer, J.F. and Perry, J.J. (1996) *Angew. Chem.*, **108**, 1410–1413; *Angew. Chem. Int. Ed.*, **35**, 1312–1315.

59 Bhattarai, K.B., Davis, A.P., Perry, J.J., Walter, C.J., Menzer, S. and Williams, D. J. (1997) *J. Org. Chem.*, **62**, 8463–8473.

60 Camiolo, S. and Gale, P.A. (2000) *Chem. Commun.*, 1129–1130.

61 Woods, C.J., Camiolo, S., Light, M.E., Coles, S.J., Hursthouse, M.B., King, M. A., Gale, P.A. and Essex, J.W. (2002) *J. Am. Chem. Soc.*, **124**, 8644–8652.

62 Anzenbacher, P., Jr. Jursíková, K., Lynch, V.M., Gale, P.A. and Sessler, J.L. (1999) *J. Am. Chem. Soc.*, **121**, 11020–11021.

63 Dukh, M., Drasar, P., Cerny, I., Pouzar, V., Shriver, J.A., Král, V. and Sessler, J.L. (2002) *Supramol. Chem.*, **14**, 237–244.

64 Miyaji, H., Anzenbacher, P., Jr. Sessler, J.L., Bleasdale, E.R. and Gale, P.A. (1999) *Chem. Commun.*, 1723–1724.

65 Anzenbacher, P., Jr. Jursikova, K. and Sessler, J.L. (2000) *J. Am. Chem. Soc.*, **122**, 9350–9351.

66 Nishiyabu, R. and Anzenbacher, P. Jr. (2006) *Org. Lett.*, **8**, 359–362.

67 Sessler, J.L., Král, V., Shishkanova, T.V. and Gale, P.A. (2002) *Proc. Natl. Acad. Sci. U.S.A.*, **99**, 4848–4853.

68 Sessler, J.L., Gale, P.A. and Genge, J.W. (1998) *Chem. Eur. J.*, **4**, 1095–1099.

69 Anzenbacher, P., Jr. Nishiyabu, R. and Palacios, M.A. (2006) *Coord. Chem. Rev.*, **250**, 2929–2938.

70 Nishiyabu, R., Palacios, M.A., Dehaen, W. and Anzenbacher, P. Jr. (2006) *J. Am. Chem. Soc.*, **128**, 11496–11504.

71 Yoon, D.-W., Hwang, H. and Lee, C.-H. (2002) *Angew. Chem.*, **114**, 1835–1837; *Angew. Chem. Int. Ed.*, **41**, 1757–1759.

72 Lee, C.-H., Na, H.-K., Yoon, D.-W., Won, D.-H., Cho, W.-S., Lynch, V.M., Shevchuk, S.V. and Sessler, J.L. (2003) *J. Am. Chem. Soc.*, **125**, 7301–7306.

73 Lee, C.-H., Lee, J.-S., Na, H.-K., Yoon, D.-W., Miyaji, H., Cho, W.-S. and Sessler, J.L. (2005) *J. Org. Chem.*, **70**, 2067–2074.

74 Sessler, J.L., Cyr, M.J., Lynch, V., McGhee, E. and Ibers, J.A. (1990) *J. Am. Chem. Soc.*, **112**, 2810–2813.

75 Sessler, J.L., Cyr, M.J. and Burrell, A.K. (1991) *SynLett*, 127–134.

76 Shionoya, M., Furuta, H., Lynch, V., Harriman, A. and Sessler, J.L. (1992) *J. Am. Chem. Soc.*, **114**, 5714–5722.

77 Sessler, J.L., Cyr, M.J., Furuta, H., Král, V., Mody, T., Morishima, T., Shionoya, M. and Weghorn, S. (1993) *Pure Appl. Chem.*, **65**, 393–398.

78 Scherer, M., Sessler, J.L., Gebauer, A. and Lynch, V. (1998) *Chem. Commun.*, 85–86.

79 Furuta, H., Cyr, M.J. and Sessler, J.L. (1991) *J. Am. Chem. Soc.*, **113**, 6677–6678.

80 Iverson, B.L., Shreder, K., Král, V., Sansom, P., Lynch, V. and Sessler, J.L. (1996) *J. Am. Chem. Soc.*, **118**, 1608–1616.

81 Sessler, J.L., Furuta, H. and Král, V. (1993) *Supramol. Chem.*, **1**, 209–220.

82 Král, V. and Sessler, J.L. (1995) *Tetrahedron*, **51**, 539–554.

83 Král, V., Andrievsky, A., Sessler, J.L. (1995) *J. Chem. Soc., Chem. Commun.*, 2349–2351.

84 Cormode, D.P., Murray, S.S., Cowley, A.R. and Beer, P.D. (2006) *Dalton Trans.*, 5135–5140.

85 Gong, J. and Gibb, B.C. (2005) *Chem. Commun.*, 1393–1395.

86 Gong, J. and Gibb, B.C. (2005) *Chem. Commun.*, 3319–3321.

87 Beer, P.D., Berry, N., Drew, M.G.B., Fox, O.D., Padilla-Tosta, M.E. and Patell, S., (2001) *Chem. Commun.*, 199–200.

88 Berry, N.G., Pratt, M.D., Fox, O.D. and Beer, P.D. (2001) *Supramol. Chem.*, **13**, 677–682.

89 (a) Beer, P.D. and Wallace, W.W.H., (2005) *"Sensing, Templation and Self-Assembly by Macrocyclic Ligand Systems"* in *Macrocyclic Chemistry, Current Trends and Future Perspectives* (ed. Gloe, K.) Springer, The Netherlands, pp.105–119. (b) Beer, P.D. and Bayly, S.R. (2005) *"Anion Sensing by Metal-Based Receptors"*, in *Topics in Current Chemistry, 255*, Springer, Berlin, pp. 125–162.

90 Wong, W.W.H., Curiel, D., Cowley, A.R. and Beer, P.D. (2005) *Dalton Trans.*, 359–364.

91 Webber, P.R.A., Drew, M.G.B., Hibbert, R. and Beer, P.D. (2004) *Dalton Trans.*, 1127–1135.

92 Wong, W.W.H., Phipps, D.E. and Beer, P.D. (2004) *Polyhedron*, 2821–2829.

93 Beer, P.D., Berry, N.G., Cowley, A.R., Hayes, E.J., Oates, E.C. and Wong, W.W.H. (2003) *Chem. Commun.*, 2408–2409.

94 Beer, P.D., Cheetham, A.G., Drew, M.G.B., Fox, O.D., Hayes, E.J. and Rolls, T.D. (2003) *Dalton Trans.*, 603–611.

95 (a) Galbraith, S.G., Plieger, P.G. and Tasker, P.A. (2002) *Chem. Commun.*, 2662–2663. (b) Miller, H.A., Laing, N., Parsons, S., Parkin, A., Tasker, P.A. and White, D.J. (2000) *Dalton Trans.*, 3773–3782.

96 Plieger, P.G., Tasker, P.A. and Galbraith, S.G. (2004) *Dalton Trans.*, 313–318.

97 Fujita, T. and Lehn, J.-M. (1988) *Tetrahedron Lett.*, **29**, 1709–1712.

98 Hossain, M.A., Llinares, J.M., Powell, D. and Bowman-James, K. (2001) *Inorg. Chem.*, **40**, 2936–2937.

99 Kang, S.O., Powell, D. and Bowman-James, K. (2005) *J. Am. Chem. Soc.*, **127**, 13478–13479.

100 Kang, S.O., Hossain, M.A., Powell, D. and Bowman-James, K. (2005) *Chem. Commun.*, 328–330.

101 Kang, S.O., Powell, D., Day, V.W. and Bowman-James, K. (2006) *Angew. Chem.*, **118**, 1955–1959; *Angew. Chem. Int. Ed.*, **45**, 1921–1925.

102 Kubik, S., Kirchner, R., Nolting, D. and Seidel, J. (2002) *J. Am. Chem. Soc.*, **124**, 12752–12760.

103 Kubik, S., Goddard, R., Otto, S., Pohl, S., Reyheller, C. and Stuwe, S. (2005) *Biosens. Bioelectron.*, **20**, 2364–2375.

104 Otto, S. and Kubik, S. (2003) *J. Am. Chem. Soc.*, **125**, 7804–7805.

105 Brooks, S.J., Gale, P.A. and Light, M.E. (2006) *Chem. Commun.*, 4344–4346.

106 Hirata, O., Takeuchi, M. and Shinkai, S. (2005) *Chem. Commun.*, 3805–3807.

107 Francesconi, O., Ienco, A., Moneti, G., Nativi, C. and Roelens, S. (2006) *Angew. Chem.*, **118**, 6845–6848; *Angew. Chem. Int. Ed.*, **46**, 6693–6696.

108 Garcia-España, E., Diaz, P., Llinares, J.M. and Bianchi, A. (2006) *Coord. Chem. Rev.*, **250**, 2952–2986.

109 Miranda, C., Escarti, F., Lamarque, L., Yunta, M.J.R., Navarro, P., Garcia-España, E. and Jimeno, M.L. (2004) *J. Am. Chem. Soc.*, **126**, 823–833.

110 Sessler, J.L. and Seidel, D. (2003) *Angew. Chem.*, **115**, 5292–5333; *Angew. Chem. Int. Ed.*, **42**, 5134–5175.

111 Seidel, D., Lynch, V. and Sessler, J.L. (2002) *Angew. Chem.*, **114**, 1480–1483; *Angew. Chem. Int. Ed.*, **41**, 1422–1425.

112 Sessler, J.L., Katayev, E., Dan Pantos, G. and Ustynyuk, Y.A. (2004) *Chem. Commun.*, 1276–1277.

113 Moyer, B.A. and Singh, R.P. (2004) *Fundamentals and Applications of Anion Separations*, Kluwer Academic/Plenum Publishers, New York.

114 Sessler, J.L., Katayev, E., Pantos, G.D., Scherbakov, P., Reshetova, M.D., Khrustalev, V.N., Lynch, V.M. and Ustynyuk, Y.A. (2005) *J. Am. Chem. Soc.*, **127**, 11442–11446.

115 Katayev, E.A., Pantos, G.D., Reshetova, M.D., Khrustalev, V.N., Lynch, V.M., Ustynyuk, Y.A. and Sessler, J.L. (2005) *Angew. Chem.*, **117**, 7552–7556; *Angew. Chem. Int. Ed.*, **44**, 7386–7390.

116 Sessler, J.L., Roznyatovskiy, V., Pantos, G.D., Borisova, N.E., Reshetova, M.D., Lynch, V.M., Khrustalev, V.N. and Ustynyuk, Y.A. (2005) *Org. Lett.*, **7**, 5277–5280.

117 Fyfe, M.C.T., Glink, P.T., Menzer, S., Stoddart, J.F., White, A.J.P. and Williams, D.J. (1997) *Angew. Chem.*, **109**, 2158–2160; *Angew. Chem., Int. Ed. Engl.*, **36**, 2068–2070.

118 Beer, P., Sambrook, M.R. and Curiel, D. (2006) *Chem. Commun.*, 2105–2177.

119 Ng, K.-Y., Cowley, A.R. and Beer, P.D. (2006) *Chem. Commun.*, 3676–3678.

10
Rotaxane and Catenane Synthesis

James A. Wisner and Barry A. Blight

10.1
Introduction

The synthesis of interlocked molecules has become commonplace over the past 25 years with the gradual development of a number of highly facile template methods for their construction. What were once laboratory curiosities have now taken a prominent place in the broad field of supramolecular chemistry, especially regarding their uses and further potential as molecular switches and machines [1]. We present here an overview of the main synthetic approaches to these molecules, with a focus on methods in which macrocyclization reactions result in interlocked products. The analysis is by no means meant to be comprehensive or exhaustive in detail, but rather to convey the variety and utility of the selected synthetic strategies in generating abiotic rotaxane and catenane superstructures.

10.1.1
General Comments

Interlocked molecules are those assemblies of two or more molecules which are linked by a so-called mechanical bond [2]. The individual molecules are not connected covalently in any way but are linked via their spatial relationship to one another. The nature of this phenomenon is such that it necessarily involves a macrocyclic component as one or more of the molecules which compose the assembly. The simplest forms of these assemblies are represented by a [2]rotaxane and a [2]catenane (Figure 10.1), where the bracketed numeral preceding the name indicates the number of individual molecules comprising the interlocked product. The synthesis of a rotaxane may be executed by a number of different routes, only one of which involves the formation of a macrocyclic component in the final
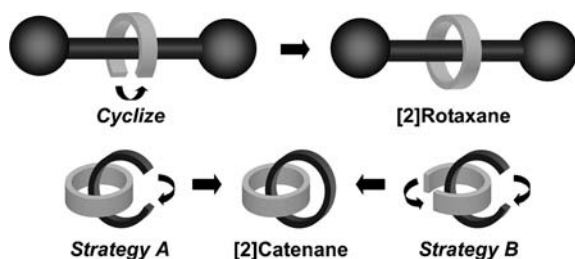
Figure 10.1 "Clipping" strategies in macrocyclization reactions resulting in interlocked products such as [2]rotaxanes and [2]catenanes.

interlocking step, which is commonly referred to as "clipping". The synthesis of a catenane requires the formation of at least one of the two (or more) catenated macrocyclic rings in the final step as a result of the topologically complex nature of the relationship between the rings. This gives rise to two different synthetic strategies for construction of a hypothetical [2]catenane, which entail either one macrocyclization step (strategy A) or two (strategy B) [3].

Interlocked structures may be synthesized in the absence of any preorganization of their precursors by statistical methods, but these are generally lower yielding and can be technically challenging [2b, 4]. The adoption of template approaches has greatly increased the efficiency, and often simplicity, of the construction of mechanically bonded species. However, the template employed and the synthetic step to enact the ring closure must be compatible. This requirement manifests itself in a couple of different considerations. First, and most obviously, the reaction conditions for ring closure must be tolerant of the functionality present in the components and not interfere with the relevant template interactions between them (i.e., break up the template). The templates used in many of the syntheses of interlocked products are often a combination of numerous weak non-covalent forces and, as such, can be highly sensitive to reaction conditions which are not considered harsh in "normal" covalent synthetic sequences (e.g., medium/ strong acids or bases, highly polar solvents). Second, the application of a template can be problematic in the case of macrocyclization reactions, which are often run under high-dilution conditions. If the template utilized is the result of an equilibrium complexation of the components, then high-dilution conditions are of little benefit unless the association constants for the relevant equilibria lie sufficiently in favor of complex formation. Luckily, many of the template methods discussed below act to organize not only the precursors with respect to one another, but also to predispose (or localize) the pendant arms of the pre-macrocyclic building blocks for their intramolecular macrocyclization. Hence, the template can serve multiple purposes and obviate the need for high dilution to reduce the formation of oligomeric and higher order cyclic species, which are often undesirable side reactions.

10.2
Macrocyclization Reactions Resulting in Interlocked Products

10.2.1
Williamson Ether Synthesis

The reaction of oxo-anions with alkyl halides or sulfonates is of central importance in the synthesis of crown ethers, and thus holds a similar position in the synthetic development of supramolecular chemistry as a whole [5]. It is no surprise then that this was the macrocyclization reaction used in the synthesis of the first metal-templated catenane by Sauvage and Dietrich-Buchecker in 1983 [6]. The authors employed a transition metal ion with a tetrahedral coordination sphere (Cu^+) to arrange two phenanthroline-based ligands (one macrocyclic (**1**) and one acyclic (**2**); strategy A) in an orthogonal and interpenetrated manner (Scheme 10.1). In the course of their investigations, they found that the polyether segment of the macrocyclic ligand must contain at least five ethyleneoxy units in order to allow efficient interpenetration by the acyclic ligand [3]. The coordination complex formed is very stable, which is likely necessary in light of the reaction conditions used to convert it to the interlocked product. The final catenate **3** (the "-ate" suffix indicating its nature as a transition-metal complex) was formed in 27% yield by reaction of the phenolate end groups of the acyclic ligand with pentaethylene glycoldiiodide and further templated using cesium carbonate as the base. Removal of the Cu^+ template to liberate the metal-free catenand **4** (the "-and" suffix indicating the ligand character of the catenane) was achieved through treatment with tetramethylammonium cyanide. The same catenate can be synthesized in 27% yield by strategy B from a Cu^+ complex of two acyclic ligands and two equivalents of the oligoethyleneoxydihalide [7]. Sauvage and coworkers have exploited these synthetic routes to produce a large number of catenanes using a variety of different dihalide linkers for the macrocyclization step, with typically similar yields [3].

An elaboration of this methodology also produced the first molecular trefoil knot **5**, which is a topologically complex macrocycle (Scheme 10.2a) [8]. The authors used a variation on strategy B to synthesize this product. In this case, rather than a single metal center, the authors began with the dinuclear double-helical template **6** (or helicate), which is intertwined and presents its terminal hydroxyl functions from the opposite ends of each of the two ligands which form the complex. Cyclization in this instance, using similar conditions to that for the catenane (strategy B), forms the knotted macrocycle in 3% yield. An even further extension is the synthesis of a doubly-intertwined [2]catenane **7** (or Solomon knot) which proceeds in 2% yield (strategy A) using a similar approach and trinuclear helicate **8** (Scheme 10.2b) [9]. The yields for both of these products can be greatly improved by using alkene metathesis for the ring closures instead [10,11].

10.2.2
Quaternization of Aromatic Amines (Menschutkin Reaction)

In the early 1980s, Stoddart and coworkers investigated the complexation of pyridinium dications (e.g., paraquat) using crown ethers [12]. The complexation of
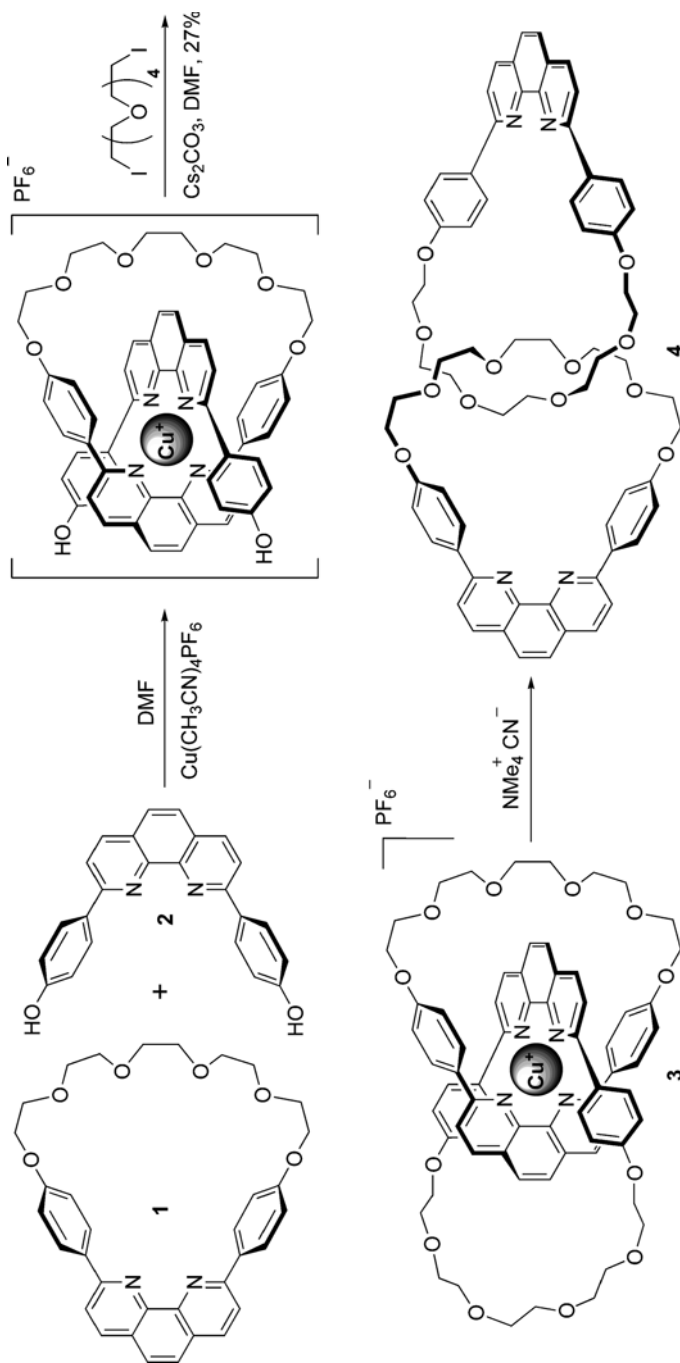
Scheme 10.1 Cu$^+$-templated catenane formation first reported by Sauvage and coworkers.
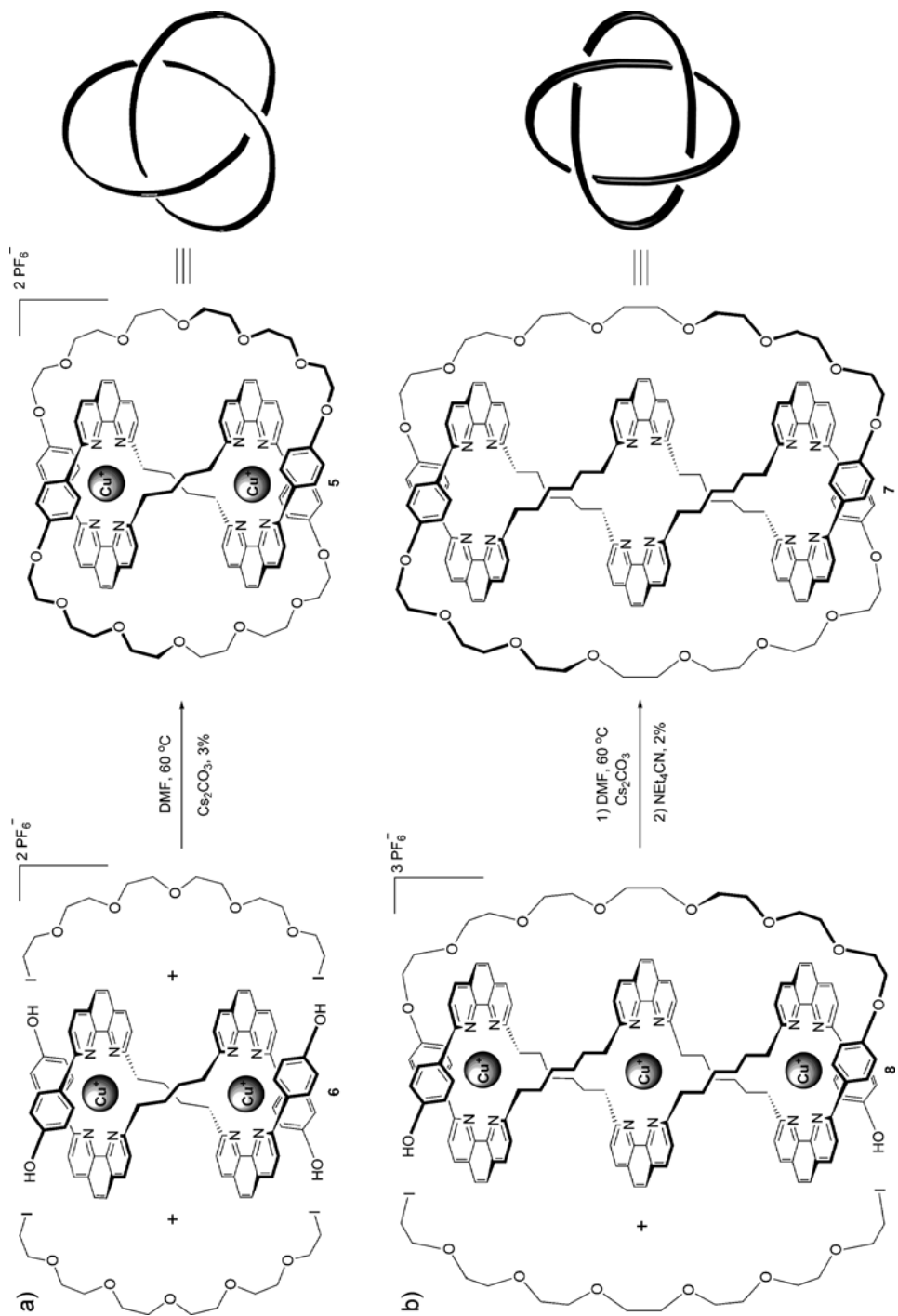
Scheme 10.2 Structural representations of the trefoil knot (a) and doubly intertwined [2]catenane (b) by Sauvage and coworkers.

these organic cations occurs through a combination of π-π stacking, ion-dipole interactions, and C–H···O hydrogen bonding. An extension of this complexation to the synthesis of interlocked species involved the introduction of bifunctional bridging units such as α,α'-dibromo-*p*-xylene, which have the potential to form tetracationic macrocyclic product **9** with 4,4'-dipyridyl [13]. The macrocycle (Scheme 10.3) can be synthesized from the dicationic U-shaped intermediate **10** and α,α'-dibromo-*p*-xylene in the absence of any template in a yield of 12% by refluxing for 18 h with MeCN as solvent. However, in the presence of a 3-molar excess of a diethyleneglycol-appended π-electron-rich hydroquinone template (**11**) and by running the reaction at room temperature for 9 days, the yield of macrocyclic product is improved to 35%; a change of solvent to DMF and the application of ultrahigh pressure enhanced the yield to 62% [14].

The macrocyclization reaction described above has been used to generate a great number of catenane (**12**) and rotaxane (**13**) architectures (Scheme 10.4) using both crown ethers [preformed macrocyclic components **14** (strategy A)] and hydroquinone-based dumbbell-shaped polyethers [preformed acyclic components **15** ("clipping")] as templates [14b, 15]. These templates are also relatively robust with regard to the substitution of different groups into both the tetracationic cyclophane and the neutral frameworks.

A representative selection of [2]catenanes synthesized by this route is given in Table 10.1[14b, 15a, 16]. It is remarkable to note that the first [2]catenane synthesized (entry 2, Table 10.1) could be isolated in 74% yield [14,16]. The final entry in the table is an example of an expanded version of the tetracationic macrocycle which incorporates a biphenylene spacer between the paraquat residues and can accommodate two π-stacked aryl rings within its cavity. The reaction results in the isolation of the [3]catenane product in 25% yield with very little (2%) [2]catenane isolated [16p]. A spectacular demonstration of the power of this approach by Stoddart and coworkers was the iterative synthesis of a [5]catenane which the authors dubbed Olympiadane after its resemblance to the Olympic rings [17].

The application of this template to the clipping of acyclic dumbbell-shaped molecules to form rotaxanes [14] has received less intensive scrutiny but involves a similar synthetic scheme and conditions. A few representative examples of [2]rotaxanes synthesized in this manner (**16–20**) are shown in Figure 10.2 [15c, 18–21]. The use of a 1,5-dihydroxynaphthalene core in these cases usually results in higher yields of the desired interlocked products [18,21].

10.2.3
Condensation of Amines with Acid Chlorides

The first examples of [2]catenanes templated by hydrogen bonding were reported in a similar time frame by both Hunter [22] and Vögtle and coworkers [23] in 1992 using nearly identical components in their syntheses (Scheme 10.5). Vögtle and coworkers simply condensed two equivalents of the diamine **21** (one equivalent acting as base) with one equivalent of 5-methoxyisophthaloyldichloride using
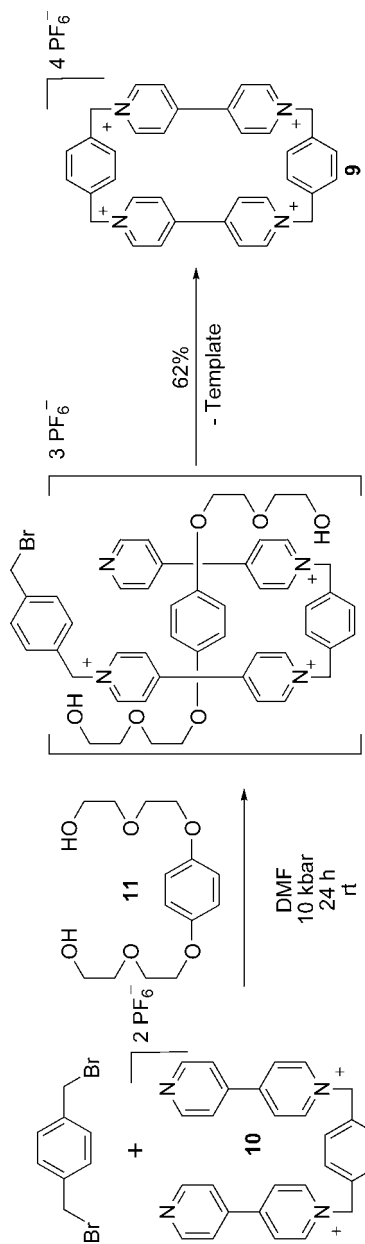
Scheme 10.3 Template-directed synthesis of a tetracationic cyclophane by Stoddart and coworkers.
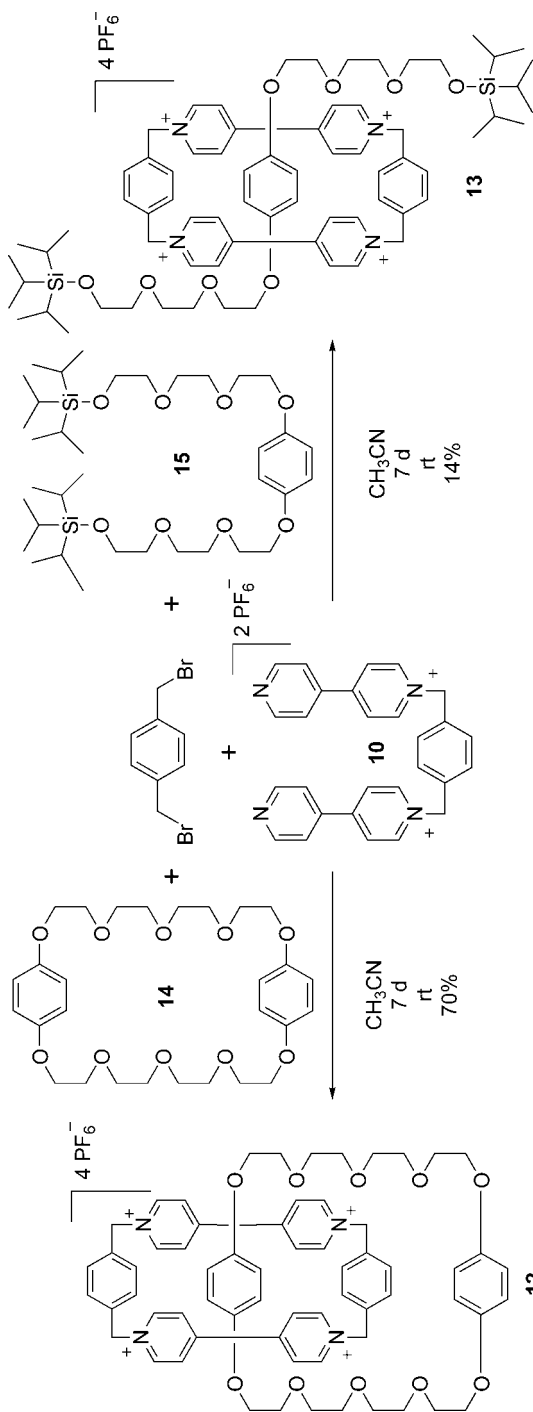
Scheme 10.4 Macrocyclization in the synthesis of a [2]catenane and [2]rotaxane reported by Stoddart and coworkers.
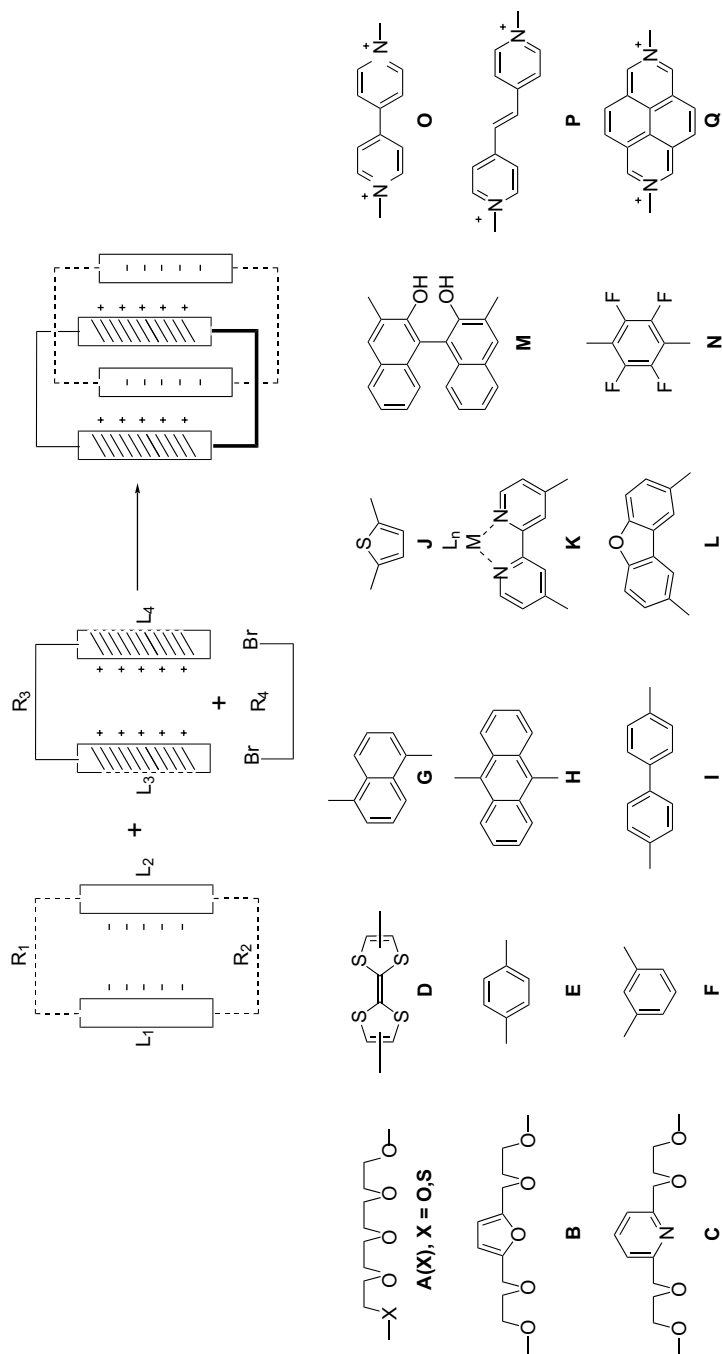
Table image 10.1

Table 10.1 Selected examples of catenane formation via quaternization of aromatic amines.

L_1	L_2	R_1	R_2	L_3	L_4	R_3	R_4	Solvent	Time	Pressure	Yield (%)	Ref.
E	E	A(O)	A(O)	O	O	E	E	MeCN	2d	$-^a$	70	14b, 15a 16a
								DMF	3d	10 kbar	74	14b, 16a
E	E	A(O)	A(O)	O	O	F	F	MeCN	–	$-^a$	0^b	16a
								DMF	3d	10 kbar	28	16a
G	G	A(O)	A(O)	O	O	E	E	DMF	10d	$-^a$	51	16b
H	E	A(O)	A(O)	O	O	E	E	MeCN	4d	$-^a$	59	16c
E	E	A(O)	A(O)	P	P	E	E	MeCN	7d	$-^a$	19	16d
								DMF	15	$-^a$	38	16d
G	G	A(O)	A(O)	P	P	E	E	DMF	15d	$-^a$	51	16d
N	N	A(O)	A(O)	O	O	E	E	MeCN	5d	$-^a$	0^b	16e
N	E	A(O)	A(O)	O	O	E	E	MeCN	5d	$-^a$	60	16f
C	C	A(O)	A(O)	O	O	E	E	MeCN	5d	$-^a$	31	16g
E	E	A(O)	A(O)	O	O	J	J	MeCN	7d	$-^a$	59	16h
E	E	B	B	O	O	E	E	MeCN	$-^b$	$-^a$	40	16i
E	E	A(S)	A(S)	O	O	E	E	DMF	4d	$-^a$	70	16j
G	G	A(S)	A(S)	O	O	E	E	DMF	4d	$-^a$	77	16j
E	E	A(O)	A(O)	O	O	L	L	MeCN	19d	$-^a$	30	16k
E	E	A(O)	A(O)	O	O	K	E	MeCN	14d	$-^a$	30	16l
M	E	A(O)	A(O)	O	O	M	E	MeCN	14d	$-^a$	24	16m
E	E	A(O)	A(O)	Q	O	E	E	MeCN	14d	$-^a$	52	16n
E	E	A(O)	A(O)	Q	Q	E	E	DMF	14d	$-^a$	73	16n
D	G	A(O)	A(O)	O	O	E	E	DMF	5d	$-^a$	23	16o
E	E	A(O)	A(O)	O	O	I	I	MeCN	7d	$-^a$	$25^c, 2^d$	16p

[a]ambient pressure;
[b]no reaction time reported;
[c][3]catenane;
[d][2]catenane.

catalytic DMAP and high dilution in chlorobenzene. This gave the [2]catenane **22** (R $=$ OMe) in 12% yield. Hunter, in an attempt to improve on the yield of the parent macrocycle he had synthesized previously, used a two-step approach wherein three quarters of the final macrocycle was synthesized first (**23**), reducing the reaction to a $1+1$ rather than a $2+2$ macrocyclization. This simplification, and the use of NEt$_3$ as the base in a methylene chloride solvent system, resulted in isolation of the [2]catenane **24** (R $=$ H) in 34% yield.

Vögtle and coworkers have explored this system further using Hunter's $1+1$ approach and different dicarbonylchloride connecting groups (e.g., 2,5-furandicarbonyldichloride), postulating a mechanism for the catenation based on the experimental data [24]. The authors posited that catenation likely involves formation of an initial macrocycle and subsequent threading of a partially reacted mixed amide/acid chloride intermediate through the macrocyclic cavity. Further intramolecular condensation of the threaded intermediate would provide the interlocked product.

Leigh and coworkers reported the synthesis of a related [2]catenane system in 1995 based on the condensation of isophthaloyldichloride and para-xylylenediamine
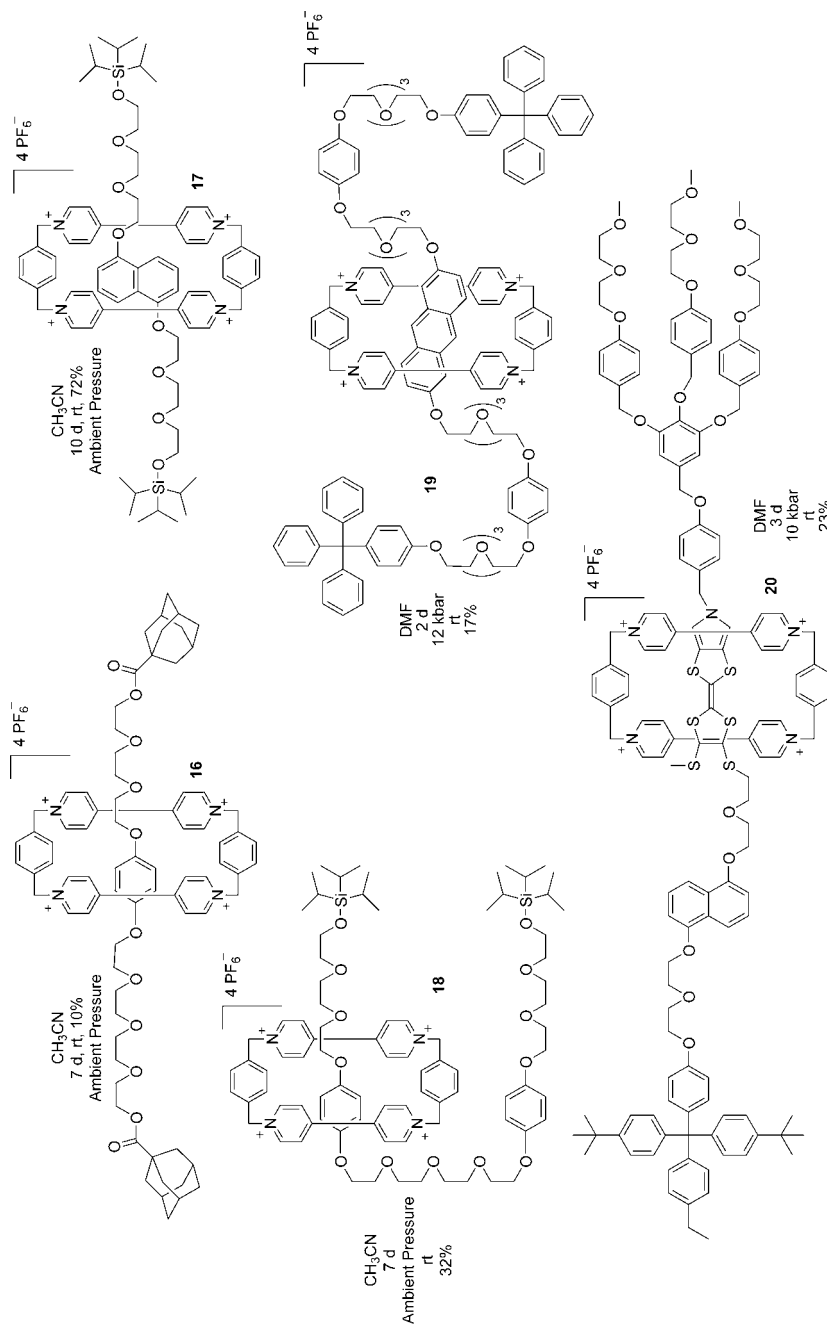
Figure 10.2 Representative examples of various "clipped" [2]rotaxanes synthesized by Stoddart and coworkers.
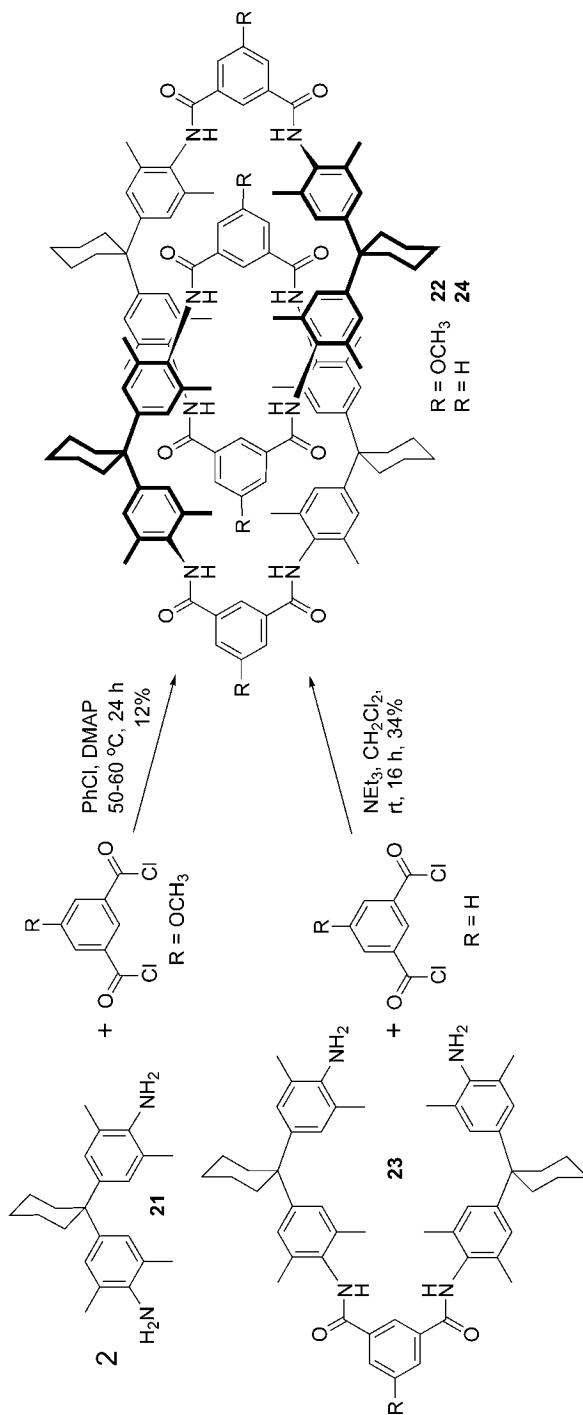
Scheme 10.5 Hydrogen bond-templated self-assembly of [2]catenanes reported by both Vögtle and coworkers and Hunter and coworkers.
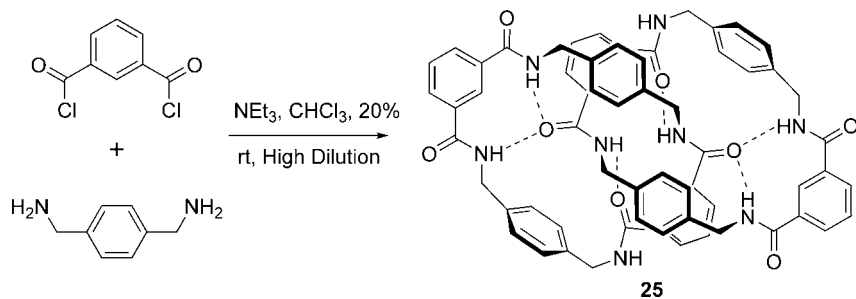
Scheme 10.6 Self-assembly of the hydrogen bond-directed [2]catenane formation by Leigh and coworkers.

in anhydrous chloroform with NEt$_3$ as base (Scheme 10.6) [25]. The reaction is exceedingly simple to execute, and [2]catenane **25** can be isolated without the aid of chromatography in 20% yield. The generality of the template was explored further using a variety of dicarbonylchloride and diamine starting materials to form a diverse array of [2]catenanes (Table 10.2) in yields ranging from 18 to 27% [26]. The authors noted that the ideal reaction concentration for catenane formation in the case of **25** was 0.02 M at 298 K in chloroform. The use of more polar solvents (e.g., DMF or acetone) in all these cases gives rise to only macrocyclic and linear products, presumably because of disruption of the hydrogen bonding template. The mechanism for catenane formation in this system has been examined theoretically, and the results support not only the hydrogen-bonding basis for templation of the catenane but also templation of the macrocycle itself from intermediate linear oligomers [27].

The macrocyclization reaction discussed above can be adapted to the formation of more constitutionally varied interlocked structures using a clipping methodology. A number of different linear subunits with sterically demanding termini (**26–31**) have been used to template the clipping of macrocycle **32** to give [2]rotaxane products (Figure. 10.3) [28]. In these schemes, the template is the limiting reagent and the pre-macrocyclic starting materials are added in a 4- to 5-fold excess to maximize the yield of interlocked species. The fumaramide-based thread **29** templates the corresponding [2]rotaxane in 97% yield, which is astonishing given that the reaction sequence involves the condensation of four components encircling a fifth [28–31]. A similar approach with preformed macrocyclic species that incorporate the same subunits yields catenated architectures with structurally dissimilar rings [32].

10.2.4
Oxidative Acetylide Coupling

The oxidative coupling of two terminal alkynes via their copper acetylide complexes to form a 1,3-butadiyne function is known variously as Glaser, Eglinton, or Hay

Table 10.2 Representative examples of [2]catenanes synthesized by Leigh and coworkers

R (S)	(2+2) Macrocycle [%]	(2+2+2+2) Catenane [%]	(3+3) Macrocycle [%]	(4+4) Macrocycle [%]	(4+4+2+2) Catenane [%]
	—[a]	20	—[a]	—[a]	–
t-Bu	25	18	trace	10	5
allyloxy	20	18	–	5	–
Br	20	20	–	7	trace
O2N	22	18	–	5	–
S (thiophene)	25	25	trace	2	–
N (pyridine)	20	27	–	6	trace
biphenyl	21	18	trace	6	–
naphthalene	19	19	–	5	–
F	20	–	–	5	–

[a] poor solubility for these products hampered all characterization attempts.
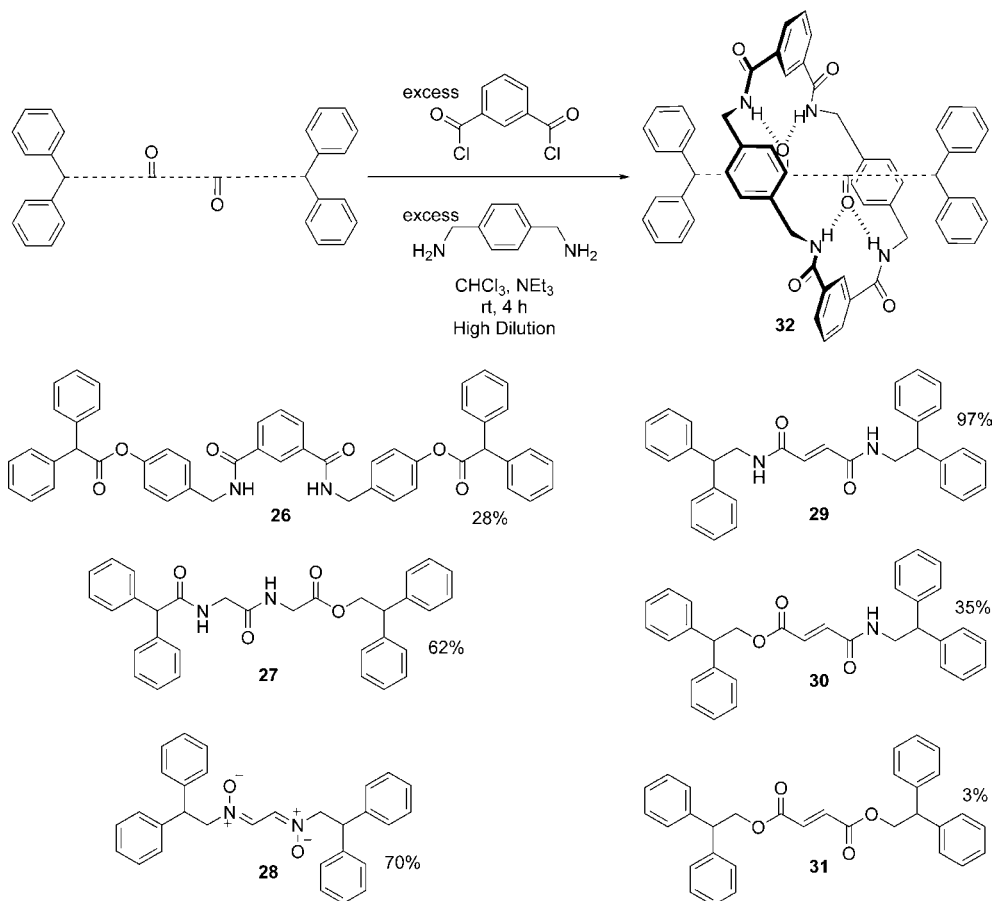
Figure 10.3 Examples of [2]rotaxane formation via hydrogen bond-templated macrocyclization reported by Leigh and coworkers.

coupling depending on the conditions used in the synthesis [33]. The reaction is highly facile and is a method of choice when constructing macrocyclic species containing 1,3-butadiynes in the backbone [34]. Given the wide precedent for this type of macrocyclization, the application of this methodology is a natural extension in the synthesis of interlocked species.

Sauvage and coworkers have explored Glaser coupling in conjunction with their Cu$^+$ template approach to synthesize multiply catenated structures [35]. The authors used a macrocyclic Cu$^+$ complex **33** pre-threaded with acyclic bis-propargyl-terminated phenanthroline co-ligand **34** as the starting material (Scheme 10.7). Oxidative coupling of this complex (pathway A) in the presence of a very large excess of CuCl and CuCl$_2$ produced a mixture of [3]- (**35**), [4]-, [5]-, [6]-, and [7]-catenate products. Characterization in this case was hampered by similar or identical NMR spectra and difficulty
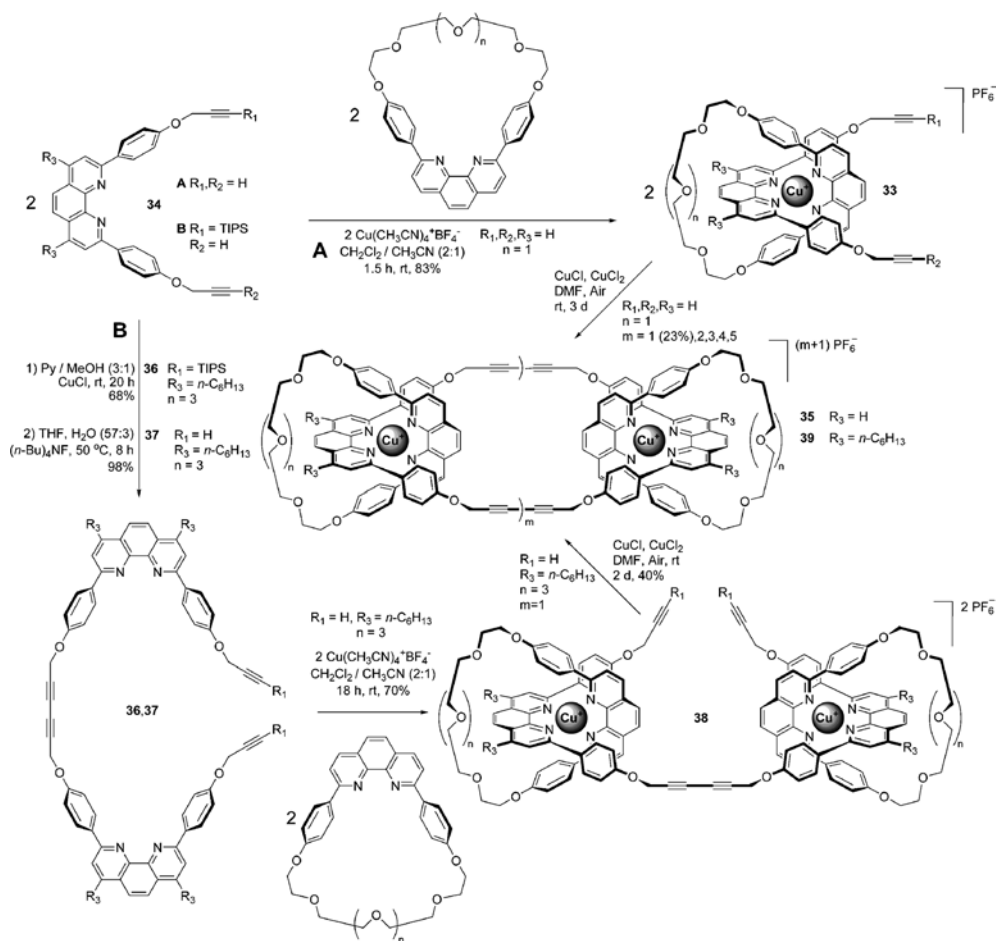
Scheme 10.7 Oxidative acetylide coupling in the formation of [3]catenanes **35** and **39** reported by Sauvage and coworkers.

in separation of the higher order [5]-, [6]- and [7]catenates. A further investigation of a related system executed in a stepwise manner (i.e., intermolecular coupling (**36**, **37**) followed by intramolecular coupling of the threaded macrocycles **38** (pathway B) resulted in an improved yield of [3]catenane **39** (40%) for the final ring closure [36]. However, the synthetic difficulty in applying Cu⁺ as both template and reagent was apparently a limiting factor.

Siegel and coworkers have recently applied a similar metal template approach with Ru(II), terpyridyl- (**40**) and pyridyl/phenanthroline-based (**41**) ligands using 20 equivalents of Cu(OAc)$_2$/MeCN to enact a double ring closure (**42–45**) in the final step, with yields of [2]catenates (**46**, **47**) ranging from 20 to 25% (Scheme 10.8) [37].
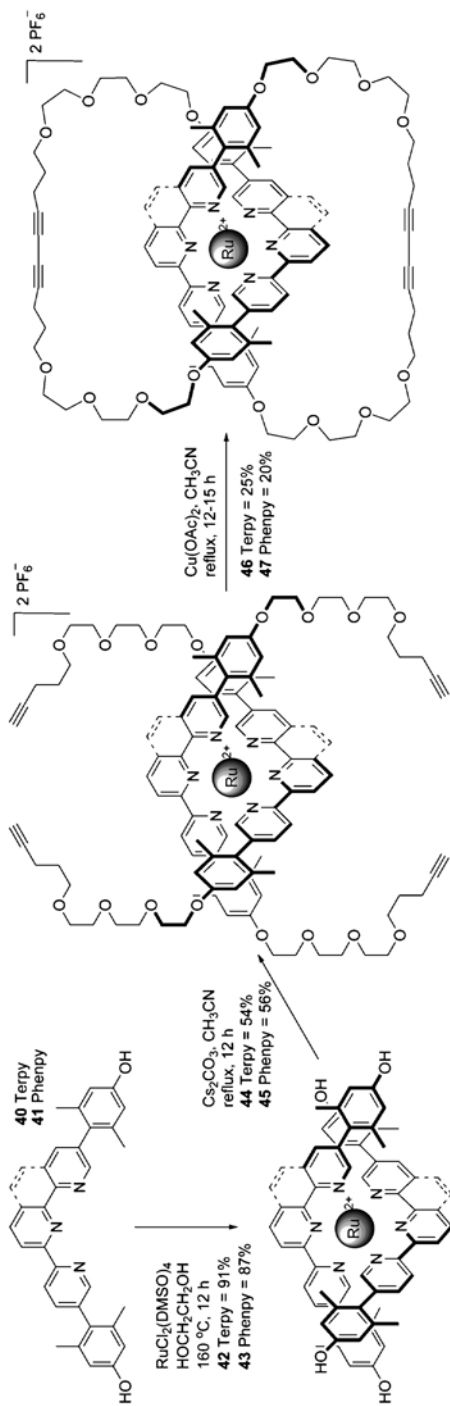
Scheme 10.8 Synthesis of a ruthenium-templated [2]catenane by Siegel and coworkers.

Bäuerle and coworkers have adapted the Cu$^+$ template (**48**) approach to [2]cate-nane synthesis using an intermediate platinum diacetylide linkage to macrocyclize each of the two rings (**49**, Scheme 10.9) [38]. Oxidation of the platinum centers in the macrocyclic rings of **50** with I$_2$ induces reductive elimination of the two acetylides to form the 1,3-butadiyne linked macrocycles (**51**). Unfortunately, the authors could not remove the copper template in this example, likely as a result of steric congestion about the metal ion in the interlocked product.

In 1997, Hamilton, Sanders, and coworkers introduced a new template for [2]catenane formation based solely on π-stacking of neutral donor and acceptor π-systems (Scheme 10.10) [39]. The authors used large excesses of CuCl/CuCl$_2$ in DMF at 50 °C to cyclize bifunctional pyromellitimide (**52**) and naphthalene diimide (**53**) monomers (2 equivalents/30 mM) in the presence of a dinaphtho-crown ether (1 equivalent) to form the corresponding [2]catenanes **54–55** and **56** in 25–33% and 29% yields, respectively. A later report in which the reactions were performed at room temperature, in spite of partial insolubility of the starting materials, raised the yields to 38% and 52%, respectively [40]. It is interesting to note that the mixed acceptor [2]catenane **56** (i.e., pyromellitimide/naphthodiimide) can be synthesized in 24% yield by reaction of equimolar amounts of all three starting materials.

A remarkable extension of this methodology to the tandem closure of both cate-nated rings using the same acetylide coupling reaction, shown in Scheme 10.11, can be achieved in the case of the pyromellitimide acceptor. Cyclization of this starting material with acyclic propargyl-terminated dinaphthyl polyether **57** produces the corresponding [2]catenane **58** in 13–16% yield in one step [41]. The same reaction run with the naphthalenediimide starting material **53** failed.

10.2.5
Alkene Metathesis

The great impact that the development of alkene metathesis has had on synthetic chemistry [42] has likewise influenced the construction of interlocked molecules. The ready availability of catalyst, high yields, mild conditions and broad functional group tolerance of the Ring Closing Metathesis (RCM) version of this reaction has prompted its use in a wide range of template approaches for rotaxane and catenane formation. The thermodynamic distribution of the products obtained from the reaction as a result of its reversible nature can lead to very high yields of mechanically bonded products in a well-designed system. A complicating factor in many of these syntheses is the presence of mixtures of E/Z isomers in the disubstituted alkene products. The subse-quent hydrogenation of the alkene is often used to remove the stereoisomerism and simplify the final purification of the interlocked species.

A number of metal-templated catenates have been prepared by RCM in conjunc-tion with a variety of 4-, 5-, and 6-coordinate metal templates using homogeneous and mixed-ligand systems. Several representative examples are given in Figure 10.4 highlighting the final alkene connection used to cyclize the ring(s). The majority of these systems follow the general approach of Sauvage and Dietrich-Buchecker's
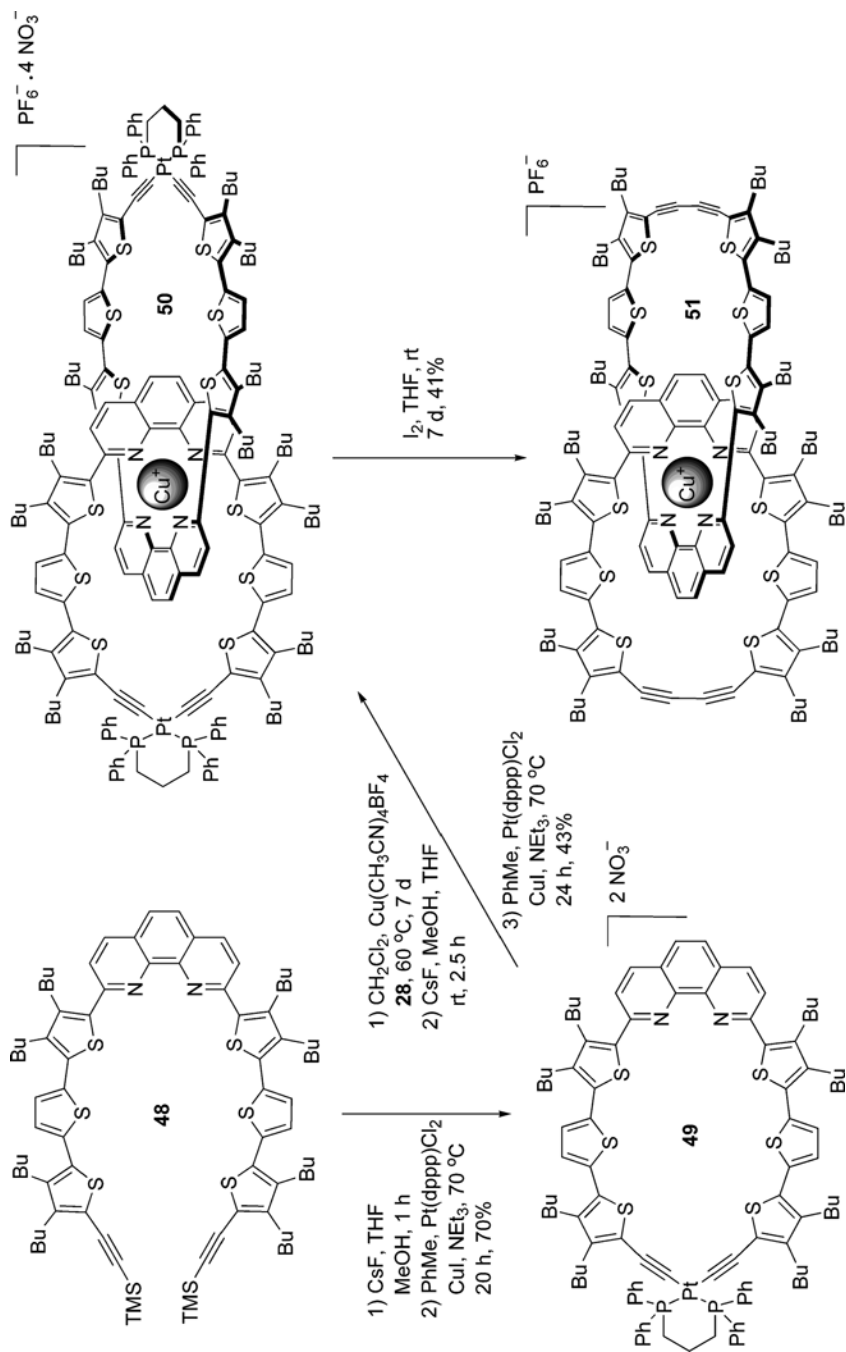
Scheme 10.9 Formation of a Pt(II)-linked, followed by a 1,3-butadiyne-linked [2]catenane reported by Bäuerle and coworkers.
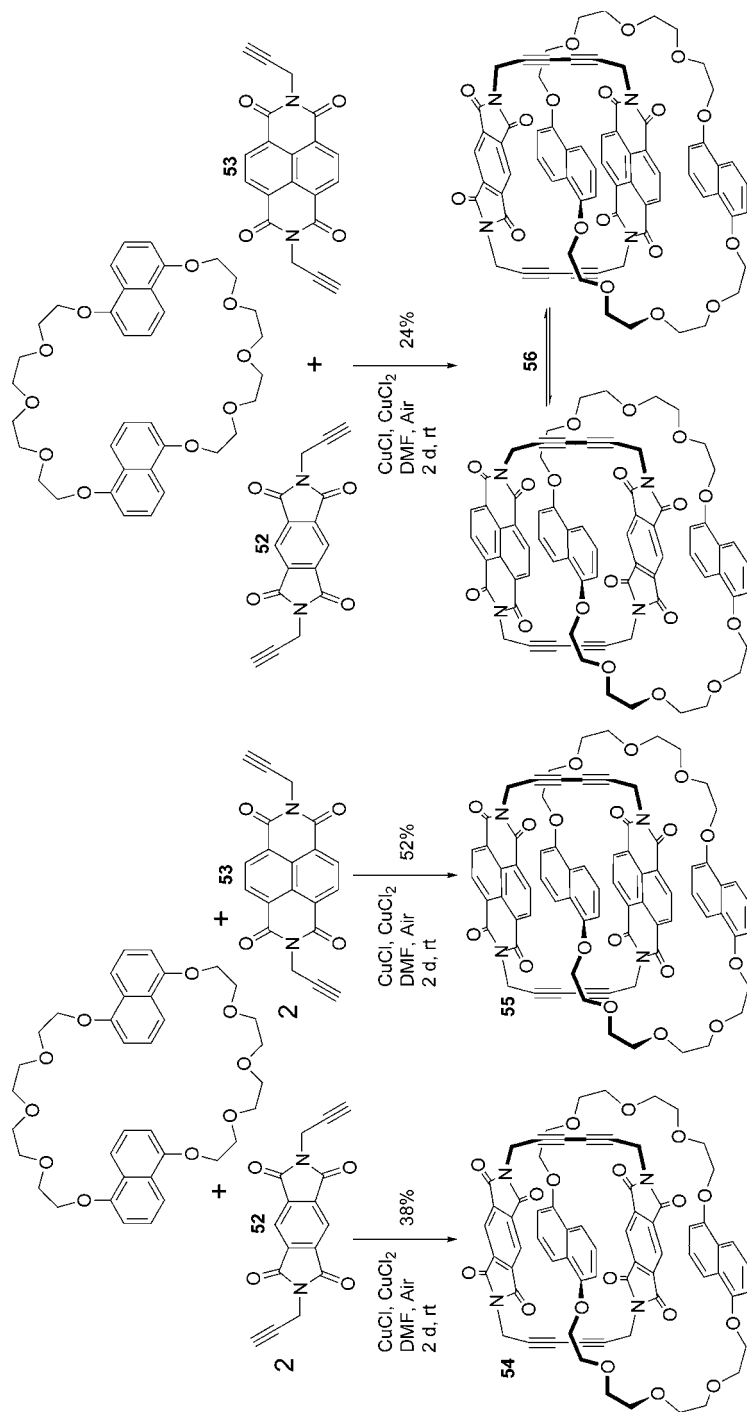
Scheme 10.10 Formation of π-donor/acceptor-templated [2]catenanes reported by Sanders and coworkers.
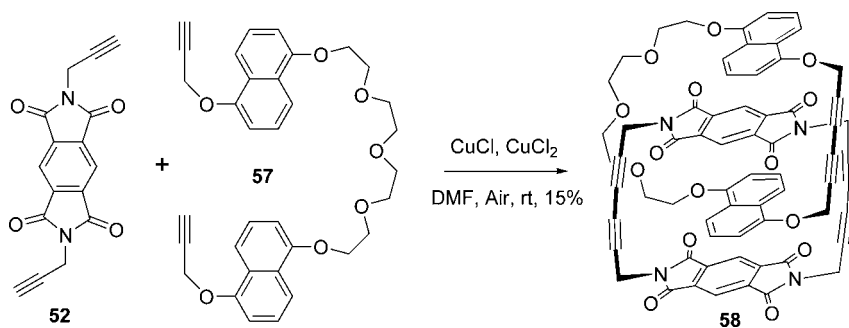
Scheme 10.11 Tandem macrocyclization and catenation via oxidative acetylide coupling reported by Sanders and coworkers.

original 3-D organization of the ligands with the metal template, which orients the pendant arms of the acyclic ligand(s) for macrocyclization (**59–62**) [43–46]. A subtly different method was applied by Leigh and coworkers. The authors employed an ostensibly 2-D square-planar palladium template and took advantage of electronic and steric influences in the intermediate metal complex to dispose the ligands appropriately (i.e., orthogonally) for formation of the final interlocked products (**63**) [47].

Sanders and coworkers have used RCM as the final ring-forming step in their neutral donor/acceptor π-stacking templated catenanes (**64** and **65**) with both pyromellitimide (**66**) and naphthodiimide (**67**) acceptors (Scheme 10.12) [48]. The addition of LiI during synthesis of the pyromellitimide-containing [2]catenane (**64**) increased the magnitude of the template interaction and resulted in a tripling of the yield to 60% [49]. X-ray crystallographic data of the corresponding [2]pseudorotaxane revealed the complexation of two Li cations by the oxygen donors of both the organic components.

The well-established secondary dialkylammonium/crown ether template introduced by Stoddart and coworkers in 1995 for the formation of interlocked molecules has been adapted for RCM to form both rotaxanes and catenanes (Scheme 10.13). Mechanically bonded products (**68**, **69**) have been synthesized by the clipping of either crown ether (**70**) around the ammonium dumbbell **71** or of the dialkylammonium component **72** around the crown ether **73** [50,51]. Higher yields were usually observed when the corresponding pre-formed macrocyclic alkenes were equilibrated with the other component of the template. Leigh and coworkers have demonstrated the adaptation of their hydrogen-bonded template methodology to RCM (Scheme 10.14), which can be used to reversibly form macrocycle **74** or [2]catenane **75** in high yields (>95%), depending on the synthetic conditions [52]. Böhmer and coworkers employed the homo- and heterodimerization of tetra-urea-functionalized calix[4]arenes (**76–78**) and RCM to synthesize [2]rotaxanes (**79**) and [2]catenanes (**80**) which have multiply interlocked topologies (Scheme 10.15) [53,54]. In these cases, the authors enact multiple ring closures at high dilution,
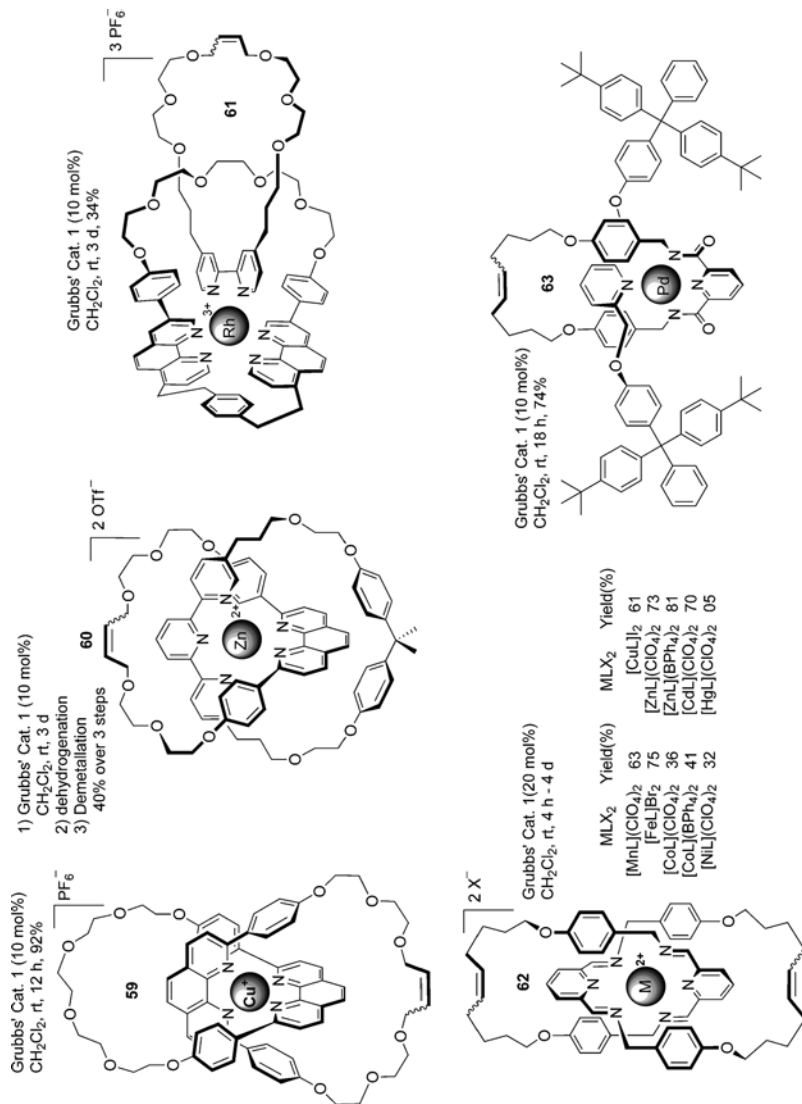
Figure 10.4 Selected examples of molecular architectures rendered interlocked via RCM.
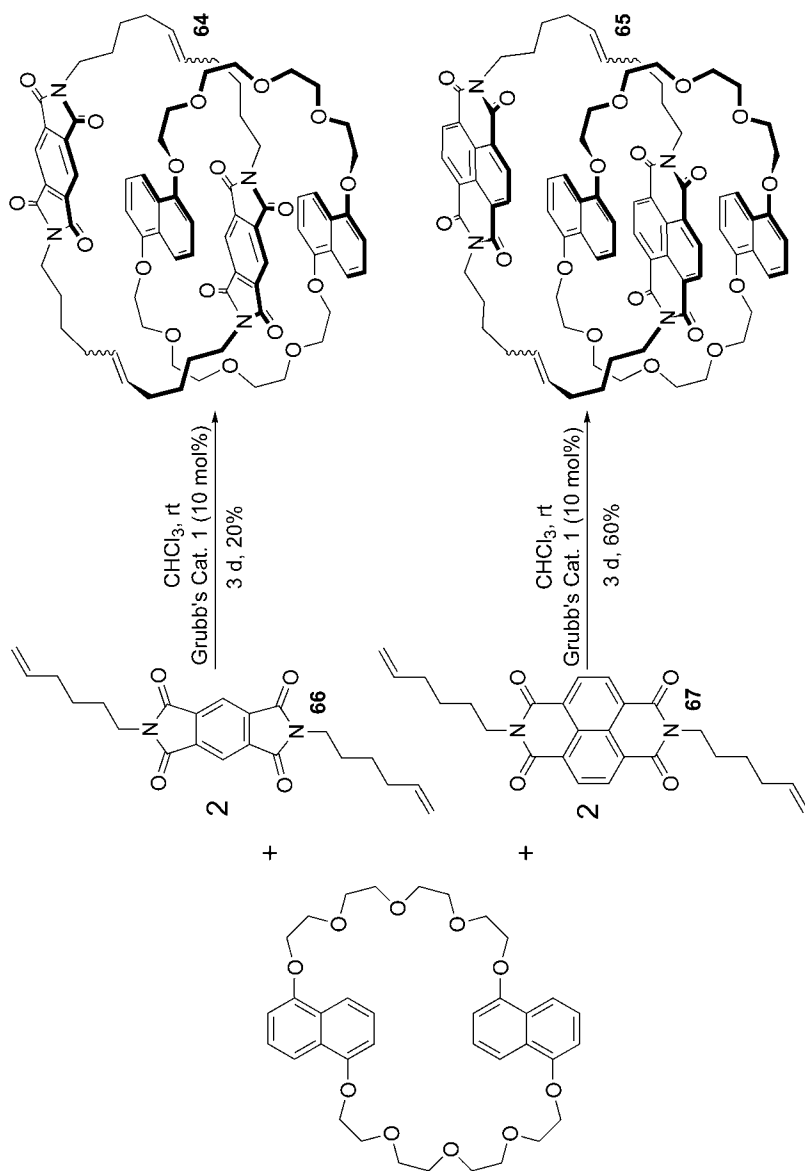
Scheme 10.12 RCM in the synthesis of [2]catenanes using the π-donor/acceptor approach by Sanders and coworkers.
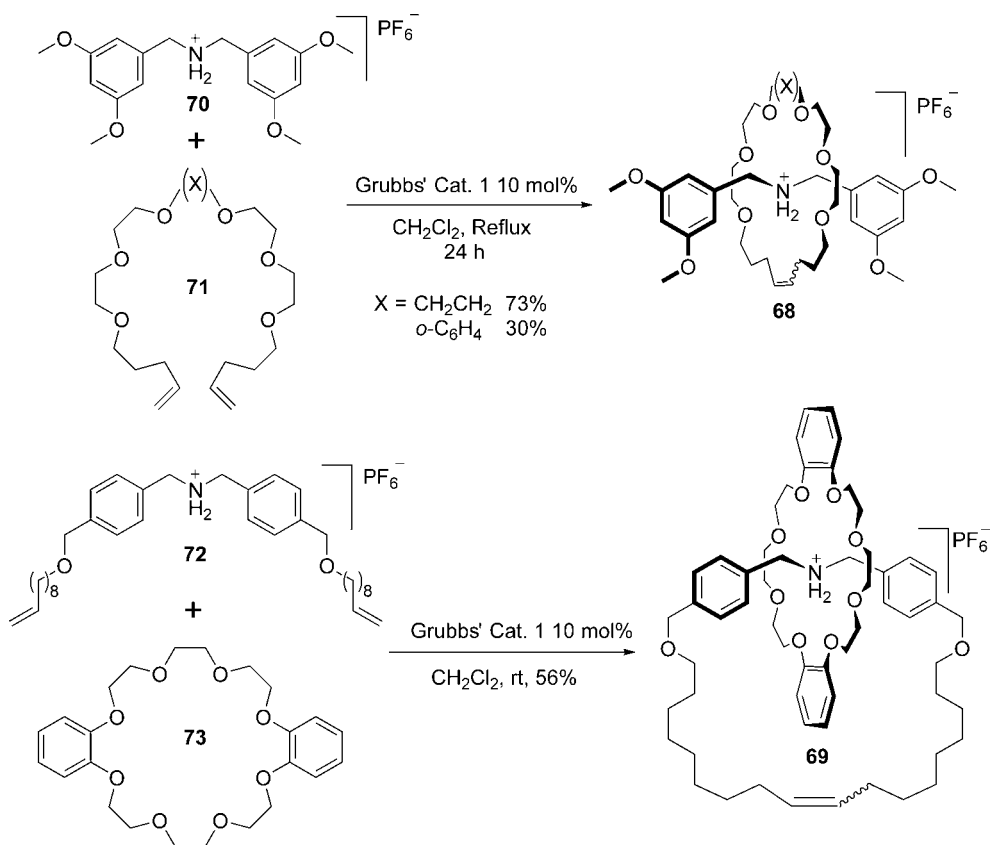
Scheme 10.13 Dialkylammonium and crown ether cyclizations via alkene metathesis.
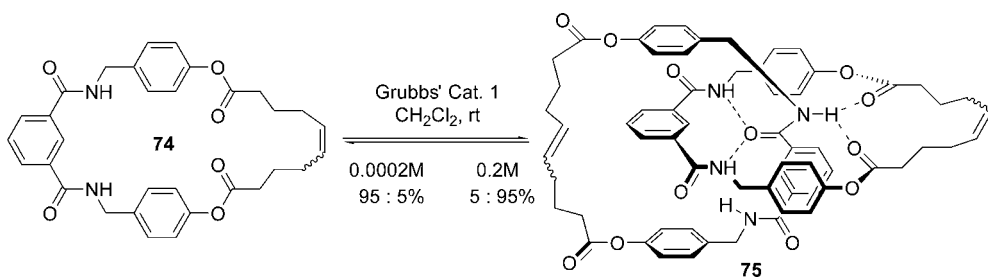
Scheme 10.14 Reversible (concentration-dependent) RCM templated by hydrogen bonding.
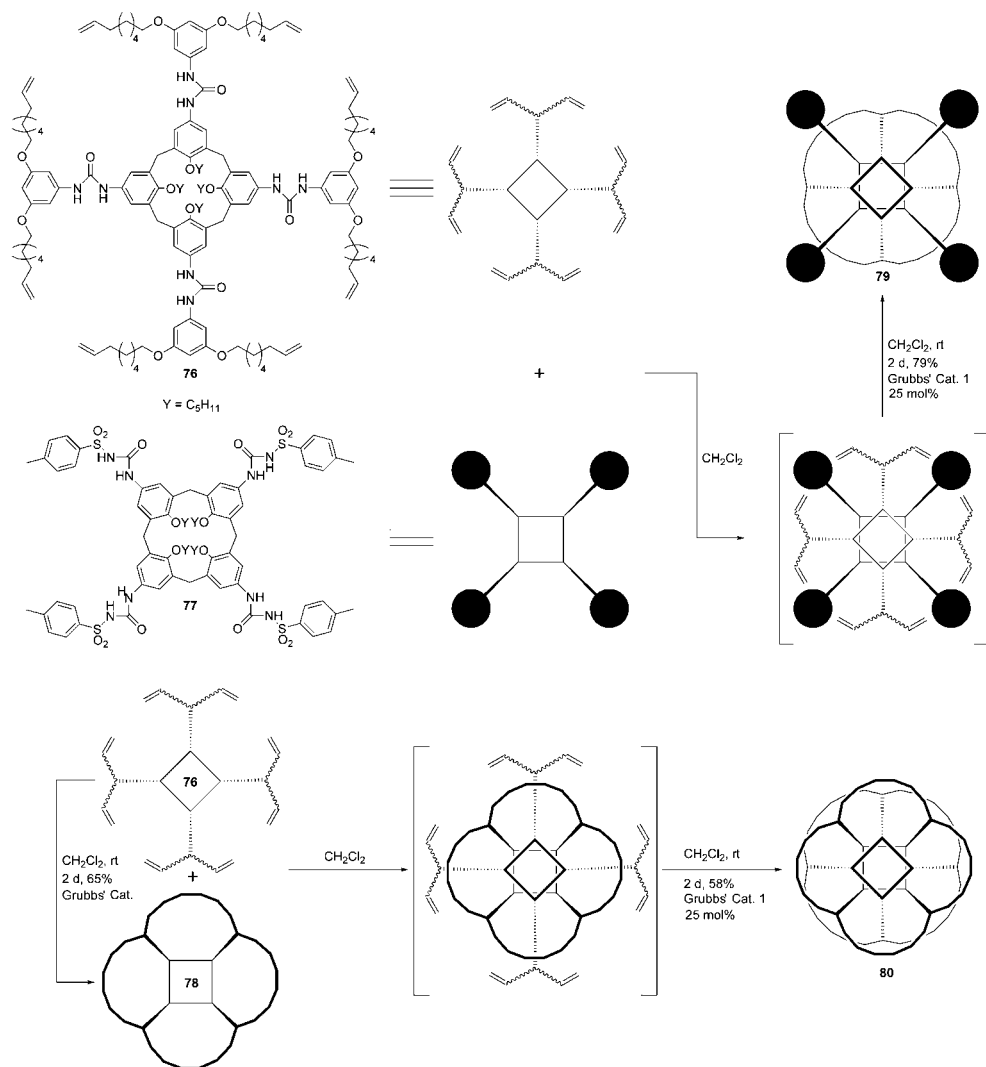
Scheme 10.15 Synthesis of multiply interlocked molecular architectures reported by Böhmer and coworkers.

followed by hydrogenation, to give the final products in 50–88% yield, depending on the particular substrates and number of connections.

The recently developed anion template methodology developed by Beer and coworkers (Scheme 10.16) has been applied in conjunction with RCM to synthesize both [2]rotaxanes (**81**) and catenanes (**82**) from their respective starting materials (**83–85**) [55,56]. In this case, the two organic components are organized orthogonally around
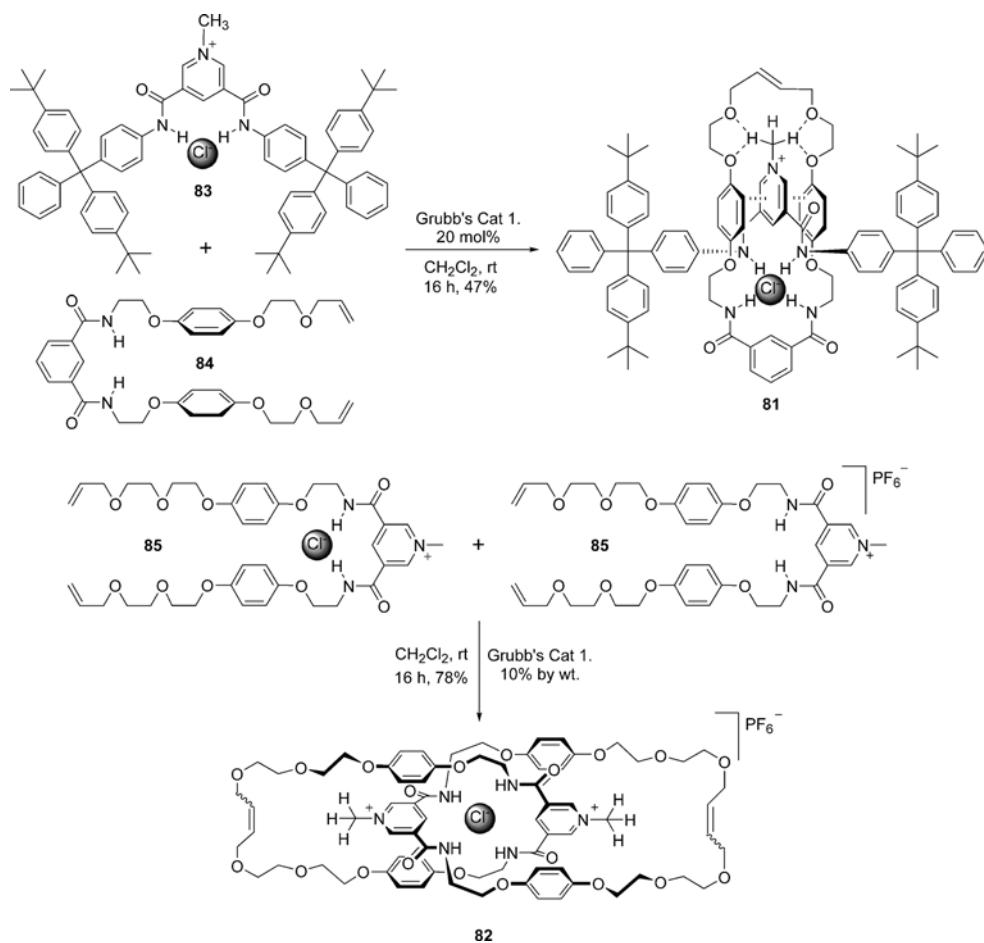
Scheme 10.16 Anion-templated [2]rotaxane and [2]catenane formation reported by Beer and coworkers.

the halide using a combination of ion pairing and hydrogen bonding. The pendant arms of the acyclic component(s) are designed to interact non-covalently with the opposing ligand, which further organizes them for ring closure. In the absence of the halide template (e.g., employing only PF_6^- salts), little or no ring-closed product is generally observed.

10.2.6
Imine Formation/Reductive Amination

The formation of a Schiff base through condensation of a primary amine with an aldehyde or ketone has recently found application in the construction of
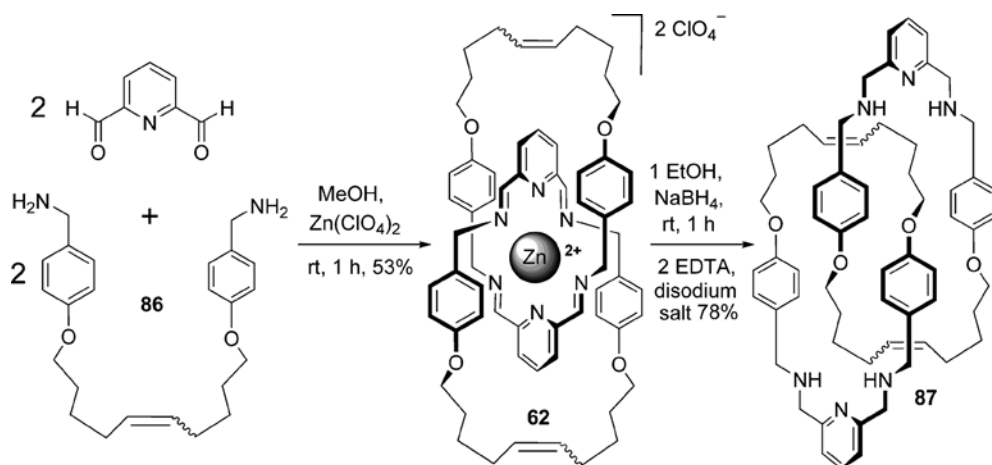
Scheme 10.17 Synthesis of **87** via imine formation reported by Leigh and coworkers.

interlocked molecules [57]. The dynamic, reversible nature of such a connection lends itself well to template synthesis, in which the thermodynamically most stable product is desired and selected through supramolecular design of the components. The resulting equilibrium distribution of species in this case may be kinetically "fixed" by reduction of the imine functions to their corresponding secondary amines.

Leigh and coworkers have modified their octahedral metal-templated approach (**62**) to form [2]catenates through imine condensation (Scheme 10.17) [46]. Instead of using RCM (Figure 10.4) to cyclize the intermediate acyclic complex formed from an existing 2,6-diiminopyridine-based ligand, the authors condensed the corresponding diamine **86** with 2,6-diformylpyridine *in situ* with the octahedral metal (Zn^{2+}) to give [2]catenate **62** in 53% yield. Though the authors state that the yields for the other metal-templated catenates by this route are uniformally higher than those following the RCM methodology, the yields were not optimized, and a follow-up report has not yet been published. The imine-containing Zn^{2+} [2]catenate synthesized by these methods was reduced with $NaBH_4$ in EtOH and demetalated with EDTA to produce the related [2]catenand **87** in 78% yield.

Nitschke and coworkers have self-assembled a [2]catenate (Scheme 10.18) [58] using a dicopper bis(phenanthrolinediimine) helicate subunit originally reported by Ziessel and coworkers [59]. Addition of an appropriately composed diamine (**88**) to 2,9- diformylphenanthroline and $Cu(MeCN)_4BF_4$ starting materials produced the [2]catenate **89** in quantitative yield. The corresponding [2]catenand **90** was generated by reduction ($NaBH_4$) and demetalation (EDTA), although the authors did not purify the product because of the small scale of the reaction. The product was identified by MS/MS analysis and the yield was estimated at >50%.
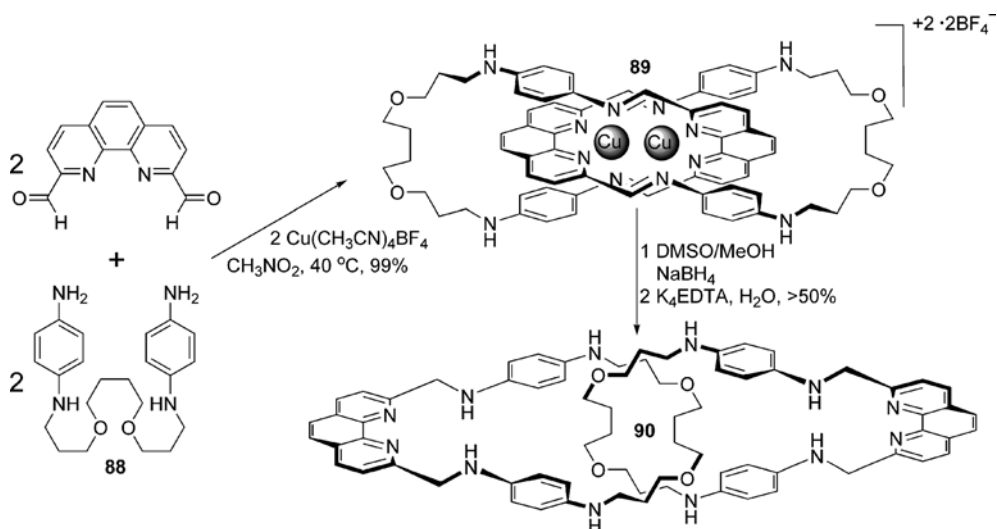
Scheme 10.18 Self-assembly of a Cu$^+$-templated [2]catenane reported by Nitschke and coworkers.

Stoddart and coworkers have used imine condensation in two different contexts to form interlocked molecules. The authors have modified the crown ether component of their dialkylammonium/DB24C8 system to incorporate reversible imine subunits which allow for dynamic clipping around dialkylammonium cation **91** [60]. Three diformyl spacers (**92–94**) have been investigated with the same acyclic diamine **95** for their thermodynamic stability and kinetics of macrocyclization (**96**). However, reduction with BH$_3$ to the kinetically trapped macrocyclic secondary diamine has only been reported for reaction of the 2,6-diformylpyridine derivative (Scheme 10.19; **97**) [60a].

A spectacular demonstration of the power of imine condensation for the formation of interlocked species was recently revealed by Stoddart and coworkers. The authors reported the first synthesis of a molecular version of the Borromean Rings, in which three rings are interlocked such that scission of any one ring releases all three (Scheme 10.20) [61]. The synthesis of this product is even more remarkable given the method used to generate it. The final interlocked product is self-assembled through condensation of six diamine (**98**), six 2,6-diformylpyridine, and six divalent transition metal components in a single synthetic step. The conversions vary in yield from a low of 36% with Co^{2+} to an astonishing 95% in the case of Zn^{2+} templation (**99**). The Zn^{2+}-templated Borromeate **99** has been further reduced (NaBH$_4$) and demetalated (EDTA), resulting in the fully interlocked (i.e., non-dynamic) Borromean link topology (**100**) [62]. It is interesting to note that the use of a 1:1 mixture of metals (Cu^{2+} and Zn^{2+}) in the self-assembly reaction results in a different product. In this case, the
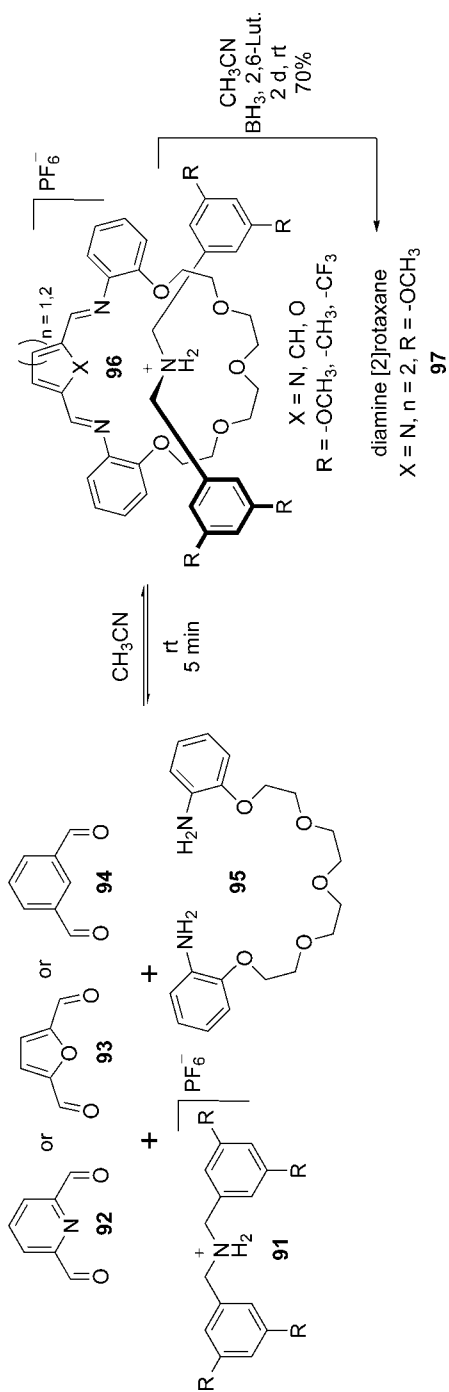
Scheme 10.19 Synthesis of various [2]rotaxanes by imine formation around a dialkylammonium dumbbell reported by Stoddart and coworkers.
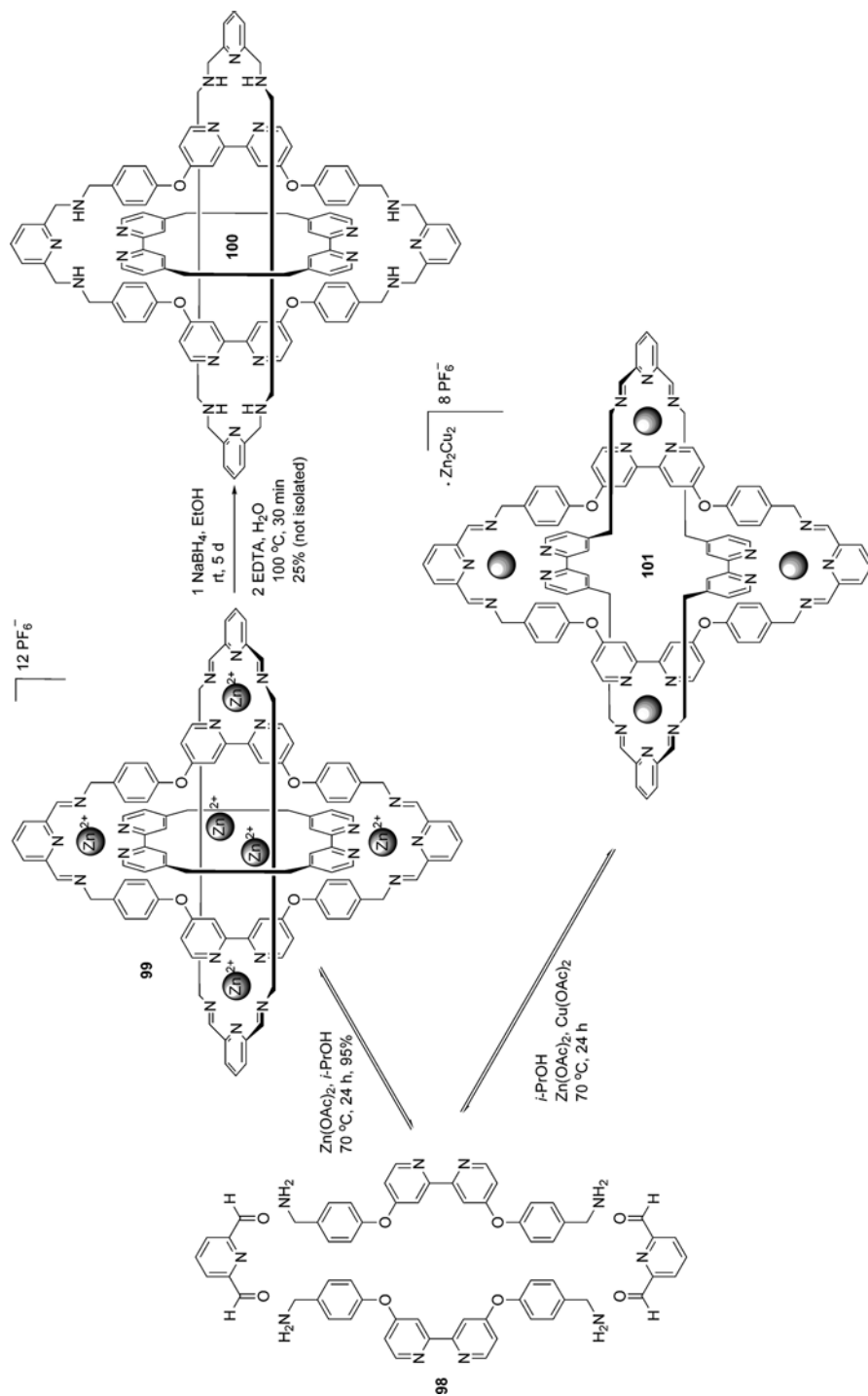
Scheme 10.20 Synthetic molecular Borromean rings and a Solomon knot reported by Stoddart and coworkers.

isolated material is in the form of a Solomon Knot or doubly intertwined [2]catenane (**101**) [63].

10.2.7
Metal-Ligand Coordination

A particularly facile synthetic method in the context of mechanically bonded molecules is the closure of one or more of the rings in the final products by using labile metal–ligand coordination as a linkage in the backbone under thermodynamic control. The underlying complication inherent in this approach is the very lability of the dative bonds used in the self-assembly of the macrocyclic component(s). Unless some method is available (e.g., solvent, temperature) to change the kinetic stability of the metal-ligand connection, the interlocked complex is forever at the mercy of equilibrium in solution. Hence, a change in the solution conditions (e.g., concentration) often changes the position of the equilibrium to give a mixture of interlocked and non-interlocked species. We will therefore focus here only on examples in which the mechanically bonded products have demonstrated kinetic stability and are isolable in the solution state without interference from further dissociation into their component parts.

In 1994, Fujita and coworkers introduced a route to [2]catenanes from the self-association of two metallacyclic rings through hydrophobic interactions in aqueous solution (Scheme 10.21) [64]. The self-assembled Pd-based macrocycle **102**, from ligand **103**, is in equilibrium at room temperature between the catenated product **104** and the free component rings. In contrast, the analogous Pt macrocycle **105** is self-assembled in water at $100\,^{\circ}$C but does not form a [2]catenane. Cooling to room temperature locks the macrocyclic geometry kinetically [65]. The addition of 5 M NaNO$_3$ and further heating to $100\,^{\circ}$C for a period of 24 h converted the macrocycle quantitatively into [2]catenane **106**, which was verified upon cooling and precipitation as the perchlorate salt. The authors describe this system as a "molecular lock", in that the catenane topology does not undergo dissociation even upon heating in water at $100\,^{\circ}$C. A similar approach has been used to self-assemble a catenated cage compound from ten separate components [66].

Very recently, Fujita and coworkers have extended this methodology to catenation in a related system at room temperature (Scheme 10.22) [67]. A solution of macrocycle **107** (2 mM) was found to be kinetically stable in 1:2 DMSO-d$_6$/D$_2$O with no catenated products observed. However, upon irradiation with UV light (Hg lamp; 330 ± 70 nm band-pass filter) the starting macrocycle is converted quantitatively into the corresponding [2]catenane **108**. Dissolution of the catenane in non-aqueous solvent (MeCN/MeOH 1:1), which would disassemble the catenane if ligand exchange were occurring, produced no change in the interlocked topology. Irradiation under these conditions disassembles the catenane into the original component rings. The authors also examined the analogous Ru-based approach, which demonstrated the same behavior.

Sauvage, Fujita, and coworkers have combined both their copper template and palladium self-assembly methodologies to form both a doubly-intertwined
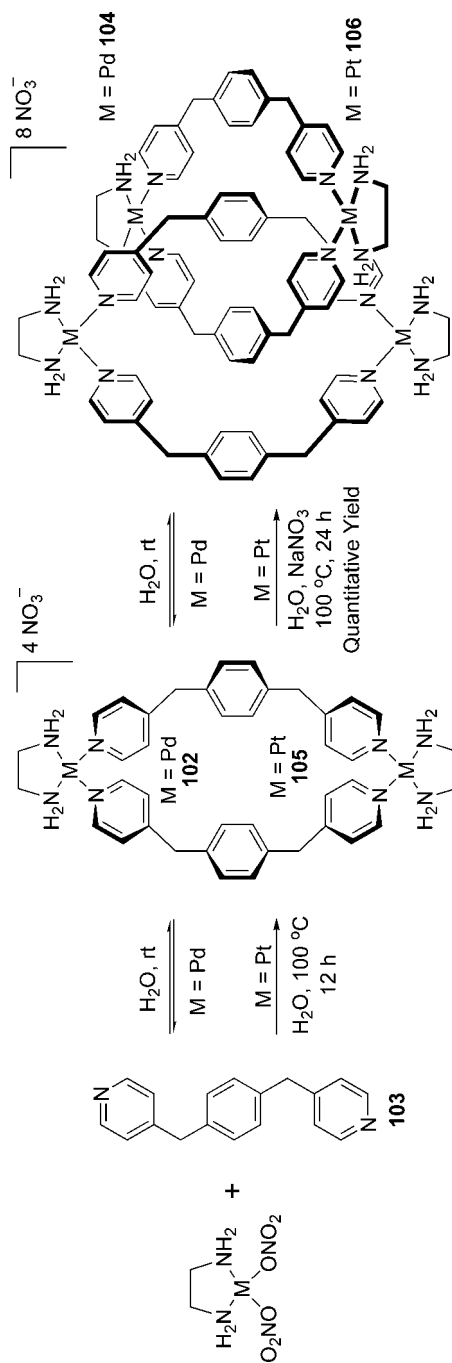
Scheme 10.21 Reversible (**104**) and non-reversible (**106**) formation of metal-based [2]catenanes by Fujita and coworkers.
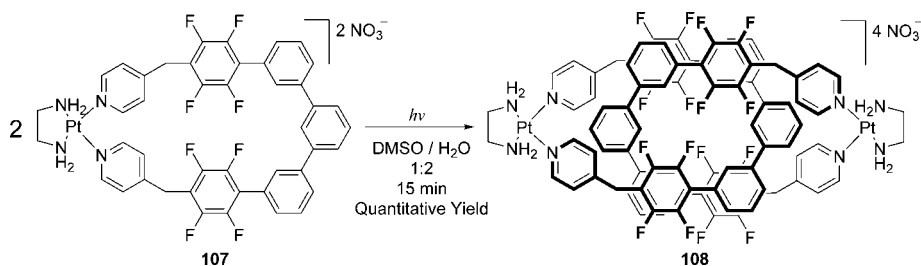
Scheme 10.22 Photoswitchable [2]catenane formation reported by Fujita and coworkers.

[2]catenane or Solomon knot (**109** from ligand **110**) and a simple [2]catenane (**111** from ligand **112**) [68,69]. The doubly intertwined [2]catenane was demonstrated by the authors to be the final products irrespective of the order in which the self-assembly and template steps were used in the synthetic sequence (Scheme 10.23). In this case, however, the Cu^+ template cannot be removed.

Jeong and coworkers have used metal-ligand coordination to form a metalomacrocyclic complex (**113**, Scheme 10.24) which closely resembles the macrocyclic component of **24** (Scheme 10.5) when cyclized [70]. The authors use dumbbell-shaped axles, similar to those pioneered by Vögtle and coworkers [71], which act as templates about which **113** ($M = Re(CO)_3Cl$) may be clipped at elevated temperature. In the case of this Re-based macrocycle, the resulting [2]rotaxanes (**114**) are stable at room temperature and may be chromatographed on silica gel. Quintela, Peinador, and coworkers have adapted Stoddart's paraquat box to include metal-ligand coordination in the backbone by replacing one *p*-xylenediyl group with a 4-picolyl subunit (Scheme 10.25) [72]. The corresponding [2]catenane **115** was formed in 85% yield by refluxing the ligand (**116**), (en)Pt(NO$_3$)$_2$, and **14** at 100 °C for 12 days.

A subtly different approach has been taken by Wisner and coworkers using a method in which the same metal center acts as both the template and the connection point in the macrocyclic backbone to form a [2]catenane [73]. The template is based on the complexation of PdCl$_2$L$_2$ complexes by the macrocycle derived from Hunter's [2]catenane synthesis [74]. In this case, the opposing isophthalamide subunits in the macrocycle hydrogen bond to the chloride ligands to form a [2]rotaxane or [2]pseudorotaxane complex [75,76]. The basic template can be adapted to form a [2]catenane by incorporating the PdCl$_2$ subunit into the backbone of the macrocycle (ligand **117** + PdCl$_2$). The resulting metallacycle is capable of self-recognition, which results in a mutually interlocked catenane- architecture (**118**, Scheme 10.26). The [2]catenane is remarkably stable given the typical lability of the Pd-N coordinate bonds used to form each macrocycle. The catenane can be chromatographed if need be and is stable to a range of normally competitive solvents. However, addition of >1 M DMSO induces the dissociation of the two rings into the parent macrocycles. The catenated topology can be easily re-established in quantitative yield by dissolution in a less competitive solvent.
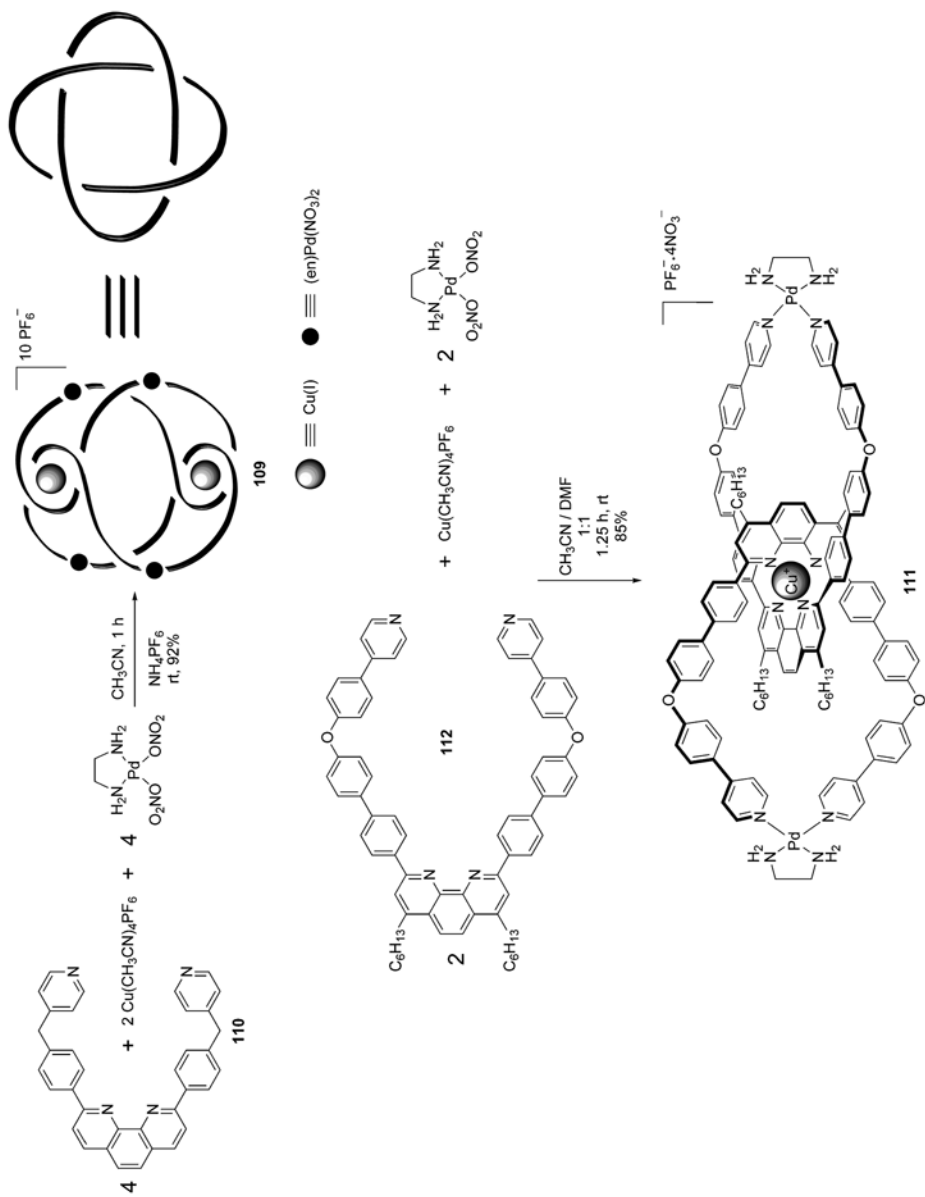
Scheme 10.23 The formation of a Solomon Knot (**109**) and a [2]catenane (**111**) reported by Sauvage, Fujita, and coworkers.
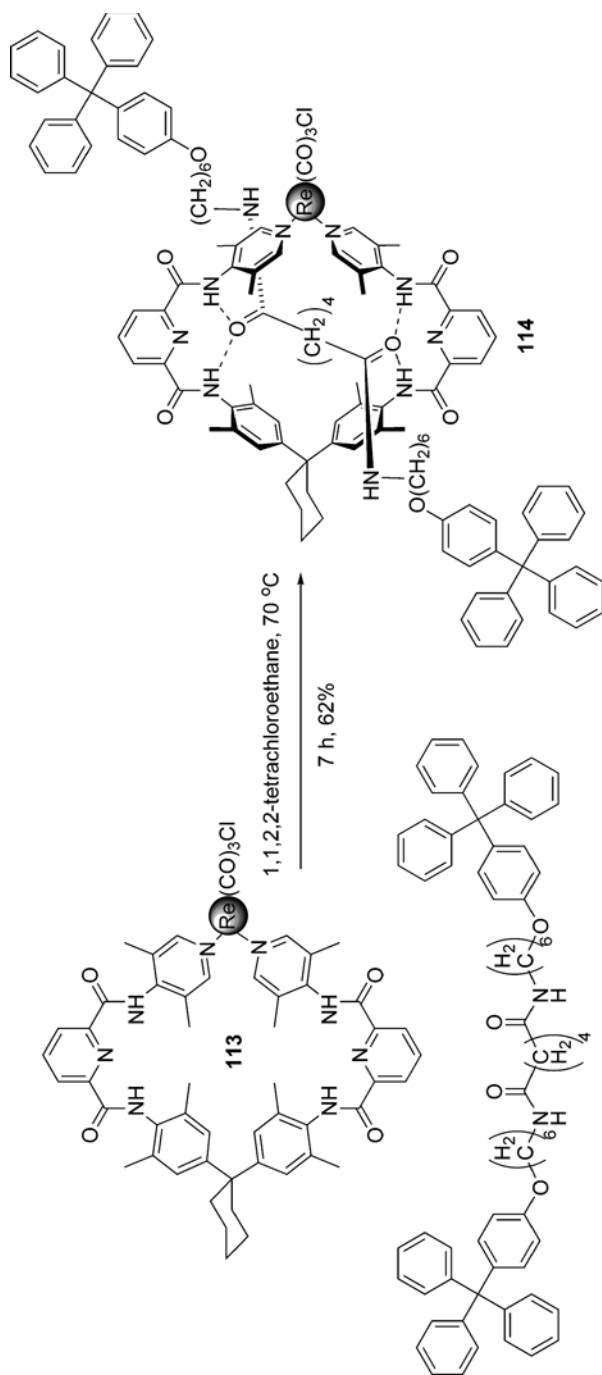
Scheme 10.24 [2]Rotaxane formation by metallomacrocyclic "clipping" reported by Jeong and coworkers.
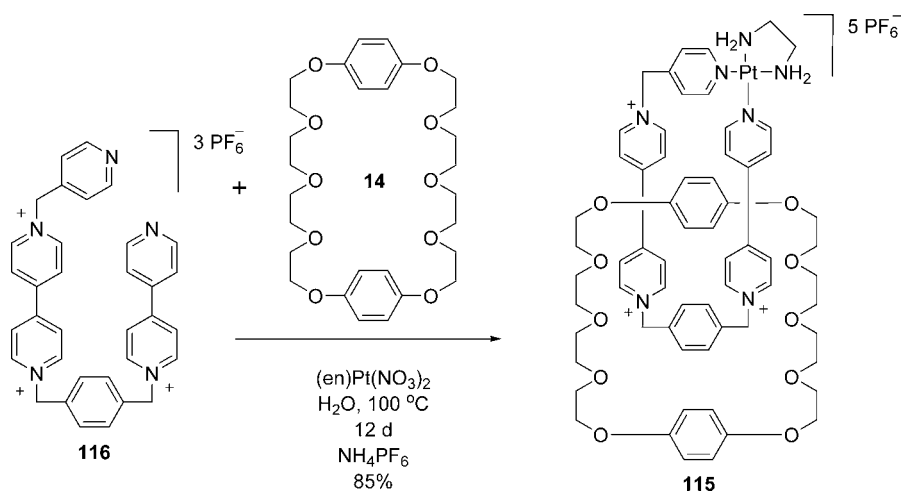
Scheme 10.25 [2]Catenane formation by metallomacrocyclic "clipping" reported by Quintela and coworkers.

10.3
Conclusions

The use of macrocyclization reactions to form interlocked molecules has progressed significantly over the last 25 years. The challenge of forming these mechanically bonded architectures has been tempered somewhat with the application of both an ever wider variety of synthetic methods and increasingly sophisticated templates. However, the exploitation of new synthetic techniques (e.g., alkene metathesis), a further understanding of the parameters which guide self-assembly (e.g., Borromean Rings), and a continuing shift from aesthetics to function will likely shape the future character of this field. The truly unique opportunities that these types of molecules offer ensures that the exploration of their syntheses will remain an exciting area of endeavor for many years to come.

10.4
Experimental: Selected Procedures

10.4.1
[2]Catenane 14 [14b, 16a]

A solution of $10 \cdot 2PF_6$ (140 mg, 0.20 mmol) in anhydrous CH_3CN (5.0 mL) was added to a stirred solution of **14** (280 mg, 0.52 mmol), also in anhydrous CH_3CN (5.0 mL). A deep yellow color ensued, and a solution of 1,4-bis(bromomethyl)benzene (56 mg, 0.20 mmol) in anhydrous CH_3CN (5.0 mL) was added. Upon stirring for 4 h, the solution turned a deep red color. The solution was stirred for a total of
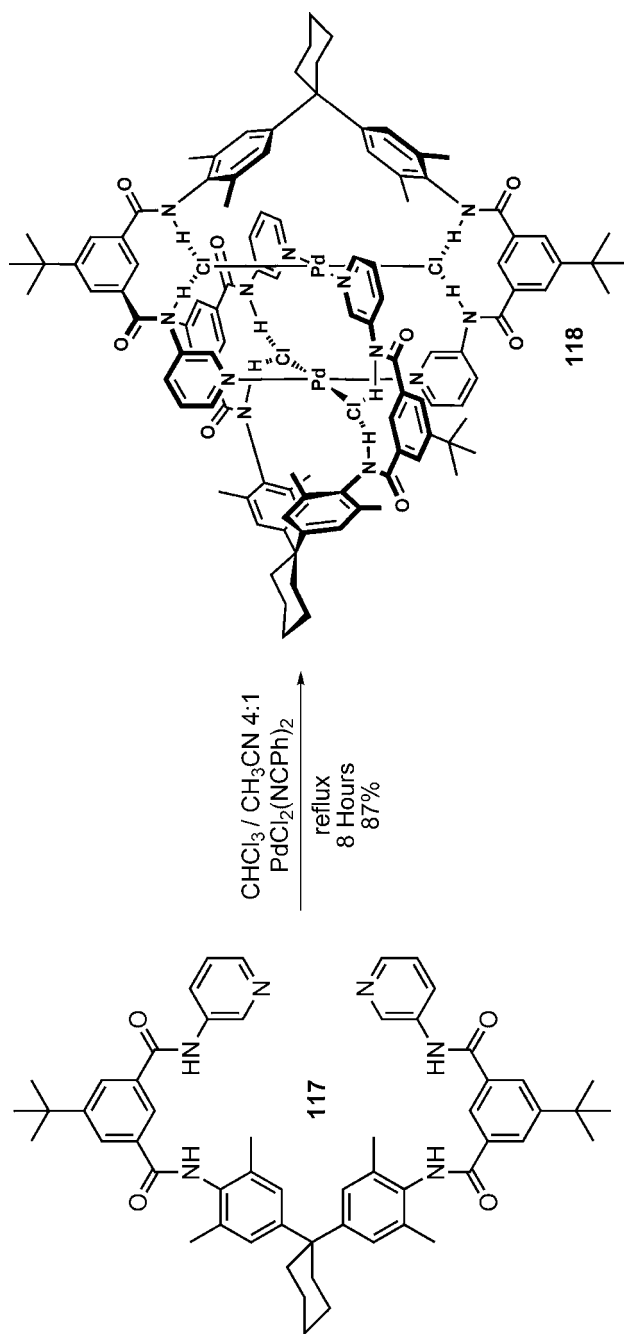
Scheme 10.26 Metallomacrocyclic/[2]catenane formation templated by second-sphere coordination of the PdCl₂ subunit reported by Wisner and coworkers.

48 h at rt, and the resulting red precipitate was filtered and washed with $CHCl_3$ (10 mL), dissolved in H_2O (30 mL), and filtered to remove any insoluble material. An aqueous solution of NH_4PF_6 was added to the filtrate until no further precipitation occurred. The precipitate was filtered off, washed with H_2O (10 mL), and dried. Recrystallization from CH_3CN and H_2O gave [2]catenane **12** (230 mg, 70% yield).

10.4.2
[2]Catenane 25 [25]

Isophthaloyldichloride (0.87 g, 4.3 mmol) and 1,4-xylylenediamine (0.58 g, 4.3 mmol), separately dissolved in anhydrous $CHCl_3$ (130 mL each), were added via syringe pump over 30 min to a stirred solution of triethylamine (1.19 g, 18.9 mmol) in anhydrous $CHCl_3$ (130 mL). Following the addition, the reaction was stirred for an additional 12 h. The precipitate was filtered off, and the filtrate was washed with 1 M aqueous HCl (3×200 mL), 5% aqueous NaOH (3×200 mL), and H_2O (3×200 mL). It was then dried with $MgSO_4$, and the volume was reduced *in vacuo* to afford 0.23 g (21%) of [2]Catenane **25**.

10.4.3
[2]Rotaxane 81 [55]

Compound **83** (0.125 g, 0.21 mmol) and compound **84** (0.125 g, 0.12 mmol) were dissolved in anhydrous dichloromethane (5 mL), and stirred for 5 min. Grubbs' catalyst (20 mol%) was then added to the solution, and the reaction mixture was stirred for an additional 16 h. Solvent was removed under reduced pressure, and the crude product chromatographed ($CHCl_3$:CH_3OH, 93:7), collecting the first yellow band eluted. The product was recrystallized by slow diffusion of diisopropyl ether into chloroform to yield brilliant yellow crystals of [2]rotaxane **81** (0.091 g, 47%).

10.4.4
[2]Catenane 118 [73]

Dipyridyl ligand **117** (0.125 g, 0.142 mmol) was dissolved in a 3:1 $CHCl_3$/CH_3CN solvent mixture (10 mL). A chloroform solution (2 mL) of *trans*-bis-benzonitrile palladium(II)dichloride (0.0543 g, 0.142 mmol) was added dropwise to the reaction mixture, which was then refluxed for 8 h. The crude reaction mixture was filtered through celite to remove any precipitate, and this was followed by the removal of solvent under reduced pressure. The resulting solid was dissolved in a minimum amount of dichloromethane and precipitated with hexanes to remove residual benzonitrile, and the precipitate was filtered to afford [2]catenane **118** (0.129 g, 87%).

Acknowledgments

We would like to acknowledge the continued support of our research by the Natural Science and Engineering Council of Canada and the University of Western Ontario.

Abbreviations

TIPS	Triisopropylsilyl
Py	Pyridine
Terpy	2,2′,6′,2″-Terpyridine
Phenpy	2-(Pyridin-2-yl)-1,10-phenanthroline
dppp	1,3-Bis(diphenylphosphino)propane
RCM	Ring Closing Metathesis
EDTA	Ethylenediamine tetraacetic acid
Lut	Lutidine
en	Ethylenediamine
TMS	Trimethylsilyl
Grubbs' Cat. 1	Generation 1 Grubbs' Catalyst

References

1 Kay, E.R., Leigh, D.A. and Zerbetto, F. (2007) *Angew. Chem.*, **119**, 72–196; *Angew. Chem. Int. Ed.*, **46**, 72–191.

2 J.-P. Sauvage and C. Dietrich-Buchecker (eds) (1999) *Molecular Catenanes, Rotaxanes and Knots: A Journey Through the World of Molecular Topology*, Wiley-VCH, Weinheim; (b) Schill, G. (1971) *Catenanes, Rotaxanes, and Knots*, Academic Press, New York.

3 Dietrich-Buchecker, C.O. and Sauvage, J.-P. (1987) *Chem. Rev.*, **87**, 795–810.

4 (a) Wasserman, E. (1960) *J. Am. Chem. Soc.*, **82**, 4433–4434; (b) Frisch, H.L. and Wasserman, E. (1961) *J. Am. Chem. Soc.*, **83**, 3789–3795; (c) Harrison, I.T. and Harrison, S. (1967) *J. Am. Chem. Soc.*, **89**, 5723–5724; (d) Harrison, I.T. (1972) *J. Chem. Soc., Chem. Commun.*, 231–232; (e) Harrison, I.T. (1974) *J. Chem. Soc., Perkin Trans.* 1, 301–304; (f) Agam, G., Graiver, D. and Zilkha, A. (1976) *J. Am.*

Chem. Soc., **98**, 5206–5214; (g) Agam, G. and Zilkha, A. (1976) *J. Am. Chem. Soc.*, **98**, 5214–5216.

5 (a) Pedersen, C.J. (1967) *J. Am. Chem. Soc.*, **89**, 7017–7036; (b) G.W. Gokel (ed.) (1991) *Crown Ethers and Cryptands*, Royal Society of Chemistry, Cambridge.

6 Dietrich-Buchecker, C.O. and Sauvage, J.-P. (1983) *Tetrahedron Lett.*, **24**, 5095–5098.

7 Dietrich-Buchecker, C.O. and Sauvage, J.-P. (1984) *J. Am. Chem. Soc.*, **106**, 3043–3045.

8 (a) Dietrich-Buchecker, C.O., Sauvage, J.-P. and Kern, J.-M. (1989) *Angew. Chem.*, **101**, 192–194; *Angew. Chem. Int. Ed.*, **28**, 189–192; (b) Dietrich-Buchecker, C.O. and Sauvage, J.-P. (1992) *New. J. Chem.*, **16**, 931–942.

9 (a) Nierengarten, J.-F., Dietrich-Buchecker, C.O. and Sauvage, J.-P. (1994) *J. Am. Chem. Soc.*, **116**, 375–376;

(b) Nierengarten, J.-F., Dietrich-Buchecker, C.O. and Sauvage, J.-P. (1996) *New. J. Chem.*, **20**, 685–693.

10 Rapenne, G., Dietrich-Buchecker, C.O. and Sauvage, J.-P. (1999) *J. Am. Chem. Soc.*, **121**, 994–1001.

11 Dietrich-Buchecker, C.O. and Sauvage, J.-P. (1999) *Chem. Commun.*, 615–616

12 (a) Allwood, B.L., Shahriari-Zavareh, H., Stoddart, J.F. and Williams, D.J. (1987) *J. Chem. Soc. Chem. Commun.*, 1058–1061; (b) Allwood, B.L., Spencer, N., Shahriari-Zavareh, H., Stoddart, J.F. and Williams, D.J. (1987) *J. Chem. Soc. Chem. Commun.*, 1061–1064; (c) Allwood, B.L., Spencer, N., Shahriari-Zavareh, H., Stoddart, J.F. and Williams, D.J. (1987) *J. Chem. Soc. Chem. Commun.*, 1064–1066.

13 (a) Odell, B., Reddington, M.V., Slawin, A.M.Z., Spencer, N., Stoddart, J.F. and Williams, D.J. (1988) *Angew. Chem.*, **100**, 1605–1608; (1988) *Angew. Chem. Int. Ed.*, **27**, 1547–1550.

14 (a) Brown, C.L., Philp, D. and Stoddart, J.F. (1991) *Synlett*, 462–464; (b) Anelli, P. L., Ashton, P.R., Ballardini, R., Balzani, V., Delgado, M., Gandolfi, M.T., Goodnow, T.T., Kaifer, A.E., Philp, D., Pietraszkiewicz, M., Prodi, L., Reddington, M.V., Slawin, A.M.Z., Spencer, N., Stoddart, J.F., Vincent, C. and Williams, D.J. (1992) *J. Am. Chem. Soc.*, **114**, 193–218.

15 (a) Brown, C.L., Philp, D. and Stoddart, J.F. (1991) *Synlett*, 459–461; (b) Philp, D. and Stoddart, J.F. (1991) *Synlett.*, 445–458; (c) Ashton, P.R., Grognuz, M., Slawin, A.M.Z., Stoddart, J.F. and Williams, D.J. (1991) *Tetrahedron Lett.*, **32**, 6235–6238; (d) Brown, C.L., Philp, D., Spencer, N. and Stoddart, J.F. (1992) *Israel J. Chem.*, **32**, 61–67.

16 (a) Amabilino, D.B., Anelli, P.-L., Ashton, P.R., Brown, G.R., Córdova, E., Godínez, L.A., Hayes, W., Kaifer, A.E., Philp, D., Slawin, A.M.Z., Spencer, N., Stoddart, J.F., Tolley, M.S. and Williams, D.J. (1995) *J. Am. Chem. Soc.*, **117**, 11142–11170; (b) Asakawa, M., Ashton, P.R., Boyd, S.E., Brown, C.L., Gillard, R. E., Kocian, Ö., Raymo, F.M., Stoddart, J. F., Tolley, M.S., White, A.J.P. and Williams, D.J. (1997) *J. Org. Chem.*, **62**, 26–37; (c) Ballardini, R., Balzani, V., Credi, A., Gandolfi, M.T., Marquis, D., Pérez-García, L. and Stoddart, J.F. (1998) *Eur. J. Org. Chem.*, 81–89; (d) Ashton, P.R., Ballardini, R., Balzani, V., Credi, A., Gandolfi, M.T., Menzer, S., Pérez-García, L., Prodi, L., Stoddart, J.F., Venturi, M., White, A.J.P. and Williams, D.J. (1995) *J. Am. Chem. Soc.*, **117**, 11171–11197; (e) Ballardini, R., Balzani, V., Credi, A., Brown, C.L., Gillard, R.E., Montalti, M., Philp, D., Stoddart, J.F., Venturi, M., White, A.J.P., Williams, B.J. and Williams, D.J. (1997) *J. Am. Chem. Soc.*, **119**, 12503–12513; (f) Gillard, R.E., Stoddart, J.F., White, A.J.P., Williams, B. J. and Williams, D.J. (1996) *J. Org. Chem.*, **61**, 4504–4505; (g) Ashton, P.R., Blower, M.A., McLean, C.H., Stoddart, J. F. and Tolley, M.S. (1994) *Synlett*, 1063–1066; (h) Ashton, P.R., Preece, J.A., Stoddart, J.F., Tolley, M.S., White, A.J.P. and Williams, D.J. (1994) *Synthesis*, 1344–1352; (i) Ashton, P.R., Blower, M. A., Iqbal, S. McLean, C.H., Stoddart, J.F., Tolley, M.S. and Williams, D.J. (1994) *Synlett*, 1059–1062; (j) Asakawa, M., Ashton, P.R., Dehaen, W., L'abbe, G., Menzer, S., Nouwen, J., Raymo, F.M., Stoddart, J.F., Tolley, M.S., Toppet, S., White, A.J.P. and Williams, D.J. (1997) *Chem. Eur. J.*, **3**, 772–787; (k) Asakawa, M., Ashton, P.R., Brown, C.L., Fyfe, M. C.T., Menzer, S., Pasini, D., Scheuer, C., Spencer, N., Stoddart, J.F., White, A.J.P. and Williams, D.J. (1997) *Chem. Eur. J.*, **3**, 1136–1150; (l) Ashton, P.R., Balzani, V., Credi, A., Kocian, O., Pasini, D., Prodi, L., Spencer, N., Stoddart, J.F., Tolley, M.S., Venturi, M., White, A.J.P. and Williams, D.J. (1998) *Chem. Eur. J.*, **4**, 590–607; (m) Ashton, P.R., Heiss, A. M., Pasini, D., Raymo, F.M., Shipway, A. N., Stoddart, J.F. and Spencer, N. (1999)

Eur. J. Org. Chem., 995–1004; (n) Ashton, P.R., Boyd, S.E., Brindle, A., Langford, S. J., Menzer, S., Pérez-García, L., Preece, J. A., Raymo, F.M., Spencer, N., Stoddart, J.F., White, A.J.P. and Williams, D.J. (1999) *New. J. Chem.*, **23**, 587–602; (o) Asakawa, M., Ashton, P.R., Balzani, V., Credi, A., Hamers, C., Mattersteig, G., Montalti, M., Shipway, A.N., Spencer, N., Stoddart, J.F., Tolley, M.S., Venturi, M., White, A.J.P. and Williams, D.J. (1998) *Angew. Chem.*, **110**, 357–361; *Angew. Chem. Int. Ed.*, **37**, 333–337; (p) Amabilino, D.B., Ashton, P.R., Brown, C.L., Cordóva, E., Godínez, L.A., Goodnow, T.T., Kaifer, A.E., Newton, S. P., Pietraszkiewicz, M., Philp, D., Raymo, F.M., Reder, A.S., Rutland, M.T., Slawin, A.M.Z., Spencer, N., Stoddart, J. F. and Williams, D.J. (1995) *J. Am. Chem. Soc.*, **117**, 1271–1293.

17 (a) Amabilino, D.B., Ashton, P.R., Reder, A.S., Spencer, N. and Stoddart, J.F. (1994) *Angew. Chem.*, **106**, 1316–1319; *Angew. Chem. Int. Ed.*, **33**, 1286–1290.

18 Bravo, J.A., Raymo, F.M., Stoddart, J.F., White, A.J.P. and Williams, D.J. (1998) *Eur. J. Org. Chem.*, 2565–2571

19 Anelli, P.L., Spencer, N. and Stoddart, J. F. (1991) *J. Am. Chem. Soc.*, **113**, 5131–5133.

20 Ballardini, R., Balzani, V., Dehaen, W., Dell'Erba, A.E., Raymo, F.M., Stoddart, J.F. and Venturi, M. (2000) *Eur. J. Org. Chem.*, 591–602

21 Jeppesen, J.O., Perkins, J., Becher, J. and Stoddart, J.F. (2001) *Angew. Chem.*, **113**, 1256–1261; *Angew. Chem. Int. Ed.*, **40**, 1216–1221.

22 (a) Hunter, C.A., (1992) *J. Am. Chem. Soc.*, **114**, 5303–5311; (b) Carver, F.J., Hunter, C.A. and Shannon, R.J. (1994) *J. Chem. Soc. Chem. Commun.*, 1277–1280; (c) Adams, H., Carver, F.J. and Hunter, C.A. (1995) *J. Chem. Soc. Chem. Commun.*, 809–810.

23 (a) Vögtle, F., Meier, S. and Hoss, R. (1992) *Angew. Chem.*, **104**, 1628–1631;

Angew. Chem. Int. Ed., **31**, 1619–1622; (b) Ottens-Hildebrandt, S., Meier, S., Schmidt, W. and Vögtle, F. (1994) *Angew. Chem.*, **106**, 1818–1821; *Angew. Chem. Int. Ed.*, **33**, 1767–1770.

24 Otten-Hildebrandt, S., Nieger, M., Rissanen, K., Rouvinen, J., Meier, S., Harder, G. and Vögtle, F. (1995) *J. Chem. Soc. Chem. Commun.*, 777–778

25 Johnston, A.G., Leigh, D.A., Pritchard, R.J. and Deegan, M.D. (1995) *Angew. Chem.*, **107**, 1324–1327; *Angew. Chem. Int. Ed.*, **34**, 1209–1212.

26 Johnston, A.G., Leigh, D.A., Nezhat, L., Smart, J.P. and Deegan, M.D. (1995) *Angew. Chem.*, **107**, 1327–1331; *Angew. Chem. Int. Ed.*, **34**, 1212–1216.

27 Leigh, D.A., Venturini, A., Wilson, A. J., Wong, J.K.Y. and Zerbetto, F. (2004) *Chem. Eur. J.*, **10**, 4960–4969.

28 Johnston, A.G., Leigh, D.A., Murphy, A., Smart, J.P. and Deegan, M.D. (1996) *J. Am. Chem. Soc.*, **118**, 10662–10663.

29 Leigh, D.A., Murphy, A., Smart, J.P. and Slawin, A.M.Z. (1997) *Angew. Chem.*, **109**, 752–756; *Angew. Chem. Int. Ed.*, **36**, 728–732.

30 Bermudez, V., Capron, N., Gase, T., Gatti, F.G., Kajzar, F., Leigh, D.A., Zerbetto, F. and Zhang, S. (2000) *Nature*, **406**, 608–611.

31 Gatti, F.G., Leigh, D.A., Nepogodiev, S. A., Slawin, A.M.Z., Teat, S.J. and Wong, J.K.Y. (2001) *J. Am. Chem. Soc.*, **123**, 5983–5989.

32 (a) Leigh, D.A., Wong, J.K.Y., Dehez, F. and Zerbetto, F. (2003) *Nature*, **424**, 174–179; (b) Hernández, J.V., Kay, E.R. and Leigh, D.A. (2004) *Science*, **306**, 1532–1537.

33 Siemsen, P., Livingston, R.C. and Diederich, F. (2000) *Angew. Chem.*, **112**, 2740–2767; *Angew. Chem. Int. Ed.*, **39**, 2632–2657.

34 Maraval, V. and Chauvin, R. (2006) *Chem. Rev.*, **106**, 5317–5343.

35 (a) Dietrich-Buchecker, C.O., Khemiss, A. and Sauvage, J.-P. (1986) *J. Chem. Soc. Chem. Commun.*, 1376–1378;

(b) Dietrich-Buchecker, C.O., Guilhem, J., Khémiss, A.-K., Kintzinger, J.-P., Pascard, C. and Sauvage, J.-P. (1987) *Angew. Chem.*, **99**, 711–714; *Angew. Chem. Int. Ed.*, **26**, 661–663; (c) Sauvage, J.-P., (1990) *Acc. Chem. Res.*, **23**, 319–327; (d) Dietrich-Buchecker, C.O., Hemmert, C., Khémiss, A.-K. and Sauvage, J.-P. (1990) *J. Am. Chem. Soc.*, **112**, 8002–8008; (e) Bitsch, F., Dietrich-Buchecker, C.O., Khémiss, A.-K., Sauvage, J.-P. and Van Dorsselaer, A. (1991) *J. Am. Chem. Soc.*, **113**, 4023–4025.

36 Kern, J.-M., Sauvage, J.-P. and Weidmann, J.-L. (1996) *Tetrahedron*, **52**, 10921–10934.

37 Loren, J.C., Gantzel, P., Linden, A. and Siegel, J.S. (2005) *Org. Biomol. Chem.*, **3**, 3105–3116.

38 Ammann, M., Rang, A., Schalley, C.A. and Bäuerle, P. (2006) *Eur. J. Org. Chem.*, 1940–1948.

39 Hamilton, D.G., Sanders, J.K.M., Davies, J.E., Clegg, W. and Teat, S.J. (1997) *Chem. Commun.*, 897–898.

40 Hamilton, D.G., Davies, J.E., Prodi, L. and Sanders, J.K.M. (1998) *Chem. Eur. J.*, **4**, 608–620.

41 (a) Hamilton, D.G., Feeder, N., Prodi, L., Teat, S.J., Clegg, W. and Sanders, J.K.M. (1998) *J. Am. Chem. Soc.*, **120**, 1096–1097; (b) Hamilton, D.G., Prodi, L., Feeder, N. and Sanders, J.K.M. (1999) *J. Chem. Soc. Perkin. Trans.* 1, 1057–1065.

42 (a) Chauvin, Y. (2006) *Angew. Chem.*, **118**, 3824–3831; *Angew. Chem. Int. Ed.*, **45**, 3740–3747; (b) Schrock, R.R., (2006) *Angew. Chem.*, **118**, 3832–3844; *Angew. Chem. Int. Ed.*, **45**, 3748–3759; (c) Grubbs, R.H., (2006) *Angew. Chem.*, **118**, 3845–3850; *Angew. Chem. Int. Ed.*, **45**, 3760–3765.

43 (a) Mohr, B., Weck, M., Sauvage, J.-P. and Grubbs, R.H. (1997) *Angew. Chem.*, **109**, 1365–1367; *Angew. Chem. Int. Ed.*, **36**, 1308–1310; (b) Weck, M., Mohr, B., Sauvage, J.-P. and Grubbs, R.H. (1999) *J. Org. Chem.*, **64**, 5463–5471.

44 Hamann, C., Kern, J.-M. and Sauvage, J.-P. (2003) *Inorg. Chem.*, **42**, 1877–1883.

45 (a) Mobian, P., Kern, J.-M. and Sauvage, J.-P. (2003) *J. Am. Chem. Soc.*, **125**, 2016–2017; (b) Mobian, P., Kern, J.-M. and Sauvage, J.-P. (2003) *Inorg. Chem.*, **42**, 8633–8637; (c) Arico, F., Mobian, P., Kern, J.-M. and Sauvage, J.-P. (2003) *Org. Lett.*, **5**, 1887–1890.

46 Leigh, D.A., Lusby, P.J., Teat, S.J., Wilson, A.J. and Wong, J.K.Y. (2001) *Angew. Chem.*, **113**, 1586–1591; *Angew. Chem. Int. Ed.*, **40**, 1538–1543.

47 (a) Fuller, A.-M., Leigh, D.A., Lusby, P.J., Oswald, I.D.H., Parsons, S. and Walker, D.B. (2004) *Angew. Chem.*, **116**, 4004–4008; *Angew. Chem. Int. Ed.*, **43**, 3914–3918; (b) Fuller, A.-M., Leigh, D.A., Lusby, P.J., Slawin, A.M.Z. and Walker, D.B. (2005) *J. Am. Chem. Soc.*, **127**, 12612–12619.

48 Hamilton, D.G., Feeder, N., Teat, S.J. and Sanders, J.K.M. (1998) *New J. Chem.*, 1019–1021.

49 Kaiser, G., Jarrosson, T., Otto, S., Ng, Y.-F., Bond, A.D. and Sanders, J.K.M. (2004) *Angew. Chem.*, **116**, 1993–1996; *Angew. Chem. Int. Ed.*, **43**, 1959–1962.

50 (a) Kilbinger, A.F.M., Cantrill, S.J., Waltman, A.W., Day, M.W. and Grubbs, R.H. (2003) *Angew. Chem.*, **115**, 3403–3407; *Angew. Chem. Int. Ed.*, **42**, 3281–3285; (b) Guidry, E.N., Cantrill, S. J., Stoddart, J.F. and Grubbs, R.H. (2005) *Org. Lett.*, **7**, 2129–2132.

51 Iwamoto, H., Itoh, K., Nagamiya, H. and Fukazawa, Y. (2003) *Tetrahedron Lett.*, **44**, 5773–5776.

52 Kidd, T.J., Leigh, D.A. and Wilson, A.J. (1999) *J. Am. Chem. Soc.*, **121**, 1599–1600.

53 (a) Vysotsky, M.O., Bolte, M., Thondorf, I. and Böhmer, V. (2003) *Chem. Eur. J.*, **9**, 3375–3382; (b) Wang, L., Vysotsky, M.O., Bogdan, A., Bolte, M. and Böhmer, V. (2004) *Science*, **304**, 1312–1314; (c) Bogdan, A., Vysotsky, M.O., Ikai, T., Okamoto, Y. and Böhmer, V. (2004) *Chem. Eur. J.*, **10**, 3324–3330.

54 Molokanova, O., Vysotsky, M.O., Cao, Y., Thondorf, I. and Böhmer, V. (2006)

Angew. Chem., **118**, 8220–8224; *Angew. Chem. Int. Ed.*, **45**, 8051–8055.

55 (a) Wisner, J.A., Beer, P.D., Drew, M.G.B. and Sambrook, M.R. (2002) *J. Am. Chem. Soc.*, **124**, 12469–12476; (b) Sambrook, M.R., Beer, P.D., Lankshear, M.D., Ludlow, R.F. and Wisner, J.A. (2006) *Org. Biomol. Chem.*, **4**, 1529–1538.

56 (a) Sambrook, M.R., Beer, P.D., Wisner, J.A., Paul, R.L. and Cowley, A.R. (2004) *J. Am. Chem. Soc.*, **126**, 15364–15365; (b) Ng, K.-Y., Cowley, A.R. and Beer, P.D. (2006) *Chem. Commun.*, 3676–3678.

57 Borisova, N.E., Reshetova, M.D. and Ustynyuk, Y.A. (2007) *Chem. Rev.*, **107**, 46–79.

58 Hutin, M., Schalley, C.A., Bernardinelli, G. and Nitschke, J.R. (2006) *Chem. Eur. J.*, **12**, 4069–4076.

59 Ziessel, R., Harriman, A., Suffert, J., Youinou, M.-T., De Cian, A. and Fischer, J. (1997) *Angew. Chem.*, **109**, 2621–2624; *Angew. Chem. Int. Ed.*, **36**, 2509–2511.

60 (a) Glink, P.T., Oliva, A.I., Stoddart, J.F., White, A.J.P. and Williams, D.J. (2001) *Angew. Chem.*, **113**, 1922–1927; *Angew. Chem. Int. Ed.*, **40**, 1870–1875; (b) Horn, M., Ihringer, J., Glink, P.T. and Stoddart, J.F. (2003) *Chem. Eur. J.*, **9**, 4046–4054.

61 (a) Chichak, K.S., Cantrill, S.J., Pease, A.R., Chiu, S.-H., Cave, G.W.V., Atwood, J.L. and Stoddart, J.F. (2004) *Science*, **304**, 1308–1312; (b) Chichak, K.S., Cantrill, S.J. and Stoddart, J.F. (2005) *Chem. Commun.*, 3391–3393.

62 Peters, A.J., Chichak, K.S., Cantrill, S.J. and Stoddart, J.F. (2005) *Chem. Commun.*, 3394–3396.

63 Pentecost, C.D., Chichak, K.S., Peters, A.J., Cave, G.W.V., Cantrill, S.J. and Stoddart, J.F. (2007) *Angew. Chem.*, **119**, 222–226; *Angew. Chem. Int. Ed.*, **46**, 218–222.

64 Fujita, M., Ibukuro, F., Hagihara, H. and Ogura, K. (1994) *Nature*, **367**, 720–723.

65 Fujita, M., Ibukuro, F., Yamaguchi, K. and Ogura, K. (1995) *J. Am. Chem. Soc.*, **117**, 4175–4176.

66 Fujita, M., Fujita, N., Ogura, K. and Yamaguchi, K. (1999) *Nature*, **400**, 52–55.

67 Yamashita, K.-i., Kawano, M. and Fujita, M. (2007) *J. Am. Chem. Soc.*, **129**, 1850–1851.

68 Ibukuro, F., Fujita, M., Yamaguchi, K. and Sauvage, J.-P. (1999) *J. Am. Chem. Soc.*, **121**, 11014–11015.

69 (a) Dietrich-Buchecker, C.O., Geum, N., Hori, A., Fujita, M., Sakamoto, S., Yamaguchi, K. and Sauvage, J.-P. (2001) *Chem. Commun.*, 1182–1183; (b) Dietrich-Buchecker C.O., Colasson, B., Fujita, M., Hori, A., Geum, N., Sakamoto, S., Yamaguchi, K. and Sauvage, J.-P. (2003) *J. Am. Chem. Soc.*, **125**, 5717–5725.

70 (a) Chang, S.-Y., Jang, H.-Y. and Jeong, K.-S. (2003) *Chem. Eur. J.*, **9**, 1535–1541; (b) Chang, S.-Y. and Jeong, K.-S. (2003) *J. Org. Chem.*, **68**, 4014–4019.

71 (a) Heim, C., Affeld, A., Nieger, M. and Vögtle, F. (1999) *Helv. Chim. Acta*, **82**, 746–759; (b) Parham, A.H., Windisch, B. and Vögtle, F. (1999) *Eur. J. Org. Chem.*, 1233–1238; (c) Seel, C., Parham, A.H., Safarowsky, O., Hübner, G.M. and Vögtle, F. (1999) *J. Org. Chem.*, **64**, 7236–7242.

72 Chas, M., Pia, E., Toba, R., Peinador, C. and Quintela, J.M. (2006) *Inorg. Chem.*, **45**, 6117–6119.

73 Blight, B.A., Wisner, J.A. and Jennings, M.C. (2007) *Angew. Chem.*, **119**, 2893–2896; *Angew. Chem. Int. Ed.*, **46**, 2835–2838.

74 (a) Hunter, C., (1991) *J. Chem. Soc., Chem Commun.*, 749–751; (b) Hunter, C. and Purvis, D.H. (1992) *Angew. Chem.*, **104**, 779–782; *Angew. Chem., Int. Ed.*, **31**, 792–795.

75 Blight, B.A., Wisner, J.A. and Jennings, M.C. (2006) *Chem. Commun.*, 4583–4585

76 Blight, B.A., Van Noortwyk, K.A., Wisner, J.A. and Jennings, M.C. (2005) *Angew. Chem.*, **117**, 1523–1528; *Angew. Chem. Int. Ed.*, **44**, 1499–1504.

Index

Supramolecular chemistry continues to be a topic of major interest in chemical research. Nowadays, with gas storage systems, pharmaceutical applications and self-assembling materials, there has been a new drive towards new synthetic methods.

Written by internationally acclaimed experts, this handy volume is the long awaited state-of-the-art work and covers all major classes of supramolecular compounds. Chapters include cyclophanes, resorcinarene and calixarene synthesis, supramolecular metallomacrocycles and macrocycle synthesis, rotaxane and catenane synthesis, cucurbiturils and porphyrins, as well as macrocyclic drugs. As a bonus each chapter contains experimental procedures allowing fast access to this fascinating type of synthetic chemistry.

François Diederich studied chemistry at the University of Heidelberg. He joined the group of Heinz A. Staab for his diploma and doctoral theses, which he completed with the synthesis of kekulene. Following postdoctoral studies with Orville L. Chapman at University of California at Los Angeles (UCLA) he returned to Heidelberg for his Habilitation at the Max-Planck-Institut für Medizinische Forschung. Subsequently, he joined the faculty in the Department of Chemistry and Biochemistry at UCLA where he became Full Professor of Organic and Bioorganic Chemistry. In 1992, he joined the Department of Chemistry and Applied Biosciences at the Swiss Federal Institute of Technology (ETH), Zürich. His research interests, documented in more than 500 publications, are currently in the entire field of supramolecular chemistry.

Peter J. Stang received his doctoral degree from the University of California at Berkeley and after postdoctoral studies at Princeton University joined the faculty at the University of Utah in Salt Lake City, where he is currently a Distinguished Professor of Chemistry and the Editor in Chief of the Journal of the American Chemical Society (JACS). He is a Member of the US National Academy of Sciences as well as a Fellow of the American Academy of Arts and Sciences and a Foreign Member of the Chinese Academy of Sciences and the Hungarian Academy of Sciences. He is the author of 410 scientific publications in the areas of supramolecular chemistry and self-assembly, polyvalent iodine chemistry, alkynyl esters and unsaturated reactive intermediates.

Rik R. Tykwinski received his BS degree from the University of Minnesota–Duluth and his PhD from the University of Utah. After postdoctoral studies at the Swiss Federal Institute of Technology (ETH), Zürich, he joined the faculty of the University of Alberta and is now Professor of Chemistry. He has published over 100 research papers concerning new synthetic methods for the synthesis of enynes and polyynes, characterization of their electronic and nonlinear optical properties, and the application of conjugated systems to supramolecular chemistry.